LEVEL

CORROSION FATIGUE OF METALS IN MARINE ENVIRONMENTS

DTIC
ELECTE
NOV 17 1981
S D
A

Metals and Ceramics Information Center

Battelle
Columbus Laboratories
505 King Avenue
Columbus, Ohio 43201

81 11 17003

SECURITY CLASSIFICATION OF THIS PAGE (When Data Entered)

REPORT DOCUMENTATION PAGE	READ INSTRUCTIONS BEFORE COMPLETING FORM

1. REPORT NUMBER	2. GOVT ACCESSION NO.	3. RECIPIENT'S CATALOG NUMBER
MCIC-81-42	AD-A107 247	

4. TITLE (and Subtitle)	5. TYPE OF REPORT & PERIOD COVERED
Corrosion Fatigue Of Metals In Marine Environments	State-of-the-Art
	6. PERFORMING ORG. REPORT NUMBER
	MCIC-81-42

7. AUTHOR(s)	8. CONTRACT OR GRANT NUMBER(s)
C. E. Jaske J. H. Payer V. S. Balint	

9. PERFORMING ORGANIZATION NAME AND ADDRESS	10. PROGRAM ELEMENT, PROJECT, TASK AREA & WORK UNIT NUMBERS
Battelle's Columbus Laboratories	

11. CONTROLLING OFFICE NAME AND ADDRESS	12. REPORT DATE
263	July 1981
	13. NUMBER OF PAGES
	262

14. MONITORING AGENCY NAME & ADDRESS(if different from Controlling Office)	15. SECURITY CLASS. (of this report)
Army Materials and Mechanics Research Center, Watertown, Massachusetts	Unclassfied
	15a. DECLASSIFICATION/DOWNGRADING SCHEDULE

16. DISTRIBUTION STATEMENT (of this Report)

Approved for Public Release; distribution unlimited

17. DISTRIBUTION STATEMENT (of the abstract entered in Block 20, if different from Report)

18. SUPPLEMENTARY NOTES

19. KEY WORDS (Continue on reverse side if necessary and identify by block number)

Corrosion fatigue	Crack propagation	Copper alloys
Fatigue	Stainless Steel	Aluminum alloys
Seawater	Nickel alloys	Titanium alloys

20. ABSTRACT (Continue on reverse side if necessary and identify by block number)

   In many engineering applications, metallic materials are used in structures, components, and machinery that are subjected to cyclic loadings and exposed to marine environments. The combined action of cyclic loading and aggressive environment often results in a significant reduction in fatigue performance compared with that obtained under cyclic loading in inert environments. Fatigue damage occurring under the conjoint action of cyclic loading and aggressive environment is generically referred to as corrosion fatigue. This damage may

(Continued)

DD FORM 1473 EDITION OF 1 NOV 55 IS OBSOLETE
1 JAN 73

467032

SECURITY CLASSIFICATION OF THIS PAGE (When Data Entered)

20. (Continued)

be a simple superposition of fatigue cracking and corrosive attack or it may be a more complex synergistic interaction of these two modes.

Examples of equipment and structures where corrosion fatigue is an important consideration are ships, offshore platforms, mining and oil drilling rigs, aircraft, navigation and communication towers, bridges, and underwater pipelines. The marine environment may be (1) full immersion in natural seawater, brackish water, or polluted seawater; (2) alternate wet/dry areas in splash, spray, or tidal zones; or (3) atmospheric exposure near saline bodies of water. In all of these cases, designers, engineers, and operators must be aware of the possible deleterious effects of corrosion fatigue on material performance and must assess the potential impact of these effects on design, safety, and reliability of engineering systems. Moreover, in military uses-for example, in aircraft, amphibious vehicles, and communication equipment-operation without failure due to corrosion fatigue is vital to defense and security operations.

This book was prepared to document and review the major factors involved in corrosion fatigue of metals in marine environments. This includes both crack initiation and crack growth. For convenient use and reference, discussions on corrosion-fatigue behavior are divided into separate chapters dealing with (1) carbon and alloy steels, (2) stainless steels, (3) nickel-base alloys, (4) copper-base alloys, (5) aluminum alloys, and (6) titanium alloys.

AUTHOR WORKSHEET

1. Report Number: MCIC-81-42

2. Title: Corrosion Fatigue of Metals in Marine Environments

3. Price: $45.00 (U.S.), $90.00 (Foreign)

4. 262 pages, 267 references, 239 figures, 39 tables

5. Authors: C. E. Jaske, J. H. Payer, V. S. Balint

6. Performing Organization: Battelle's Columbus Laboratories

7. Abstract:

In many engineering applications, metallic materials are used in structures, components, and machinery that are subjected to cyclic loadings and exposed to marine environments. The combined action of cyclic loading and aggressive environment often results in a significant reduction in fatigue performance compared with that obtained under cyclic loading in inert environments. Fatigue damage occurring under the conjoint action of cyclic loading and aggressive environment is generically referred to as corrosion fatigue. This damage may be a simple super-position of fatigue cracking and corrosive attack or it may be a more complex synergistic interaction of these two modes.

Examples of equipment and structures where corrosion fatigue is an important consideration are ships, offshore platforms, mining and oil drilling rigs, aircraft, navigation and communication towers, bridges, and underwater pipelines. The marine environment may be (1) full immersion in natural seawater, brackish water, or polluted seawater; (2) alternate wet/dry areas in splash, spray, or tidal zones; or (3) atmospheric exposure near saline bodies of water. In all of these cases designers, engineers, and operators must be aware of the possible deleterious effects of corrosion fatigue on material performance and must assess the potential impact of these effects on design, safety, and reliability of engineering systems. Moreover, in military uses- for example, in aircraft, amphibious vehicles, and communication equipment-operation withou failure due to corrosion fatigue is vital to defense and security operations.

This book was prepared to document and review the major factors in- volved in corrosion fatigue of metals in marine environments. This includes both crack initiation and crack growth. For convenient use and reference, discussions on corrosion-fatigue behavior are divided into separate chapters dealing with (1) nickel-base alloys, (4) copper-base alloys, (5) aluminum alloys, and (6) titanium alloys.

8. This report discusses the importance of corrosion-fatigue in marine environments such as ships, offshore platforms, oil rigs, aircraft, bridges, and pipelines.

9. This report will be useful to: oil industry, aircraft maintenance, communications groups, pipeline companies, military organizations.

10. Chemical Industry, Metallurgical Industries, Municipal and State Road Maintenance Groups, Oil and Gas Companies: Industries interested in this report.

11. Organizations who may have mailing lists: American Society for Metals, National Association of Corrosion Engineers, American Insititute of Mining, Metallurgical and Petroleum Engineers, American Institute of Chemical Engineers.

12. Keywords: Corrosion fatigue, Fatigue, Seawater, Crack propagation, Stainless Steel, Nickel alloys, Copper alloys, Aluminum alloys, Titanium alloys.

13. Applicable NTIS Scope-Note Fields: 71G 71J 71N 800

Date _12 Nov 1981_   NTIS Control #_____

TO: Defense Technical Information
            Center - DTIC
        Cameron Station
        Alexandria, Virginia 22314

FROM: NTIS, Input Branch
        5285 Port Royal Road
        Springfield, Virginia 22161

Report # _MCIC - 81 - 42_   ADA # _A107247_

Title: "_Corrosion Fatigue of Metals in Marine_".

Subject report is [ ] Standard Process [X] STG report. STG - Special
Technology Group.   [ ] Computer Product [ ] Follow up date_____

[ ] The report will be accessioned by DDC. The form noting the ADA numbe
    is returned.

[ ] The report has been assigned the ADA number noted above and is return
    to NTIS for processing.

[ ] DDC will not process the report. It is returned to NTIS

. . . .

Mag Tape Price_____
PC & MF Price _45.50 MF 45.50_   Source _MCIC_ _field 3_

Stock Quantity _102_   Source Share _30.50_
            Bin - B9   _NTI$_   _15.00_
Comments:

field 4
P C   E 19
M F   E 19   _Dottie Adams_
                                    ————————————————
                                    Signature (for billing)

Copy when completed to
Finance Branch

DOD Report Action Request
(Replaces NTIS-164 5-72)

Please return to NTIS - Information Services Branch, Room 301, Yorktown Building.
Attention: Dottie Adams

CORROSION FATIGUE OF METALS IN MARINE ENVIRONMENTS

C. E. Jaske, J. H. Payer, and V. S. Balint
Battelle's Columbus Laboratories

CORROSION FATIGUE OF METALS
IN MARINE ENVIRONMENTS

by

C. E. Jaske
J. H. Payer
V. S. Balint

Battelle's Columbus Laboratories
Columbus, Ohio 43201

ACKNOWLEDGMENT

Accession For

NTIS GRA&I

DTIC TAB

Unannounced

Justification

$75.50

By NTIS

Distribution/

Availability Codes

Avail and/or

Dist   Special

A 21

TABLE OF CONTENTS

TABLE OF CONTENTS
(Continued)

TABLE OF CONTENTS
(Continued)

TABLE OF CONTENTS
(Continued)

LIST OF FIGURES

LIST OF FIGURES
(Continued)

Page

LIST OF FIGURES
(Continued)

Page

LIST OF FIGURES
(Continued)

LIST OF FIGURES
(Continued)

LIST OF FIGURES
(Continued)

Page

LIST OF FIGURES
(Continued)

LIST OF FIGURES

LIST OF FIGURES
(Continued)

LIST OF TABLES

LIST OF TABLES

CHAPTER 1
INTRODUCTION

In many engineering applications, metallic materials are used in structures, components, and machinery that are subjected to cyclic loadings and exposed to marine environments. The combined action of cyclic loading and aggressive environment often results in a significant reduction in fatigue performance compared with that obtained under cyclic loading in inert environments. Fatigue damage occurring under the conjoint action of cyclic loading and aggressive environment is generically referred to as corrosion fatigue. This damage may be a simple superposition of fatigue cracking and corrosive attack or it may be a more complex synergistic interaction of these two modes.

Examples of equipment and structures where corrosion fatigue is an important consideration are ships, offshore platforms, mining and oil drilling rigs, aircraft, navigation and communication towers, bridges, and underwater pipelines. The marine environment may be (1) full immersion in natural seawater, brackish water, or polluted seawater; (2) alternate wet/dry areas in splash, spray, or tidal zones; or (3 atmospheric exposure near saline bodies of water. In all of these cases, designers, engineers, and operators must be aware of the possible deleterious effects of corrosion fatigue on material performance and must assess the potential impact of these effects on design, safety, and reliability of engineering systems. Moreover, in military uses—for example, in aircraft, amphibious vehicles, and communication equipment—operation without failure due to corrosion fatigue is vital to defense and security operations.

This book was prepared to document and review the major factors involved in corrosion fatigue of metals in marine environments. This includes both crack initiation and crack growth. Background information was obtained by searching technical literature through eight different sources—(1) Chemical Abstracts, (2) Metals Abstracts, (3) Metals and Ceramics Information Center (MCIC), (4) Engineering Index, (5) Copper Data Center, (6) National Technical Information Service, (7) Defense Technical Information Service, and (8) Proceedings of Offshore Technology Conferences. Unpublished and proprietary papers and reports were excluded unless permission was obtained to release the results contained therein. Thus, most of the information was from documents published in the open literature.

For convenient use and reference, discussions on corrosion-fatigue behavior are divided into separate chapters dealing with (1) carbon and alloy steels, (2) stainless steels, (3) nickel-base alloys, (4) copper-base alloys, (5) aluminum alloys, and (6) titanium alloys. Representative plots and tabulations of important data and factors influencing them are presented, but exhaustive plots and tabulations of all available data, such as might be found in handbooks, are not included because these are beyond the scope of this review. A general background for corrosion fatigue is presented in Chapter 2, which briefly discusses experimental procedures, general phenomena and mechanisms, variables affecting corrosion of metals in marine environments, and use of fatigue data in design.

CHAPTER 2
BACKGROUND FOR CORROSION FATIGUE IN MARINE ENVIRONMENTS

This chapter provides perspective and background for the discussions of corrosion-fatigue behavior presented in ensuing chapters. Four areas—(1) experimental procedures, (2) phenomena and mechanisms, (3) variables affecting corrosion, and (4) design use of fatigue data—are briefly reviewed.

Experimental Techniques and Procedures in Corrosion-Fatigue Testing

The experimental techniques, apparatus, and specimen configurations used in corrosion-fatigue testing are basically the same as those used in general fatigue testing.[1] Environmental effects are induced by submerging the specimen test section in an aqueous solution, by enclosing it in a chamber with controlled gaseous composition, or by dripping, splashing, spraying, or wicking a solution onto the test section surface. Smooth (unnotched) and notched specimens are used to develop S-N curves in fatigue-life studies. Fracture-mechanics-type, precracked specimens are used to generate fatigue-crack-propagation data. To assist in understanding experimental results and data presented in succeeding chapters, it is instructive to briefly review experimental methods commonly used in corrosion-fatigue testing. In certain special cases, structural components or prototypical hardware may be subjected to corrosion-fatigue testing. Usually, however, laboratory specimens with simple configurations and well-defined states of loading are used in corrosion-fatigue evaluations of materials. It is these specimens that are of interest in this review.

Fatigue-Life Studies

The majority of corrosion fatigue experiments are performed on specimens loaded in bending or on specimens loaded uniaxially. Torsion and more complex multiaxial loading states are not often used in corrosion-fatigue work.

The simplest and the first widely used fatigue testing machines are of the rotating bending type. One example of this type is the R. R. Moore rotating-beam fatigue machine shown schematically in Figure 1. The loading produces a constant moment in the test section. As the specimen rotates, a fully reversed sinusoidal stressing pattern is repeatedly produced on its surface. The R. R. Moore rotating-beam fatigue machine has an hourglass-shaped test section as shown in Figure 2. However, cylindrical test-section specimens are also often used in rotating bending experiments. For example, Figure 3 shows the cylindrical specimen used by Ebara et al.[2] In some variations of rotating bending fatigue machines, cantilever bending is used as in the McAdam-type machines that have been used extensively in corrosion-fatigue studies by the U.S. Navy at Annapolis, Maryland (e.g., see References 3 and 4) and at the Francis L. LaQue Corrosion Laboratory in Wrightsville Beach, North Carolina[5,6]. Although only smooth specimens are illustrated in Figures 2 and 3, circumferential grooves can be introduced to study notch effects. Although these conventional rotating bending machines are fairly simple, highly reliable, and easy to use, they are restricted to round specimens and the mean cyclic stress is always zero. Webb et al[7] have developed a special rotating bending machine

3
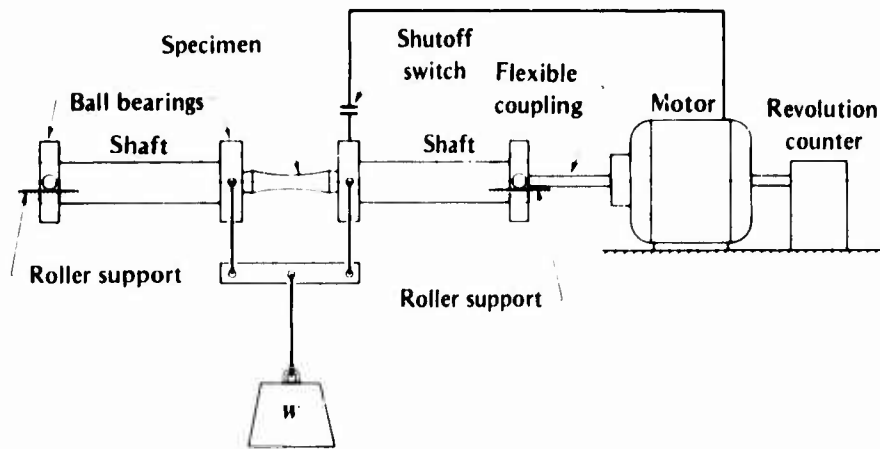
FIGURE 1. Schematic of R. R. Moore Rotating Beam Fatigue Machine[8]

3-7/16

$1\frac{23}{32}$

3/4   1-15/16

0.495 diam.

3/16 → 3/16 →   d = 0.200 to 0.400

5/8 taper per foot
grind to fit gage

Relief 0.010 deep

R = 3.5 to 10

No. 4 drill — 1/2 deep,
1/4 — 20 tap — 7/15 deep,
60° csk

Tolerances
Fractions ± 1/64
Decimals ± .005
except as noted

All dimensions in in. (1 in. = 25.4 mm)
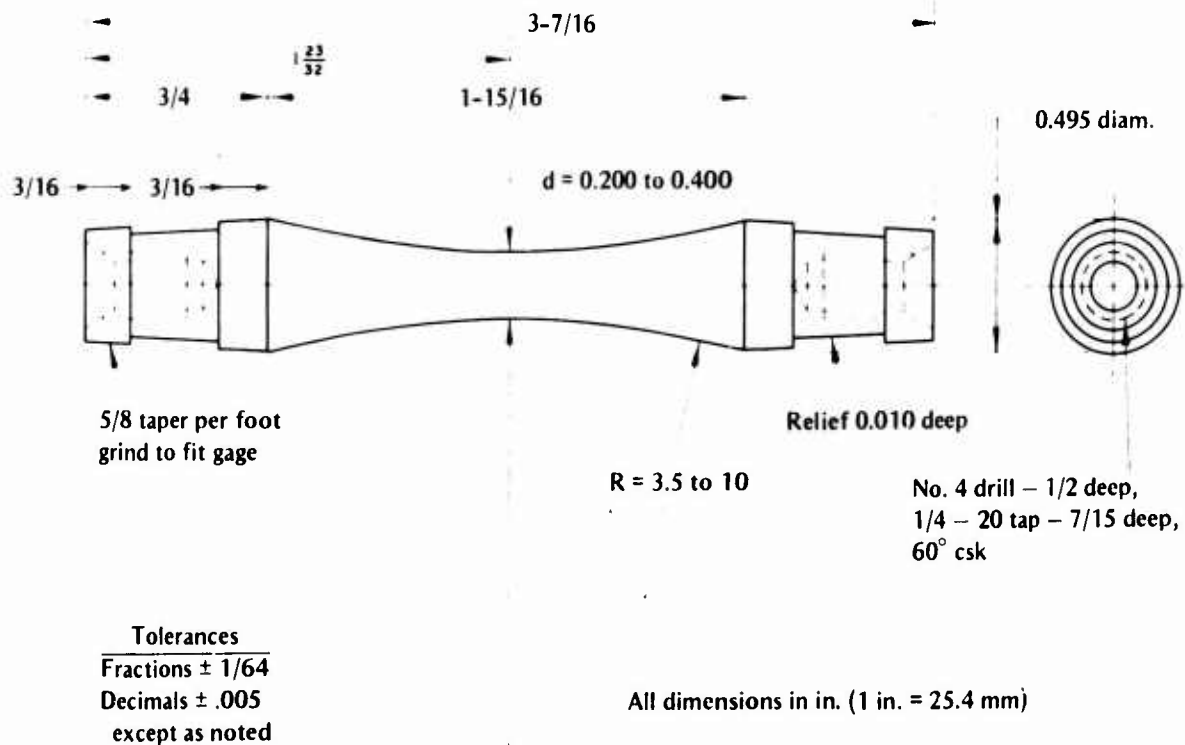
FIGURE 2. R. R. Moore Rotating Beam Specimen

All dimensions are approximate and in inches.

0.6 ± 0.0004   1R   0.4 ± 0.0004

— 1.5 —
— 2 —
— 8.25 —
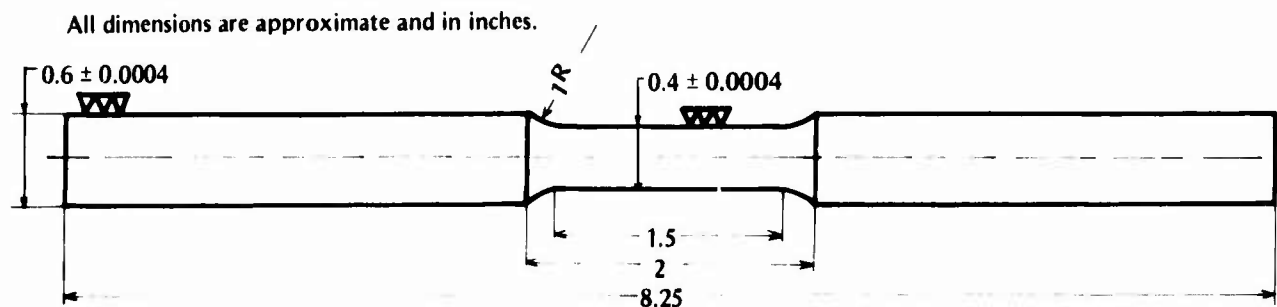
FIGURE 3. Cylindrical Test Section Rotating Beam Specimen[2]

that uses large, 3-in. (76.2-mm)-diameter hollow specimens. A special device is inserted inside these specimens so that they can be axially preloaded to a desired level of tensile mean stress, with the cyclic stress being applied by rotating bending. With rotating bending, the peak stress and strain are difficult to determine if yielding occurs. Thus, these machines are best-suited to long-life fatigue testing where the cyclic stress-strain response is nominally elastic.

The other simple type of fatigue test is repeated bending with cantilever, three-point bending, or four-point bending loading. The loading is usually mechanical with fixed-displacement control by means of a rotating adjustable cam/crank arrangement. Load control can be achieved by using a closed-loop electrohydraulic system in place of the mechanical loading, but this is not commonly used for corrosion-fatigue testing. A schematic of the cantilever, fixed-deflection machine is shown in Figure 4. The test specimen cross section need not be circular (as with rotating bending), and sheet and plate specimens of rectangular cross section are frequently employed. This type of machine was used in an extensive study of the corrosion-fatigue behavior of bronze propeller alloys, and, as is often done, the specimen test section was tapered (see Figure 5) to produce a constant-stress, test-section region. The same type of specimen has also been used for corrosion-fatigue testing at the U.S. Navy's David W. Taylor Naval Ship Research and Development Center.[10] Again, these machines are simple, highly reliable, and easy to use. With repeated bending, different levels of mean tensile stress can be easily introduced. As with rotating bending, the peak stress and strain are difficult to determine if yielding occurs, a problem which was encountered and addressed by Jaske et al.[9] Also, with fixed-displacement loading, the applied tensile load will decrease as cracking occurs and the crack will not propagate as rapidly as it would if load control were employed. It is even possible that the cracks may arrest and become nonpropagating.

Uniaxially loaded specimens are used widely in corrosion-fatigue evaluation of metals, and recommended practices for conducting axial-load fatigue tests have been published.[11,12] Specimens can have a variety of cross-sectional shapes, various mean stresses can be employed, and the axial stress and strain within the specimen test section can be defined clearly and measured easily. Testing machines used for axial loading of specimens are more complex than those described above, slightly more prone to breakdowns, and generally more costly to operate. However, the advantages of uniaxial loading usually offset these factors. Axial-load fatigue systems can be driven by mechanical oscillators, mechanical drives, resonant drives, electromagnetic shakers, hydraulic pulsators, and electrohydraulic actuators.[1] Actually, with appropriate fixturing, these driving devices can be used to test specimens in repeated bending or torsion. Since many of these devices are not commonly used in corrosion-fatigue testing and since discussions on their use are available elsewhere, only two of the most commonly used types, mechanical and electrohydraulic, are described here.

A schematic of a mechanically driven fatigue-test system often used to apply sinusoidal axial loading (constant amplitude) to a specimen is shown in Figure 6. Cyclic load is applied by means of an adjustable cam (driven by a rotating motor), connecting rod, and lever arrangement. Flexure plates are used to minimize bending of the specimen. The mean load may be mechanically fixed (when specimen length changes are negligible) by adjusting the spindle shown in Figure 6 or by using a hydraulic load-maintainer piston that compensates for small length changes in the specimen. This type of system is relatively economical to operate but is limited mainly to long-life fatigue testing where the cyclic stress-strain response is nominally elastic.

The most versatile and widely used kind of fatigue testing system is the closed-loop, servo-controlled electrohydraulic system. During the past 15 years, this type of fatigue testing system has received widespread and rapidly increasing use in fatigue laboratories primarily because of its versatility (e.g., many applications are described in Reference 13). A schematic of one such typical system[1] is shown in Figure 7. The major components are the load frame, the

6
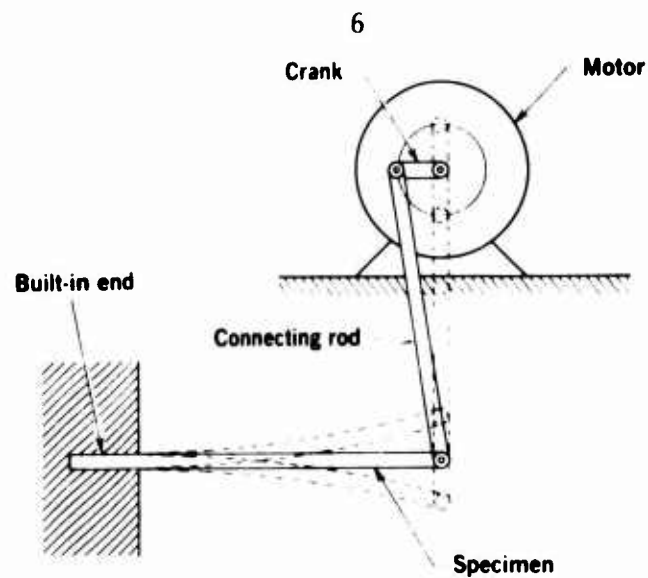
FIGURE 4. Schematic of Cantilever Repeated Bending Fatigue Machine[8]
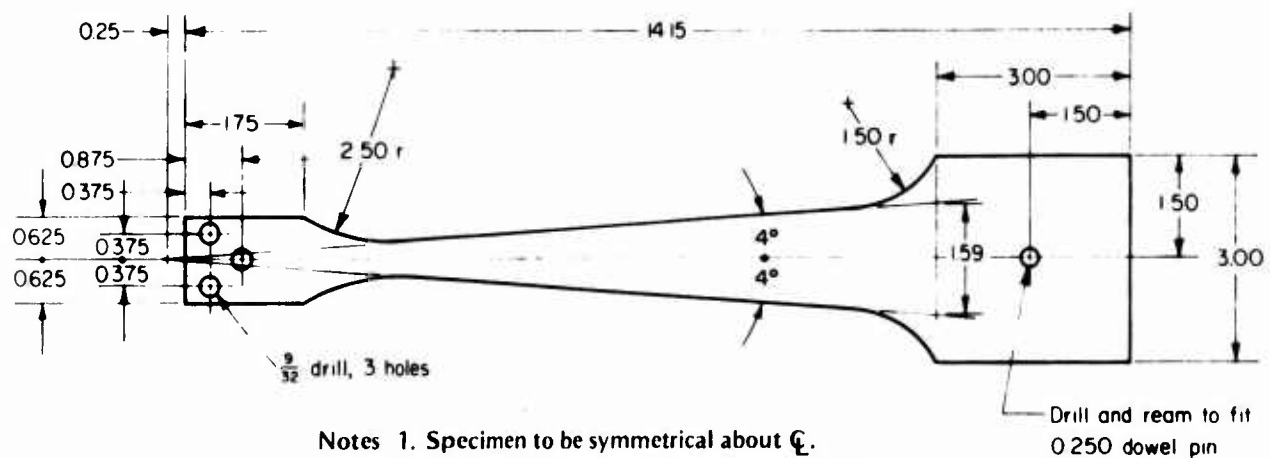
Notes 1. Specimen to be symmetrical about ₵.
2. Specimen thickness shall be 0.400 ± .001 in.
3. All dimensions in inches.

FIGURE 5. Cantilever Bending Specimen[9]

1. Specimen
2. Specimen grips
3. Load proving ring.
4. Fixed head assembly
5. Mean load spindle
6. Moving head assembly
7. Load lever
8. Connecting rod
9. Variable cam motor
10. Shut-down contact
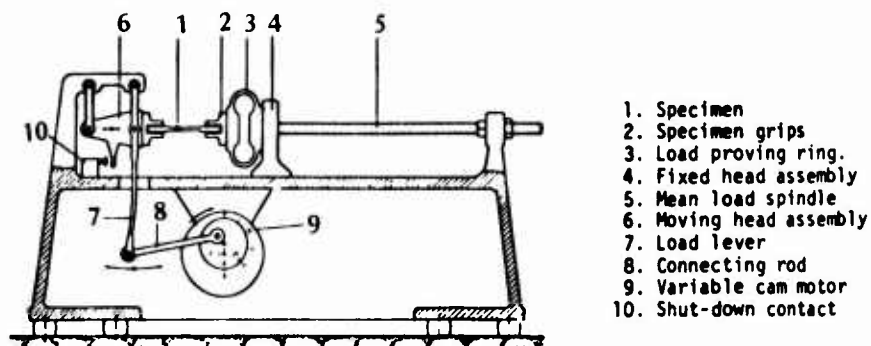
FIGURE 6. Schematic Illustration of Mechanically Driven Fatigue Test System[1]
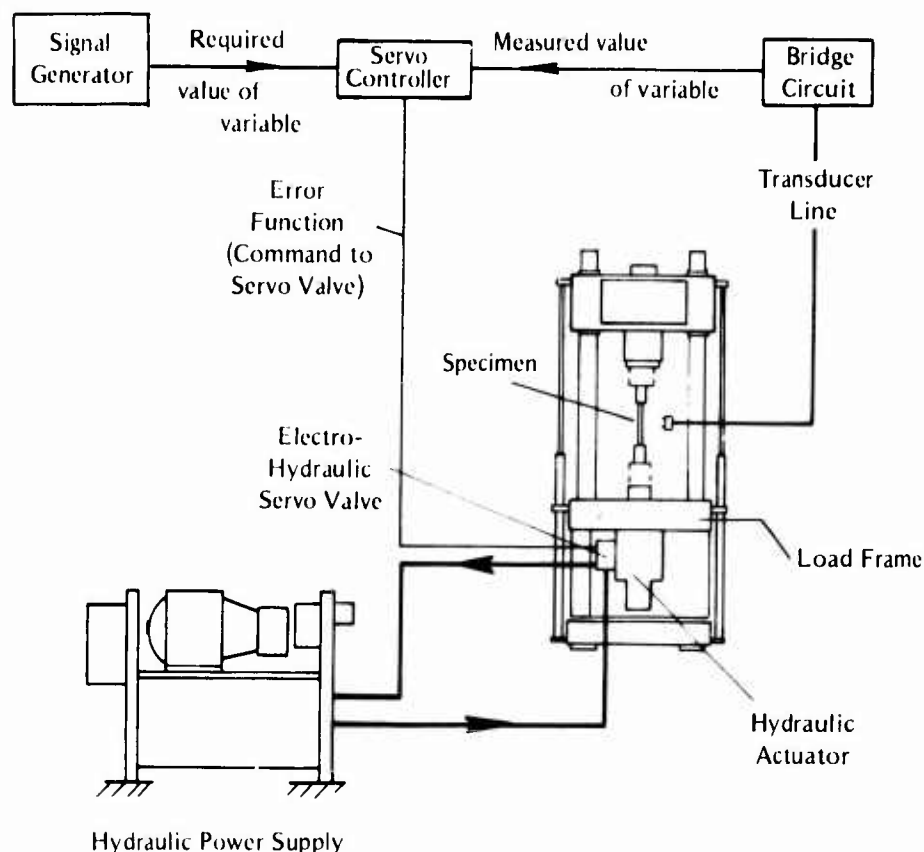
FIGURE 7. Schematic of a Typical Closed-Loop, Electrohydraulic Fatigue Testing System[1]

hydraulic actuator, the hydraulic power supply, the electrohydraulic servo-valve, the servo-controller, the signal generator, the specimen, and a load, displacement, and/or strain transducer. Within the capabilities of the hydraulic system response, the variable measured by the transducer (usually load, displacement, or strain) can be programmed to follow any arbitrary waveform produced by the signal generator. Therefore, real-service-type, variable-amplitude loading histories can be imposed on the specimen. With this type of system, fatigue experiments can be easily automated and interfaced with digital programmers, analog computers, digital computers, and hybrid combinations of these devices.[1] Closed-loop electrohydraulic test systems are used routinely in many corrosion-fatigue studies.

Examples of the most commonly employed axial-load fatigue-specimen configurations are shown in Figure 8.[11] Specimens usually have either circular (Figure 8, a and b) or rectangular (Figure 8, c and d) cross sections. The test-section area normally is either constant-size (Figure 8, a and c) with uniform axial stress in the gage length or hourglass shaped (Figure 8, b and d) with maximum axial stress at the minimum cross-sectional area. The grip ends may be clamped directly in special fixtures or machined with threads, button ends, pinholes, or bolt holes for attachment to loading fixtures. The test section may contain notches, welds, or other simulated fabrication details. The surface condition and residual stresses play an important role in fatigue initiation. Machined and polished surfaces are often used. In many cases, however, the surface may be prepared to a condition that simulates service applications. Further details on fatigue-specimen design are available in the literature. [1,11-13]
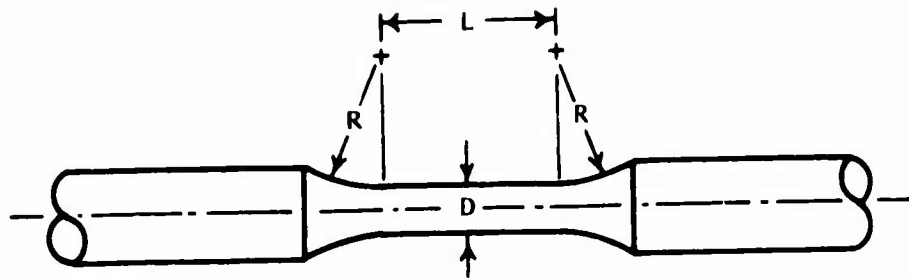
a. Specimens with Tangentially Blending Fillets Between the Test Section and the Ends
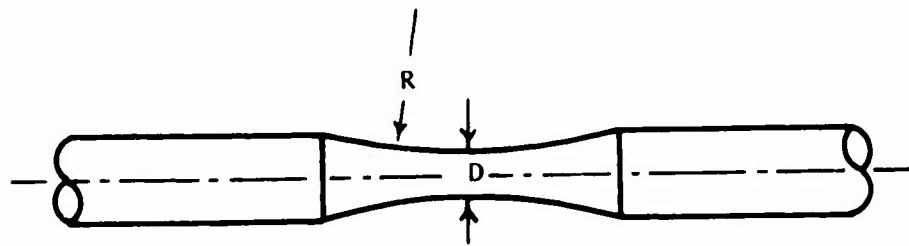
b. Specimens with a Continuous Radius Between Ends
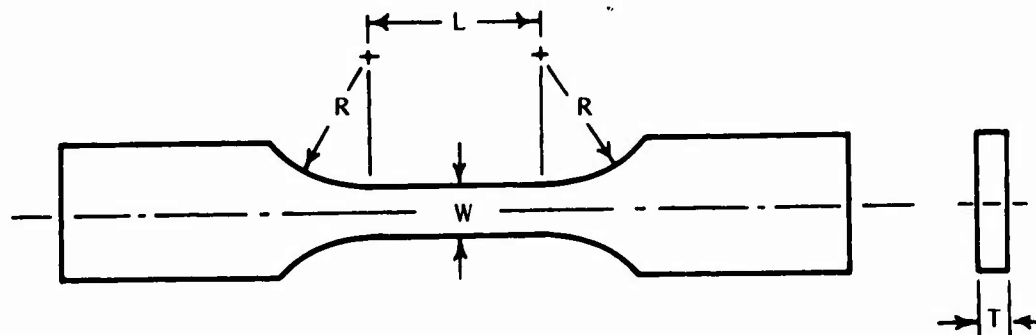
c. Specimens with Tangentially Blending Fillets Between the Uniform Test Section and the Ends
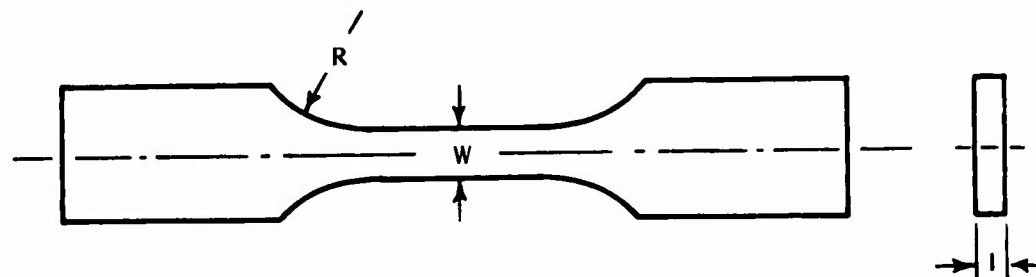
d. Specimens with Continuous Radius Between Ends

FIGURE 8. Typical Configurations of Axial-Load Fatigue Specimens[11]

Fatigue-Crack-Growth Studies

The fatigue testing machines used in fatigue-crack-growth studies are the same as those used in the fatigue-life studies described above, with the exception of rotating beam machines, which generally are not preferred for these types of experiments. Procedures for conducting fatigue-crack-growth tests at rates above 4×10^{-7} in./cycle (10^{-8} m/cycle) have been developed[14] and evaluated by workers at a number of laboratories[15]. Similarly, procedures for threshold [growth rates near or below 4×10^{-7} in./cycle (10^{-8} m/cycle)] studies are being developed and evaluated.[16] Basically, crack length, a, is measured as a function of the applied number of loading cycles, N. Knowing this relationship, the cyclic crack growth rate, da/dN, can be obtained at particular points during the test. At corresponding points, the range (and mean level) of the linear elastic stress intensity factor, ΔK, can be determined. Thus, information on da/dN values as a function of ΔK can be developed.

Two standard types of specimens are recommended for fatigue-crack-growth rate testing.[14] The compact-type (CT) specimen shown in Figure 9 allows the use of test material to be minimized, but it is "not recommended for tension-compression testing because of uncertainties introduced into the K calibration".[14] The center-cracked-tension (CCT) specimen shown in Figure 10 requires more material but is suitable for both tension-tension and tension-compression testing (providing that buckling is prevented). It also is more practical for testing thin plate and sheet materials. Single-edge-notch (SEN), double, edge-notch, and surface-flaw specimens also are used in fatigue-crack-growth studies. For example, Figure 11 shows an SEN specimen used at the U.S. Naval Research Laboratory, Marine Corrosion Research Laboratory, in Key West, Florida.[17] This particular SEN specimen configuration is used for cantilever bending, whereas other types of SEN specimens are sometimes tested under axial loading. All of these specimen types are employed in corrosion-fatigue-crack-growth studies.
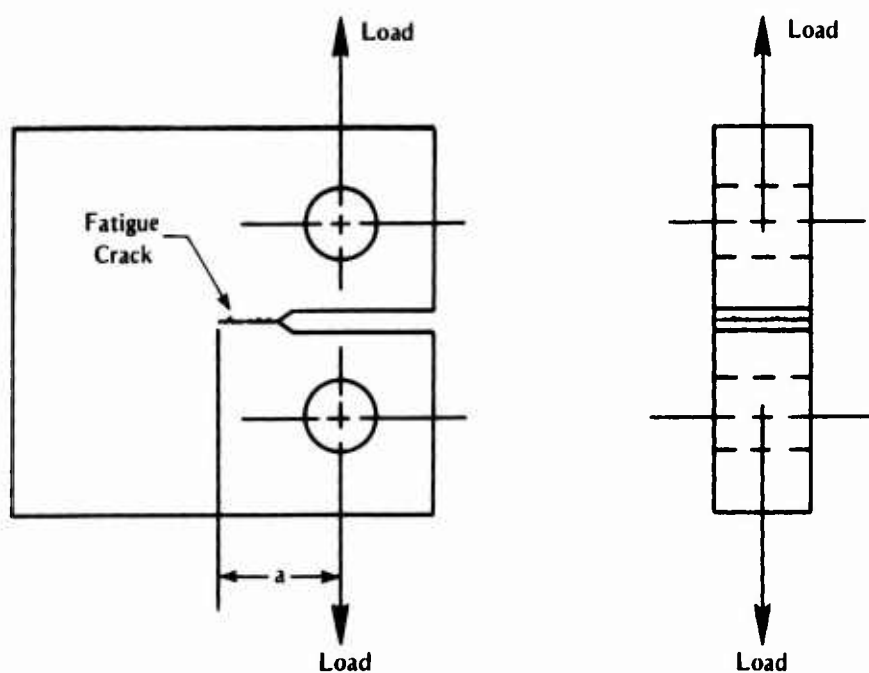
FIGURE 9. Compact-Type (CT) Specimen Used in Fatigue–Crack–Growth Testing

FIGURE 10. Center-Cracked-Tension (CCT) Specimen Used in Fatigue–Crack-Growth Testing

FIGURE 11. Example of a Single-Edge-Notch (SEN)
Specimen Used in Fatigue-Crack-Growth Testing[17]

Environmental Control

General kinds of aqueous solutions are used to simulate marine environments in corrosion-fatigue experiments. These include fresh natural seawater, seawater with organic species removed (usually shipped to an inland laboratory site), synthetic seawater solutions such as ASTM standard synthetic seawater[18], brackish waters, and sodium chloride solutions.

In comparing results obtained by different investigators or in using data to provide design guidelines for particular service applications, it is important to remember that these variations in water composition may have a significant influence on corrosion-fatigue behavior.

In most marine-environment corrosion-fatigue experiments, the specimen test section is totally immersed in the aqueous solution. Sometimes the solution is dripped or sprayed onto the specimen surface. With the latter methods, the surface may be kept moist continuously or it may be allowed to become alternately wet and dry for certain periods. Immersion is usually achieved by enclosing the specimen test section with a chamber through which water is flowed, as illustrated in Figures 12 through 15. The flow rate is, typically, just fast enough to ensure a constant supply of well-aerated water with minimal contamination and to avoid stagnant conditions. In some cases, however, the flow rate is fast enough to examine the effects of increased water velocity on the corrosion-fatigue process. Simple chambers for small ~0.25 to 0.5-in. (6 to 12-mm)-diameter, round specimens used in fatigue-life testing are shown in Figures 12 and 13. Figure 14 shows a larger, ~1.5 by 1-in. (38.0 by 25.4-mm) cross section, welded specimen tested to determine fatigue life under axial loading.[19] A CCT specimen with three cracks along its length[19] is shown in Figure 15. Each crack has a separate environmental chamber so that the effects of three environments can be evaluated under identical loading histories. These chambers and associated fittings, flow lines, reservoirs, and pumps are normally made from plastic (nonmetallic) materials to avoid introduction of undesired metallic ions into the water and to prevent possible unintended galvanic effects.
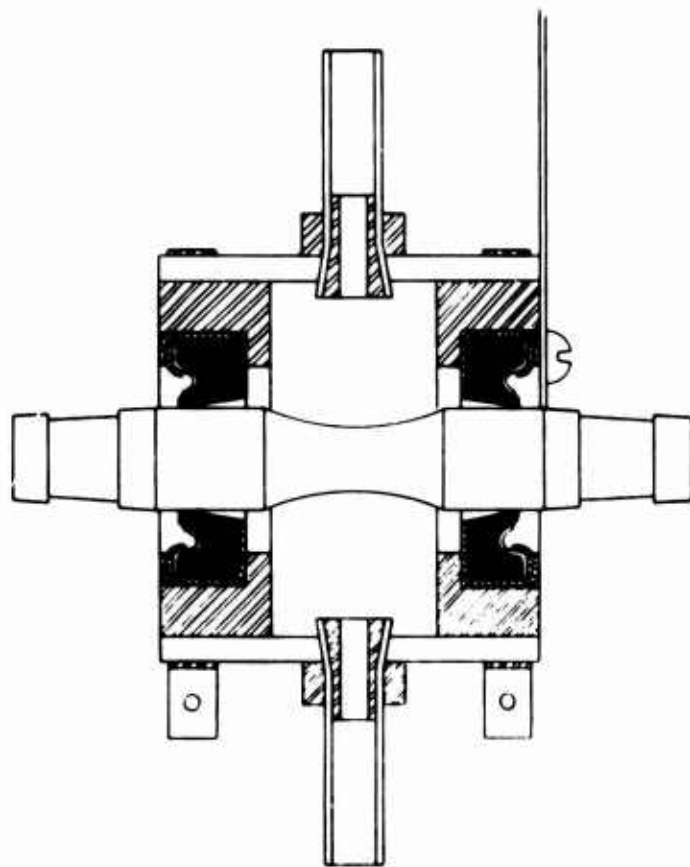
FIGURE 12. Rotating Beam Specimen With a Test Chamber for Corrosive Fluids[1]

FIGURE 13. Axial-Load Fatigue Specimen With Chamber
for Testing in Water Environment[1]

Important environmental variables that may significantly influence corrosion-fatigue damage should be controlled or monitored. As mentioned above, the water composition and flow rates should be controlled carefully and the controlled values should be reported. In addition, water temperature, level of dissolved oxygen, pH level, pressure, and electrochemical potential should be controlled or measured. Most fatigue experiments are conducted at ambient temperatures of about 68 to 77 F (20 to 25 C). In some cases, however, higher or lower temperatures are used by either heating or chilling the water reservoir. Most corrosion-fatigue testing is carried out at ambient atmospheric pressure, although some work has been done at high pressures to simulate conditions that may be encountered in deep waters. Typically, seawater will have 5 to 10 ppm dissolved oxygen, 30 to 35 ppt salinity, and 7.8 to 8.2 pH level. Variations within these ranges generally are expected to have little influence on corrosion-fatigue behavior. However, larger variations or values outside of these ranges may significantly affect corrosion fatigue.

Most corrosion-fatigue experiments in marine environments are carried out under free-corrosion conditions. It is desirable to measure the free-corrosion potential during such experiments, but often this is not done. In some experiments, the specimens are anodically or cathodically polarized. Anodic polarization usually is employed in studies to examine the influence of accelerated corrosion rates on the corrosion-fatigue-damage process. Cathodic polarization is used to simulate the effects of commonly used cathodic protection methods on
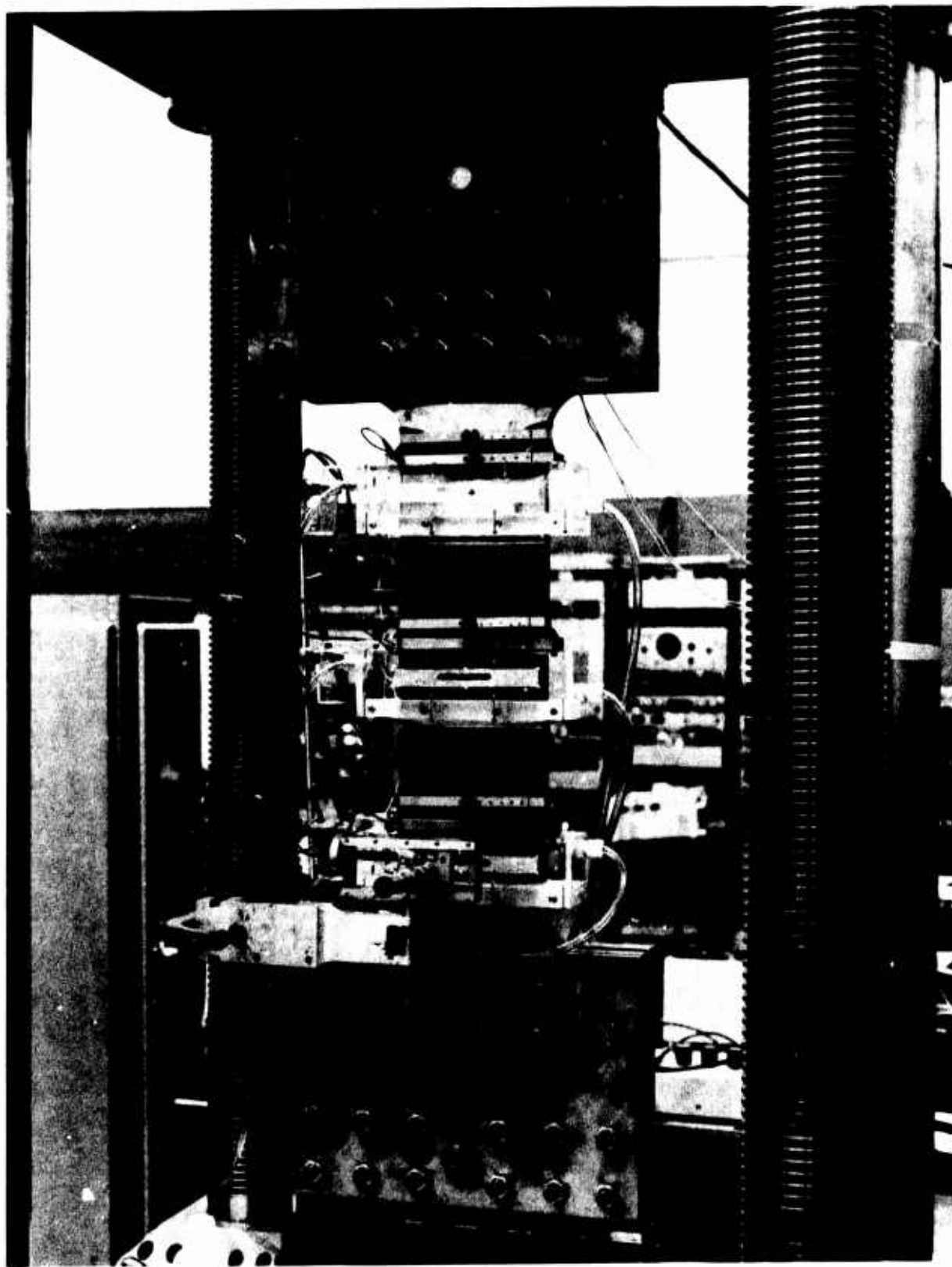
7112-5

FIGURE 14. Example of Setup for Corrosion-Fatigue Testing in Seawater With Cathodic Polarization[19]
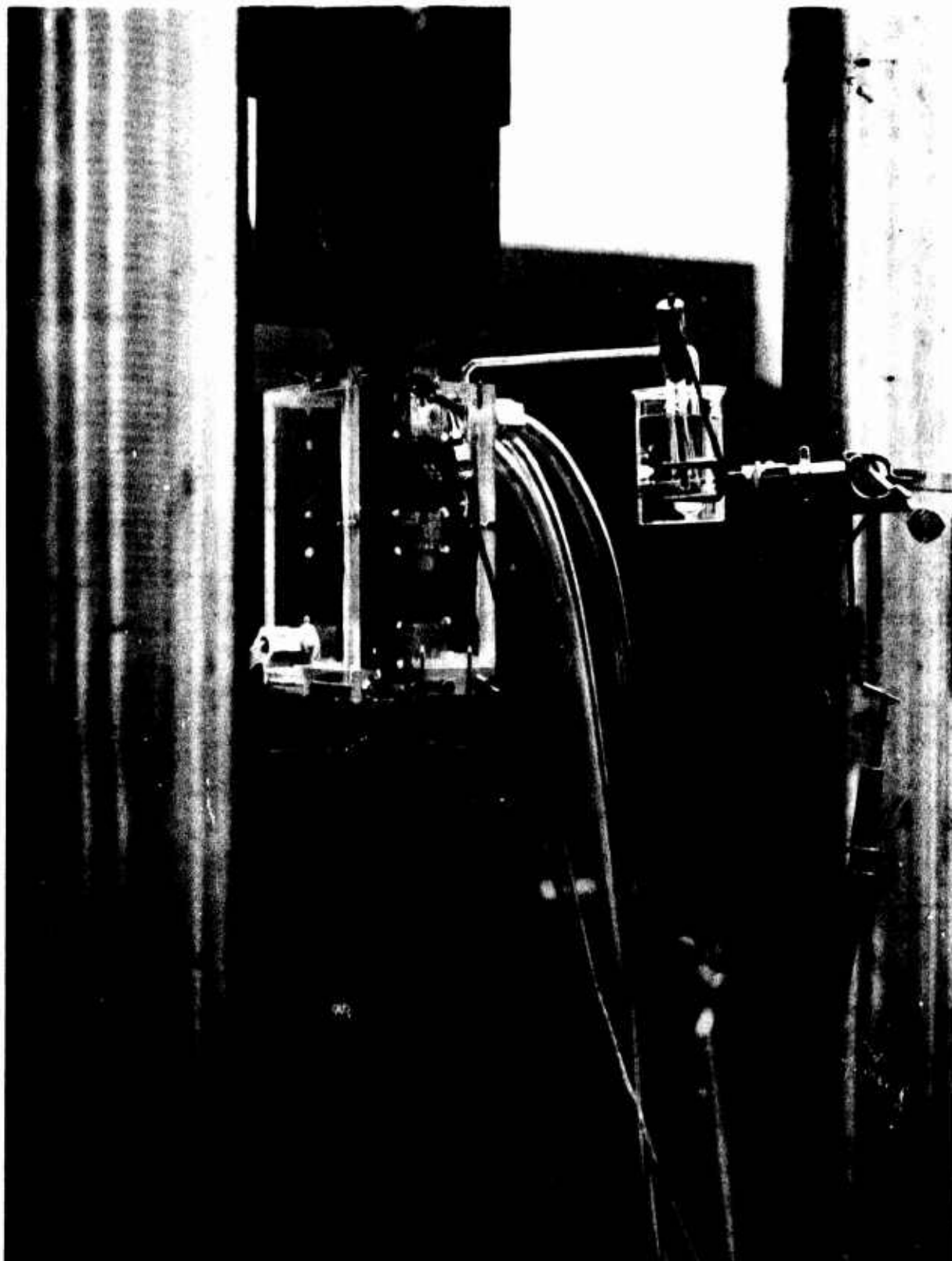
7112-1

FIGURE 15. Example of Test Setup for Corrosion-Fatigue-Crack Growth Experiments
in Seawater With Cathodic Polarization[19]

corrosion-fatigue performance. Usually, potential is maintained potentiostatically in laboratory studies and variations in applied current density are monitored during the course of testing. In some cases, cathodic polarization is provided by coatings, such as zinc, or by sacrificial anodes connected to the specimen. Since the electrochemical potential can significantly influence corrosion-fatigue behavior, it is important to take this variable into account in evaluating data.

Environmental conditions also can be affected by coatings applied to the metal surface and by inhibitors added to the water. When considering such factors, it is important to make sure that they reasonably simulate situations that can be used or may be encountered in actual service.

Phenomena and Mechanisms of Corrosion Fatigue in Aqueous Environments

The important general phenomena and mechanisms involved in corrosion fatigue of metals in aqueous environments are briefly reviewed. This review provides background and perspective for later detailed discussions of specific types of metals in marine environments. Fatigue-crack initiation and propagation are discussed separately.

Wei and Speidel[20] have pointed out that a large number of variables can influence corrosion fatigue behavior. They have listed these variables in three categories—mechanical, metallurgical, and environmental. Those from their list that are important in this review are given below:

Mechanical Variables

- Maximum stress or stress-intensity factor

- Cyclic stress or stress-intensity range

- Cyclic loading frequency

- Cyclic load wave form (constant amplitude loading)

- Load interactions in variable amplitude loading

- State of stress

- Residual stress

- Crack size and shape, and their relation to component size and geometry.

Metallurgical Variables

- Alloy composition

- Distribution of alloying elements and impurities

- Microstructure and crystal structure

- Heat treatment

- Mechanical working

- Preferred orientation of grains and grain boundaries (texture)

- Mechanical properties (strength, fracture toughness, etc).

Environmental Variables

- Temperature
- Concentration of damaging species in aqueous or other liquid environments
- Electrochemical potential
- pH
- Coatings, inhibitors, etc.

This extensive list emphasizes the complexity of corrosion-fatigue behavior. With such a large number of variables, a complete evaluation of all the factors involved in corrosion fatigue cannot be justified economically. In most studies, all but a few of these are held constant while those of primary importance to the investigator(s) are varied. When evaluating and comparing data from different sources, it is important to know all of these variables so that proper evaluations and comparisons can be made. For example, some results appear, at first glance, to be contradictory. However, when all the variables are considered, this apparent contradiction can be explained and taken into account.

Fatigue-Crack Initiation

Mechanisms of corrosion-fatigue-crack initiation in aqueous environments have been characterized as belonging in at least one of four categories.[21,22]

(1) Pitting, where crack nucleation is related to pits formed by corrosive attack

(2) Preferential dissolution of highly deformed material acting as a local anode with undeformed material acting as a local cathode

(3) Film rupture, where protective surface films such as oxides are cracked by cyclic deformation, allowing corrosion to occur

(4) Surface energy reduction caused by adsorption of environmental species and enhancement of microcrack propagation.

None of these mechanisms adequately explains crack initiation by corrosion fatigue in aqueous environments in general. The crack-initiation mechanism is a function of both the material and environment. In other words, changes in the type of metal or alloy may change the initiation mechanism, and, even when the material is the same, changes in environmental conditions may alter the mechanism of crack initiation. Furthermore, no complete, well-accepted model of the corrosion-fatigue-crack-initiation process has been developed for any material/environment system.

Fatigue-crack initiation is a localized process usually occurring at some point on the surface of the metal. When this surface is exposed to an aggressive environment, the fatigue-cracking process is accelerated. Thus, it is a highly localized corrosion process rather than a general one, and the local rate of damage accumulation is more important than the overall damage rate. In some cases, changes in environmental variables can alter the local rates of damage accumulation and cause the critical location of fatigue-crack initiation to be changed. For example, fatigue-crack-initiation sites may shift from slip steps within grains to grain boundaries when the environment becomes more aggressive. The localized nature of corrosion-fatigue-crack initiation and the competing damage processes make it difficult to conduct experiments to identify the controlling mechanisms of crack nucleation.

One commonly observed process of corrosion-fatigue-crack initiation is that persistent slip bands, which are formed by emergence of slip steps or an intrusion-extrusion slip mechanism, are preferentially attacked by the corrosive medium which causes local stress intensification that subsequently leads to earlier cracking.[21] Corrosion increases the density of the persistent slip bands, and this produces an increased number of sites for crack initiation.[22] A simple model [22] of this type of process is illustrated in Figure 16 where the ease of plastic deformation at the surface is increased by unlocking dislocations at preferentially attacked slip-band steps. This type of process has been observed to occur for low-carbon steels and copper in aqueous solutions. Application of anodic currents for both of these materials showed a "critical" rate of corrosion (local not general) associated with corrosion-fatigue damage. With low-carbon steel, crack initiation was always transgranular when anodic currents were applied. The behavior with copper implies a shift in the region of preferential attack from persistent slip bands to grain boundaries with the increased anodic potentials.
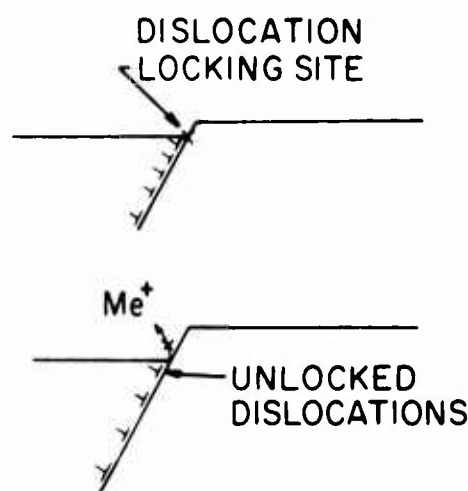
FIGURE 16. Schematic of Simple Model for
Corrosion-Enhanced Crack Nucleation at
Emerging Slip Step[22]

With low-carbon steels, it is found that cathodic protection can increase fatigue-crack-initiation resistance up to or slightly above levels observed with comparable tests in air.[23] This protection is afforded by reducing the rate of local corrosion attack at persistent slip bands, and the potential for corrosion-fatigue protection was found to be essentially the same as that for protection from general uniform corrosion.[22] Furthermore, the formation of a calcareous scale is found to be an important factor in mitigating corrosion-fatigue-crack initiation in seawater.[23] However, with higher strength heat-treated steels (e.g., AISI 4140 steel), cathodic protection at levels used to inhibit general corrosion produces a decrease in fatigue-crack-initiation resistance that is believed to be caused by a hydrogen-embrittlement mechanism.[22]

The role of pitting in corrosion fatigue is not completely understood. Materials that show corrosion pitting tend to be susceptible to corrosion fatigue, but corrosion fatigue also is observed when no pitting occurs. For low-carbon steels in aqueous sodium chloride solutions, careful studies show that cracks do not necessarily initiate at pits and that it is more likely that pits associated with fatigue cracking are formed after cracking takes place.[21] However, in studies of a martensitic 13Cr stainless steel, Ebara et al[2] found that pitting played an important part in promoting fatigue-crack initiation in solutions ranging from 3×10^{-4} to 3 percent NaCl. Their data are shown in Figure 17. No pitting was observed for tests in distilled water, but
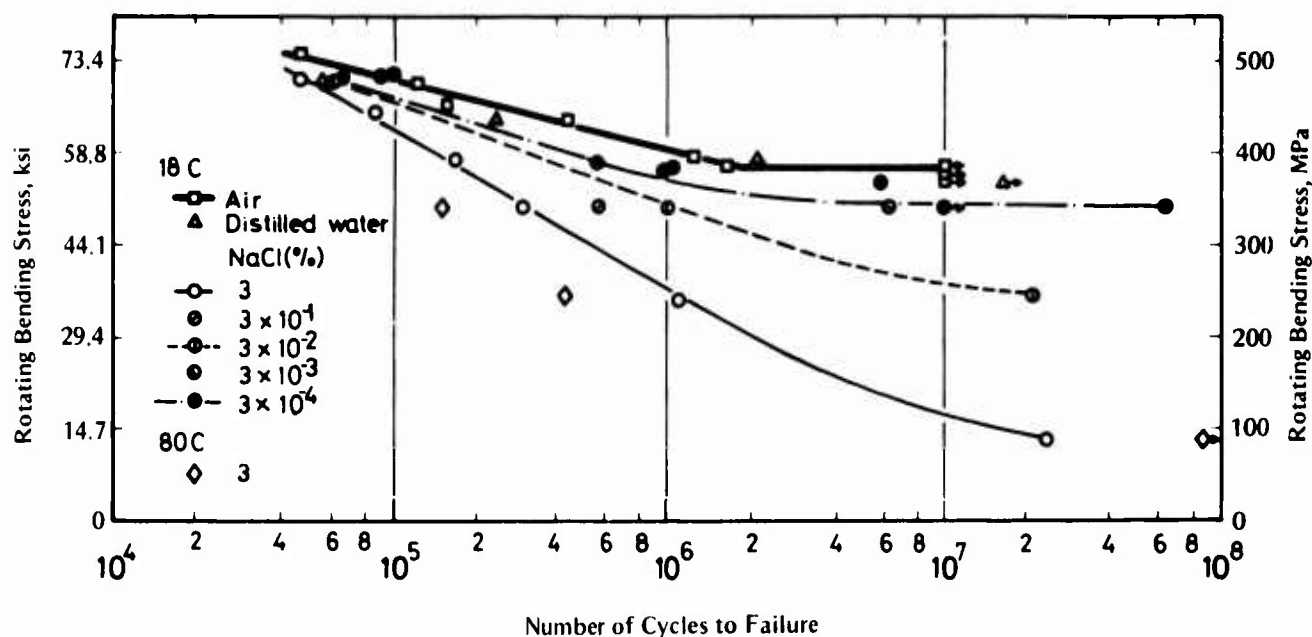
FIGURE 17. Corrosion-Fatigue Resistance of Martensitic 13Cr Stainless Steel[2]

pitting was observed for tests in all of the other aqueous solutions. When pitting occurred (NaCl solutions), fatigue resistance was decreased; but when no pitting occurred (distilled water), fatigue resistance was the same as that observed for tests conducted in air. There is also evidence that pitting may be important in low-cycle, corrosion-fatigue-crack initiation for high-strength aluminum alloys.[22,24] These results again point out the need to consider each material/environment system separately.

Duquette[22] has reviewed recent studies which indicate that long-life, corrosion-fatigue-crack nucleation in 7075-T6 aluminum alloy and its high-purity analogue in NaCl solutions may be caused by localized hydrogen embrittlement. There is evidence that cathodically produced hydrogen diffuses more rapidly by a dislocation transport process, and it is hypothesized[22] "...that hydrogen may collect at the semicoherent precipitate-matrix interface, ...". Localized embrittlement of this interface would then be responsible for easier crack nucleation. For 7075-T6 aluminum alloy, the type of stress state also strongly influences corrosion-fatigue resistance. As shown in Figure 18, fatigue resistance in NaCl solution was drastically lower than that in air for axial fatigue loading but was only slightly lower for torsic i loading.[22] In torsion the hydrostatic stress component is zero, while in uniaxial tension it is one-third the maximum stress. Thus, it appears that a hydrostatic stress component is required for the localized hydrogen embrittlement to occur.

In alloys that are strengthened by precipitates, the nature of the precipitates influences fatigue life in corrosive environments.[25] In high-strength aluminum alloys with coherent shearable precipitates, dislocation movement is concentrated within planar bands of intense slip. These bands are more sensitive to localized corrosion, and hence the fatigue resistance is much lower in an aqueous environment than it is in dry air. When the alloys are modified to make the precipitates incoherent, which promotes dislocation looping (i.e., precipitates are made nonshearable), the slip becomes more diffuse and little effect of aqueous environment on corrosion-fatigue resistance is observed. Hahn and Duquette[26] have made similar observations for a copper-base alloy. When these types of alloys are overaged to produce incoherent precipitates, their strength is markedly decreased, so that, even if the environment attack is
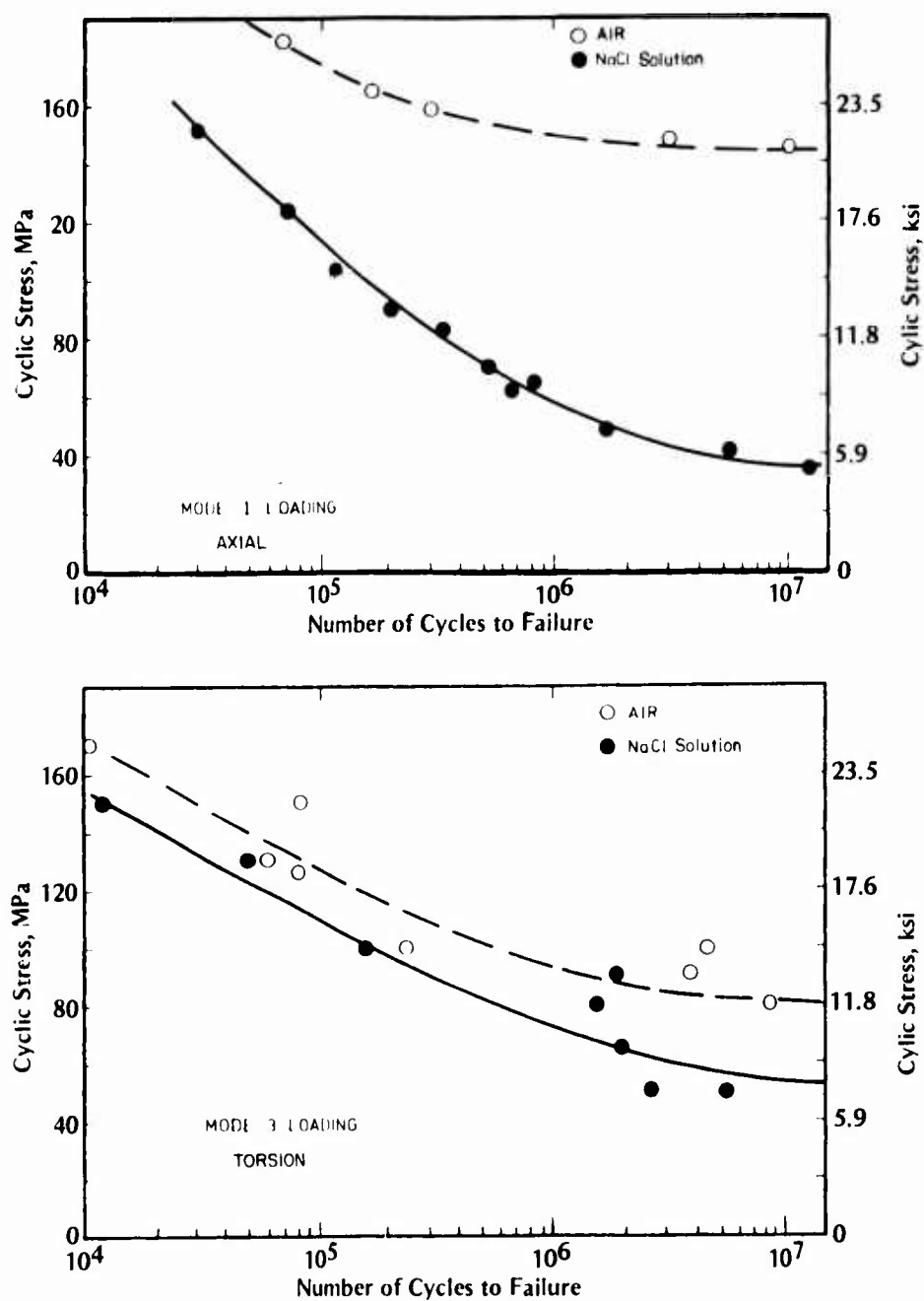
FIGURE 18. Corrosion-Fatigue Behavior of 7075–T6 Aluminum Alloy in Air and in Aerated Sodium Chloride Solution[22]

negligible, their actual corrosion-fatigue strength may be lower than that of their higher strength, peak-aged counterpart. Maximizing the amount of unrecrystallized structure also increased homogeneous slip behavior and reduced environmental degradation in the corrosion-fatigue resistance of the high-strength aluminum alloys.[25]

According to the above information, corrosion-fatigue cracking usually initiates in a transgranular fashion at surface discontinuities associated with slip bands, which is similar to commonly observed fatigue-crack-initiation processes in air. With corrosive attack, however, the initiation process is intergranular or a mixture of transgranular and intergranular cracking. Factors generally observed to promote a change from the transgranular mode to the intergranular mode are (1) decreased cyclic frequency, (2) increased mean stress (applied or residual), (3) decreased strain (or stress) amplitude, and (4) increased environmental attack. In addition to altering the basic environmental composition, factor (4) can be affected by anodic polarization which increases anodic dissolution or by cathodic polarization which increases chances of localized hydrogen embrittlement. When the mode of crack initiation is shifted from transgranular to intergranular, fatigue resistance normally is greatly decreased. Therefore, it is of major importance to consider all four factors and their possible influence on the mode of crack initiation when evaluating corrosion-fatigue resistance of metals.

The preceding comments and observations on corrosive-fatigue-crack initiation are based mainly on data for smooth, unnotched specimens. When the local environment in the notch is similar to the bulk environment, then there is a direct correspondence between initiation processes at the notch root and on the surface of smooth specimens. For example, Mitchell[27] has shown that the corrosion-fatigue life of notched coupons ($K_t = 2.52$) of 7075-T73 aluminum alloy tested in 3.5 wt % NaCl solution can be predicted using the local stress-strain approach with baseline data from smooth specimens tested in the same environment. A similar observation was made for fatigue data on notched specimens of a 0.35 wt % carbon steel tested in synthetic seawater.[28] If the local environment in the notch were altered, however, such correlations would not be expected. Under certain combinations of notch geometry and water-flow conditions, the local environment at the notch root may become quite different from the bulk environment. For example, the solution in the notch could be relatively stagnant and allow a concentration cell to form in the notch. Therefore, to properly evaluate notch effects in corrosion fatigue, the local environment near the notch root should be adequately characterized.

In this discussion of corrosion-fatigue-crack initiation, the common theme of a local process of damage accumulation and cracking is obvious. An understanding of the mechanisms of corrosion-fatigue cracking requires study of local damage and local environmental attack. This emphasis on localized phenomena also applies to fatigue-crack-growth processes discussed next.

Fatigue-Crack Growth

Corrosion-fatigue-crack growth normally is thought of in terms of the applied stress intensity related to some apparent threshold for stress-corrosion cracking, K_{Iscc}, under static loading. McEvily and Wei[29] have categorized corrosion-fatigue-crack growth as falling into one of the three types of behavior illustrated in Figure 19. In Type A behavior, there is a synergistic interaction of cyclic and corrosive crack-growth mechanisms at all but very rapid rates of crack growth, where the mechanical aspects are dominant because cracking occurs more rapidly than chemical and/or transport processes involved in corrosion fatigue. Corrosion-fatigue-crack growth in the aluminum-water system is a typical example of this Type A behavior.[29,30,31] With Type B response, there is no environmental effect below the
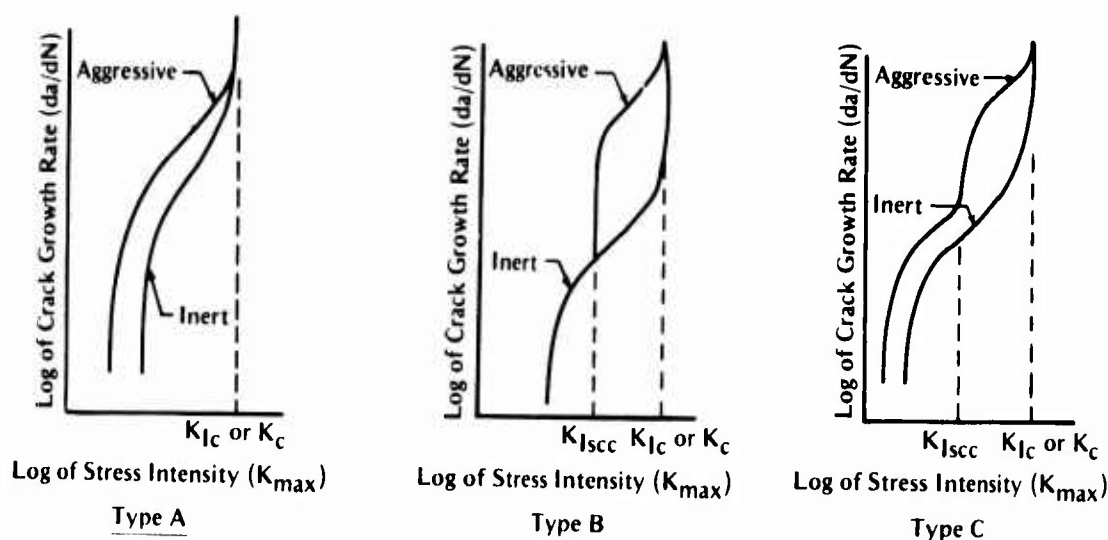
FIGURE 19. Illustration of Three Types of Corrosion–Fatigue–Crack Growth Behavior[29]

threshold K_{Iscc} observed in sustained-load crack-growth studies. Above K_{Iscc}, sustained-load crack growth contributes substantially to the cyclic-crack-growth component. The hydrogen-steel system is representative of Type B behavior.[29,30] Wei[30] points out that Type B corrosion-fatigue-crack growth depends on range of stress intensity, maximum level of stress intensity, cyclic frequency, and shape of loading wave form, and that the effects of these four variables can be reasonably well accounted for by use of the Wei and Landes superposition model.[32] With this model, the total crack growth rate, $(da/dN)_t$, is the sum of that due to pure fatigue, $(da/dN)_f$, and that due to stress-corrosion cracking, $(da/dN)_{scc}$:

$$(da/dN)_t = (da/dN)_f + (da/dN)_{scc} \tag{1}$$

or

$$(da/dN)_t = (da/dN)_f + \int_0^T (da/dt) \, K(t) \, dt \quad . \tag{2}$$

Type C response is intermediate to the extremes of Types A and B and is the behavior which is typical of most alloy-environment systems.[30] The behavior tends to be similar to that of Type A systems below K_{Iscc}. To include the synergistic corrosion-fatigue component of cyclic crack growth, $(da/dN)_{cf}$, Wei[30] has proposed a more general form of Equation (1):

$$(da/dN)_t = (da/dN)_f + (da/dN)_{scc} + (da/dN)_{cf} \quad . \tag{3}$$

Support for this phenomenological model was obtained from analysis of results of experiments on AISI 4340 steel in distilled water and water vapor.[30] Wei[30] emphasizes that this is a multidisciplinary problem and that an understanding of corrosion fatigue requires combined application of (1) fracture machanics, (2) surface analysis, and (3) metallurgical techniques.

Kraft and Cullen[33] have suggested a methodology for organizing corrosion-fatigue-crack growth data. Their approach is based on a tensile ligament instability model. It includes one parameter to account for cyclic stress-strain response of the crack-tip ligament material. Another hybrid parameter accounts for interaction between stress-strain behavior (monotonic and cyclic) and corrosive attack or stress-relaxation behavior. A parametric mapping scheme is

then used to correlate actual data with the model. The anomalous effects of stress ratio and frequency often observed in corrosion-fatigue-crack growth are approximated reasonably well by this model for data on two titanium alloys, one aluminum alloy, and three steels. The model works best for the high-strength alloys, which includes five of the above six materials. For a medium-strength API X-65 steel, the authors note that the strength is below the level for which their model is strictly applicable, and the correlation with actual data is not as good as that for the five other alloys.

Four of the anomalous types of data on corrosion-fatigue-crack growth which Krafft and Cullen[33] believe should be accounted for in any modelling scheme are illustrated schematically in Figure 20. Saltwater causes a dramatic increase in the effect of stress ratio for the Ti-8-1-1 alloy. Decreasing frequency yields marked changes in crack growth rates for API X-65 steel in saltwater with cathodic protection, for Ti-6-4 alloy in saltwater, and for AISI 4340 steel 400 F (204 C) temper in fresh water. There are some regions at lower ΔK levels where frequency has no effect on da/dN. In other regions, at medium ΔK levels, decreased frequency yields large increases in da/dN. Where the curves are almost horizontal, da/dN is almost independent of ΔK. Where the curves are almost vertical, da/dN increases rapidly for very small increases in ΔK. All of these factors cannot be properly accounted for if data are not available over a wide range of ΔK values, frequencies, and stress ratios. As pointed out by two reviewers[23,34], examination of the pertinent variables over a broad range of values is required for a proper understanding of corrosion-fatigue-crack growth. Many apparent contradictions and discrepancies in the literature arise from a failure to do this extensive exploration. Thus, in evaluating data for this report, those studies that have thoroughly investigated a wide range of variables are emphasized.

Understanding the mechanisms of corrosion-fatigue-crack growth requires consideration of the kinetics of the various processes. The major processes that take place during corrosion-fatigue-crack growth are illustrated schematically in Figure 21. First, the reactants present in the bulk environment must be supplied to the crack-tip region. The local solution near the crack tip generally will be different in nature from the bulk solution. The difficulties and
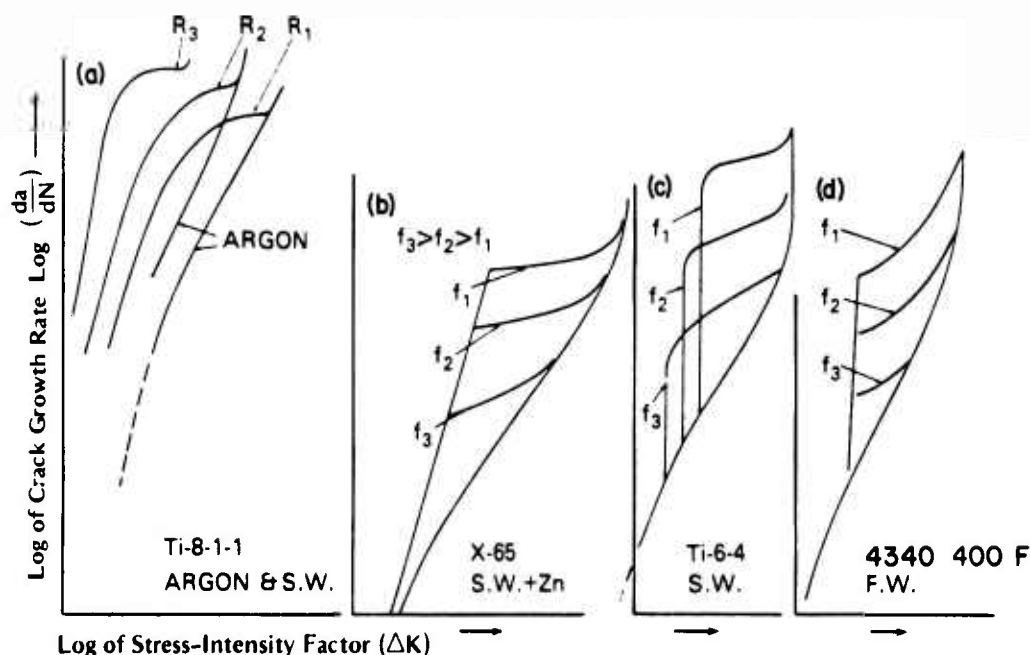
FIGURE 20. Anomalous Behaviors Observed in Corrosion-Fatigue-Crack Growth Data[33]

Legend

1. Supply of reactants to crack tip
2. Chemical reaction with newly exposed metal
3. Adsorption of deleterious species
4. Diffusion of species to plastic zone
5. Removal of reacted products

Bulk Environment

Crack Tip

Plastic Zone
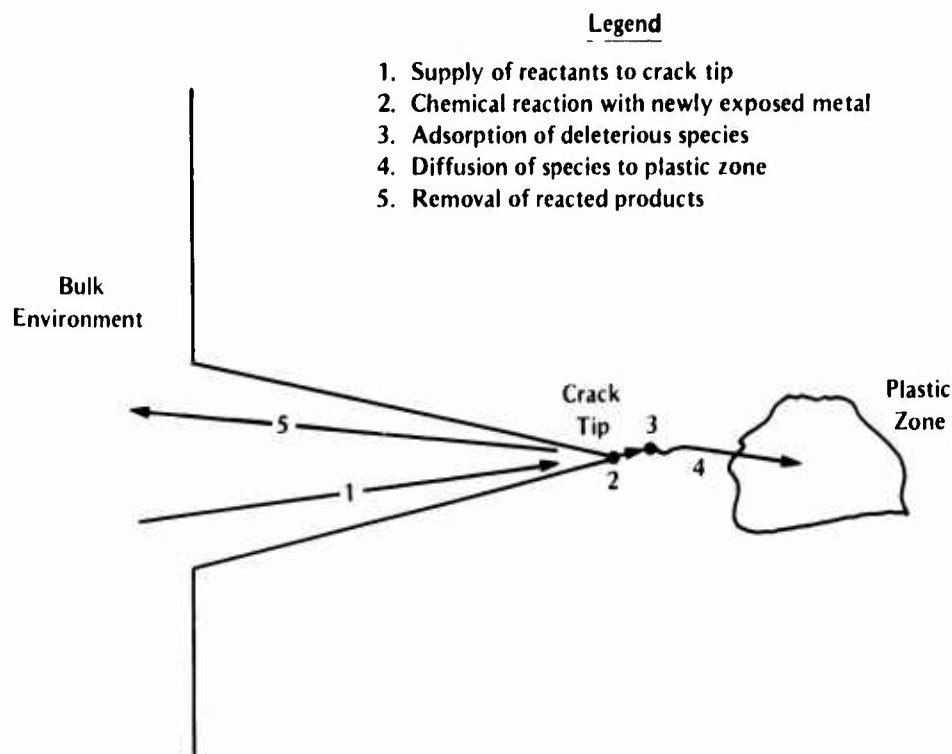
FIGURE 21. Schematic of Processes Involved Near Crack Tip During Corrosion Fatigue

complexities of modelling this aspect have been discussed by Hartt et al.[35] It is also important to note that the local crack-tip chemistry may be affected by the presence of corrosion products. Therefore, the rate of removal of these products is important. A buildup of products in the crack tip may alter the local stresses just by its physical influence on crack closure.

As newly cracked material is produced near the crack tip by fatigue processes, this material reacts with the local environment. Thus, the mechanical fracturing process synergistically interacts with the chemical attack. In the simplest case, anodic dissolution of material at the crack is responsible for the environmental contribution to corrosion-fatigue-crack growth. The highly deformed material in the plastic zone ahead of the crack contains a high concentration of slip bands which are more susceptible to corrosive attack than the surrounding metal, just as in the case of crack initiation at slip bands. In highly aggressive environments at high levels of ΔK, where the plastic zone is fairly large, the anodic dissolution of material at the crack tip is sometimes rapid enough to cause blunting of the crack. This blunting normally causes a decrease in crack growth rate, so it is not often of much engineering concern. Also, corrosion attack may occur at grain boundaries, resulting in intergranular rather than transgranular crack growth. In fact, these two modes of crack growth may be competing. A transition from transgranular to mixed or to intergranular crack growth in corrosion fatigue, if observed, usually takes place with decreased ΔK level, increased K_{max} level, decreased cyclic frequency, and increased environmental attack.

The corrosion reaction at the crack tip may produce a deleterious chemical species. (For example, hydrogen ions are produced by the cathodic reaction in aqueous solutions.) This species (e.g., hydrogen) is absorbed at the metal surface. It then diffuses to the zone ahead of the crack tip where it causes localized damage (e.g., hydrogen embrittlement). The diffusion transport process most likely is along dislocation pipes or grain boundaries, rather than by bulk diffusion. This localized hydrogen-embrittlement process is thought to be responsible for accelerated corrosion-fatigue-crack growth in a high-strength steel[36] and in a high-strength

aluminum alloy[37] in water/water vapor environments. For the steel, surface reaction kinetics were rate controlling, whereas either surface reaction kinetics or transport of water vapor to the crack tip was rate controlling for the aluminum alloy (depending on vapor pressure and time of exposure). In these cases, the localized production of hydrogen from the surface reaction is promoted by the continued exposure of new cracked surfaces under cyclic loading. For medium- and high-strength steels in saltwater or seawater, cathodic protection is observed to accelerate cyclic crack growth by a localized hydrogen-embrittlement mechanism (for example, see References 38 and 39). The fatigue-crack growth behavior is of the Type B class in these cases.

It is often postulated that fatigue loading may cause the rupture of protective films that would otherwise form on crack surfaces and reduce environmental attack. If such a mechanism is operative, then at low cyclic frequencies the protective film formation should be rate controlling. At still lower frequencies there would be no further increase in crack growth rates. This mechanism probably plays a role in some corrosion-fatigue behavior, but direct experimental evidence for it is difficult to develop.

Loading history can have a significant influence on crack growth behavior in corrosive environments. Since most real structures are subjected to variable-amplitude loading spectra in actual service, loading-history effects are important to consider. Variable-amplitude loading will not only alter the plastic-zone size and residual stress fields, but it may alter the mechanisms of crack growth in aggressive environments. Frequency and wave form are important to consider. Generally, decreased frequency accelerates crack growth rates in aggressive environments. Wave form is important in water-steel systems but has only a small influence in aluminum-water systems.[20] Thus loading-history effects must be studied for each material-environment system of interest.

Just as with corrosion-fatigue-crack initiation, corrosion-fatigue-crack growth is localized. At least six types of mechanisms may play a role in environmentally assisted fatigue-crack growth:

(1) Supply of reactants to and removal of products from crack-tip region

(2) Surface/environment reaction to produce a deleterious chemical species (e.g., hydrogen) which diffuses into zone ahead of crack-tip and promotes accelerated growth (e.g., by localized hydrogen embrittlement)

(3) Anodic dissolution at crack tip

(4) Repeated production of new, freshly fractured crack surfaces by fatigue cracking

(5) Rupture of protective surface films by cyclic straining

(6) Buildup of scale and corrosion products in crack opening which influences crack closure and effective local stress intensity at crack tip.

The relative importance of these possible mechanisms (and others) must be evaluated separately for each individual metal-environment system.

Variables Affecting Corrosion of Metals in Seawater

Most of the information in this section is taken from "Corrosion of Metals in Marine Environments" by Boyd and Fink.[40] Corrosion behavior can play a significant role in both the initiation and propagation of corrosion-fatigue cracks. The variables affecting the corrosion and protection of metals in seawater, including physical and geographical locations, and the

various factors influencing the corrosivity of seawater are discussed. General forms of corrosion, e.g., galvanic, localized, and erosion corrosion, are described. The corrosion characteristics of the major alloy systems are discussed because each has a distinct corrosion behavior and responds differently to the different variables. A brief discussion of the protection methods employed under marine-environment conditions is also included.

Types of Marine Exposure

The behavior of a metal in the marine environment depends on the exposure conditions. The resistance to corrosion attack of metals varies, depending upon the specific environmental zone to which the metal is exposed. The marine environment can be divided into distinct types of exposure: marine atmosphere, splash zone, tidal zone, shallow seawater, continental shelf, deep ocean, and mud.

In marine atmospheric exposure, the intensity of attack is influenced greatly by the amount of salt particles or mist which collects on the metal surface. The corrosivity of the salt deposition varies with wind velocity and direction, height above the water, and surface exposure. Variations in geographical localities affect such factors as temperature, time of wetness, seasonal changes, dew cycle, rainfall, solar radiation, and dust and pollution.

Materials in the splash zone are continually wet with well-aerated seawater, and corrosivity is consequently quite high. Biofouling is not a factor in this exposure. During intense storms the splash zone is exposed to a combination of high wind and water velocities, which can lead to combined erosion/corrosion damage.

There are two major considerations in differentiating the tidal zone from the splash zone: exposure time and biofouling. First, surfaces in the tidal zone are in contact with well-aerated seawater only part of the day, and second, biofouling is a factor in this environment. Erosion is not as severe in the tidal zone as in the splash zone.

The depth of seawater is an important factor because its properties vary with depth. At shallow depths, the oxygen supply is normally at or close to saturation. Biological activity, plant and animal, is at a maximum. The temperatures are warmer relative to those at moderate and great depths at most localities. Pollution and chemical contamination, especially sulfide and ammonia, are more notable in the shallow waters. Furthermore, the dilution of seawater at harbors and estuaries causes changes in the resistivity and in the formation of protective mineral scales. On the continental shelf, water depths range up to approximately 1000 feet (300 meters). Oxygen content can decrease with depth. Temperatures also tend to drop with depth. The velocity of seawater may drop to low values in many localities. Beyond depths of 60 to 100 feet (18 to 30 meters), any biofouling is entirely animal. The amount of biofouling also decreases with distance from the shore. In deep-ocean exposure, the oxygen content varies depending upon the ocean, values of pH decrease from surface values as pressure increases, and the temperature is near 32 F (0 C).

The physical, chemical, and biological properties of marine muds vary nearly as widely as they do for soils on land. Because of saltwater, the marine muds typically have low resistivity (i.e., they are good electrolytes) and are therefore quite corrosive. Oxygen concentrations at the metal surface are typically low.

Factors Affecting Corrosion in Seawater

The factors affecting corrosion of metals in seawater may be classified as chemical, physical, and biological (see Table 1). Alone or in combination, these factors determine a metal's corrosion behavior and the forms of corrosion damage to which the metal is susceptible.

The *dissolved oxygen* content is a major factor affecting the corrosivitiy of seawater. Oxygen content varies with geographic location, temperature, and depth. The effects of oxygen content separate metals into two groups: active metals and passive metals. The former do not develop protective oxide films and higher oxygen concentrations increase corrosion damage. The latter metals depend upon an oxide (passive) film for their protection, and a supply of dissolved oxygen is required to maintain passivity. At too low oxygen levels, the passive metals undergo localized corrosion, e.g., pitting and crevice corrosion. Other dissolved gases that can greatly increase the corrosivity of seawater are carbon dioxide, hydrogen sulfide, and sulfur dioxide. In addition, ammonia is particularly damaging to copper alloys.

TABLE 1. Factors Affecting Corrosion in Seawater

Chemical	Physical	Biological
Dissolved Gases	Velocity	Biofouling
Oxygen	Air bubbles	Hard-shell types
Carbon dioxide	Suspended silt	Types without hard shells
		Mobile and semimobile types
Chemical Equilibrium	Temperature	Plant Life
Salinity		Oxygen generation
pH		Carbon dioxide consumption
Carbonate solubility		Hydrogen sulfide generation
	Pressure	Animal Life
		Oxygen consumption
		Carbon dioxide generation

Salinity is defined as the total weight in grams of solid matter in 1000 grams of water. Sodium chloride (NaCl) is the most abundant dissolved constituent of seawater. The chloride content is sometimes used as an indicator of the corrosivity of seawater. The average salinity of natural seawater is 35,000 ppm. Because of high salinity, seawater has low resistivity and high corrosivity. Corrosion currents can flow readily between the anodes and cathodes through the highly conductive seawater.

The effects of pH on corrosion vary from metal to metal, but, in general, more acidic waters are more corrosive. The pH is a measure of the acidity or alkalinity of a solution. Seawater normally has a pH of 8.2, which is mildly alkaline. Variations in pH can affect the formation and growth of calcareous deposits and the stability of other protective films. Variations in pH result from corrosion reactions, sea life, and dissolved gases.

Calcareous-scale deposition forms carbonate-bicarbonate scales on metals and protects them from corrosion. Calcium, magnesium, and strontium are constituents of natural seawater that can precipitate under alkaline conditions, and thus form deposits on metallic surfaces.

Calcareous-scale formation is temperature and pH dependent, and scales form more readily in warmer waters and in alkaline solutions.

The effects of velocity vary, depending on the metal-environment system. Metals which form passive films frequently show improved corrosion resistance at higher velocities and poor corrosion resistance in stagnant waters. In the high-velocity seawater, oxygen necessary for the formation and stability of the passive films is continuously available at the metal surface. Erosion damage is more severe at higher velocity and when entrained air or solids increase.

The temperature of seawater varies with geographic location and depth. In general, corrosion reaction rates increase with increasing temperature. The rate of corrosion of steel essentially doubles with each 10-degree temperature rise. Other factors in seawater are also affected by temperature, and the overall effect on corrosion can vary. For example, gas solubility, calcareous deposition, and growth of marine life are all temperature dependent.

Pressure has only a secondary affect on corrosion. The pressure affects gas solubility, pH, and marine life, which in turn can affect corrosion.

Marine fouling on the surfaces of marine structures can affect corrosion. For many passive metals, these organisms shield surfaces from the oxygen needed to maintain passivity. For other metals, biofouling can reduce attack. The intensity of attack varies with location. In tropical waters, fouling can occur all year, whereas in arctic waters fouling is almost nonexistent. Biological fouling can cause damage to paint and coatings of structures and also create mechanical overloading conditions in structural components. The biological action of marine life can consume or generate dissolved gases in the seawater. Hydrogen sulfide can be produced by the action of sulfate-reducing bacteria and decaying marine life.

Forms of Corrosion in Marine Environments

In addition to corrosion fatigue, several other forms of corrosion occur in seawater: general, crevice, galvanic, pitting, stress corrosion cracking, erosion-corrosion, impingement, and cavitation. The various forms are distinguished by the morphology of the damage. Specific alloy systems are susceptible to specific forms of attack, e.g., mild steels are susceptible to general corrosion and stainless steels are susceptible to pitting, crevice corrosion, and stress-corrosion cracking. These forms of corrosion can be precursors to corrosion fatigue and create initiation sites, or they can act simultaneously with corrosion fatigue and contribute to the damage.

General corrosion is a uniform dissolution of the metal surface which can be measured by weight loss. The rusting of steel in marine environments typifies this form of corrosion.

There are several forms of localized corrosion: pitting, crevice corrosion, corrosion fatigue, and stress-corrosion cracking. With these forms, the bulk of the metal surface is undamaged while local areas are severely damaged. Metals that rely upon passive films for their corrosion resistance are susceptible to these forms of corrosion. Stress-corrosion cracking and corrosion fatigue require the combined action of stress and a corrosion reaction. Crevice corrosion is a form of localized corrosion occurring in crevices and other shielded sites such as overlapping surfaces or beneath corrosion and biofouling deposits. The metal in the crevice becomes anodic to the metal outside the crevice region and is damaged. Limited access to fresh seawater within the crevice results in differences in oxygen concentration, metal-ion concentration, and pH.

Galvanic corrosion occurs when dissimilar metals are in electrical contact and exposed to a corrosive environment. A potential difference exists between the metals, and one metallic member becomes active (acts as an anode) and the other member becomes a cathode. The potential difference between the dissimilar metals creates current flow between the metals and corrosion occurs at the anodic member. The magnitude of the potential difference is a function of the metals themselves and the environment. The temperature, oxygen concentration, pH, and other factors can affect the severity of galvanic corrosion. Furthermore, which metal in the galvanic couple will be the anode is determined by the environment as well as by the metal composition. For this reason published galvanic series for metals in seawater must be used with caution. Changes in the environment can significantly affect the position of a metal in the galvanic series.

Erosion corrosion is a form of corrosion influenced by the velocity of a corrosive medium relative to the metallic surface. Air bubbles and suspended solids and other matter are the erosive species. Most metals are susceptible to this combination of mechanical abrasive wear and corrosion deterioration. Erosion-corrosion attack usually exhibits a directional pattern, depending on the velocity, amount of suspended materials, and direction of corrosive medium flow.

Impingement and cavitation attack are also velocity-associated types of corrosion. Under turbulent conditions, seawater containing entrapped air and gas bubbles can impinge a metallic surface. This action can destroy protective films and also lead to metal removal at the surface. Impingement can occur where design conditions create abrupt changes in the direction of the medium flow or in the cross-sectional area of the flow containments. This form of attack is observed at sharp bends in piping.

Cavitation damage results from the formation and subsequent collapse of vapor-filled bubbles on a metallic surface. Under turbulent flow conditions, bubbles develop because of pressure changes associated with changes in cross sections or vibrations. These rapidly collapsing bubbles can destroy protective films and promote mechanical removal of metal. Cavitation damage occurs on propellers and other marine structures where rapidly flowing seawater changes direction, which results in pressure changes in the seawater.

Corrosion Behavior of Major Alloy Systems

Each major alloy system has a distinct corrosion behavior in seawater. The forms of corrosion and the important environmental variables are different for each alloy. A summary of the alloys' behavior, from the report by Boyd and Fink[40], is repeated here.

Plain-carbon steel is the most widely used metal in marine service, but it is chosen for its other properties and not because of its resistance to corrosion. In the atmosphere, the rust coat formed offers no protection but tends to flake off. In the splash zone, the attack is several times that for complete immersion, while in the tidal zone, the rate is between that in the splash zone and that under submerged conditions. Steel corrodes typically at 3 to 4 mpy* in quiet seawater, with higher rates being observed as the velocity is increased. Local pitting is often observed and must be provided for in design. Under submerged conditions, steel's corrosion behavior is governed by the reaction at the cathode. Since the depolarization of the cathodic reaction is governed by the amount of oxygen arriving at the surface, higher oxygen levels are usually accompanied by higher rates of attack. At the local cathode, hydroxyl ions may be formed and the solution becomes more alkaline. The increased alkali may promote deposition of a protective calcareous scale. This, in turn, retards the rate of corrosion.

---

*mpy = mil (0.001-in.) per year and 1 mpy = 0.0254 mm/year.

Unlike plain-carbon steel, high-strength, low-alloy steels develop a tight protective rust coat in the atmosphere. Small combined additions of several elements, such as copper, chromium, nickel, manganese, silicon, etc., totalling about 2 to 3 percent, may reduce the attack by 50 percent or more, as compared with that for unalloyed steel. Low-alloy steels also experience less corrosion attack than plain-carbon steel in the splash zone. Under water, the protective rust coat does not form and the corrosion rate is about the same as that for plain-carbon steel.

Stainless steels depend on their passive film for resistance to corrosion. They perform well in the atmosphere and splash zone. In quiet seawater, passivity tends to break down at crevices, under deposits, etc., and the local pitting is more rapid than that on steel. Passivity is promoted by keeping the surface clean and free of biofouling and deposits. A seawater velocity of 5 fps or higher will prevent fouling and promote passivity of austenitic stainless grades. In general, martensitic and most ferritic grades do not retain their passive state as readily as austenitic grades and are not recommended for below-water applications without some protection.

Nickel alloys with about 30 to 40 percent nickel and 20 to 30 percent chromium (balance iron plus other elements) also depend on a passive film for protection. Like stainless steels, these alloys pit in seawater, but they are more resistant than the steels in this respect. Nickel-base copper alloys, e.g., Monel-400, are resistant to the atmosphere but pit in quiet seawater. The pits tend to be shallower and broader than those typically found on stainless steels. The most resistant of the nickel-based alloys are those containing 15 percent or more chromium and 10 percent or more molybdenum. Hastelloy C-276 is an example. These alloys are completely resistant to all environmental zones, and are equaled, in this respect, by titanium.

Copper-base alloys are resistant to corrosion in marine environments and are widely used in seawater. The cupronickels are among the most resistant in seawater service and show less tendency to pit than the nickel-copper alloy, Monel-400. Aluminum brass and many of the bronzes, such as those with aluminum, aluminum-nickel, or tin, are resistant to corrosion. The presence of hydrogen sulfide in polluted seawater greatly increases the corrosion damage to copper alloys.

Titanium is completely resistant to corrosion in all the environmental zones. In seawater service at temperatures above 250 F (121 C)*, there is some tendency for crevice attack to take place, e.g., at flanged connections. Stress-corrosion cracking of titanium alloys will occur under tension in seawater where a crack of sufficient acuity is present.

Aluminum alloys in the 5000 series and Alloy 6061 are resistant to marine environments, but crevices and galvanic couples should be avoided. Heat treatments have a marked effect on the corrosion behavior, and can promote stress-corrosion cracking. Pitting is a problem with many alloys, particularly those in the 2000 and the 7000 series.

Beryllium is a light metal that is prone to pitting in seawater and other saline solutions. Magnesium is not used as a structural material under water.

For special applications, the refractory metals may be used in marine atmospheres. Of the group, tantalum (like titanium) is completely resistant to seawater. Platinized tantalum, like platinized titanium, is excellent as an impressed-current anode. Although information is scanty, all the refractory metals appear to have good-to-excellent resistance in marine environments. Precious metals like platinum, gold, and silver are used in marine applications for electronic and electrical applications, and their corrosion resistance is excellent.

Zinc or cadmium provides corrosion protection to steel as a sacrificial metal coating. Lead, with an addition of silver, is used as an impressed-current anode, and zinc serves as a sacrificial anode. Tin is cathodic to steel and therefore is not suitable as a protective coating for steel.

---

*In pressurized systems.

Corrosion Protection in Marine Environments

Methods of corrosion protection in marine environments are (a) use of the most corrosion-resistant alloys, (b) application of coatings, and (c) application of cathodic protection. The summary of corrosion behavior of metals in seawater presented above outlines a broad range of corrosion resistance. A common method of corrosion control in marine environments is to use construction materials that have adequate inherent corrosion resistance along with the other required properties. Where a material having insufficient corrosion resistance is used, additional protection must be provided. The most common methods of providing corrosion protection are coatings and cathodic protection.

Metallic and nonmetallic coatings are used extensively to protect metals in seawater. Generally, their function is to isolate the underlying structure from the corrosive solution by creating a protective barrier. For example, the more corrosion-resistant metals are applied to steel surfaces by cladding, weld overlaying, or flame spraying. Several kinds of nonmetallic coatings are used for corrosion protection.

Barrier coatings for corrosion protection must maintain their integrity to be effective. Corrosion damage can be concentrated and severe at flaws in the coating. Where corrosion-resistant metallic coatings are used, a detrimental galvanic couple is set up at a flaw in the more noble coating. This galvanic action can significantly affect both corrosion and corrosion-fatigue behavior.

Cathodic protection is broadly applied to metallic structures in seawater. The high-conductivity seawater provides a low resistance path for cathodic protection currents and enhances uniform current distribution. Both impressed current systems using inert anodes and sacrificial systems using more active metal anodes, e.g., zinc and aluminum, are widely applied.

Cathodic protection causes several changes in the corrosion environment which can greatly affect the corrosion and corrosion-fatigue behavior of a metal. The oxidizing potential of the metal surface is shifted to a potential range where dissolution is suppressed or significantly reduced. Corrosion, stress-corrosion cracking, and corrosion-fatigue processes are all potential dependent. In addition to potential changes, cathodic protection causes changes in the corrosive solution at the metal surface. The solution in contact with the metal being protected increases in pH and becomes more alkaline. Both corrosion processes and the formation of calcareous deposits are affected by solution pH. Another significant effect of cathodic protection is the generation of hydrogen on the metal surface. Much of the hydrogen is released from the surface as bubbles of hydrogen gas; however, some of the hydrogen enters the metal. The mechanical properties and susceptibility to cracking of a metal are strongly influenced by dissolved hydrogen.

Use of Fatigue Data in Design

To appreciate the importance of understanding corrosion fatigue, it is instructive to review the major steps typically involved in fatigue design. These steps are illustrated in the block diagram in Figure 22. In assessing the potential for corrosion-fatigue damage, the designer must estimate both the operational history and the environmental history and the relation between them. From the system operational history, the loading histories for various components are determined, and these, in turn, are used to determine local stress-srain histories in critical areas where corrosion fatigue may take place. At these same critical

1. Estimation of Operational and Environmental History of System

2. Computation of Corresponding Loading History for Components of System

3. Computation of Stress-Strain History and Estimation of Local Environment History Near Critical Areas (e.g., Notches, Welds, Flaws of Components (It may be necessary to include the influence of environment on deformation response in some cases.)

4. Assessment of Probable Corrosion-Fatigue Damage — Initiation or Propagation of Cracks — at Critical Locations in Components

5. Comparison of Probable Damage with Performance, Reliability, and/or Safety Criteria

FIGURE 22. Major Steps in Typical Fatigue Design Process

locations, the correspondng history of environment must be determined. For example, it may be important to know whether changes in flow rate, concentration, or temperature occur at high or low levels of cyclic stressing. Next the fatigue damage is determined using existing data and damage-accumulation rules. Finally, the computed fatigue damage is compared with appropriate criteria for satisfactory performance, reliability, and safety of the component.

The corrosion-fatigue behavior of metals in marine environments is important in the fourth step illustrated in Figure 22, fatigue-damage assessment. The information on corrosion-fatigue resistance is only one aspect of this damage-assessment process, and the total aspects usually addressed in the fatigue-design process must be considered.

Fatigue Life Curves Versus Crack Growth Rates

Two different types of basic corrosion-fatigue data are used in current fatigue-damage-assessment approaches. One is fatigue-life curves and the other is crack-growth-rate information. Both types of data normally are based upon results from constant-amplitude cycling of specimens. Therefore, some cumulative damage rule, such as Miner's linear cycle fraction rule, must be employed to assess fatigue damage under variable-amplitude loading.

Fatigue-life curves are presented as plots of stress or strain (or log of stress or log of strain) versus log of the number of cycles to failure, as shown schematically in Figure 23. These are commonly referred to as S-N curves. The failure criterion may be either initiation of a specified size of crack or complete fracture of the specimen. In the latter case, both the process of initiation of a detectable-size crack and its propagation to a critical size are involved in determining the total life of the specimen. Fatigue-crack-growth data are obtained from specimens
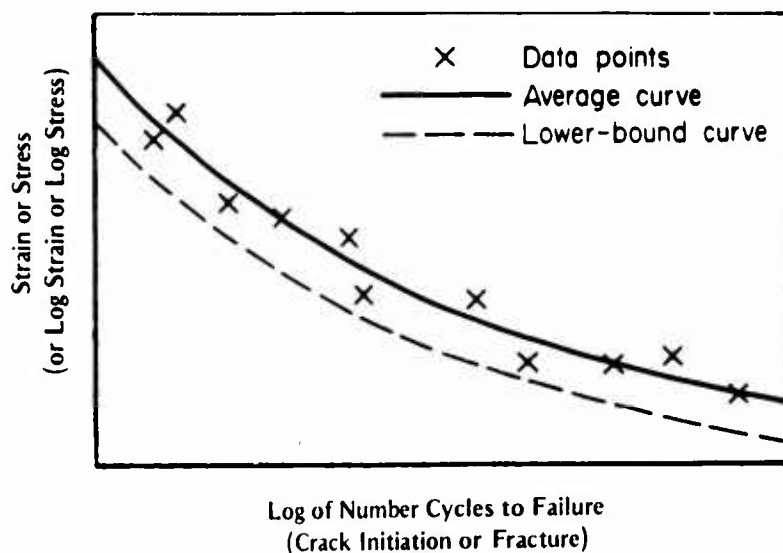
FIGURE 23. Schematic of Typical Fatigue-Life Curve (S-N Curve)

after a detectable-size crack has been initiated. Records of crack length versus number of loading cycles are differentiated to obtain cyclic crack-growth-rate (da/dN) data. The logarithm of crack growth rate is usually correlated with the logarithm of the linear elastic stress intensity factor, K, as illustrated in Figure 24. Corrosion-fatigue information reported in the literature and subsequently discussed in this report thus is presented either as fatigue-life curves or as fatigue-crack-growth curves.

When significant environmental effects on fatigue behavior are observed, the fatigue performance of metallic materials is usually degraded. Thus, corrosion causes lowering of the
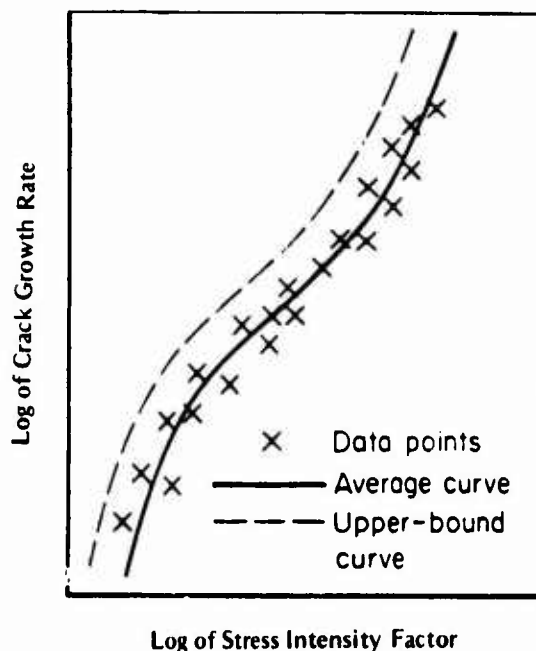
FIGURE 24. Schematic of Typical Fatigue-Crack Growth-Rate Curve

average fatigue-life curve (Figure 23) or raising of the average fatigue-crack-growth-rate curve (Figure 24). Since the designer typically is concerned with conservative-bound curves (dashed ones in Figures 23 and 24), it also is important to consider the effect of corrosive environment on the data scatter. For if corrosive effects increase scatter as well as shift the average curve, the net effect on the lower-bound fatigue-life curve or on the upper-bound, fatigue-crack-growth curve is worse than just a shift in this average curve. Unfortunately, most corrosion-fatigue studies are not extensive enough to assess data scatter quantitatively, and comparisons between results of tests conducted in different environments are based upon average trends in the data, which is the case in the present report. However, it should be remembered that if in fatigue design the conservative-bound curves are shifted by the same amount as the average curves are observed to be displaced, it is tacitly implied that the environmental effects do not increase data scatter.

Prediction of Corrosion-Fatigue Damage

Most of the currently popular approaches to fatigue design can be separated into (1) those dealing with predicting crack-initiation life or (2) those dealing with predicting crack-growth behavior. The local stress-strain concept, which has been reviewed by Leis[41] and by Dowling[42], predicts fatigue life in terms of the formation of an engineering-size crack. The assumption is made that by computing the local stress-strain history at critical locations in complex structures (notches and other discontinuities), the cyclic life will be the same as that for an unnotched (smooth) specimen subject to the same history in the laboratory. In other words, the fatigue-damage-accumulation process is taken to be the same in both cases. For this to be valid, significant microstructural features should be small compared with the size of the notch root so that the surface material at the critical location behaves in a fashion similar to that of material on a smooth specimen surface under comparable stress-strain histories. In addition, the crack size at initiation must be small enough "to ensure similitude between the early growth rates at notch roots and in smooth specimens".[43] For this reason, Leis and Forte[43] used an initiation crack length of 0.005 in. (125 m). As the notch root increases in acuity, the initial crack length needed to meet the similitude requirement decreases[44,45], which led Dowling[46] to recommend that a crack length of about one-tenth the notch-root radius be used to define crack initiation. The important point is that the size of an initiated crack is really a variable quantity. This must be remembered when evaluating and comparing published fatigue-life data. In the context of corrosion fatigue, aggressive aqueous environments normally are found to accelerate the crack initiation process in metals and alloys. That is, the average and lower-bound curves shown in Figure 23 are shifted downward by environmental effects.

Fatigue-crack-growth data are used in the fracture-mechanics approach to fatigue analysis. This approach can be employed either (1) as a life analysis or (2) as a damage-tolerance analysis.

In life analysis, the structure is assumed to contain defects from the start of its life and the severity of these defects is represented by an equivalent crack-like initial flaw. The growth of this equivalent flaw to failure then determines the life of the structure. It is important to realize that this equivalent flaw may not be physically realistic; it is just the initial flaw that gives the appropriate life. If the equivalent flaw size is unique for a given structure and load histories of interest, then this concept is useful. For generalized variable-amplitude loading, this approach seems to work fairly well, but the equivalent initial size is sometimes a function of loading, i.e., it is nonunique.[43]

The damage-tolerance concept recognizes that at some time cracks may develop in a structure, and the growth of these cracks is then computed. Using a risk analysis, a critical strength and the associated critical crack size are calculated. The time for a crack to grow from some detectable size to the critical size is determined next. An inspection interval shorter than this time period can be established so that damage can be detected well before failure occurs. Thus, the damage-tolerance approach assumes that if cracks exist or develop they will be detected and repaired before failure can take place. This philosophy inherently requires highly reliable methods for inspecting and detecting cracks in the structure.

With either the life analysis or the damage-tolerance analysis, the growth of a crack is computed using fracture mechanics and experimentally measured fatigue-crack-growth data. In aggressive aqueous environments, the crack growth rate normally is accelerated compared with that in less aggressive environments such as air. In other words, the effect of aggressive environment generally is to cause a shift in the curves shown in Figure 24. In some cases, the environmental attack at or near the crack tip is so great that the crack growth rate is actually decreased because of crack-tip blunting by the corrosive action. Since this deceleration of crack-growth-rate effect is conservative from a design viewpoint, it is not of as much concern as the more commonly observed acceleration effect.

Rather than simply accepting shorter crack-initiation lives and/or higher crack growth rates in corrosive environments, the designer may choose to employ protective methods, such as coatings, inhibitors, and electrochemical polarization, to reduce the influence of environment on the fatigue-damage process. Both organic and inorganic coatings are used. The coatings must be tight, adherent, and ductile. The major problem with them is that corrosion-fatigue damage is likely to occur locally at any discontinuity or break in the coating, and the entire coating system is no stronger in resistance to corrosion-fatigue damage than its weakest point. Inhibitors are effective only in closed systems where the supply of aqueous environment is controlled. This is generally not the case for most marine structures. Application of an electrochemical potential (cathodic or anodic protection) is commonly employed to reduce overall general corrosion. For example, cathodic protection is used extensively to limit general corrosion of steel offshore structures. It is found to effectively inhibit corrosion-fatigue-crack initiation, but it is not always effective in retarding fatigue-crack growth and may even accelerate the rate of crack growth in some instances.[23] The intent at this stage of this review is simply to point out that protective measures can be considered in design. More detailed discussions of protective methods are presented later.

CHAPTER 3
CORROSION-FATIGUE DATA FOR CARBON AND ALLOY STEELS

Many kinds of structures used in marine environments, such as ships, offshore platforms, drilling rigs, harbor works, and underwater pipelines, are made from carbon and alloy steels. Even though such steels are susceptible to corrosion, they are used widely because of their relatively low cost, ease of fabrication, availability, and range of strength levels. Since steels are subject to corrosive degradation in marine environments, the loss in fatigue resistance due to corrosion must be taken into account in engineering design, or protection from environmental attack must be employed. Because of their extensive use, there are a great deal of corrosion-fatigue data on carbon and alloy steels. To facilitate presentation, discussions of these data have been separated according to three categories of steels:

1. Low- and medium-strength structural steels with ultimate tensile strengths of about 100 ksi (690 MPa) or less

2. Steels used in construction of ships

3. High-strength steels with an ultimate strength of about 100 ksi (690 MPa) or more.

In some cases the distinctions among these categories are rather slight so there may be some overlap in the discussions. Category 1 includes low-carbon and low-alloy structural steels, such as those used in offshore structures. These steels are generally used in the as-rolled or normalized condition and are easy to fabricate and weld. The ship steels—Category 2—are mainly those of the HY-series or other steels specifically identified for ship construction. Many of the other steels could be used for ships but these are also employed in other applications. The high-strength steels in Category 3 are more highly alloyed than those in Categories 1 and 2. These steels are typically quenched and tempered to produce lower temperature transformation products, such as martensite, or they are given aging treatments to promote precipitation hardening. The high-chromium, precipitation-hardened steels, such as 17-4 PH steel, are included in this final category. Although they could be referred to as stainless steels, they are commonly considered for applications where high-strength steels are employed rather than for those where stainless steels are employed.

Low- and Medium-Strength Structural Steels

In recent years, shortages have given a strong impetus to exploration, drilling, and production of oil and gas in offshore environments, which has in turn led to an increased interest in the corrosion-fatigue behavior of structural steels commonly used in these applications. With this increased interest, there has been a great increase in the research activity in this technical field.

In addition to the literature review made during this study, recent reviews[23,28,47,48] of corrosion fatigue of steels in marine environments were employed in preparing this book. The review of Jaske et al[23,28] emphasized both fatigue life (S-N) and crack growth data for welded carbon steels used in fixed offshore platforms. Ishiguro[47] reviewed S-N results from recent

studies carried out in Japan. This review was limited to base-metal behavior and did not include welded material. Knight[48] concentrated on S-N curve data for weldments, with only a brief discussion of crack growth data.

In this section, fatigue-life (S-N) data are discussed first. Crack-growth-rate information is then reviewed. As pointed out earlier, S-N data are generally based on total life and thus incorporate both crack initiation and crack growth, but cyclic crack growth rate is not treated explicitly. Also, the portion of life during crack growth depends on stress/strain level, notch acuity, specimen size, and aggressiveness of environment. Therefore, in comparing and evaluating S-N-type results, these variables must be taken into account and comparisons made carefully.

Fatigue-Life Data

Available corrosion-fatigue-life data on low- and medium-strength structural steels reviewed in this study are summarized in Table 2. Unless otherwise indicated, specimens were completely immersed in the indicated type of aqueous environment at room temperature [about 68 to 77 F (20 to 25 C)] during testing. The approximate cyclic life range over which S-N curves were developed is indicated under the column heading Type of Data. A similar data summary developed in Japan (as reported by Ishiguro)[47] is given in Table 3. Most of these data are for tests carried out using a 1 percent or 3 percent sodium chloride solution. In some cases, artificial formulations that were chemically similar to natural seawater were employed; these are designated by the term synthetic seawater. In a few investigations, the tests were performed using a natural seawater environment. The salient factors that have been shown to influence corrosion-fatigue life of these steels are discussed in the following paragraphs. Where appropriate, examples of representative data are presented, but exhaustive presentations of all pertinent data are not given because of the limitations on the size and scope of this book. Other sources of similar data, however, are cited so that the reader can pursue the subject in more detail.

Effect of Stress Amplitude (Smooth Specimens). For constant-amplitude fatigue cycling of steels in air, the cyclic life (N) increases as stress amplitude (S) decreases until a stress amplitude corresponding to $N = 10^6$ to 10^7 cycles is reached, whereupon further decreases in stress amplitude show large increases in cyclic life or often no failure within the testing duration. The stress amplitude where cyclic life rapidly becomes quite large and below which fatigue failures are not expected is commonly referred to as the fatigue limit. For free-corrosion conditions in saline solutions, the S-N curve continues to decrease at longer lives with no apparent fatigue limit, as shown by the examples of Figures 25 and 26. It is particularly interesting to note that the S-N curve for 1 percent NaCl solution in Figure 26 continues decreasing well past 10^8 cycles to failure. Although the authors showed a cusp in this S-N near 10^8 cycles to failure, it might have been equally valid to pass a smooth curve through the data points. Typically, values of 10 to 20 ksi (70 to 140 MPa) are reported for the corrosion-fatigue strength (CFS) in saline solutions at 10^7 cycles. (For example, see Table 3.) The corresponding value from Figure 26 is 13 ksi (90 MPa), which is in this range, but at 10^9 cycles to failure the CFS is only about 2 ksi (14 MPa). In their tests of of mild steel in flowing seawater, Kirk et al[71] found a similarly low value of 2 ksi (14 MPa) at 10^8 cycles to failure. At higher stress amplitudes, the curves for mild steel in air and seawater generally converge, as shown in Figures 25 and 26. In the short-life or low-cycle fatigue regime (less than about 50,000 cycles to failure for these steels), the environmental effect on fatigue life is small at frequencies of about 1 Hz or more because the inelastic strain

TABLE 2. Corrosion-Fatigue-Life Data for Carbon and Low-Alloy Steels

Alloy	Condition or Treatment	Tensile Strength, ksi (MPa) Ultimate	Yield	Type of Specimen	Type of Loading	Cyclic Frequency, Hz	Environment(a)	Types of Data	Notes	References
Mild steel		66 (457)	45 (311)	Smooth plate	Reversed bending	0.33 to 50	3% NaCl	Strain-N curves 10^4-10^7	Bars and painted, cathodic protection, open circuit to -1.1 V SCE	49
Mild steel		66 (457)	45 (311)	Smooth plate	Reversed bending	0.33	Seawater	S-N curves 10^4-10^6		49
Mild steel		67 (460)	49 (336)	Smooth plate	Reversed bending	0.33	Seawater	S-N curves 10^4-10^6		49
Mild steel		48 (328)		Smooth plate	Reversed bending	0.33	Seawater	S-N curves 10^4-10^6		49
Low (≤0.01) C steel		~47 (~320)	~29 (~200)	Smooth plate	Reversed bending	17.7	3% NaCl	Strain-N curves 10^5-10^7	Effects of alloying elements	50
SM41 steel		~57 (~390)	27-36 (185-250)	Smooth bar	Rotating bending	41.7	3% NaCl	S-N curves 10^5-10^7		51
S45C steel		~80 (~550)	44-55 (300-380)	Smooth bar	Rotating bending	41.7	3% NaCl	S-N curves 10^5-10^7	Effects of grain size and dissolved oxygen	51
SM50A steel		79 (542)	55 (381)	Smooth bar		20	3% NaCl	S-N curves 10^5-10^7		52
Corten 50A steel		82 (563)	59 (405)	Welded and notched	Axial and rotating bending, respectively	20	3% NaCl	S-N curves 10^5-10^7		52
Marina		78 (536)	68 (468)			20	3% NaCl	S-N curves 10^5-10^7		52
0.11 C steel		84 (578)	68 (470)	Smooth plate	Axial tension	0.17	Seawater	Strain-N curves 10^2-10^5		53
0.09 to 0.20 C steel	Q and T	81-84 (559-578)	55-68 (382-470)	Smooth plate	Reversed bending	25	Seawater	S-N curves 10^5-10^7	Periodic overloads	53
0.26 C steel		125 (862)	120 (827)	Notched bar	Axial tension	7.5	3% NaCl	S-N curves 10^4-10^7	Galvanized coating	54
0.02-0.05 C steel	Galvanized	40-47 (275-320)		Smooth sheet	Reversed bending	30	3% NaCl	S-N curves 10^5-10^7		55
0.05-0.07 C steel	Hot-rolled	46-53 (315-370)		Smooth sheet	Reversed bending	30	96 hr salt spray before test only	S-N curves 10^4-10^7		55
S541 steel		61 (471)	44 (300)	Smooth and notched bar	Reversed bending	0.1 to 0.5	3% NaCl	S-N curves 10^4-10^7	Effects of sand blasting	56
SM50A steel		88 (604)	75 (520)			0.1 to 0.5	3% NaCl	S-N curves 10^4-10^7	At coating, Zn plating, and cathodic protection at -1 V SCE	56
0.06C steel		73 (491)	57 (396)			0.1 to 0.5	3% NaCl	S-N curves 10^4-10^7		56
0.09 C steel		73 (501)	51 (352)			0.1 to 0.5	3% NaCl	S-N curves 10^4-10^7		56
Mild steel	Cold rolled	87 (600)	77 (530)	Fillet welded lap joint	Axial at R = -0.33	0.17 and 8	3% NaCl drip	S-N curves 10^4-10^7	Surface dried between drips	57
ASTM A245 steel	Hot rolled	87 (600)	55 (379)	Smooth plate	Reversed bending	29.2	Synthetic seawater	S-N curves 10^5-10^8		58
AISI 1035 steel	Normalized	87 (600)	55 (379)	Smooth bar	Reversed bending	10	3% NaCl	S-N curve 10^5-10^7	3 anodic currents, varying pH level	59
AISI 1018 steel	Stress relieved	76 (522)	69 (473)	Smooth bar	Rotating bending	30	3% NaCl	S-N curves 10^5-10^7	Anodic currents, varying pH level	60
AISI 1018 steel	Stress relieved	80 (552)	69 (473)	Smooth bar	Rotating bending	30	3% NaCl	S-N curves 10^5-10^7	Aeration, cathodic protection	61
AISI 1020 steel	Hot rolled	72 (496)	46 (317)	Smooth and notched bar	Axial at R = 0	12.5	Synthetic seawater	S-N curves 10^5-10^8	Cathodic protection	62
HT-50 steel		90 (617)	73 (500)	Smooth and notched sheet	Axial at R >> 0	0.0028 to 3.33	1% NaCl	S-time plots	Small secondary cycles	63, 64
0.37 C steel		100 (689)	68 (469)	Smooth and notched sheet	Reversed bending	0.0028 to 0.045	1% NaCl	Strain-N curves 10^2-10^4	Plastic strain, corrosion potential	65
AISI 1036 steel	Normalized	63 (431)	28 (196)	Smooth bar	Rotating bending	33.3	1% NaCl	S-N curves 10^5-10^9	pH from 6.6 to 14*	66
0.16 C steel	Normalized	59 (407)	29 (200)	Smooth bar	Rotating bending	3 and 50	1% NaCl	S-N curves 10^5-10^8	Cathodic protection -1 V SCE	67
0.15 C steel	Drawn	106 (731)		Smooth wire	Rotating bending	50	1% NaCl	S-N curves 10^5-10^8	Tuftrided steel	68, 69
0.17 C steel		60 (414)		Smooth bar	Rotating bending	50	Synthetic seawater	S-N curves 10^5-10^8		70
Mild steel				Smooth bar	Reversed axial	24.2	Seawater	S-N curves 10^5-10^8		5, 71
AISI 1020 steel	Cold rolled	94 (648)	47 (324)	Smooth bar	Reversed axial	14,200	3% NaCl at 50 F	S-N curves 10^6-10^9	2,000 psia (13.8 MPa) pressure	73
AISI 1020 steel	Cold rolled	80 (552)	51 (352)	Smooth bar	Reversed axial	20,000	3% NaCl at 50 F	S-N curves 10^6-10^9	2,000 psia (13.8 MPa) pressure	73
ASTM A537A steel				Smooth bar	Reversed axial	20,000	Synthetic seawater	S-N curve 10^6-10^9	1,000 psia (6.9 MPa) pressure	74
AISI 1020 steel				Smooth bar	Reversed axial	14,200	Synthetic seawater	S-N curve 10^6-10^9	Cathodic protection	75
0.35 C steel		88 (607)	47 (324)	Smooth plate	Reversed bending	4.1 and 42.5	Synthetic seawater	S-N curves 10^5-10^7		76
0.44 C steel	Normalized	95 (655)	51 (352)	Notched plate	Reversed bending	30.8	Seawater	S-N curve 10^5-10^7	Cathodic protection	77
AISI 1018 steel				Notched plate	Reversed bending	30.8	Seawater and 3% NaCl	Fatigue limit-10^7	Cathodic protection	78
AISI 1018 steel				Notched plate	Reversed bending	3.3 and 30.8	Seawater and 3% NaCl	Fatigue limit-10^7	Cathodic protection, notch geometry	79, 80
AISI 1018 steel				Notched bar	Rotating bending	25	Brine drip at 55 and 91 F	S-N curves 10^5-10^8	Temperature	81
0.22 C steel	Normalized	72 (496)	28 (193)	As-welded plate	Rotating bending	25	1% NaCl	S-N curves 10^5-10^7		81
0.15 C steel	Normalized	63 (434)	28 (193)	Notched bar	Rotating bending	36.7	1% NaCl	S-N curves 10^5-10^7	Cathodic protection	82
0.35 C steel	Normalized	83 (572)	50 (345)	Notched bar	Rotating bending	36.7	1% NaCl	S-N curves 10^5-10^7		83
Carbon steel		82 (569)	40 (274)	Notched plate	Reversed bending	0.17	3% NaCl at 68 to 194 F	N-temperature	Cathodic protection	84
0.18 C steel		65 (449)	37 (256)	Smooth and notched, base and weld metal plate	Wave-load bending	0.0017 to 16.7	3% NaCl drip	Deflection-N 10^3-3×10^4	Temperature, low-cycle, oxygen level	84, 93
0.18 C steel		65 (449)	32 (223)	Notched plate, base metal and weld metal	Wave-load bending	Wave history	Seawater	S-N curves 10^5-10^7	Protective coating	28
AISI 1018 steel	Hot rolled			Smooth and notched beam and weld metal	Reversed bending	33.3	Synthetic seawater	S-N data 10^4-10^7	Cathodic protection	85, 86
AISI 1020 steel										
API K-45 steel		79 (542)	62 (425)	Smooth	Bending	5	Synthetic seawater	S-N data 10^4-10^7	Cathodic protection	87
Steel 45		80-85 (549-588)	41-49 (279-338)	Smooth	Bending	85	3% NaCl	S-N data 10^5-10^7	Ni-Cr coating	88
BS 4360/50D steel				Smooth plate	Reversed bending	0.23	Synthetic seawater	S-N data 10^6-10^7		89
BS 970 En 1 steel				Smooth and welded plate	Reversed bending	0.23	Synthetic seawater	S-N data 10^5-10^6	3 types of welds	90
BS 4360/50D V-cut				Smooth and welded plate	Reversed bending	0.23	Synthetic seawater	S-N data 10^5-10^6	Painted surface	90
ASTM A-441	Normalized	76 (524)	50 (345)	Notched and welded plate	Bending at R = -0.33	0.1 and 0.2	Seawater	S-N data 10^3-10^6	Cathodic protection	91
ASTM A-441	Q and T	76 (524)	50 (345)	As-welded plate	Bending at R = -0.33	33.3	Seawater	2 data ~ 10^9	Cathodic protection	91
ASTM A-337 B	Normalized	76 (524)	50 (345)	As-welded plate	Axial at R = 0 and 0.5	3.67	Synthetic seawater	S-N curves 10^5-10^6		92
NVE 36 steel	Normalized	71-90 (490-618)	51 (355)	Welded T-joints	Bending at R = 0.1	0.125 and 1	Seawater drip	S-N curves 10^5-10^6	Residual stress	94, 95
BS 4360/50 D steel		71-90 (490-620)	50 (345)	Welded transverse joints	Bending at R = 0 and -1	0.167	Synthetic seawater	S-N curves 10^4-10^7	Cathodic protection	96, 97
Euronorm Fe 510 steel(b)		86-103 (590-710)	71 (490)	Welded T-joints	Bending at R = 0.1 and -1	0.2	Synthetic seawater	S-N curves 10^5-10^6	Plate thickness, weld procedures	98, 99
Si 52 E steel		77 (530)	54 (370)	Butt-welded plate	Bending at R = 0	1	Synthetic seawater	S-N curves 10^4-10^6		100
BS 4360/50D steel		77 (530)	54 (370)	Butt-welded plate	Bending at R = 0	1	Synthetic seawater	S-N curves 10^5-10^7	Cathodic protection	101
OX 602E	Q and T	93 (640)	78 (540)	Welded transverse joint	Bending at R = 0	1	Synthetic seawater	S-N curves 10^5-10^7		
BS 4360/50D steel		78 (538)	54 (370)	Butt-welded plate	Bending at R = -1 to +0.18	0.167	Synthetic seawater at 50 to 54 F	S-N curves 10^5-10^7	Cathodic protection	102
ABS DH32	Normalized	78 (538)	57 (391)	Butt-welded plate	Axial at R = 0.1	1 and 7.5	Seawater at 39 and 68 F	S-N data 10^5-10^6	Constant amplitude and narrow-band random loading	19
SM41A steel		68 (471)	48 (333)	Smooth plate	Reversed bending	31.7	3% NaCl at 86 F	S-N curves 10^5-10^8		103
1.0%C steel		103 (703)	61 (412)	Smooth bar	Rotating bending	24.2	Saltwater(c)	CFS(d) at 10^7	Painted coatings, cathodic protection	4

(a) Unless noted water temperature was 68 to 77 F.
(b) Same as BS 4360/50D steel.
(c) Severn River water with one-sixth to one-third the salinity of seawater.
(d) CFS denotes corrosion-fatigue strength.

TABLE 3. Corrosion-Fatigue-Life Data for Steels From Recent Studies in Japan[47]

Alloy	Condition or Treatment	Tensile Strength, ksi (MPa)		Environment	Type of Load	Cyclic Frequency, Hz	Temp, F	Diameter or Thickness, in. (mm)	CFS(a) at 10^7 Cycles	
		Ultimate	Yield						ksi	(MPa)
Mild Steel										
Mild steel	1652 F, N	60 (412)	—	10% saline water	Rotary bending	38.3	RT	1.14 (29) φ wire	9.5	(66)
Carbon steel		51 (355)	35 (238)	3% saline water	Spray	Plane bending	28.3	43	0.16 (4)	13.7	(94)
Mild steel		63 (434)	49 (335)	Seawater	Immersion	Plane bending	20.8–24.2	RT	0.13 (3.2)	9.2(b)	(64)
S 15 C	1652 F, FC; 1202 F, T	58 (402)	28 (196)	1% saline water	Immersion	Plane bending	35	RT	0.50 (12.8)	19.6	(135)
SS 41	1652 F, FC; 1202 F, T	66 (457)	47 (326)	Seawater	Drop	Plane bending	24.2	RT	0.59 (15)	7.8	(54)
SM 41 B		53 (366)	41 (285)	Synthetic seawater	Immersion	Axial	0.17	86	0.32 (8) φ wire	17.1	(118)
SM 50 B		77 (531)	51 (349)	Synthetic seawater	Immersion	Axial	0.17	86	0.32 (8) φ wire	15.6	(108)
SS 41		61 (421)	44 (300)	3% saline water	Immersion	Plane bending	0.50	RT	0.24 (6)	8.5(c)	(59)
Low-Alloy Steel										
SM 50		88 (604)	75 (520)	3% saline water	Immersion	Plane bending	0.50	RT	0.24 (6)	~12	(~80)
Atmospheric-corrosion-resistant steel		71 (491)	57 (396)	3% saline water	Immersion	Plane bending	0.50	RT	0.24 (6)	~10	(~70)
Atmospheric-corrosion-resistant steel		73 (501)	51 (352)	3% saline water	Immersion	Plane bending	0.50	RT	0.24 (6)	~10	(~70)
HT 60		92 (637)	74 (513)	Synthetic seawater	Drop	Rotary bending	24.5	86	0.47 (12) φ wire	12.8	(88)
Low-alloy steel		—	115 (794)	Synthetic seawater	Drop	Rotary bending	24.5	86	0.47 (12) φ wire	11.4	(78)
Low-alloy steel		137 (941)	104 (716)	Synthetic seawater	Drop	Rotary bending	24.5	86	0.47 (12) φ wire	11.4	(78)
HT 80		123 (847)	116 (803)		Drop	Rotary bending	25	RT		11.4	(78)
SM 50		74 (510)	48 (333)		Drop	Rotary bending	25	RT		14.2	(98)

TABLE 3. (Continued)

Alloy	Condition or Treatment	Tensile Strength, ksi (MPa) Ultimate	Yield	Environment		Type of Load	Cyclic Frequency, Hz	Temp. F	Diameter or Thickness, in. (mm)	CFS(a) at 10⁷ Cycles ksi	(MPa)
Low-Alloy Steel (Cont.)											
Seawater-corrosion-resistant steel		80 (554)	53 (365)	Synthetic seawater	Drop	Rotary bending	24.5	86	0.47 (12) φ wire	11.8	(81)
Seawater-corrosion-resistant steel		86 (590)	—	Synthetic seawater	Drop	Rotary bending	24.5	86	0.47 (12) φ wire	14.9	(103)
Seawater-corrosion-resistant steel		99 (680)	89 (615)	Synthetic seawater	Drop	Rotary bending	24.5	86	0.47 (12) φ wire	16.8	(116)
Atmospheric-corrosion-resistant steel		81 (559)	55 (382)	Synthetic seawater	Immersion	Plane bending	25–36.7	86	b = 0.71 (18) h = 0.13 (3.2)	19.9	(137)
Atmospheric-corrosion-resistant steel		82 (569)	67 (461)	Synthetic seawater	Immersion	Plane bending	25–36.7	86	b = 0.71 (18) h = 0.13 (3.2)	13.5	(93)
HT 50		77 (529)	50 (343)	Seawater	Immersion	Rotary bending	48.3	86	0.04 (10)	8.8	(61)
HT 60		88 (606)	70 (479)	Seawater	Immersion	Rotary bending	48.3	86	0.04 (10)	13.8	(95)
HT 60	As rolled	96 (665)	70 (480)	Seawater		Plane bending	0.50	86		—	
Medium-Carbon Steel											
CK 45	N	101 (694)	—	3% saline water		Plane bending	0.50	RT		16.4	(113)
S 45 C	1652 F, 30 min	97 (668)	61 (423)	3% saline water		Plane bending	38.3	RT	0.04 (10)	14.9	(103)
Semihard steel	1472 F, N	84 (577)	—	10% saline water	Drop	Plane bending	38.3	RT	1.4 (29) φ wire	10.1(d)	(70)
Cast Iron											
FC 19	1472 F, N	31 (216)	—	3% saline water	Drop	Plane bending	38.3	RT	0.59 (15)	10.0(d)	(70)
FC 23		40 (273)	—	3% saline water	Drop	Plane bending	38.3	158	0.59 (15)	12.8	(88)
Acicular carbon cast iron			—	Synthetic seawater		Plane bending	38.3	158	0.59 (15)	5.4	(37)
High-Carbon Steel											
Steel wire	Drawing, 1886 F patenting	199 (1375)	—	Aerated seawater		Plane bending	38.3	158	0.59 (15)	9.2	(64)

(a) CFS denotes corrosion-fatigue strength.
(b) At 2 x 10⁷ cycles to failure.
(c) At 4 x 10⁶ cycles to failure.
(d) At 10⁸ cycles to failure.
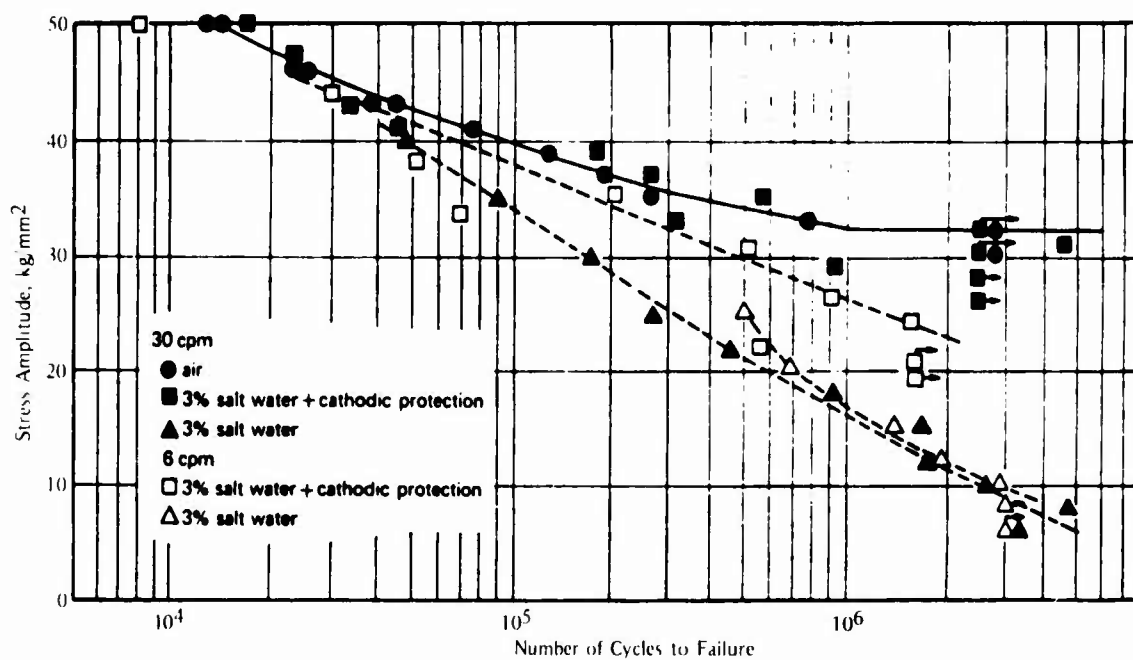
FIGURE 25. Stress-Fatigue-Life Plot for Reversed-Bending Corrosion Fatigue of As-Rolled SM50A (0.17 C-1.35 Mn-0.35 Si) Steel[56]
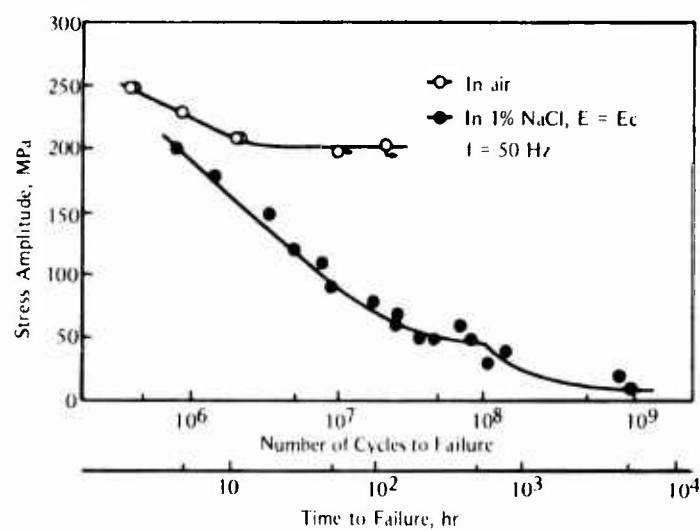
FIGURE 26. Stress-Fatigue-Life Plot for Rotating-Bending Corrosion Fatigue of a 0.16 C-0.49 Mn-0.27 Si Steel[67]

range is large and the total test time is short. At very low frequencies (0.003 to 0.05 Hz), there can be an environmental effect on low-cycle fatigue resistance, as shown by the results of Endo et al[65] in Figure 27. However, this effect is much less than that observed in the long-life or high-cycle fatigue regime. The major effects of environment on lowering corrosion-fatigue resistance are thus most evident at lower stress amplitudes in the long-life fatigue regime.

Effect of Stress Ratio. Increasing the stress ratio, R (R = minimum stress/maximum stress), or the level of mean stress reduces the stress amplitude associated with a specific cyclic life in the long-life regime for fatigue tests in air. Most of the data summarized in Tables 2 and 3 are for fully reversed cycling (i.e., R = -1 or mean stress of zero). For these steels, no study on the effects of R on corrosion fatigue of base-metal specimens in saline solutions was found. Changes in R values have been included in several studies of welded specimens in these environments.[92,96-99,102] At 2×10^6 cycles to failure, Havens and Bench[92] found that increasing R from 0 to 1/2 reduced the CFS from an amplitude of 11 ksi (76 MPa) to 10 ksi (69 MPa), i.e., a small effect. In tests of as-welded specimens at lives up to 10^7 cycles to failure, others[96-99,102] have found no significant influence of stress ratio in corrosive solutions. Knight[48], in his review, came to a similar conclusion for stress ratios above -1 (i.e., mean stress greater than zero), but he did point out that CFS appears to increase with increasing compressive mean stress. The data of Wildschut et al[98] and Vaessen and deBack[99] show that residual stress pays a significant role in the above work. With as-welded samples, they found only a small R effect for tests in seawater (see Figure 28). When samples were stress relieved, however, a significant decrease in CFS was discovered as R was increased from -1 to 0.1 (see Figure 29). Thus, in as-welded specimens, the tensile residual stress is usually high enough when coupled with small stress amplitudes in corrosive environments that there is little influence of tensile mean stress on CFS. When little residual stress is present and/or when stress amplitudes are increased because of protection from the environment, then an R effect is expected.
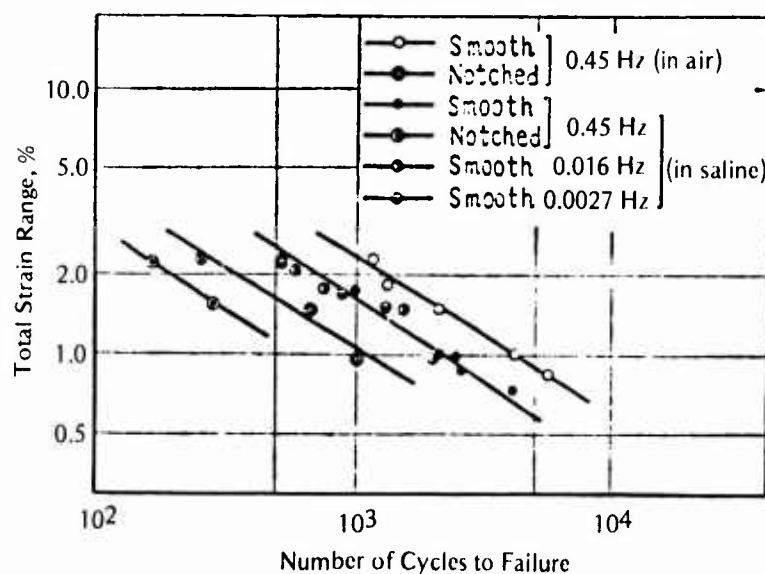
FIGURE 27. Low-Cycle Corrosion-Fatigue Resistance of a 0.37C-0.87Mn-0.58Si Steel at Very Low Frequencies[65]
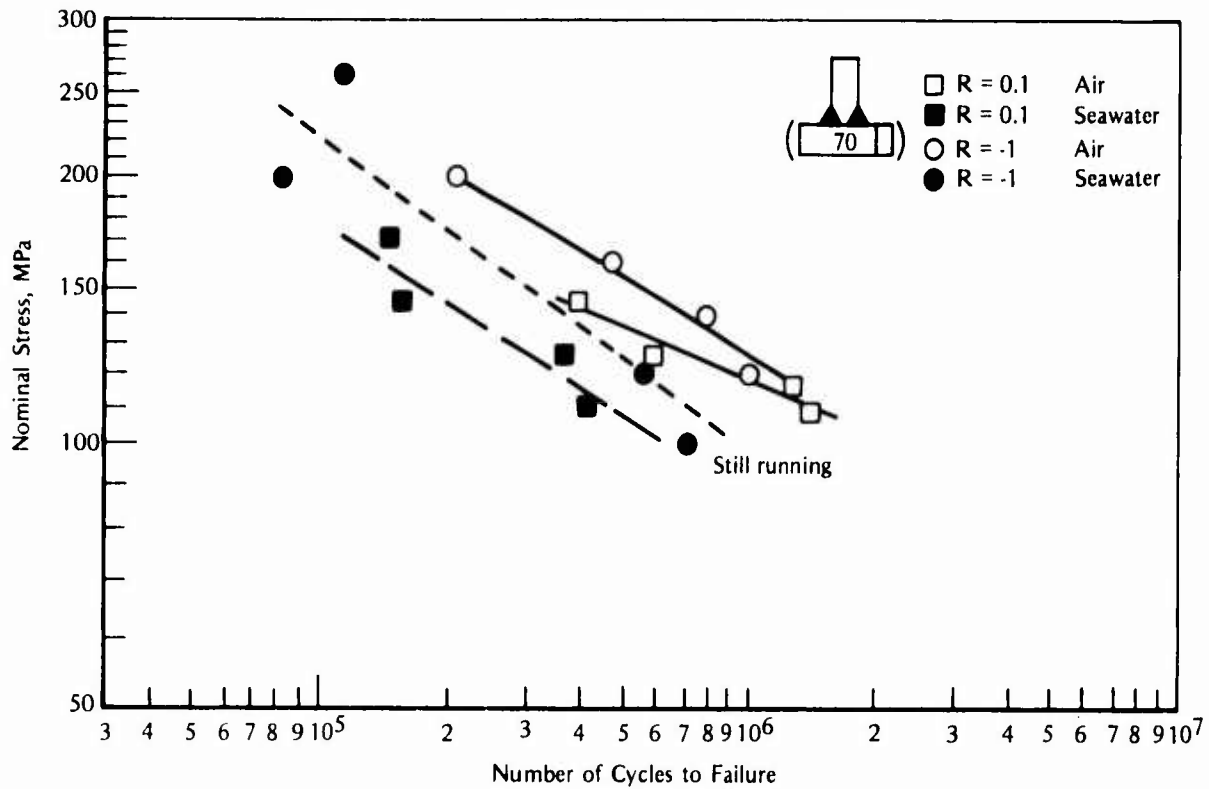
FIGURE 28. Fatigue Behavior of As Welded Specimens
of Euronorm Fe 510 Steel at Two Stress Ratios[99]
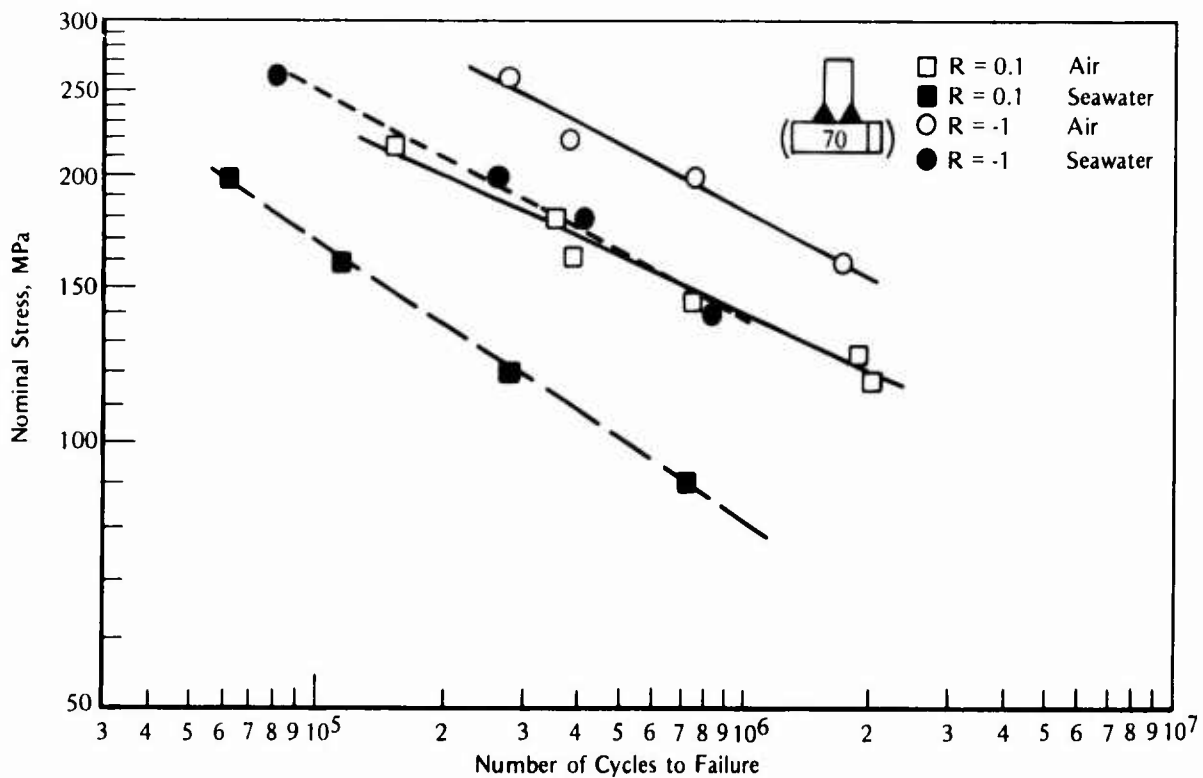
FIGURE 29. Fatigue Behavior of Welded and Stress-
Relieved Specimens of Euronorm Fe 510 Steel at Two
Stress Ratios[99]

Effect of Strength and Microstructure. For fatigue of structural steel in air, increasing strength typically produces increased high-cycle fatigue strength, and increasing ductility typically promotes improved low-cycle fatigue resistance. Since low-cycle fatigue behavior of these steels is not strongly influenced by marine environments, ductility is still expected to be the primary factor in determining low-cycle corrosion-fatigue resistance. High-cycle CFS of carbon and low-alloy steels has been shown to be approximately independent of tensile strength in saltwater and in contaminated fresh water[104], as illustrated in Figure 30. When the environment is not very aggressive, such as distilled water or dry air, the fatigue strength tends to increase with ultimate strength. Similar data reported by Ishiguro[47] are shown in Figure 31. In
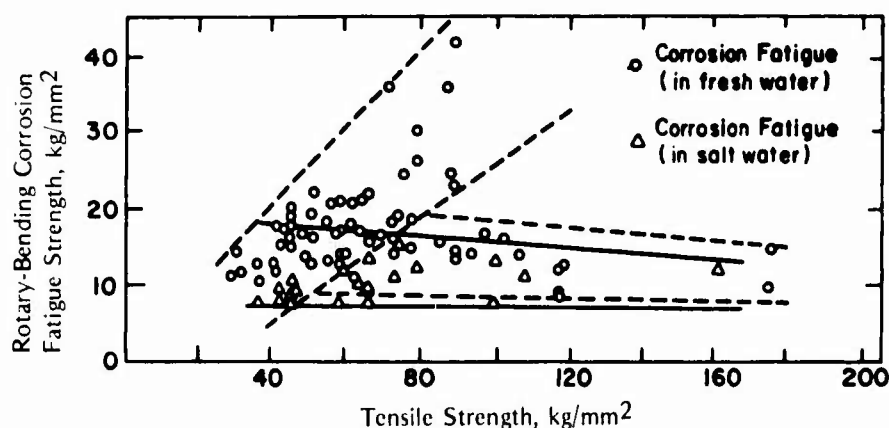
FIGURE 30. Correlation Between Ultimate Tensile Strength and Corrosion-Fatigue Strength at 10^7 Cycles to Failure for Carbon and Alloy Steels[104]

Bending frequency: 1,450 to 3,000 cpm
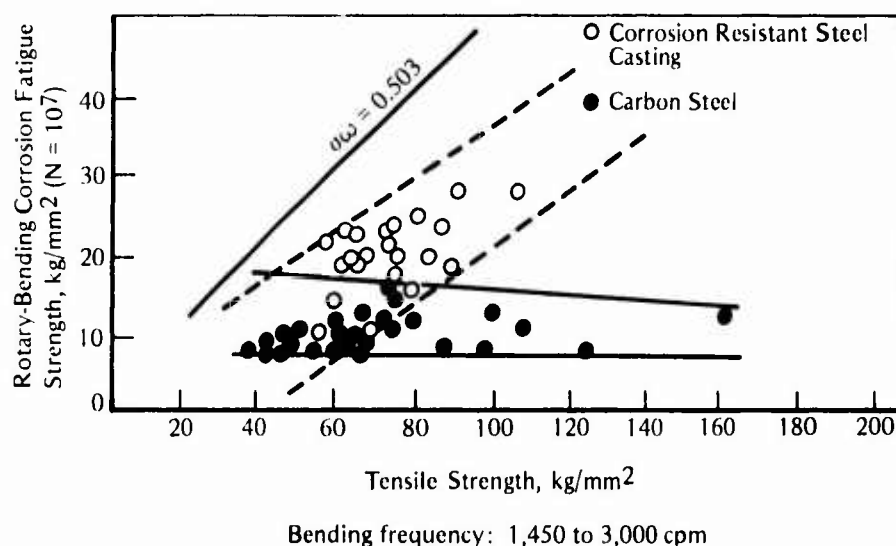
FIGURE 31. Correlation Between Ultimate Tensile Strength and Corrosion-Fatigue Strength at 10^7 Cycles to Failure of Carbon and Alloy Steels in Saltwater and Seawater[47]

this case, the data show no benefit of increased tensile strength for corrosion fatigue of carbon steels. Corrosion-resistant structural steels (with small additions of alloying elements such as Cr, Nb, Cu, and Ni) show increased CFS at higher tensile strengths. Microstructural features known to improve tensile strength and high-cycle fatigue strength in air thus seem to be of little benefit in aggressive aqueous solutions. Decreasing the ASTM grain size of a carbon steel from No. 4 to No. 8 improved fatigue strength in air but made no difference in a 3 percent NaCl solution[51], as illustrated in Figure 32. A similar trend was observed for changing the microstructure from lamellar pearlite to dispersed cementite[51], as shown in Figure 33. Thus, unless adequate protection from corrosive attack is maintained, the high-cycle corrosion-fatigue resistance will not be significantly improved by factors that normally increase fatigue strength in air. Such factors will be effective only if corrosion protection is achieved and maintained. However, as discussed later, the commonly used method of cathodic protection may make high-strength steel more susceptible to a localized hydrogen-embrittlement process during corrosion fatigue, and thus enhance the type and/or rate of damage.

Notch Effects. Notches act as stress concentrators and thereby promote fatigue cracking at the notch root. Several of the studies listed in Table 2 employed notched specimens.[52,54,56,62-65,77-82,84,87,91,93] For low-cycle fatigue, Endo et al[65] showed that notches still have a significant effect on fatigue life in saline solution. In other words, corrosion-fatigue life was less than in-air fatigue life for notched specimens. Generally, the long-life fatigue results for notched specimens show behavior trends similar to those for smooth specimens. The effects of corrosion and geometric stress concentration are typically additive. That is to say, notched specimens of the steels show lower fatigue strength in saltwater and seawater than they do in air. Therefore, the corrosion-fatigue process does more than produce a notch or discontinuity that acts as a stress concentrator. It has been noted by Dugdale[81] and by Hartt[77] that the nonpropagating cracks usually present in notched carbon steel specimens tested in air just below the fatigue limit no longer persist in corrosive media. It is believed that corrosion acts to keep these cracks growing to produce eventual failure.

Welded Joints. Many steel structures are assembled and fabricated using welded joints. The welded areas are often critical locations where corrosion-fatigue damage is likely to occur. In as-welded components, geometric configuration plays a dominant role in that corrosion-fatigue cracking often initiates at the toe of the weld where a stress raiser or notch is present. In addition to the pure notch effect, the metallurgical structure of the material in this region is altered from that of the base material by the welding process. Weld specimens were used in several studies.[19,52,96-102] All of the specimens were weldments except those used in the work of Watanabe and Mukai[93], where rotating-bending specimens were made from weldments. Most of those were tested as welded. In some cases, stress-relieving and weld-dressing procedures were employed.

For smooth specimens from weldments, only a slight reduction in low-cycle fatigue resistance occurred in saltwater-drip environment compared with that occurring in air.[93] For welded specimens, the low-cycle fatigue resistance under free-corrosion conditions is not markedly affected by corrosion conditions because significant plastic flow occurs in the local region where cracking initiates. However, in long-life or high-cycle fatigue, the environment causes a significant decrease in fatigue strength. As discussed before (see Figures 28 and 29), residual stress significantly influences the CFS of welded specimens. Thus, in the worst case, as-welded specimens tend to behave like samples with a tensile mean stress present. Then, reducing the applied mean stress will improve fatigue resistance only when the weldment has been fabricated with low residual stresses or heat treated to relieved residual stresses.
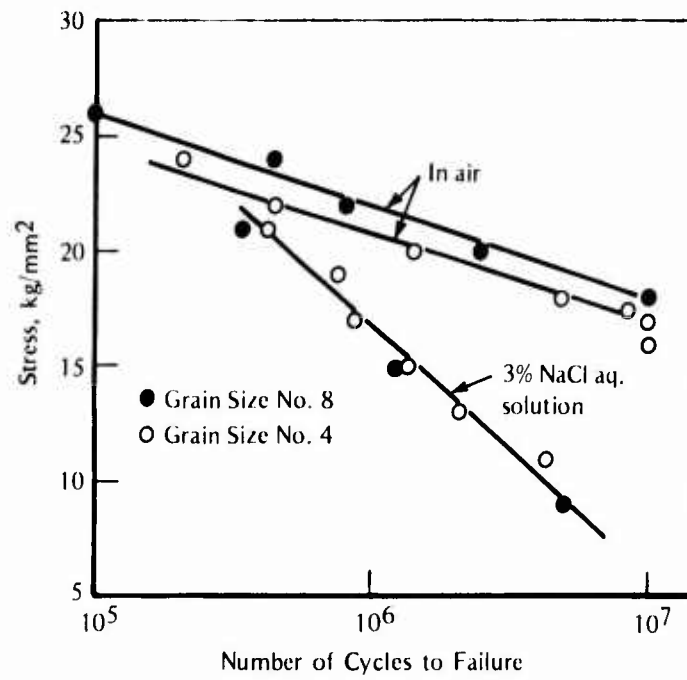
FIGURE 32. Effect of Grain Size on Fatigue
Behavior of a 0.18C Steel[51]
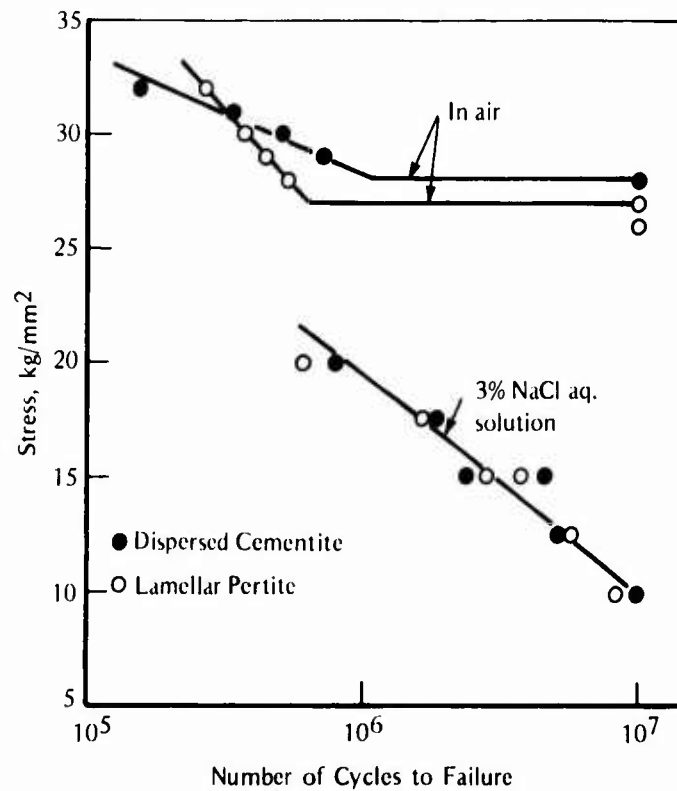
FIGURE 33. Effect of Cementite Configuration
on Fatigue Behavior of a 0.45C Steel[51]

Booth[97] shcwed that the grinding of weldments produced an improvement in fatigue strength for specimens tested in synthetic seawater, as illustrated in Figure 34. This improvement, however, was not as large as that observed in tests carried out in air. Vaessen and de Back[99] found that both grinding and plasma dressing imprcved fatigue resistance in synthetic seawater. In contrast, they observed that TIG dressing and modification of the weld toe angle (from 70 degrees to 45 degrees) gave only a slight improvement in CFS.

Effect of Cyclic Frequency. In low-cycle fatigue, decreasing the frequency has little effect on cyclic life except at very low frequencies (0.003 to 0.05 Hz or less)[85], as mentioned earlier (see Figure 27). Decreased cyclic frequency causes marked reductions in high-cycle fatigue strength under free-corrosion conditions. Several studies on the effects of frequency were conducted.[19,49,57,63-65,67,76,79,80,93-95] The work of Endo and Miyao[76] clearly showed a significant decrease in corrosion-fatigue strength as frequency decreased from 42.5 to 4.1 Hz, as illustrated in Figure 35. Since the S-N curves tend to diverge at lower stress amplitudes, the detrimental effect becomes worse as stress amplitude becomes lower. Figure 36 from the work of Nishioka et al[56] shows the influence of decreasing frequency on the corrosion-fatigue (free corrosion) strength of a number of steels tested in saline solutions. Over the regime of existing data and typical frequencies, corrosion-fatigue strength (at 10^6 cycles to failure) generally decreased by a factor of two. This point is important to remember when using data developed in the laboratory, where test frequencies are normally 20 to 40 Hz, for field applications where the actual loading frequency of a structure is more typically in the range 0.1 to 1 Hz. Figure 36
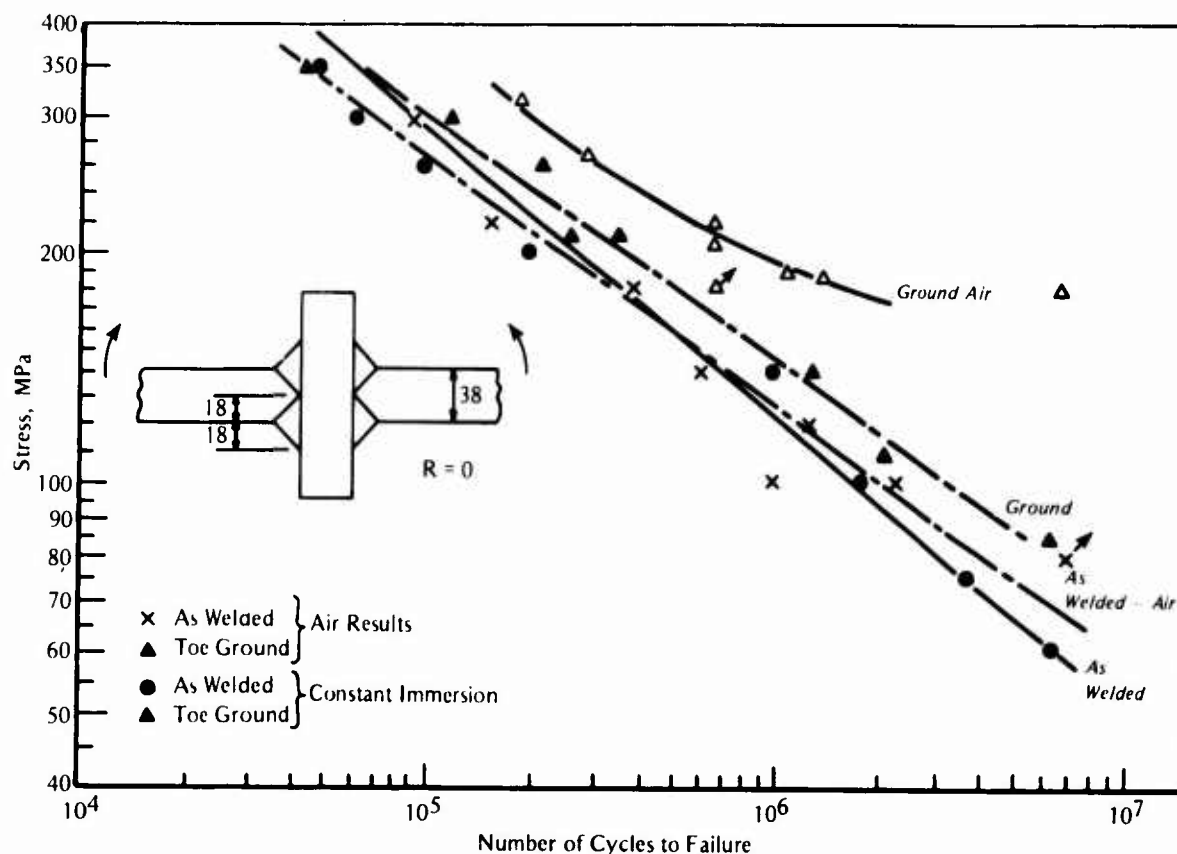
FIGURE 34. Effect of Welding Grinding of BS4360, Grade D Steel Plate Weldments on Corrosion-Fatigue Behavior in Synthetic Seawater[97]
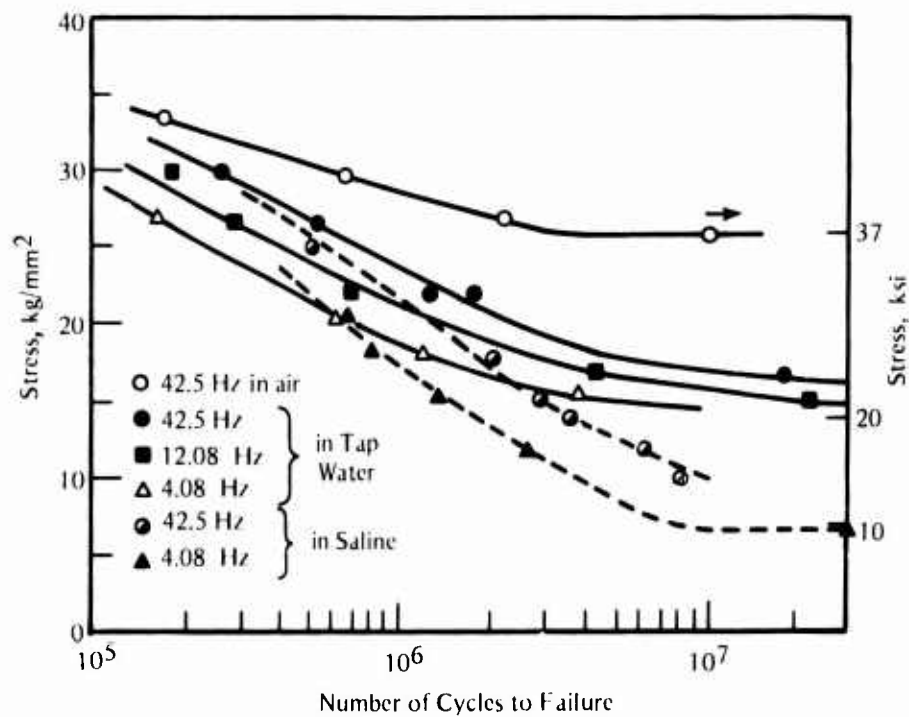
FIGURE 35. Effect of Cyclic Frequency on Corrosion-Fatigue Strength of a 0.44C Normalized Steel in 1 Percent NaCl Solution[76]
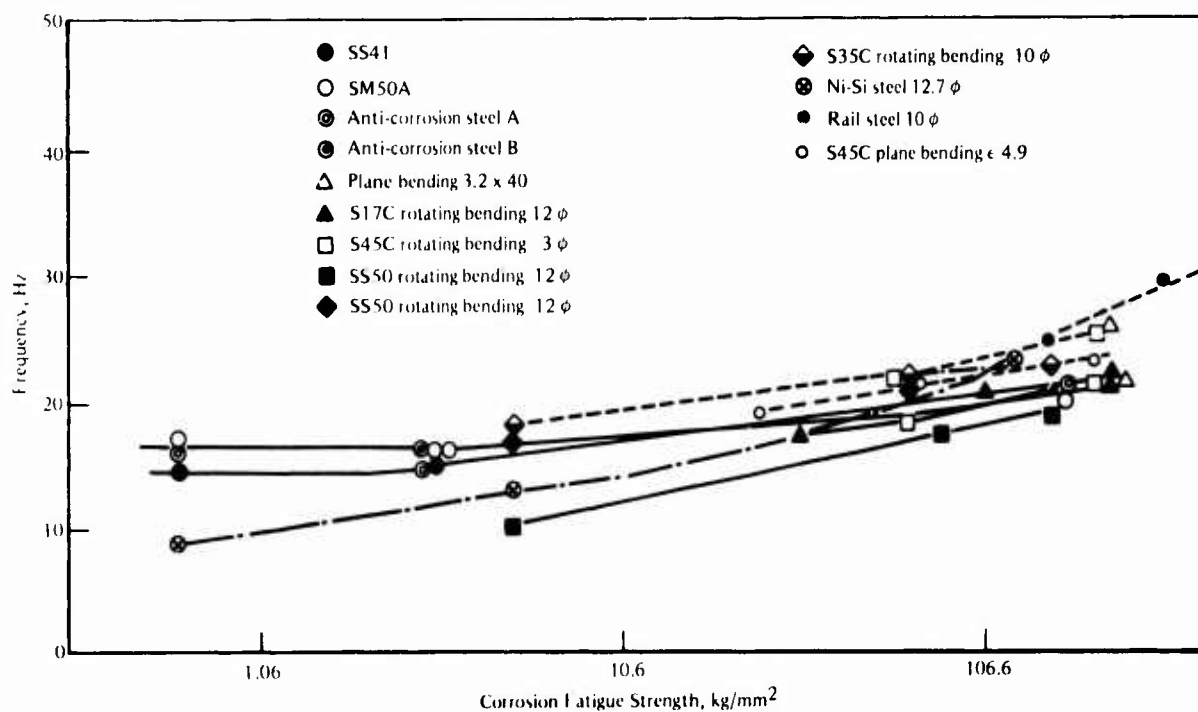
FIGURE 36. Influence of Cyclic Frequency on Corrosion-Fatigue Strength of Several Carbon and Alloy Steels Tested in Saline Solutions[56]

shows that with some corrosion-resistant steels there appears to be a saturation in the frequency effect at lower frequencies. Thiruvengadam et al[72-74] found that even at frequencies as high as 20 kHz there is still a corrosion-fatigue effect, compared with the results of similar tests carried out in air.

Load-History Effects. Almost all of the results summarized in Table 2 are for constant-amplitude cycling, whereas in actual service the cycling usually will be of variable amplitude. In tests of notched specimens, Mehdizadeh[54] found that periodic tensile overloads improved corrosion-fatigue resistance in a 3 percent NaCl solution. These overloads were undoubtedly beneficial because they produced compressive residual stress at the notch root. Endo and Komai[63,64] showed that the low-cycle, corrosion-fatigue life of a steel not susceptible to stress-corrosion cracking (static load) was markedly reduced by superposition of small secondary cycles (high R ratio) upon the main trapezoidal cyclic waveform. Holmes[102] investigated the corrosion-fatigue behavior of weldments in synthetic seawater and under narrow-band random loading. His results are shown in Figures 37 and 38, where the number of cycles to failure is shown as a function of the rms stress amplitude. On this basis, the random loading results fell slightly below the constant-amplitude ones, but exhibited the same slope of S-N curves. For R = -1 to + 0.2 (Figure 37), mean stress appeared to have little influence. Since these were as-welded specimens, this behavior is expected and would also occur in constant-amplitude loading as well as in random loading. The results were not dependent upon changing from a stationary to nonstationary Rayleigh distribution, but appeared to be influenced somewhat by changing to a La Place distribution. These results are limited and should not be generalized to other cases until further work is done.

Effect of Environmental Variables. Five major environmental variables influence the corrosion-fatigue behavior of steels in marine environments: temperature, oxygen level, pH, pressure, and water velocity. Electrochemical potential is another major environmental factor, but this is discussed separately in the next section. Gould[70], Dugdale[81], and Watanabe and Mukai[93] have all shown that increased temperature in the range 55 to 113 F (13 to 45 C) results in decreased fatigue resistance. Above about 122 F (50 C), the low-cycle fatigue results of Watanabe and Mukai[93] show a saturation in the temperature effect, as shown in Figure 39. Similar data are not available for high-cycle fatigue behavior.

Low-cycle fatigue strength was not very sensitive to oxygen level[93], as shown in Figure 40, which is not surprising in view of the small effect of environment on low-cycle fatigue of such steels. In high-cycle fatigue, the level of dissolved oxygen is important.[51,61]

The work of Duquette and Uhlig[61], illustrated in Figure 41, shows dramatically the importance of oxygen level. The fatigue limit in deaerated 3 percent NaCl solution is the same as that in air. In aerated 3 percent NaCl, fatigue life is markedly reduced and no fatigue limit is apparent. Masumoto and Akaishi[51] reported the CFS as a function of oxygen level and their data are reproduced in Figure 42. Below 0.01 cc/l, the effect of oxygen level is extremely important. Above 0.01 cc/l and up to the saturated level of 1.98 cc/l, the corrosion-fatigue life is relatively independent of oxygen level. Thus, in the range of oxygen levels normally encountered in marine environments, a deleterious corrosion-fatigue effect is anticipated. Only when the oxygen is reduced to extremely low levels, $\ll 0.01$ cc/l, will the fatigue limit be restored to that in air, as shown in Figure 41.

Over a broad range of pH (4 to 10), the value of pH has little influence on fatigue resistance.[60,66] The data of Radd et al[66] are shown in Figure 43. Values of pH below four
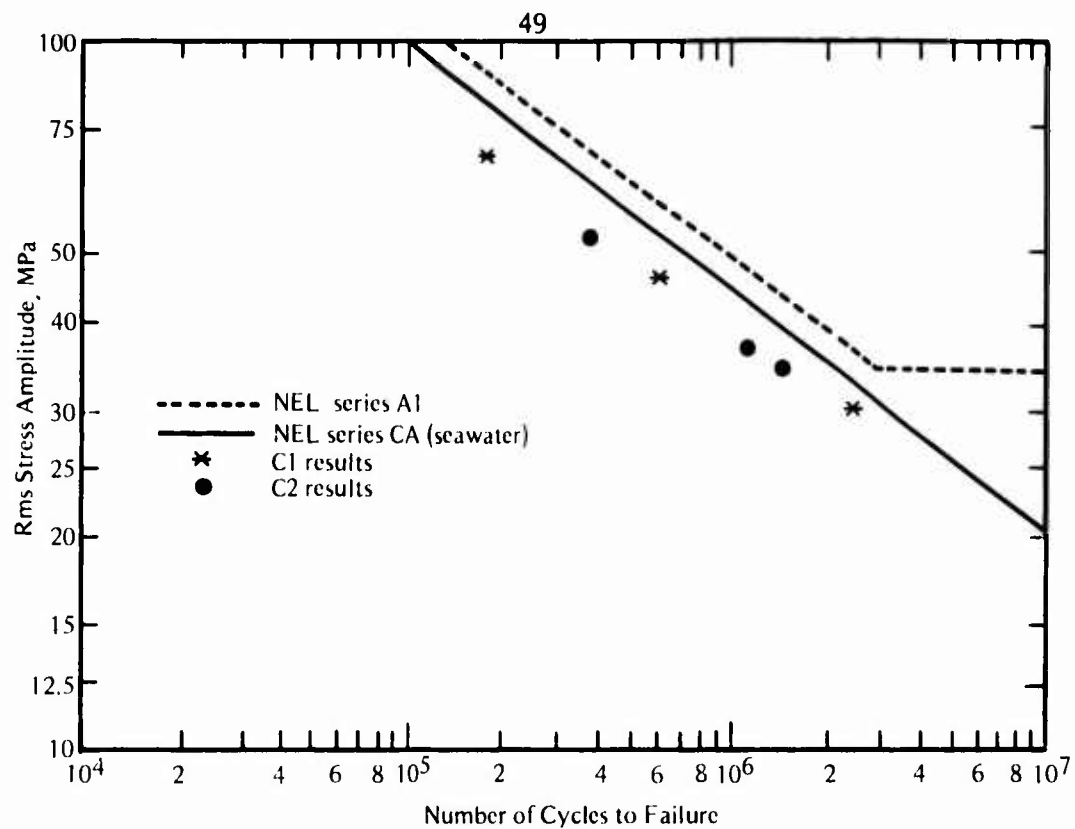
FIGURE 37. Corrosion Fatigue of Weldments Under Narrow-Band Random
Loading at Different Mean Stress Levels (R = -1 to 0.2)[102]
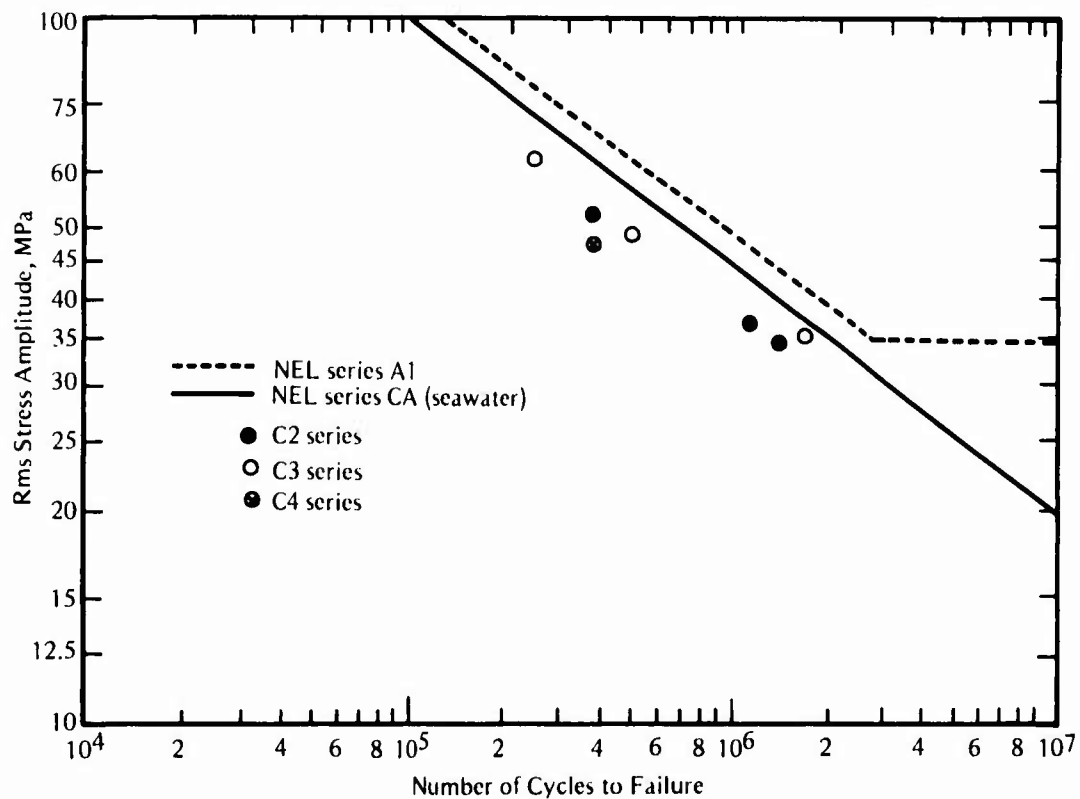
FIGURE 38. Corrosion Fatigue of Weldments Under Narrow-Band Random
Loading with Three Different Types of Load Spectra[102]
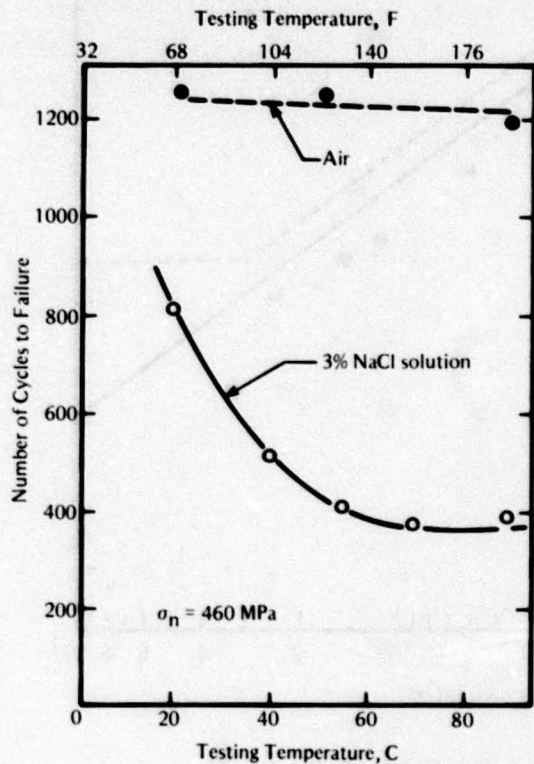
FIGURE 39. Effect of Water Temperature on Low-Cycle Fatigue Life of Notched Specimens of a 0.18C Steel[93]
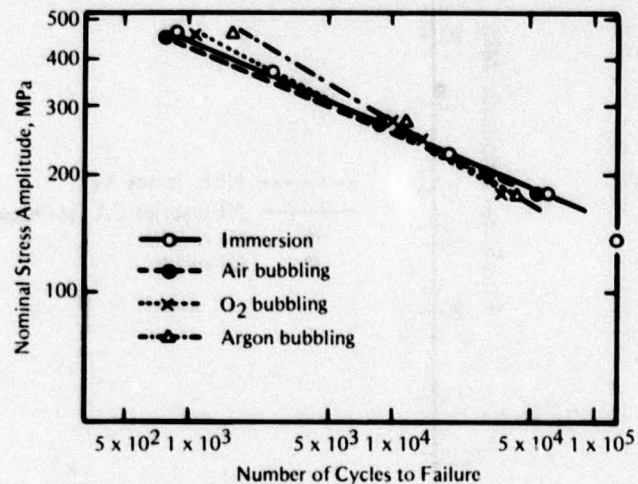
FIGURE 40. Effect of Aeration on Low-Cycle Fatigue Resistance of Notched Specimens of a 0.18C Steel in 3 Percent NaCl Solution[93]
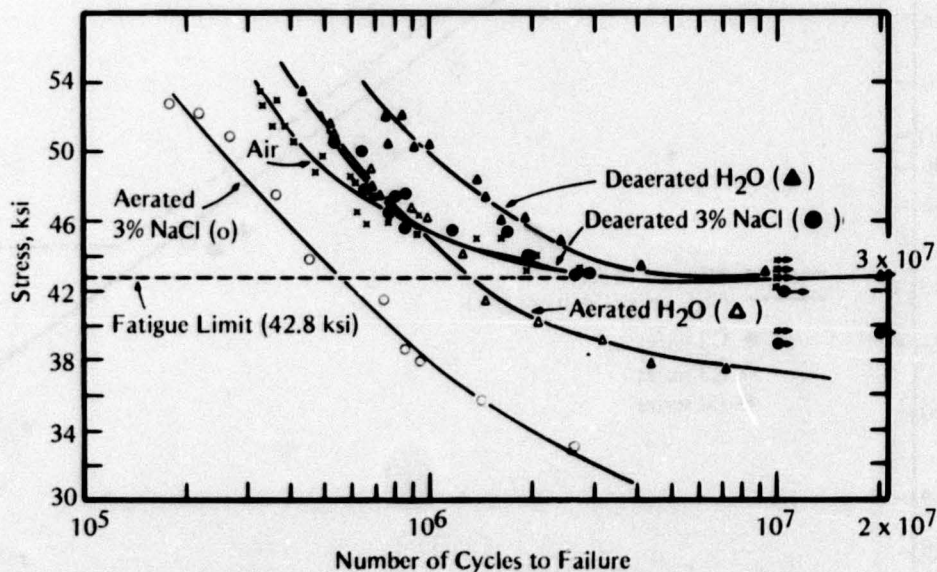
FIGURE 41. Effect of Aeration on Corrosion Fatigue Strength of AISI 1018 Steel in 3 Percent NaCl Solution[61]
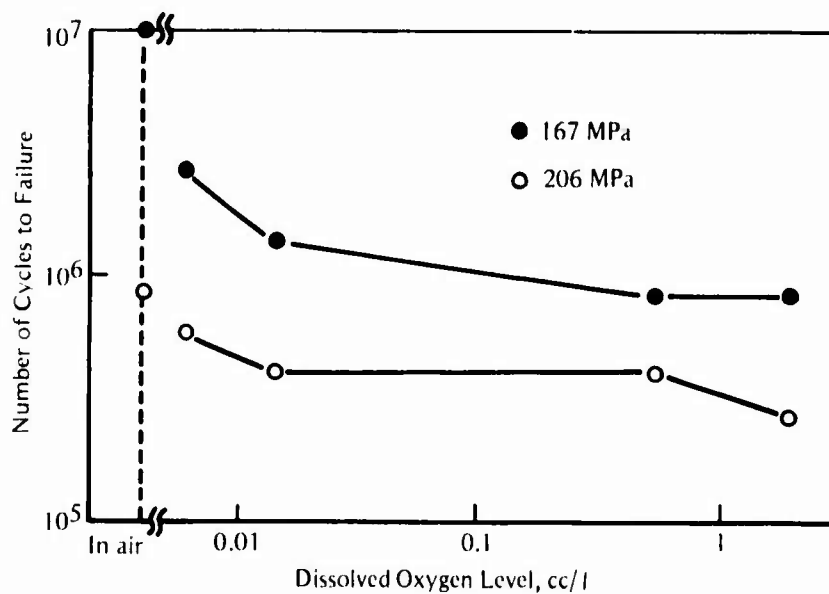
FIGURE 42. Effect of Dissolved Oxygen Level on Corrosion Fatigue
of SM41 Steel in 3 Percent NaCl Solution[51]
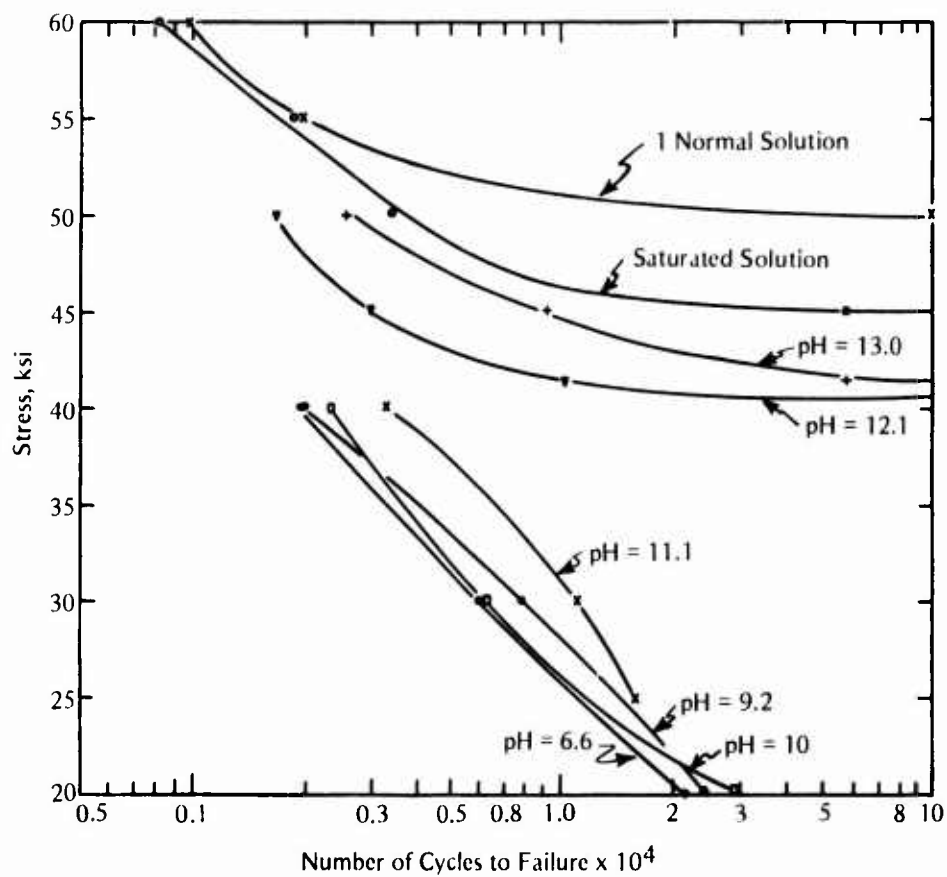
FIGURE 43. Effect of pH Level on Corrosion Fatigue of AISI 1036
Steel in 3 Percent NaCl Solution[66]

decrease fatigue resistance and those above 10 improve fatigue resistance.[60,66] At a pH of about 12, the corrosion-fatigue strength approaches the fatigue limit for tests in air.[60]

Increased hydrostatic pressure of 1000 to 2000 psi (6.9 to 13.8 MPa) causes a marked reduction in CFS[73,74] compared with results of tests conducted in 3 percent NaCl solution at ambient pressure. The reason for this effect is not known but it is thought to be related to increased chemical reaction kinetics at high pressure. This hydrostatic-pressure effect is important to keep in mind for deep-water application.

Protective Methods. Examination of Table 2 shows that the use of cathodic protection for improving corrosion-fatigue resistance has been examined by many investigators. It has been found that the CFS of these steels can be restored to (or raised somewhat above) the levels observed in air when cathodic protection is employed. Restoration of the in-air fatigue limit requires a more negative cathodic protection potential. This level for adequate cathodic protection from corrosion-fatigue damage is similar to that for adequate protection from general uniform corrosion, which is typically about -0.783 V SCE (or -0.85 V Cu/CuSO$_4$); however, the protection potential is affected by the environment. There is some indication that overprotection to levels of -0.933 V SCE (or -1.00 V Cu/CuSO$_4$) or less may be detrimental to corrosion-fatigue resistance.

The data in Figure 44 provide an example of the restoration of the in-air fatigue limit for an overprotection case (-1.00 V SCE) and a slow cyclic frequency of 3 Hz.[67] For this same level (-1.0 V SCE), Nishioka et al[56] found cathodic protection to be effective at a cyclic frequency of 0.5 Hz but less effective at 0.1 Hz. (See Figure 25 presented earlier.) Minami et al[49] mention such a frequency effect with cathodic protection and point out that it may be related to a hydrogen-embrittlement process. In their results at 0.33 Hz and in seawater, they noted a decrease in the effectiveness of cathodic protection at levels below -1.0 V SCE, as illustrated in Figure 45. Thus, the combination of very low frequency ($\leq$0.1 Hz) and overprotection ($\leq$-1.0 V SCE) appears to be detrimental to corrosion-fatigue resistance.

Nichols[58], Hudgins et al[62], and Hartt et al[77-80] emphasize the importance of the formation of a calcareous scale consisting of CaCO$_3$ and Mg(OH)$_2$ in achieving adequate cathodic protection from corrosion fatigue. This scale cannot form in NaCl solutions, so it is important to use actual seawater or well-formulated synthetic seawater in evaluating the effects of cathodic protection. With the formation of such a scale, adequate protection of smooth fatigue specimens can be achieved more readily at moderate cathodic potential levels in the region of about -0.73 V SCE. Also, the current-density requirements for maintaining this potential markedly reduce with scale formation. However, Hartt et al[77] found that a lower potential of -0.78 V SCE was required for notched samples. To explain this finding, it is suggested that the local environment at the notch root may be different from that on the surface and/or the effective potential at the notch root may be diminished from the applied nominal value.

Hooper and Hartt[105] showed that the fatigue limit of notched specimens was above that in air for optimum protection conditions of about -1.1 to -1.25 V SCE in seawater, as shown in Figure 46. For potentials less than -1.25 V SCE, a detrimental effect resulted from overprotection. When these same investigators used a frequency of 3.3 Hz rather than 31 Hz, the curve was shifted to higher strengths and potentials, as shown in Figure 47. Thus, adequate protection was achieved more readily at the lower frequency. In Figure 46, there are two data points at -1.0 V SCE in 3 percent NaCl solution, representing failures that occurred in the no-failure region of the seawater data. This is direct evidence that use of actual seawater rather than 3 percent NaCl solution can influence results of cathodic-protection studies.

Time to Failure, hr
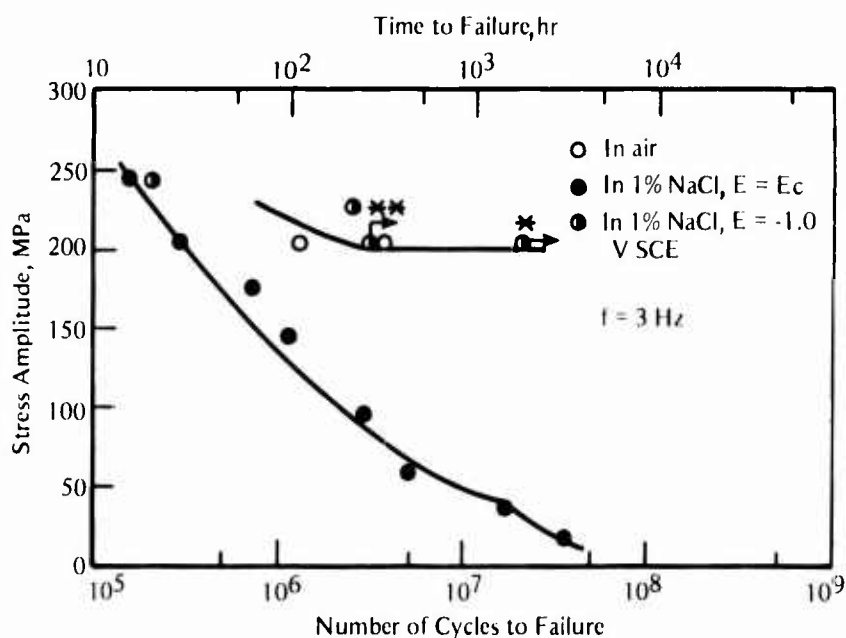
FIGURE 44. Effect of Cathodic Protection on Corrosion
Fatigue of a 0.16 C Steel[67]
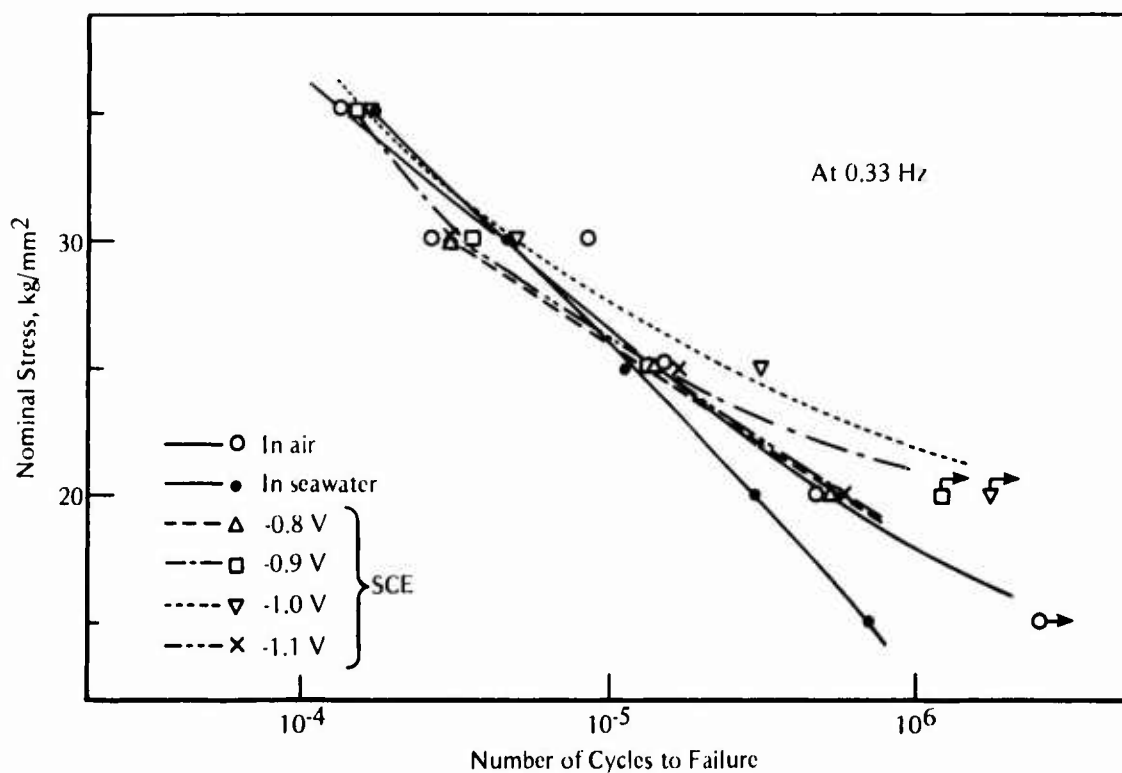
FIGURE 45. Effect of Level of Cathodic Protection on Corrosion Fatigue of a 0.14 C Steel[49]
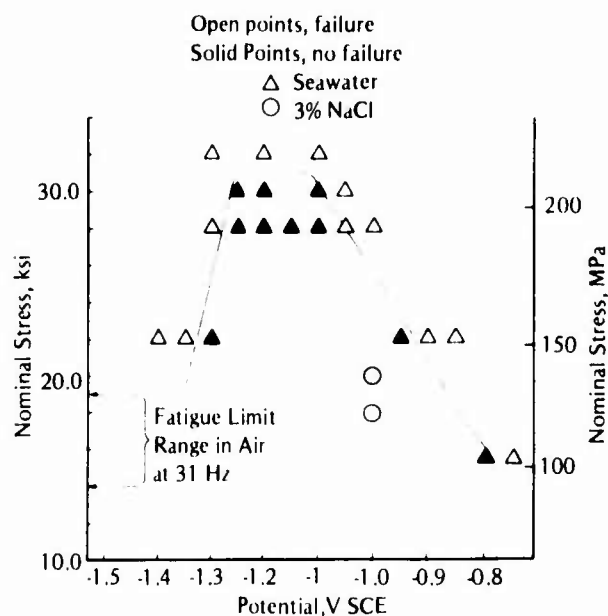
FIGURE 46. Corrosion-Fatigue Strength of AISI 1018 Steel (Notched) to Failure as a Function of Cathodic Potential[105]
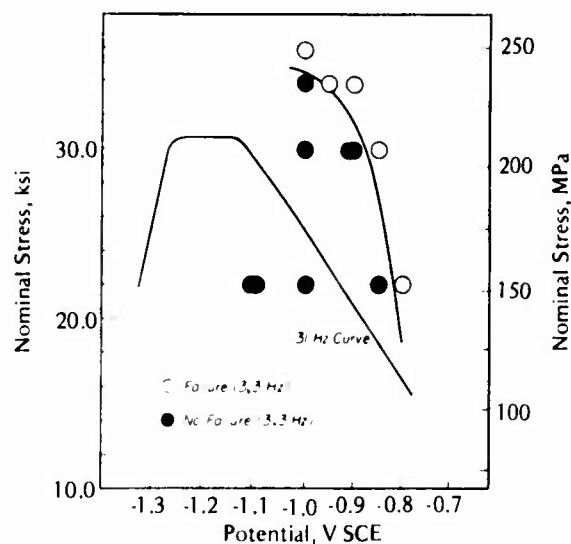
FIGURE 47. Effect of Frequency on Corrosion-Fatigue Strength of AISI 1018 Steel (Notched) at 10[7] Cycles to Failure as a Function of Cathodic Potential[79]

Using synthetic seawater at 5 to 8 C, Booth[97] investigated the influence on corrosion-fatigue behavior of cathodically protecting as-welded specimens to a level of -0.85 V Ag/AgCl. These data are compared with a USA design curve (solid line) and UK design curve (dashed line) in Figure 48.[97] These are all at a frequency of 0.167 Hz, so they involve long test times. Except for cycles approaching 10[7], all of these data are above the design curves. Intermittent immersion is just as detrimental as continuous immersion. Stress ratio has no significant effect in seawater without protection. With protection, increased stress ratio (from R = -1 to R = 0) is slightly deleterious at long lives ($\geq$10[6] cycles). At short lives (<10[6] cycles), there is little benefit of cathodic protection, but at long lives ($\geq$10[6] cycles) cathodic protection improves fatigue resistance. It is particularly significant that protected specimens showed no failures at stress amplitudes of 7.25 ksi (50 MPa) or less.

Coatings can effectively protect against corrosion-fatigue damage as long as they remain intact and are not scratched or cracked by fatigue cycling. The CFS of a carbon steel at 10[6] cycles in 3 percent NaCl can be improved fourfold by means of a chromium-nickel diffusion coating.[88] Part of this improvement is related to inducing favorable compressive residual stresses during the coating procedure. The effects of aluminum and zinc coatings were examined by Nishioka et al.[56] They found both coatings to be satisfactory, with aluminum being better than zinc in the high-cycle fatigue regime. They summarized their data in the normalized plot in Figure 49. Data above the 45-degree line show that the coating improved CFS over that under free-corrosion conditions. Data falling near 1.0 on the ordinate show CFS values comparable to those in air. The aluminum coating was better than zinc and/or chromium and gave good results at low frequencies of 0.5 and 0.1 Hz. Both aluminum and zinc are sacrificial coatings on steel and they corrode preferentially to steel. Thus, they provide cathodic protection as well as being barrier coatings. Painting can improve fatigue resistance up to or above values observed for tests in air.[49,103] However, cracks or scratches on the painted surface can significantly reduce CFS, and repaired coatings were not as satisfactory as good initial ones.[103] Combined use of both paints and cathodic protection is recommended for the most effective protection from corrosion-fatigue damage.[103]
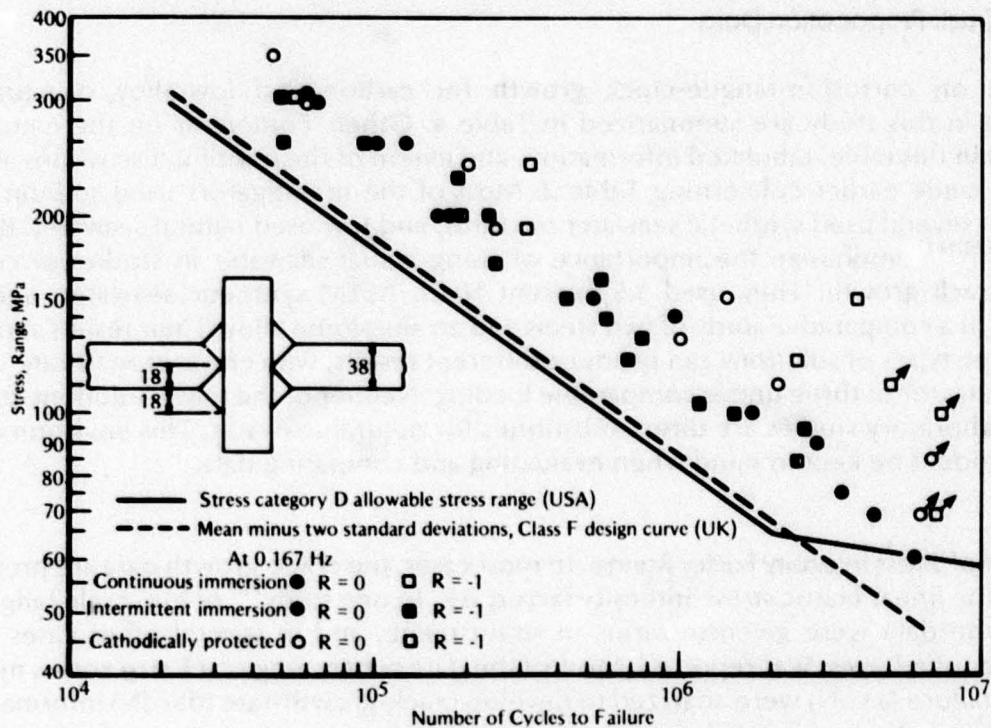
FIGURE 48. Effect of Cathodic Protection on Corrosion Fatigue of As-Welded Specimens of BS4360/50D Steel in Synthetic Seawater[97]
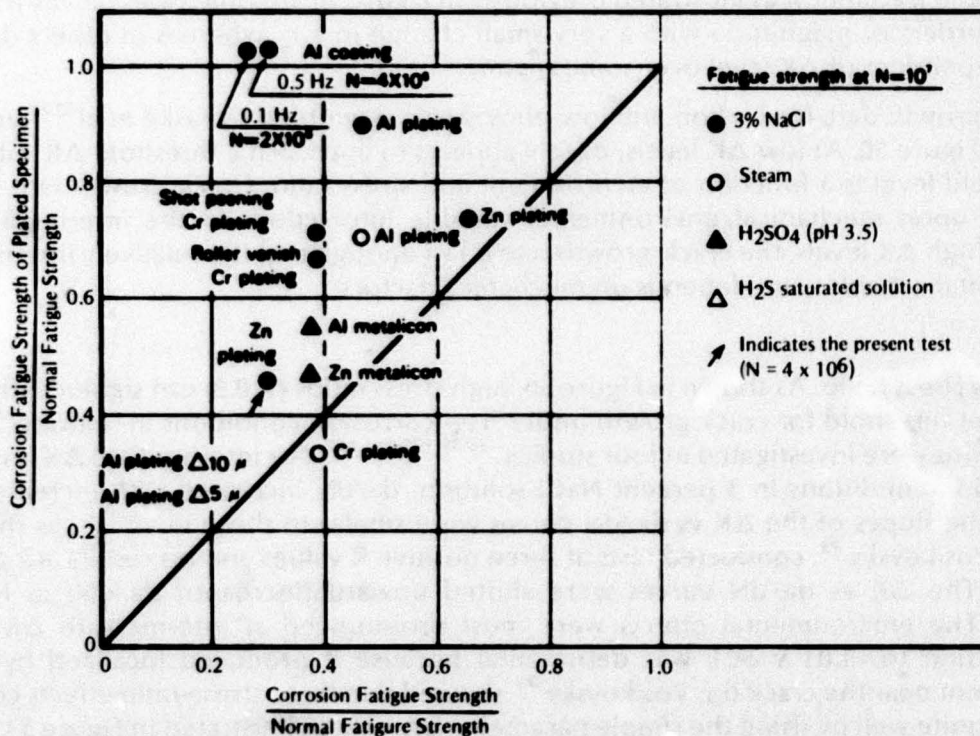
FIGURE 49. Effect of Coating and Plating on Corrosion-Fatigue Strength of Carbon Steels at 10[7] Cycles to Failure[56]

Fatigue-Crack-Propagation Data

Data on corrosion-fatigue-crack growth for carbon and low-alloy structural steels reviewed in this study are summarized in Table 4. Other comments on the nature of the headings in this table, tabulated information, and extent of the ensuing discussions are similar to those made earlier concerning Table 2. Most of the investigators used sodium chloride solutions, several used synthetic seawater mixtures, and few used natural seawater. Bogar and Crooker[126,127] emphasize the importance of using actual seawater in studies of corrosion-fatigue-crack growth. They used 3.5 percent NaCl, ASTM synthetic seawater, and natural seawater in a comparative study of two steels and an aluminum alloy. Their results showed that these three types of solutions can produce different results, with crack-growth-rate variations of up to a factor of three under comparable loading. Neither of the saline solutions commonly used in laboratory studies are direct substitutes for natural seawater. This environmental difference should be kept in mind when evaluating and comparing data.

Effect of Stress Intensity Factor Range. In most cases, the crack growth data are presented in terms of the linear elastic stress-intensity factor, ΔK. In one study[108] of low-cycle fatigue-crack growth, the data were given in terms of strain range, and in several other cases only the nominal applied stress was reported. Most of the data concerning crack size versus number of cycles to failure (a vs N) were analyzed to develop crack-growth-rate (da/dN) information. In a few instances, basic a vs N data are reported for given nominal stress ranges. As shown schematically in Figure 24 earlier, da/dN increases as ΔK increases, and the log ΔK vs log da/dN curve usually has a sigmoidal shape for tests in air. When environmentally enhanced crack growth occurs, the ΔK vs da/dN curves often have unusual shapes and vary more with stress ratio and frequency, as illustrated previously in Figure 20. In some cases da/dN increases by several orders of magnitude with a very small change in ΔK, whereas in others da/dN is almost independent of ΔK level over some regime.

Crack growth data for carbon and low-alloy steels assembled by Jaske et al[23,28] are summarized in Figure 50. At low ΔK levels, da/dN appears to approach a threshold ΔK value, but this threshold level is a function of environment and stress ratio. Crack growth rate is quite dependent upon mechanical/environmental variable interactions in the intermediate ΔK regime. At high ΔK levels, the crack growth rate is fast enough that it is relatively insensitive to environmental variables and depends on mechanical factors.

Effect of Stress Ratio. As shown in Figure 50, high stress ratios (> 0.8) can significantly lower the apparent threshold for crack growth under free-corrosion conditions in seawater. Stress-ratio variations were investigated in four studies.[38,39,106,111,122] For intermediate ΔK levels and free-corrosion conditions in 3 percent NaCl solution, da/dN increased with increased K_{max} levels and the slopes of the ΔK vs da/dN curves were similar to those in air[111], as shown in Figure 51. Vosikovsky[39] conducted tests at three positive R values and his results are given in Figure 52. The ΔK vs da/dN curves were shifted upward (increased da/dN) as R value increased. The environmental effects were most pronounced at intermediate ΔK levels. Overprotection to -1.03 V SCE was detrimental because it produced localized hydrogen embrittlement near the crack tip. Vosikovsky[39] showed that these stress-ratio effects could be correlated quite well by using the simple parameter $\Delta K + 4R$, as illustrated in Figure 53. At low ΔK levels, these data for saltwater environment appear to approach the same threshold level as that observed for tests in air, whereas Haagensen's data[121] in seawater showed a different threshold (Figure 50).

TABLE 4. Corrosion-Fatigue-Crack Growth Data for Carbon and Low-Alloy Steels

Alloy	Condition or Treatment	Tensile Strength, ksi (MPa) Ultimate	Yield	Type of Specimen	Type of Loading	Cyclic Frequency, Hz	Environment(a)	Types of Data	Notes	References
ASTM A301B steel	Normalized	68 (469)	48 (331)	Surface-cracked, cantilever beam	Reversed bending	0.08	3.5% NaCl	Strain range da/dN		108
ASTM A302B steel	Normalized	80 (552)	58 (400)	cantilever beam	Reversed bending	0.08	3.5% NaCl	Strain range da/dN		108
ASTM A516-60 steel	Normalized		44 (301)	CTS	Axial at R = 0.1	0.1 and 1	3.5% NaCl	ΔK vs da/dN	Cathodic protection, specimen thickness	109
0.15C steel				SEN	Axial	0.23	3.5% NaCl at 86 to 176 F	a vs N	Three maximum stress levels	110
Mild steel						0.05 to 5	3% NaCl	ΔK vs da/dN		111
ASTM A537 steel	Quenched and tempered	82 (565)	62 (427)	SEN-base and weld metal	Axial		3.5% NaCl at 30 and 75 F	ΔK vs da/dN		112
API X-65 steel		83 (570)	66 (458)	SEN	Axial at R = 0.2	0.01 to 15	3.5% NaCl	ΔK vs da/dN	Cathodic protection	113
API X-70 steel		98 (673)	77 (527)	SEN	Axial at R = 0.05 to 0.7	0.1 to 10	3.5% NaCl	ΔK vs da/dN	Cathodic protection	39
0.16C steel	Normalized	58 (402)	28 (196)	Notched bar	Rotating bending	0.005 to 23.3	1% NaCl	a vs N		114
0.16C steel	Normalized	58 (402)	28 (196)	SEN	Reversed bending	0.002 to 16.7	1% NaCl	a vs N		114
0.16C steel	Normalized	58 (402)	28 (196)	Notched bar	Rotating bending	0.008 to 30	1% NaCl	a vs N	Cathodic protection	115
HT-50 steel	Hot rolled	89 (617)	73 (500)	Double-edge notched	Axial R = 0 and > 0	0.065 to 30	1% NaCl	a vs N and ΔK vs da/dN	Small secondary stress	63, 64
S15C steel	Normalized	56 (385)	35 (242)	Notched bar	Rotating bending	25	0.5N NaCl	a vs N and ΔK vs da/dN	pH 5.3 and 11.2	116
AISI 1020 steel	Hot rolled			SEN	Reversed bending	33.3	Synthetic seawater	ΔK vs da/dN		85, 86
St 42 and 52 steel				Notched plate	Bending		Synthetic seawater	ΔK vs da/dN		117
ST 52 steel		80 (549)	52 (361)	SEN	Bending R = 0.6 to 0.8	0.2	Synthetic seawater	ΔK vs da/dN	Synthetic seawater saturated with H2S also	118
ASTM A441 steel	Normalized	76 (524)	50 (345)	Surface cracked, cantilever beam	Bending at R = -0.33	0.1 and 0.2	Seawater	a vs N and ΔK vs da/dN	Cathodic protection	91
BS 4360/D steel	Normalized	77 (530)	54 (370)	MSEN	Axial at R = 0	1	Synthetic seawater at 53 F	ΔK vs da/dN	Cathodic protection	119, 120
0.17C steel	Normalized	85 (586)	65 (440)	SEN	Axial at R > 0	6.5	Seawater	ΔK, nmₛ vs da/dN	Random loading	119, 121
Mild steel					R = 0.64 and -1		Brine	ΔK vs N		106
Mild steel		62 (430)	46 (315)	Double-edge notched	Axial at R = 0.6		3% NaCl	ΔK vs N	Cathodic protection	107
BS 4360/50D steel		78 (540)	54 (370)	CTS	Axial at R = 0.1 to 0.85	0.1	Seawater at 41 to 50 F	ΔK vs da/dN	Cathodic protection	38, 122
BS 4360/50D steel		78 (540)	54 (370)	SEN	Axial at R = -1	0.1	Seawater at 41 to 50 F	ΔK vs da/dN	Cathodic protection, tidal immersion	122
BS 4360/50D steel		78 (540)	54 (370)	Surface-cracked, cantilever beam	Bending at R = -1	0.1	Seawater at 41 to 50 F	a vs N		122
BS 4360/50D steel		78 (540)	54 (370)	CTS	Axial at R < 0.1	0.05 to 10	Seawater at 41 to 68 F	ΔK vs da/dN	Cathodic protection	123
BS 4360/50D steel		77 (530)	54 (370)	MSEN	Axial at R = 0.02 to 0.06	0.17 to 1	Synthetic seawater at 53 F	ΔK vs da/dN	Cathodic protection	124
API X-65 steel				CTS	Axial at R = 0.25	0.01 to 1	3.5% NaCl	ΔK vs da/dN	Cathodic protection	125
ABS DH32 steel	Normalized	78 (538)	57 (391)	Center-notched, butt-welded plate	Axial at R = 0.1	0.5 to 10	Seawater at 39 and 68 F	ΔK vs da/dN	Cathodic protection	19
0.25C steel	Reinforcing bar	59 (410)			R = 0.07	10	3.5% NaCl	ΔK vs da/dN		48

(a) At 68 to 77 F unless noted.

Stress Intensity Factor Range (ΔK), ksi $\sqrt{\text{in.}}$

API X65 steel, Vosikovsky

St 42, Bristoll and Opdam

ASTM A537 steel, Socie and Antolovich

Carbon steel, Haagensen

Band of data for structural steels in air, Barsom

Crack Growth Rate, (da/dN), mm/cycle

Crack Growth Rate (da/dN), in./cycle

Saltwater, free corrosion (0.1 Hz)

Saltwater, cathodic potential (0.1 Hz)

Air

Synthetic seawater, free corrosion

Seawater at -1 C

Seawater at 24 C

Air (R > 0.8)

Air

Seawater, free corrosion (R > 0.8)

Stress Intensity Factor Range (ΔK), MN/m$^{3/2}$

FIGURE 50. Corrosion-Fatigue-Crack Growth Behavior of Low- and Medium-Strength Structural Steels in Seawater and Saltwater[23,28]
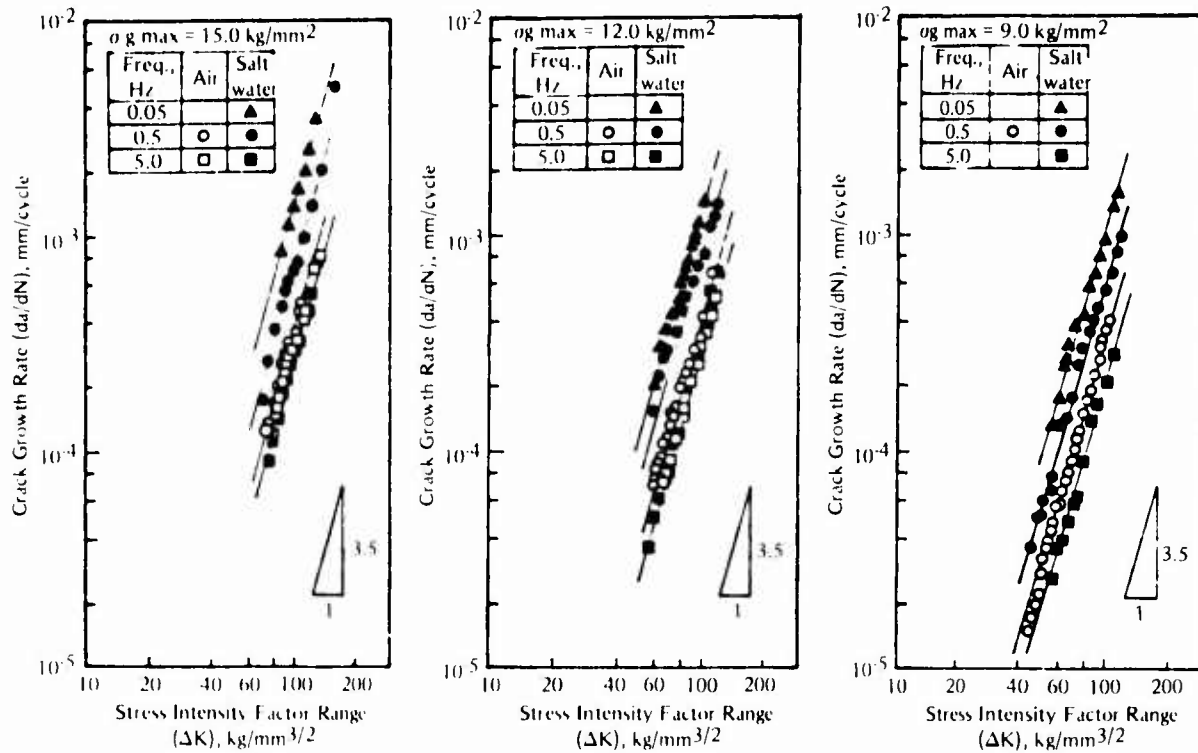
FIGURE 51. Corrosion-Fatigue-Crack Growth Rate for Mild Steel
in 3 Percent NaCl Solution[111]

a. Free Corrosion

b. Zn Potential, -1.03 V SCE
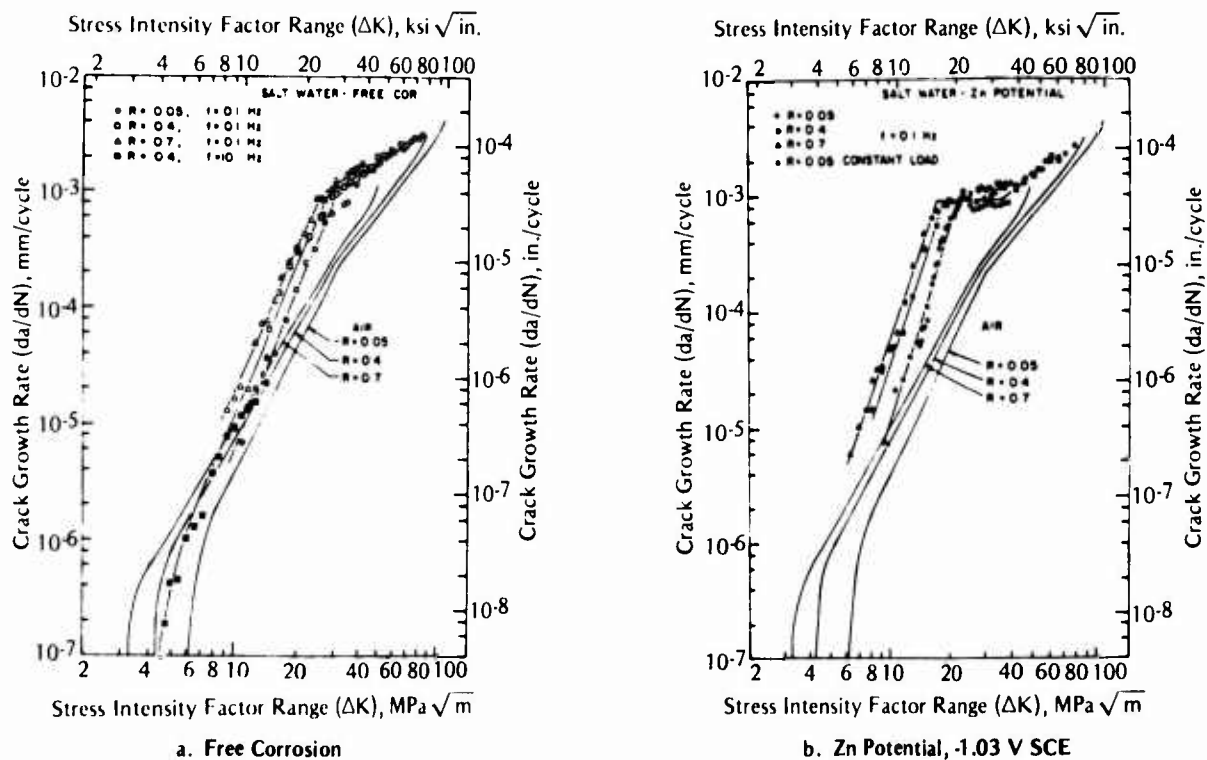
FIGURE 52. Corrosion-Fatigue-Crack Growth Rates for API X-70 Steel in 3.5 Percent NaCl Solution[39]
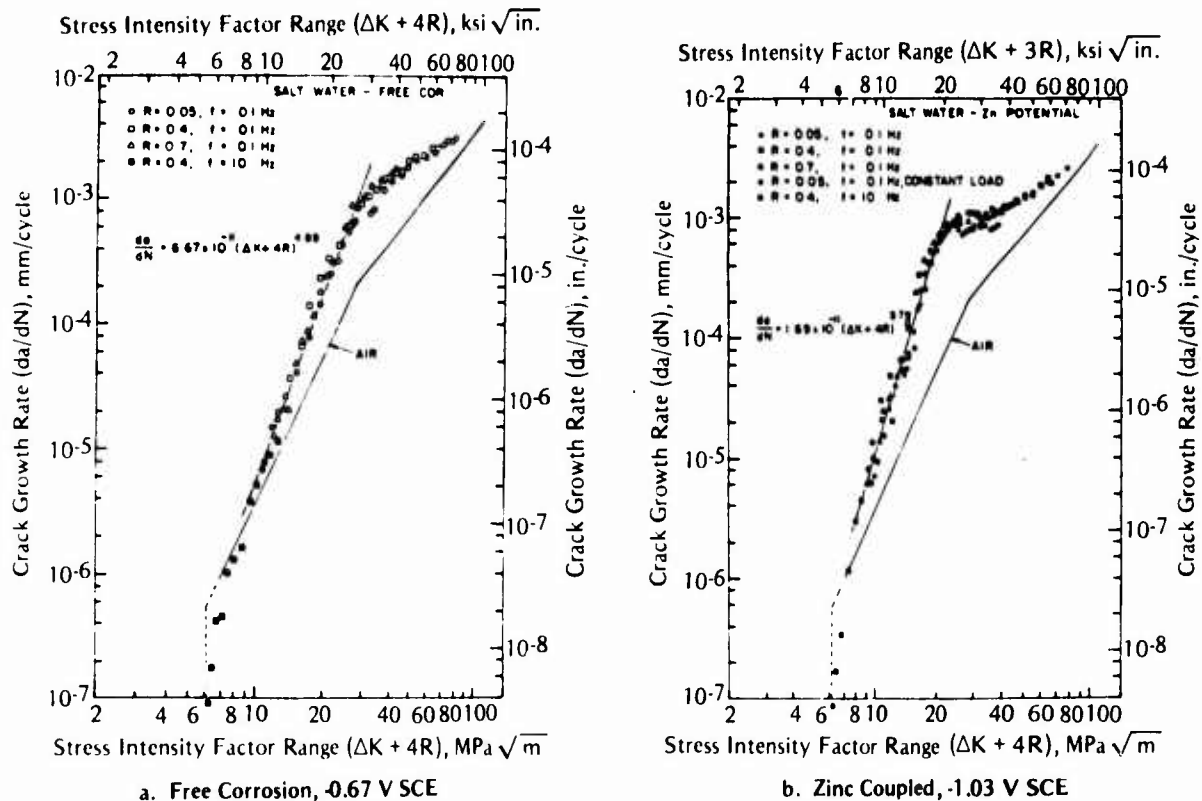
FIGURE 53. Normalized Corrosion-Fatigue-Crack Growth Rates for API X-70 Steel at Several Stress Ratios[39]

Scott and Silvester[38,122] conducted experiments in seawater at 5 to 10 C and at three potentials; their results are presented in Figures 54, 55, and 56. The crack growth rates were accelerated by the seawater environment and by increasing stress ratio. There is an upper bound curve for all of the data except intermediate ΔK levels with cathodic protection, where sharp bumps in the ΔK vs da/dN curves, similar to those reported by Vosikovsky, were found. At low ΔK levels some points are labelled as experimental artifacts because calcareous deposits formed in the crack tip and decreased the effective local stress intensity; hence the da/dN values decreased. When R ratio was increased on the same specimen, crack growth rates were initially higher, which is also indicated as an artifact in the figures. Thus, increasing R ratio increases crack growth rate in these steels, and the apparent threshold level at high R values (≥ 0.8) is lower in seawater than in NaCl solution.

Effect of Strength and Microstructure. Within this class of steels, there appear to be no significant effects of strength level or microstructure on crack growth behavior. In general, the corrosion behavior of these steels is similar, so no major differences would be anticipated in that respect. However, no systematic study of these factors has been undertaken, so the effects may simply be masked by scatter in the data or may not have been studied.

Welded Specimens. Welded specimens were used in two studies.[19,112] Socie and Antolovich[112] found that welded ASTM A537 steel gave the same corrosion-fatigue-crack-growth rates in both air and 3.5 percent NaCl at 75 F (24 C) and that these growth rates were similar to those for base metal. Their data were limited to intermediate ΔK levels and the cyclic
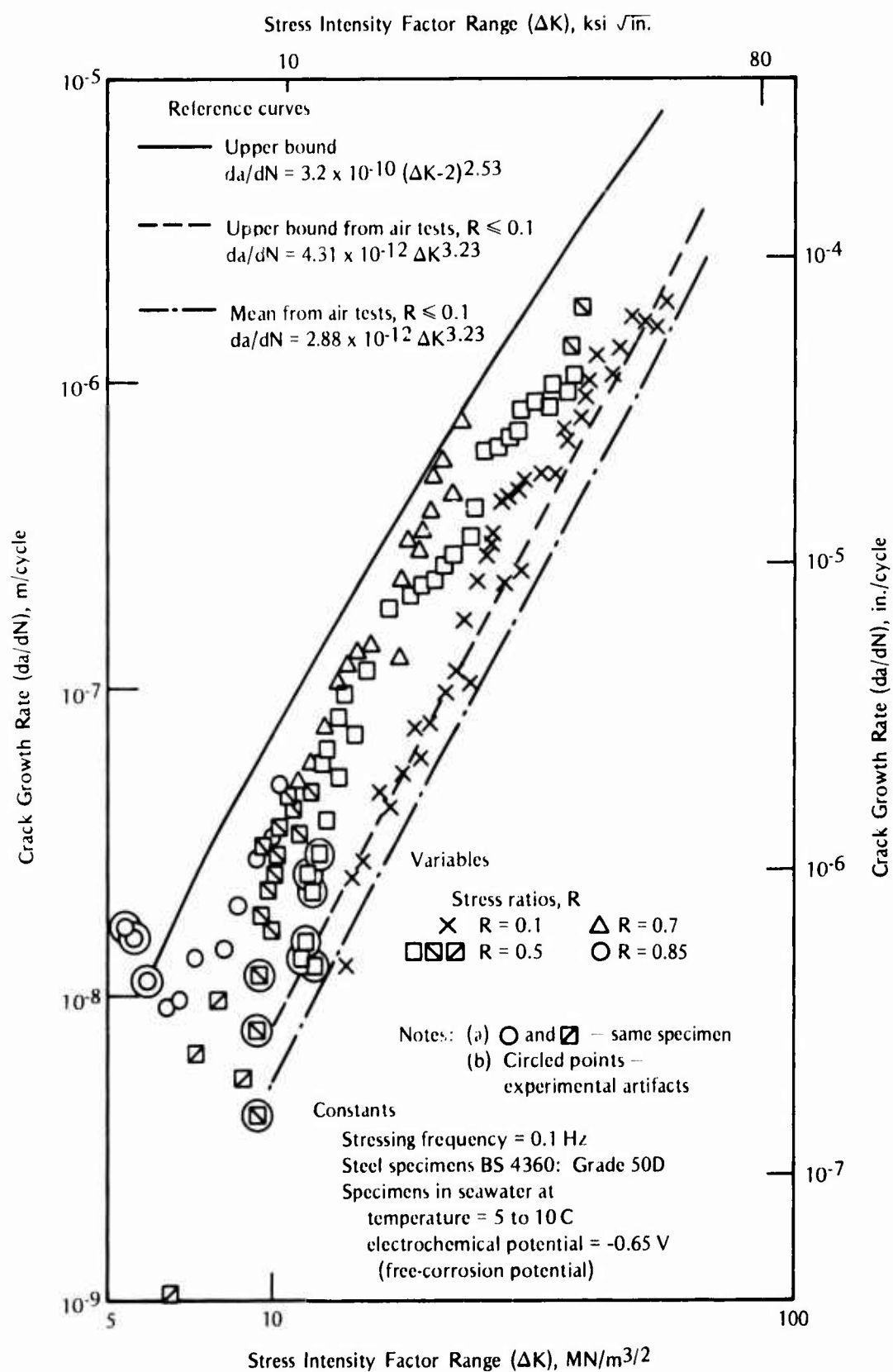
FIGURE 54. Crack-Growth Data for Specimens at an Electrochemical Potential of -0.65 V Ag/AgCl[38]
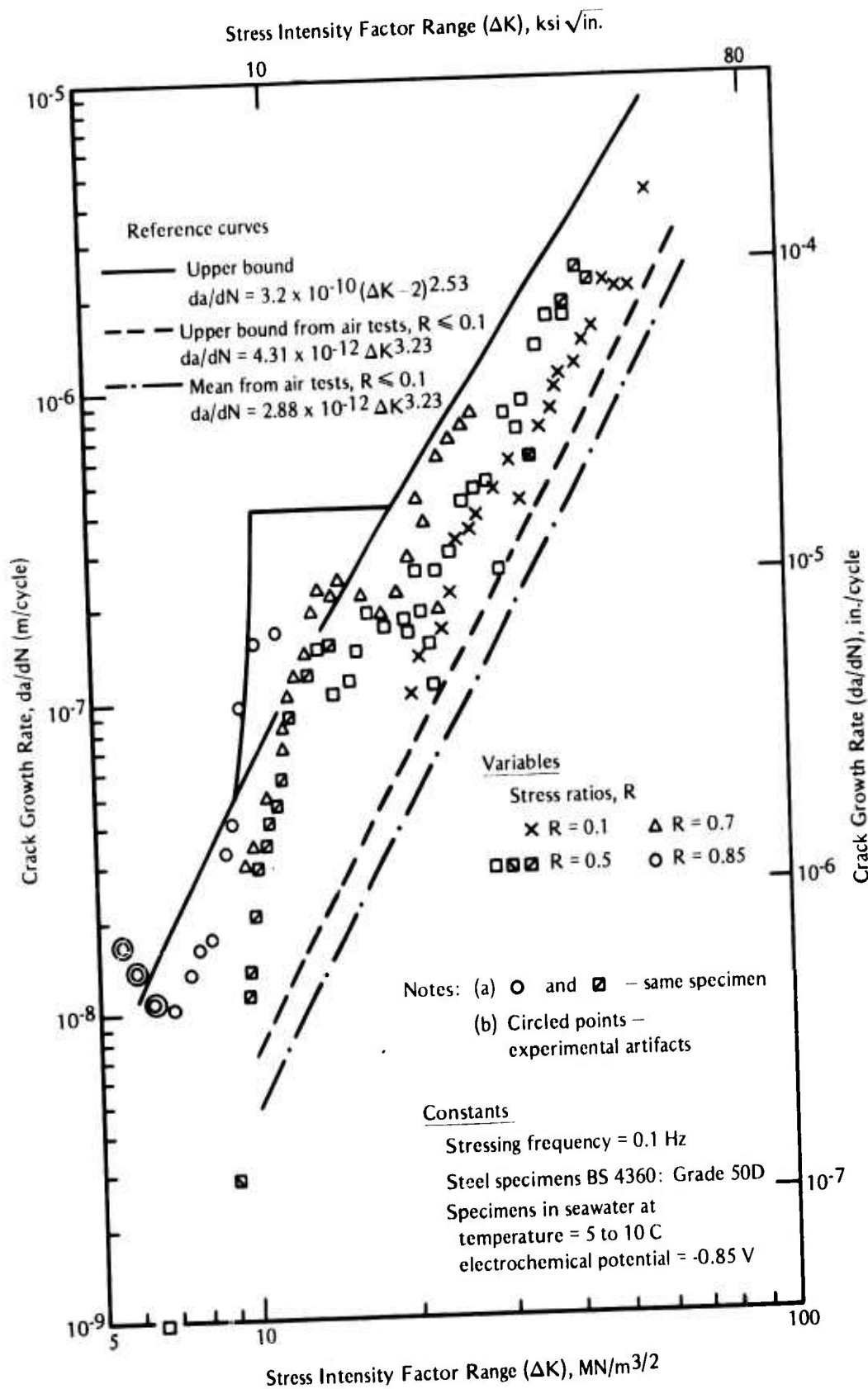
FIGURE 55. Crack-Growth Data for Specimens at an
Electrochemical Potential of -0.85 V Ag/AgCl38
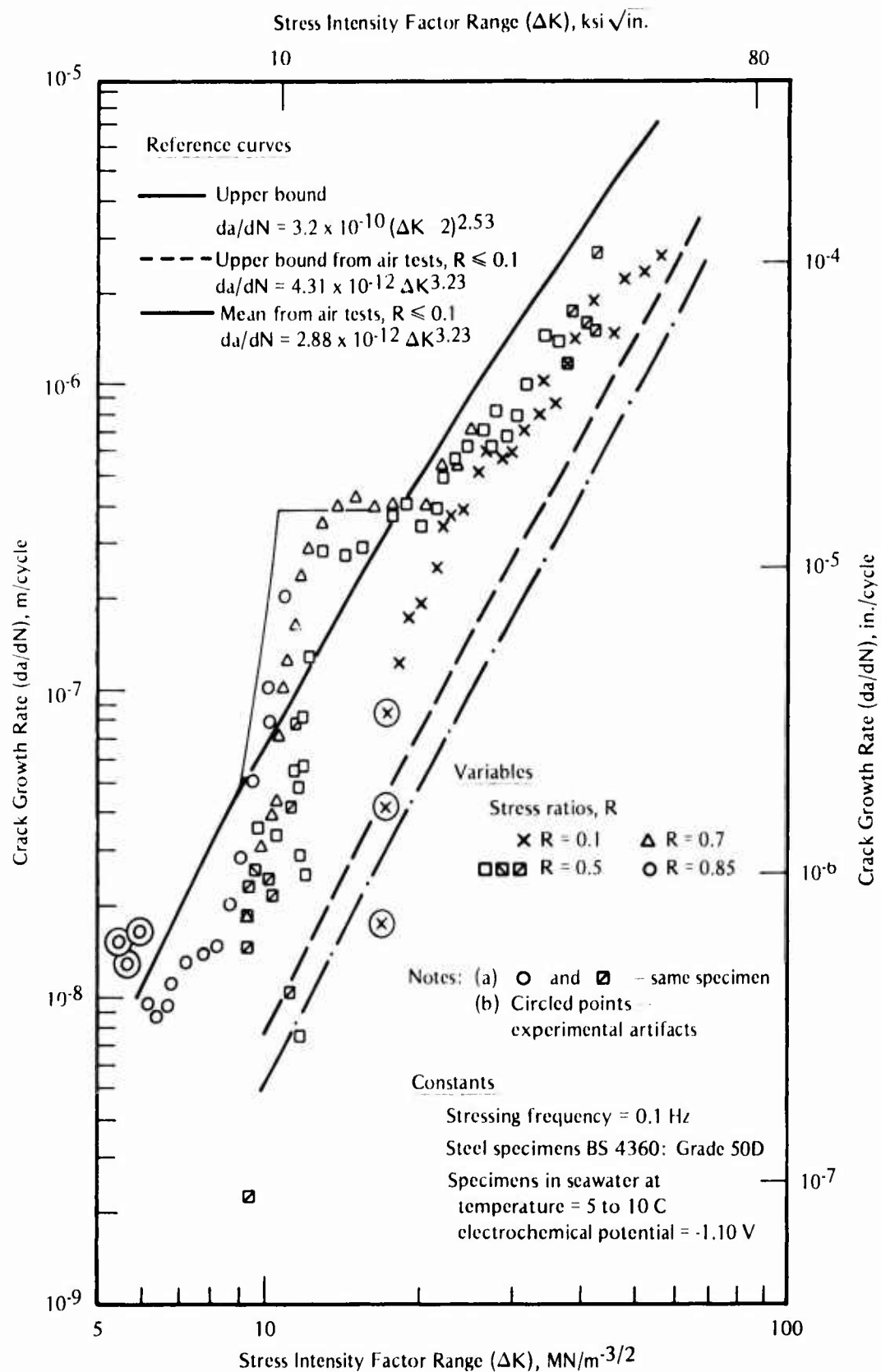
FIGURE 56. Corrosion-Fatigue-Crack Growth Rate for Specimens at an
Electrochemical Potential of -1.10 V Ag/AgCl[38]

frequency was not reported. The frequency was probably above 1 Hz where little environmental effect would be expected based on tests of base metal. Jaske et al[19] conducted no tests on base metal but grew cracks at the toe of the weld near the heat-affected zone in welded specimens. At R = 0.1, with a frequency of 10 Hz, and in seawater at 68 F (20 C), their results were similar to those typically measured in air, except that a definite kink (similar to those in Figure 57) in the ΔK vs da/dN curve was found in the region of ΔK = 12.74 to 16.38 ksi $\sqrt{\text{in.}}$ (14 to 18 MPa/m$^{3\,2}$. In seawater at 39 F (4 C), they found about a factor of 4 increase in da/dN [near $\Delta K \simeq 9.5$ ksi $\sqrt{\text{in.}}$ (10 MPa/m$^{3\,2}$)] only when the frequency was reduced to 0.5 Hz and cathodic overprotection (-1.0 V Cu/CuSO$_4$) was applied. At higher values of cathodic potential (i.e., less negative) and/or a lower frequency of 0.5 Hz, there was no significant increase in da/dN. These results for welds show trends similar to those observed for base metal, but they are limited to a narrow range of variables.
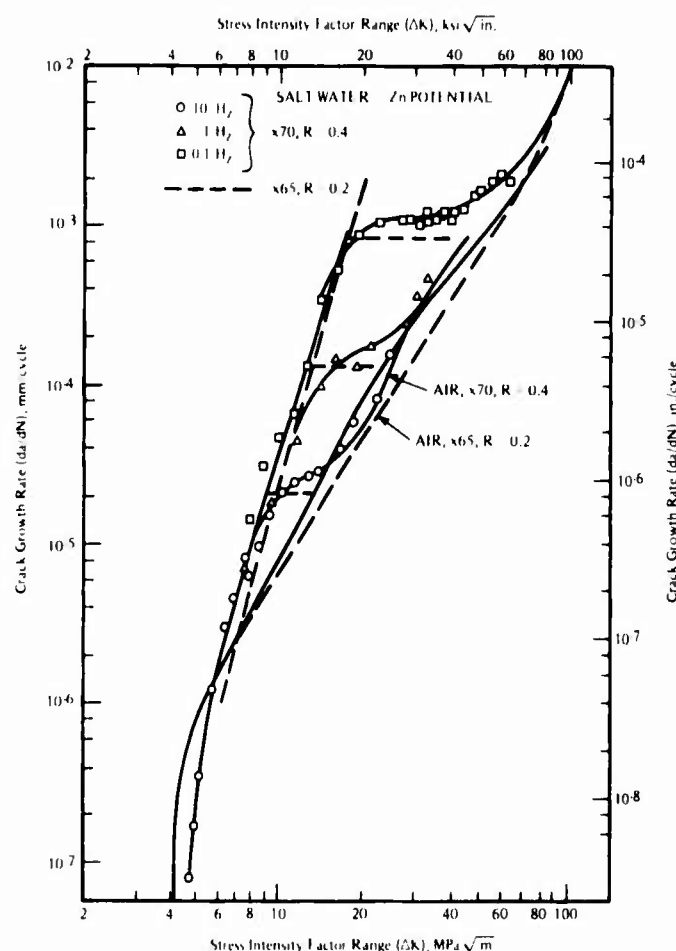
FIGURE 57. Corrosion-Fatigue-Crack Growth Rates in
3.5 Percent NaCl Solution at Zinc Potential, R = 0.4,
and Three Frequencies[39, 113]

Effect of Cyclic Frequency. Effects of cyclic frequency changes from 0.002 to 30 Hz have been investigated as indicated in Table 3. It is generally observed that lower frequencies cause increased da/dN values at intermediate ΔK levels (see Figures 20, 51, and 57). Vosikovsky[39,113] found very similar frequency effects for both API X-65 and X-70 steels tested in 3.5 percent NaCl solution (Figure 57). At reduced frequencies, the kink in the curves for overprotection conditions (Zn potential, -1.03 V SCE) is shifted to higher da/dN values and ΔK levels. Scott and

Silvester[123] found that decreasing the frequency from 10 to 1 Hz had little effect on crack growth rate but that decreasing it to 0.1 and 0.05 Hz resulted in crack growth rates about four to five times those in air, when ΔK was about 18.20 ksi $\sqrt{in.}$ (20 MPa/m$^{3/2}$) at R = 0.1, and in seawater at 68 F (20 C). Below this ΔK level, there was no significant frequency effect. Detailed discussions of frequency effects on crack growth of these steels are included in References 23 and 28.

Load-History Effects. Even under constant-amplitude cycling the shape of the loading wave form has a significant influence on corrosion-fatigue-crack-growth behavior of high-strength steels[128-130], which are discussed later. However, no such data were found for low-strength steels. Endo and Komai[63,64] found that small secondary stress fluctuations had no significant influence on crack growth but that larger secondary fluctuations accelerated crack growth. In one study[119,121], crack growth under narrow-band random loading of specimens immersed in seawater was investigated. The center frequency was 6.5 Hz and the da/dN data were correlated using ΔK_{rms}, as shown in Figure 58. Contrary to other studies the crack growth rate was accelerated in the seawater compared with that in air, even at the fairly high frequency of 6.5 Hz. The random-loading data give a shallower slope than the constant-amplitude-loading data. At $\Delta K \geq 4.5$ ksi$\sqrt{in.}$ (5 MPa/m$^{3\,2}$), the constant-amplitude data give a conservative upper bound on da/dN values for random loading in seawater, but such may not be the case for ΔK values below 4.5 ksi $\sqrt{in.}$ (5 MPa/m$^{3/2}$), where no data are available. More experimental data on variable-amplitude cycling corrosion-fatigue-crack growth are needed.

Effect of Environmental Variables. Effects of variations in water temperature from 30 to 176 F (-1 to 80 C) were evaluated in a combination of four investigations.[19,110,112, 123] Crack-growth rates increased about a factor of two as temperature increased from 30 to 39 F (-1 to 4 C) up to 68 to 75 F (20 to 24 C) in the intermediate ΔK regime. For example, see the curves for data of Socie and Antolovich[112] in Figure 50. At low ΔK levels, the results of Scott and Silvester[123] showed that increasing temperature from 41 to 68 F (5 to 20 C) had little effect. Temperatures in the range 39 to 68 F (4 to 20 C) were also found to have little effect at low ΔK levels in the work of Jaske et al.[19]

Oxygen levels of 1 mg/l and 7 to 8 mg/l (air saturation) were investigated by Silvester.[123] The reduction in oxygen level significantly decreased crack growth rates under free-corrosion conditions, but had no significant influence under cathodic protection at -0.8 V Ag/AgCl and -1.0 V Ag/AgCl.

Changing the pH from 5.3 to 11.2 had no significant effect on the rate of crack growth in 0.5N NaCl solution at 77 F (25 C).[116]

Cathodic Protection. Once a dominant crack exists and is propagating by corrosion fatigue, surface coatings and paints provide little effective protection. Thus, a large number of the studies listed in Table 3 examined cathodic protection as a possible means of offsetting the detrimental influence of saline environments on crack growth. Most of the results show that cathodic protection does not reduce the crack growth rates significantly. Furthermore, overprotection to potentials less than -0.78 V SCE can be detrimental and can increase growth rates to levels above those observed under free-corrosion conditions at intermediate levels of ΔK, especially at frequencies below 1 Hz. In a few cases, however, it was found that moderate protection ($\gtrsim$-0.78 V SCE) can be beneficial compared with free-corrosion conditions when cracks are shallow and the environment is not stagnant.
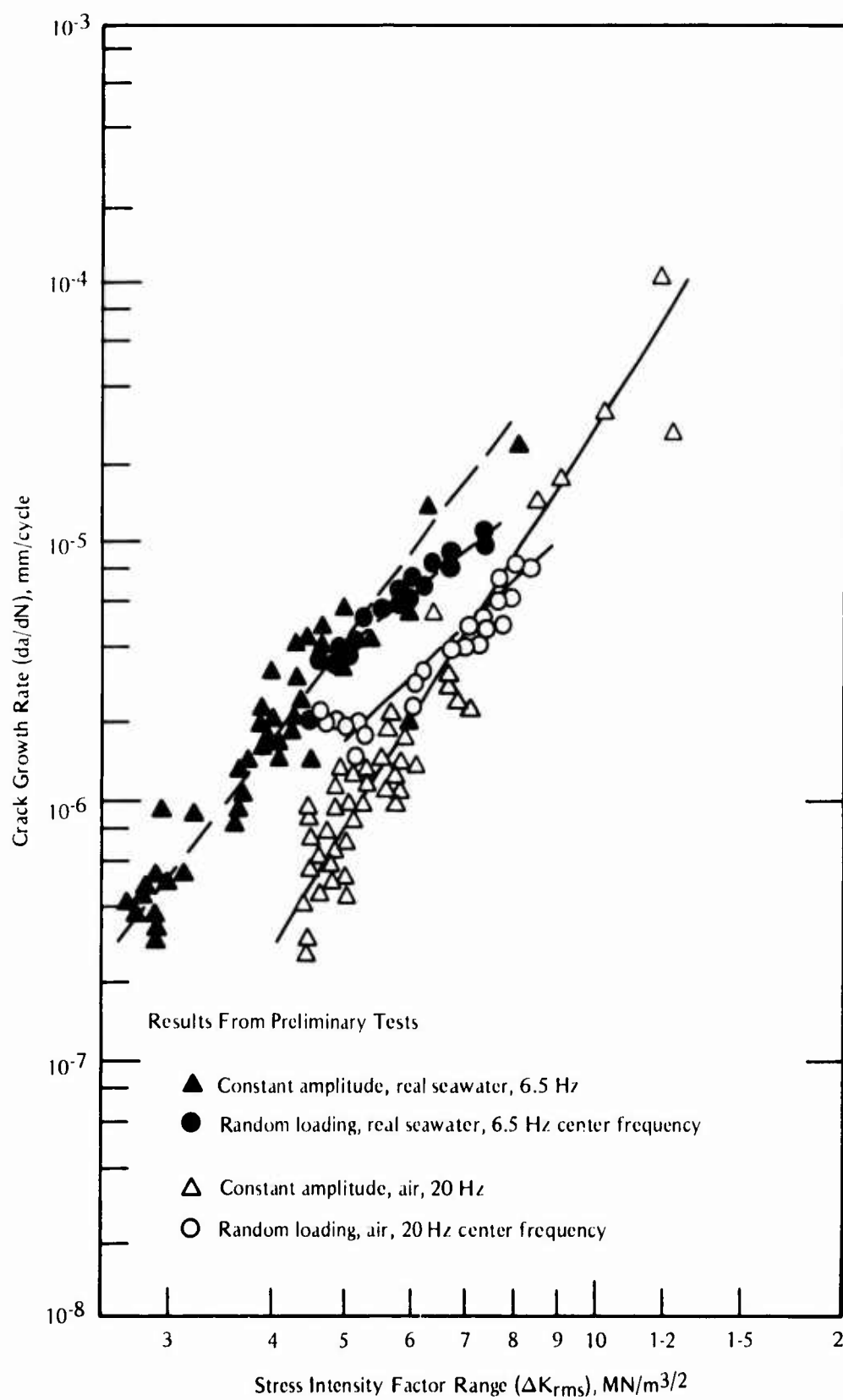
FIGURE 58. Corrosion-Fatigue-Crack Growth Rate for a Normalized 0.17C Steel Under Narrow-Band Random Loading[119]

Endo et al[115] found that in 1 percent NaCl solution, protection to -0.8 V SCE was beneficial at frequencies below 1.67 Hz and above 0.008 Hz, but detrimental at a frequency of 30 Hz. They also found that more negative potentials (<-0.8 V SCE) were generally detrimental at all frequencies because of localized hydrogen embrittlement. Their specimens had relatively shallow [0.039 to 0.118 in. (1 to 3 mm)] surface cracks. Scott and Silvester[123] showed that a moderate potential of -0.7 V Ag/AgCl was somewhat beneficial, but that more commonly used potentials in the range -0.8 to -1.0 V Ag/AgCl were of no benefit in decelerating corrosion-fatigue-crack-growth rates. Bardal et al[124] found cathodic potentials of -0.8 and -1.1 V SCE to be beneficial for shallow [0.039 to 0.118 in. (1 to 3 mm deep)] surface cracks but of no benefit for deeper 0.118 to 275 in. (3 to 7 mm) surface cracks for ΔK levels near 9.10 ksi $\sqrt{}$ in. (10 MPa/m$^{3\,2}$). They used synthetic seawater at 54 F (12 C) and slow cyclic frequencies (0.17 to 1 Hz). Kochera et al[91] found cathodic protection to be beneficial at -0.8 V Ag/AgCl for a long, shallow crack in flowing seawater. At -1.2 V Ag/AgCl in stagnant seawater, they found cathodic protection to be of no benefit. A similar influence of water-flow conditions was observed by Sullivan and Crooker[109], as shown in Figure 59, for A516-60 steel coupled to zinc (-1.1 V Ag/AgCl) in 3.5 percent NaCl solution. Under flowing conditions, the cathodic protection was of no benefit, nor was it detrimental; in a still solution, however, a detrimental effect was seen. Thus, moderate cathodic protection of these steels is effective only when fresh solution can be supplied to the crack-tip region continually, the cracks are relatively shallow surface cracks, and the stress ratio is ≤0.1.
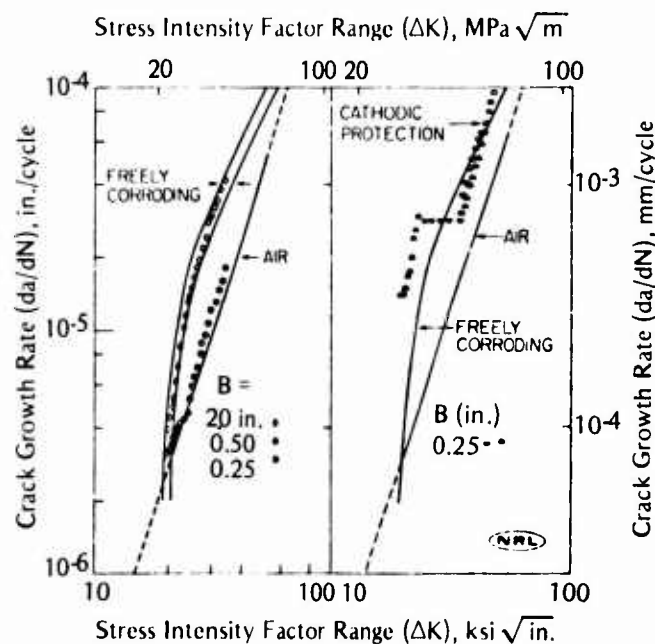
FIGURE 59. Corrosion-Fatigue-Crack Growth Rate for A516-60 Steel Coupled to Zinc and in a 3.5 Percent NaCl Solution[109]

Left: Flowing solution (0.5-inch specimen at 1 Hz)
Right: Still solution.

As shown in Figures 52 and 53, overprotection can accelerate fatigue-crack-growth rates, and decreasing the frequency increases this detrimental effect, as shown in Figure 57[39]. The results of Scott and Silvester[38] (see Figures 54, 55, and 56) show similar detrimental effects of cathodic protection. The effect is slight at -0.85 V Ag/AgCl but somewhat more prominent at -1.00 V Ag/AgCl. These kinks in the ΔK vs da/dN curve are evident only for R ≥ 0.5 and not for

R = 0.1. So, in more general situations where residual stress may be present (increasing R) and cracks may not be shallow, cathodic protection provides no reduction in crack growth rate over that under free-corrosion conditions. In addition, care should be taken to avoid overprotection in critical regions where fatigue cracks may grow, because this can significantly accelerate crack growth rates at intermediate ΔK levels.

Ship Structural Steels

Corrosion-fatigue data for ship structural steels are summarized in Table 5. These are mainly for the HY-series of 3 to 5 Ni-Cr-Mo-V steels. Other steels that may be used in ships as well as in other marine structures are covered in the preceding and subsequent sections of this Chapter. Many of the general trends in behavior and effects of mechanical and environmental variables are similar to those for the low- and medium-strength steels discussed previously. Thus, earlier detailed discussions are not repeated here. Instead, features and information peculiar to these steels are emphasized. Both fatigue-life data and crack growth data are included in Table 5, but data of each type are covered separately in the discussion that follows.

Fatigue-Life Data

Most of the fatigue-life data are for rotating bending, high-cycle fatigue tests or reversed bending, low-cycle fatigue tests. In two studies[131,132], plane bending fatigue tests were conducted in the high-cycle fatigue-life regime. Major factors influencing the fatigue-life behavior are discussed below.

Effect of Stress Amplitude (Smooth Specimens). Gross and Czyryca[133] conducted an extensive fatigue study of the HY-series steels in Severn River water. Their low-cycle fatigue tests ($\leq 10^4$ cycles) were conducted at 0.017 Hz and their high cycle tests ($>10^4$ cycles) at 24.2 Hz. The stress versus fatigue life curves from this study are summarized in Figure 60. The ordinate is pseudo stress amplitude, S_{PE}, and

$$S_{PE} = E\Delta\epsilon/2 \quad ,$$

where E is elastic modulus and $\Delta\epsilon$ is total strain range. For nominally elastic cycling at long lives, S_{PE} is the actual stress amplitude. However, at short lives where cyclic plasticity is present, S_{PE} is greater than the actual stress amplitude. Near 10^3 cycles to failure, the environmental effect is small, but at longer lives the environmental degradation of fatigue strength in Severn River water (compared with that in air) is clearly evident. At 10^8 cycles to failure, the fatigue strength of HY-100 is slightly better than that of HY-80 or HY-130/150, and the fatigue strength of all three steels is superior to that of HT structural steel. As with the low-and medium-strength steels, no fatigue limit is apparent in saltwater, and the fatigue strengths of 9 to 12 ksi (62 to 83 MPa) are within the range cited earlier for these other steels but are somewhat above the typical values for plain carbon steels.

Effect of Stress Ratio. Only Macco's[132] study of welded HY-130 steel examined stress-ratio effects. His results are shown in Figure 61. Butt-weld plates, plates with tee welds, and base metal were evaluated in seawater at R = -1, but only tee welds were tested at R = 0 and +1/3. The ordinate in Figure 61 is maximum stress, so the stress amplitude associated with a certain cyclic life decreased as R increased. This is the normally expected effect of stress ratio.

TABLE 5. Corrosion-Fatigue Data for Ship Steels

Alloy	Condition or Treatment	Tensile Strength, ksi (MPa) Ultimate	Yield	Type of Specimen	Type of Loading	Cyclic Frequency, Hz	Environment(a)	Type of Data	Notes	References
HY-80 steel		>80 (>552)	>80 (>552)	Smooth plate	Reversed bending	0.17	3.5% NaCl	N-potential	Cathodic protection	134, 135
3.25-Ni steel		>55 (>379)	>55 (>379)	Smooth bar base metal and IN-625 weldment	Rotating bending	23.3	Seawater	S-N curves 10⁵-10⁸		131
Clad 3.25-Ni steel		>80 (>552)	>55 (>379)	Smooth plate	Reversed bending	23.3	Seawater	S-N curves 10⁷-10⁸	IN-625 cladding	131
HY-130 steel				Smooth plate	Reversed bending	0.017	Saltwater(b)	Strain-N curves 10²-10⁵	Cathodic protection	136
HT steel		67 (464)	41 (284)			0.017 and 24.2	Saltwater(b)	S-N curves 10²-10⁸		133
HY-80 steel		104 (715)	88 (609)	Smooth and notched beams	Rotating bending and reversed bending	0.017 and 24.2	Saltwater(b)	S-N curves 10²-10⁸	Notch effects	133
HY-100 steel		120 (825)	105 (726)			0.017 and 24.2	Saltwater(b)	S-N curves 10²-10⁸		133
HY-130/150 steel		155 (1070)	147 (1010)			0.017 and 24.2	Saltwater(b)	S-N curves 10²-10⁸		136
HY-80 steel		105 (726)	87 (602)	Smooth and notched beams- base and weld metal	Reversed bending	0.0003 to 3.33	Saltwater(b), seawater,	Strain-N curves 10²-10⁵	Cathodic protection,	137
HY-130 steel		150 (1030)	141 (970)			0.0003 to 3.33	synthetic seawater	Strain-N curves 10²-10⁵	frequency, notches	137
HY-100 steel		121 (834)	107 (738)	Smooth bar	Rotating bending	1.25 to 24.2	Saltwater(b)			136
HY-130 steel		153 (1054)	147 (1015)	SEN	Bending at R = 0	0.0167 and 0.167	Seawater	ΔK vs da/dN	Cathodic protection	17
HY-80 steel		>80 (>552)	>80 (>552)	SEN	Axial at R = 0	0.001 to 10	3.5% NaCl	ΔK vs da/dN	Cathodic protection	139
.25-Ni steel		>80 (>552)	>55 (>379)	SEN	Axial	10	3.5% NaCl	ΔK vs da/dN		131
Clad 3.25-Ni steel		>80	>55 (>379)	SEN	Axial	10	3.5% NaCl	ΔK vs da/dN	IN-625 cladding	131
HY-80 steel		99 (680)	81 (556)	CTS	Axial at R = 0.1 and 0.8	10 and 60	Seawater	ΔK vs da/dN	Cathodic protection	140
Q1(N) steel		106 (730)	90 (619)	CTS-base plate and weld metal	Axial at R = 0	0.0014	2.6% NaCl	ΔK vs da/dN		141
HY-100 steel		128 (883)	112 (769)		Axial at R = 0	0.0014	2.6% NaCl	ΔK vs da/dN		141
HY-140 steel	Q and T	153 (1055)	140 (965)	CTS-base and weld metal	Axial at R = 0	10	Synthetic seawater	ΔK vs da/dN	HAZ cracks	142
HY-130 steel	Q and T	150 (1034)	144 (993)	SEN	Axial at R = 0.05 to 0.9	0.01 to 10	3.5% NaCl	ΔK vs da/dN	Cathodic protection	143
HY-80 steel				Deep-side-grooved	Axial at R = 0.15	0.008	Seawater	ΔK vs da/dN	Cathodic protection.	144
HY-130 steel				Deep-side-grooved	Axial at R = 0.30	0.008	Seawater	ΔK vs da/dN	wave form effects	144
HY-130 steel			147 (1015)	SEN	Bending at R = 0	0.167	Seawater, synthetic seawater, 3.5% NaCl	ΔK vs da/dN	Effect of solution chemistry	126, 127
HY-130 steel		140 (969)	132 (913)	CTS	Axial	0.005 to 2.5 Hz	3.5% NaCl at 41 to 185 F	ΔK vs da/dN	Frequency, temperature	145
HY-130 steel				CTS-base and weld metal	Axial at R = 0.05	0.0017 and 0.17	Seawater	ΔK vs da/dN	Cathodic protection	146
HY-130 steel		150 (1034)	143 (986)	CTS	Axial	0.05 to 2.5	3.5% NaCl at 77 to 185 F	ΔK vs da/dN	Frequency, temperature	147
HY-80 steel		103 (710)		Smooth bar	Reversed axial	20,000	3% NaCl at 50 F	S-N curves 10⁷-10⁹	2000 psig pressure	73
HY-130 steel		160 (1130)		Smooth bar	Reversed axial	20,000	3% NaCl at 50 F	S-N curves 10⁷-10⁹	2000 psig pressure	73
HY-80 steel				Tapered box beam, welded construction	Bending under spectrum Loading		Synthetic seawater	Life and crack growth data	Cumulative damage assessment	148
HY-130 steel		151 (1040)	145 (996)	Smooth-base metal, T-welds and butt welds	Bending at R = -1, 0, and +1/3	1 to 33.3	Seawater	S-N curves 10⁵-10⁸	Goodman diagrams	132

(a) Water temperature is 68 to 77 F unless otherwise noted.
(b) Severn River water with salt content one-third to one-sixth that of seawater.
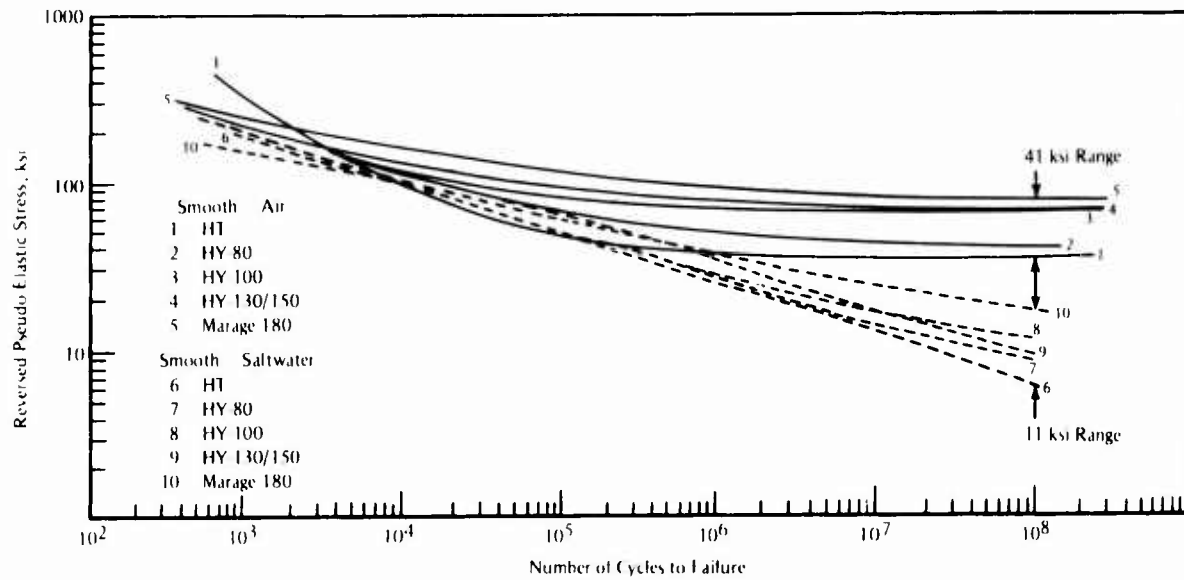
FIGURE 60. Effect of Stress on Fatigue Life for Smooth Specimens of HY-Series Steels in Severn River Water[133]
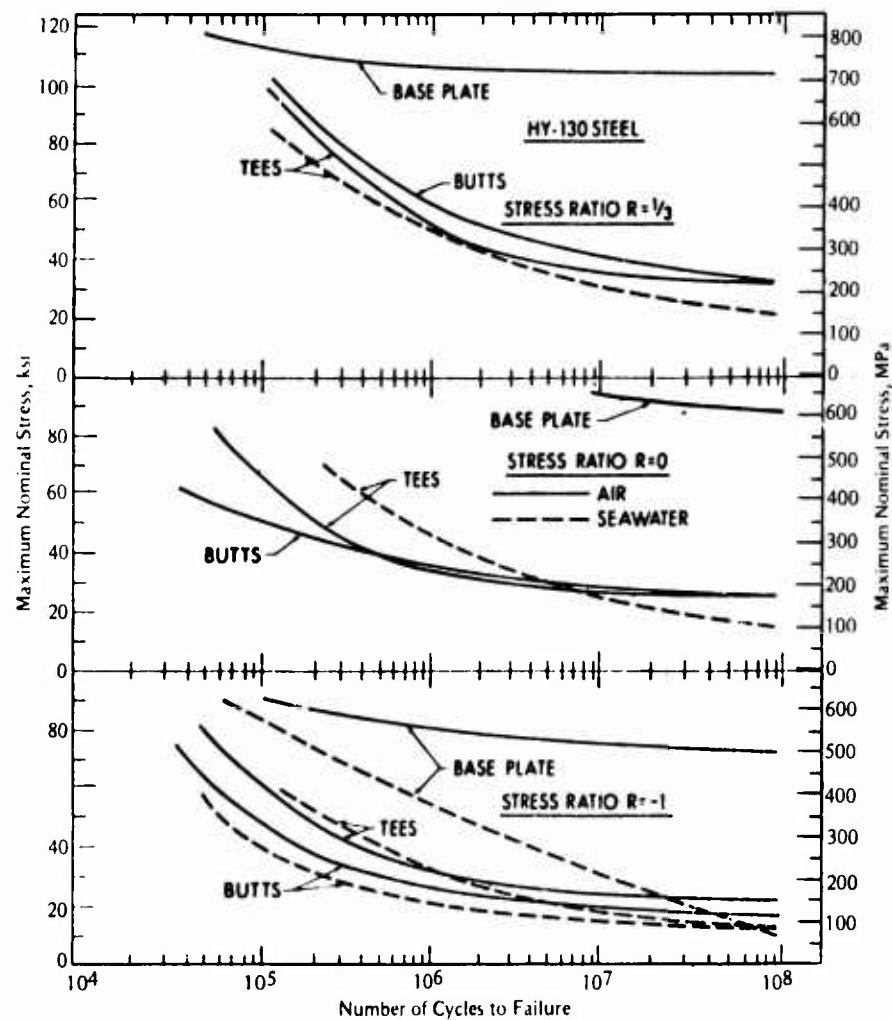
FIGURE 61. Effect of Stress Ratio on Corrosion-Fatigue Behavior of HY-130 Steel Welds[132]

Effect of Strength. As noted above, the strength variations from 80 to 130 ksi (544 to 884 MPa) minimum yield had little influence on low-cycle corrosion-fatigue resistance and only a small influence on the high-cycle (10^8) fatigue strength. Actually the HY-100 steel was slightly superior to the HY-80 and HY-130 steels at 10^8 cycles (see Figure 60). Overall, tensile-strength level has little effect on the corrosion-fatigue strength of these steels under free-corrosion conditions.

Notch Effects. For notched specimens in saltwater, the low-cycle corrosion-fatigue resistance is improved with increasing tensile-strength level from that of HY-80 to that of HY-130 steel[133,137], as shown in Figure 62. At 10^8 cycles to failure, the HY-100 steel is slightly superior to the HY-80 and HY-130 steels, which have about the same corrosion-fatigue strength. This is the same type of comparative behavior among these three steels as that for smooth specimens compared at 10^8 cycles to failure.
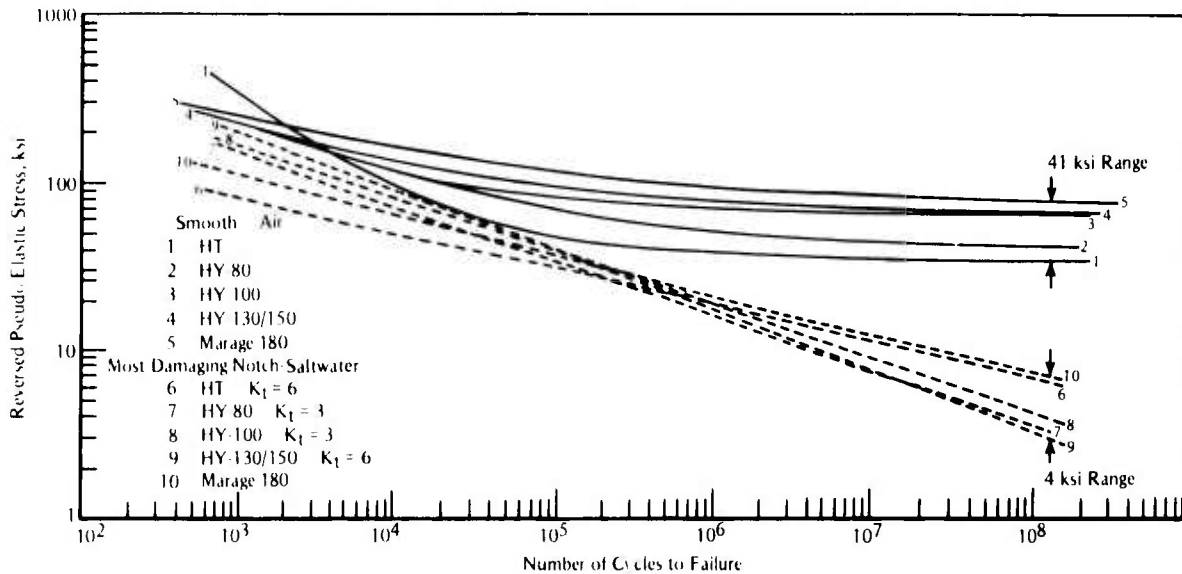
FIGURE 62. Effect of Stress on Fatigue Life for Notched Specimens of
HY-Series Steels in Severn River Water[133]

Welded Joints. For low-cycle fatigue, weldments of HY-130 steel were superior to those of HY-80 steel.[137] At shorter lives, weldments of HY-130 steel were inferior to base metal in CFS but little difference between them was observed at 10^8 cycles to failure.[132] (See Figure 61.)

Beach et al[148] evaluated welded box beams of HY-80 and HY-130 steels in synthetic seawater. The tests were conducted using a variable-amplitude spectrum of load cycling. Cracking initiated in both slot welds and butt welds. When crack initiation occurred at butt welds, the cyclic lives were about one-half those when crack initiation occurred at slot welds. Fatigue lives in saltwater were similar to those in air for the weldments studied because the lives in air were much shorter than expected. Stress concentration factors for the as-welded condition were estimated to be about 3.0. To correlate analytical predictions with actual failures in saltwater environments, the authors found it was necessary to assume that either a stress concentration factor of 2.4 to 6.7 was present and/or that the local residual stress was from 0 to 20 ksi (0 to 140 MPa). Thus, the effect of welded construction on corrosion-fatigue life was somewhat worse than analytically predicted.

Effect of Cyclic Frequency. No data were found on effect of cyclic frequency on fatigue resistance of the HY-series steels. However, it is expected that the frequency effects should be similar to those discussed for low- and medium-strength steels earlier.

Loading-History Effects. In the study of Beach et al[148], tapered box beams of HY-80 and HY-130 steels were fatigue tested under a variable-amplitude loading history in a synthetic seawater environment. Predictions of cumulative damage were made by using Miner's rule based on nominal stress history and S-N curves for notched ($K_t \approx 3.0$) specimens. Mean stress was accounted for by using the Goodman relation. In saltwater, predicted lives were close to or within a factor of 2 of the actual ones. In air, predictions of cyclic life were nonconservative by a factor of about 30. This difference in predictions was primarily related to the beams having similar cyclic lives in both air and saltwater, whereas the predicted lives were much longer for tests in air than for those in saltwater.

Effect of Environmental Variables. Jolliff[73] found that the corrosion-fatigue strength (CFS) (high cycle at 20 kHz) of HY-80 was not affected by 2000-psi hydrostatic pressure in 3 percent NaCl solution. In contrast, the CFSs of HY-130, AISI 1020, and ASTM A537 A steels were all significantly reduced under the same pressure as compared with their CFSs under atmospheric pressure. No other data on environmental effects were found. It is expected that temperature, pH, and oxygen level will have effects similar to those explained previously for low- and medium-strength steels.

Protective Methods. Cladding 3.25-Ni steel with Inconel 625 was found to increase the CFS (at 10^8 cycles) from 7 ksi (50 MPa) to 15 ksi (100 MPa) over that of the unclad steel.[131] These tests were conducted in reversed bending at 23.3 Hz and in seawater.

Cathodic protection was evaluated in three investigations.[134,136,137] In low-cycle fatigue, where a major portion of specimen life consists of crack propagation, cathodic overprotection is detrimental to fatigue resistance of HY-130 steel[136,137,149]. Figure 63 from References 134 and 135 shows that optimum cathodic protection from low-cycle corrosion-fatigue damage of HY-130 steel was obtained at a potential of about -0.75 V Ag/AgCl. However, at potentials near -1.0 V Ag/AgCl or less, the cathodic protection reduces fatigue strength to below that under free-corrosion conditions. Vassilaros and Czycryca[137] reported that, for cathodic potentials of -1.05 and -1.40 V SCE, the high-cycle ($>10^4$ cycles to failure) fatigue strength of HY-130 steel base plates and weldments was increased up to values approaching the fatigue strengths determined in air. Thus, cathodic overprotection of HY-130 steel appears to be effective in improving this steel's corrosion-fatigue-crack-initiation resistance, but not in altering its crack-growth resistance.

Fatigue-Crack-Growth Data

Except for one study[148], where crack length versus number of blocks of cycling was reported, all crack growth data were reported as ΔK versus da/dN curves.

Effect of Stress-Intensity-Factor Range. The general influence of ΔK level on corrosion-fatigue-crack-growth behavior of these HY-series steels is basically the same as that described earlier for low- and medium-strength structural steels. For example, consider the data of
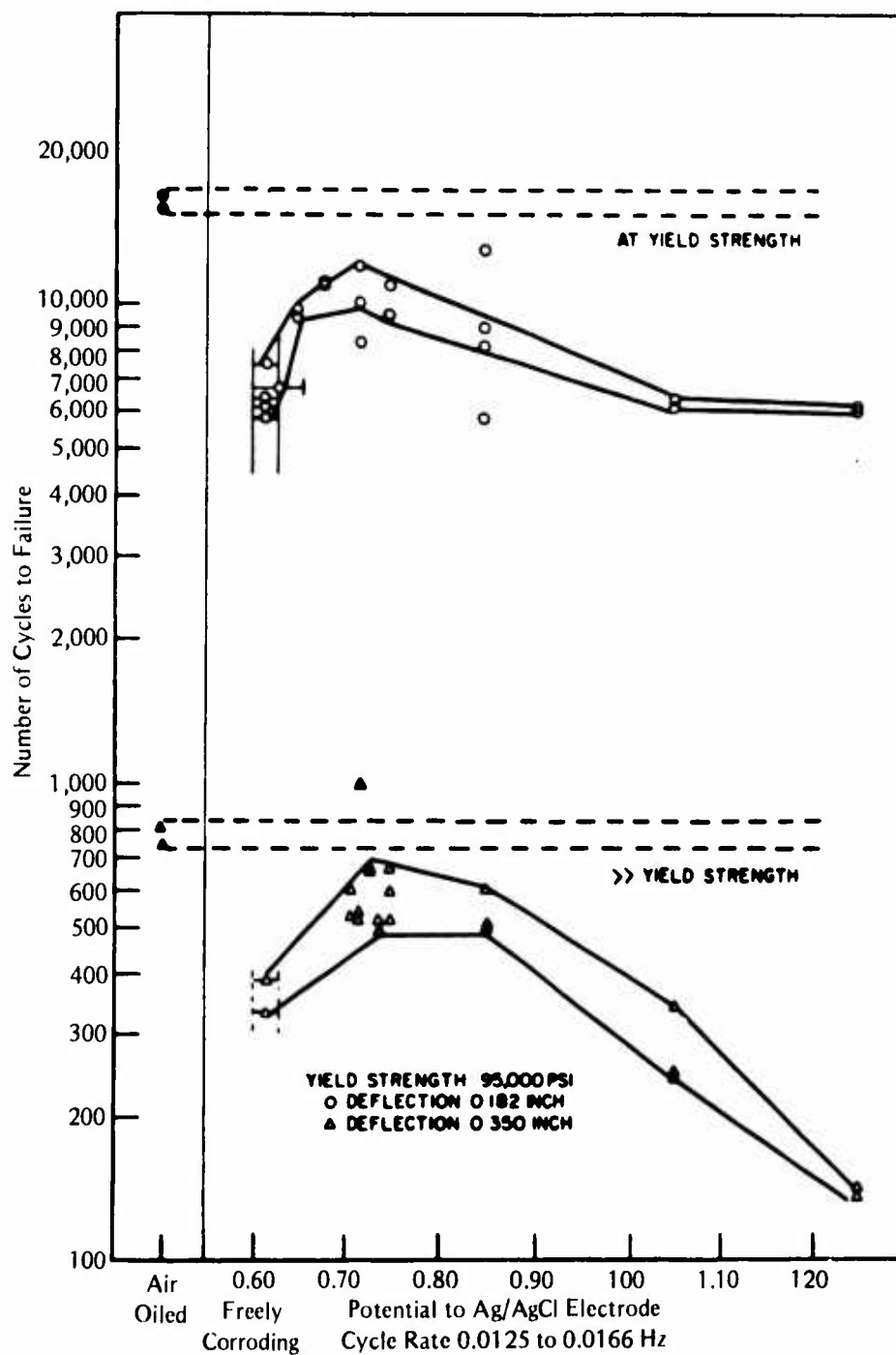
FIGURE 63. Effect of Potential on Low-Cycle Corrosion-Fatigue Life of HY-130 Steel in Solution[135]

Vosikovsky[143] for HY-130 steel in 3.5 percent NaCl solution shown in Figure 64. Detrimental effects of corrosion are typically more evident at intermediate levels of ΔK. Little environmental effect is observed at high and low ΔK values. Compared with similar data on low- and medium-strength steels (X65, X70, or A516-60), the HY-130 steel shows only about half as much acceleration in da/dN values due to environment.[143] The data of Congleton et al[144] also show a similar higher resistance to corrosion-fatigue-crack growth for HY-130 compared with that for

a. Free Corrosion, -0.67 V SCE

b. Zinc Coupled, -1.03 V SCE
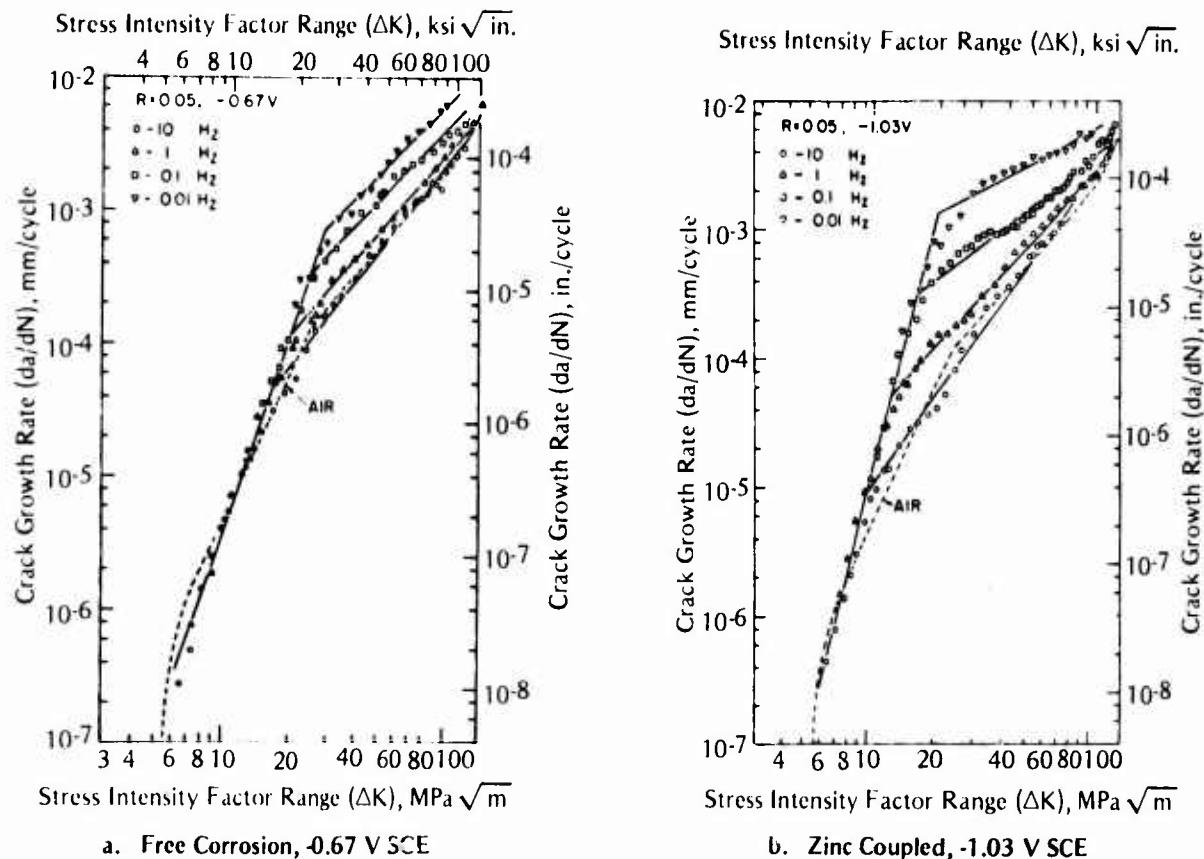
FIGURE 64. Corrosion-Fatigue-Crack Growth Behavior of HY-130 Steel in 3.5 Percent NaCl Solution[143]

the lower strength HY-80. Thus, improved resistance to corrosion-fatigue-crack growth is exhibited by the HY-130 steel, but not by the lower strength HY series steels.

Effect of Stress Ratio. Hartt and Adamson[140] found that increasing the stress ratio from 0.1 to 0.8 significantly shifted the ΔK vs da/dN curve to the left (faster growth rates), as shown in Figure 65. From comparisons with results for several other steels, they felt that HY-80 steel is superior for applications where ΔK is low and R is high. Vosikovsky[143] used R values of 0.05, 0.7, and 0.9 in his work on HY-130 steel. Similarly to the previously discussed results for API X-65 and X-70 steels, he found the simple parameter $\Delta K + 3R$ could correlate stress ratio effects. The correlation for HY-130 steel is shown in Figure 66.

Welded Joints. Welded specimens were used in four of the studies[141,142,146,148] listed in Table 5. At 10 Hz cyclic frequency, synthetic seawater environment had no effect on crack growth rates in weldments of HY-140 steel.[142] However, at a much lower frequency of 0.0014 Hz, Knight[141] found that crack growth rate was accelerated by factors up to 4.5 for both base metal and weldments of Q1(N) and HY-100 steel in a 2.6 percent NaCl solution. At 0.0017 and 0.17 Hz, Davis[146] observed accelerated crack growth rate in seawater (compared with that in air) at ΔK levels below about 63.70 ksi $\sqrt{\text{in.}}$ (10 MPa/m$^{3/2}$), but not at higher ΔK levels, for HY-130 steel. The weld-metal-crack-growth behavior was no worse than that of the base metal.
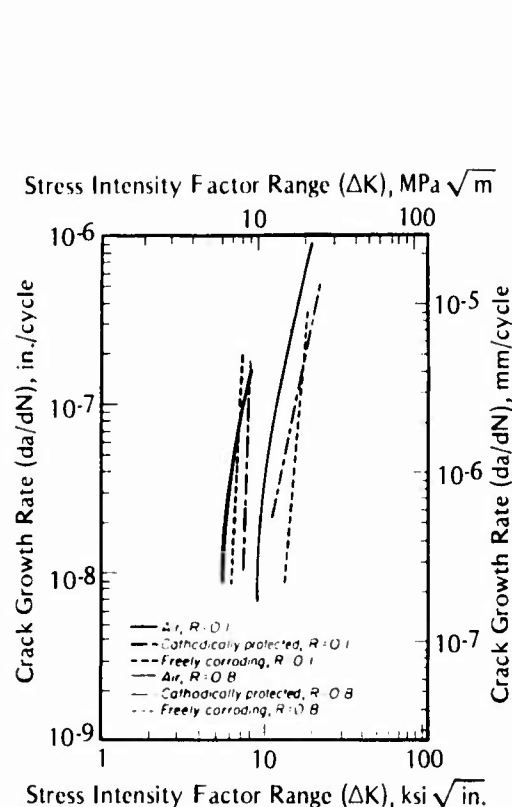
FIGURE 65. Effect of Stress Ratio on
Corrosion-Fatigue-Crack Growth Rate of HY-80
Steel in Seawater[140]
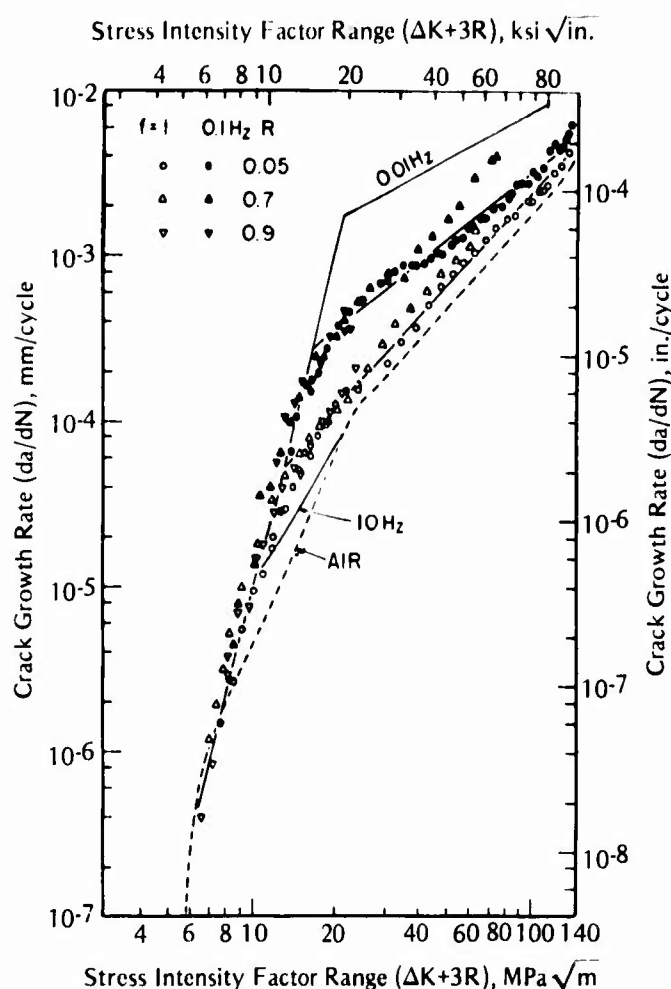
FIGURE 66. Corrosion-Fatigue-Crack Growth Rate of
HY-130 Steel at Three Stress Ratios[143]

Beach et al[149] found that corrosion-fatigue-crack-growth rates in welded box beams of HY-80 and HY-130 steel were conservatively predicted using crack-growth data for base metal in saltwater. Overall, the data indicate that corrosion-fatigue-crack-growth rates are no higher in weld metal than in base metal for these steels in marine environments.

Effect of Cyclic Frequency. Frequency effects were investigated in four studies.[139,143,145,147] Gallagher's results[139] for HY-80 steel, presented in Figure 67, showed that da/dN increased as frequency increased from 0.001 to 10 Hz. The crack growth rates at 10 Hz approached those for a vacuum environment for a high ΔK level (78 ksi $\sqrt{in}$.) but were significantly above them for an intermediate ΔK level (39 ksi $\sqrt{in}$.). Gallagher et al[147] found that, for K_{max} levels below K_{Iscc}, the corrosion-fatigue-crack-growth rates for HY-130 steel in 3.5 percent NaCl increased as frequency decreased at temperatures from 77 to 185 F (25 to 85 C), as shown in Figure 68. In an extension of this work on HY-130 steel, Ryder and Gallagher[145] found that there was still a frequency effect at 41 F (5 C). Vosikovsky's results[143] (see Figure 64) show no significant corrosion effect for cycling at 10 Hz, but at 1 Hz to 0.01 Hz, the da/dN values increased with decreased frequency at intermediate ΔK levels. Therefore, all these studies are in agreement in that they show a detrimental effect of decreased cyclic frequency below 10 Hz at intermediate ΔK values.
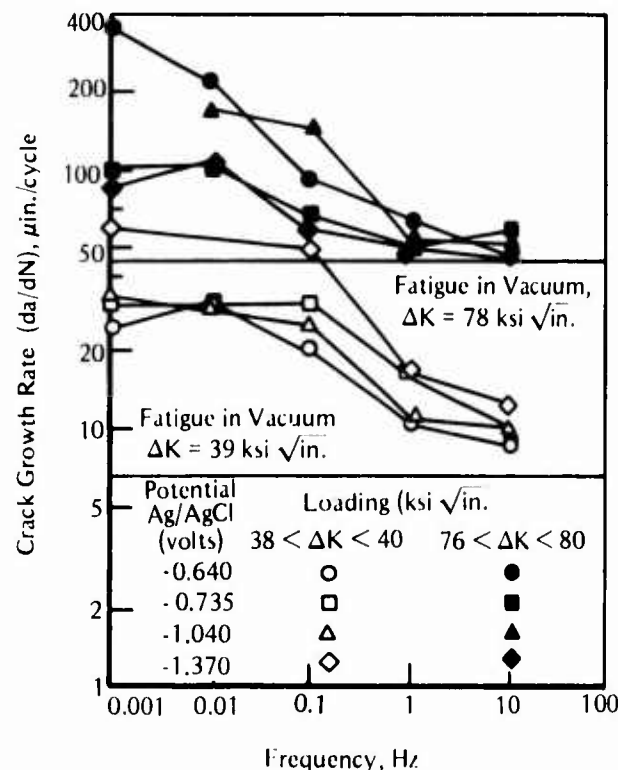
FIGURE 67. Effect of Frequency on Corrosion-
Fatigue-Crack-Growth Rate for HY-80 Steel
in 3.5 Percent NaCl Solution[139]
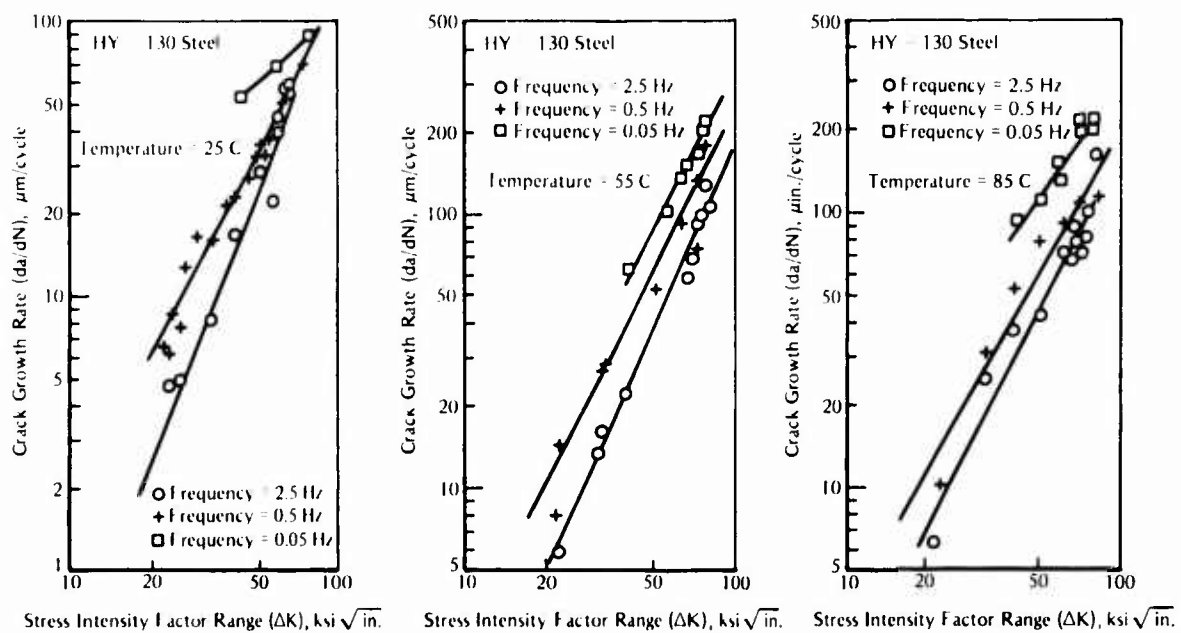
FIGURE 68. Effect of Frequency and Temperature on Cyclic
Corrosion-Fatigue-Crack Growth Rates for HY-130 Steel in
3.5 Percent NaCl Solution[147]

Loading-History Effects. Beach et al[148] measured corrosion-fatigue-crack-growth rates in HY-80 and HY-130 steel welded beams. The beams were subjected to a variable-amplitude loading spectrum. Crack-growth-rate predictions using the Paris relation with retardation effects included gave the best agreement with actual data but were still somewhat conservative.

Effect of Environmental Variables. Gallagher and coworkers[145,147] (see Figure 68) found that increased temperature gave increased da/dN values in the range 41 to 185 F (5 to 85 C). The accelerating influence of increased temperature was most significant at the lowest K levels of their study (about 20 ksi $\sqrt{\text{in.}}$).

No data on the effects of oxygen level, pH, and pressure variation were found for these steels. It is expected that their influence on corrosion-fatigue-crack-growth behavior is similar to that for the low- and medium-strength steels discussed earlier.

Bogar and Crooker[126,127] reported that for intermediate ΔK levels, da/dN values for HY-130 steel were significantly higher in flowing natural seawater than in flowing 3.5 percent NaCl solution. Their results are shown in Figure 69. Thus, actual seawater should be used to realistically assess the effects of marine environment on crack growth in these ship steels.
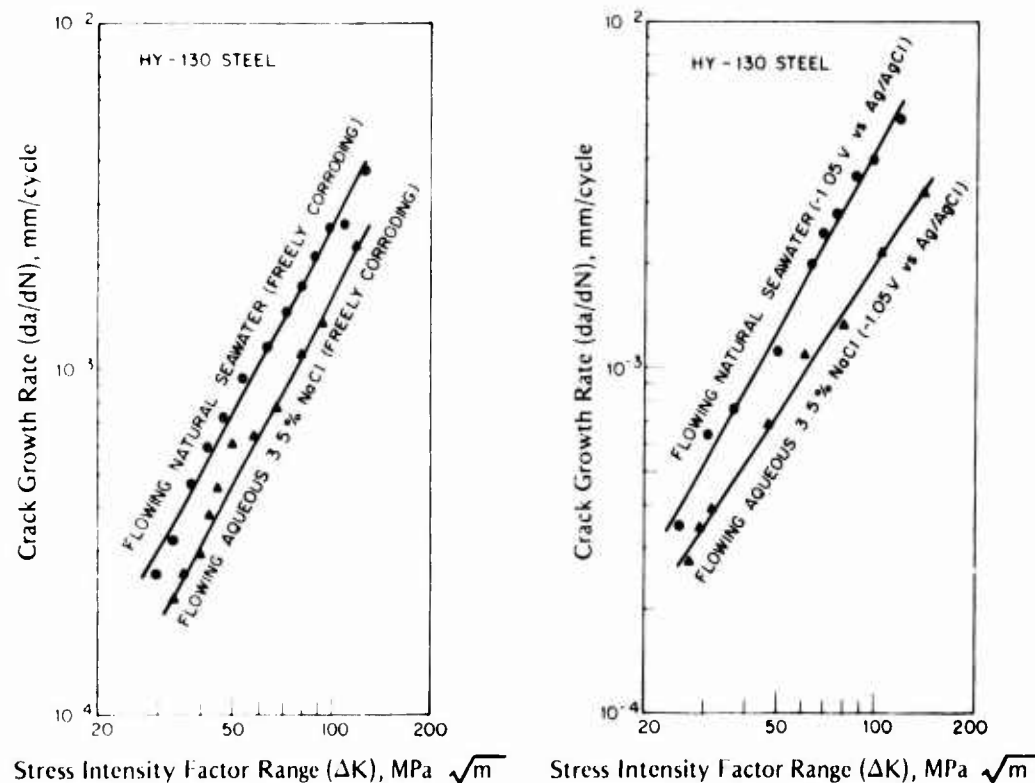
FIGURE 69. Effect of Type of Water on Corrosion-Fatigue-Crack Growth in HY-130 Steel[127]

Protective Methods. The influence of IN-625 cladding on corrosion-fatigue-crack growth of a 3.25-Ni steel in 3.5 percent NaCl solution was investigated by Hasson et al.[131] At low ΔK levels (near 20 ksi $\sqrt{\text{in.}}$), the clad steel had da/dN values similar to those of the unclad steel. At higher levels of ΔK (up to 60 ksi $\sqrt{\text{in.}}$), the clad steel showed significantly increased da/dN

values. These data resulted from tests at 10-Hz cyclic frequency, where the corrosive environment should have little effect on crack growth rate. No baseline data for the clad steel in air were presented, so it may be possible that the cyclic crack growth behavior of the clad steel is inherently different from that of the unclad steel.

Cathodic protection was found to provide no benefit over free-corrosion conditions in terms of increased crack-growth resistance. In fact, overprotection is likely to be detrimental at intermediate ΔK levels (see Figure 64) because it produces localized hydrogen embrittlement of material near the crack tip. Furthermore, the deleterious effects of overprotection become worse at lower frequencies, as shown by Gallagher's[139] data for HY-80 given in Figure 70. Detrimental effects of cathodic overprotection were found also for HY-130 steel in natural seawater[17], as demonstrated by the results in Figure 71. Note that the detrimental effect increased when the cyclic frequency was decreased from 0.167 to 0.0167 Hz. At ΔK levels near 10 MN/m$^{3\,2}$, Hartt and Adamson[140] found no deleterious influence of cathodic protection to -0.78 V SCE in flowing seawater for HY-80 steel at cyclic frequencies of 10 and 60 Hz. The data of Bogar and Crooker [126,127] for HY-80 steel (Figure 69) show that the deleterious effect of overprotection is larger in flowing natural seawater than in flowing 3.5 percent NaCl solution. The above data show that no increase in crack growth resistance results from using cathodic protection for the HY-series steels and that cathodic overprotection combined with low-cyclic frequency can be quite detrimental at intermediate levels of ΔK.
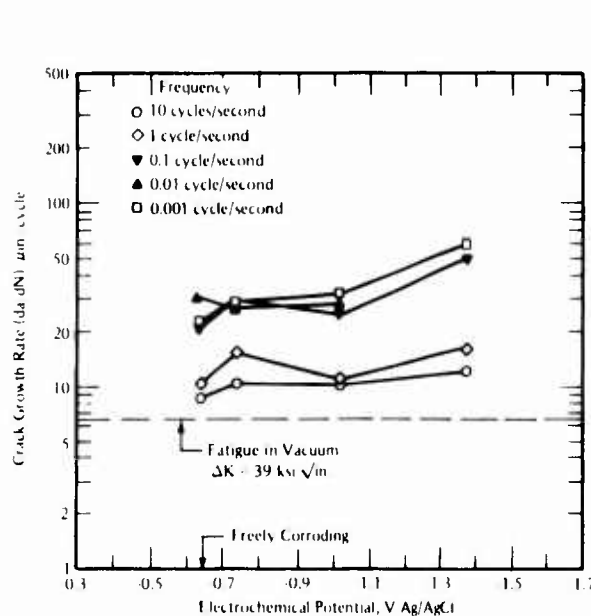
FIGURE 70. Effect of Cathodic Potential on Corrosion-Fatigue-Crack Growth of HY-80 Steel in 3.5 Percent NaCl Solution[139]
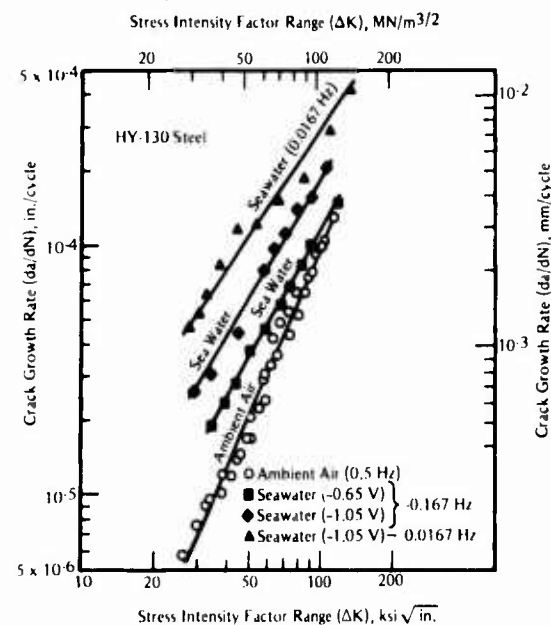
FIGURE 71. Corrosion Fatigue of HY-130 in Natural Seawater with Cathodic Protection and at Low-Cyclic Frequencies[17]

High-Strength Steels

Corrosion-fatigue data for high-strength steels are summarized in Tables 6 and 7. The steels listed in Table 6 are alloy steels heat treated to produce tensile strengths in the range of about 100 to 300 ksi (690 to 2070 MPa). These steels generally are not used to fabricate large structural members as are the low- and medium-strength steels. Instead, they are used in machinery, equipment, and selected critical structural components where the high-strength

TABLE 6. Corrosion-Fatigue Data for High-Strength Steels

Alloy	Condition or Treatment	Ultimate ksi (MPa)	Yield ksi (MPa)	Type of Specimen	Type of Loading	Cyclic Frequency, Hz	Environment(a)	Types of Data	Notes	References
Maraging 180 (12Ni-5Cr-3Mo)	Annealed and aged	202 (1390)	197 (1360)	Smooth and notched beams	Rotating bending and reversed bending	0.017 and 24.2	Saltwater(b)	S-N curves 10^2-10^8	Notch effects	133
AISI 4340 steel	Q and T	—	>220 (>1517)	SEN	Axial at R = 0	0.001 to 5	3.5% NaCl	da/dt vs frequency	da/dt at > K_{ISCC}	139
Type 135 steel	Q and T	159 (1096)	144 (993)	Smooth sheet	Axial: mean stress = 517 MPa	0.2 to 20	Seawater, drilling mud	S-N curves 10^4-10^7	Zinc coatings	150
18Ni maraging steel		>250 (>1724)	200-250 (1379-1724)	Smooth bar	Rotating bending	24.2	Seawater	S-N curves 10^6-10^8	Mild steel coating, cathodic protection	5, 71
12-5-3 maraging steel		—	166-205 (1145-1413)	Smooth bar	Rotating bending	24.2	Seawater	S-N curves 10^6-10^8	Mild steel coating	71
9Ni-4Co-0.20C steel		196 (1351)	185 (1276)	Smooth and notched bar, smooth and notched plate	Rotating bending and reversed bending	0.0042 to 24.2	Saltwater(b)	S-N curves 10^3-10^8		151
18Ni-5Cr-3Mo steel		202 (1393)	197 (1358)			0.0042 to 24.2	Saltwater(b)	S-N curves 10^3-10^8		151
18Ni-8Co-3Mo steel		192 (1324)	183 (1262)			0.0042 to 24.2	Saltwater(b)	S-N curves 10^3-10^8		151
10Ni-8Co-2Cr-1Mo steel		207 (1427)	191 (1317)			0.0042 to 24.2	Saltwater(b)	S-N curves 10^3-10^8		151
Astralloy-V steel	N and T	178 (1227)	141 (972)	Smooth and notched bar	Rotating bending	24.2	Saltwater(b)	S-N curves 10^4-10^8		152
Cr-Ni-Mo-Co-Cu-B steel	Q and T	156-172 (1080-1190)	94-112 (650-770)	Smooth bar	Rotating bending	10	Seawater	S-N curves 10^6-10^8	Cathodic protection	153
Ni steel	Q and T	—	—	Simulated propeller shaft	Rotating bending		Saltwater(b)	N for 1 shaft	Monel inlay	154
AISI 4340 steel	VAR, Q and T	194 (1338)	—	Smooth bar	Axial at R = 0.8 and rotating bending	33 and 50	3.5% NaCl	S-N curves 10^5-10^7	Cadmium plate, chromium plate, and tungsten carbide coat	155
AISI 4140 steel(c)	Hot rolled	115 (793)	96 (662)	Smooth bar	Rotating bending	30	3% NaCl	S-N curves 10^5-10^7		156
AISI 4140 steel	Q and T	175 (1207)	164 (1131)	Smooth bar	Rotating bending	30	3% NaCl	S-N curves 10^5-10^7	Heat treatments to different hardnesses, aerated and deaerated	156
AISI 4140 steel	Q and T	221 (1524)	204 (1407)	Smooth bar	Rotating bending	30	3% NaCl	S-N curves 10^5-10^6		156
AISI 4140 steel	Q and T	315 (2172)	242 (1669)	Smooth bar	Rotating bending	30	3% NaCl	S-N curves 10^5-10^6		156
18Ni maraging steel	Q and T	300 (2069)	286 (1972)	Smooth sheet	Reversed bending	12	3.5% NaCl	S-N curves 10^5-10^6	Anodic polarization	157
18Ni maraging steel		—	—	Notched plate	Reversed bending	0.083	3% NaCl	Data at τ 772 MPa for 16 alloy variations	Cathodic polarization	158
AISI 6150 steel	Q and T	261 (1800)	197 (1358)	Smooth bar	Rotating bending	30	3% NaCl	S-N curves 10^4-10^7	Effects of shot peening	159
Composite low-alloy steel	Q and T (R_c = 48)	—	—	Center-notched plate	Axial at R > 0	15	3.5% NaCl	a vs N	Armor plate	160
AISI 8635 steel	Q and T	106 (731)	—	Threaded elements	Axial	0.1	3.5% NaCl	S-N curves 10^4-10^5	Type of thread preparation	161
Improved plow steel		—	—	Single wire and wire rope	Axial at R > 0	60 to 120	Synthetic seawater	S-N curves 10^5-10^7		162
0.8Kh2G2M steel		—	—	Steel wire	Reversed bending	0.13	3% NaCl	Strain-N curves 10^2-10^3	Effect of no nickel in alloy	163
AISI 4340 steel	Q and T	149 (1029)	132 (912)	Notched bar	Rotating bending	0.23 and 23.3	1% NaCl	S-N curves 10^4-10^6 at 23.3 Hz only; a vs N curves at both frequencies		164
AISI 4340 steel	Q and T	228 (1569)	195 (1343)	Notched bar	Rotating bending	23.3	1% NaCl		Effects of heat treatment, cathodic polarization	164
AISI 4340 steel	Q and T	264 (1824)	218 (1500)	Notched bar	Rotating bending	0.23 and 23.3	1% NaCl			164
1C-1Cr steel	Hot rolled	206 (1420)	140 (965)	Smooth bar	Rotating bending	25, 50, and 100	0.004, 0.4, 4 and 25% NaCl	Initiation-propagation	2-stage tests	165
9Ni-4Co-0.20C steel	Q and T	201 (1386)	183 (1262)	SEN	Bending at R = 0	0.083	3.5% NaCl	ΔK vs da/dN		166
10Ni-2Cr-1Mo-8Co steel	Austenitized and aged	208 (1434)	193 (1331)	SEN	Bending at R = 0	0.083	3.5% NaCl	ΔK vs da/dN		166
833M30 steel	Q and T	—	196 (1350)	CTS	Axial at R = 0.5	0.25 to 32	3.5% NaCl	ΔK vs da/dN	Effect of frequency, dry hydrogen gas also	125
833M30 steel	Q and T	—	196 (1350)	CTS	Axial at R = 0.31 to 0.9	75 to 120	3.5% NaCl	ΔK vs da/dN	Vacuum, hydrogen gas, H2S also	167
833M30 steel	Q and T	196 (1350)	196 (1350)	CTS	Axial at R = 0.1 and 0.8	4 to 64	3.5% NaCl	ΔK vs da/dN	Wave-shape effects	129
5CN steel		155 (1066)	—	SEN	Bending at R = 0.1	70	0.1 M NaCl	ΔK vs da/dN	pH = 0 and 7	168
5CNM steel		164 (1133)	—	SEN	Axial at R = 0.1	70	0.1 M NaCl	ΔK vs da/dN	Frequency effect	169
18Ni maraging steel	250 grade	187 (1289)	184 (1269)	CTS	Axial at R = 0.25	0.1 to 10	3.5% NaCl	ΔK vs da/dN	Frequency effect, pH = 7 and 13.5	170
12Ni-5Cr-3Mo maraging steel		187 (1289)	184 (1269)	CTS	Axial at R = 0.25	0.1 to 10	3% NaCl	ΔK vs da/dN	Wave form effect	130
12Cr steel		—	150 (1020)	Notched bar	Rotating bending	0.1	3% NaCl	ΔK vs da/dN	Temperature effect	171
AISI 4340 steel	Q and T	—	190 (1290)	SEN	Axial at R > 0; Axial at R = 0.1	10; 0.0005 to 10	1 to 7% NaCl, to 180 F; 3.5% NaCl	da/dt vs frequency; ΔK vs da/dN	da/dt relative to K_{ISCC}; 25 kinds of loading wave forms	147
SNCM2 steel	Q and T	131 (960)	116 (799)	SEN	Axial at R = 0.1	0.05 and 0.5	3% NaCl	ΔK vs da/dN		128
3.7Ni steel	Q and T	130 (886)	119 (807)	Smooth bar	Rotating bending	24.2	Saltwater(b)	CFS(d) at 10^7		4
Ni-Cr steel	Q and T	138 (940)	123 (836)	Smooth bar	Rotating bending	24.2	Saltwater(b)	CFS(d) at 10^7		4
ASTM A517F steel	Q and T	118 (814)	107 (738)	Surface-cracked, cantilever beam	Reversed bending	0.08	3.5% NaCl	Strain range vs da/dN		108

(a) Water temperature is about 68 to 77 F unless otherwise noted.
(b) Severn River water with one-sixth to one-third the salinity of seawater.
(c) Part of a study of effects of high-strength heat treatments.
(d) CFS denotes corrosion-fatigue strength.

TABLE 7. Corrosion-Fatigue Data on Precipitation-Hardened Stainless Steels

Alloy	Condition or Treatment	Tensile Strength, ksi (MPa)		Type of Specimen	Type of Loading	Cyclic Frequency, Hz	Environment	Types of Data	Notes	References
		Ultimate	Yield							
13Cr-8Ni-2Mo PH steel	Annealed and aged 4 hr at 566 C	183 (1260)	176 (1210)	SEN	Bending at R = 0	0.083	3.5% NaCl	ΔK vs da/dN		166
17-4 PH steel	VM-H1050	160 (1105)	154 (1060)	SEN	Bending at R = 0	0.167	Seawater	ΔK vs da/dN	Cathodic protection	17
17-4 PH steel	AOM-H1050	171 (1178)	163 (1125)	SEN	Bending at R = 0	0.167	Seawater	ΔK vs da/dN	Cathodic protection	17
17-4 PH steel	AOM-H1150	149 (1025)	135 (931)	SEN	Bending at R = 0	0.167	Seawater	ΔK vs da/dN	Cathodic protection	17
17-4 PH steel	VM-H1050	160 (1105)	154 (1060)	SEN	Bending at R = 0	0.167	Synthetic seawater, seawater, 3.5% NaCl	ΔK vs da/dN	Effect of bulk solution chemistry	126, 127
17-4 PH steel	AOM-H1050	171 (1178)	163 (1125)	SEN	Bending at R = 0	0.167		ΔK vs da/dN		126, 127
17-4 PH steel	H1100	153 (1054)	101 (697)	Smooth-base metal, T-welds, and butt welds	Bending at R = -1, 0 and +1/3	1 to 33.3	Seawater	S-N curves 105-108	Goodman diagrams	132
17-4 PH steel				Smooth butt weldments	Axial at R = -1	14,200	Synthetic seawater	S-N curves 105-108	Cathodic protection	172
17-4 PH steel				Tapered box beam, welded construction	Bending under spectrum loading		Synthetic seawater	Fatigue-life and crack-growth data	Cumulative damage assessment	148

capability is needed to produce desired performance. Table 7 contains data for precipitation-hardened stainless steels. They are discussed in this chapter rather than in the later one on stainless steels because of their high-strength levels.

As with the ship steels, many of the general behavior patterns and influences of environmental and mechanical variables are similar to those discussed extensively for the low- and medium-strength steels. Thus, factors and effects peculiar to the high-strength steels are emphasized in this section, and earlier detailed discussions are not repeated here. Both fatigue-life and crack-growth data are included in Tables 6 and 7. Data of each type are addressed separately in the following discussion.

Fatigue Life

About two-thirds of the studies in Table 6 and three of the studies in Table 7 involved development of fatigue-life data. Most of the experiments were conducted on specimens tested in rotating bending. In some cases, plane bending or axial loading was used. The main variables influencing fatigue-life behavior are discussed below.

Effect of Stress Amplitude (Smooth Specimens). As with the steels discussed earlier, fatigue life increases as stress amplitude decreases and no indication of a fatigue limit is observed for freely corroding conditions in marine environments. Good examples of typical S-N curves for high-strength steels are shown in Figure 72, from the work of Schwab and Czyryca.[151] The ordinate values are pseudo stress amplitude based on strain range, which are the same as those of Figure 60 discussed earlier. Fatigue limits are apparent for tests in air but not for those in saltwater. At short lives, the environmental degradation is negligible or small, but at long lives it is quite significant.

Effect of Stress Ratio. None of the fatigue-life studies in Table 6 included stress ratio as a variable. It is expected that increasing R values would result in decreased stress-amplitude levels associated with a given cyclic life, just as for lower strength steels. In Reference 132, stress ratios of R = -1.0 and 0 were used in fatigue tests of 17-4 PH steel base-plate and butt-weld specimens in seawater. The resulting S-N curves are shown in Figure 73. At 10^8 cycles to failure, corrosion-fatigue strength (stress amplitude) decreased from 15 ksi (100 MPa) to 12 ksi (83 MPa) as R increased from -1 to 0.

Effect of Strength. As shown in Figures 30 and 31 presented earlier, increased tensile strength does not significantly improve the high-cycle corrosion-fatigue strength of steels, under free-corrosion conditions in saline solutions. Thus, unless high-strength steels are protected in some manner, little benefit derives from using them in marine environments if they are subjected to cyclic loading. For this reason, many of the studies noted in Table 6 involved investigations of protective methods.

In two investigations[156,164], heat treatment of the same low-alloy steel to various strength levels was a major variable. Lee and Uhlig[156] tested AISI 4140 steel heat treated to four tensile strengths in 3 percent NaCl solution. For intermediate life levels of 10^5 and 10^6 cycles to failure, corrosion-fatigue strength increased as tensile strength increased. However, the slope of the S-N curve became steeper as tensile strength became higher so that extrapolating these data to long lives of 10^8 cycles or more shows little increase in CFS. Endo et al[164] quenched and
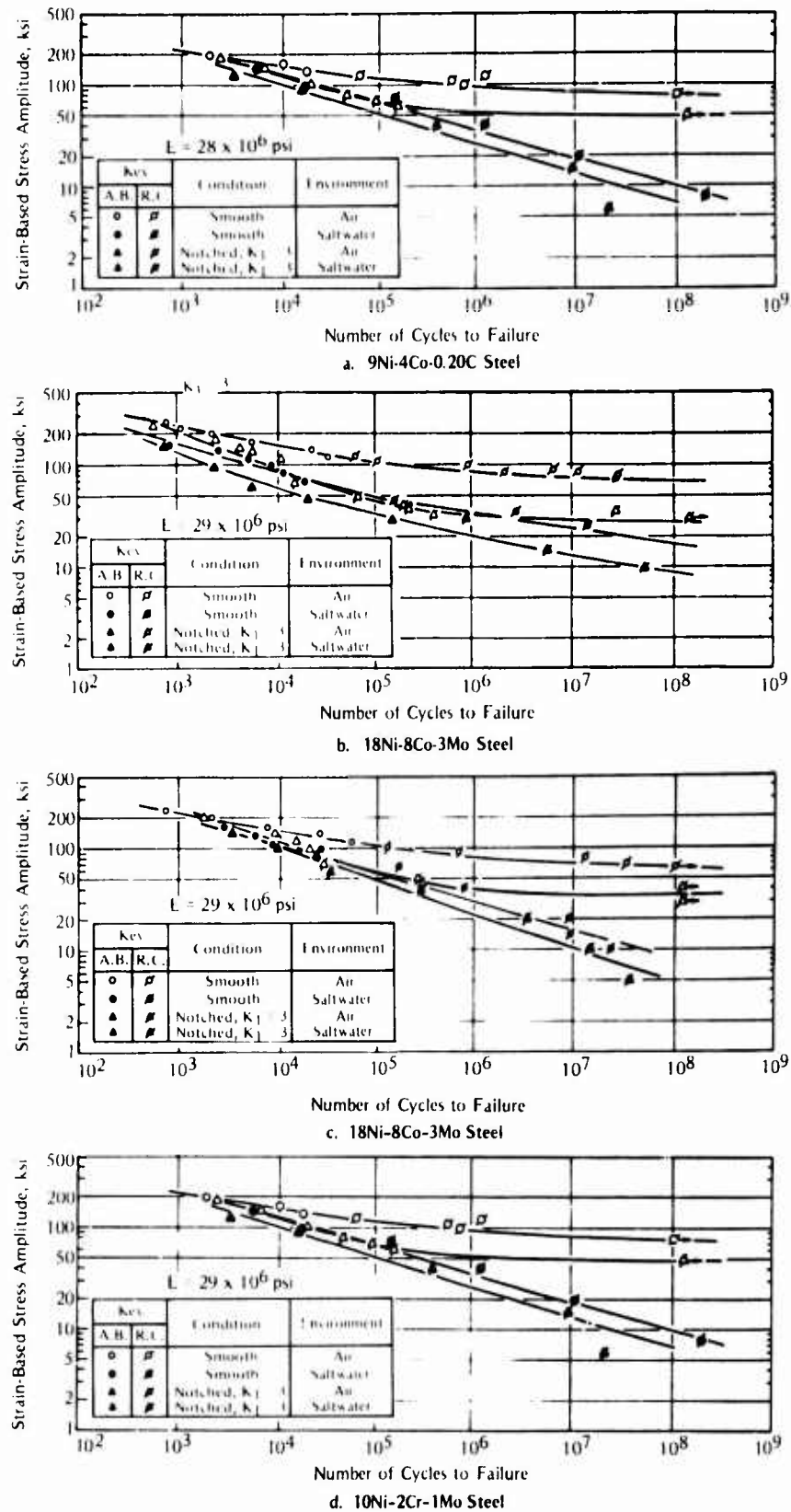
FIGURE 72. Corrosion Fatigue of Four High-Strength Steels in Severn River Water [151]

tempered AISI 4340 steel to three strength levels and conducted corrosion-fatigue tests of notched specimens in 1 percent NaCl solution. Increased tensile strength correlated with increased notched CSF in argon gas (inert) environment, but correlated with slightly decreased notched CFS in 1 percent NaCl solution. These authors believed that the increased degradation at high-strength levels was related to the increased sensitivity of the steel to hydrogen embrittlement.

Notch Effects. Fatigue-life (S-N) curves were developed for smooth and notched specimens of all four steels evaluated in Reference 151 (see Figure 72). In each case, the long-life CFS is significantly reduced by the introduction of a notch $K_t = 3.0$. When significant plasticity occurs in the low-cycle fatigue regime, the notch effect becomes much smaller or negligible. In general, similar behavior is observed for other high-strength steels. Thus, just as for the steels discussed earlier, notch effects are significant in marine environments.

Welded Joints. None of the experimental work listed in Table 6 contains data on welded specimens of the high-strength steels. This is probably because such steels are not generally used in welded construction.

The three fatigue-life studies [132,148,172] of 17-4 PH steel listed in Table 7 all involved tests of weldments. Macco's [132] results (see Figure 73) showed that butt weldments had S-N curves almost identical to those for base-plate material when tested in seawater. Preiser's [172] work did not include tests of base metal for comparison. Beach et al [148] obtained quite accurate predictions of corrosion-fatigue life for two welded box-beam specimens of 17-4 PH steel tested in saltwater and under spectrum loading. They used Miner's rule base nominal stress, the Goodman relation for stress-ratio effects, and base-metal data for notched specimens with $K_t = 3.0$. These data indicate that the CFS of 17-4 PH steel weldments is similar to that of base-plate material in marine environments.

Effect of Cyclic Frequency. For the studies listed in Tables 6 and 7, only Pettit et al [150] made a direct evaluation of the effect of cyclic frequency on CFS. For Type 135 drill pipe steel at corrosion-fatigue lives in the range of 10^4 to 10^5 cycles, reducing the cyclic frequency from 20 to 1 Hz reduced cyclic life by a factor of approximately 2 in seawater. A further reduction from 1 to 0.2 Hz caused a further cyclic-life reduction of only about 20 percent. In the work reported in References 132, 133, and 151, low frequencies were used for short-life tests conducted in reversed bending and high frequencies were used for long-life fatigue tests. It is anticipated that reduced frequency will give reduced CFS for these steels just as for the other steels discussed previously.

Loading-History Effects. Only the welded, box-beam specimens of 17-4 PH steel evaluated in Reference 148 were tested under a variable-amplitude loading history. As mentioned earlier in the section on welded joints, cumulative damage based on a nominal stress, S-N curves for $K_t = 3.0$, and Miner's rule gave good fatigue-life predictions for the two cases evaluated.

Environmental Variables. None of the studies listed in Tables 6 and 7 examined the influence of temperature, pressure, or water velocity or corrosion-fatigue life. These factors are expected to have effects similar to those discussed for other steels earlier.
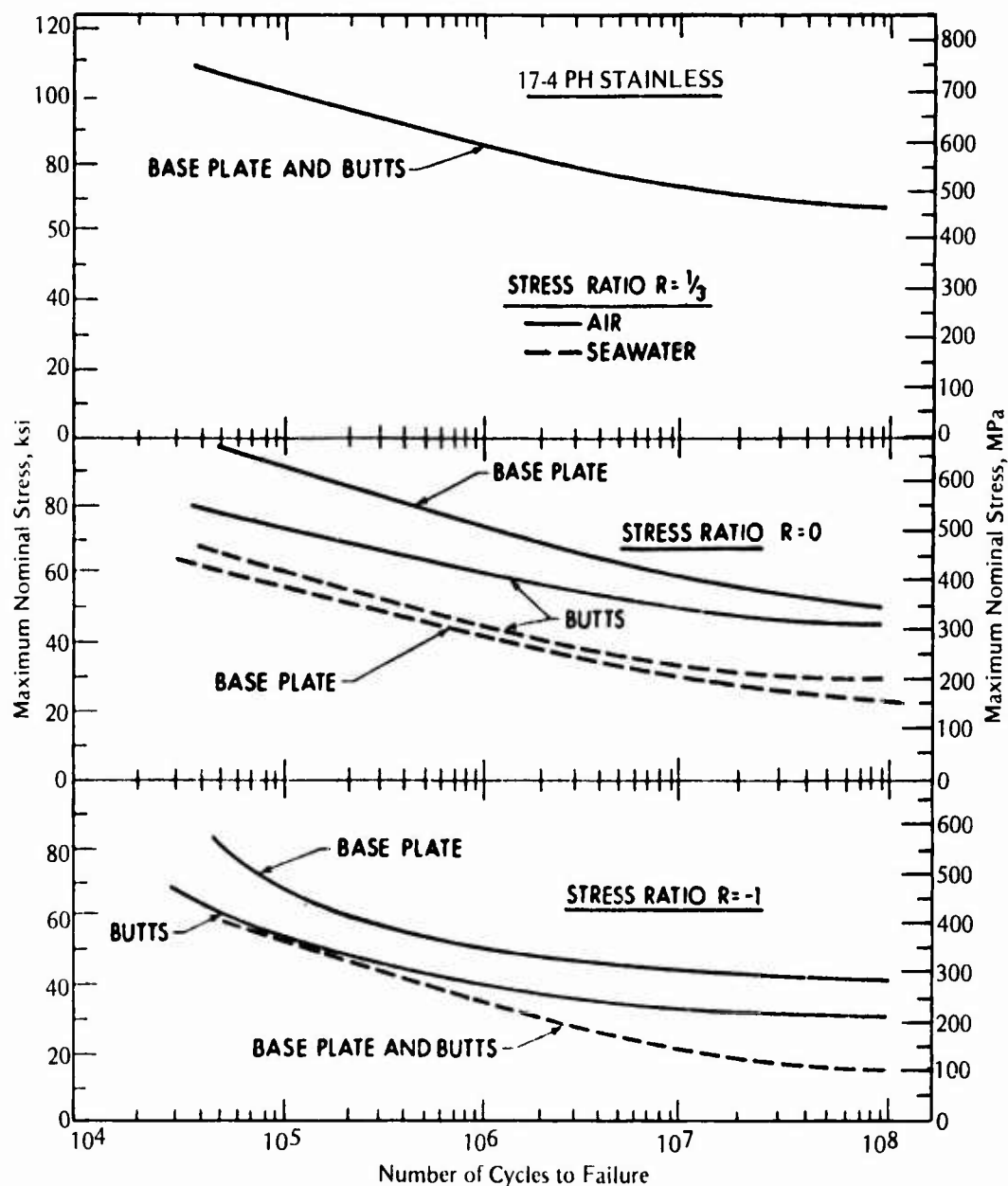
FIGURE 73. Effect of Stress Ratio on Corrosion Fatigue of 17-4PH Steel (H1100) in Seawater[132]

Lee and Uhlig[156] showed that that AISI 4140 steel specimens heat treated to a 115-ksi (793-MPa) tensile strength had the same corrosion-fatigue resistance when tested in deaerated 3 percent NaCl solution as specimens tested in air. This is an agreement with other work on AISI 1018 steel[61] discussed earlier (see Figure 41). Pettit et al[150] found that reducing the oxygen level from 6 to 0.02 ppm had little effect on the corrosion-fatigue behavior of Type 135 steel in seawater, which is in agreement with Masumoto and Akaishi's[51] work on SM41 steel discussed earlier (see Figure 42). The reduction of oxygen to a very low level is necessary to improve corrosion-fatigue resistance of steels. Within the normal range of oxygen levels in seawater, variations in oxygen content appear to have little influence on corrosion-fatigue strength.

Pettit et al[150] also examined the effect of seawater drilling muds on the corrosion-fatigue resistance of Type 135 steel. The muds had pH levels of 9 and 11.5 to 12.0, and the cyclic frequency for these experiments was 1 Hz. In plain seawater, cyclic lives were 200,000 to 300,000 cycles for their loading conditions. But in the seawater muds, cyclic lives were from 40,000 to 250,000 cycles. Thus, the higher pH levels did not provide improved corrosion-fatigue resistance in these mud environments.

Protective Methods. Kirk et al[71] used a 0.010-in. (0.254 mm)-thick flame-sprayed coating of mild steel to improve the CFS (at 10^8 cycles) of two maraging steels tested in natural seawater. The 18Ni maraging steel's CFS was increased from 5 ksi (34 MPa) to 24 ksi (165 MPa) by this coating process. For the 12-5-3 maraging steel, the corresponding increase was from 7 ksi (48 MPa) to 39 ksi (260 MPa). Thus, in both cases, the flame-sprayed coating of mild steel gave about a factor of 5 improvement in CFS (at 10^8 cycles).

Harbage[154] found no improvement in corrosion-fatigue resistance for a Monel inlay on a Ni-steel shaft.

Levy and Morrossi[155] evaluated AISI 4340 steel with cadmium plating, chromium coating, and tungsten carbide coating in a 3.5 percent NaCl solution. For R = -1 loading in rotating bending, these coatings increased CFS (at 10^7 cycles) to 4 to 4-1/2 times that for uncoated steel in saltwater or to 76 to 86 percent of the fatigue strength in air. For axial loading at R = 0.8, there was a much greater difference in performance among these three coatings. The cadmium-plated steel showed no environmental effect (test results for 3.5 percent NaCl compared those for air). Comparing CFS (at 10^7 cycles) in 3.5 percent NaCl with that in air, the chromium-coated steel showed a 45 percent decrease in fatigue strength and the tungsten carbide-coated steel showed a 60 percent decrease in fatigue strength due to the saltwater. Thus, considering both stress ratios, the cadmium-plated steel showed the best protection overall.

Baxa et al[159] showed that shot peening the surface of AISI 6150 steel specimens improved corrosion-fatigue life by a factor of about 10 (one order of magnitude) in 3 percent NaCl solution. This improvement was thought to be derived from the beneficial effect of compressive residual stresses on the surface. Even with this improvement, the CFS (at 10^7 cycles) was still almost a factor of 4 below the fatigue limit in air for unpeened material.

In their study of Type 135 steel, Pettit et al[150] evaluated the use of cathodic protection by means of flame-sprayed and electroplated zinc coatings. The flame-sprayed zinc gave little or no improvement over smooth specimens tested in seawater because grit blasting of the surface prior to flame spraying was detrimental to the fatigue resistance. Electroplated zinc coating increased the CFS in seawater (compared with that of smooth uncoated specimens), but decreased the CSF in air.

Cathodic protection to -0.85 V SCE increased the CFS (at 10^8 cycles) of the 18Ni maraging steel tested by Kirk et al[71] to 15 ksi (103 MPa). This was three times the value under free-corrosion conditions but below the value of 24 ksi (165 MPa) for flame-sprayed mild steel coating (discussed above). Taniguchi et al[153] found that cathodic protection to -0.80 V SCE improved CFS (at 5×10^7 cycles) by a factor of 1.4 compared with that under freely corroding conditions in seawater, but even with this improvement, the CFS was only about 80 percent of the fatigue limit in air. However, Hutchings and Sanderson[158] showed that the low-cycle fatigue resistance of 18Ni maraging steel was generally decreased by cathodic polarization to -1.0 V SCE, especially for alloying/tempering conditions that were conducive to hydrogen embrittlement. It appears that cathodic protection can be of some benefit in improving the CFS of high-strength steels, but it does not improve fatigue resistance up to levels observed for

tests conducted in air. Since many of these steels are more susceptible to hydrogen embrittlement than lower strength steels, it is likely that cathodic overprotection would be detrimental to their corrosion-fatigue resistance.[164]

Fatigue-Crack-Growth Data

Most of the fatigue-crack-growth data are reported in terms of cyclic crack growth rate, da/dN. However, in two studies [139,147], the time-based crack growth rate, da/dt, was used to characterize behavior. In two other studies[160,164], only data on crack growth rate versus number of cycles to failure were reported.

Effect of Stress Intensity Factor Range. The influence of stress intensity factor range is similar to that for the low- and medium-strength steels and ship steels discussed previously. Environmental effects are small or negligible at low and high ΔK levels, but they can be quite significant and detrimental at intermediate levels of ΔK. Low-alloy (Ni-Cr-Mo) steels, such as AISI 4340[139,147] and 835M30[125,129,167], can show marked acceleration of crack growth rates under certain conditions. In contrast, some of the more highly alloyed steels, such as 9Ni-4Co-0.20C, 10Ni-2Cr-1Mo-8Co, and 17-4 PH steels, show good resistance to fatigue-crack propagation and less sensitivity to deleterious environmental effects than other steels of comparable tensile strength.[166]

Effect of Stress Ratio. Only Austen and Walker[129,167], in their work using 835M30 steel (a quenched and tempered martensitic Ni-Cr-Mo steel), examined the influence of stress ratio on corrosion-fatigue-crack growth of one of these high-strength steels. For tests at 75 Hz and in a 3.5 percent NaCl solution, they found no effect of varying R from 0.31 to 0.73.[167] However, at R = 0.8 and 0.9, there were accelerated crack growth rates, especially at low ΔK values. At a lower frequency of 4 Hz, increasing R from 0.1 to 0.8 gave large increases in da/dN values[129], as shown in Figure 74. At R = 0.1, K_{max} was below K_{Iscc} and results showed little environmental effect compared with in-air data. At R = 0.8, K_{max} was above K_{Iscc} and the environmental effect was quite dramatic. Thus, high R ratios can be quite deleterious to corrosion-fatigue-crack-growth resistance of high-strength steels because they may cause K_{max} to be greater than K_{Iscc}.

Welded Joints. No corrosion-fatigue-crack-growth data for welded high-strength steels were found, except for the results of Beach et al[148] on 17-4 PH steel-welded box beams. These beams were tested under spectrum loading and in synthetic seawater. Using linear-elastic fracture mechanics methodology, Beach et al were able to obtain reasonably accurate prediction of crack growth behavior in these welded beams. The baseline data for their predictions were from tests of base-plate material, so the corrosion-fatigue-crack-growth behavior of the weldment was not significantly different from that expected for base plate in this one study.

Effect of Cyclic Frequency. The effect of cyclic frequency was investigated in six studies.[125,129,139,147,169,170] It was typically found that decreased frequency caused increased da/dN values. Gallagher et al[139,147] showed that the effect of frequency depended upon whether K_{max} was below or above K_{Iscc} for AISI 4340 steel in 3.5 percent NaCl solution, as shown in Figure 75. In vacuum, da/dt depends only on the number of applied cycles and, therefore, the da/dt versus frequency curve for a given K is a 45-degree straight line (Figure
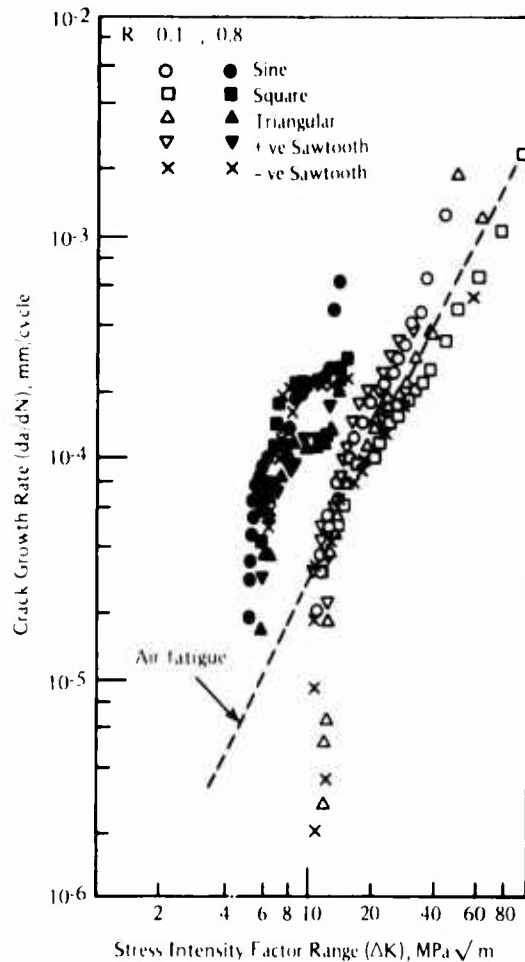
FIGURE 74. Corrosion-Fatigue-Crack Growth Behavior
of 835M30 Steel in 3.5 Percent NaCl Solution and at a
Cyclic Frequency of 4 Hz[129]
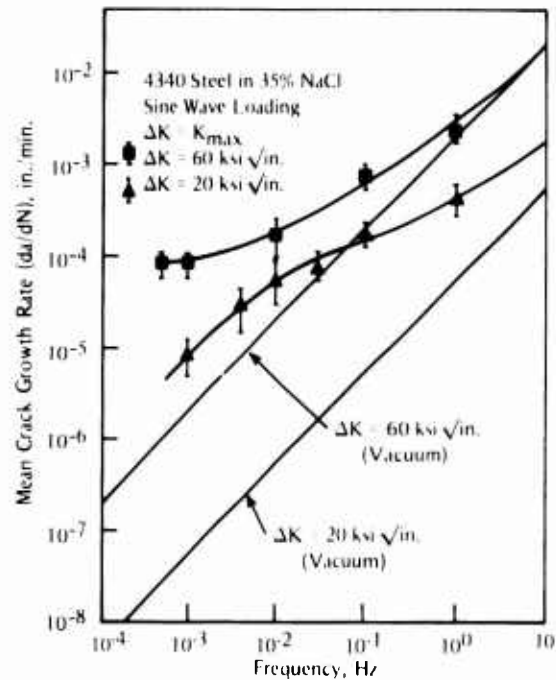
FIGURE 75. Corrosion-Fatigue-Crack Growth Behavior
of AISI 4340 Steel Above ($\Delta K = 60$ ksi $\sqrt{in.}$) and Below
($\Delta K = 20$ ksi $\sqrt{in.}$) K_{Iscc}[147]

75). At high frequencies in 3.5 percent NaCl, the da/dt values asymptotically approach those in vaccum. At lower frequencies, environmental attack causes accelerated da/dt values. Above K_{Iscc}, da/dt tends to approach a constant value at low frequencies where stress-corrosion crack growth dominates. Below K_{Iscc}, da/dt approaches a 45-degree slope with frequency (at low-frequency values where environmental effects are cycle dependent). Thus, below K_{Iscc} the time-dependent environmental effect was most evident at intermediate frequencies in the range of about 0.01 to 1 Hz.

In their studies at 835M30 steel in 3.5 percent NaCl solution, Austen and Walker[125,129] varied frequency from 64 Hz to 0.25 Hz. As shown in Figure 76, da/dN values dramatically increased with decreased frequency at intermediate ΔK values, whereas there was little frequency effect at very high and very low values of ΔK. These curves are similar to those discussed earlier for low- and medium-strength steel in saltwater with cathodic overprotection (see Figures 52 and 53). Thus, frequency effect and localized hydrogen embrittlement can easily occur in high-strength steels, even without cathodic protection, because these steels are more susceptible to hydrogen embrittlement than the lower strength steels.
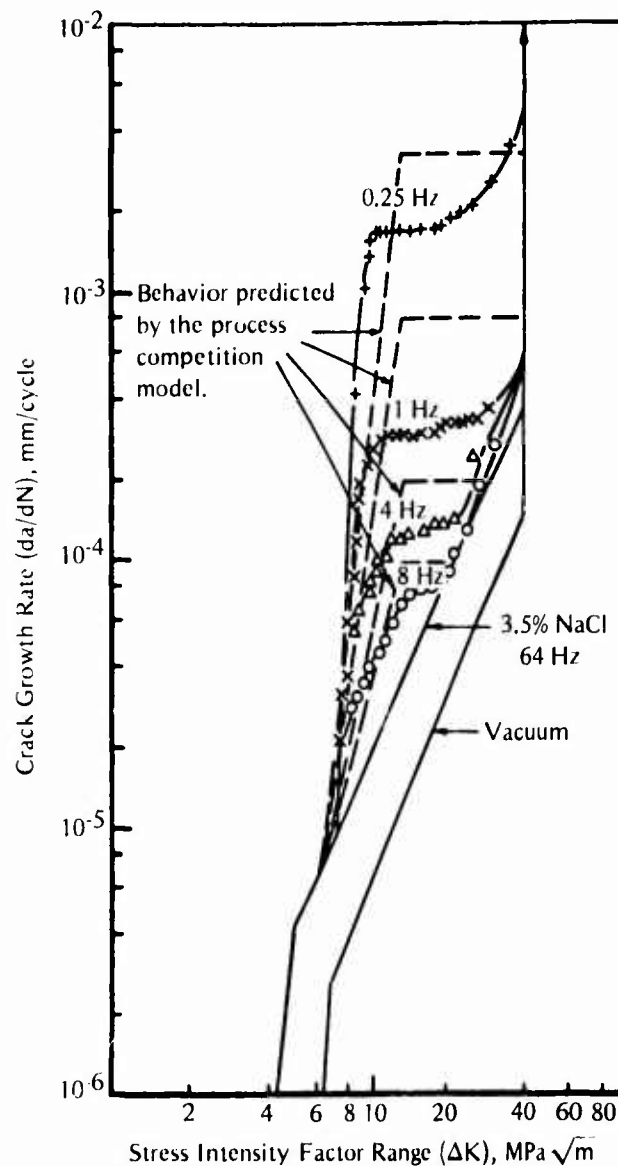
FIGURE 76. Effect of Cyclic Frequency on Corrosion-Fatigue-Crack
Growth Rate of 835M30 Steel in 3.5 Percent NaCl Solution[129]

Barsom[170] and Pettit et al[169] investigated frequency effects for maraging steels in saltwater environment. At intermediate ΔK levels, Barsom[170] found that da/dN increased as frequency decreased (see Figure 77) for 12Ni-5Cr-3Mo steel. Pettit et al[160] found similar behavior for 18Ni maraging steel (see Figure 78). Their data tend to converge at low ΔK values just as those for other steels discussed previously. Barsom[170] did not obtain data at low ΔK values, but close examination of the data points in Figure 77 suggests a slight tendency toward such convergence. With these more highly alloyed steels, there is no sharp knee and plateau region in the ΔK vs da/dN plot such as those seen in Figure 76. Thus, the susceptibility to localized hydrogen embrittlement at low frequencies is not evident in these maraging steels under free-corrosion conditions.
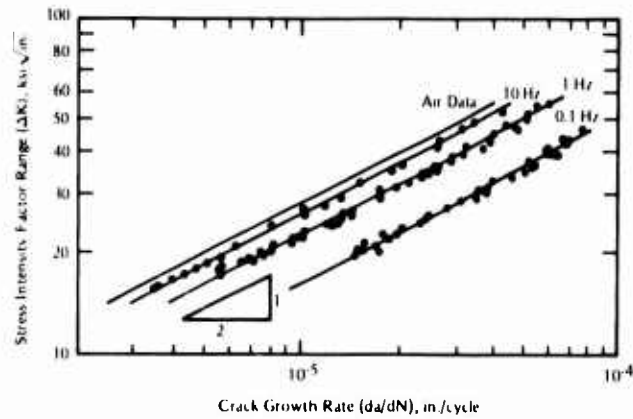
FIGURE 77. Effect of Cyclic Frequency on Corrosion-Fatigue-Crack
Growth of 12Ni-5Cr-2Mo Steel in 3 Percent NaCl Solution[170]
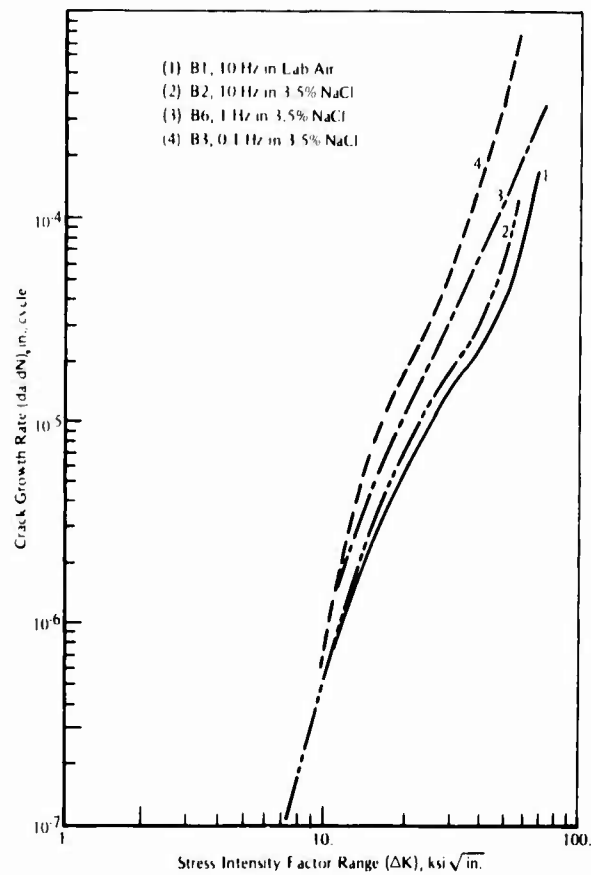
FIGURE 78. Effect of Cyclic Frequency on Corrosion-Fatigue-Crack Growth
Rate of 18Ni Maraging Steel in 3.5 Percent NaCl Solution[169]

close to those observed for tests in air. However, when the loading time was low (sinusoidal, triangular, and positive sawtooth), a marked acceleration of crack growth rate was observed. Thus, for this steel, the environmental attack occurs during the time period of rising load. Austen and Walker[129] found similar wave shape effects in their work on 835M30 steel (see Figure 74) at $K_{max} < K_{Iscc}$. However, when $K_{max} > K_{Iscc}$, they found square-wave loading to be the most detrimental, as expected.

Load-History Effects. The influence of wave shape was addressed in three studies.[128-130] Barsom[130] found that wave shape had an important influence on da/dN values for 12Ni-5Cr-3Mo steel in 3 percent NaCl solution, as shown in Figure 79. In these tests, K_{max} was less than K_{Iscc}. For square and negative, sawtooth loading wave forms where the loading portion of the cycle was quite rapid (compared with the hold and/or unloading portions), da/dN values fell

Kawai and Koibuchi[128] conducted an extensive evaluation of the effects of 25 different wave-form shapes. They tested specimens of a quenched and tempered martensitic Ni-Cr-Mo steel (SNCM2 or BS830M31) in 3 percent NaCl solution. As illustrated in Figure 80, they separated each wave form into four different components (T_1, T_2, T_3, and T_4 for analysis of their

T   Period of a stress wave (sec)
T1 Stress increasing time
T2 Maximum stress hold time
T3 Stress decreasing time
T4 Minimum stress hold time
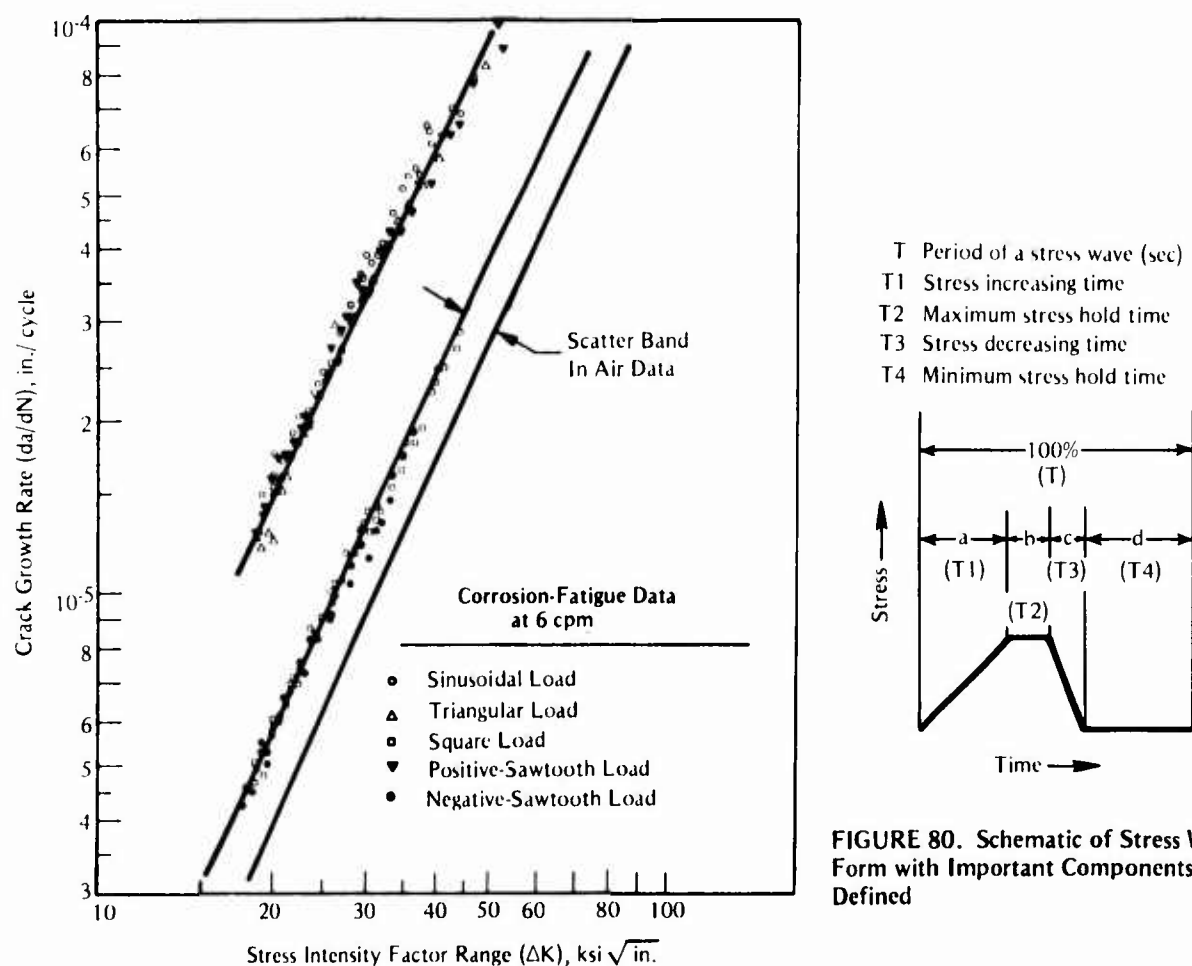
FIGURE 80. Schematic of Stress Wave Form with Important Components Defined

FIGURE 79. Effect of Wave Shape on Corrosion-Fatigue-Crack Growth Rate of 12Ni-5Cr-3Mo Steel in 3 Percent NaCl Solution[130]

results. They found that T_1 and the combination of T_2, T_3, and T_4 were the two dominant factors in quantifying wave-form effects. Thus, they were able to quantify the accelerating effect of wave form on corrosion-fatigue-crack growth in terms of two parameters

$$(T/T_1) \; (\Delta K^m/T_1) \quad ,$$

as shown in Figure 81. They also obtained a similar correlation for published data on HY-80 and HY-130 steels.
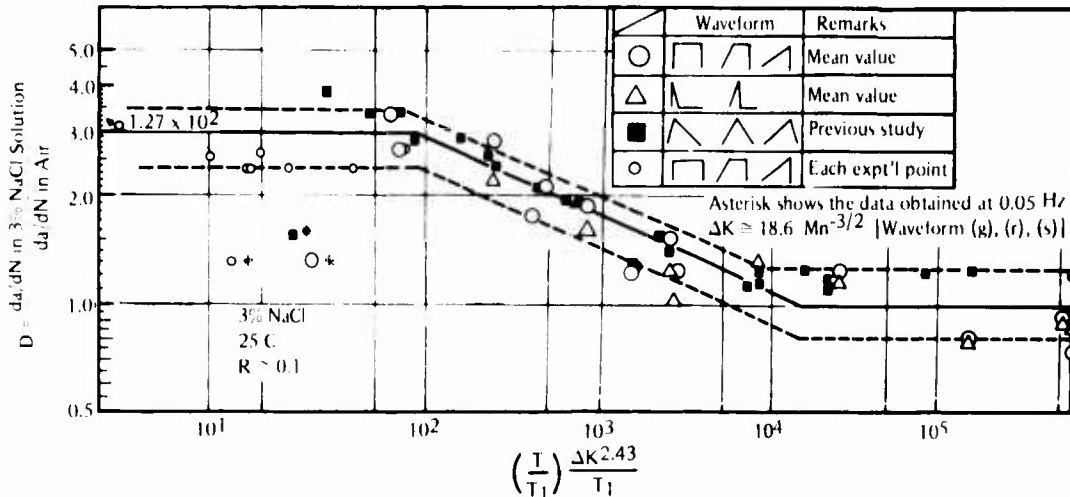
FIGURE 81. Quantification of the Effect of Wave Forms on Corrosion-Fatigue-Crack Growth of SNCM2 Steel in 3 Percent NaCl Solution[128]

For welded box beams of 17-4 PH steel, Beach et al[148] conducted tests under variable-amplitude block histories. Using linear-elastic fracture mechanics methods, they were able to predict crack growth data in saltwater when they used the Paris relation without incorporating retardation effects.

Effect of Environmental Variables. None of the studies listed in Tables 6 and 7 examined the influence of oxygen level, pressure, or water velocity on corrosion-fatigue-crack growth. Eisenstadt and Rajan[171] tested a 12Cr steel at 10-Hz cyclic frequency and in salt solutions ranging from 0 to 7 percent NaCl. At 70 F (21 C), increasing salinity caused a very slight increase in crack growth rate (see Figure 82). At 151 F (71 C), a crack growth rate increased rapidly as salinity increased from 0 to 4.5 percent but increased only slightly from 4.5 to 7 percent salinity. Thus, the maximum temperature influence occurred at about 4.5 percent NaCl. Data for this salt level and other temperatures are shown in Figure 83. The indicated stress levels correspond to intermediate-level ΔK values. In this range, it is apparent that increased temperature results in increased crack growth rate, which is in accord with previously discussed results for other steels.

The data of Barsom[170] shown in Figure 77 were for a solution of pH = 7. When the pH was increased to 13.5·(3 percent NaCl), the ΔK vs da/dN curve was the same for 0.1, 3, and 10 Hz, and was below the curve for tests in air. This result indicates that the increased pH significantly reduced environmental attack and that some corrosion fatigue actually may have occurred in the tests in air. Austen et al[168], in tests of two 5Ni steels (5CN and 5CNM) in 0.1M NaCl solution, found that changing the pH from 7 to 0 had no significant influence on the ΔK vs da/dN curve.
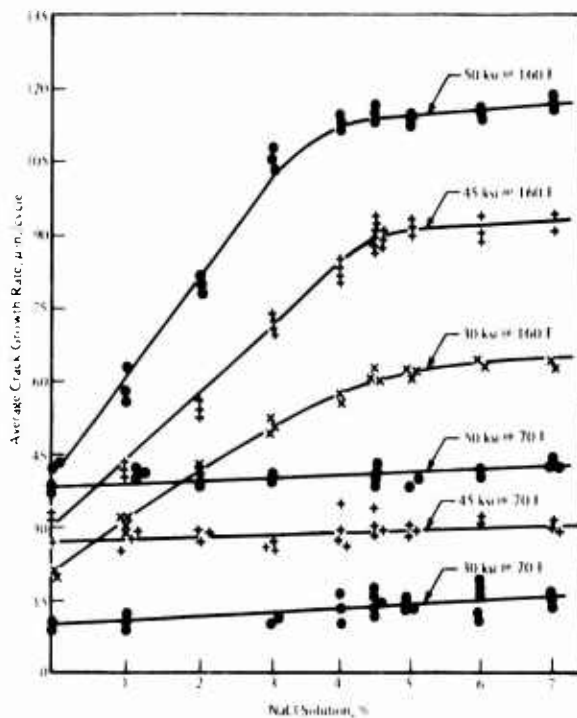
FIGURE 82. Effect of Salt Concentration on Average Crack Growth Rate for 12Cr Steel[171]
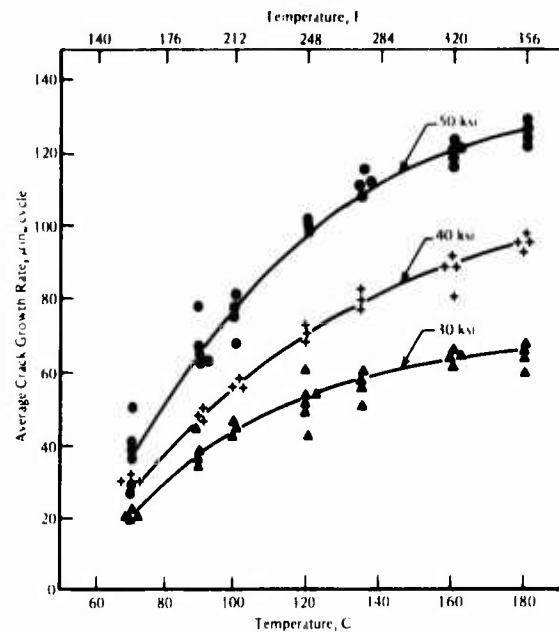
FIGURE 83. Effect of Temperature on Average Crack Growth Rate of 12Cr Steel in 4.5 Percent NaCl Solution[171]

Thus, very high pH (≥ 3) appears to be beneficial, but other pH levels seem to have little influence on crack-growth-rate behavior.

As mentioned in the earlier discussion of ship steels, Bogar and Crooker[126,127] used natural seawater, 3.5 percent NaCl solution, and ASTM synthetic seawater in their study on HY-130 steel. Their work also included two heats of 17-4 PH steel, H1050 temper, the results for which are presented in Figure 84. For the argon-oxygen melted heat, there was only a slight difference in corrosion-fatigue behavior for the three types of water. However, for the
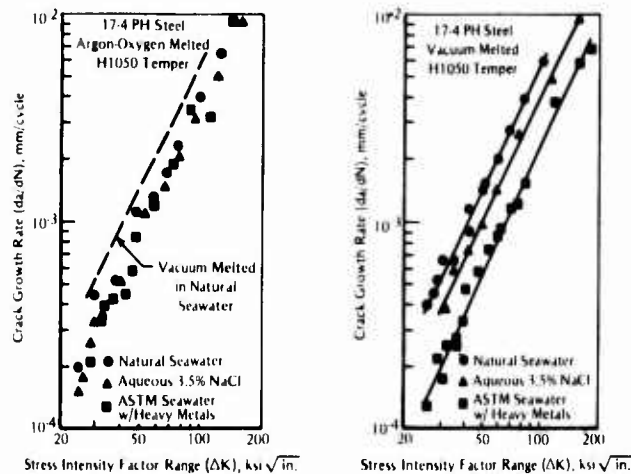
FIGURE 84. Effect of Type of Flowing Water on Corrosion-Fatigue-Crack Growth Rate of 17-4 PH Steel[127]

vacuum-melted steel, a significant effect of water type was observed. Natural seawater produced the highest growth rates, ASTM seawater produced the slowest, and the rates with 3.5 percent NaCl were intermediate. As mentioned before, natural seawater should be used to most accurately reflect the effects of marine environment on corrosion-fatigue-crack growth. Furthermore, one might have erroneously concluded that the vacuum-melted material was superior to the argon-oxygen-melted material based on tests in ASTM seawater only. In natural seawater, the argon-oxygen-melted steel is actually the superior steel. This was also the only alloy studied by Bogar and Crooker that showed little effect from changes in the environmental chemistry.

Cathodic Protection. None of the studies of high-strength steels listed in Table 6 examined the effect of cathodic protection on crack growth. Since these steels generally are susceptible to hydrogen embrittlement, it is likely that cathodic protection would not retard the acceleration of crack growth rates observed in marine environments. Furthermore, it is quite likely that cathodic overprotection would be detrimental in the same manner as was discussed earlier for many of the lower strength steels.

Crooker et al [17] studied the influence of cathodic protection on corrosion-fatigue-crack growth of 17-4 PH steel (vacuum melted, argon-oxygen melted/H1050, and argon-oxygen melted/H1150) in natural seawater. Their results are shown in Figures 85, 86, and 87. The crack growth resistance of the argon-oxygen melted (AOM) H1050 temper material (Figure 86) was much poorer than that of the vacuum melted and AOM/H1150 materials in air. Under free-corrosion conditions (-0.2 and -0.3 V Ag/AgCl), the AOM materials (Figures 86 and 87) exhibited better crack growth resistance than the vacuum-melted (VM) material (Figure 85). The best crack growth resistance in freely corroding seawater was obtained for the AOM/H1150 material. However, with cathodic polarization to -0.65 V Ag/AgCl, the VM material showed no increase in da/dN values, whereas the AOM materials showed significant increases. Thus, with the cathodic polarization, the VM material and the AOM/H1150 material showed similar behavior, and whereas the AOM/H1050 material showed slightly higher da/dN values. The overall observation is that cathodic polarization is of no benefit and can be detrimental to corrosion-fatigue-crack-growth resistance of the 17-4 PH steels.

FIGURE 87. Corrosion-Fatigue-Crack Growth
Rate for 17-4 PH AOM-H1150 Steel[17]

FIGURE 86. Corrosion-Fatigue-Crack Growth
Rate for 17-4 PH AOM-H1050 Steel[17]

FIGURE 85. Corrosion-Fatigue-Crack Growth Rate for
17-4 PH (Vacuum Melted H1050 Temper) Steel[17]

CHAPTER 4
CORROSION-FATIGUE DATA FOR STAINLESS STEELS

The corrosion-fatigue data for stainless steels are compiled in Table 8. The chromium stainless steels are listed first, followed by the chromium-nickel stainless steels (austenitic and duplex and high-alloy ferritic stainless steels). For each alloy, the type of corrosion-fatigue data in the reference article is described, as well as the specimen type, the loading, and the environment. The stainless steels have a corrosion resistance superior to that of steel in seawater; however, they are susceptible to localized forms of corrosion, e.g., pitting and crevice corrosion, which can lessen corrosion-fatigue resistance.

Chromium Stainless Steels

The nominal chemical compositions of chromium-based stainless steels are presented in Table 9. Chromium contents range from approximately 12 to 20 weight percent. Nickel, molybdenum, and copper are common alloying elements.

Redmon[173] reported corrosion-fatigue data in seawater for three cast martensitic stainless steels: CA-15, CA-6NM, and a modified CA-6NM. These stainless steels are used for shafts, valves, and pumps in aggressive environments. The corrosion fatigue tests were performed in natural seawater at ambient temperature. Smooth, cantilever-beam specimens were rotated at 1450 rpm, producing a loading frequency of 24.2 Hz. The results are shown in Figure 88. At 10^8 cycles to failure, all three stainless steels had corrosion-fatigue strengths of 5 ksi (35 MPa) or less. No fatigue limit was observed for any of the steels. The CA-6NM steel modified with 1.5 percent Mo exhibited the highest corrosion-fatigue resistance, while CA-15 steel had the lowest. The differences in corrosion-fatigue resistance were greater at lower stress levels. All three steels exhibited some pitting corrosion during exposure to seawater.

Jaske et al[9] investigated the corrosion-fatigue behavior of CA-6NM stainless steel in seawater at a frequency of 3.3 Hz, which is seven times lower than the frequency used by Redmond in the above study. Jaske's data are presented along with Redmond's data in Figure 89. Large, Krouse-type, plate-bending specimens were machined from large castings, which were made to simulate material used in ship propellers. Fatigue experiments were carried out under fully reversed, constant-amplitude loading. A check analysis for chromium and molybdenum indicated 14.51 and 0.24 weight percent, respectively.

In experiments by Jaske et al and by Redmond, actual seawater was used; the primary difference was that the data of Jaske et al were for a lower frequency. There appears to be a slightly degrading effect of lower frequency, but overall, both sets of data show a similar trend in behavior. The data show quite low corrosion-fatigue strength near 10^7 to 10^8 cycles. Extrapolation to 10^8 cycles would give a value of 10 ksi (69 MPa) or less, which is no more (and perhaps less) than that for bronze alloys (see Chapter 6 on copper-base alloys) which are commonly used for ship propellers. It should be noted that these tests were run under freely corroding conditions and that the specimens showed signs of crevice corrosion near the gripping fixtures. In actual practice, cathodic protection is applied to propellers. With cathodic protection, the corrosion-fatigue resistance should be much improved.

TABLE 8. Summary of Corrosion Fatigue Data for the Stainless Steels

Alloy	Condition or Treatment	Tensile Strength, ksi (MPa)		Type of Specimen	Type of Loading	Frequency, Hz	Environment	Types of Data	References
		Ultimate	Yield						
CA-6NM	Austenitized at 1922 F 1½ hr, tempered at 1120 F 2 hr	19.2 (1130.4)	15.4 (1104.7)	Smooth	Rotating cantilever	23.3	Seawater	SN curve 10^5-10^8	173
Modified C..-6NM	Austenitized at 1922 F 1½ hr, tempered at 1120 F 2 hr	19.2 (1130.3)	15.5 (1105.2)	Smooth	Rotating cantilever	23.3	Seawater	SN curve 10^5-10^8	173
CA-15	Austenitized at 1823 F 1½ hr, air cooled, tempered at 1120 F 2 hr	17.4 (118.1)	14.7 (100.2)	Smooth	Rotating cantilever	23.3	Seawater	SN curve 10^5-10^8	173
CA-6NM	Machined from a large casting	108 (745)	100 (690)	Krause type, smooth beam	Bending	3.3	Seawater	SN curve 10^6-10^7	9
14Cr	1800 F 1 hr, quenched in oil, 1075 F 2 hr, air cooled	178.1 (1211.0)	101.7 (691.5)	Smooth	Rotating beam	24	Air, freshwater, saltwater	SN curves 10^4-10^8	4
14Cr	1800 F 1 hr, quenched in oil, 1200 F 2 hr, air cooled	117.4 (798.3)	45.0 (306)	Smooth	Rotating beam	24	Air, freshwater, saltwater	SN curves 10^4-10^8	4
14Cr	1700 F 1 hr, furnace cooled	94.4 (641.9)	37.5 (255)	Smooth	Rotating beam	24	Air, freshwater, saltwater	SN curves 10^4-10^8	4
20Cr-0.9Cu		87.9 (597.7)	40.5 (275.4)	Smooth	Rotating beam	24	Air, freshwater, saltwater	SN curves 10^4-10^8	4
13Cr-6Ni	Quenched and tempered	117.7 (800.6)	95.5 (649.7)	Center notched	Tensile, bending, stress	Air 11.67, H_2O 4.0	Air, seawater	Crack growth rate diagrams	174
13Cr-1Ni	1796 F 3 hr, air RT 1094 F 8 hr, air RT	92.8 (557.1)	64.7 (439.9)	Center notched	Tensile, bending, stress	Air 11.67, H_2O 4.0	Air, seawater	Crack growth rate diagrams	174
16Cr-5Ni	1832 F 18 hr, air R, 1094 F 12 hr, air RT	121.7 (827.7)	100.6 (684.4)	Center notched	Tensile, bending, stress	Air 11.67, H_2O 4.0	Air, seawater	Crack growth rate diagrams	174
18Cr-6Ni-1Co-1Mo	Cast, 1652 F 10 hr, air cooled	137.08 (932.1)	49.91 (339.4)	Smooth	Rotating beam		Air, seawater 212 F, pH 2-10	SN curves 10^6-10^8	175
1Kh 14NDL Stainless Steel		98.8 (671.8)	73.2 (497.8)	Smooth and notched	Symmetrical bending		Air, seawater, $K_2Cr_2O_7$	Fatigue and corrosion-fatigue curves	75
13Cr SUS41011	1778 F ½ hr quenched in oil, 1688 F ½ hr cooled in water	112.5 (765)	95.6 (650)	Smooth	Rotating cantilever	60	0.03% NaCl 3% NaCl	SN curve, SN data, effect of aeration, stress concentration, temperature and surface roughness	176-179
403	Austenitized at 1760 F 2.5 hr, oil quenched, tempered at 2237 F 4 hr	110.5 (751.4)	93.5 (635.8)	Notched	Compact tension fracture-toughness specimens and 1T-WOL specimens(a)		Air, seawater	Crack growth rate diagrams	180
AISI 403-12Cr	1742 F 1 hr, air cooled, 1202 F 1 hr	114 (775.2)	100 (689)	Compact tension	Torsion-tension	10-40	0.01M and 1M NaCl	Crack growth rate	181
AISI 410	Magnetized and unmagnetized						Air, seawater	Time, stress to failure, X-ray diffraction studies, residual magnetic flux measurements during air-fatigue tests	182
AISI 304	Wrought	116 (79.0)		Smooth	Rotating cantilever	24	Seawater	Corrosion-fatigue strength	5
AISI 304L	Wrought	12.5 (85.0)		Smooth	Rotating cantilever	24	Seawater	Corrosion-fatigue strength	5
AISI 316	Wrought	11.0 (75.0)		Smooth	Rotating cantilever	24	Seawater	Corrosion-fatigue strength	5

TABLE 8. (Continued)

Alloy	Condition or Treatment	Tensile Strength, ksi (MPa)		Type of Specimen	Type of Loading	Frequency, Hz	Environment	Types of Data	References
		Ultimate	Yield						
AISI 316L	Wrought	11.6 (79.0)		Smooth	Rotating cantilever	24	Seawater	Corrosion-fatigue strength	5
Austenitic, Z6 CND 17.12	2012 F 30 min, water-cooled	12.0 (82.0)	4.8 (33.0)	Smooth	Rotating cantilever	0.5, 20, 50	Air, 3% NaCl	Fatigue-crack growth rate	177, 183
Austenitic Ti, stabilized, Z6 CNDT 17.12	2012 F 30 min, water-cooled	113.6 (193.0)	4.3 (29.0)	Smooth	Rotating cantilever	0.5, 20, 50	Air, 3% NaCl	Fatigue-crack growth rate	179, 182 / 171, 183
Duplex, Z3 CNDU 21.7	2102 F 30 min, water-cooled	13.8 (94.0)	9.3 (63.0)	Smooth	Rotating cantilever	0.5, 20, 50	Air, 3% NaCl	Fatigue-crack growth rate / SN curves 10^5-10^8	171, 182
Ferritic, ZO CD 26.1	1670 F 30 min, water-cooled	10.1 (69.0)	-.2 (49.0)	Smooth	Rotating cantilever	0.5, 20, 50	Air, 3% NaCl	Fatigue-crack growth rate	177, 182
X2CrNiN1810		94.70/93.67 (644/637)	43.38/42.64 (295/290)	Smooth and notched	Rotating beam	11.67, 100, 2000	3% NaCl solution, aerated, nonaerated, pH of 1, 3, 7, air	CFS at 2×10^7 cycles, corrosion data	184
X2CrNiMoN1813		94.55 (643)	43.52 (296)	Smooth and notched	Rotating beam	11.67, 100, 2000	3% NaCl solution, aerated, nonaerated, pH of 1, 3, 7, air	CFS at 2×10^7 cycles, corrosion data	184
X3CrNiMoN17135		105.14 (715)	52.79 (359)	Smooth and notched	Rotating beam	11.67, 100, 2000	3% NaCl solution, aerated, nonaerated, pH of 1, 3, 7, air	CFS at 2×10^7 cycles, corrosion data	184
X2CrNiMoN 225		108.23/105.88 (736/720)	75/70.59 (510/480)	Smooth and notched	Rotating beam	11.67, 100, 2000	3% NaCl solution, aerated, nonaerated, pH of 1, 3, 7, air	CFS at 2×10^7 cycles, corrosion data	184
X10CrNiTi 189		88.52/89.26 (602/607)	39.26/41.9 (267/285)	Smooth and notched	Rotating beam	11.67, 100, 2000	3% NaCl solution, aerated, nonaerated, pH of 1, 3, 7, air	CFS at 2×10^7 cycles, corrosion data	184
X10CrNiMoTi 181		89.26/89.7 (607/610)	40.88/43.8 (278/298)	Smooth and notched	Rotating beam	11.67, 100, 2000	3% NaCl solution, aerated, nonaerated, pH of 1, 3, 7, air	CFS at 2×10^7 cycles, corrosion data	184
ETi19123n C 26	Welding rod material	90.7/91.6 (617/624)	61.7/62.79 (430/427)	Smooth and notched	Rotating beam	11.67, 100, 2000	3% NaCl solution, aerated, nonaerated, pH of 1, 3, 7, air	CFS at 2×10^7 cycles, corrosion data	184
EKb19153Mn8N20t	Welding rod material	103.0/103.97 (701/707)	72.35/73.0 (492/497)	Smooth and notched	Rotating beam	11.67, 100, 2000	3% NaCl solution, aerated, nonaerated, pH of 1, 3, 7, air	CFS at 2×10^7 cycles, corrosion data	184
ETi19123n C26	Welding rod material	90.88/88.9 (618/605)	67.5/66.0 (459/449)	Smooth and notched	Rotating beam	11.67, 100, 2000	3% NaCl solution, aerated, nonaerated, pH of 1, 3, 7, air	CFS at 2×10^7 cycles, corrosion data	184
EKb1874n C20t	Welding rod material	99.26/93.97 (675/639)	66.7/65.7 (454/447)	Smooth and notched	Rotating beam	11.67, 100, 2000	3% NaCl solution, aerated, nonaerated, pH of 1, 3, 7, air	CFS at 2×10^7 cycles, corrosion data	184
EKb25?MoNb20t	Welding rod material	120.1/123.5 (817/840)	88.6/93.2 (603/634)	Smooth and notched	Rotating beam	11.67, 100, 2000	3% NaCl solution, aerated, nonaerated, pH of 1, 3, 7, air	CFS at 2×10^7 cycles, corrosion data	184
ETi2283n C26	Welding rod material	119.26 (811)	91.4 (622)	Smooth and notched	Rotating beam	11.67, 100, 2000	3% NaCl solution, aerated, nonaerated, pH of 1, 3, 7, air	CFS at 2×10^7 cycles, corrosion data	184
AISI 316				Boiler test piece type K70B(20)	Rotation under cantilever loading, pre-corroded	50	Air	SN curves 10^3-10^8 with prior corrosion	185
Ferralium							Seawater	SN curves	186

(a) 1T-WOL denotes thick wedge opening load, crack growth specimen.

TABLE 9. Nominal Chemical Compositions of the Chromium Stainless Steels

| Alloy | Major Alloying Elements, wt % | | | Reference |
	Cr	Ni	Other	
CA-6NM	11.7	3.9	0.5 Mo, 0.5 Mn, 0.5 Si	173
Modified CA-6NM	11.7	3.9	1.5 Mo, 0.5 Mn, 0.5 Si	173
CA-15	12.5	0.6	0.5 Mn, 0.5 Si	173
14-Cr	14.5	0.2	0.3 Mn, 0.2 Si, 0.38 C	4
20Cr-0.9Cu	20.9	0.2	0.9 Cu, 0.3 Mn, 0.6 Si, 0.19 C	4
13Cr-6Ni	12.4	5.8	1.6 Mo, 0.5 Mn, 0.3 Si	174
13Cr-1Ni	13.5	0.7	0.7 Mn, 0.4 Si	174
16Cr-5Ni	16.0	4.7	1.0 Mo, 0.8 Mn, 0.4 Si	174
18Cr-6Ni-1Co-1Mo	18	6	1.0 Mo, 0.6 Mn, 0.3 Si, 1.0 Co	175
1Kh14NDL	13.5	1.4	1.3 Cu, 0.5 Mn, 0.3 Si	75
SUS 410J1	12		0.5 Mo, 0.4 Mn, 0.4 Si	176, 178, 179
SUS 410J1	12.4		0.5 Mo, 0.5 Mn, 0.3 Si	2
AISI-403	12.5	0.3	0.5 Mo, 0.4 Mn, 0.3 Si	180
AISI-403	11.7	–	0.1 Mo, 0.5 Mn, 0.3 Si	181
AISI-410	12.5		0.5 Mn, 0.3 Si	182

McAdam[4] determined the corrosion-fatigue resistance of alloys for springs. Included in this evalation were a 14Cr stainless steel and a 20Cr-0.9Cu stainless steel. These alloys were selected for their high elastic limit relative to many of the corrosion resistant steels. Three sets of curves for the 14Cr steel are presented in Figure 90a. These show the fatigue behavior of this steel in air and fresh water at three hardnesses. The furnace-cooled (fully annealed steel) specimen and the specimen given a spring temper had essentially the same corrosion-fatigue limit. Further data were reported for the behavior in saltwater. Tests in saltwater with salinity approximately one-third that of seawater revealed lower corrosion fatigue limits at 10^8 cycles for the 1075 F (579 C) temper steel but equal limits for the 1200 F (649 C) temper. For the 1200 F (649 C) temper, corrosion-fatigue limits were 36 ksi (248 MPa) in fresh water and seawater. For the 1075 F (579 C) temper, corrosion fatigue limits were 37.5 ksi (259 MPa) and 27 ksi (186 MPa) in fresh water and saltwater, respectively.

The fatigue and corrosion-fatigue curves for a 20Cr-0.9Cu steel are shown in Figure 90b after McAdam.[4] The corrosion-fatigue limit in saltwater was considerably lower than that in fresh water, 30 ksi (207 MPa) and 40 ksi (279 MPa), respectively.

Tenge and Gjertsen[174] determined the corrosion-fatigue-crack propagation rates in air and in seawater for three stainless steel propeller alloys: 13Cr-6Ni, 13Cr-1Ni, and 16Cr-5Ni. The study was concerned with the rate of propagation of fatigue cracks initiating from sharp surface cracks. The 13Cr-6Ni and 16Cr-5Ni steels were cast in test blocks for the study, while
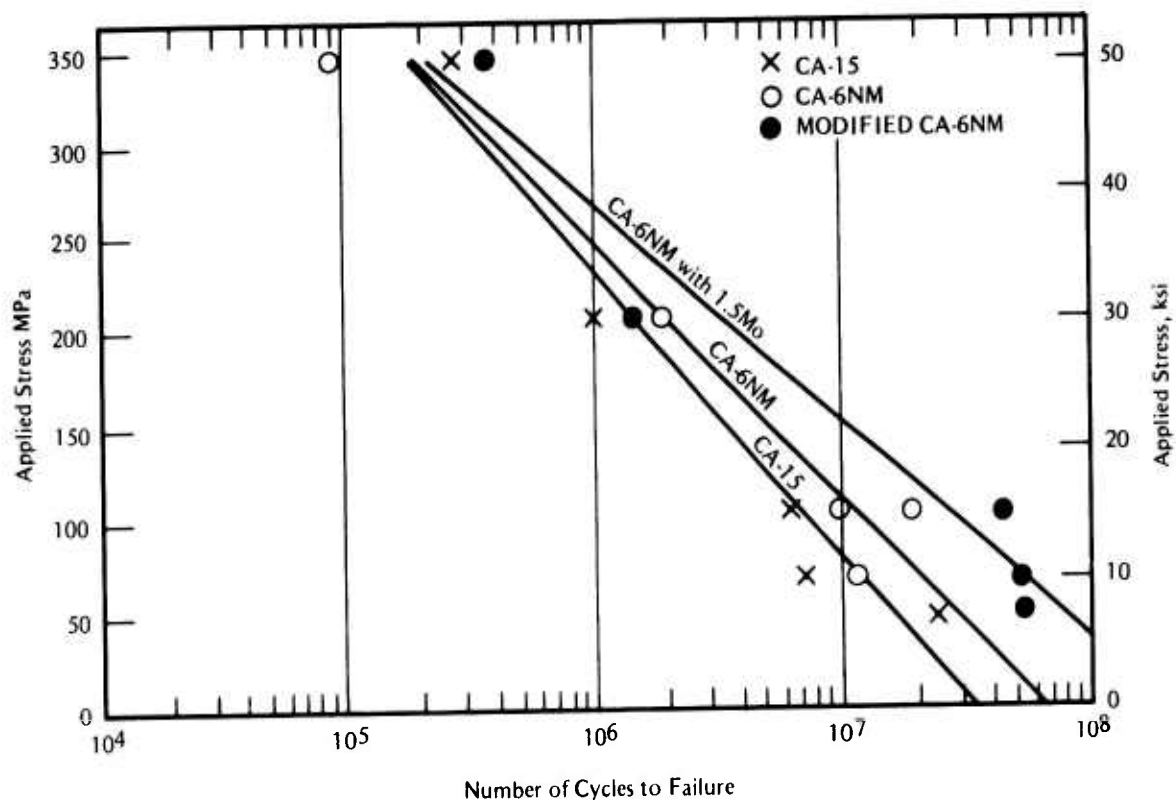
FIGURE 88. Corrosion Fatigue Behavior in Ambient Temperature Seawater[173]
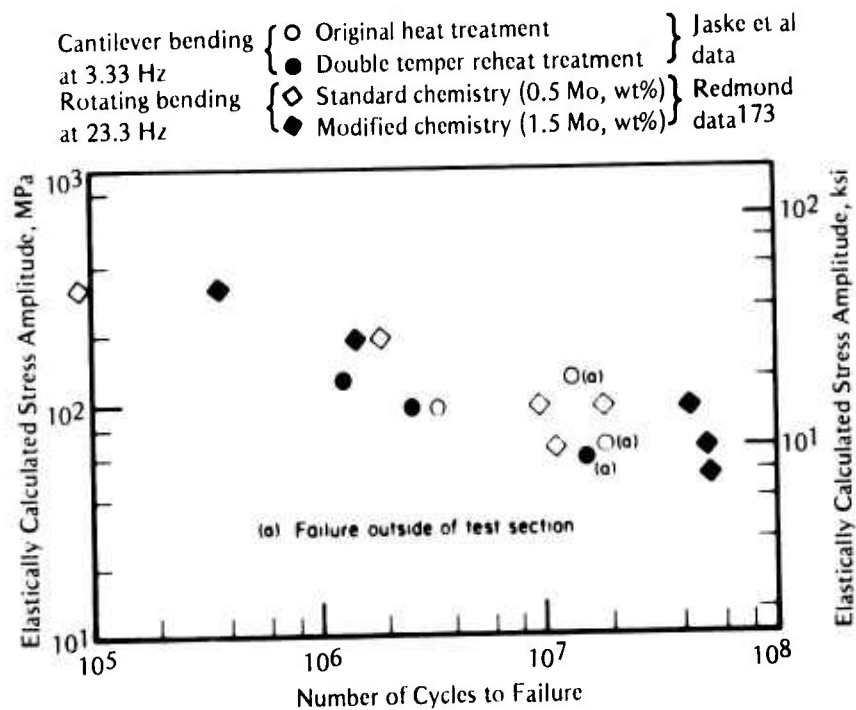
FIGURE 89. Corrosion Fatigue of CA-6NM Steel in
Flowing Seawater Environment (Zero Mean Stress)[9]
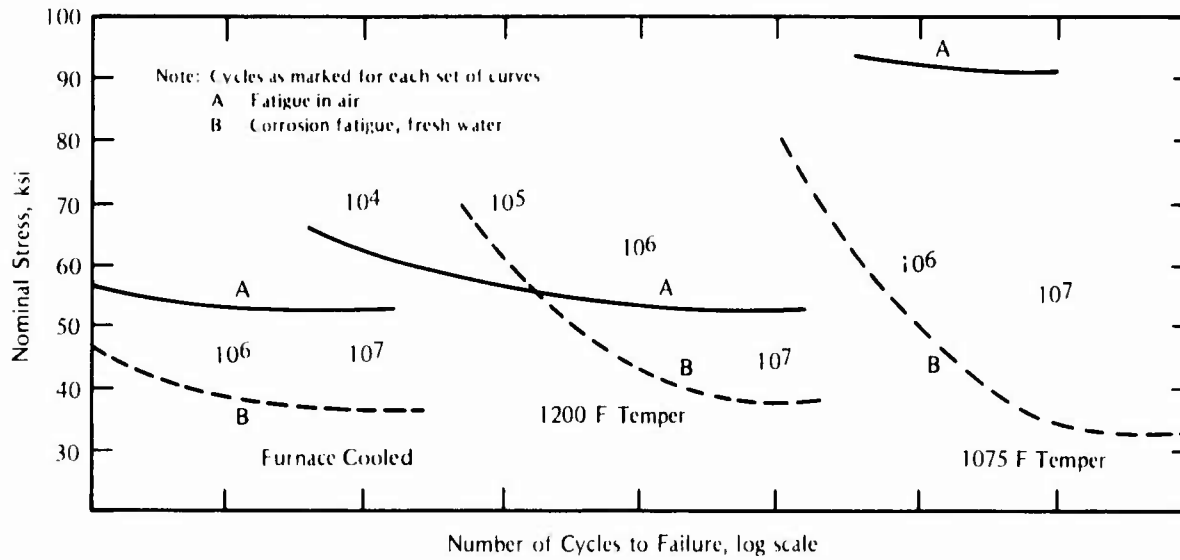
a. 14Cr Steel
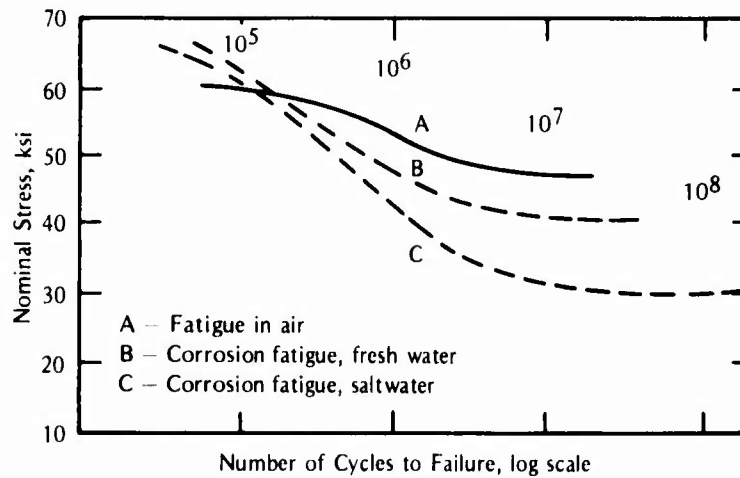
b. 20Cr + 0.9Cu

FIGURE 90. Fatigue and Corrosion-Fatigue Curves
for Two Types of Stainless Steels[4]

the 13Cr-1Ni steel was taken from a broken propeller blade. The mechanical properties of the 13Cr-1Ni steel deviate significantly from the properties normally attained for this alloy. The authors attribute this deviation to an incorrectly performed heat treatment and state that the corrosion-fatigue data are not representative of properly heat-treated 13Cr-1Ni steel. Corrosion-fatigue tests were made with precracked, center-notched specimens. A constant mean stress with superimposed dynamic stress was applied. Tests in air were made at a frequency of 11.7 Hz, while those in seawater were made at 4 Hz. A 3 percent NaCl solution was used at 70 C, with continual aeration to maintain constant oxygen concentration.

The crack growth rates for the three steels in air and seawater are shown in Figures 91 and 92, respectively. In air, all three steels showed a decrease in growth rate below a stress intensity factor (ΔK) of 7.03 to 8.44 ksi (10 to 12 $kg/mm^{3/2}$). A significantly lower crack growth rate was

16Cr-5Ni Steel
13Cr-6Ni Steel
13Cr-1Ni Steel

$m = 2.4$ $C = 2.10 \times 10^{-9}$

$m = 2.4$ $C = 6.08 \times 10^{-9}$

$m = 2.6$ $C = 1.15 \times 10^{-9}$

$\sigma_{mean} = 7$ kg/mm^2
Seawater at
240 cpm

Stress Intensity Factor Range (ΔK), kg/mm$^{3/2}$

Crack Growth Rate (da/dN), mm/cycle

FIGURE 92. Crack Propagation Rates for Three Propeller Steels in Seawater[174]

16Cr-5Ni Steel
13Cr-6Ni Steel
13Cr-1Ni Steel

$m = 2.8$ $C = 2.52 \times 10^{-10}$

$m = 2.7$ $C = 9.03 \times 10^{-10}$

$m = 2.6$ $C = 1.03 \times 10^{-9}$

$m = 7.4$ $C = 7.41 \times 10^{-15}$

$m = 6.5$ $C = 1.82 \times 10^{-1/4}$

$m = 6.2$ $C = 2.44 \times 10^{-13}$

$\sigma_{mean} = 7$ kg/mm^2
Air at 700 cpm

Stress Intensity Factor Range (ΔK), kg/mm$^{3/2}$

Crack Growth Rate (da/dN), mm/cycle

FIGURE 91. Crack Growth Rates for Three Propeller Steels in Air[174]

observed for the 16Cr-5Ni steel than for the other two steels over the entire ΔK range. In seawater, the 13Cr-1Ni steel was characterized by a propagation rate higher than that of the other two steels. The propagation rates in seawater for the 13Cr-1Ni and 16Cr-5Ni were greater than those in air, while for the 13Cr-6Ni steel, propagation rates in air and in seawater were similar. The authors suggest that the data were too limited to generalize on the relative behaviors of the steels tested. The investigation demonstrated that sharp cracks 0.12 to 0.20 in. (3 to 5 mm) in depth can lead to fracture of a propeller within 4 to 12 months.

Corrosion-fatigue data for an 18Cr-6Ni-1Co-1Mo steel for propellers were presented by Udea et al.[175] The behavior of specimens machined from a test ingot and results of ship tests of a propeller for over 3-1/2 years were described. The alloy was compared with a conventional nickel-aluminum bronze (a widely used propeller alloy). The S-N curves for the 18Cr-6Ni-1Co-1Mo steel and a nickel-aluminum bronze are presented in Figure 93. The corrosion fatigue strength in seawater after 10^8 cycles was about 38 ksi (265 MPa) or almost twice that of a nickel-aluminum bronze casting at 2×10^7 cycles. The 18Cr-6Ni-1Co-1Mo steel in the ship test performed well. After 3 years and 7 months, both the pressure and backside surfaces of the propeller kept their metallic luster and dye-penetration-test results were satisfactory.

An investigation[75] was made of the corrosion-fatigue strength of 1Kh14NDL steel (13.5Cr-1.4Ni-1.3Cu) and the effectiveness of its protection by cathodic polarization. For comparison, 35 steel (a carbon steel) was also tested. The fatigue tests were made with reversed bending of 0.39-in. (10-mm)-diameter samples, both of uniform cross section and with a round notch. The corrosion-fatigue life of smooth and notched specimens is shown in Figure 94 in synthetic seawater and in air. The fatigue limit for smooth specimens at 50×10^6 cycles in seawater was 50 percent of that in air. For notched specimens in seawater, the corresponding decrease was 30 percent of the notched-specimen fatigue limit in air.

The effect of cathodic protection on corrosion-fatigue strength is shown in Figure 95 where the corrosion-fatigue limit for 1Kh14NDL steel is given as a function of oxidizing potential. The potential was controlled by impressed cathodic currents. Corrosion-fatigue strength was increased by cathodic protection. The potentials of the stainless steel when galvanically coupled to mild steel, zinc, and magnesium are marked on the curve. At 0.9 V, the corrosion-fatigue limit for smooth specimens was equal to that in air. For notched specimens, cathodic protection increased the corrosion-fatigue limit by more than 1.7 times the fatigue limit in air. The corrosion-fatigue limits for notched specimens in seawater with and without cathodic protection, in air, and in a 3 percent $K_2Cr_2O_7$ solution are shown in Figure 96. The entire curve for the steel in seawater with cathodic protection lies above the curve for that in air. The curve for the steel in a 3 percent $K_2Cr_2O_7$ solution, where no corrosion of the stainless steel was observed, also lies above the curve for the steel in air. The authors conclude that the complete suppression of corrosion of the stainless steel accounts for the improved fatigue properties. The suggestion that hydrogen generated during the cathodic protection improves the fatigue properties is refuted by the results in the $K_2Cr_2O_7$ solution, where hydrogen is not generated. Similar effects of cathodic protection and inhibited solutions were reported by the authors for carbon steel.

The corrosion-fatigue behavior of a 13Cr stainless steel used for blades of a compressor driving turbine was investigated by Ebara et al.[2,176,178] They carried out rotating-bending fatigue tests on 13Cr stainless steel (SUS 410J1) in NaCl and NaOH solutions at various concentrations. Their results in sodium chloride solutions are summarized here. The SUS 410J1 martensitic stainless steel was oil quenched after heating to 975 C for 1 hour and then tempered at 700 C for 2 hours.
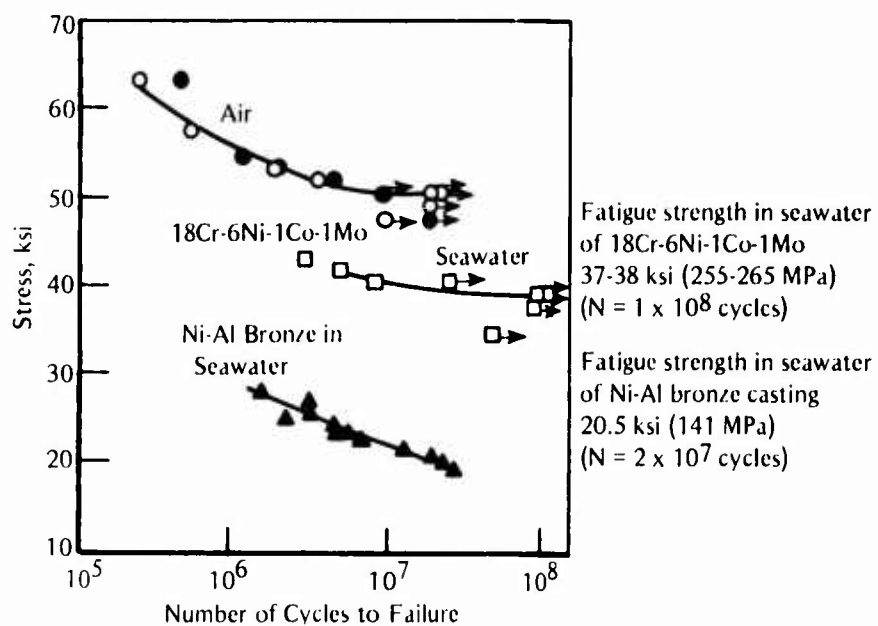
FIGURE 93. Corrosion-Fatigue Strength of an
18Cr-6Ni-1Co-1Mo Steel and a Nickel-
Aluminum Bronze Casting[175]
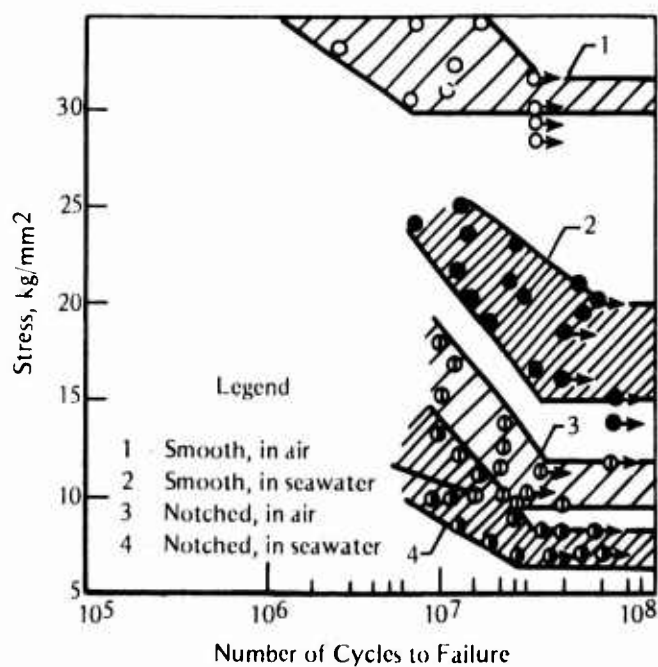
FIGURE 94. Corrosion-Fatigue Strength of
Smooth and Notched 1Kh14NDL Steel in
Seawater and Air[75]
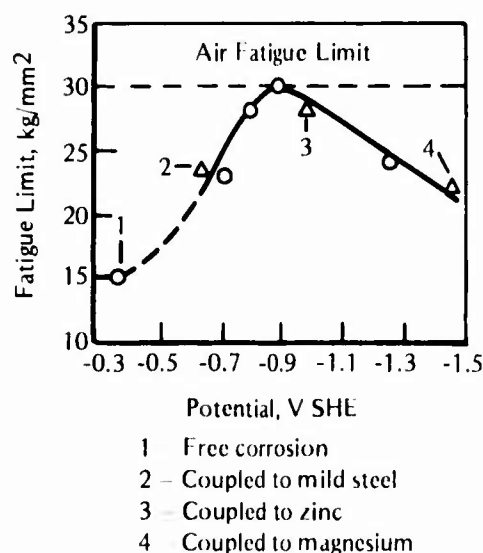
FIGURE 95. Relationship of the Corrosion Fatigue Limit of 1Kh14NDL Steel in Seawater to the Sample Potential[75]

1 — Free corrosion
2 — Coupled to mild steel
3 — Coupled to zinc
4 — Coupled to magnesium

1 — In air
2 — In seawater
3 — In seawater with zinc cathodic protection
4 — In a 3 percent solution of $K_2Cr_2O_7$
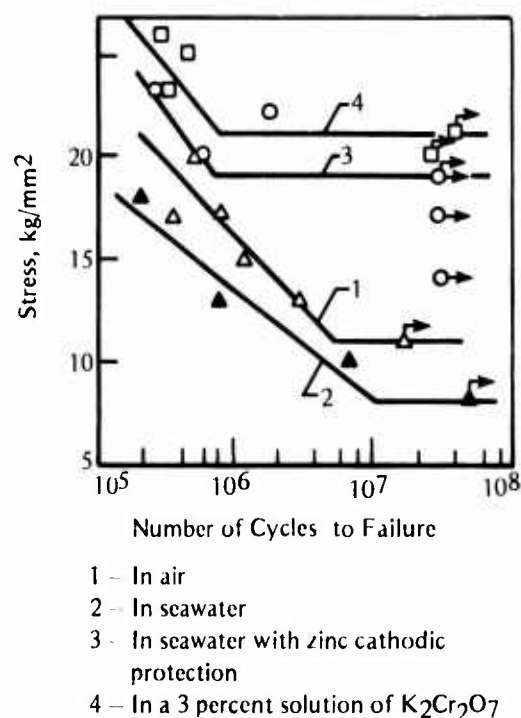
FIGURE 96. Corrosion-Fatigue Curves for Notched Samples of 1Kh14NDL Steel[75]

Corrosion-fatigue test results for smooth bar specimens in various concentrations of NaCl aqueous solutions are presented in Figure 97. In the 3 percent NaCl solution, fatigue strength at 10^7 cycles was about 17.6 ksi (120 MPa), or about 30 percent of that in air [approximately 58.8 ksi (400 MPA)]. For decreasing NaCl contents in aqueous solution, fatigue life at the same stress level increased, as shown in Figure 98. The effect of NaCl concentration on the fatigue limit at 6×10^6 cycles is shown in Figure 99. Even in low-concentration (3×10^{-4} percent) NaCl aqueous solution, fatigue strength was reduced. In contrast, no decrease in fatigue strength was observed in distilled water.

The corrosion-fatigue-test results for plain bar specimens within the long-life range (about 200 days) in 0.03 percent NaCl aqueous solution are shown in Figure 100. Fracture occurred after 6×10^8 cycles with a rotating bending stress of 13.97 ksi (95 MPa). No fracture occurred at the bending stresses of 7.50 and 17.35 ksi (51 and 118 MPa); however, cracks and corrosion pits were observed on the specimen surface. Thus, even in such a dilute environment as a 0.03 percent NaCl aqueous solution, the long-life-range fatigue strength decreased to a level of about 25 percent of that limit in air.

While no reduction in fatigue strength was observed in distilled water, the influence of steam on fatigue life has been recognized at high stress levels. Figure 101 shows the effect of steam and steam plus 3 percent NaCl on the corrosion-fatigue strength. With decreasing stress, the influence of steam was decreased, and no influence was recognized at the fatigue limit.

In the environment with steam and 3 percent NaCl, the decrease in corrosion-fatigue strength within the long-life range was severe (about a factor of 2). These differences in the magnitude of decrease in corrosion-fatigue strength at low stress levels in a mild (steam) environment compared with that in an aggressive (steam plus 3 percent NaCl) environment may be related to differences in the corrosion-fatigue mechanism in these two environments. Further fatigue tests were conducted in 3 percent NaCl aqueous solution at 140 and 176 F (60 C and 80 C), and the results are shown in Figure 102. In the 176 F (80 C) solution of NaCl, fatigue strength of a smooth specimen at 10^8 cycles was about 14.71 ksi (100 MPa), which equals
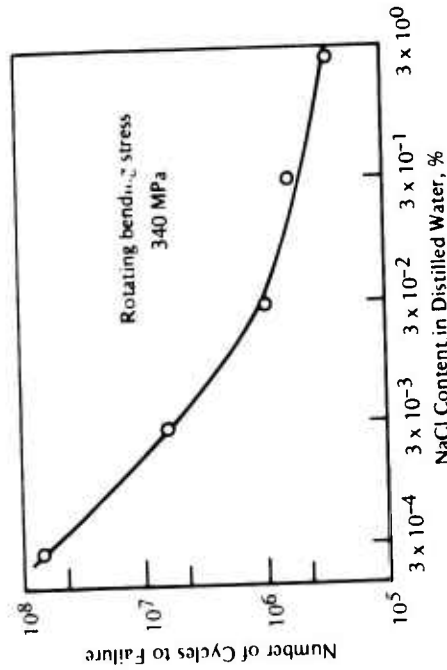
FIGURE 98. Influence of NaCl Concentration in Distilled Water on Corrosion-Fatigue Strength of 13 Cr Steel Specimens at Rotating Bending Stress of 340 MPa[178]

FIGURE 100. Corrosion-Fatigue Strength of 13 Cr Steel Specimens in 0.03 Percent NaCl Solutions in Long-Term Tests[178]
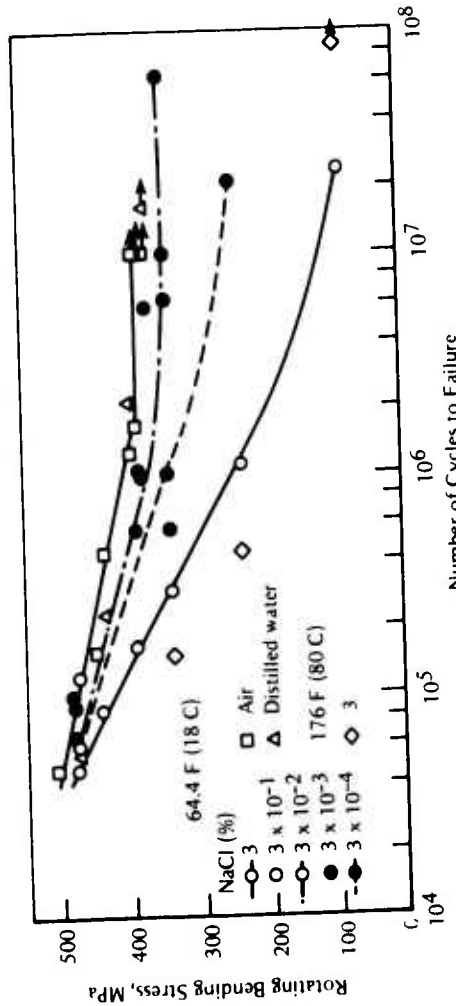
FIGURE 97. Corrosion-Fatigue Strength of 13 Cr Steel Specimens in Various Concentrations of NaCl Solutions[178]
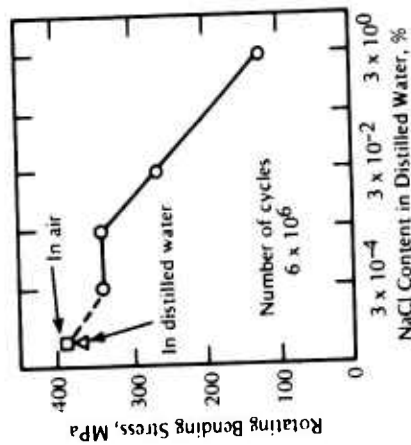
FIGURE 99. Influence of NaCl Concentrations on Corrosion-Fatigue Strength of 13 Cr Steel Specimens at 6 x 10^6 Cycles to Failure[178]

approximately 25 percent of the fatigue limit in air. Corrosion-fatigue strength in the long-life range on the notched specimen under the same environment was not much different from that of the smooth specimen. Both notched and smooth specimens showed the same nominal fatigue strength in both solutions of NaCl at both 140 and 176 F (60 C and 80 C).

In a further investigation of the 13Cr stainless steel (SUS 410J1), Ebara et al[179] studied the effects of (a) aeration and deaeration, (b) stress concentration, and (c) surface roughness on corrosion fatigue in NaCl solutions. The corrosion-fatigue strength of the 13Cr steel in air and in aerated and deaerated 3 percent NaCl aqueous solution at 176 F (80 C) is shown in Figure 103. The corrosion-fatigue strength at 5×10^7 cycles in aerated 3 percent NaCl aqueous solution is 13 ksi (88 MPa), which is about one-fourth the fatigue limit 53 ksi (368 MPa) in air. The comparable corrosion-fatigue strength in deaerated 3 percent NaCl aqueous solution is 38 ksi (265 MPa), which is about 3 times higher than the strength in aerated solutions. The degree of decrease of fatigue strength in deaerated solutions compared with the decrease in fatigue limit in air is about 30 percent. Thus, the detrimental effect of oxygen is large. Although corrosion pits were observed at the crack-initiation sites in both aerated and deaerated solutions, the corrosion was more severe in aerated solutions, as evidenced by the buildup of rust on the samples.

For the experiments on the influence of stress concentration factor (K_t) and surface roughness, Wöhler-type rotating bending fatigue testing machines were used. The effect of stress concentration factor on fatigue strength in air and in 3 percent NaCl solution is shown in Figure 104. Considering the fatigue limits, stress concentration had a significant effect in air, but only a slight effect in 3 percent NaCl solution. The corrosion-fatigue strengths in air and in 3 percent NaCl as a function of stress concentration factor are shown in Figure 105. From these two figures, it can be seen that corrosion-fatgue strengths (K_t = 2.6 and K_t = 3.3) in these two media are almost equal in the range 10^6 to 10^8 cycles.

The relation between stress concentration factor (K_t) and fatigue notch factor (K_f) in air and 3 percent NaCl aqueous solution (N = 5×10^7 cycles) is shown in Figure 106. It is clear from the figure that $K_f \simeq K_t$ in air, but $K_f < K_t$ in the small-K_t range in 3 percent NaCl aqueous solution. When $K_t > 2.5$, K_f was almost constant at a value $K_f \simeq 2$. The authors note that the influence of stress concentration depends upon the corrosive environment.

The corrosion-fatigue-test results for the specimens with different surface roughness in the air and 3 percent NaCl aqueous solution at room temperature are shown in Figure 107. In both environments, the difference in corrosion-fatigue strength due to difference in surface roughness to the extent of 5 to 13 μ was not significant. Figure 108 shows the effect of surface roughness on the corrosion-fatigue-test results in a 3 percent NaCl solution at 176 F (80 C). Round specimens 0.39 in. (10 mm) in diameter were used for the tests. The fatigue strength was slightly decreased in 3 percent NaCl solution at a surface roughness of 1 μ as compared with that at 15 μ. Overall, these results indicate that surface roughness does not greatly affect the fatigue life of 13Cr stainless steel in seawater.

Data on fatigue-crack-growth rate (da/dN) were generated for Type 403 (12 percent Cr) stainless steel blading material in various marine turbine environments.[180] Tests were conducted in air, distilled water, seawater, and sulfurous acid at 75 F (23.9 C) and 200 F (93 C) and in high and low (40 ppm to < 1 ppm) oxygen content steam at 212 F (100 C). Very low crack-growth-rate data (da/dN = 10^{-9} in./cycle) were also generated in air, steam, and brine-saturated-steam environments. All tests were conducted with compact tension (CT) specimens under constant load amplitude conditions, and the results were expressed in terms of fracture mechanics parameters.
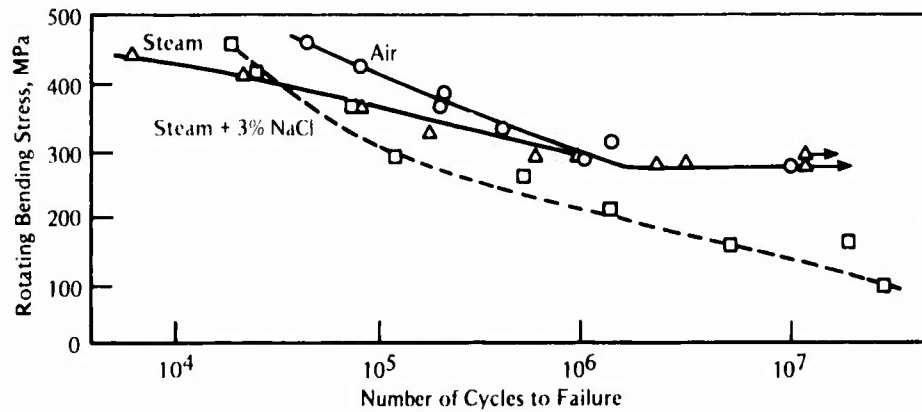
FIGURE 101. Corrosion-Fatigue Strength for 13 Cr Steel in Steam and Steam Plus 3 Percent NaCl Environment[178]
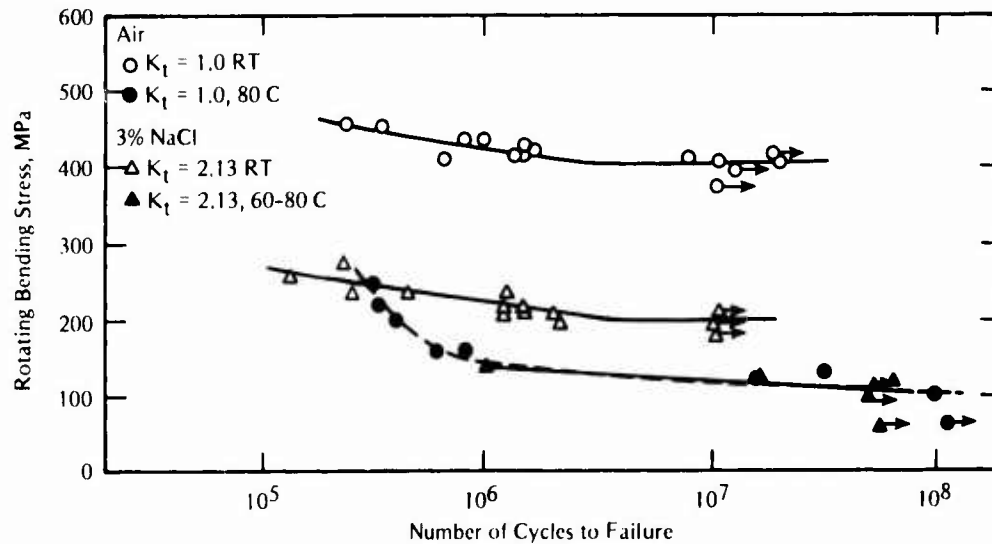
FIGURE 102. Corrosion-Fatigue Strength for 13 Cr Steel in 3 Percent NaCl Solutions at 140 and 176 F (60 and 80 C)[178]
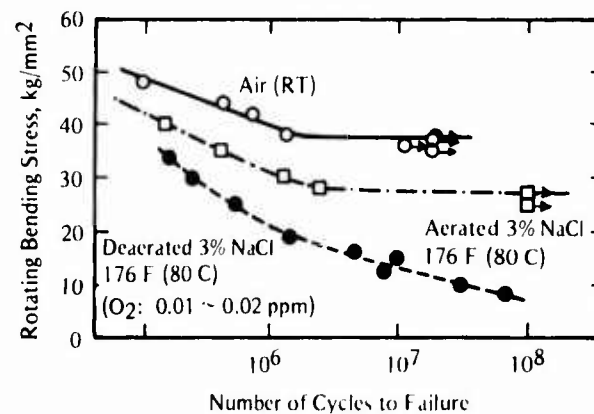
FIGURE 103. Corrosion Fatigue Strength of 13Cr
Steel in Air and in Aerated and Deaerated 3 Percent
NaCl Solution at 176 F (80 C)[179]
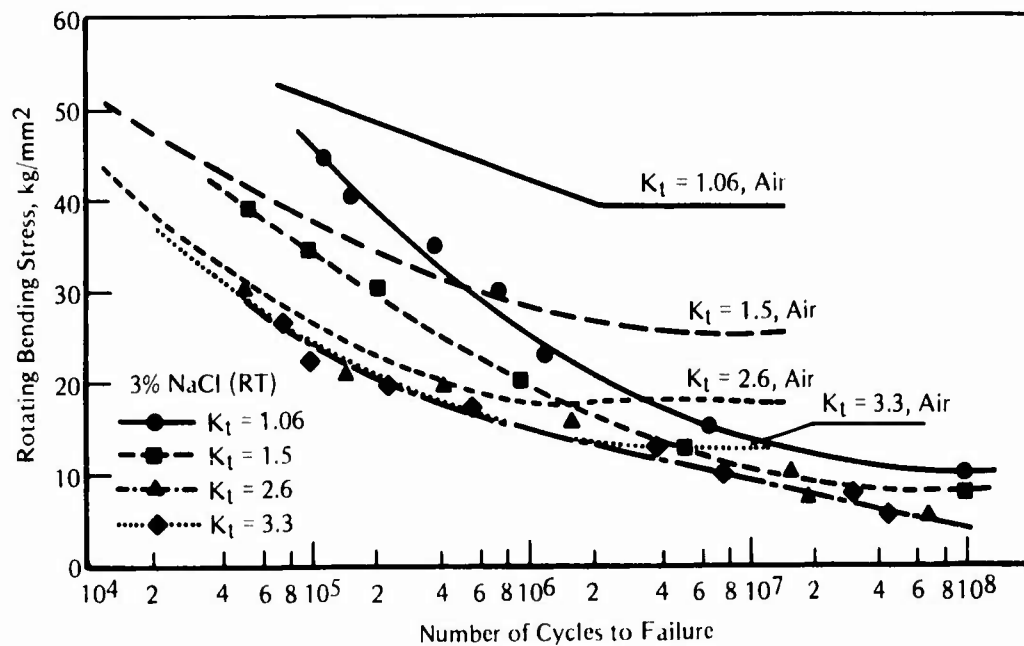
FIGURE 104. Influence of Stress Concentration Factor (K_t) on Corrosion-Fatigue Strength in Air and in 3 Percent NaCl Aqueous Solution[179]
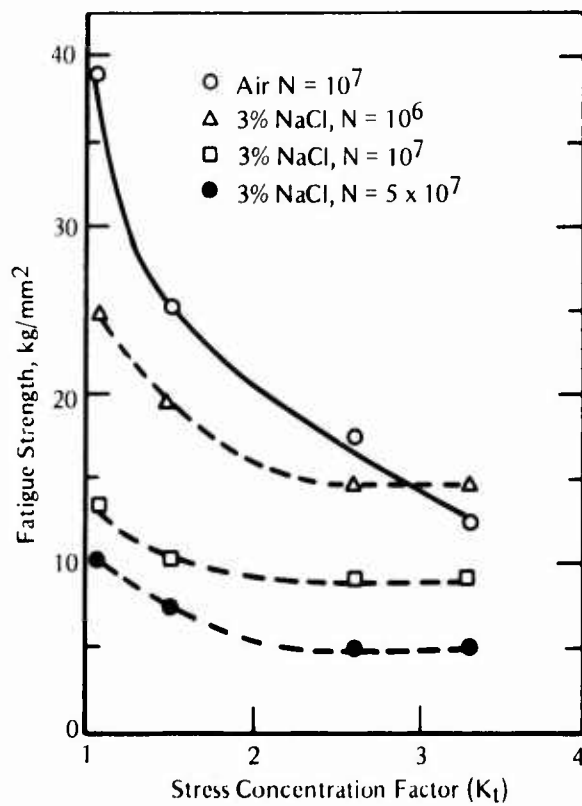
FIGURE 105. Relation Between Stress Concentration Factor and Fatigue Strength in Air and in 3 Percent NaCl Aqueous Solution[179]
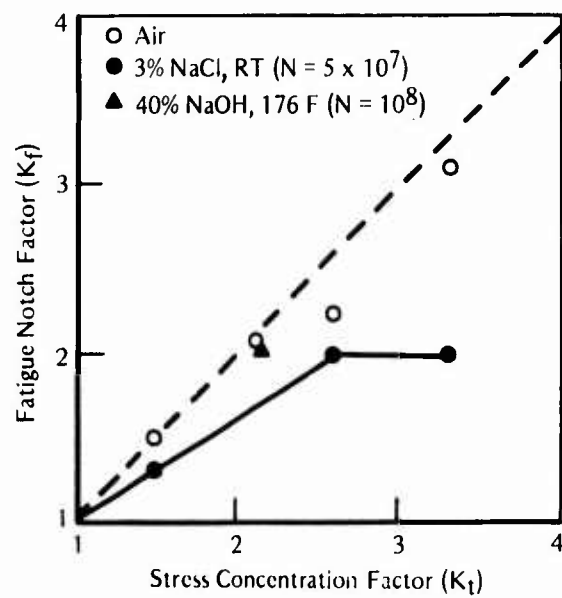
FIGURE 106. Relation Between Stress Concentration Factor and Fatigue Notch Factor[179]
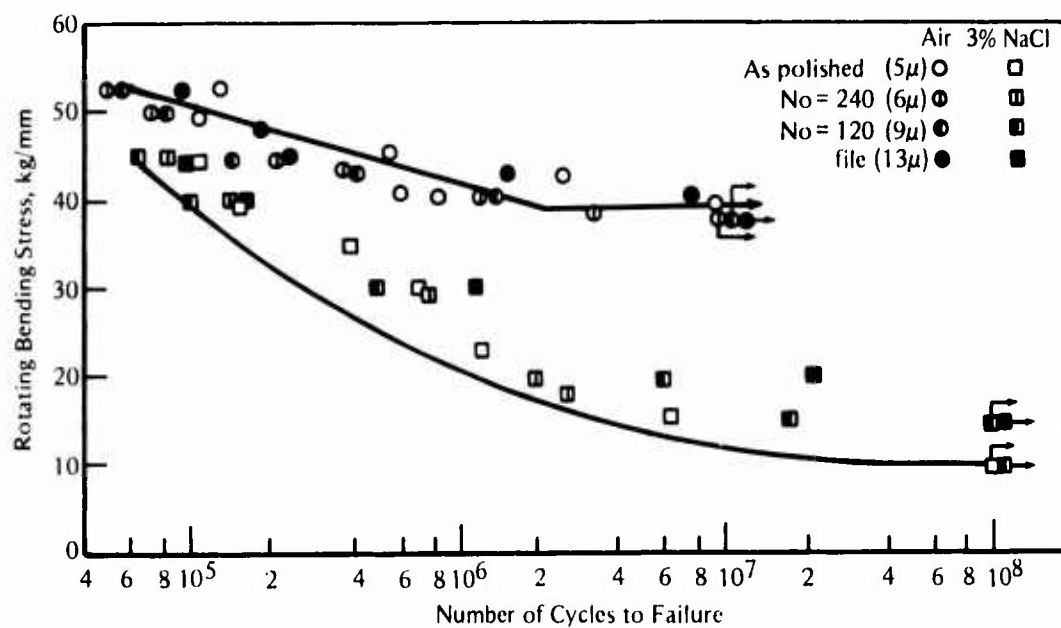
FIGURE 107. Influence of Surface Roughness on Corrosion-Fatigue
Strength in Air and in 3 Percent NaCl Aqueous Solution at Room
Temperature[179]
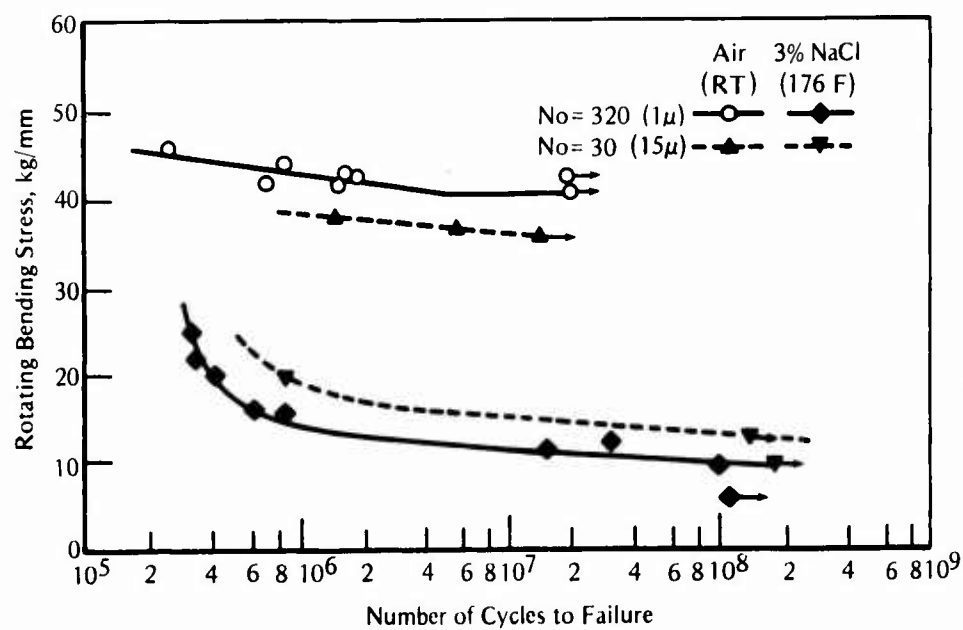
FIGURE 108. Influence of Surface Roughness on Corrosion-Fatigue
Strength in Air and in 3 Percent NaCl Aqueous Solution at 176 F (80 C)[179]

Fatigue-crack-growth rates of Type 403 stainless steel in seawater at room temperature and in seawater and distilled water at 200 F are presented in Figures 109 and 110, respectively. At room temperature the results of tests in seawater and distilled water fell within the same scatterband established for air tests. Very little data scatter was encountered in the tests. At 200 F (93 C) the fatigue-crack-growth rates in seawater and distilled water were essentially identical, but they were lower than that in air. The effects of various marine turbine environments on the fatigue-crack-growth rates are summarized in Figure 111.

The following conclusions were drawn from the study by Clark.[180] The fatigue-crack-growth rates for Type 403 stainless steel blading material conform to the generalized fracture mechanics crack growth rate law where

$$\frac{da}{dN} = C_o\, \Delta K^n \quad.$$

The room-temperature fatigue-crack-growth rates for Type 403 stainless steel tested in air, distilled water, seawater, and sulfurous acid at pH levels of 3 and above are essentially identical and can be summarized by the crack-growth-rate equation:

$$\frac{da}{dN} = 1.6 \times 10^{-9}\, \Delta K^{2.4}\ (\text{in./cycle, ksi } \sqrt{\text{in.}}).$$
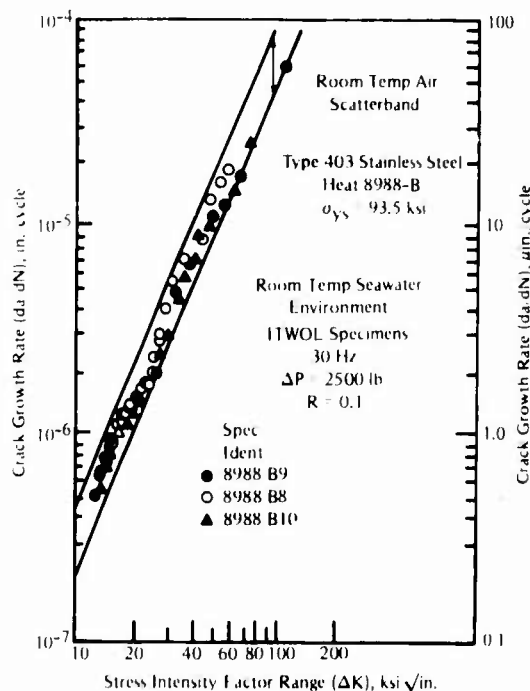
FIGURE 109. Fatigue-Crack Growth Rate of Type 403 Stainless Steel (Room Temperature — Seawater Environment)[180]
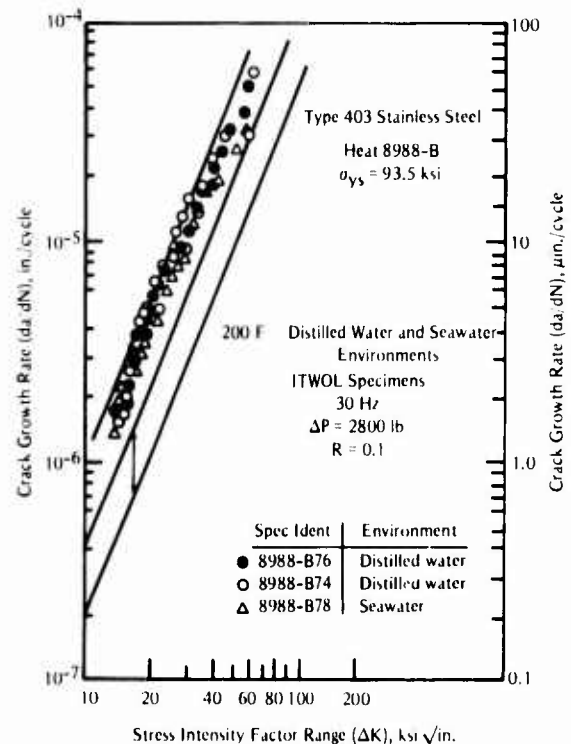
FIGURE 110. Fatigue-Crack Growth Rate of Type 403 Stainless Steel in 200 F Distilled Water and Seawater Environments
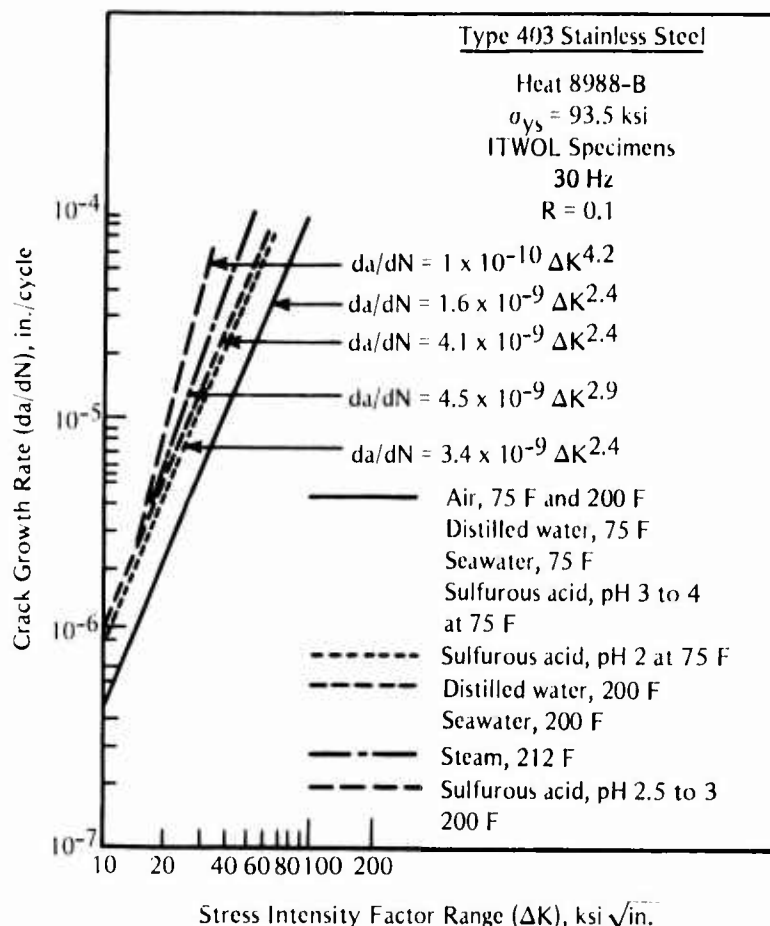
FIGURE 111. Effect of Various Marine Turbine Environments on the
Fatigue-Crack Growth Rate of Type 403 Stainless Steel[180]

At 200 F, however, the water (distilled and seawater), steam, and sulfurous acid environments increased the rate of fatigue crack growth in Type 403 stainless steel by factors of approximately 2.5, 3, and 5, respectively, over that in air.

Abrego and Begley[181] investigated the fatigue-crack-growth behavior of Type 403 (12Cr) stainless steel in aqueous solutions at 212 F (100 C). Their results for tests in sodium chloride solutions are summarized here. Tests were run at two concentrations of sodium chloride, 1 M and 0.01 M at pH 2, 7, and 10.

Figure 112 shows the effect of test frequency on the fatigue-crack-growth rates in 0.01 M NaCl, pH 10, 212 F (100 C). These results are similar to the crack growth rates obtained in water. The sample cycled at 40 Hz had a crack growth rate faster than that in air. At $\Delta K \geq 13.65$ ksi $\sqrt{in}$. (15 MPa $\sqrt{m}$), crack growth rates increased with decreasing frequency. This frequency effect was similar to the water results. The threshold stress intensity factor range, ΔK_{th}, obtained in 0.01 M sodium chloride, 212 F (100 C), pH 2 and 10 was identical to that obtained in water. Solution pH had little influence on ΔK_{th}.

Figure 113 shows the fatigue-crack-growth rates in 1 M sodium chloride at 10 Hz, pH 2, 7, and 10 at 212 F (100 C). The crack growth rate in 1 M sodium chloride was almost identical to that obtained in water, which also coincided with the growth rates obtained in 0.01 M NaCl,
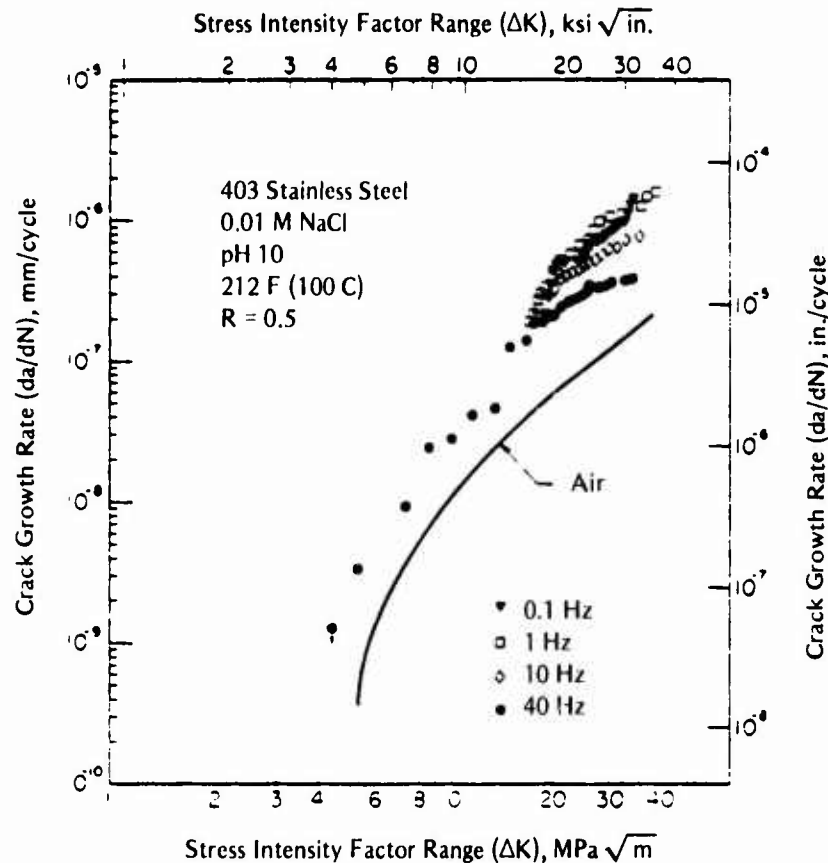
FIGURE 112. Fatigue-Crack Growth Rates as a Function of ∆K
for 403 Stainless Steel Tested at Various Frequencies[181]

pH 10, 212 F (100 C). Consequently, the detrimental effects of the chloride anion concentration and solution pH were no worse than those produced by boiling water.

The authors concluded that NaCl either of low (0.01 M) or of high (1 M) concentration does not produce a fatigue-crack-growth rate either lower or higher than that produced by water alone. The anions did produce a shift in the open-circuit potential, which was pH dependent, but this shift was not significant in terms of fatigue-crack-growth rates.

Collins[182] investigated the effect of residual magnetism on corrosion-fatigue properties of Type 410 stainless steel compressor blades. Residual magnetism was beneficial in improving the corrosion-fatigue strength of Type AISI-410 tested in a synthetic seawater environment. The corrosion-fatigue strength of magnetized blades was improved 56 percent, and survival time was increased 37 percent as compared with that of nonmagnetized blades. The improvement was attributed to a reduction in the rate at which dislocations cross slip to broaden slip planes which are preferentially attacked by the corrosion media. X-ray diffraction studies confirmed an interaction of dislocations and magnetic domain walls.
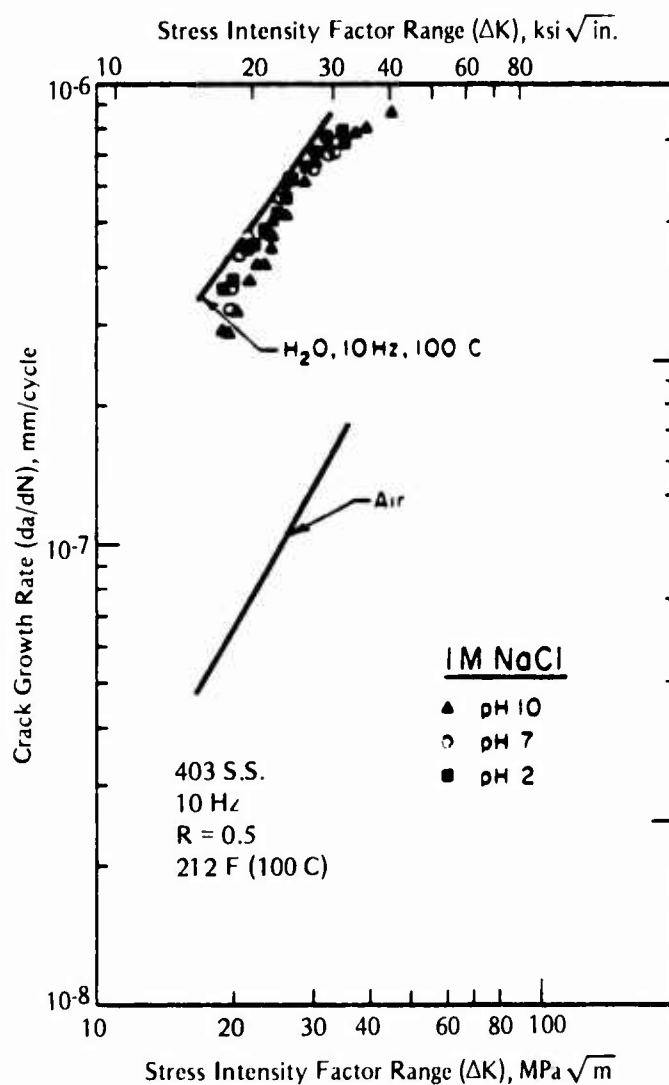
FIGURE 113. Fatigue-Crack Growth Rates as a Function
of ΔK for 403 Stainless Steel Tested at 10 Hz[181]

Austenitic, Duplex, and Cr-Mo
Ferritic Stainless Steels

The nominal compositions of stainless steels discussed in this section are presented in Table 10. Austenitic stainless steels were primarily of the following types: AISI 304, AISI 316, and the titanium-stabilized grades. Several austenitic/ferritic, duplex stainless steels were investigated. Only limited data were available for the Cr-Mo ferritic stainless steels. Nearly all of the data reported were for fatigue life, and only a few studies measured crack growth.

Sedricks and Money[5] evaluated AISI 304 and 316 stainless steels and the low-carbon grades AISI 304L and 316L in seawater using smooth cantilever beam specimens rotating at 1450 rpm (24.2 Hz). They defined a corrosion-fatigue strength (CFS) as the lowest alternating stress at

TABLE 10. Nominal Chemical Composition of Austenitic, Duplex, and Cr-Mo Ferritic Stainless Steels

| | Major Alloying Elements, wt % | | | | |
Alloy	Cr	Ni	Mo	Other	Reference
AISI 304	19	10	—	2 Mn, 0.08 C	5
AISI 304 L	19	10	—	2 Mn, 0.03 C	5
AISI 316	18	12	2.5	2 Mn, 0.08 C	5
AISI 316 L	18	12	2.5	2 Mn, 0.03 C	5
Z6 CND 17.12	17	10.7	2.2	1.9 Mn, 0.55;	177, 183
Z5 CNDT 17.12	16.8	11.6	2.2	0.4 Ti, 1.6 Mn, 0.6 Si	177, 183
Z3 CNDU 21.7	21.1	6.2	2.4	0.05 N, 1.7 Mn, 0.5 Si	177, 183
Z0 CD 26.1	26.2	0.1	1.0	0.007 N, 0.001 C, 0.21 Si	177, 183
X2CrNiN1810	18.2	10	0.4	0.14 N, 1.7 Mn, 0.5 Si	184
X2CrNiMoN1813	17.4	12.5	2.4	0.11 N, 2 Mn, 0.5 Si	184
X3CrNiMoN17135	16.8	13.5	4.2	0.15 N, 1.9 Mn, 0.4 Si	184
X2CrNiMoN225	23	5.5	2.9	0.13 N, 1.7 Mn, 0.4 Si	184
X10CrNiTi189	17.3	9.7	0.5	0.5 Ti, 1.9 Mn, 0.5 Si	184
X10CrNiMoTi1810	17.6	11.8	2.2	0.5 Ti, 1.9 Mn, 0.5 Si	184
ETi199nC26	18.9	9.4	—	1 Si, 0.7 Mn,	184
EKb19153Mn8N20	18.1	15.3	2.8	0.3 S; 7.5 Mn, 0.1 N	184
ETi19123nC26	17.7	11.8	2.6	1 Si, 0.9 Mn;	184
EKb18171nC20	17.4	16.5	4.1	0.2 Si, 2.2 Mn	184
EKb257MoNb20	23.0	8.1	1.4	0.3 S, 0.7 Mn, 0.1 Nb	184
ETi2283nC26	23.8	9.0	3.2	1 Si, 0.8 Mn, 0.17 N	184
AISI 316	16.8	11.6	2.4	1.7 Mn, 0.4 Si	185
Ferralium	25	5	2.5	3 Cu, 0.2 N	186
0Cr18Ni10Ti	18	10	—	Ti stabilized	187

which an alloy survived 100 megacycles in a test lasting 48 days. Their results for these austenitic stainless steels are presented in Figure 114. Data points for a mild steel and Alloy 800 were included for comparison. There was little distinction among the corrosion-fatigue strengths of the austenitic stainless steels. Generally the behavior was erratic and wide scatter in the data was observed. The erratic behavior was ascribed to the tendency for these alloys to pit in low-velocity seawater. The authors suggest that the corrosion-fatigue strength increases with increasing resistance to pitting corrosion.

Amzallag and his co-workers[177,183] studied corrosion-fatigue-crack initiation and growth in four types of stainless steels: two types of austenitic steels (Z6 CND 17.12 and titanium-stablized Z6 CNDT 17.12), a ferritic steel (Z0 CD 26.1), and an austenitic/ferritic duplex steel (Z3 CNDU 21.7). Rotating-bending tests at 50 Hz were used to produce fatigue life curves with corrosion-fatigue strengths being measured at 3×10^7 cycles. Fatigue-crack-growth tests were conducted under sinusoidal tension-tension loading (at R = 0.1) at frequencies from 0.5 to 20 Hz. Results of rotating-bending tests are summarized in Table 11. The increasing order of resistance to corrosion fatigue was the austenitic stainless steel (low), austenitic-ferritic steel, and ferritic steel (high). This ranking is attributed to the stainless steels being passive under the test conditions and having a protective film to prevent corrosion. The ferritic steel, which had the most protective film and the passive film that would re-form most rapidly, was the least damaged by the 3 percent NaCl. The authors concluded that resistance to corrosion fatigue in
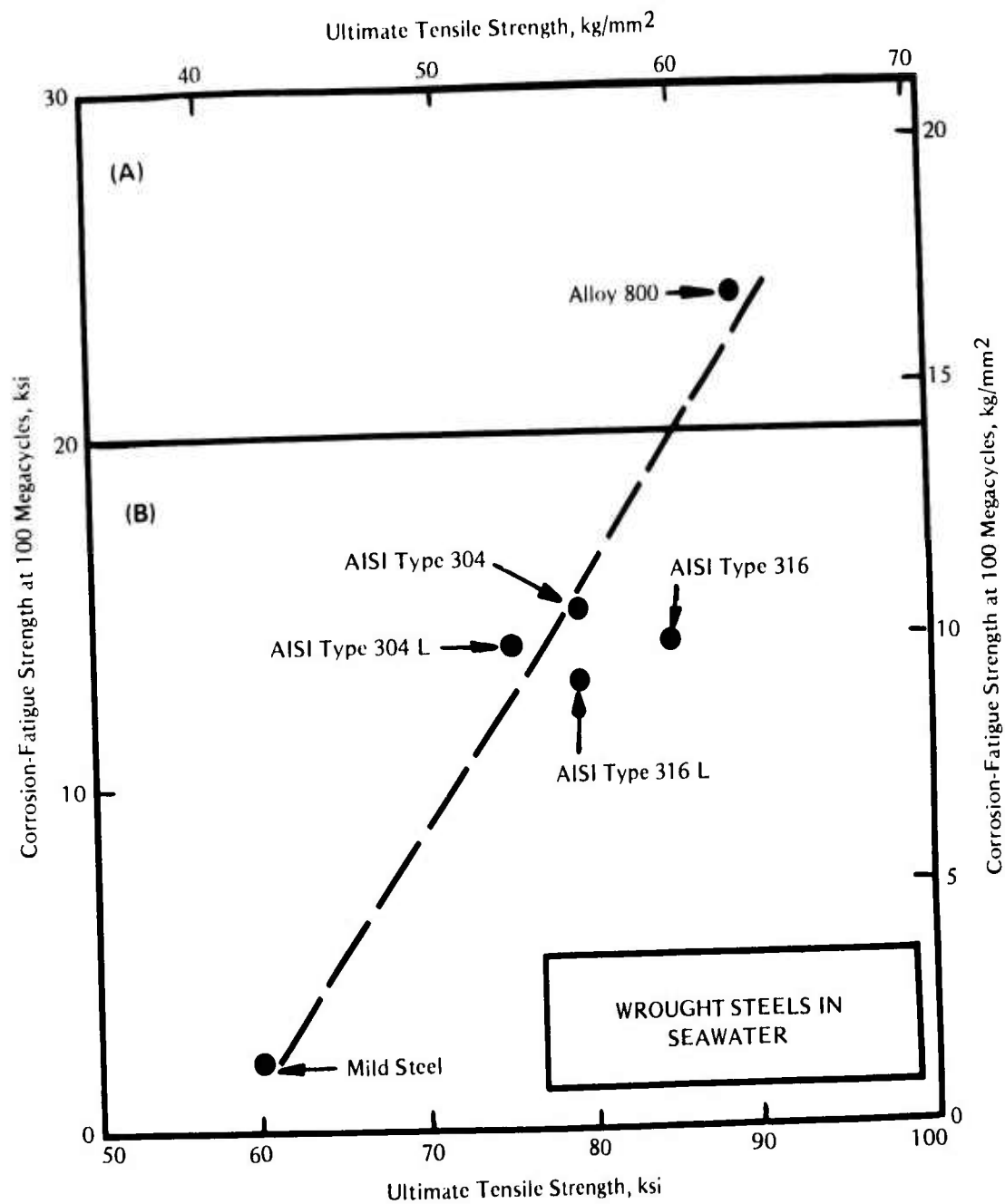
FIGURE 114. Corrosion-Fatigue Strength of Austenitic Stainless Steels, Mild Steel, and Alloy 800 as a Function of Ultimate Tensile Strength[5]

TABLE 11. Corrosion-Fatigue Strength of Stainless Steels in Air and in 3 Percent NaCl at 3×10^7 Cycles [177]

Alloy	Air		3% NaCl Solution (pH = 6)	
	Fatigue Limit, ksi (MPa)	Fatigue Limit / Tensile Strength	Tensile Strength, ksi (MPa)	Corrosion-Fatigue Strength / Tensile Strength
Z6 CND 17.12	47 (320)	0.57	34.6 (235)	0.42
Z6 CNDT 17.12	49 (335)	0.52	40 (270)	0.42
Z3 CNDU 21.7	58.8 (400)	0.62	42.6 (290)	0.45
Z0 CD 26.1	51.5 (350)	0.74	45.6 (310)	0.65

the passive state depends on both the resistance to fatigue in air (mechanical properties) and the ability to form and maintain a protective film in the corrosive solution (corrosion resistance).

The effect of imposed potential on the corrosion-fatigue behavior of the ferritic steel, Z3 CNDU 21-7, is shown in Figure 115. The results of rotating-bending tests in 3 percent NaCl at open circuit and with imposed potentials of 0.2, 0.05, and 0 V SCE are presented. At a potential where significant localized corrosion was observed (0.2 V SCE), the steel was severely damaged by corrosion fatigue. At 0.05 V SCE near the open-circuit potential, localized corrosion is still possible and could be accelerated by applied stress because of damage to the passive film. A significant improvement in corrosion-fatigue resistance was observed at a potential of 0 V SCE, where the passive film is quite stable and re-forms rapidly when damaged.

Crack growth rates (da/dN) in air as a function of stress intensity factor (ΔK) for the four stainless steels are shown in Figure 116. The curves for the two austenitic steels (A and B) were almost identical. For values of ΔK greater than 27.30 ksi $\sqrt{in.}$ (30 MPa $\sqrt{m}$), the lowest crack growth rate was observed for the ferritic steel (D), followed by the austenitic-ferritic steel (C) and the austenitic steels. For austenitic steels tested at a frequency of 20 Hz, the corrosive solution had no influence on crack growth rate. The da/dN values were identical to those obtained in air. For the austenitic-ferritic steel at high values of ΔK, a significant increase in crack growth rate was observed. As shown in Figure 117, the effect was even greater at the lower frequency of 0.5 Hz. Similar damage by the corrosive solution was observed for the ferritic steel (Figure 118). The authors rationalize these results on the basis of an acceleration of anodic dissolution at the crack tip under the effect of increasing applied stress. The degree of protection and stability of passive films were the primary corrosion parameters in rotating beam tests for crack initiation; however, the anodic dissolution and repassivation of films were the primary corrosion parameters in the crack growth tests.

Bock[184] investigated the corrosion-fatigue behavior of nitrogen-alloyed, austenitic and ferritic-austenitic stainless steels. The alloys were tested in 3 percent NaCl solution at 104 F (40 C) and over a range of pH and redox potential. The behavior of welding rods of matching composition was compared with that of the wrought alloys. The work was done to support materials selection for heat exchangers in corrosion solutions.

A matrix of tests was performed. Parameters studied were pH, aeration versus deaeration, smooth versus notched specimens, and rotation frequency. The results of rotating beam tests for the wrought alloys in pH 1, 3, and 7 NaCl solutions and in air are summarized in Table 12.
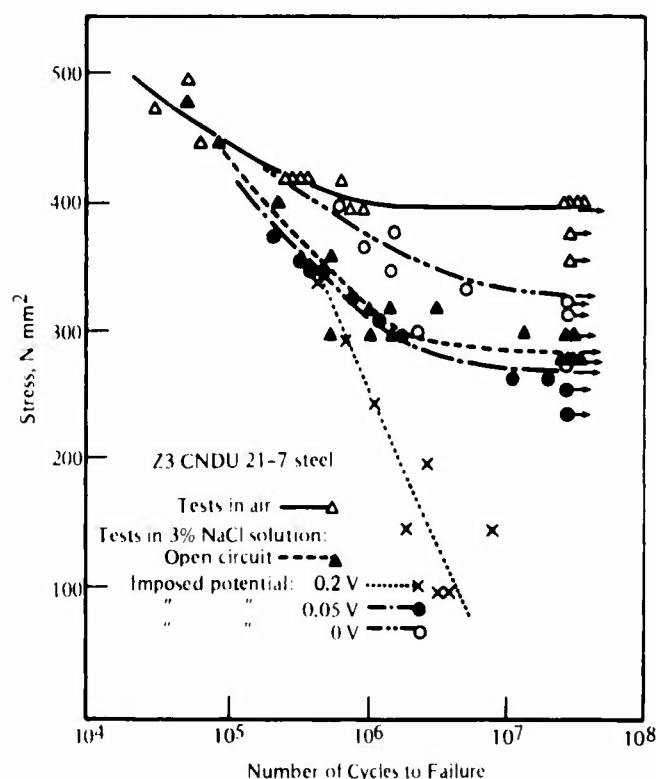
FIGURE 115. Effect of Applied Potential on Corrosion–Fatigue Behavior of a Ferritic Stainless Steel in 3 Percent NaCl[177]
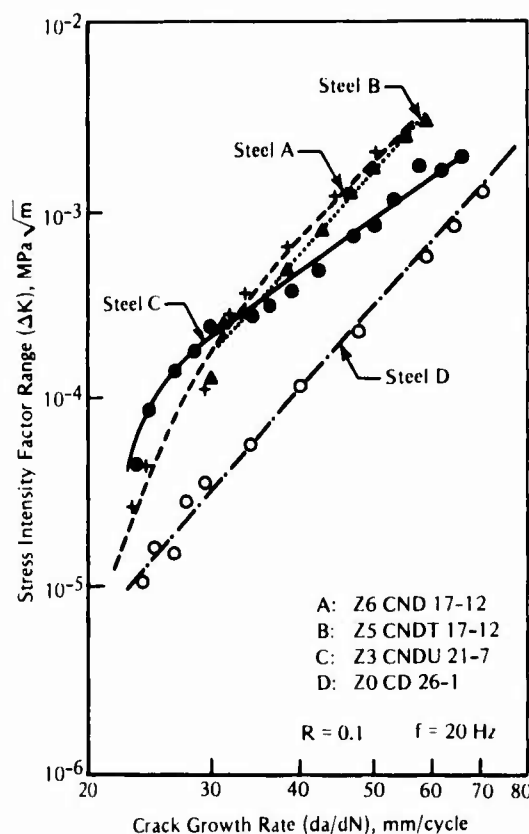
FIGURE 116. Crack Growth Rates in Air for Two Austenitic Stainless Steels (A and B), an Austenitic–Ferritic Steel (C), and a Ferritic Steel (D)[177]

Lower pH (more acidic) solutions were more damaging than the pH 7, neutral solution. At pH 7, the fatigue resistance was essentially the same as that in air or slightly lower. The fatigue resistance of notched specimens was lower than that of smooth specimens; however, similar trends were observed for notched or smooth specimens in the corrosive solutions. Deaeration increased the corrosion-fatigue damage, which is to be expected for an alloy that derives corrosion resistance from a passive protective film. The austenitic-ferritic steel, X2CrNiMoN225, was the most fatigue resistant.

Data on corrosion-fatigue strength at 2×10^7 cycles as a function of test frequency (10 to 200 Hz) are summarized in Table 13. No major effect of frequency was observed, which is to be expected for this fairly high range of cyclic frequency. The results for weld rods are summarized in Table 14. In general the effects of the corrosive solution were similar for weld rod and the wrought steels.

Journeaux et al[185] examined the effect of prior corrosion on the fatigue resistance of an AISI-316 steel in air. Specimens were exposed to a 0.5 M NaCl solution, and pitting was stimulated by applied currents. Effects of the pits on fatigue resistance are shown in Figure 119. Wöhler-type rotating beam tests in air resulted in lower fatigue strength of the pitted specimens over the entire range of cycles.
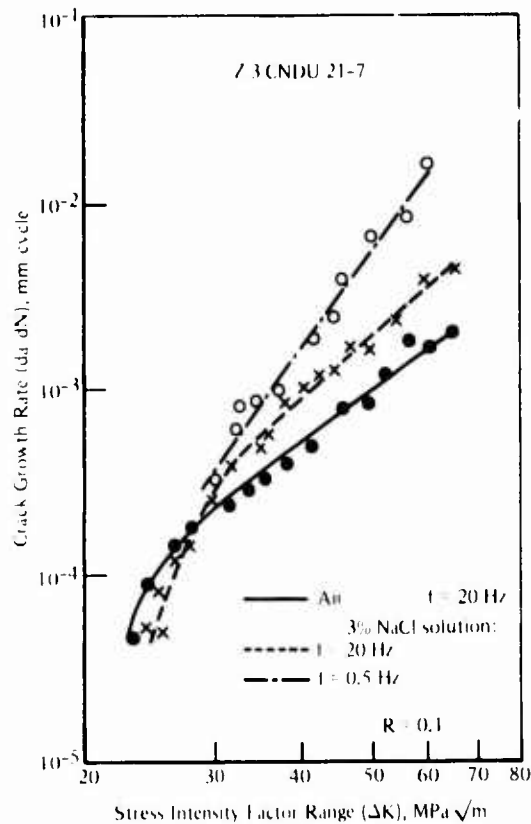
FIGURE 117. Crack Growth Rates in 3 Percent NaCl for an Austenitic–Ferritic Stainless Steel[177]
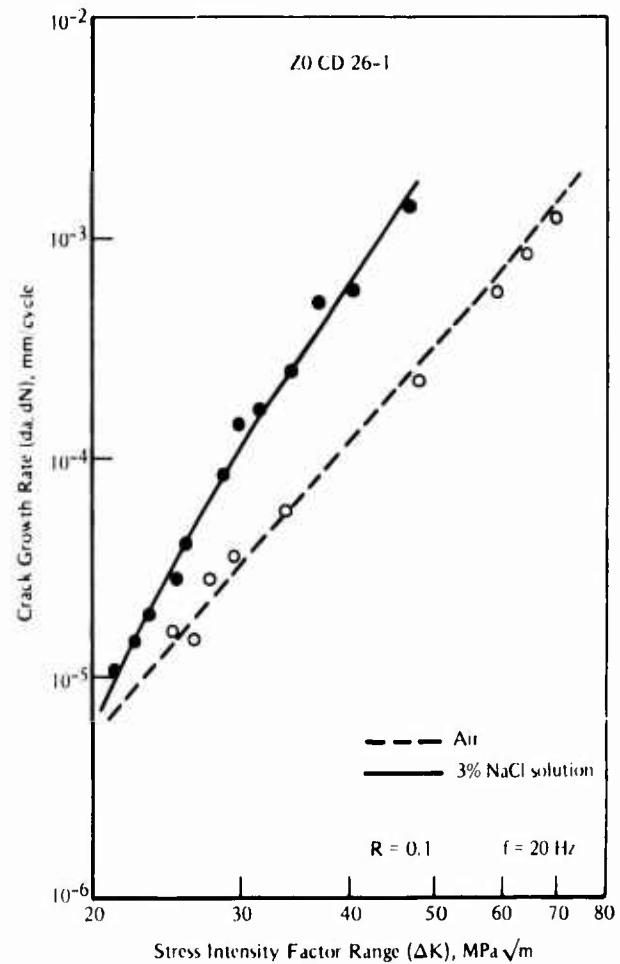
FIGURE 118. Crack Growth Rates in 3 Percent NaCl for a Ferritic Stainless Steel[177]
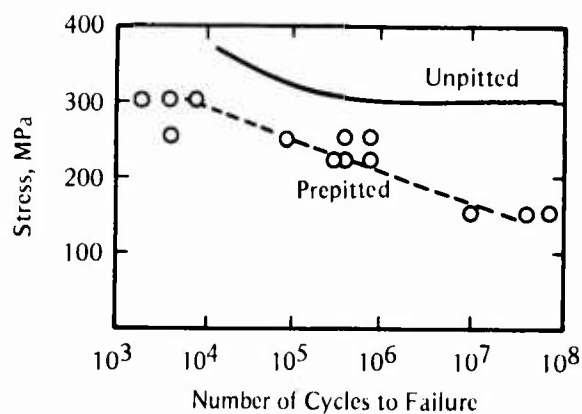
FIGURE 119. Effect of Prior Corrosion (Pits) on Corrosion-Fatigue Strength of AISI 316 Stainless Steel in Air[185]
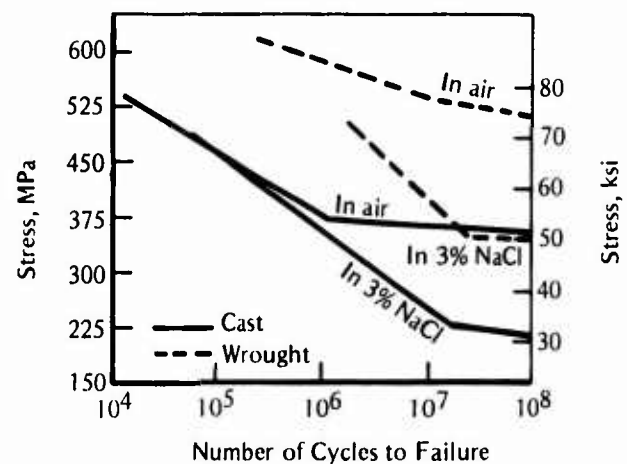
FIGURE 120. Corrosion-Fatigue Strength of Ferralium in Air and Seawater[186]

TABLE 12. Effect of pH on Corrosion-Fatigue Strength of Stainless Steels at 100 Hz in 3 Percent NaCl Solution at 104 F (40 C) [184]

Alloy	Type of Specimen	pH 1 Aerated	pH 1 Deaerated	pH 3 Aerated	pH 3 Deaerated	pH 7 Aerated	pH 7 Deaerated	In Air
					Corrosion-Fatigue Strength[a], ksi (MPa)			
X2CrNiN 1810	Smooth	2.0 (148)	6.8 (47)	29 (200)	23.9 (165)	42 (290)	39 (269)	46.4 (320)
	Notched	6.8 (47)	5.8 (40)	10.9 (75)	6.7 (46)	18.7 (129)	16 (110)	23.2 (160)
X10CrNiTi 189	Smooth		18.4 (127)		31.8 (219)		46 (317)	46.4 (320)
	Notched		9.9 (68)		23.2 (160)		27 (186)	29 (200)
X2CrNiMoN 1813	Smooth	21 (145)	21 (145)	32 (220)	32 (220)	37.7 (260)	39.9 (275)	44.2 (305)
	Notched	12 (83)	12 (83)	17.7 (122)	18.9 (130)	20.2 (139)	21.8 (150)	32 (220)
X10CrNiMoTi 1810	Smooth		32 (220)		30.7 (260)		47.9 (330)	47.6 (328)
	Notched		19 (131)		33.2 (229)		34.8 (240)	30.5 (210)
X3CrNiMoN 17135	Smooth	20 (138)	15.8 (109)	39 (269)	38.3 (264)	42.8 (295)	36.3 (250)	38.9 (268)
	Notched	9.3 (64)	10.1 (70)	12.6 (87)	12.6 (87)	28.3 (195)	28.3 (195)	27.4 (189)
X2CrNiMoN 225	Smooth	30.5 (210)	27.6 (190)	53 (365)	47.8 (330)	61 (420)	61.7 (425)	66.5 (458)
	Notched	22.4 (154)	17.8 (123)	30.5 (210)	30.5 (210)	36.4 (251)	33.4 (230)	34.8 (240)

(a) At 2×10^7 cycles

TABLE 13. Effect of Frequency on the Corrosion-Fatigue Limit of Stainless Steels in 3 Percent NaCl Solution at 104 F (40 C) [177]

Alloy	Frequency, Hz	Corrosion-Fatigue Limit[a], ksi (MPa) Air	pH 3
X2CrNiN 1810	200	43.5 (300)	
	100	46.4 (320)	23.9 (165)
	10.7	47.9 (330)	30.5 (210)
X10CrNiTi 189	200	46.4 (320)	
	100	46.4 (320)	31.8 (219)
	10.7	47.9 (330)	30.5 (210)
X2CrNiMoN 1813	200	46 (317)	
	100	44.3 (305)	32 (220)
	10.7		
X10CrNiMoTi 1810	200	47.8 (329)	
	100	47.6 (328)	37.7 (260)
	10.7	50.6 (349)	
X3CrNiMoN 17135	200	43.5 (300)	
	100	38.9 (268)	38.3 (264)
	10.7	46.4 (320)	34.8 (240)
X2CrNiMoN 225	200	64.6 (445)	--
	100	66.5 (458)	47.9 (330)
	10.7	66.5 (458)	47.9 (330)

(a) Smooth specimens in deaerated solution after 2×10^7 cycles.

TABLE 14. Corrosion-Fatigue Strength of Stainless Steel Weld Rods in 3 Percent NaCl Solution
at 104 F (40 C) [177] , 100 Hz

Weld-Rod Alloy	Type of Specimen	Type of Environment	pH	Fatigue Strength[a], ksi (MPa)
EKb 18174nC 20+	Smooth	Deaerated	Air	30.5 (210)
EKb 257MoNb 20+	Smooth	Deaerated	1	31.5 (217)
EKb 257MoNb 20+	Smooth	Aerated	1	34.7 (239)
EKb 257MoNb 20+	Smooth	Deaerated	3	50.8 (350)
EKb 257MoNb 20+	Smooth	Aerated	3	50.8 (350)
EKb 257MoNb 20+	Smooth	Deaerated	7	62.7 (432)
EKb 257MoNb 20+	Smooth	Aerated	7	63.9 (440)
EKb 257MoNb 20+	Smooth	Deaerated	Air	56.6 (390)
EKB 18174nC 20+	Smooth	Deaerated	1	21 (145)
EKb 18174nC 20+	Smooth	Aerated	1	22.3 (154)
EKb 18174nC 20+	Smooth	Deaerated	3	29 (200)
EKb 18174nC 20+	Smooth	Aerated	3	29 (200)
EKb 18174nC 20+	Smooth	Deaerated	7	30.5 (210)
EKb 18174nC 20+	Smooth	Aerated	7	30.5 (210)
EKb 18174nC 20+	Smooth	Deaerated	Air	30.5 (210)
ETi 2283nC 26	Smooth	Deaerated	1	31.5 (217)
ETi 2283nC 26	Smooth	Deaerated	3	49.3 (340)
ETi 2283nC 26	Smooth	Deaerated	7	58 (400)
ETi 2283nC 26	Smooth	Deaerated	Air	59.5 (410)

(a) After 2×10^7 cycles.

The corrosion-fatigue behavior of Ferralium, a duplex ferritic/austenitic stainless steel, was reported by Richardson et al [186] The fatigue-life curves for the wrought and cast alloy in air and in seawater are shown in Figure 120. Exposure to seawater significantly reduced the fatigue strength of the alloy in either the wrought or the cast form.

Karpenko et al[187] investigated the corrosion-fatigue strength of a 0Cr18Ni10Ti stainless steel under axial cyclic loads in 3 percent NaCl solution at 446 F (230 C). The fatigue strength at 5×10^6 cycles in tension-compression tests in air and in 3 percent NaCl at 446 F (230 C) was 24 ksi (167 MPa) and 21 ksi (147 MPa), respectively. The full fatigue-life curves are shown in Figure 121. Similar behavior was observed for tension-tension tests, as shown in Figure 122. The fatigue strengths (maximum stress) at 2×10^6 cycles were 57 ksi (392 MPa) in air and 46 ksi (314 MPa) in 3 percent NaCl at 446 F (230 C). This damage from exposure to high-temperature chloride solutions is in contrast to room-temperature results, where no appreciable damage was observed for smooth, austenitic steel specimens.
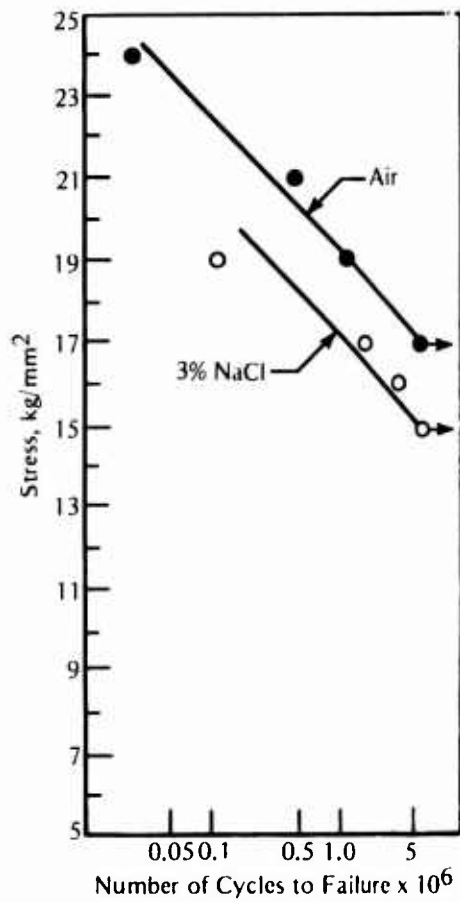
FIGURE 121. Corrosion–Fatigue Behavior of an Austenitic Stainless Steel (0Cr18Ni10Ti) Tested in Tension–Compression in Air and 3 Percent NaCl at 446 F (230 C)[187]
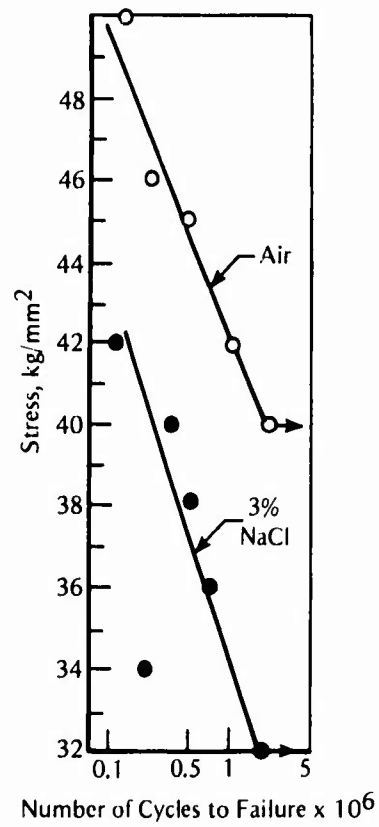
FIGURE 122. Corrosion–Fatigue Behavior of an Austenitic Stainless Steel (0Cr18Ni10Ti) Tested in Tension–Tension in Air and 3 Percent NaCl at 446 F (230 C)[187]

CHAPTER 5
CORROSION-FATIGUE DATA FOR NICKEL, NICKEL ALLOYS, AND COPPER-NICKEL ALLOYS

The corrosion-fatigue data for nickel, nickel alloys, and copper-nickel alloys are summarized in Table 15. The nickel and nickel alloys are listed first, followed by the copper-nickel alloys. For each alloy, the types of corrosion-fatigue data in the reference article are described, along with the type of specimen, loading, and environment. All of these alloys have corrosion resistance superior to that of steel in seawater, and therefore they are used for critical applications where corrosive conditions prevail. The corrosion-fatigue results for these alloys are all presented as fatigue-life (S-N)-curve data. No data on corrosion-fatigue-crack growth were found for these alloys in the literature.

Nickel and Nickel Alloys

Very few corrosion-fatigue data were available for nickel and nickel alloys. In general, these corrosion-resistant alloys exhibit good corrosion-fatigue resistance.

Unalloyed Nickel

McAdam[3] studied fatigue and corrosion of a series of alloy systems. Fatigue tests were conducted using a cantilever-rotating beam type of specimen. The specimens were smooth (unnotched) and the cyclic frequency was 1450 rpm. Fatigue and corrosion-fatigue graphs for unalloyed nickel are shown in Figure 123. Two sets of curves are presented. The curves at the upper right are for cold-rolled nickel which was given a low-temperature anneal [600 F (315 C) for 2 hours] to relieve internal stress with practically no reduction in strength. The curves at the lower left are for a fully annealed nickel [1400 F (760 C) for 1 hour]. The tensile strengths were 131.7 ksi (908 MPa) and 77.6 ksi (535 MPa), respectively. Each of the two families of curves has its own scale for number of cycles to failure, with the decades identified by the numbers above the curves. The stress scale on the ordinate is the same for all curves.

Fatigue behavior in air is indicated by the solid curves in Figure 123, and corrosion-fatigue results in fresh water and saltwater are represented by the broken lines. The saltwater was river water with approximately one-third the salinity of seawater. The most striking effect is that the corrosion-fatigue limits for the strain-hardened and fully annealed nickel are practically the same. Cold working increases the fatigue limit (air) approximately in proportion to the increase in tensile strength; however, cold working had little effect on the corrosion-fatigue limit. This effect was also observed for steel, where composition and heat treatment were found to influence the corrosion-fatigue limit only through their influence on corrosion resistance and not on mechanical properties. The results are nearly identical in fresh water and saltwater.

At high stresses, the corrosion-fatigue plots correspond to the fatigue plots. As the stress level decreases, the fatigue and corrosion-fatigue curves diverge. The curves clearly separate at approximately 1 million and 4 million cycles for the strain hardened and annealed nickels, respectively, at a frequency of 1450 rpm.

123

TABLE 15. Corrosion–Fatigue Data for Nickel, Nickel Alloys, and Copper–Nickel Alloys

Alloy	Condition or Treatment	Tensile Strength (ksi) Ultimate	Yield	Type of Specimen	Type of Loading	Cyclic Frequency	Environment	Types of Data	Notes	References
Nickel	Cold rolled and low anneal (1400 F, 1 hr)	77.6	19.3(a)	Smooth	Rotating cantilever	1450 rpm	Air, fresh water, saltwater(c)	S-N curves 10^4-10^8		3
Nickel	Cold rolled and low anneal (600 F, 2 hr)	131	86(a)	Smooth	Rotating cantilever	1450 rpm	Air, fresh water, saltwater(c)	S-N curves 10^4-10^8		3
IN-120 (Exptl Alloy)		205		Smooth	Rotating cantilever	1450 rpm	Seawater	CFS at 10^8 cycles(b)	Comparison of grain size	5
Inconel 718		189		Smooth	Rotating cantilever	1450 rpm	Seawater	CFS at 10^8 cycles(b)	G.S. = 0.004 in. (0.01 mm)	5
Inconel 718		189		Smooth	Rotating cantilever	1450 rpm	Seawater	CFS at 10^8 cycles(b)	G.S. = 0.003 in. (0.068 mm)	5
Inconel 718		189		Smooth	Rotating cantilever	1450 rpm	Seawater	CFS at 10^8 cycles(b)	G.S. = 0.006 in. (0.152 mm)	5
Inconel 625		149		Smooth	Rotating cantilever	1450 rpm	Seawater	CFS at 10^8 cycles(b)	G.S. = 0.004 in. (0.01 mm)	5
Inconel 625		129		Smooth	Rotating cantilever	1450 rpm	Seawater	CFS at 10^8 cycles(b)	G.S. = 0.003 in. (0.068 mm)	5
Hastelloy C		108		Smooth	Rotating cantilever	1450 rpm	Seawater	CFS at 10^8 cycles(b)		5
Incoloy 800		89		Smooth	Rotating cantilever	1450 rpm	Seawater	CFS at 10^8 cycles(b)		5
Medium Cr-High Ni Alloy		112.3	57.6	Smooth	Rotating cantilever		Air, fresh water, saltwater	S-N curves 10^4-10^8		4
Monel K-500		176		Smooth	Rotating cantilever	1450 rpm	Seawater	CFS at 10^8 cycles(b)		5
Monel	Cold rolled, low anneal	127.2	84.5(a)	Smooth	Rotating cantilever		Air, fresh water, saltwater(c)	S-N curves 10^4-10^8		3
Monel	Cold rolled, full anneal	81.9	28.2(a)	Smooth	Rotating cantilever		Air, fresh water, saltwater(c)	S-N curves 10^4-10^8		3
48Ni-48Cu	Cold rolled, as received	85.8	47.5(a)	Smooth	Rotating cantilever		Air, fresh water, saltwater(c)	S-N curves 10^4-10^8		3
48Ni-48Cu	Cold rolled, full anneal	78	26(a)	Smooth	Rotating cantilever		Air, fresh water, saltwater(c)	S-N curves 10^4-10^8		3
21Ni-78Cu	Cold worked, low anneal	62.4	34.3(a)	Smooth	Rotating cantilever		Air, fresh water, saltwater(c)	S-N curves 10^4-10^8		3
21Ni-78Cu	Cold worked, full anneal	47.3	9.2(a)	Smooth	Rotating cantilever		Air, fresh water, saltwater(c)	S-N curves 10^4-10^8		3
20Ni-79Cu	Cold worked, low anneal	61.0	32.0	Notched and smooth	Rotating cantilever		Air, fresh water, saltwater(c)	S-N curves 10^5-10^8		4
20Ni-79Cu	Cold worked, full anneal	47.5	7.3	Notched and smooth	Rotating cantilever		Air, fresh water, saltwater(c)	S-N curves 10^5-10^8		4
63Ni-35Cu	Cast	74.0	27.2	Smooth	Rotating cantilever	1450 rpm	Air, saltwater	CFS at 5 x 10^7 cycles		190
65Ni-30Cu	Cast	52.4	25.0	Smooth	Rotating cantilever	1450 rpm	Air, saltwater	CFS at 5 x 10^7 cycles		190
63Ni-30Cu-2.85i	Cast	92.3	72.2	Smooth	Rotating cantilever	1450 rpm	Air, saltwater	CFS at 5 x 10^7 cycles		190
66Ni-28Cu-3.65i	Cast	136.5	102.2	Smooth	Rotating cantilever	1450 rpm	Air, saltwater	CFS at 5 x 10^7 cycles		190
CDA 722	Solution treated	45.0	15.9	Smooth	Axial, fully reversed	20 Hz	0.5N NaCl	S-N vs applied current		26
CDA 722	Solution treated and aged	58.0	34.0	Smooth	Axial, fully reversed	20 Hz	0.5N NaCl	S-N vs applied current		26
Monel	Tempered 575 F, 4 hr, cold drawn, polished	101.0	88.0	Smooth	Rotating cantilever, stressless	1780 cpm	60- and 390-day exposure to seawater prior to testing	S-N curves 10^6-10^8		188
Monel	Cold drawn, tempered 1000 F, 2 hr, oxidized	91.0	66.5	Smooth	Rotating cantilever, stressless	1780 cpm	60- and 90-day exposure to seawater prior to testing	S-N curves 10^6-10^8		188
Monel	Cold drawn, tempered 1000 F, 2 hr, polished	91.0	66.5	Smooth	Rotating cantilever, stressless	1780 cpm	60- and 90-day exposure to seawater prior to testing	S-N curves 10^6-10^8		188
Monel	Hot rolled, smooth machined	84.0	38.0	Smooth	Rotating cantilever, stressless	1780 cpm	60- and 390-day exposure to seawater prior to testing	S-N curves 10^6-10^8		188
45-55 Ni-Cu	800 F, 2 hr, cold drawn	75.0	63.0	Smooth	Rotating cantilever, stressless	1780 cpm	60- and 390-day exposure to seawater prior to testing	S-N curves 10^3-10^8		188
Cu-Ni 70/30	Weldment	84.9	49.2				Seawater	Corrosion performance		189
Cu-Ni 90/10	Weldment	66.7	36.3				Seawater	Corrosion performance		189

(a) Elastic limit -- the highest stress which results in no appreciable permanent deformation after removal of the load.
(b) CFS -- corrosion fatigue strength defined as the alternating stress at which a given material survived 100 megacycles in a test lasting 48 days.
(c) Severn River water having a saline content about one-third that of seawater.
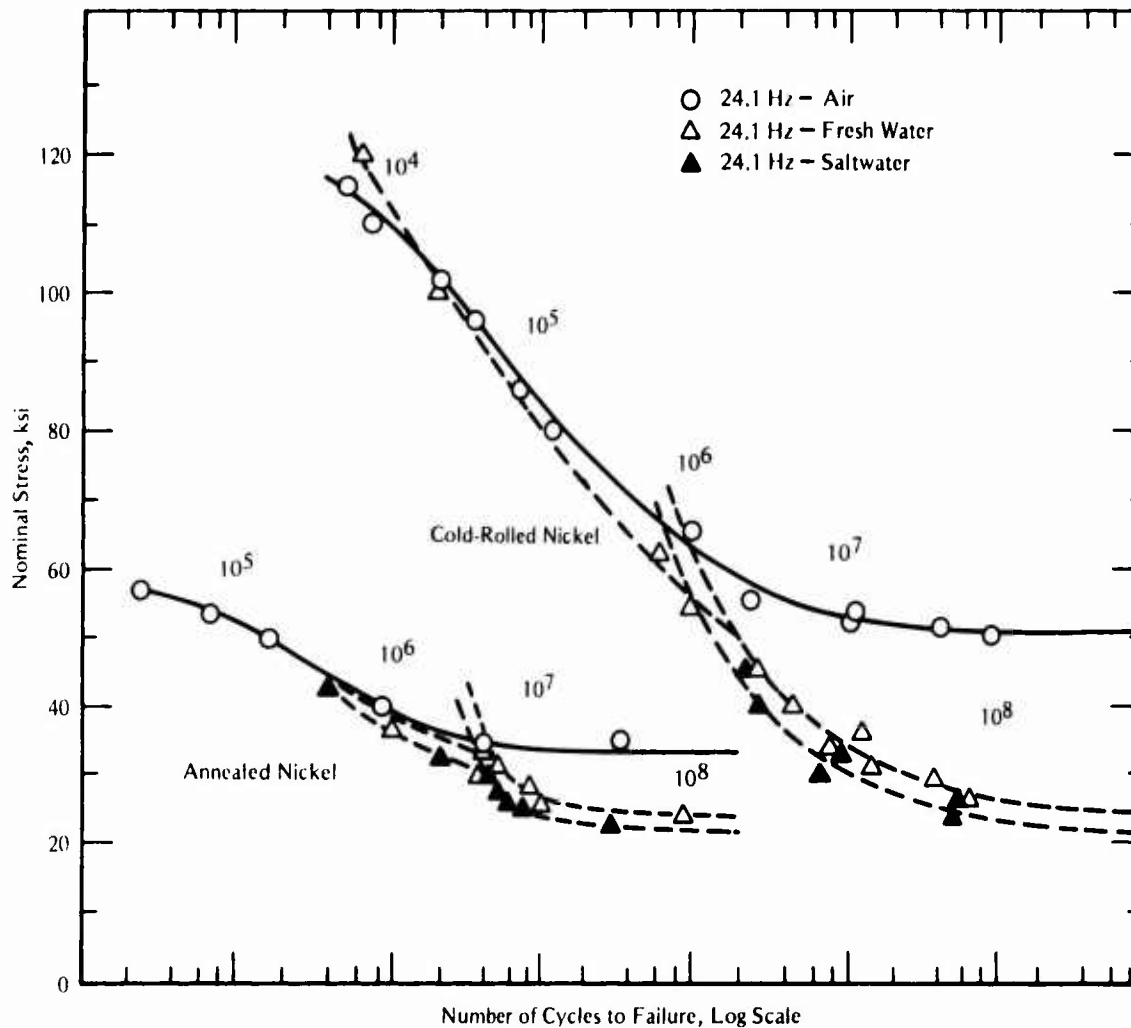
FIGURE 123. Fatigue and Corrosion Fatigue of Nickel[3]

Nickel Alloys

The nominal chemical compositions of nickel alloys discussed in this section are presented in Table 16. Nominal nickel contents range from 32 to 77 weight percent.

Sedricks and Money[5] evaluated a number of nickel alloys in seawater using smooth (unnotched) cantilever beam specimens rotating at 1450 rpm. Most alloys do not exhibit a fatigue limit when tested in seawater; thus, for purposes of or comparison, corrosion-fatigue strength was defined as the minimum alternating stress at which a given alloy survived 100 megacycles in a test lasting 48 days.

The results for nickel alloys obtained by Sedricks and Money[5] are summarized in Figure 124. The long-life corrosion-fatigue strength is directly proportional to ultimate tensile strength for these alloys. None of the alloys showed evidence of corrosion at the termination of the tests, and all failures occurred as a result of a single crack. These features are believed to be related to the high resistance of these alloys to localized corrosion attack, which is

TABLE 16. Nominal Chemical Compositions of the High-Nickel Alloys

| Alloy | Major Alloying Elements, wt % | | | | | |
	Ni	Cr	Fe	Mo	Co	Other
Inconel Alloy 718	Bal	19	17	3	—	5Cb, 0.8Ti, 0.6Al
Inconel Alloy 625	Bal	21	2.5	9	—	3.6 (Ta + Cb)
Hastelloy C	Bal	16	5	16		4W
IN-120(a)	Bal	21		4	14	2.5Ti, 2 (Cb + Ta)
Incoloy Alloy 800	32	21	Bal		—	0.4Ti, 0.4Al
Inconel Alloy 600	Bal	16	7			
Incoloy Alloy 825	40	20	32	2.8		1.7Cu, 1.1Ti, 0.2Al
Medium Cr, High Ni Alloy	34.7	10.9	Bal		—	0.39C, 1.1Mn, 0.15Si

(a) An experimental alloy at the time the data were published.
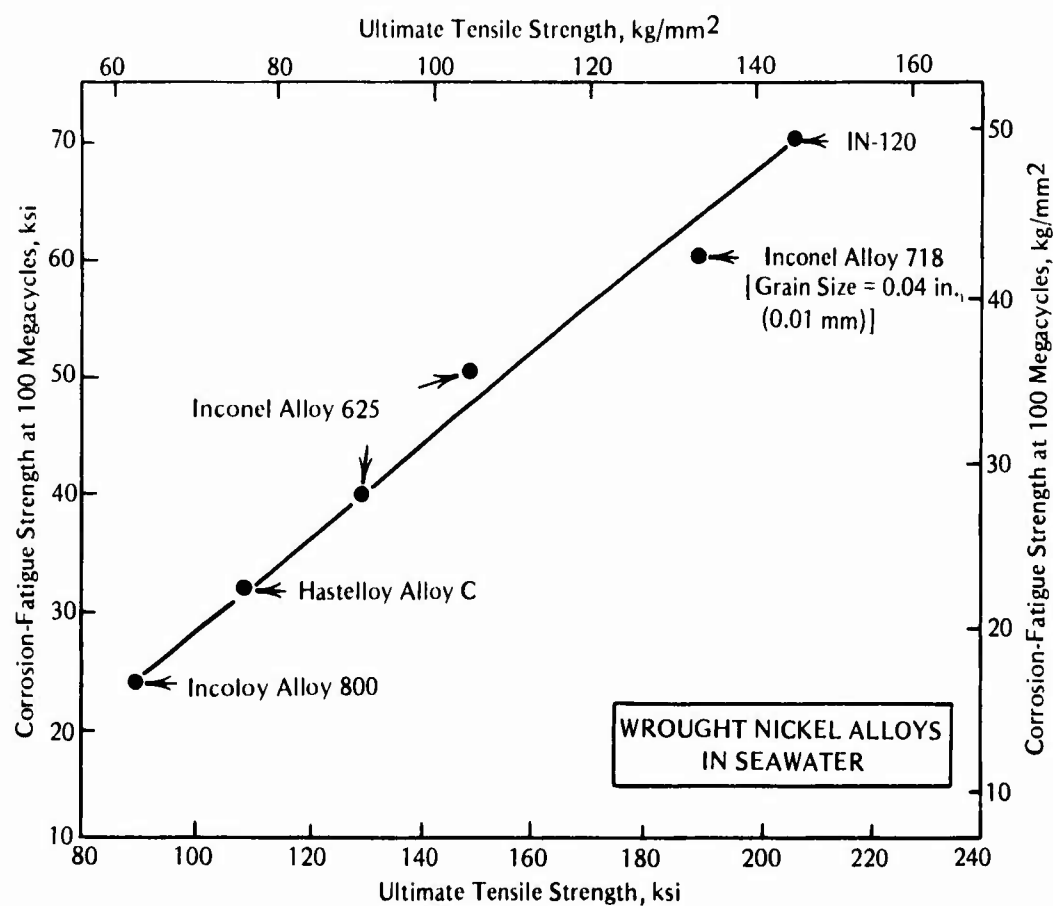
FIGURE 124. Variation of Corrosion-Fatigue Strength With Ultimate Tensile Strength for Various Nickel Alloys[5]

evidenced by their extremely good resistance to pitting corrosion. Thus, high pitting resistance correlated with good resistance to the localized attack at slip bands usually associated with corrosion-fatigue-crack initiation. In these cases, the crack-initiation mechanism is similar to that which occurs for tests in air. Therefore, properties such as ultimate tensile strength, which correlate with fatigue strength in air, also correlate with corrosion-fatigue strength.

The effect of grain size on corrosion-fatigue strength of Inconel Alloy 718 was examined[5], and the results are shown in Figure 125. Both fatigue strength in air and corrosion-fatigue strength in seawater increased with decreasing grain size. The differences are not related to changes in tensile strength since both the .0004 in. (.01 mm) and .003 in. (.068 mm) grain size materials had the same tensile strength 189 ksi (1303 MPa). Nor is this effect related to differences in pitting resistance since the effect is observed in air and in seawater. With high corrosion resistance, the correspondingly high resistance of nickel alloys to corrosion fatigue in seawater correlates well with high ultimate tensile strength and small grain size. These same factors normally give enhanced fatigue resistance in an air environment.

McAdam[4] reported corrosion-fatigue data for a medium chromium-high nickel (10.9Cr-34.7Ni) alloy in air, fresh water, and saltwater. His results are presented in Figure 126. The alloy was selected in a study of spring materials, because it had a higher elastic limit (E.L. in the figure) than many of the corrosion-resistant steels. Even though the corrosion-fatigue resistance in saltwater is significantly reduced from that in fresh water, or in air, the alloy is more corrosion-fatigue resistant than ordinary steels.
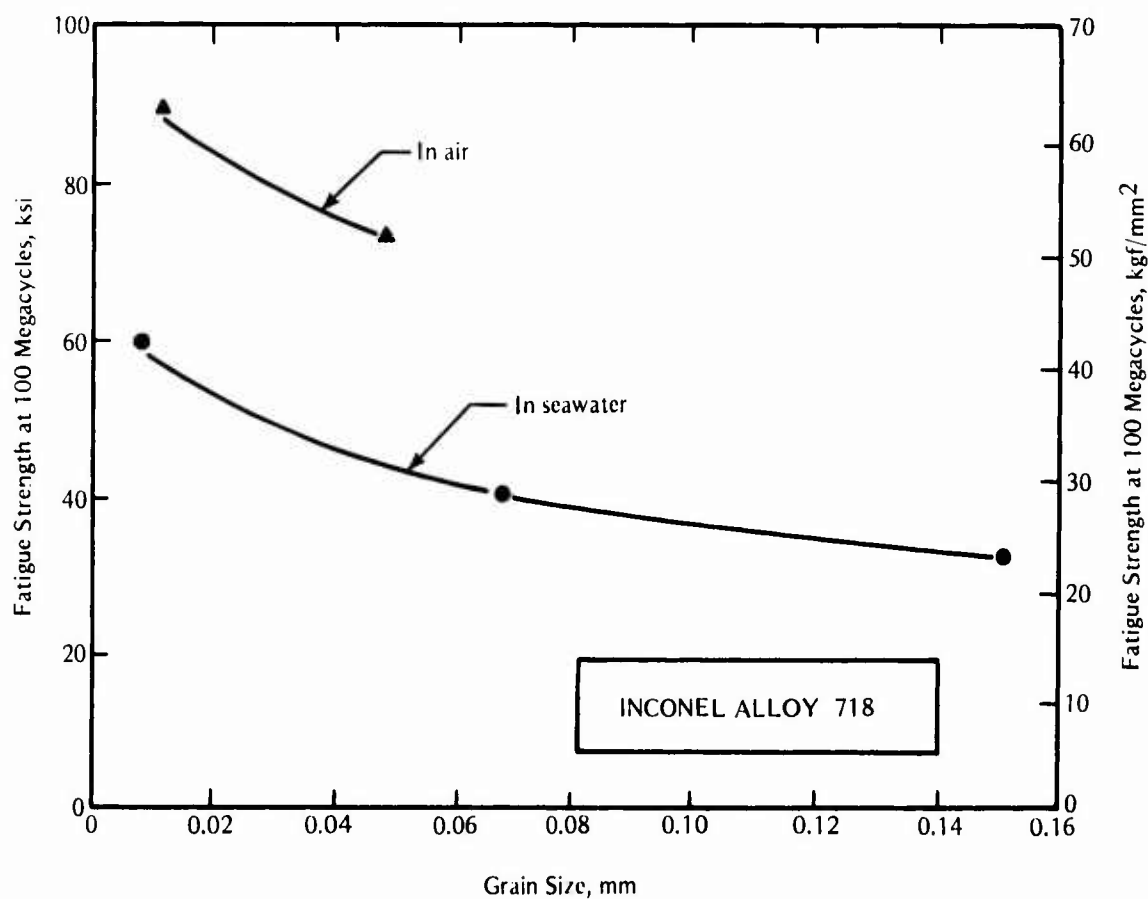
FIGURE 125. Effect of Grain Size on Corrosion-Fatigue Strength of Inconel Alloy 718 at 100 Megacycles[5]
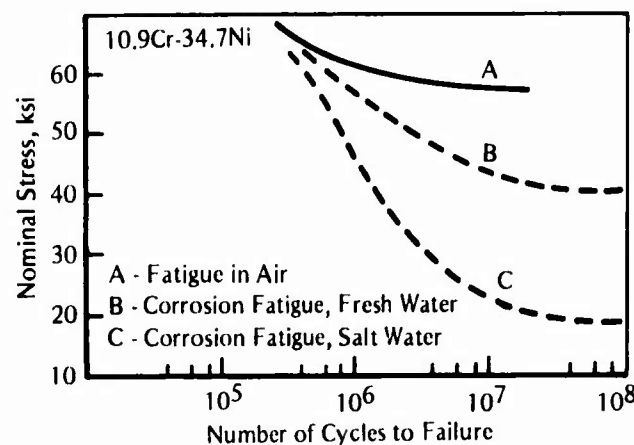
FIGURE 126. Fatigue and Corrosion-Fatigue Curves for Medium Chromium–High Nickel Alloy[4]

Copper-Nickel Alloys

Smooth Specimens in Fresh and Saltwater

Copper-nickel alloys are widely used in seawater because of their high corrosion resistance. (For corrosion-fatigue data on these alloys see Table 15.) The nominal chemical compositions of alloys discussed in this section are given in Table 17. The data for other copper alloys are given in Chapter 6.

The corrosion-fatigue strength of wrought Monel Alloy k.-500 with an ultimate tensile strength of 176 ksi (1214 MPa) was 26 ksi (179 MPa) in seawater.[5] The data were obtained using smooth, cantilever beam specimens rotating at 1450 for a maximum duration of 100 megacycles (approximately 48 days). The corrosion-fatigue strength was defined as the minimum alternating stress at which the alloy survived 100 megacycles.

The fatigue and corrosion-fatigue graphs for Monel are shown in Figure 127 from McAdam.[3] Two sets of curves are presented. The curves at the upper right are for cold-rolled Monel which was given a low-temperature anneal (425 C for 3 hours). This heat treatment relieved internal stress with practically no reduction in strength. The curves at the lower left are for a fully annealed Monel (760 C for 1 hour). The tensile strengths were 127.7 ksi (880 MPa) and 81.9 ᵏ (565 MPa), respectively. Each family of curves has its own scale for number of cycles to failure, with the decades identified by the number above the curves. The stress scale on the ordinate is the same for all curves.

The corrosion-fatigue limits for cold-rolled and fully annealed Monel were practically the same.[3] As was found for nickel, there is much less difference between the corrosion-fatigue limit in fresh water and that in saltwater. This is in contrast to the behavior of steels, where exposure to saltwater greatly reduced the corrosion-fatigue limit below that in fresh water. At higher stresses, the corrosion-fatigue curves for Monel were slightly above the air fatigue curves. The point at which the corrosion-fatigue curve started to rapidly descend below the air-fatigue curve was at about 1 million cycles for cold-rolled Monel and at about 2 million cycles for fully annealed Monel.

TABLE 17. Nominal Chemical Compositions of the Copper-Nickel Alloys

| Alloy | Major Alloying Elements, wt % | | | | | Reference |
	Ni	Cu	Fe	Mn	Other	
Monel K-500	66	29	1.0	0.7	3Al, 0.6Ti	5
Monel	68	29	1.5	1.0	—	188
Monel	67	29	1.8	1.0	—	3
45Ni-55Cu	45	54	0.5	0.5	—	188
48Ni-48Cu	48	48	1.1	1.9		3
21Ni-78Cu	21	78	0.5	0.2		3
20Ni-79Cu	20	79	0.4	0.3	—	4
29Ni-67Cu	29	67	2.8	1.4	—	4
40Ni-57Cu	40	57	1.1	1.8	—	4
63Ni-35Cu	63	35	0.9	0.7	0.7Al	190
65Ni-30Cu	65	30	1.6	0.8	0.9Al	190
63Ni-30Cu-2.8Si	63	30	2.3	0.5	2.8Si, 1.5Al	190
66Ni-28Cu-3.6Si	66	28	1.5	0.6	3.6Si	190
CDA 722	16	72	0.9	0.7	0.6Cr	26
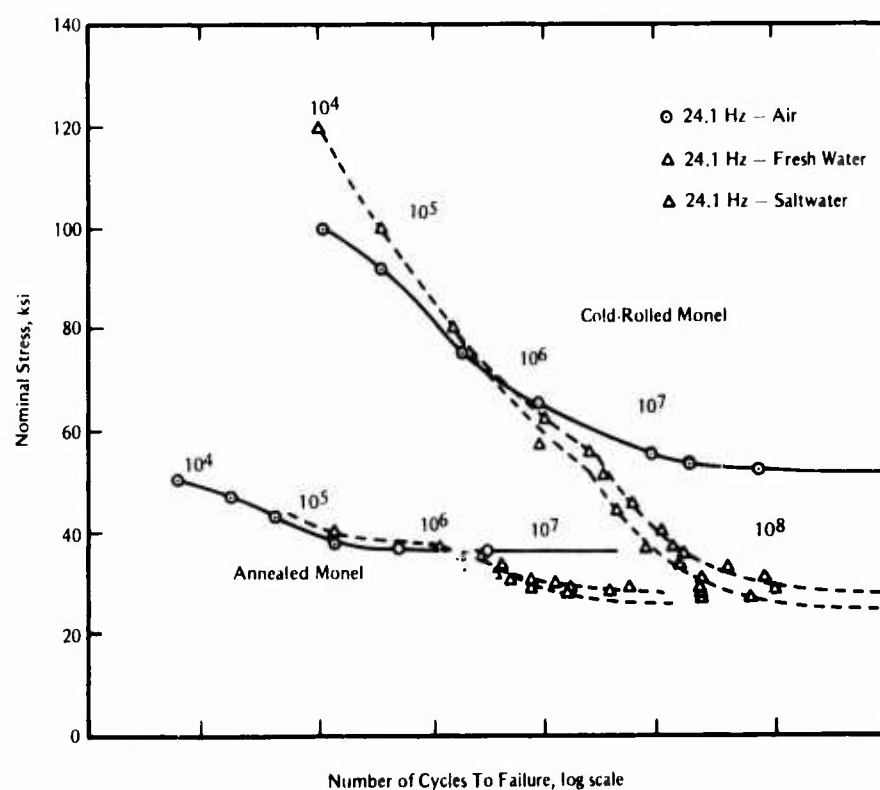
FIGURE 127. Fatigue and Corrosion Fatigue of Monel[3]

Three pairs of graphs arranged from left to right with increasing nickel content are shown in Figure 128[3]. The two graphs to the left are for electrolytic copper, the two in the middle are for a 21Ni-78Cu alloy, and the two on the right are for a 48Ni-48Cu alloy. The shape of the fatigue life (S-N) curves is the same as that observed for nickel and Monel. For the 48Ni-48Cu alloy, rapid descent of the corrosion-fatigue curve below the air-fatigue curve did not occur until nearly 10 million cycles; however, the corrosion fatigue limits were no higher than those for the 21Ni-78Cu alloy or for Monel. For the 21Ni-78Cu alloy, practically no difference was observed between corrosion-fatigue behavior in fresh water and that in saltwater, and the corrosion-fatigue limit was approximately the same as that for Monel. For the annealed 21Ni-78Cu alloy tested in water environments, the corrosion-fatigue-data curve did not drop below that for in-air test data. Therefore, it was only after strengthening by cold work that an intrinsic corrosion-fatigue effect was observed for the alloy. Similar results were observed for cold-worked and hot-rolled copper, where the corrosion-fatigue data curves from tests in water environments remained on or above that for in-air test data. This behavior did not result from a lack of chemical reaction in the corrosion-fatigue tests. The surfaces of copper specimens tested in water environments were heavily coated with films of corrosion products. Either the copper was not sensitive to localized corrosion or the general corrosion process did not produce enough metal loss to significantly increase the actual net-section stress significantly.
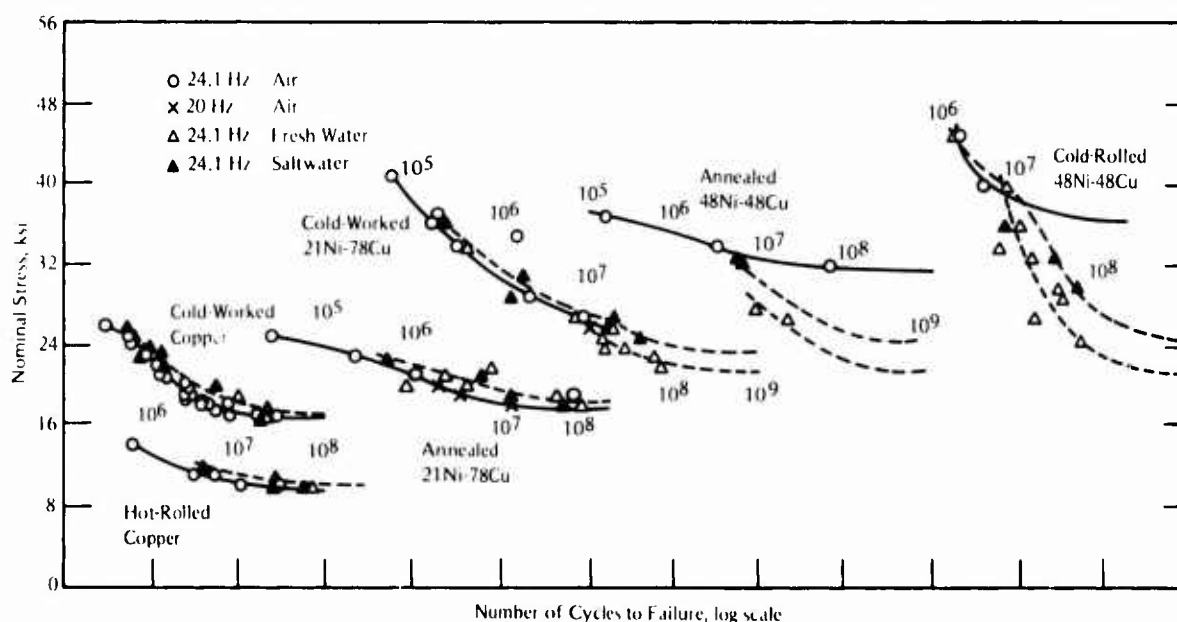
FIGURE 128. Fatigue and Corrosion Fatigue of 48Ni-48Cu Alloy, 21Ni-78Cu Alloy, and Copper[3]

McAdam's data for several copper-nickel alloys are summarized[205] in Table 18. McAdam[4] observed that for the copper-nickel alloys, those fully annealed had a nominal fatigue limit above their elastic limit and even above their yield point because the specimen surface layer yielded and underwent cyclic plastic deformation. If sufficient cyclic hardening occurred, the outer surface would have stabilized with nominally elastic cyclic stress-strain response. However, it is possible that some cyclic inelasticity still remained, in which case the nominal stress values would be lower than the actual stress at the surface. Thus, care should be taken in using the reported stress levels for data on the fully annealed alloys. This cyclic plasticity and associated cyclic hardening behavior was characteristic of all fully annealed alloys of only one microconstituent (alpha solid solution).

TABLE 18. Summary of Corrosion-Fatigue Data for Various Copper-Nickel Alloys[191]

Composition of Alloy, percent				Condition	Corrosion-Fatigue Strength, ksi (MPa)			Number of Cycles x 10^6
Copper	Nickel	Iron	Manganese		Air	Tap Water	Saltwater	
78	21	0.51	0.29	Cold drawn, tempered	35.8 (243)	30 (204)		100
				Annealed	22.6 (154)	22.6 (154)	22.6 (154)	100
67.11	28.6	2.83	1.35	Cold drawn, tempered	50.6 (344)	29 (200)		50
				Annealed	126.5 (860)	29 (200)		50
56.6	40.3	1.09		Annealed	42 (285.6)	39 (268)		50
53.5	45	0.38	1.03	Cold drawn, tempered	57.6 (391.7)	27 (91)	31 (211)	100
				Annealed	42.2 (287)	31 (211)	32 (218)	100
29.54	67.5	1.76	0.95	Cold drawn, tempered	73.2 (198)	34 (228)	39 (268)	100
				Annealed	50 (340)	37 (249)		50

For fully annealed alloys, the fatigue limit increased rapidly with nickel content up to nickel concentrations of about 45 percent.[4] Beyond this concentration, the fatigue limit remained essentially constant with increasing nickel. Cold-rolled, nickel-copper alloys in 1-inch (25.4 mm) -diameter rods with tensile strengths of 135 to 140 ksi (931 to 965 MPa) had a fatigue limit of greater than 50 ksi (345 MPa). To obtain this fatigue limit, a mild anneal was required after cold working to relieve internal stresses.

Stewart and Williams[190] reported corrosion-fatigue strengths for two cast Cu-Ni and two cast Cu-Ni-Si alloys in seawater. Rotating cantilever beam tests at 1450 rpm (24.2 Hz were run in brackish estuary water with one-third to one-sixth the salinity of seawater. Smooth, tapered specimens were used. The fatigue and corrosion-fatigue strengths are given in Table 19. The data for the cast alloys were more scattered than those typically obtained for wrought alloys. The corrosion-fatigue strengths at 5×10^7 cycles ranged from 10 to 13 ksi (69 to 90 MPa). No clear effect of silicon was observed.

TABLE 19. Fatigue and Corrosion-Fatigue Strengths of Cast Cu-Ni and Cu-Ni-Si Alloys in Saltwater [190]

Alloy	Tensile Strength, ksi (MPa)	Yield Strength, ksi (MPa)	Fatigue Strength[a], ksi (MPa)	Corrosion-Fatigue Strength[a], ksi (MPa)
63Ni-35Cu	74.0 (510)	27.2 (188)	18 (124)	12.5 (86)
65Ni-30Cu	52.4 (361)	25.0 (172)	12 (83)	10 (69)
63Ni-30Cu-2.85	92.3 (636)	72.2 (498)	15 (103)	11 (76)
66Ni-28Cu-3.6Si	137 (941)	102 (703)	16 (110)	13 (90)

(a) At 5×10^7 cycles.

The effect of heat treatment on the fatigue and corrosion-fatigue of a Cu-Ni-Cr alloy, CDA 722, was investigated by Hahn and Duquette.[26] Fully reversed cycling fatigue tests of axially loaded specimens were performed in air and in 0.5 N NaCl solution. Tests were conducted under conditions of free corrosion and with applied anodic currents. The alloy was heat treated to produce a solution-treated structure and a precipitation-hardened structure. The fatigue-life curves are shown in Figure 129. Exposure to the aqueous solution under free-corrosion conditions did not significantly affect the fatigue resistance of the solution treated alloy, but the precipitation-hardened alloy showed a significant reduction in fatigue resistance when exposed to the sodium chloride solution. However, the precipitation-hardened material still had higher corrosion-fatigue strength than the solution-treated material in the range of cyclic lives studied (10^5 to 10^7 cycles). The difference in behavior between these two heat treatments is related to the distribution of slip. In the solution-treated material, slip was diffused and not localized where it would be highly sensitive to corrosive attack. In contrast, the dispersion-strengthened material exhibited well-defined planar arrays of slip. The localized regions where these planar slip bands are exposed at the metal surface were subject to localized corrosive action, resulting in the observed reduction in corrosion-fatigue life compared to that in air.
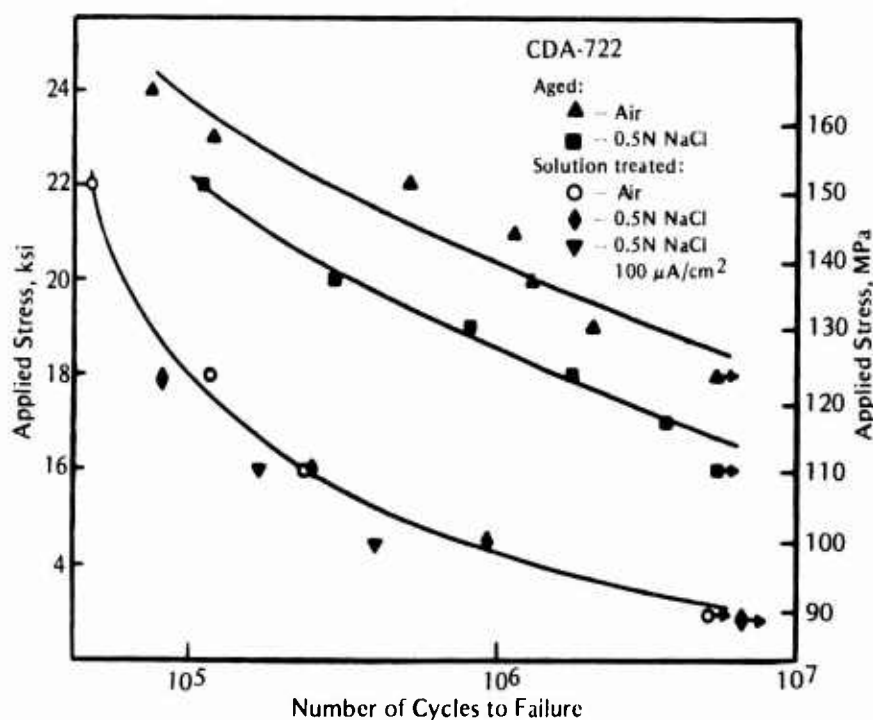
FIGURE 129. Corrosion-Fatigue Strength of Solution-Treated and Age-Hardened Alloy CDA-722 in Laboratory Air and in Aerated 0.5 N NaCl Solution Under Free-Corrosion Conditions at 20 Hz[26]

Small applied anodic currents decreased the corrosion-fatigue resistance of the alloy in either heat-treated condition. Increasing the anodic currents to approximately 600 μA/cm^2 resulted in a further decrease in fatigue resistance. At a current greater than 600 μA/cm^2, the fatigue resistance increased because of blunting of microcracks by anodic dissolution. In both heat treatments, fatigue in air resulted in mixed transgranular-intergranular crack initiation and propagation. Applied anodic currents increased the relative amount of intergranular cracking.

Gross and co-workers investigated the low-cycle fatigue behavior of nonferrous alloys for submarine heat exchangers and saltwater piping applications.[192,194] Low-cycle, flexural fatigue tests were carried out using beam specimens subjected to completely reversed bending strain. A cycle rate of 5 cpm with essentially a square wave was used. Alloys investigated included Monel, Cufenloy 40, Cupro-Nickel 707, 70-30 Cupro-Nickel and 90-10 Cupro-Nickel. From the limited test results, the authors conclude that saltwater corrosion had little effect on low-cycle fatigue life. Wrought Monel and forged Ni-Al bronze had the highest fatigue (air) strengths, whereas gun metal and valve bronze had the lowest fatigue strengths.

Effect of Prior Corrosion on Fatigue Strength

The effects of prior corrosion on the fatigue strength of Monel and a 45Ni-55Cu alloy (Constantan) were investigated by Ellinghausen.[188] Prior corrosion was carried out with the specimens completely submerged in slowly moving seawater for periods of 60 and 390 days. The corroded specimens were tested at various stresses to establish the stress-cycle relationship up to 10^8 cycles. All fatigue tests were made at 1780 cpm with rotating cantilever beam specimens. The results are summarized in Table 20. The long-life fatigue strength of both Monel and the 45Ni-55Cu alloy was lowered after exposure to seawater prior to the fatigue tests.

TABLE 20. Effect of Prior Corrosion in Seawater on Fatigue Properties of Monel and a 45Ni-55Cu Alloy[188]

Alloy	Condition	Surface Finish and Prior Exposure in Seawater	Tensile Strength, ksi (MPa)	Fatigue Strength, ksi (MPa)	
				10^7 Cycles	10^8 Cycles
Monel metal	Cold drawn, tempered 575 F, 4 hr	Polished, not exposed	101 (686.8)	14 (97)	28 (193)
		Polished, 60 days		27 (186)	22 (152)
		Polished, 340 days		25 (172)	21 (145)
Monel metal	Cold drawn, tempered 1000 F, 2 hr	Oxidized, not exposed	91 (619.8)	28 (193)	21 (145)
		Oxidized, 60 days		27 (186)	
		Oxidized, 390 days		21 (145)	16 (110)
Monel metal	Cold drawn, tempered 1000 F, 2 hr	Polished, not exposed	91 (619.8)	35 (241)	31 (214)
		Polished, 60 days		30 (207)	—
		Polished, 390 days		24 (166)	—
Monel metal	Hot rolled	Smooth machined, not exposed	84 (571)	32 (221)	31 (214)
		Smooth machined, 60 days		30 (207)	29 (200)
		Smooth machined, 390 days		23 (159)	—
Constantan 45-55 Ni-Cu	Cold drawn, tempered 800 F, 2 hr	Smooth machined, not exposed	75 (510)	32 (221)	31 (214)
		Smooth machined, 60 days		22 (152)	21 (145)
		Smooth machined, 390 days		19 (131)	17 (117)

Corrosion Fatigue of Welds

The performance in seawater of several copper-alloy weld fabrications was investigated by Newcombe.[189] The aim of the work was to support development of welding for maintenance and modification of existing copper-alloy cast components. Two precipitation-hardened Cupro-Nickel alloys, 90-10 and 70-30 Cu-Ni, were included in the study. These alloys were of interest because of their near matching composition with that of wrought Cupro-Nickel alloys used for seawater piping. Low-cycle, corrosion-fatigue tests using reverse bend, cantilever beam specimens were performed on variations of a 90-10 Cu-Ni cast alloy. No fatigue-life data were reported, and the results were described only qualitatively. The Cupro-Nickel alloy specimens showed that crack initiation at the free surface was associated essentially with grain boundaries. Some selective attack of cored areas from which cracks had developed was observed.

CHAPTER 6
CORROSION-FATIGUE DATA FOR COPPER-BASE ALLOYS

Corrosion-fatigue data for copper-base alloys are summarized in Table 21. Data on the Cu-Ni alloys are presented in Chapter 5, and are not repeated herein. Examination of the entries in Table 21 shows that almost all of the studies listed reported data in terms of corrosion-fatigue life—either as fatigue-life (S-N) curves or as corrosion-fatigue strength (CFS). Data on corrosion-fatigue-crack growth were reported in only two studies[195,196]. Therefore, the bulk of this chapter concentrates on fatigue-life data, and only a brief section on fatigue-crack-growth data is presented.

Fatigue-Life Data

General Discussion

Most of the corrosion-fatigue data for copper alloys are for smooth specimens tested in rotating bending or reversed bending (R = -1) at high cyclic frequencies (20 to 50 Hz). The objective of the studies has been to obtain an experimental measure of the corrosion-fatigue strength in the high-cycle life regime. Typically, the corrosion-fatigue strengths at 10^8 cycles to failure or fatigue-life (S-N) curves from which these values could be determined were reported. Data on CFS at 10^8 cycles to failure for copper-base alloys tested in saline solutions or in salt-spray environments are summarized in Table 22. In general, the CFSs for these alloys are as high as, or even somewhat higher than, those for carbon and low-alloy steels under free-corrosion conditions, but are not as high as those for some of the highly corrosion-resistant alloys. The copper-base alloys are fairly easy to fabricate and are used extensively in cast components to avoid high fabrication costs. Many of the experimental data on these alloys have been developed to aid in their application in ship components, such as shafts and propellers.

Corrosion-fatigue data for electrolytic copper[3] provide a baseline for comparison with the various copper-base alloys. The fatigue-life (S-N) curves for this type of copper are shown in Figure 130. The corrosion-fatigue strength in a salt-water solution is slightly greater than that in air. Masuda and Duquette[197] found no environmental degradation in fatigue strength when high-purity copper was tested in a 0.5 N NaCl solution under free-corrosion conditions. However, applied anodic currents ≥ 10 $\mu A/cm^2$ decreased the CFS and caused a shift from transgranular to intergranular cracking. Duquette et al[199] found that the CFS of a Cu-7.8Al alloy was significantly reduced in 0.5 N NaCl solution compared with that in air, as shown in Figure 131. Even with this significant reduction, the CFS (at 10^7 cycles) of the Cu-7.8Al alloy was about 70 percent greater than that of pure copper under the same test conditions. The pure copper exhibited wavy slip behavior and exposure to NaCl solution did not affect its crack-initiation behavior. The Cu-Al alloy exhibited planar as slip behavior because of its lower stacking fault energy, and the mode of crack initiation changed from transgranular to intergranular when the alloy was exposed to the NaCl solution. Hahn and Duquette[26] made similar observations for a Cu-Ni alloy. (See Chapter 5 on nickel-base alloys). Thus, alloying

TABLE 21. Corrosion-Fatigue Data for Copper Alloys

Alloy	Condition or Treatment	Tensile Strength, ksi (MPa) Ultimate	Yield	Type of Specimen	Type of Loading	Cyclic Frequency, Hz	Environment(a)	Types of Data	Notes	References
Electrolytic Copper	Cold-worked	47 (316)	21 (144)	Smooth bars	Rotating bending	24.2	Saltwater(b)	S-N curves 10^6-10^8		3
Electrolytic Copper	Fully annealed	31 (212)	4.5 (31)	Smooth bars	Rotating bending	24.2	Saltwater(b)	S-N curves 10^6-10^8		3
High-Purity Copper	Fully annealed	32 (220)	4.5 (31)	Smooth bars	Axial at R = 0.11 to 0.18	30	0.5N NaCl	S-N curves 4×10^5-10^7	Anodic polarization	197
99.99% Copper	Annealed	—	—	Smooth bars	Rotating bending	28.3	2M NaCl (pH = 5)	N at 21 ksi (145 MPa)	Examined corrosion products	198
α Brass (70Cu-29Zn)	Annealed	35 (239)	4.3 (29)	Smooth bars	Rotating bending	28.3	2M NaCl (pH = 5)	N at 30 ksi (207 MPa)	Examined corrosion products	198
Copper	CW + annealed	63 (432)	16 (110)	Smooth bars	Axial at R ~ 0.1	30	0.5N NaCl	S-N curves 10^6-10^7	Wavy slip, anodic currents	199
Cu-7.9Al	CW + annealed	81 (561)	56 (383)	Smooth bars	Axial at R ~ 0.1	30	0.5N NaCl	S-N curves 10^5-10^7	Planar slip	4
95Cu-5Sn	CW + annealed	55 (382)	20 (137)	Smooth bars	Rotating bending	24.2	Saltwater(b)	CFS(c) at 10^8		4
92Cu-8Sn	CW + annealed	—	—	Smooth bars	Rotating bending	24.2	Saltwater(b)	CFS(c) at 10^8		4
Ni-Al Bronze	As forged	116 (798)	78 (536)	Smooth bars	Rotating bending	36.7	Saltwater(b)	S-N curves 10^6-10^8		200
Al Bronze	Extruded and drawn	80 (551)	46 (318)	Smooth bars	Rotating bending	36.7	Saltwater(b)	S-N curves 10^6-10^8		200
Be Bronze	Extruded and drawn	94 (646)	74 (511)	Smooth bars	Rotating bending	36.7	3% NaCl spray	S-N curves 10^6-10^8		200
P Bronze	Rolled and drawn, normalized	62 (426)	61 (420)	Smooth bars	Rotating bending	36.7	3% NaCl spray	S-N curves 10^6-10^8		200
Be Bronze	Solution treated	72 (497)	—	Smooth bars	Rotating bending	36.7	3% NaCl spray	CFS(c) at 5×10^7		201
Be Bronze	STA	182 (1255)	—	Smooth bars	Rotating bending	36.7	3% NaCl spray	CFS(c) at 5×10^7		201
84Cu-14Zn-1.6Sn	Cast	28 (192)	14 (96)	Smooth bars	Rotating bending	24.2	Saltwater(b)	CFS(c) at 5×10^7		190
86Cu-6Zn-7.6Sn	Cast	22 (150)	14 (99)	Smooth bars	Rotating bending	24.2	Saltwater(b)	CFS(c) at 5×10^7		190
Mn Bronze (4 heats)	Cast	71-85 (490-590)	28-31 (192-211)	Smooth bars	Rotating bending	24.2	Saltwater(b)	CFS(c) at 5×10^7		190
Al-Mn Bronze (2 heats)	Cast	103-111 (709-764)	66-90 (454-709)	Smooth bars	Rotating bending	24.2	Saltwater(b)	CFS(c) at 5×10^7		190
Mn-Ni Bronze	Cast	87 (603)	42 (288)	Smooth bars	Rotating bending	24.2	Saltwater(b)	CFS(c) at 5×10^7		190
Al-Ni Bronze (2 heats)	Cast	67-73 (462-506)	44-51 (300-349)	Smooth bars	Rotating bending	24.2	Saltwater(b)	CFS(c) at 5×10^7		190
Al-Ni-Fe Bronze	Cast	88 (607)	40 (278)	Smooth bars	Rotating bending	24.2	Saltwater(b)	CFS(c) at 5×10^7		190
Al Bronze	Cast	86 (590)	32 (222)	Smooth bars	Rotating bending	24.2	Saltwater(b)	CFS(c) at 5×10^7		190
Si Bronze	Cast	50 (342)	25 (172)	Smooth bars	Rotating bending	24.2	Saltwater(b)	CFS(c) at 5×10^7		190
Cu-Be Alloy (2 heats)	Cast + aged	120-150 (825-1034)	—	Smooth bars	Rotating bending	24.2	Saltwater(b)	CFS(c) at 5×10^7		190
Cu-Ni-Be Alloy	Cast + aged 2 hr at 400 C	32 (221)	—	Smooth bars	Rotating bending	24.2	Saltwater(b)	CFS(c) at 5×10^7		190
Cu-Ni-Be Alloy	Cast + aged 4 hr at 350 C	108 (743)	—	Smooth bars	Rotating bending	24.2	Saltwater(b)	CFS(c) at 5×10^7		190
Cu-Co-Be Alloy	Cast + aged 2 hr at 500 C	49 (338)	—	Smooth bars	Rotating bending	24.2	Saltwater(b)	CFS(c) at 5×10^7		190
Tobin Bronze		59 (403)	—	Smooth bars	Rotating bending	24.2	Exposure to seawater 60 and 390 days prior to testing in air	Strain-N 10^3-10^6		188
CMA-1 (Mn-Ni-Al) Bronze	Cast	105 (726)	47 (324)	Smooth bars	Rotating bending		Salt spray	S-N curves 10^6-10^8		202
α Brasses (3 types)	Cast	82-105 (564-726)	34-65 (232-448)	Smooth bars	Rotating bending		Seawater	CFS(c) at 10^8		202
Ni-Al Bronze	Cast	92-103 (633-710)	36-43 (247-293)	Smooth bars	Rotating bending		Seawater	CFS(c) at 10^8		202
Mn Bronze CA865	Cast (5 heats)	73 (503)	28 (194)	Smooth bars	Rotating bending	24.2	Seawater	S-N curves 10^5-10^8		5,6
Ni-Al Bronze CA955	Cast (6 heats)	87 (600)	37 (255)	Smooth bars	Rotating bending	24.2	Seawater	S-N curves 10^6-10^8		5,6
Ni-Al Bronze CA955HT	Cast (1 heat)	115 (793)	—	Smooth bars	Rotating bending	24.2	Seawater	S-N curves 10^6-10^8		5
Mn-Ni-Al Bronze CA957	Cast	101 (694)	47 (324)	Smooth bars	Rotating bending	24.2	Seawater	S-N curves 10^6-10^8		192
Gun Metal	Cast	39 (267)	16 (108)	Smooth bars	Rotating bending	24.2	Saltwater(b)	Strain-N 10^3-10^6	87Cu-8.4Sn-3.5Zn	192
Valve Bronze	Cast	28 (193)	16 (109)	Smooth plate and smooth bar	Reversed bending and rotating bending	0.083 and 24.2	Saltwater(b)	Strain-N 10^3-10^8	88Cu-5.6Sn-3.8Zn-1.6Pb	192,194
Ni-Al Bronze	Cast	97 (671)	42 (290)	Smooth bars	Rotating bending	24.2	Saltwater(b)	Strain-N 10^4-10^8	80Cu-5.2Ni-10.3Al-3.7Fe	192,194
Mn-Ni-Al Bronze	Forged	103 (712)	52 (357)	Smooth bars	Rotating bending	24.2	Saltwater(b)	Strain-N 10^4-10^8	81Cu-4.5Ni-10.6Al-2.8Fe	192,194
LMtsZn Brass	Cast	85 (589)	43 (299)	Smooth bars	Rotating bending	50	Saltwater(b)	Strain-N 10^4-10^6	75Cu-12.5Mn-2.2Al-2.4Al	192
LAMtsZn Brass	Cast	60 (415)	33 (226)	Smooth bar	Rotating bending	50	3% NaCl	S-N curve 10^6-2×10^7	55Cu-3Mn-1Fe-41Zn	203
Br.AZhMts Bronze	Cast	63 (431)	40 (275)	Smooth bar	Rotating bending	50	3% NaCl	S-N curve 10^6-2×10^7	70Cu-2Al-4Mn-2Fe-22Zn	203
Br.AZhMts Bronze	Cast	58 (402)	33 (226)	Smooth bar	Rotating bending	50	3% NaCl	S-N curve 10^6-2×10^7	86Cu-8Al-2Fe-4Mn	203
Br.ANZhMts Bronze	Cast	81 (559)	38 (265)	Smooth bar	Rotating bending	50	3% NaCl	S-N curve 10^6-2×10^7	82Cu-10Al-4Fe-4Mn	203
80Cu-10Al-5Fe-5Ni	Cast	71 (490)	43 (294)	Smooth bar	Rotating bending	50	3% NaCl	S-N curve 10^6-2×10^7	82Cu-8.5Al-4Ni-1.5Fe-4Mn	203
80Cu-10Al-5Fe-5Ni	As-cast and extruded	116-131 (800-900)	—	Smooth bar	Rotating bending	50	Synthetic seawater	S-N curves 10^5-10^8		204
86Cu-10Al-2Co-1Ni	As-cast and extruded	107-115 (734-790)	—	Smooth bar	Rotating bending	50	Synthetic seawater	S-N curves 10^5-10^8		204
86Cu-10Al-2Co-2Fe	As-cast and extruded	113-117 (779-809)	—	Smooth bar	Rotating bending	50	Synthetic seawater	S-N curves 10^5-10^8		204

TABLE 21. (Continued)

Alloy	Condition or Treatment	Tensile Strength, ksi (MPa)				Type of Specimen	Type of Loading	Cyclic Frequency, Hz	Environment[a]	Types of Data	Notes	References
		Ultimate		Yield								
Al Bronze	Cast	97	(670)	36	(246)	Smooth base metal and weld metal plate	Reversed bending	0.00028 and 0.0028	Seawater, 45-82 F	Deflection-N 10^4-10^5	78Cu-9.5Al-5Fe-1Mn	189
Al-Si Bronze	Cast	71	(490)	25	(170)	Smooth plate	Reversed bending	0.0028	Seawater, 45-82 F	Deflection-N 10^4-10^5		189
Gun Metal	Cast	42	(290)	20	(135)	Smooth plate	Reversed bending	0.0028	Seawater, 45-82 F	Deflection-N 10^4-10^5		189
AlZn Bronze	Cast	–		–		Smooth			Seawater	CFS(c) at 2×10^7 vs potential	81Cu-4Fe-2Mn-9Al-5Ni	205
8Mn-Al-2Ni Bronze	Cast	95	(652)	43	(294)	Smooth bars	Axial at R = -1 and 0.3	185	Seawater(d)	S-N curve 10^6-10^8	Mean stress diagrams at 2×10^9 (extrapolated)	206
Mn Bronze	Cast	71-77	(490-529)	28-34	(190-233)	Smooth bars	Axial at R = -1 and 0.3	185	Seawater(d)	Estimated CFS(c) at 2×10^9		206
LiMnZn Brass	Cast	68	(471)	–		Smooth bars	Rotating bending	50	Seawater	S-N curves 10^5-2×10^7	Cathodic protection	207
Mn Bronze	Cast propeller	50	(343)	26	(176)	Smooth, notched, and welded bars	Rotating bending	24.2	Saltwater(b)	S-N curves 10^5-10^8	Welds, notches, actual propeller casting	194,195,208
Mn Bronze	Cast plate	–		–		CTS, weld metal	Axial at R = 0	16.7	Saltwater(b)	ΔK vs da/dN	Weld metal	195
Mn Bronze	Cast plate	71	(490)	31	(211)	Smooth bars	Rotating bending	24.2	Saltwater(b)	S-N curve 10^6-10^8		208
Ni-Al Bronze	Cast plates	75-85	(514-585)	33-36	(230-245)	Smooth, notched, and welded bars	Rotating tending	24.2	Saltwater(b)	S-N curves 10^6-10^8	Weld metal, notches	208
Mn-Ni-Al Bronze	Cast plates	82-97	(563-672)	42-44	(289-300)	Smooth, notched, and welded bars	Rotating bending	24.2	Saltwater(b)	S-N curves 10^6-10^8	Weld metal, notches	194,208
Mn Bronze	Cast					Smooth, hollow bars	Rotating bending + constant axial	28-33	3% NaCl	S-N curves 10^7-10^8	Effect of mean stress	?
Ni-Al Bronze	Cast							28-33	3% NaCl	S-N curves 10^7-10^8		?
Mn-Ni-Al Bronze	Cast							28-33	3% NaCl	S-N curves 10^7-10^8		?
Mn Bronze	Cast					Smooth bars	Rotating bending	50	3% NaCl	CFS(c) at 10^8		?
Ni-Al Bronze	Cast							50	3% NaCl	CFS(c) at 10^8		?
Mn-Ni-Al Bronze	Cast							50	3% NaCl	CFS(c) at 10^8		?
Al Bronze						Smooth plate	Reversed bending	0.0028 and 0.17	Seawater, 50 to 135 F	Strain-N curves 10^4-10^7	Frequency, water temperature	209
Ni-Al Bronze	Swaged bar + 24 hr anneal at 1697 F	128	(882)	58	(400)	Smooth bars	Axial at R = -1	2 and 20	0.5N NaCl	S-N curves 10^5-10^7	Frequency, anodic and cathodic currents	210
Mn Bronze	Cast block	53-66	(365-455)	25-30	(170-210)	Smooth plates	Bending with mean stress > 0	3.33	Seawater at 45 to 54 F	S-N curves 10^6-10^8	Low frequency, effect of mean stress, large castings	9
Ni-Al Bronze	Cast block	72	(496)	28	(193)	Smooth plates		3.33	Seawater at 45 to 54 F	S-N curves 10^6-10^8		9
Mn-Ni-Al Bronze	Cast block	62	(427)	32	(221)	Smooth plates		3.33	Seawater at 45 to 54 F	S-N curves 10^6-10^8		9
Ni-Al Bronze	Cast propellers	73	(500)	26	(182)	Smooth and notched bars and plates	Rotating and reversed bending	50 and 16.7	Seawater	S-N curves 10^5-10^8	Small and large specimens	196
Ni-Al Bronze	Cast propeller and block	76	(522)	30	(205)	CTS	Axial at R = 0	2.5 and 5	Synthetic seawater	ΔK vs da/dN	Frequency, large castings	196

(a) Water at about 68 to 77 F unless noted.
(b) Severn River water with one-third to one-sixth salinity of seawater.
(c) CFS denotes corrosion-fatigue strength.
(d) Two weeks' exposure to seawater before fatigue testing in seawater.

TABLE 22. Corrosion–Fatigue Strength of Copper Alloys in Saline Solutions at R = -1

Alloy	Condition or Treatment	Corrosion-Fatigue Strength at 10^8 Cycles, ksi (MPa)		Reference
Electrolytic Copper	CW	16.5	(114)	3
Electrolytic Copper	FA	10.0	(69.0)	3
95Cu-5Sn	CW	22.0	(152)	4
92Cu-8Sn	CW	19.0	(131)	4
84Cu-14Zn-1.6Sn	Cast	5.5	(37.9)	190
86Cu-6Zn-7.6Sn	Cast	6.0	(41.4)	190
30% α Brass	Cast	11.9	(81.9)	202
20% α Brass	Cast	14.3	(98.8)	202
5% α Brass	Cast	9.6	(66.4)	202
Mn Bronze	Cast (4 heats)	9.0-12.5	(62-86)	190
Mn Bronze	Cast (5 heats)	8.0	(55.2)	5,6
Mn Bronze	Cast	7.5	(52)	206
Mn Bronze	Cast	7.0	(48.3)	208
Mn Bronze	Cast	10.8	(74.1)	7
Mn Bronze	Cast	9.0	(61.8)	7
Mn Bronze	Cast	10.1	(70)	9
Mn-Ni Bronze	Cast	9.5	(65.5)	190
LMtsZh Brass		11.4	(78.4)	203
LMtsZh Brass		12.8	(88.2)	207
LAMtsZh Brass		15.6	(108)	203
Gun Metal	Cast	7.5	(51.7)	192
Valve Bronze	Cast	10.0	(69.0)	192
P Bronze	Rolled and drawn	25.8	(178)	200
Si Bronze	Cast	13.0	(89.6)	190
Be Bronze	CW	39.0	(269)	200
Be Bronze	ST	30.5	(210)	2
Be Bronze	STA	35.6	(246)	2
Cu-Be Bronze	Cast + aged	13.5	(93)	190
Cu-Be Bronze	Cast + aged	15.5	(107)	190
Cu-Ni-Be Bronze	Cast + aged	7.7	(53.1)	190
Cu-Ni-Be Bronze	Cast + aged	12.5	(86.2)	190
Cu-Co-Be Bronze	Cast + aged	7.0	(48.3)	190
Al Bronze	Extruded and drawn	22.0	(151)	200
Al Bronze	Cast	23.5	(162)	190
Ni-Al Bronze	Forged	32.7	(226)	200
Al-Ni Bronze	Cast (2 heats)	8.0	(55.2)	190
Al-Ni-Fe Bronze	Cast	20.0	(138)	190
Ni-Al Bronze	Cast	22.4	(154)	202
Ni-Al Bronze	Cast (6heats)	12.5	(86.2)	5,6
Ni-Al Bronze	Cast	15.0	(103)	5
Ni-Al Bronze	Cast	18.0	(124)	192,194
Ni-Al Bronze	Forged	28.0	(193)	192,194
80Cu-10Al-5Fe-5Ni	Extruded	24.2	(167)	204
80Cu-10Al-5Fe-5Ni	Cast	22.8	(157)	204
86Cu-10Al-2Co-1Ni	Extruded	24.2	(167)	204
86Cu-10Al-2Co-1Ni	Cast	25.6	(176)	204
86Cu-10Al-2Co-2Fe	Extruded	27.0	(186)	204

TABLE 22. (Continued)

Alloy	Condition or Treatment	Corrosion-Fatigue Strength at 10^8 Cycles, ksi (MPa)		Reference
86Cu-10Al-2Co-2Fe	Cast	27.0	(186)	204
Ni-Al Bronze	Cast	12.0	(83)	208
Ni-Al Bronze	Cast	17.9	(124)	7
Ni-Al Bronze	Cast	15.7	(108)	7
Ni-Al Bronze	Swaged bar	26.1	(180)	210
Ni-Al Bronze	Cast	12.0	(82.7)	9
Ni-Al Bronze	Cast	15.6	(108)	196
Al-Mn Bronze	Cast (2 heats)	16.0	(110)	190
CMA-1 (Mn-Ni-Al) Bronze	Cast	20.2	(139)	202
Mn-Ni-Al Bronze	Cast	9.0	(62.0)	5
Mn-Ni-Al Bronze	Cast	12.0	(82.7)	208
Mn-Ni-Al Bronze	Cast	12.3	(84.9)	7
Mn-Ni-Al Bronze	Cast	13.2	(91.1)	7
Mn-Ni-Al Bronze	Cast	13.0	(89.6)	9
Br. AZhMts Bronze		14.2	(98.0)	203
Br. AZhMts Bronze		21.3	(147)	203
Br. ANZhMts Bronze		15.6	(109)	203
AZhN Bronze	Cast	18.5	(127)	205
8Mn-8Al-2Ni Bronze	Cast	11.4	(78.4)	206

increases the CFS of copper but not to the point where it equals that observed for these copper alloys tested in air, and the alloyed materials are more susceptible to environmental effects than pure copper.

Cold working increased the CFS of copper from 10 to 16.5 ksi[3] (69 to 114 MPa). Comparing these values with those for other wrought materials listed in Table 22 shows that alloying increases the CFS. The CFS values for the wrought copper-based alloys typically ranged from 20 to 40 ksi (138 to 276 MPa). In contrast, cast materials had lower CFS values, ranging from 5 to 25 ksi (34 to 172 MPa). Thus, for applications where corrosion fatigue is critical, the wrought materials would be superior to the cast ones. However, cast products are often much more economical than wrought ones, and if welding of the wrought materials is required, this may offset any advantage they have over cast materials.

Typical examples of corrosion-fatigue curves for four cast copper alloys tested in air and saltwater are shown in Figures 132 through 135.[192] The ordinate in these plots in psuedo stress amplitude which is directly proportional to total strain range and is actually the applied stress, only under nominally elastic cyclic stress-strain conditions, as explained earlier in the chapter on carbon and low-alloy steels. Within the data scatter, environmental effects are small at short lives ($\leq 10^5$ cycles to failure). At long lives, low-strength alloys (e.g., valve bronze in Figure 133) show slightly improved CFS just as with pure copper, but higher strength alloys (e.g., Ni-Al bronze in Figures 134 and 135) show somewhat decreased CFS in saltwater compared with that in air. Also, the CFS of wrought material (Figure 135) is typically better than that of its cast counterpart (Figure 134).
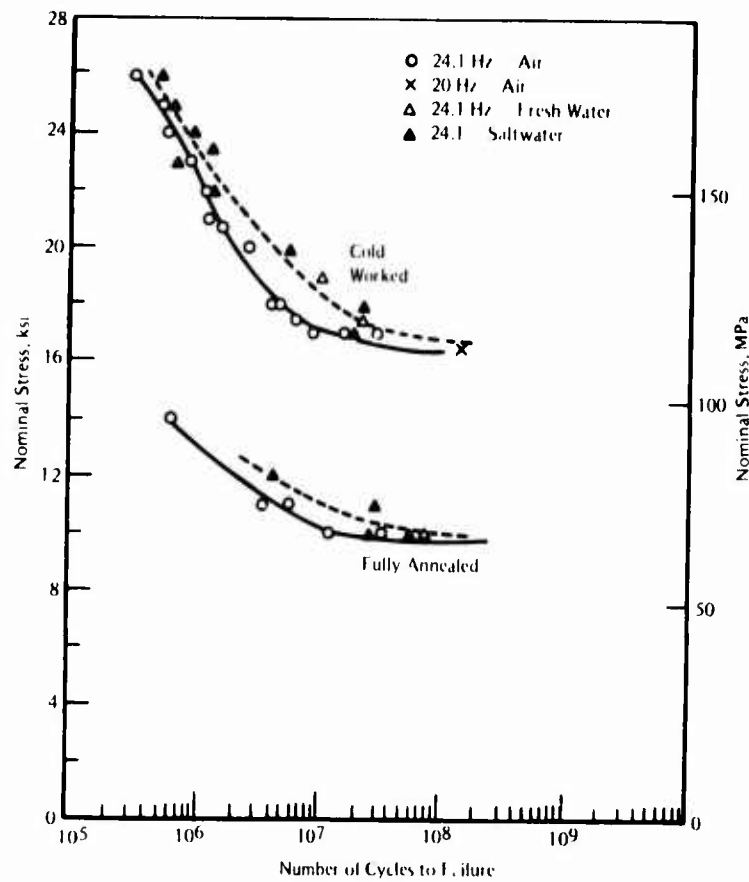
FIGURE 130. Corrosion-Fatigue Behavior of Electrolytic Copper in Severn River Water[3]
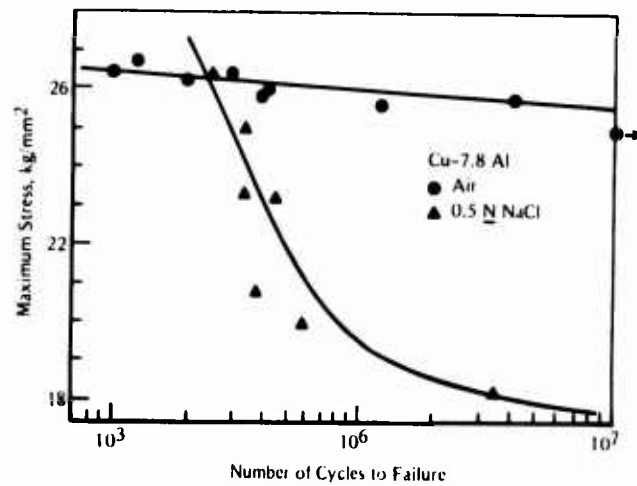
FIGURE 131. Corrosion Fatigue of Cu–7.8Al Alloy[199]
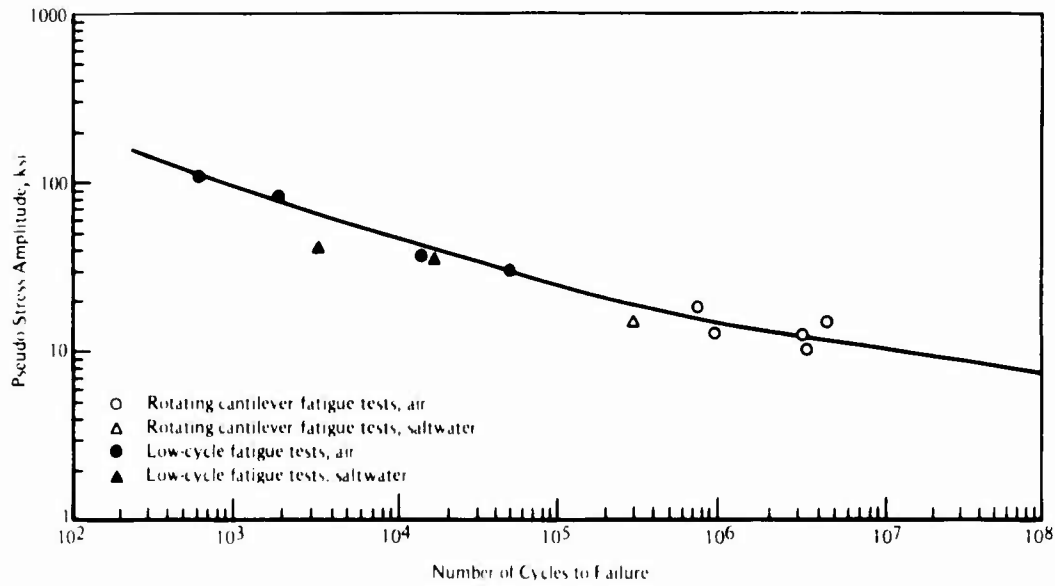
FIGURE 132. Corrosion Fatigue of Cast Gun Metal in Severn River Water [192]
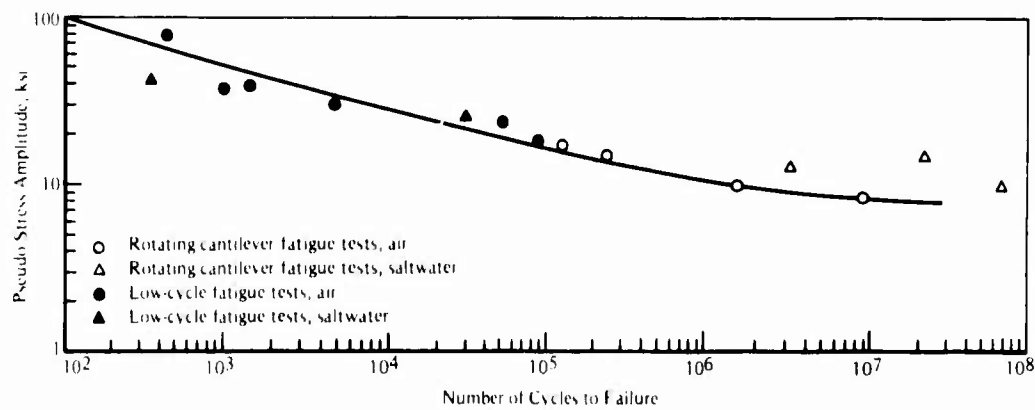
FIGURE 133. Corrosion Fatigue of Cast Valve Bronze in Severn River Water [192]
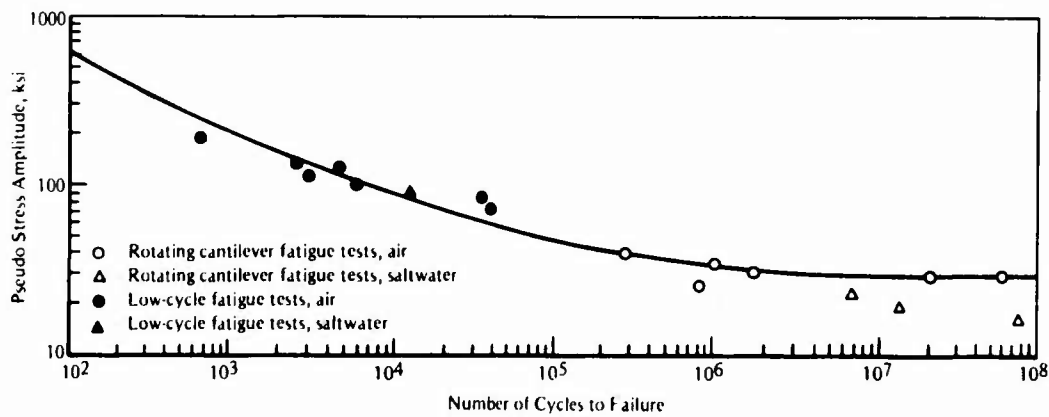
FIGURE 134. Corrosion Fatigue of Cast Ni-Al Bronze in Severn River Water [192]
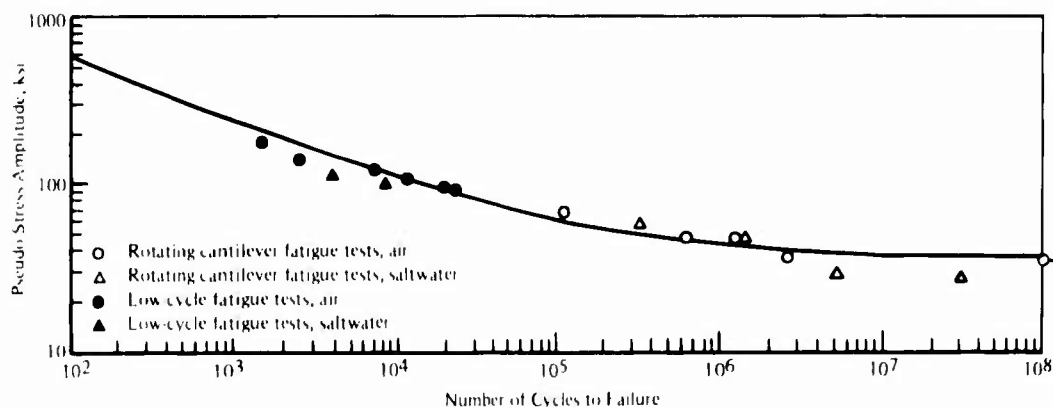
FIGURE 135. Corrosion Fatigue of Forged Ni-Al Bronze in Severn River Water [192]

Effect of Alloy Composition

The two Cu-Sn alloys[4] listed in Table 22 had CFS values of 22 and 19 ksi (152 and 131 MPa), which are about 15 to 30 percent greater than that of the electrotytic copper in the cold-worked (CW) condition. The two Cu-Zn-Sn alloys (cast) had the lowest CFS of any alloy listed in Table 22.

The high-tensile-strength brasses or manganese bronzes had fairly low CFS values, ranging from 7.0 to 15.6 ksi (48.3 to 108 MPa). Gun metal and valve bronze[192] had similar CFS values—7.5 and 10.0 ksi (51.7 and 69.0 MPa), respectively. The P bronze and Si bronze had moderate CFS values for the product forms tested. A Mn-Ni bronze[190] had a fairly low CFS, 9.5 ksi (66 MPa).

The wrought Be bronzes[2,200] had the highest CFS values of all the copper alloys listed in Table 21, ranging from 30.5 to 39 ksi (210 to 269 MPa). The cast Be bronzes[190] had moderately high CFS values, 13.5 and 15.5 ksi (93 and 107 MPa). One of the Cu-Ni-Be alloys[190] had good CFS, 12.5 ksi (86.2 MPa), but another Cu-Ni-Be alloy and a Cu-Co-Be alloy had fairly low CFS values, 7.7 and 7.0 ksi (53.1 and 48.3 MPa), respectively.

With the exception of two Al-Ni bronzes[190] all of the Al and Ni-Al types of bronzes had moderately good to quite good corrosion-fatigue resistance, with CFS values ranging from 12.0 to 27.0 ksi (82.7 to 186 MPa) for castings and from 22.0 to 32.7 ksi (151 to 226 MPa) for wrought products. The two Al-Ni alloys[190] with low CFS values, 8 ksi (55.2 MPa), contained only about 1 weight percent Fe or less and about 4.4 weight percent Al or less. In contrast, the Al and Ni-Al bronzes typically contained 8 to 11 weight percent Al and 3 to 5 weight percent Fe.

The Mn-Ni-Al bronzes (cast) generally had fairly high CFS values, ranging from 12 to 21.3 ksi (82.7 to 147 MPa), although in one case[5] a surprisingly low value of only 9 ksi (62 MPa) was reported. In subsequent analyses and discussions[6], no good reason for this lower than expected value was found.

The Mn bronzes (or high-tensile-strength brasses), the Ni-Al bronzes, and the Mn-Ni-Al bronzes are widely used in propellers. A comparative summary of the corrosion-fatigue strength of these three alloys, by Jaske et al[9], is shown in Figure 136. This figure shows that at 10^8 cycles to failure, the Mn bronze typically had a CFS of about 10 ksi (70 MPa), while the Ni-Al and Mn-Ni-Al bronzes had a higher CFS, about 12 ksi (83 MPa).

Note: Shaded area shows scatter band of specimen failures.

1 Jaske et al in seawater } Cantilever bending at 3.33 Hz

2 May in seawater
3 Webb et al in 3% NaCl solution } Rotating bending
4 Czyryca and Niederberger in Severn at 20 to 30 Hz
   River Water

a. At 10^6 Cycles to Failure

b. At 10^8 Cycles to Failure
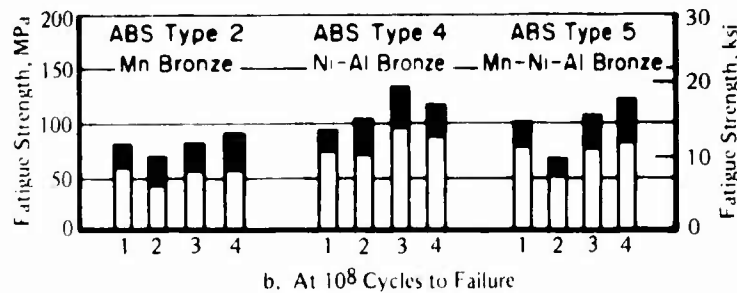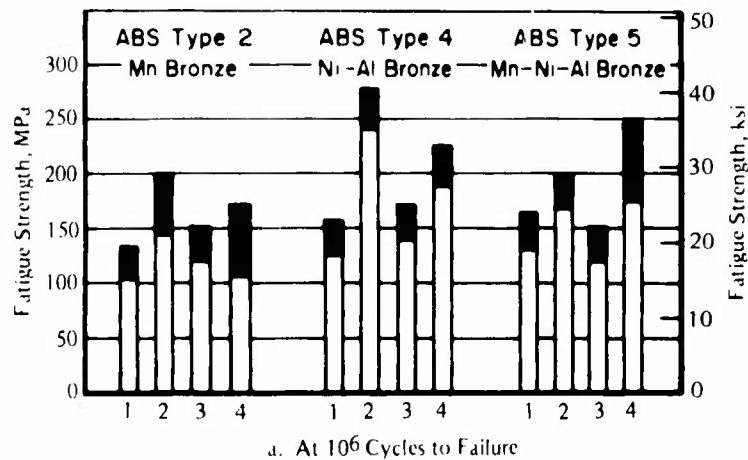
FIGURE 136. Comparative Corrosion-Fatigue Strength of Three Cast Bronze Alloys for Fully Reversed Loading (Zero Mean Stress)[9]

Effect of Stress Ratio

The effect of stress ratio (R) on long-life corrosion-fatigue resistance has been evaluated for propeller alloys.[7,9,206] In general, increased R (above -1) is detrimental to corrosion-fatigue life. Jaske et al[9] analyzed their data using both the Goodman-type relation and the Smith-Watson-Topper (SWT) parameter.[211] They found that the SWT parameter provided a better correlation of stress ratio (or mean stress) effects than the Goodman relation. The parameter defines an equivalent fully reversed strain amplitude. ε_{eq}, in terms of the strain amplitude, ε_a, the actual maximum stress, S_{max}, the elastic modulus, E, and a material constant, m:

$$\varepsilon_{eq} = (\varepsilon_a)^m (S_{max}/E)^{1-m}$$

For the nominally elastic cyclic stress-strain amplitudes which are observed for these alloys in the long-life regime ($>10^6$ cycles to failure), the parameter reduces to an equivalent stress amplitude, S_{eq},

$$S_{eq} = (S_a)^m (S_{max})^{1-m} \quad ,$$

where S_a is the actual stress amplitude. Using this parameter with $m = 1/2$, gives

$$S_{eq} = (S_a S_{max})^{1/2} \quad ,$$

which they found worked quite well, as shown in Figures 137 and 138.[9]

Notch Effects

The effect of notches on corrosion-fatigue resistance was addressed in four of the studies[190,194-196] listed in Table 21. These were all studies of cast propeller alloys. No results for notched specimens of wrought materials were found. For rotating bending specimens with a circumferential notch of $K_t = 3$, Czyryca and Niederberger[208] found that the notches had no significant influence on the nominal CFS of Mn bronze, Ni-Al bronze, or Mn-Ni-Al bronze castings. Their results for these three cast alloys are shown in Figures 139, 140, and 141. For specimens with sharp surface notches ($K_t = 5.2$ and 9.7) tested in plane bending, Tokuda et al[196] found that CFS was reduced about 50 percent below that of unnotched specimens of Ni-Al bronze cast material, as shown in Figure 142. The scatter band of Czyryca and Niederberger's[208] data for both smooth and notched specimens is included for comparison. Tokuda et al[196] also tested unnotched specimens of cast Ni-Al bronze in rotating bending and their results agree quite well with the data of Czyryca and Niederberger[208], as shown in Figure 143. Thus, the data indicate that sharp surface notches will reduce the CFS of these cast propeller alloys under plane bending, whereas circumferential notches ($K_t \sim 3$) have no significant influence on CFS in rotating bending.

Welded Joints

Welded material was used in two of the studies[189,208] listed in Table 21. Newcombe[189] tested specimens of butt-welded Al bronze and Al-Si bronze cast plates under reversed cantilever bending at 0.0028 Hz and in seawater, with temperatures varying (not controlled) from 45 F (7 C) to 82 F (28 C). The specimens were cycled under deflection control and cyclic lives in the range 10^4 to 10^5 were obtained. Welded specimens of Al bronze had about two times the cyclic life of base-metal specimens. No failures were obtained for Al-Si specimens, so for this alloy no data on effect of welding were obtained. However, all of the Al-Si alloy specimens were tested for about twice the number of cycles or more than those of the Al bronze under similar test conditions, so the Al-Si bronze had better low-cycle corrosion-fatigue resistance than the Al bronze. Czyryca and Niederberger[208] conducted corrosion-fatigue tests (rotating beam) for weldments of three cast propeller alloys—Mn bronze, Ni-Al bronze, and Mn-Ni-Al bronze. As shown by the data in Figures 144, 145, and 146, weld-metal and weldment specimens had CFS values within the scatter bands of base-metal data. For these small specimens, taken from welded plates, stress-relieved material had about the same CFS as the as-welded material. However, even with as-welded material there may have been signficant stress relief from the fabrication process that would not occur with large as-welded components. If tensile residual stresses are present in actual welded hardware, it would be expected that these would reduce CFS in the same manner as would imposed tensile mean stresses (see earlier discussion of stress-ratio effects). Other than possible reduction in CFS because of the residual stress, the results indicate that welding does not degrade the CFS of these cast bronze alloys.
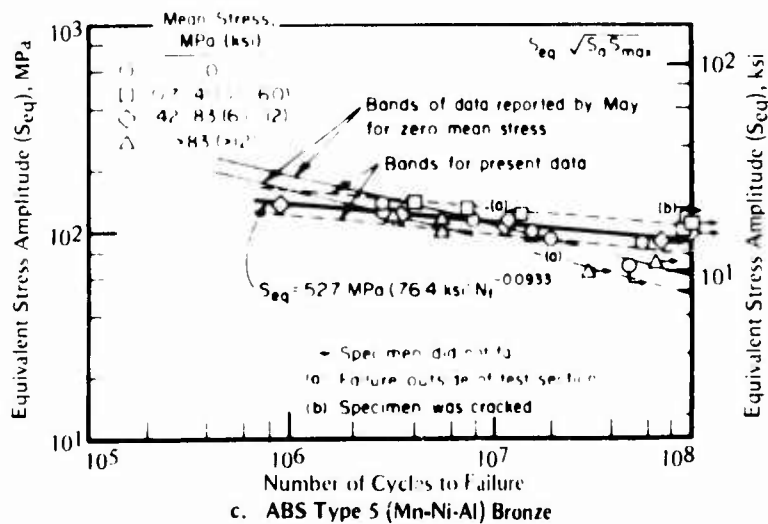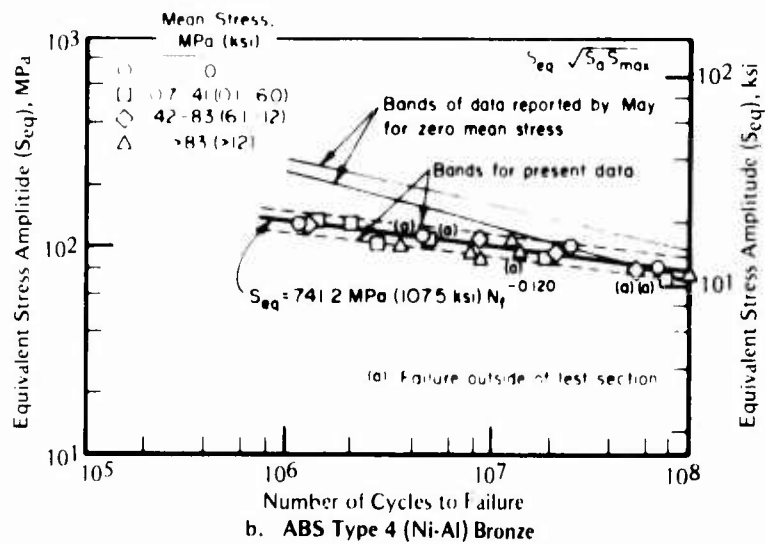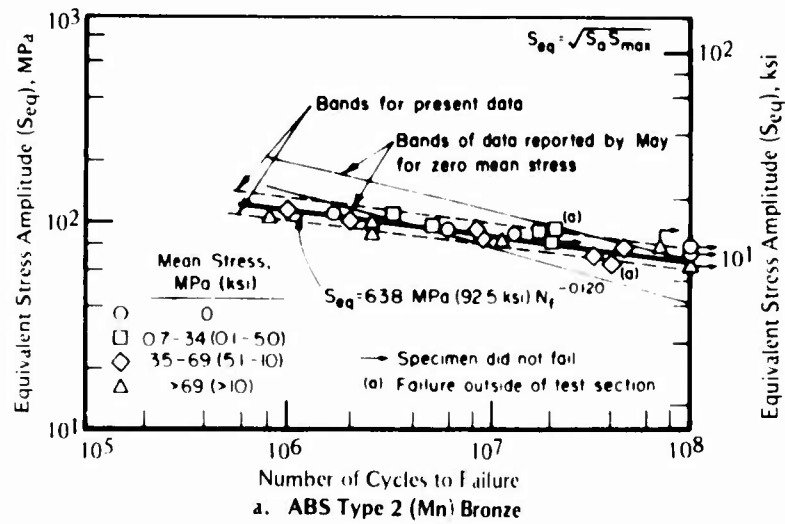
FIGURE 137. Corrosion Fatigue Life as a Function of the Equivalent
Stress Parameter (Flowing Seawater Environment)[9]
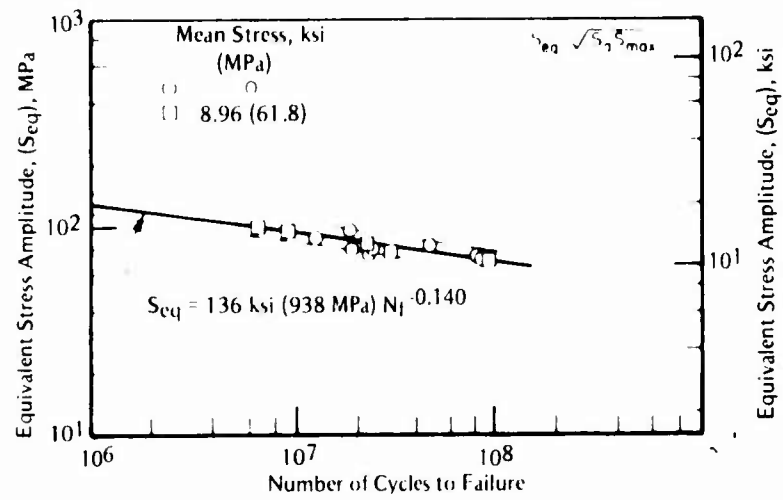
a. High Tensile Brass (Similar to ABS Type 2)
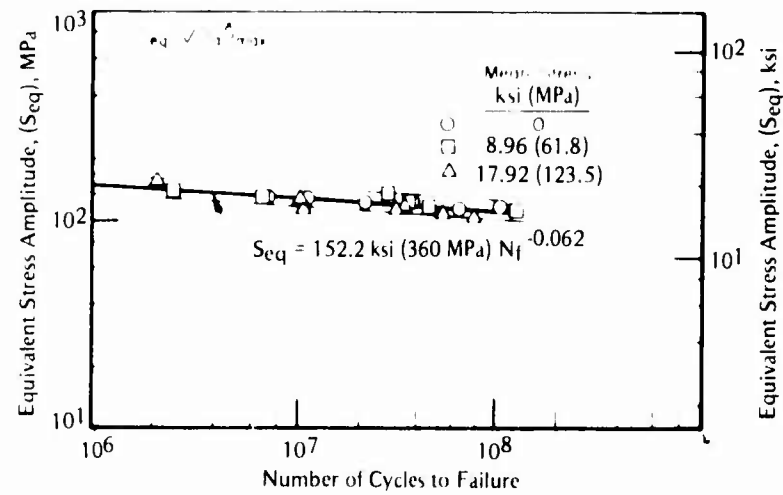
b. Ni-Al Bronze (Similar to ABS Type 4)
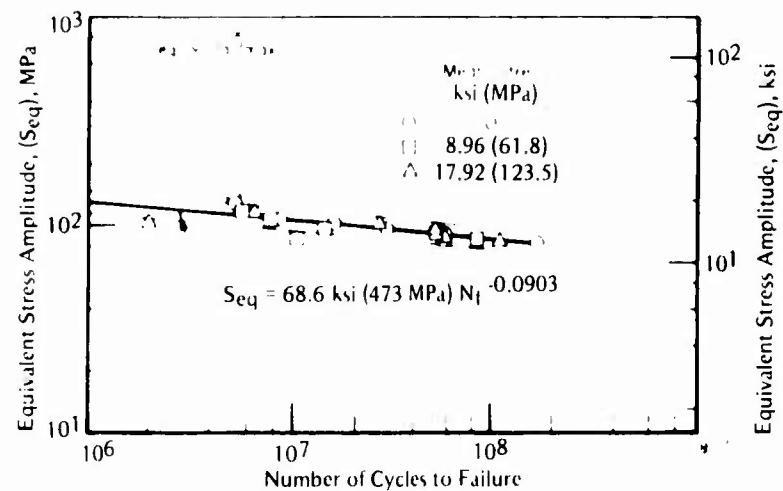
c. Mn-Al Bronze (Similar to ABS Type 5)

FIGURE 138. Corrosion Fatigue Life as a Function of the Equivalent Stress Parameter for 3 Percent NaCl Environment[9]
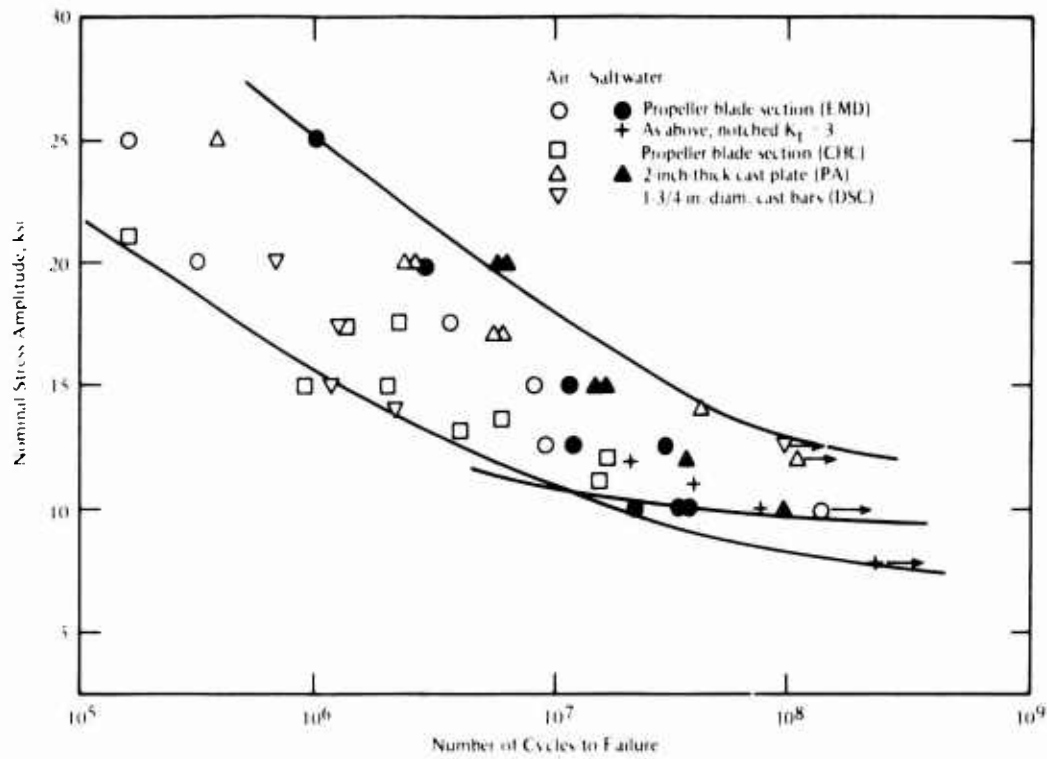
FIGURE 139. Rotating Beam Fatigue Data for Mn Bronze Castings[208]
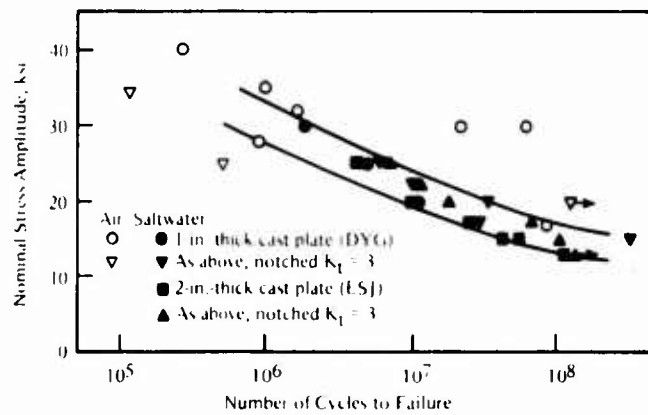
FIGURE 140. Rotating Beam Fatigue Data
for Ni-Al Bronze Castings[208]
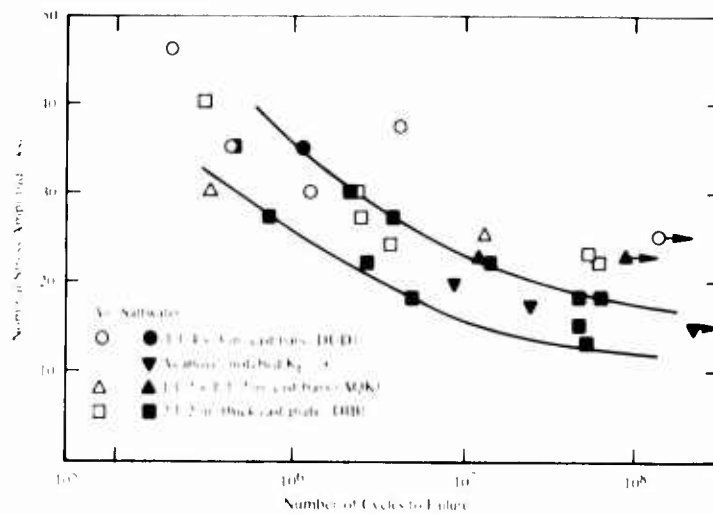
FIGURE 141. Rotating Cantilever–Beam Fatigue Data for Cast Mn-Ni-Al Bronze[141]
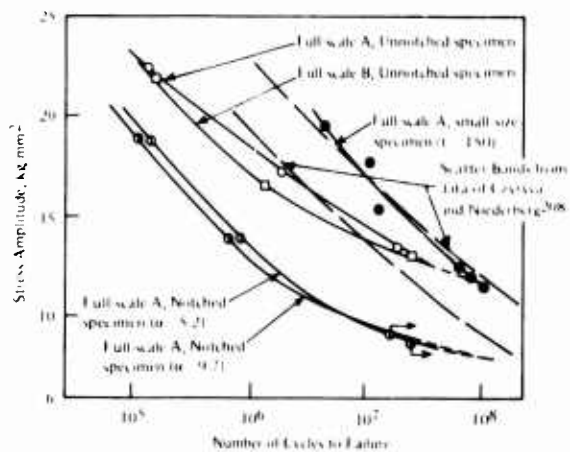
FIGURE 142. Corrosion Fatigue (Seawater) of Specimens Under Plane Taken From Cast Ni-Al Bronze Propeller[196]
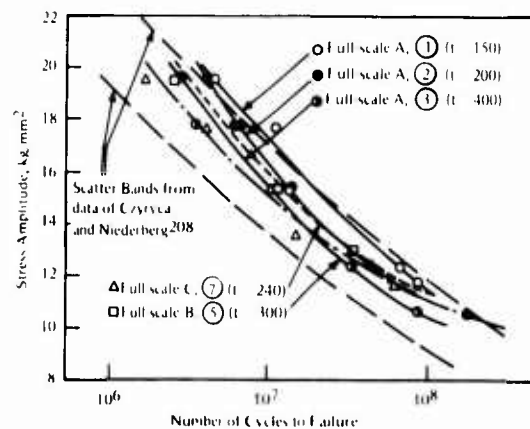
FIGURE 143. Corrosion Fatigue (Seawater) of Specimens Under Rotating Bending Taken From Cast Ni-Al Bronze Propellers[196]
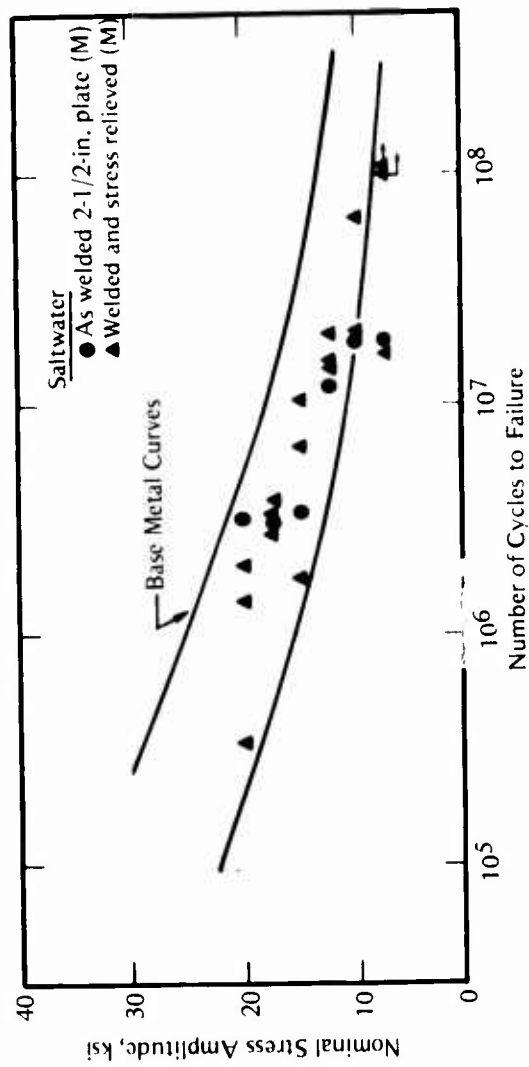
FIGURE 144. Rotating Beam Corrosion-Fatigue Data for Weldments of Cast Mn Bronze[208]
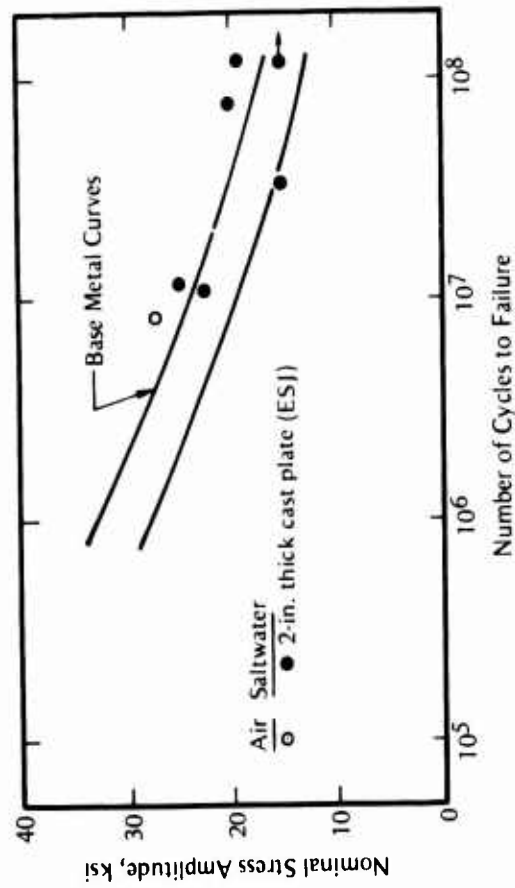
FIGURE 145. Rotating Beam Corrosion-Fatigue Data for Weldments of Cast Ni-Al Bronze[208]
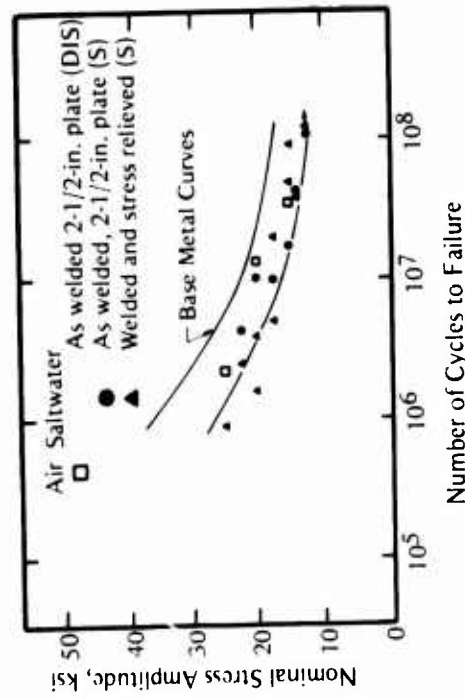
FIGURE 146. Rotating Beam Corrosion-Fatigue Data for Weldments of Cast Mn-Ni-Al Bronze[208]

Effect of Cyclic Frequency

The effect of cycling at low frequencies (<5 Hz) was investigated in four of the studies[9,189,209,210] listed in Table 21. Newcombe[189] showed that decreasing the frequency from 0.0028 to 0.00028 Hz decreased low-cycle corrosion-fatigue life of a cast Al bronze by about a factor of two, as shown in Figure 147. However, when frequency was decreased from 0.17 to 0.0028 Hz, Cross[209] found that there was no significant change in low-cycle corrosion-fatigue resistance of Al bronze in seawater, as shown in Figure 147. Cross's data[209] at 0.0028 Hz agree fairly well with Newcombe's data[189] at the same cyclic frequency.

FIGURE 147. Effect of Cyclic Frequency and Water Temperature on Low-Cycle Corrosion Fatigue of Al Bronze in Seawater[189, 209]
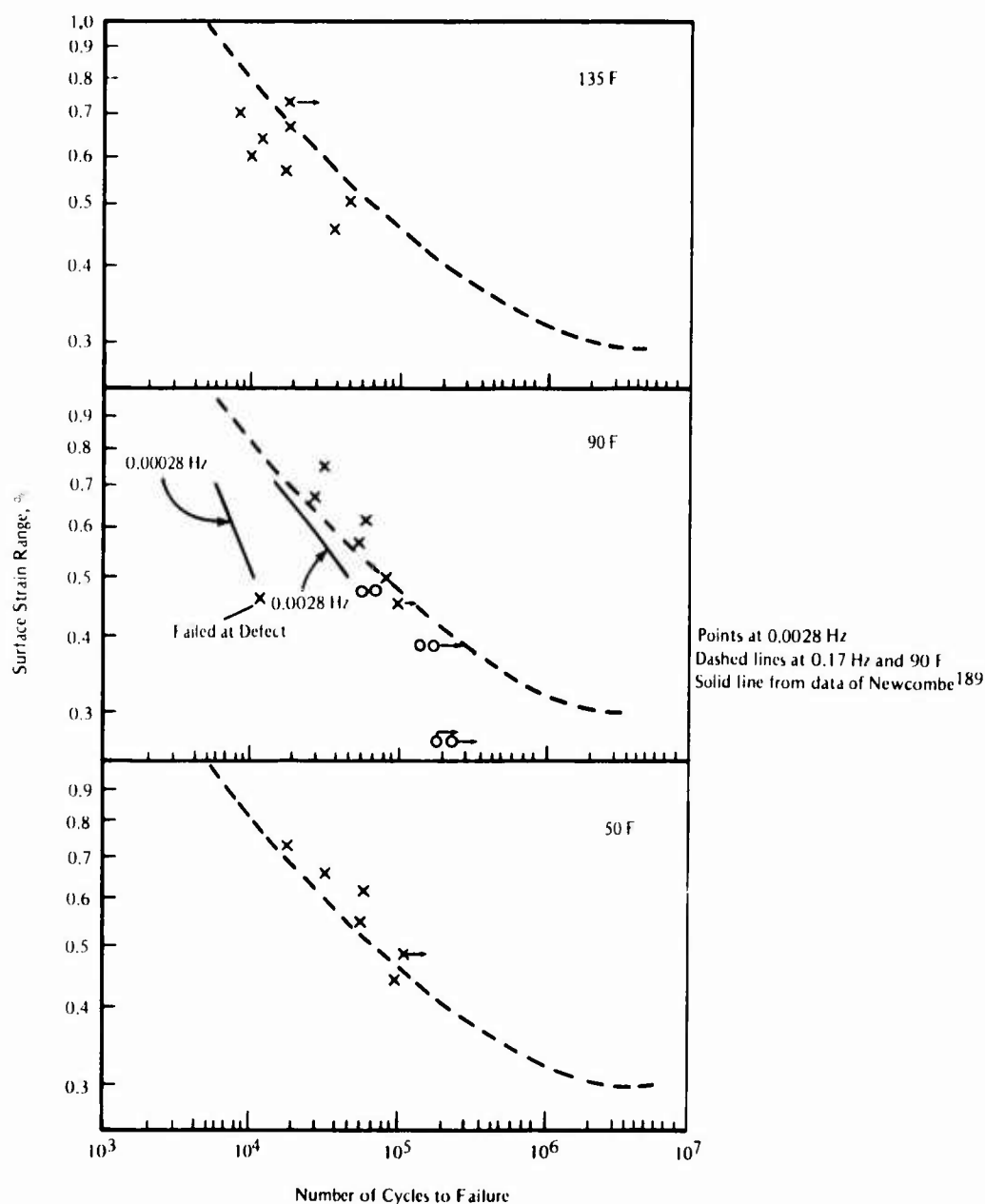
Collins and Duquette[210] found that decreasing the cyclic frequency significantly decreased the corrosion-fatigue resistance of a wrought Ni-Al bronze alloy in 0.5 N NaCl solution. Their results are presented in Figure 148. At 10^6 cycles to failure, CFS decreased from 40 ksi (276 MPa) at 20 Hz to 31 ksi (213 MPa) at 2 Hz. When Jaske et al[9] tested a cast Ni-Al bronze of the same nominal chemical composition, they found that a reduced cyclic frequency of 3.33 Hz (compared with 20 to 30 Hz) had little or no effect on CFS at 10^8 cycles to failure (see Figure 136). Their data at 10^6 cycles to failure are biased by the fact that plane bending lowers CFS at shorter lives than does rotating bending. For example, compare May's[6] data with that of Jaske et al[9] in Figure 137 or compare the data of Tokuda et al[196] for small-size specimens under rotating beam bending with that for full-scale specimens under plane bending in Figure 142.

The difference in frequency effect between the wrought Ni-Al bronze alloy and its cast counterpart seems to be related to the difference in microstructures developed in processing each material. In both cases, the materials contained large equiaxed α grains. In the cast material, the region between these α grains was a mixture of well-distributed and a self-annealing eutectoid, whereas in the wrought bar this region contained well-defined α platelets intermixed with the eutectoid. In the bar, the area between the primary α grains was preferentially corroded and the lower frequency enhanced this corrosive attack.

No such enchancement of localized corrosion was noted with the cast material. However, such enhancement was not specifically looked for in the work of Jaske et al[9], and they conducted no experiments at a higher cyclic frequency. Thus, further work needs to be done to confirm whether the above hypothesized microstructural influence is truly an accurate explanation of the results.
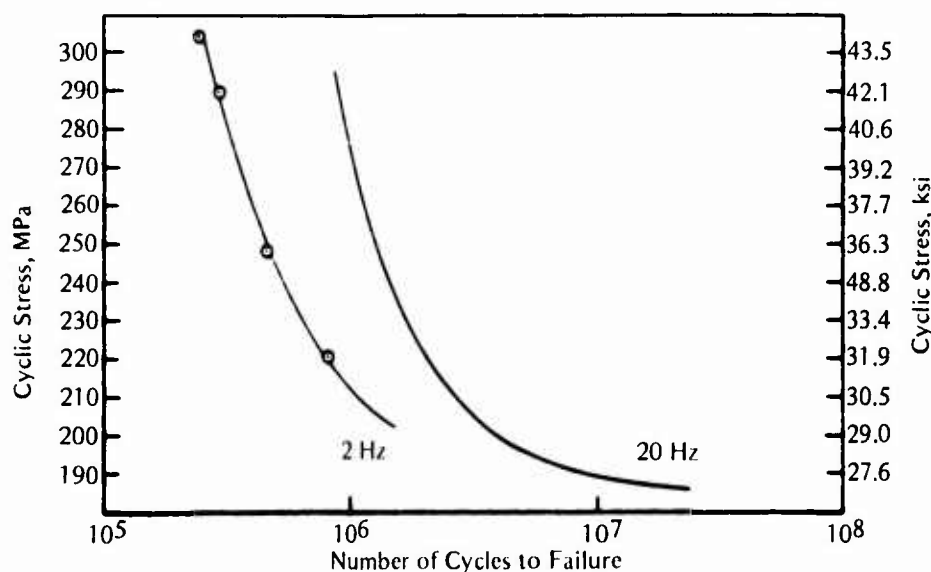
FIGURE 148. Effect of Frequency on Corrosion-Fatigue Resistance of Ni-Al Bronze in 0.5 N NaCl Solution at Room Temperature[210]

Effect of Environmental Variables

No systematic comparison of the influence of various types of saline environments on the CFS of copper alloys was found in this review. Taken as a whole, the results listed earlier in Table 22 indicate that the CFS of these copper alloys is not significantly affected by variations in

solution composition, such as ~3 percent NaCl solution, natural seawater, brackish saltwater, and synthetic seawater. However, such effects may be masked by variations in data from study to study. Jaske et al[9] used flowing natural seawater at 45 F (7 C) to 54 F (12 C) in their investigation of propeller alloys and obtained results and trends similar to those of studies carried out in warmer seawater, brackish saltwater, and 3 percent NaCl solution (see Figure 136).

In his study of Al bronze, Cross[209] used seawater at temperatures of 50 F (10 C), 90 F (32 C), and 135 F (57 C). (See Figure 147 presented earlier.) There was little difference in low-cycle corrosion-fatigue resistance between 50 F (10 C) and 135 F (32 C), but it was slightly reduced (by about a factor of 2 on cyclic life) at 135 F (57 C).

No data were found on the effects of pH level, oxygen content, pressure, or water velocity on the corrosion-fatigue behavior of copper alloys in marine environments.

Effect of Cathodic Protection

In three cases[197,199,210], it was shown the anodic polarization increased localized attack and reduced CFS of copper alloys. In all three cases, anodic polarization enhanced the tendency for intergranular cracking as opposed to transgranular cracking normally observed under free-corrosion conditions.

Since anodic polarization decreases CFS, it might be expected that cathodic polarization increases it and provides a means of protection from corrosion-fatigue damage. For cycling at 20 Hz, Collins and Duquette[210] found that cathodic protection improved the corrosion-fatigue resistance of wrought Ni-Al bronze in 0.5 N NaCl solution, as shown in Figure 149. At 10^7 cycles to failure, the CFS under free-corrosion conditions was about 27 ksi (186 MPa) and
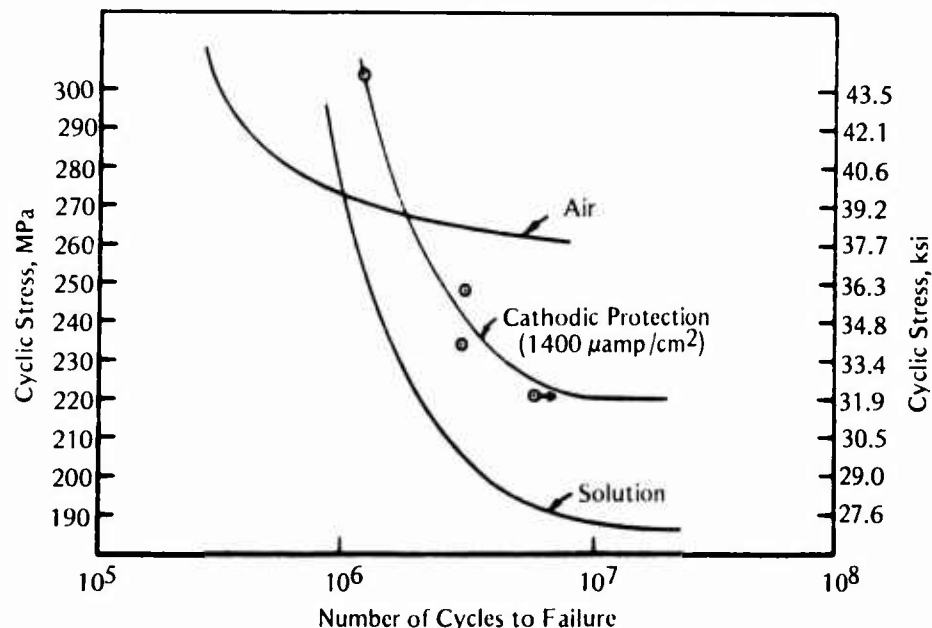
FIGURE 149. Effect of Applied Cathodic Current on Corrosion-Fatigue Resistance of Ni-Al Bronze in 0.5 N NaCl at Room Temperature[210]

under cathodic protection it was increased to about 32 ksi (221 MPa), which was still below the value of 38 ksi (262 MPa) obtained in air. Thus, cathodic protection improved CFS but not up to the levels of fatigue strength measured in air.

Veingarten et al[207] carried out experiemts on a LMtsZh (55Cu-3Mn-1Fe-35Ni) brass propeller alloy in seawater. Their results are presented in Figures 150 and 151. Cathodic polarization to -0.800 V increased CFS compared with that under free-corrosion conditions and gave fatigue resistance slightly above that for tests in air. Polarization to -0.900 and -1.050 V gave further improvements in CFS to levels well above those for tests in air. However, at -1.200 V, the CFS was decreased back to the levels observed for tests in air. Thus, cathodic protection appears to enhance resistance to corrosion-fatigue-crack initiation, but overprotection can be detrimental.
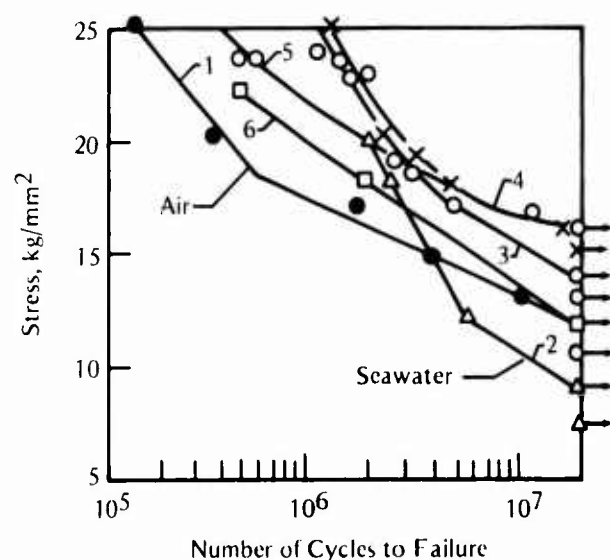
1 – In air
2 – In seawater without polarization
3 – In seawater at a potential of -0.8 V
4 – In seawater at a potential of -0.9 V
5 – In seawater at a potential of -0.105 V
6 – In seawater at a potential of -1.2 V

FIGURE 150. Fatigue Curves for Specimens of Brass LMtsZh 55-3-1[207]
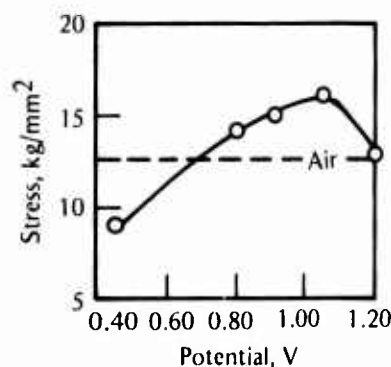
FIGURE 151. Corrosion-Fatigue Limit (at 2×10^7 cycles) of Brass LMtsZh 55-3-1 as a Function of Polarization Potential[207]

Fatigue-Crack-Growth Data

Only two of the investigations[195,196] listed in Table 21 developed corrosion-fatigue-crack growth data for copper alloys. In both cases, the stress ratio was zero. Gatzoulis et al[195] tested weld-metal specimens of cast Mn bronze in brackish saltwater at a frequency of 16.7 Hz. The results of their study are presented in Figure 152. At this high frequency, there was no environmental effect on crack growth rate. Weld metal was more resistant to crack growth than base metal for tests in air. Tokuda et al[196] developed crack-growth data for cast Ni-Al bronze in synthetic seawater at lower frequencies of 2.5 and 5 Hz. Their results are shown in
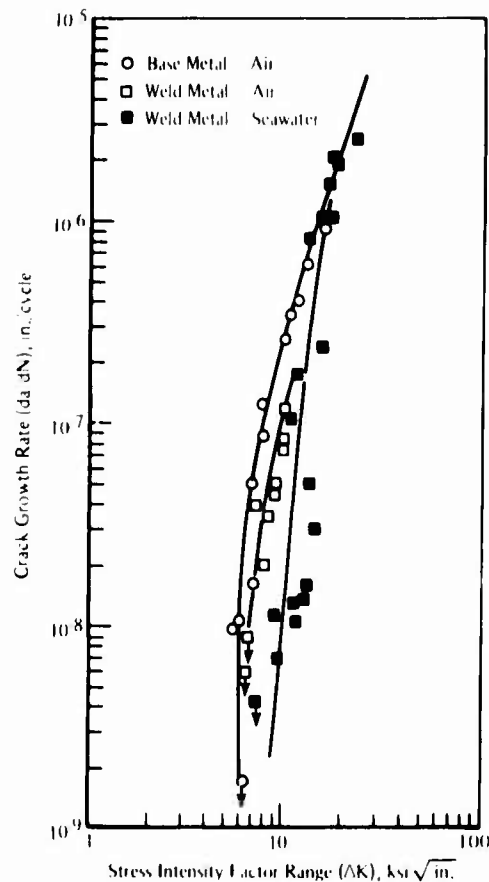
FIGURE 152. Fatigue-Crack Growth Results at 16.7 Hz for Manganese Bronze[195]

Figures 153 and 154, with weld-metal curves for the Mn bronze[195] added for comparison. At 5 Hz, crack growth rate was increased by a factor of about 3 to 4 in the synthetic seawater compared with that in air (see Figure 153). Also, decreased frequency (to 2.5 Hz) gave slightly increased crack growth rates (see Figure 154). Crack growth rates for the Ni-Al bronze at these lower frequencies were higher than those of the Mn bronze weld metal at a higher frequency. It appears that at higher frequencies ($\geq$10 Hz), marine environment has little effect on corrosion-fatigue-crack growth rate. However, at lower frequences ($\leq$5 Hz), exposure to such environments can accelerate crack growth rates. At this point, data on corrosion-fatigue-crack growth in copper alloys are quite limited, so these specific results for propeller alloy bronzes should not be generalized.
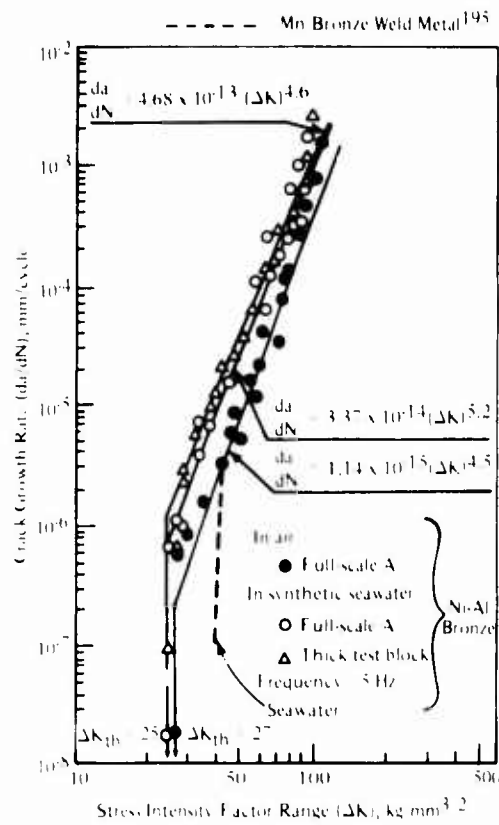
FIGURE 153. Effect of Environment on Fatigue Crack Growth Rate[196]
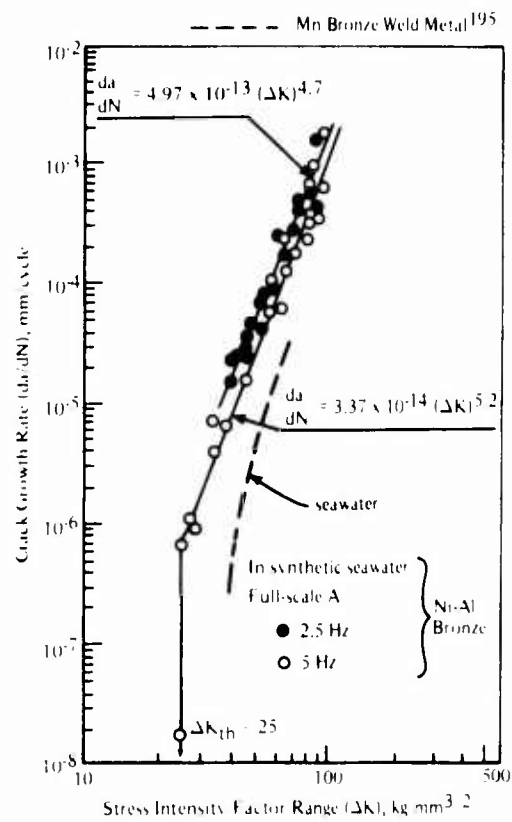
FIGURE 154. Effect of Frequency on Corrosion-Fatigue Crack Growth Rate[196]

CHAPTER 7
CORROSION-FATIGUE DATA FOR ALUMINUM ALLOYS

Corrosion-fatigue data are presented for aluminum alloys in seawater or saltwater. Four series of alloys are covered: the 2XXX, 5XXX, 6XXX, and 7XXX alloys. The 2XXX Al-Cu and 7XXX Al-Zn-Mg alloys can be heat treated to high strength levels but have only moderate corrosion resistance. They have been used primarily in the aerospace and aircraft industries. The 5XXX Al-Mg alloys are nonheat-treatable, medium-strength alloys and are used widely in marine applications because of their good resistance to corrosion in a marine atmosphere. Very little data was found for the 6XXX series of alloys since they have only limited application in the marine and aircraft and aerospace industries. It is observed that, in general, the presence of moisture and sodium chloride solutions accelerates corrosion-fatigue-crack growth rates for aluminum alloys, especially at low frequencies and low stress intensity factor (ΔK) levels.

2XXX Series Aluminum Alloys

Solution heat treatment or artificial aging is required to impart optimum mechanical properties to Al-Cu alloys. These 2XXX-series alloys are used in the aircraft and aerospace industries. The alloys reviewed and the corresponding reference numbers of the articles in which the data appeared are listed in Table 23. Data for the 2XXX series aluminum alloys are summarized in Table 24. RR58 and LM30 are British alloys* and D16T and D16AT are Soviet alloys.

TABLE 23. 2XXX Series Aluminum Alloys Reviewed

Alloy	Alloy Composition, wt %									References
	Si	Cu	Mg	Mn	Fe	Ni	Li	Zn	Al	
2014	0.8	4.4	0.5	0.8	—	—	—	—	Bal	212, 213
2020	—	4.5	.	—	—	—	1.3	—	Bal	212
2024	—	4.4	1.5	0.6	—	—	—	—	Bal	212, 213, 215, 216
2219	—	6.3	—	0.3	—	—	—	.	Bal	217
RR58	0.23	2.64	—	0.03	1.15	0.1	—	—	Bal	218, 219
LM30	18.0	4.5	—	0.3	1.1	0.1	—	—	Bal	219
D16T	0.3	4.1	1.6	0.5	0.4′	0.1	—	0.24	Bal	220 – 222
D16AT	—	4.2	1.6	1.5	—	—	—	0.5	Bal	220, 222, 223

*Alloy LM30 should be classified as a 4XXX series alloy but is placed in this chapter for comparison purposes.

PRECEDING PAGE BLANK—NOT FILMED

TABLE 24. Summary of Corrosion-Fatigue Data for the 2XXX Series Aluminum Alloys

Alloy-Condition	Tensile Strength, ksi (MPa) Ultimate	Yield	Type of Specimen	Frequency, Hz	Environment	Type of Loading	Types of Data	Notes	References
2219-T87			Single-edge-notched cantilever		3.5% NaCl	Zero-to-tension, constant load		Basic crack propagation appeared to be completely unaffected by salt water environment	217
2014-T6	69.1 (476)	—	Repeated bending	No mention	Actual fatigue testing done in laboratory air	Repeated plane bending		Fatigue following corrosion-induced attack	212
2014-T6	67.5 (462)	—	Repeated bending	No mention	Methods used to corrode material: continuous fog (spray), cyclic fog spray, and continuous immersion	Repeated plane bending			212
2014-T6	65.3 (447)	—	Repeated bending	No mention		Repeated plane bending			212
2014-T6-clad	69.3 (477)	—	Repeated bending	No mention		Repeated plane bending			212
2014-T6-clad	68.9 (472)	—	Repeated bending	No mention		Repeated plane bending			212
2014-T6-clad	68.7 (474)	—	Repeated bending	No mention		Repeated plane bending			212
2020-T651	83.1 (573)	—	Dogbone with holes	No mention	Fretted,[b] tested in 3.5% NaCl solution	Uniaxial tension,[a] maneuver spectrum		(1) Prior to corrosive exposure, most specimens were subjected to a "fretting" program which produced a condition in the specimen test holes similar to that in repeatedly loaded aircraft holes containing "nonfilling" hole fasteners	214
2024-T851	68.2 (470)	—	Dogbone with holes	2		Uniaxial tension, maneuver spectrum			214
2024-T351	66.8 (461)	—	Dogbone with holes	2	Fretted, alternately immersed in 3.5% NaCl for 30 days and then tested in air	Uniaxial tension, maneuver spectrum			214
2020-T651	83.1 (537)	—	Dogbone with holes	2		Uniaxial tension, maneuver spectrum			214
2024-T851	68.2 (470)	—	Dogbone with holes	2	Fretted, alternately immersed in 3.5% NaCl solution for 30 days and tested in distilled H_2O	Uniaxial tension, maneuver spectrum			214
2020-T651	83.1 (573)	—	Dogbone with holes	2		Uniaxial tension, maneuver spectrum			214
2020-T651	83.1 (573)	—	Dogbone with holes	2	Fretted, alternately immersed in 3.5% NaCl solution for 30 days	Uniaxial tension, maneuver spectrum			214
2020-T651-Alodine[c]	83.1 (573)	—	Dogbone with holes	2		Uniaxial tension, maneuver spectrum		(2) Alodine protective coating in the hole	214
2024-T851	68.2 (470)	—	Dogbone with holes	2	Fretted, alternately immersed in 3.5% NaCl solution	Uniaxial tension, maneuver spectrum			214
2024-T351	66.8 (461)	—	Dogbone with holes	2	Nonfretted, alternately immersed in 3.5% NaCl solution and tested in air	Uniaxial tension, maneuver spectrum			214
2020-T651	83.1 (573)	—	Dogbone with holes	2		Uniaxial tension, maneuver spectrum			214
2020-T651[d]	83.1 (573)	—	Dogbone with holes	2	Fretted, alternately immersed for 30 days in 3.5% NaCl solution and tested in 3.5% NaCl solution until a crack was detected; then reworked and tested in air	Uniaxial tension, maneuver spectrum		Determine the additional life which could be obtained if the corrosive holes were reworked to remove cracks after detection (3) As opposed to constant amplitude loadings	214
RRS8[d]	65 (448)	53 (365)	Crack-line-loaded Double-cantilever beam	0.15	3.5% NaCl solution @69.8 F	Axial, R=0	Crack growth vs N FCG vs ΔK		218
D16AT[e]	(h)	(i)	Flat	1.5	3.0% NaCl solution	Pure bending	S-N diagrams from 6×10^4 to 10^6 cycles	Effect of magnetic treatments on corrosive media	227
D16T[f,g]	—	—	Flat some with rivet holes	8.33	3.0% NaCl solution	Pure symmetrical bending	S-N curves from 7×10^4 to 5×10^6		222

TABLE 24. (Continued)

Alloy-Condition	Tensile Strength, ksi (MPa) Ultimate	Yield	Type of Specimen	Frequency, Hz	Environment	Type of Loading	Types of Data	Notes	References
D16AT (clad)	-	-	Flat some with rivet holes	8.33	3.0% NaCl solution	Pure symmetrical bending			220
D16AT clad	65 (447)	46 (314)		8.33	3.0% NaCl solution	Pure symmetrical flexure	S-N cures from 8×10^4 to 5×10^6 cycles		
D16T unclad	66 (456)	46 (314)		8.33	3.0% NaCl solution	Pure symmetrical flexure			
D16AT (clad)			Sheet with single- and double-stitch welds with and without polymer coating	41.67	3.5% NaCl solution containing 0.196 H_2O_2	Asymmetric cyclic tensile pulse	S-N curves from 2×10^5 to 10^7 cycles	Effect of polymer coatings	223
2024-T8	69 (471)		Single-edge notched	1.0	3.5% NaCl solution	Constant-amplitude (FCP)		Influence of environment on retardation	224
2014-T6			Rotating beam	33.33	Artificial seawater	Cantilever rotating bending			213
2024-T4			Rotating beam	33.33	Artificial seawater	Cantilever rotating bending			213
2618A T851	67 (460)		Center notched	25, 1, 0.1, 0.01	3 g/l NaCl solution			Influence of environment on crack propagation	225
2024 T351	70 (477)		Center notched	25, 1, 0.1, 0.01	3 g/l NaCl solution				225
2024-T3	70.5 (486)	45.7 (315)	Center-cracked	2.0	3.5% NaCl solution	Remote loading; wedge force loading		Influence of environment on fatigue-crack growth rate under conditions where the mechanical aspects of fatigue are less dominant	226
2024-T4	72 (496)		Rotating beam	60	Salt spray of 20 wt % NaCl at 95 F for various lengths of time (2 hours to 32 days); rinsed in distilled H_2O, dried, and fatigue tested in laboratory air	Rotating bending		Effects of corrosion pitting on fatigue behavior found to serve as stress raisers	215
2024-T4	72 (496)		Rotating beam	60		Rotating bending			215
2024-T4	71 (490)		Rotating beam	60		Rotating bending			215
2024-T4	70 (483)		Rotating beam			Rotating bending			215
RR58(d)	65 (450)		Double Cantilever beam		3.5% NaCl solution				219
2024-T851			WOL specimens, center cracked tension, surface-cracked part-through cracked Wedge open loading, ≈ compact tension, though they are actually different	20-0.1	3.5% NaCl solution				169
D16 Duralumin(i)	55 (37?)	40 (275)	Cylindrical with circular V-shaped grooves; smooth, no grooves	46.6	3.0% NaCl solution			Fatigue limits	221

(a) See note (1) in Notes column. (b) See note (2) in Notes column. (c) See note (3) in Notes column. (d) An Al-Cu-Mg alloy belonging to the series 2000. (e) Al-4.1 Cu-1.6 Mg-0.5 Mn-1.5 Zn. (f) Al-4.1 Cu-1.6 Mg-0.4 Fe-0.3 Si-0.1 Ni-0.04 Ti.

(g) See note (3) in Notes column. (h) 42 daN/mm². (i) Al-3.8 Cu-1.23 Mg-0.53 Mn-0.50 Fe-0.53 Si.

(e) Specimens were anodized. (f) 30 daN/mm².

Alloy 2014

The effect of prior corrosion on the fatigue behavior of clad and bare Alloy 2014-T6 was studied by Person.[212] Tapered repeated-bending specimens of bare 2014-T6 were corroded by a continuous fog spray (ASTM-B-368-65) of 5 percent NaCl plus 0.026 percent $CaCl_2$ acidified to a pH of 3.0 with acetic acid, for 48 and 168 hours. The clad 2014-T6 specimens were corroded by continuous immersion in 3.5 percent seasalt plus 10 percent H_2O_2 in H_2O for 96 and 168 hours. The pH was not adjusted. The two exposure-time periods were used to provide two sets of specimens, one with light pitting and one with heavy pitting. Fatigue testing was carried out under constant deflection conditions.

The tensile properties for each alloy were measured after corrosion in the laboratory. The unclad 2014-T6 exhibited the greatest decrease in tensile properties. The average tensile properties for both materials are given in Table 25. Fatigue-life curves are presented in Figure 155 for specimens of Alloy 2014-T6 under the following conditions: (1) no prior corrosion and

TABLE 25   Average Tensile Properties for Bare and Clad 2014-T6 Test Materials

(Transverse Direction)

Material	Ultimate Tensile Strength, ksi	Yield Strength, ksi	Elongation in 1.4 Inches, %
0.125-Inch 2014-T6			
Uncorroded	69.1	62.3	11.0
Light	67.5	60.7	8.5
Heavy	65.3	59.5	5.5
Decrease Caused by Heavy Pitting	5.5%	4.5%	50.0%
0.160-Inch Clad 2014-T6			
Uncorroded	69.3	62.5	10.0
Light	68.9	62.3	11.0
Heavy	68.7	62.4	11.0
Decrease Caused by Heavy Pitting	0.9%	0.2%	---

fatigued in air, (2) prior corrosion to produce light pitting and fatigued in air, and (3) prior corrosion to produce heavy pitting and fatigued in air. The presence of corrosion pitting lowered the fatigue strength of bare 2014-T6, with the heavily pitted specimens showing the greatest decrease in strength. Fatigue-life curves for clad 2014-T6 under the same conditions are presented in Figure 156. Again, the presence of corrosion pitting lowered the fatigue strength with respect to that of the uncorroded control specimens. For the clad 2014-T6 there was not much difference between the strength of the lightly corroded specimens and that of the heavily pitted specimens. The bare 2014-T6 exhibited a decrease in fatigue strength of about 60 percent for the heavily pitted specimens compared with that of the uncorroded control specimens. The clad 2014-T6 exhibited a decrease in fatigue strength of about 25 percent for the lightly pitted specimens and 33 percent for the heavily pitted specimens compared with that of the uncorroded control specimens. All these results are for a fatigue life of 10^8 cycles to failure. It was also reported that the effects of prior corrosion are less in the high stress-low cycle range. This is particularly noticeable for the clad 2014-T6 since the data points for all conditions seem to lie together until approximately 10^5 cycles.
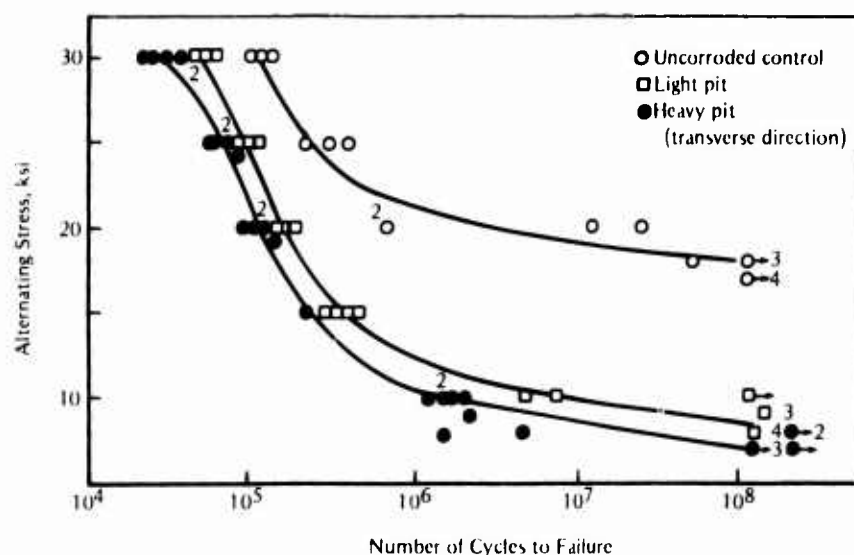
FIGURE 155. Effect of Heavy and Light Corrosion
Pitting on Repeated Bending Fatigue Properties of
0.125-Inch-Thick Bare 2014-T6 Sheet[212]
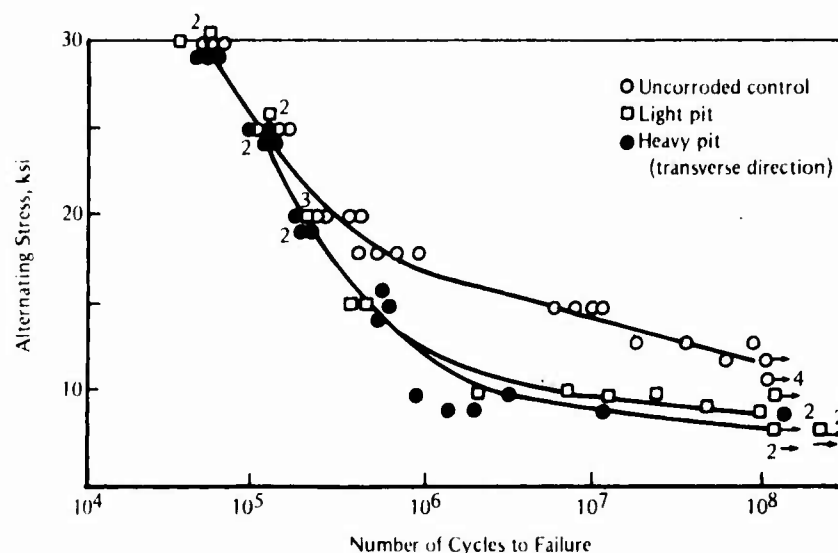
FIGURE 156. Effect of Heavy and Light Corrosion
Pitting on Repeated Bending Fatigue Properties of
0.160-Inch-Thick Clad 2015-T6 Sheet[212]

Austin[213] examined the rotating bending fatigue behavior of Alloy 2014-T6 in air and seawater. His results are plotted in Figure 157. At the stress levels studied, the seawater environment reduced cyclic life by more than an order of magnitude compared with that in air.

Alloys 2020 and 2024

Austin[213] also studied the corrosion-fatigue resistance of Alloy 2024-T4 (see Figure 157). The results were similar to those for Alloy 2014-T6. The artificial seawater environment produced more than an order of magnitude reduction in cyclic life compared with that in an air environment.
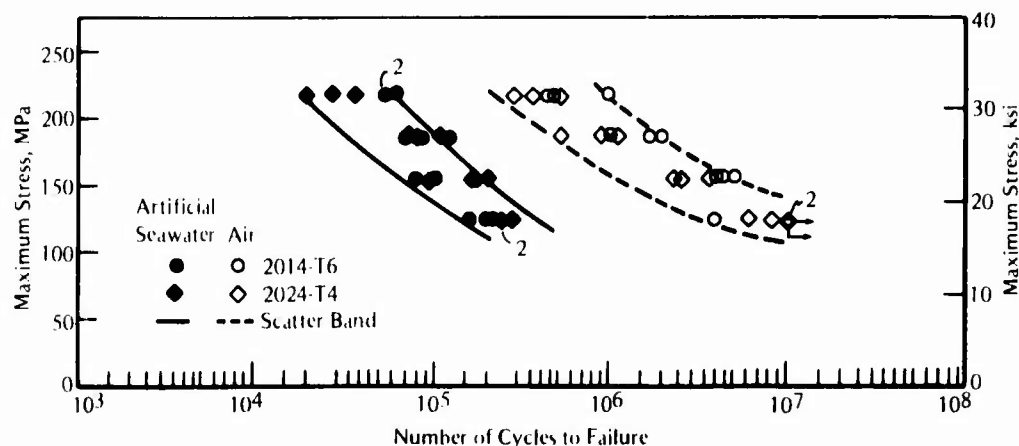
FIGURE 157. Rotating Bending Fatigue of Alloys 2014-T6 and 2024-T4 in Air and Artificial Seawater[213]

The behavior of Alloys 2020-T651, 2024-T851, 2024-T351, 7075-T651, and 7075-T73 was evaluated in spectrum fatigue tests by Gruft and Hutcheson.[214] The materials are typical aircraft wing materials. Because Alloy 7075 is also a typical aircraft wing material, it is appropriate to report its behavior in this section for comparison purposes. Other 7XXX series alloys are discussed in a later section of the chapter. Axially loaded flat specimens with prefretted countersunk holes were tested under a maneuver-type spectrum loading for several adverse environmental conditions. Some tests were conducted on specimens with a (1) MIL-5541 "Alodine" protective coating in the hole, (2) with "as-is" holes made from actual Alloy 2020-T651 wings skins with a 5-year previous exposure, or (3) with holes that had been reworked to restore fatigue life. Alodine is a chromate-containing conversion coating used on aluminum alloys. The test environment, materials, and results are summarized in Table 26. Maneuver spectrum loadings are variable-amplitude-loading spectrums which simulate actual service conditions.

There was no significant difference between the results for specimens with the countersunk holes and those for specimens made with "as-is" holes from actual wing skins. Also, reworking of specimens with cracks did not restore the fatigue life to the level of that for control specimens. All visible fatigue cracks and corrosion damage could be removed, but this did not remove all corrosion-fatigue damage. The Alodine protection of Alloy 2020-T651 was beneficial, although total fatigue life was still considerably reduced.

The effect of prior corrosion pitting on the fatigue life of Alloy 2024-T4 was investigated by Harmsworth.[215] Pits can act either as stress raisers, accelerating fatigue damage in a manner similar to that for notched fatigue specimens, or as cavities of corrosion concentration where stress-corrosion cracks may form. Rotating beam specimens were drilled to simulate a theoretical stress concentration of corrosion pits, K_t = 1.8 to 2.8, and were suspended in a 20 percent NaCl salt-spray environment at 95 $\pm$ 2 F for periods of 2 hours to 32 days. The specimens were then tested at 60 Hz in laboratory air. The fatigue-life curves for Alloy 2024-T4 specimens subjected to prior corrosion are plotted in Figure 158. Results from specimens with no prior corrosion exposure are shown for reference. The fatigue lives decreased as a result of corrosion exposure of the specimens prior to testing. Metallographic analysis indicated all cracks initiated from areas of corrosion which branched off from the main corrosion pits.

Fatigue-crack growth tests on flat specimens of Alloy 2024-T3 in air and seawater were performed by Figge and Hudson.[216] These specimens were axially loaded, R = 0, either at 0.67 Hz for maximum stress levels of 50, 40, 30 and 25 ksi (346, 276, 206, and 173 MPa) or at 20 Hz for

TABLE 26. Summary of Corrosion-Fatigue Results for Alloys 2020, 2024, and 7075[214]

Test Environment	Group	Alloys Tested	Discussion and Results
Nonfretted, non-exposed, and tested in air	A	2020-T651, 2024-T851, 2024-T351, 7075-T651, 7075-T	Reference Group — fatigue life of specimens in air if they were not prefretted. Order of decreasing fatigue lives was: 7075-T651, 2020-T651, 7075-T73, 2024-T351, 2024-T851.
Fretted, nonexposed, and tested in air	B	2020-T651, 2020-T651A[a], 2024-T351, 7075-T73, 7075-T651, 7075-T651A, 2024-T851	Control Group — representative of aircraft loaded hole conditions with no corrosive damage. Relative order of fatigue life remained the same as that for Group A.
Fretted, nonexposed, and tested in 3.5 percent NaCl solution	C	Same specimens as Group B	Total fatigue life reduced to 66 to 89 percent of that for Group B. Alloy 7075-T651 had highest fatigue life. Alloy 2024-T851 had lowest fatigue life.
Fretted, alternately immersed in 3.5 percent NaCl solution for 50 days, tested in air	D	Same materials as Group A	Total life reduced to 39 to 73 percent of that for Group B. Alloy 7075-T651 had highest fatigue life. Alloy 2024-T851 had the lowest fatigue life.
Fretted, alternately immersed in 3.5 percent NaCl solution for 30 days, tested in distilled water	E	2020-T651, 7075-T651	Slightly less degradation than for Group F. Results imply that presence of salt during cycling is necessary for significant degradation when moist conditions exist.
Fretted, alternately immersed in 3.5 percent NaCl solution for 30 days, tested in 3.5 percent NaCl solution	F	Same specimens as Group B	Total life reduced to 21 to 55 percent of that for Group B. Fatigue life of Alloys 7075-T651 and 7075-T73 reduced to 20 percent of that for Group B. Alloy 2024-T351 had greatest resistance, retaining 55 percent of the Group B life. Relative order of fatigue life was 2024-T351, 7075-T651, 2020-T651, 2024-T851, 7075-T73.

(a) An Alodine protective coating was applied to the hole area before testing.
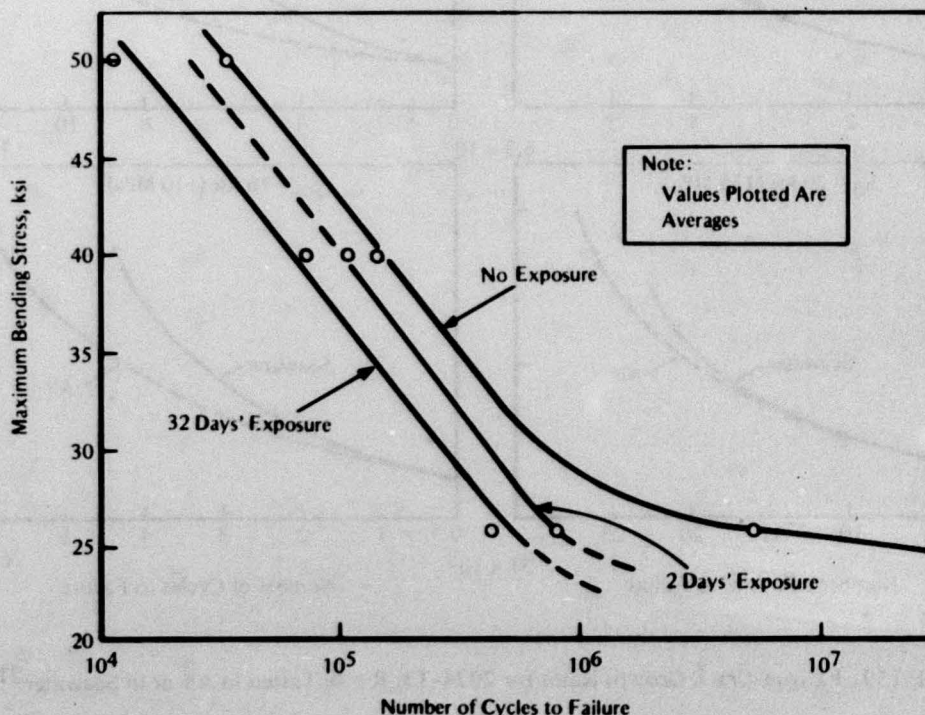
FIGURE 158. Fatigue Life of 2024-T4 Aluminum Alloy Specimens Subjected to Pitting Corrosion[215]

maximum stress levels of 20 and 16 ksi (138 and 110 MPa). Fatigue-crack growth rates at these stress levels for 2024-T3 in air and in seawater are shown in Figure 159. The fatigue-crack growth rate in seawater was approximately one and one-half times higher than that in air at the lowest stress level, 16 ksi (110 MPa). At the higher stress levels, seawater had a less deleterious effect, and at the highest stress level, 50 ksi (346 MPa), the fatigue-crack growth rate in air was approximately twice as high as that in seawater, which indicates that the corrosion caused crack blunting.
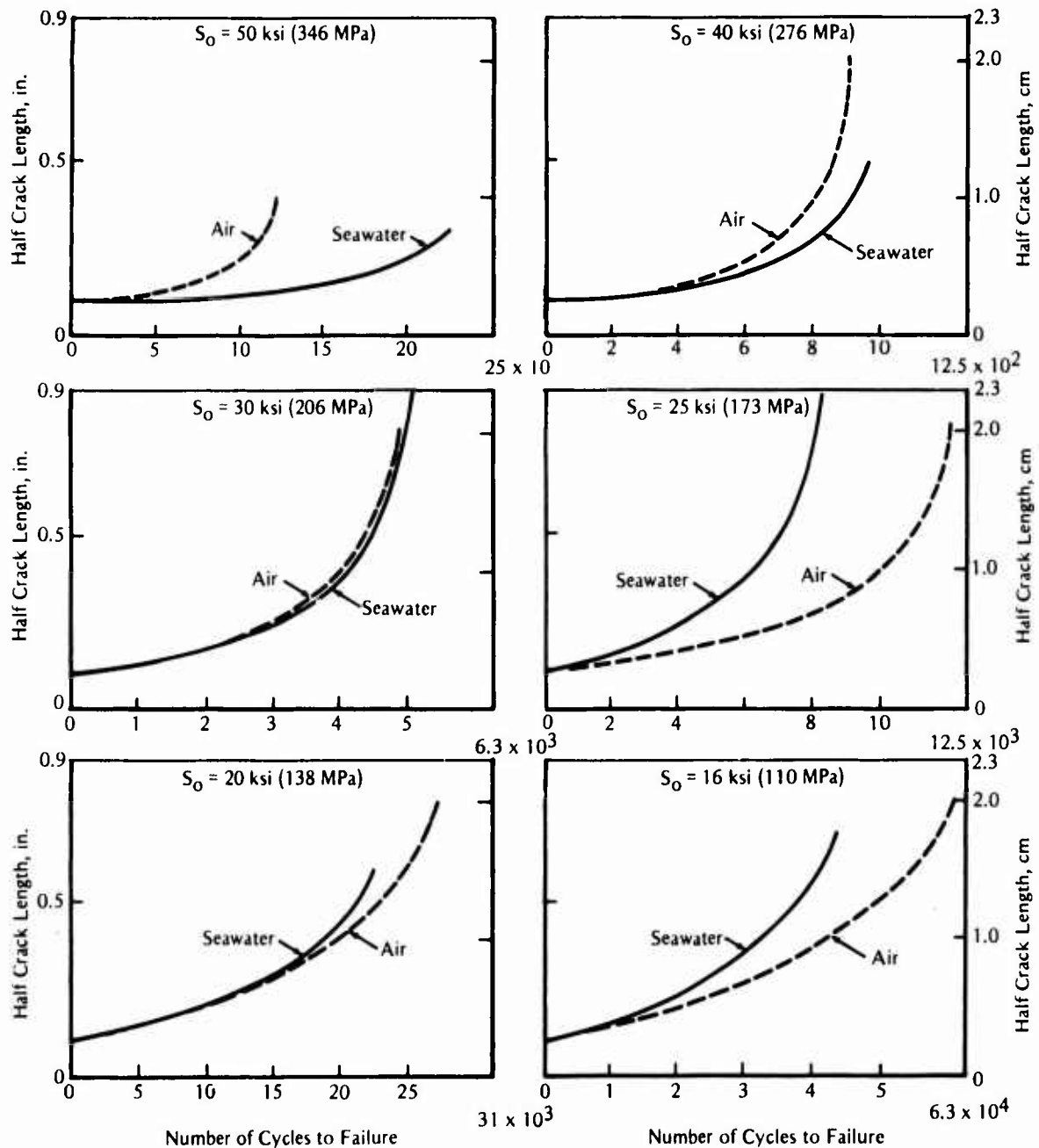
FIGURE 159. Fatigue-Crack Growth Rates for 2024-T3, R = 0, Tested in Air or in Seawater[216]

Alloy 2219

Crooker[217] found that the high-strength, low-toughness alloy, 2219-T87, was completely unaffected by flowing 3.5 percent NaCl solution under high-amplitude nominally elastic loading conditions. Single-edge-notched cantilever specimens were cycled at R = 0 under constant amplitude loading at 0.1 Hz. The fatigue-crack growth data for Alloy 2219-T87 in air and saltwater are plotted in Figure 160. This alloy is insensitive to the saltwater environment under these conditions.

Soviet Alloys—D16T and D16AT

Corrosion-fatigue tests were performed[221] on deformed and undeformed specimens of D16 Duralumin (Al-3.8Cu-1.23Mg), in 3.0 percent NaCl solution. Notched and smooth specimens were pulled in a standard tensile machine to a stress equal to 80 percent of the ultimate tensile strength before fatigue testing. Corrosion-fatigue results for these specimens are compared (Figure 161) with those for specimens exposed in the same environment which
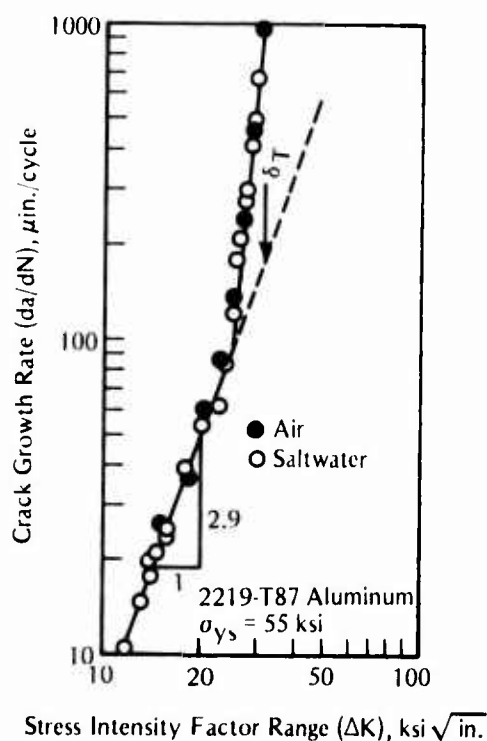
FIGURE 160. Fatigue-Crack Growth Rate as a Function of Stress Intensity Factor Range for 2219-T87 Aluminum in an Ambient Room Air Environment and in 3.5 Percent NaCl Saltwater[217]
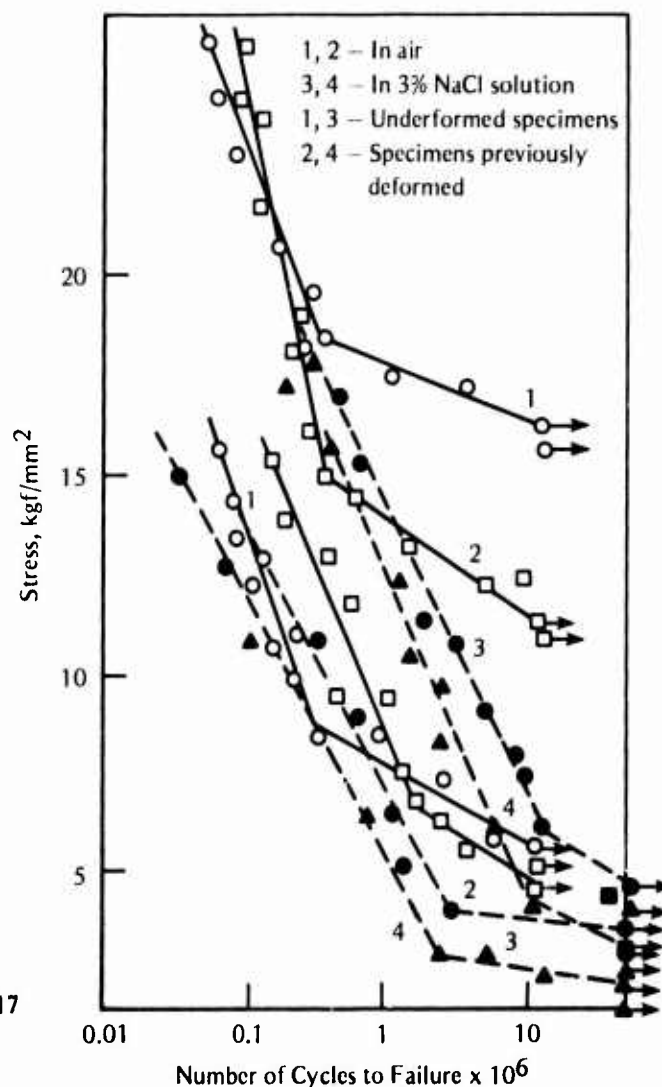
FIGURE 161. Fatigue of (a) Smooth and (b) Notched D16 Duralumin Specimens[221]

did not receive any prestressing. For the entire range of applied stresses, fatigue lives of all the previously deformed specimens were lower than those of the corresponding undeformed specimens. The prior tensile deformation reduced the fatigue life in air and in 3 percent NaCl solution. Based upon 10^7 cycles to failure, the decrease in fatigue strength between the undeformed and deformed specimens was greater for the smooth specimens than for the notched specimens. The authors attributed this reduced influence of notch sensitivity to corrosion at the notch root, which reduced the stress concentration at that location.

The protection of Alloys D16T and D16AT (clad D16T) by anodizing and cladding was studied by Karlashov et al.[220] Specimens were tested under conditions of fully reversed flexure at 8.33 Hz in air, tap water, condensate, and 3.0 percent NaCl solution. The condensate solution was used to simulate typical solutions found under the floor in an aircraft fuselage during operation. Cladding slightly increased corrosion-fatigue resistance in 3.0 percent NaCl solution but decreased resistance in air. Fatigue-life curves for specimens of clad Alloy D16AT and unclad Alloy D16I are plotted in Figure 162. In tap water, the fatigue resistance of Alloy D16AT was found to be the same as that of Alloy D16T. In the condensate, the fatigue resistance of Alloy D16AT was slightly better than that of Alloy D16T.
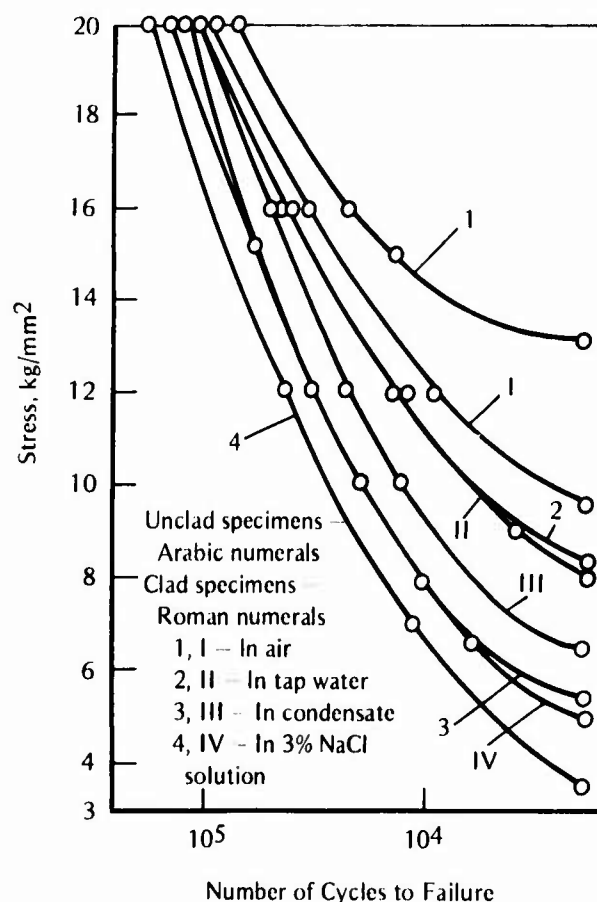
FIGURE 162. Fatigue Life for Unclad and Clad D16 Alloy Specimens[220]

In a more recent paper, Karlashov et al[222] discussed the effects of cladding and subsequent anodizing of Alloy D16T specimens, both smooth and with rivet holes. Results for the smooth specimens are shown in Figure 163. From this figure it can be seen that the unclad, anodized D16T had the best fatigue resistance in both the air and the saltwater environments. In the saltwater, the unclad, uncoated D16T exhibited the worst fatigue resistance. Anodizing did raise the corrosion-fatigue resistance of this alloy, whereas cladding proved to be
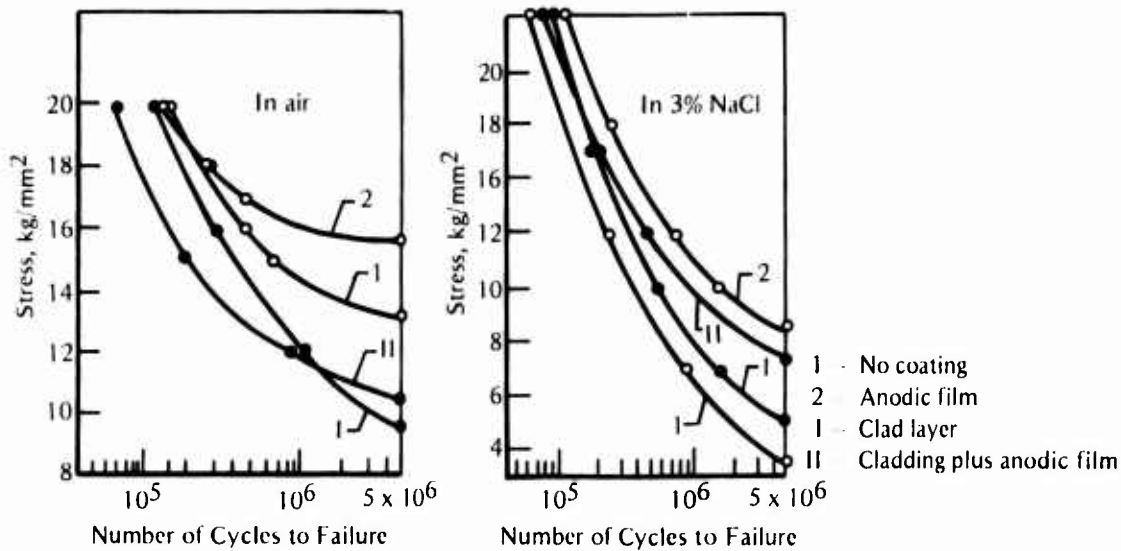
FIGURE 163. Fatigue Life for Alloy D16T Specimens[222]

detrimental. Results of corrosion-fatigue tests performed on specimens containing rivet holes simulating actual component fabrication are shown in Figure 164. In air, the fatigue lives for both the clad and the clad plus anodized specimens are shorter than those for both the uncoated and the anodized specimens. The presence of an anodic film appears to be beneficial, especially in the low-stress, high-cycle range. In the 3.0 percent NaCl solution, the anodized Alloy D16T specimens, clad and unclad, were superior to the untreated clad specimens and the bare specimens. The test results are qualitatively summarized in Table 27.

Shavyrin et al[223] found that polymer adhesive coatings on single and double-seam lap-welded joints of Alloy D16AT alloy and on butt-jointed welds of Alloy D20 increased the fatigue strength in air and in a 3.0 percent NaCl solution containing 0.1 percent H_2O_2. Fatigue-life curves for each type of weld, coated and uncoated, in each environment, are shown in
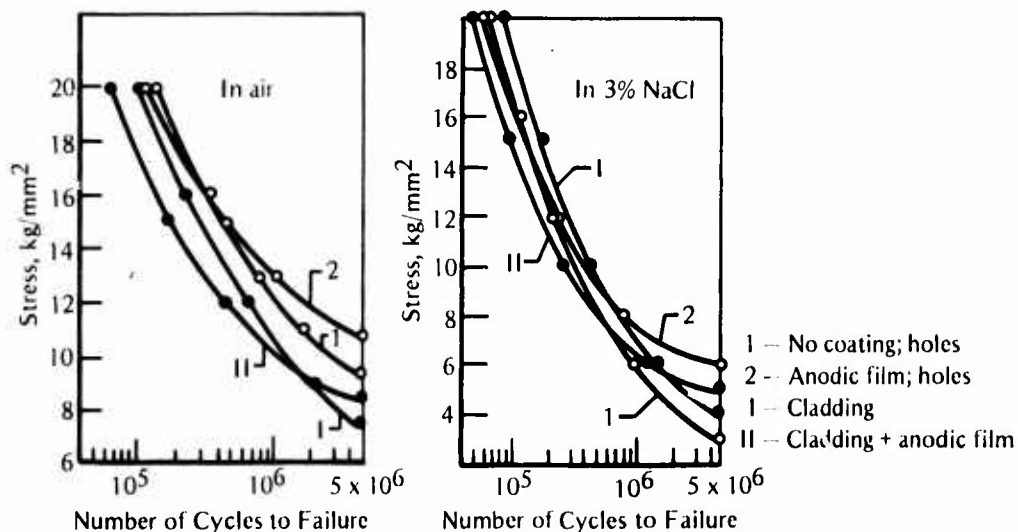
FIGURE 164. Fatigue Life for D16T Specimens Containing Rivet Holes[222]

TABLE 27. Relative Order of Fatigue Strengths for Alloys D16T and D16AT at 5 x 10⁶ Cycles

Smooth Specimens		Specimens With Rivet Holes	
In Air	In 3.0% NaCl Solution	In Air	In 3.0% NaCl Solution
D16T anodized	D16T anodized	D16T	D16T anodized
D16T	D16AT anodized	D16T anodized	D16AT anodized
D16AT anodized	D16AT	D16AT anodized	D16AT
D16At	D16T	D16AT	D16T

Figure 165. The relative order of fatigue strengths of these welds at 10^7 cycles to failure is shown in Table 28. The coating creates a continuous film on the metallic surface by filling in all the macroscopic and microscopic surface irregularities, which reduces the effect of such surface stress raisers on crack initiation and at the same time acts as a barrier against the environment. Also, the curing of the polymer on the metallic surface could create compressive stresses at the metallic surface, which could be a possible factor in the increased corrosion-fatigue strength.

a. Single-Seam Lap Joints   b. Double-Seam Lap Joints   c. Butt-Jointed, Welded

LEGEND

◐ 1 — With polymer coatings, in air
◕ 2 — With polymer coatings, in corrosion medium
● 3 — Without coating, in air
○ 4 — Without coating, in corrosive medium
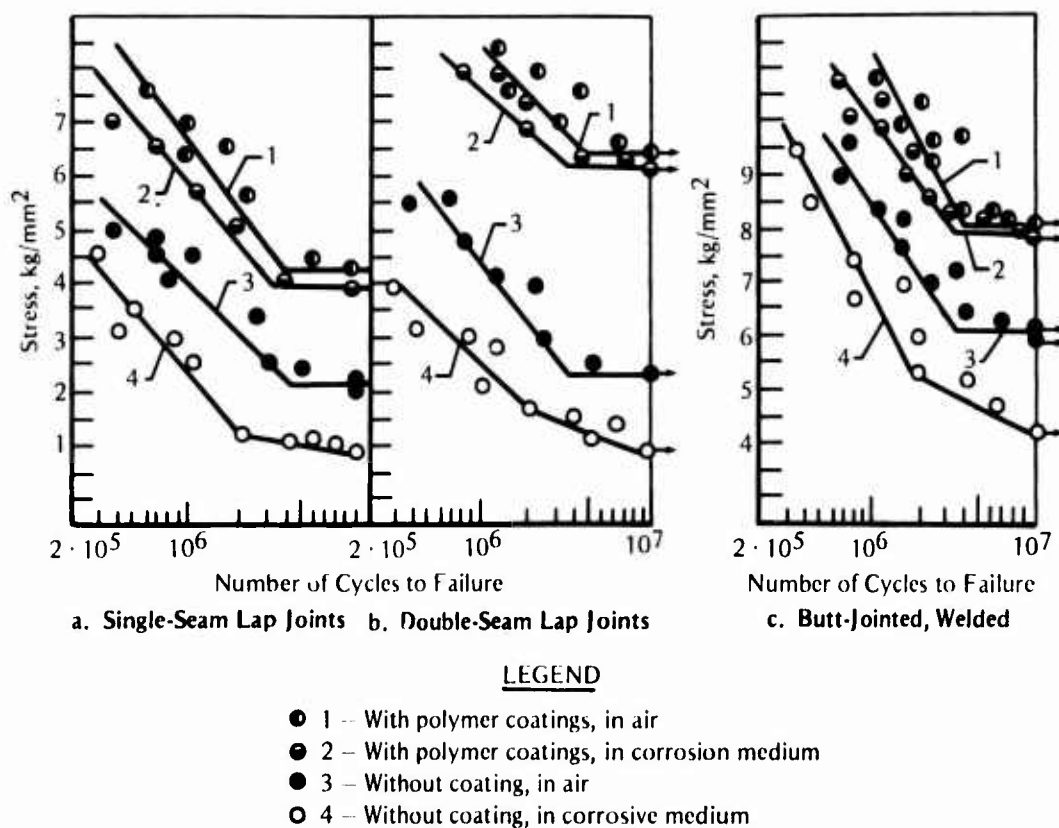
FIGURE 165. Fatigue and Corrosion-Fatigue Curves for Welded Specimens of Alloys D16AT and D20[223]

TABLE 28. Relative Order of Fatigue Strengths for Alloy D16AT Lap
Joints and Alloy D20 Welds[223]

Alloy D16AT		Alloy D20 Butt-Jointed Welds
Single-Seam Lap Joints	Double-Seam Lap Joints	
Specimens with polymer coatings in air	Specimens with polymer coatings in air	Specimens with polymer coatings in air
Specimens with polymer coatings in saltwater	Specimens with polymer coatings in saltwater	Specimens with polymer coatings in saltwater
Specimens with no coatings in air	Specimens with no coatings in air	Specimens with no coatings in air
Specimens with no coatings in saltwater	Specimens with no coatings in saltwater	Specimens with no coatings in saltwater

British Alloys

The fatigue-crack-growth rates of RR58, a Cu-Al alloy which is nominally the same as Alloy 2618Al, were investigated by Branco et al.[218] Contoured double-cantilever-beam specimens of Alloy RR58 were tested in laboratory air, in air with 50 percent relative humidity, and in a 3.5 percent NaCl solution at 0.15 Hz with a tensile sinusoidal wave. Results of these tests at a constant mean stress intensity are shown in Figure 166. Since the stress intensity factor (ΔK) was constant, a linear dependence of crack growth on number of cycles was observed. Crack growth rates increased in the 3.5 percent NaCl solution compared with those in air at the same mean stress intensity and ΔK values. Crack growth rates for RR58 as a function of ΔK for different levels of constant mean stress intensity are shown in Figure 167. At intermediate ΔK
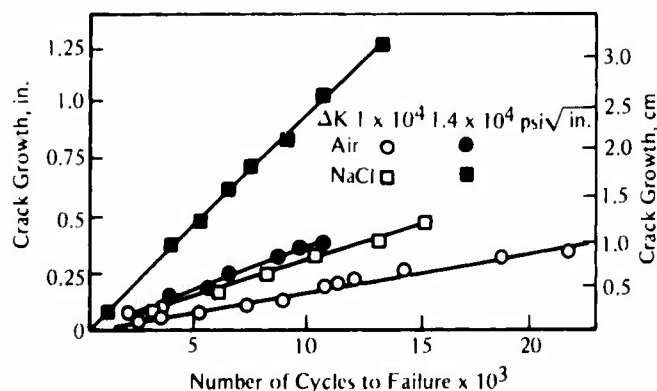
FIGURE 166. Crack Growth in RR58 for a Constant Mean Stress Intensity of 7500 psi $\sqrt{\text{in.}}$ in Air and in 3.5 Percent NaCl Solution at 0.15 Hz[218]
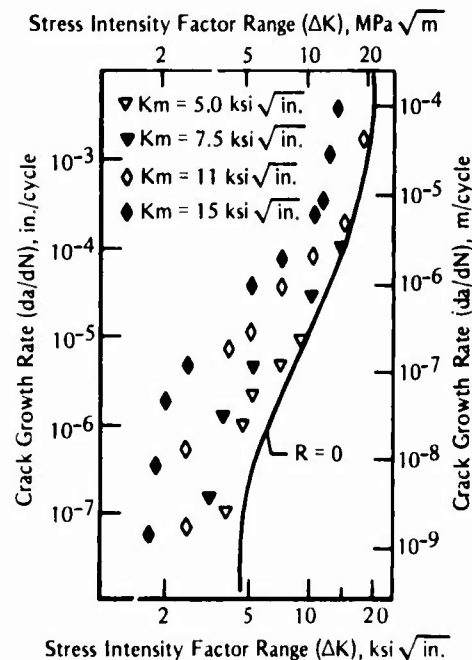
FIGURE 167. Crack Growth Rate Versus ΔK for RR58 in 3.5 Percent NaCl Solution at 0.15 Hz[218]

To compare data points in the curve for R = 0, note that at R = 0, $\Delta K = 2K_m$.

levels, crack growth rates decreased with increased constant mean stress intensity. It was shown that the saltwater environment lowered the threshold value for crack growth and caused an increase in crack growth rates. The threshold ΔK level decreased as the mean levels of ΔK increased.

The effect of a 3.5 percent NaCl solution on the corrosion-fatigue-crack growth in RR58 and LM30 aluminum alloys was investigated by Radon.[219] LM30 is a chill cast Al-Si alloy. Double-cantilever beams of the materials were tested at 0.15 and 35 Hz with (1) R = 0 at various ΔK and mean stress intensity levels, (2) specific mean stress intensity levels, and (3) specific ΔK values. Crack growth rates for Alloy RR58 specimens in laboratory air and in 3.5 percent NaCl solution at four ΔK levels are shown in Figure 168. In the NaCl solution, the cyclic crack growth rates increased by a factor of about 2.5 (compared with those in air) at ΔK levels of 12.49 ksi $\sqrt{\text{in.}}$ (13.73/MN/m$^{3\,2}$) and 16.56 ksi $\sqrt{\text{in.}}$ (18.03 MN/m$^{3\,2}$). But at ΔK levels of 17.89 ksi $\sqrt{\text{in.}}$ (19.66 MN/m$^{3\,2}$) and higher, the crack growth rates remained nearly the same in both environments. The crack growth rates for LM30 tested in air and in 3.5 percent NaCl solution are plotted in Figure 169. In region III, LM30 experienced very high crack growth rates. Otherwise, the investigator observed that the cyclic crack growth of LM30 was comparable to that of RR58. The authors support the theory that the environment can corrode and embrittle the material at the crack tip and subsequently increase the rate of crack growth.
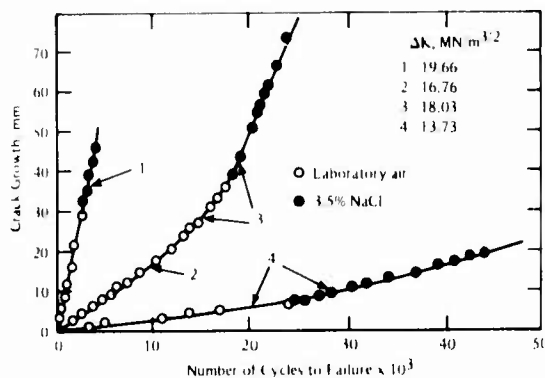
FIGURE 168. Crack Growth for Alloy RR58 Specimens at Various Values of ΔK and R = 0 in Laboratory Air and in 3.5 Percent NaCl at 0.15 Hz[219]
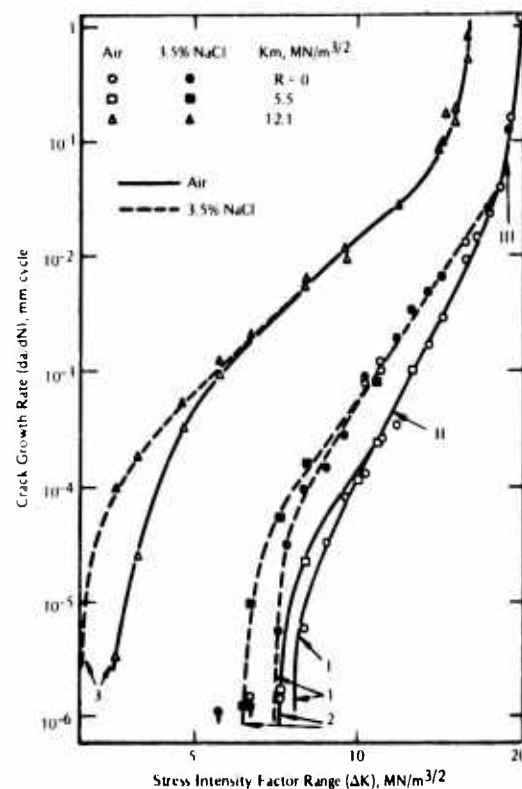
FIGURE 169. Crack Growth Rate as a Function of ΔK for LM30 in Laboratory Air and in 3.5 Percent NaCl at 0.25 Hz[219]

5XXX Series Aluminum Alloys

The 5XXX series of aluminum alloys are nonheat-treatable alloys used extensively for marine applications, particularly in the shipbuilding industry. These alloys are known for high resistance to stress corrosion and general corrosion attack, high strength, high toughness, and good fabricability. The alloys reviewed in this section and the corresponding reference numbers of the articles in which the data appeared are listed in Table 29. Alloys 5086 and 5456 are the most commonly used alloys, with -H32, -H321, -H117, and -H116 being the most common tempers. The corrosion-fatigue data reviewed for these alloys are summarized in Table 30.

TABLE 29. 5XXX Series Aluminum Alloys Reviewed

Alloy	Nominal Alloy Compositions, wt %				References
	Al	Mn	Mg	Cr	
5456	93.9	0.8	5.1	0.12	10, 17, 132, 151, 217, 228 – 232
5086	95.4	0.4	4.0	0.15	10, 73, 132, 213, 230, 233
5083	94.7	0.7	4.4	0.15	230
5052	97.5		2.5		213

Alloys 5456, 5086, and 5052

The effect of notch depth on the corrosion-fatigue life of Alloy 5456-H343 in 3.5 percent NaCl solution was investigated by Tinkel.[232] Tests were performed on cantilever beam specimens, either smooth or notched. The notches were semielliptical surface cracks with depths of approximately 0.002 in. (0.05 mm), 0.0115 in. (0.292 mm), and 0.025 in. (0.635 mm) with a root radius of 0.0015 in. (0.038 mm) to 0.002 in. (0.05 mm). The results of these tests are shown in Figure 170. Sensitivity to 3.5 percent NaCl increased in the higher (10^6 to 10^7) cyclic range. At 10^7 cycles, the smooth specimens had the best fatigue strength in both air and 3.5 percent NaCl. The effects of notches on the average fatigue limit (or fatigue strength) at 10^7 cycles are summarized in Table 31. It can be seen that Alloy 5456-H343 is notch sensitive to the corrosive effects of 3.5 percent NaCl solution under deflection-controlled loading.

Results of high-cycle fatigue tests of rotating tapered cantilever beams for Alloy 5456-H117 in air and in Severn River water at three stress ratios (R) are shown in Figure 171.[10] For R = 0, data from tests on Alloy 5086-H116 were incorporated into the curves. These curves indicate that the two alloys have similar corrosion-fatigue behavior at this ratio. The saltwater exposure caused a dramatic reduction in fatigue strength in the cyclic range above about 10^6 cycles to failure for all stress ratios. The authors constucted a modified Goodman diagram for Alloy 5456-H116, as shown in Figure 172. The fatigue strengths at 10^6 cycles to failure for this alloy in air and in saltwater at each stress ratio are given in Table 32. The fatigue lives in air and saltwater at 2×10^4 to 2×10^5 cycles are shown in Figure 173. Data for both environments lie within a scatterband because the effect of saltwater on fatigue life is negligible at high stress corrosion. The low and high-cycle 2×10^4 to 10^8 cycles-to-failure data are incorporated into a single plot in Figure 174. There appeared to be a fatigue limit in the air environment, but there was no indication of one in saltwater.

TABLE 30. Summary of Corrosion-Fatigue Data for the 5XXX Series Alloys

Alloy Type – Condition	Tensile Strength, ksi (MPa)		Type of Specimen	Type of Loading	Frequency, Hz	Environment	Types of Data	References
	Ultimate	Yield						
5456-H116	53.8 (365.84)		Single-edge notched	Cantilever, R=0	0.167	Natural seawater	Fatigue-crack growth rate (da/dN) vs. crack tip stress intensity range (ΔK) under free corroding and potentiostat-controlled electrochemical conditions da/dN vs ΔK	17
5456-H321		34 (231.2)	Single-edge notched	Cantilever	0.1	3.5% NaCl solution		217
CS19(a)	61.6 (418.8)		Smooth-round	Axial stress, R=-1.0	18.3	Substitute ocean water; ASTM P1141-52	Maximum stress vs number of cycles to failure	234
CS19 type alloy	63.8 (433.8)		Smooth-round	Axial stress, R=-1.0	18.3	Substitute ocean water; ASTM P1141-52		234
5456-H117	52.9 (359.7)		Smooth-round	Axial stress, R=-1.0	18.3	Substitute ocean water; ASTM P1141-52		234
5456-H117	52.9 (359.7)	30 (204)	As welded-plate	Axial stress, R=-1.0	3.0	Substitute ocean water; ASTM P1141-52	Evaluation of weldments, maximum stress vs number of cycles to failure	234
CS19 type alloy H117 temper	63.8 (433.8)	35 (238)	As welded-plate	Axial stress, R=-1.0	3.0	Substitute ocean water; ASTM P1141-52		234
5456-H117	52.9 (359.7)		Weld bead dressed-plate	Axial stress, R=-1.0	3.0	Substitute ocean water; ASTM P1141-52		234
CS19 type alloy H117 temper	63.6 (433.8)		Weld bead dressed-plate	Axial stress, R=-1.0	3.0	Substitute ocean water; ASTM P1141-52		234
5456-H117	51.0 (346.8)		Cantilever beam-tapered	Constant load, R=1, 0, 1/3	33.33	Fresh Severn River water(b)		10
5086-H116	46.0 (312.8)		Cantilever beam-tapered	Constant load, R=-1, 0, 1/3	33.33	Fresh Severn River water(b)		10
5456-H117	51.0 (346.8)		Cantilever beam-tapered and dog boned	Constant load, R=0	0.233	Natural seawater		10
5086-H116	46.0 (312.8)		Cantilever beam-tapered	Constant load, R=0, 0.125, 0.25, 0.50, 0.75	0.233	Natural seawater		10
5456-H117	51.0 (346.8)		Compact tension	R=0, 0.125, 0.25, 0.50, 0.75	30	Natural seawater		10
5456-H117	46.0 (312.8)		Double cantilever beam		30	Natural seawater		10
5086-H116	42 (285.6)		Rotational cantilever beams	Rotating cantilever-beam tests, R=-1	24.17	Severn River water		230
5083-H116	46 (312.8)					Severn River water		230
5456-H116	51 (346.8)					Severn River water		230
5086-H117	42 (285.6)					Severn River water		230
5086-H117	42 (285.6)					Natural seawater		230
5086-H32	51 (346.8)					Severn River water		230
5456-H321	39 (265.2)					Severn River water		230
5086-H112	47 (319.6)					Severn River water		230
5456-H311						Natural seawater		230
5086-H116(c) 5356 filler	40.5 (275.4)					Natural seawater		230
5456-H117(c) 5556 filler	45.5 (275.4)					Natural seawater		230
5456-H321(c) 5556 filler						Severn River water		230
5456-H343	56.4 (383.5)		Smooth and surface notched untapered	Cantilever beam	30	3.5% NaCl solution	S-N curves from 10^4 to 10^7 cycles	232
5052-H34			Smooth-hour glass	Rotating bending	33.3	Artificial seawater	S-N curves from 10^3 to 10^7 cycles	213
5086-H34			Smooth-hour glass	Rotating bending	33.3	Artificial seawater		
5052-H32			Smooth-hour glass	Rotating bending	33.3	Artificial seawater		
5086-H34			Polished, center-cracked plate	Axial, R=0.1	20	Natural seawater	Crack growth rate vs stress intensity, application of applied potential	233
5086-H116 unwelded, welded	46.3 (314.8)	31.5 (214.2)	Tapered plate	Cantilever bending, R=1/3, 0, -1	33.3	Natural seawater	S-N curve from 10^4 to 10^8 cycles	132
5456-H117 unwelded, welded	57.2 (388.9)	45.2 (307.4)	Tapered plate	Cantilever bending, R=1/3, 0, -1	33.3	Natural seawater	Fatigue strengths, constant life diagram	132
5456-H116			Single-edge notched	Cantilever bending, R=0	0.17	Natural seawater	FCG vs ΔK, effect of dissolved oxygen	231
5086-H116			Smooth cylindrical, continuous radius		33.3	Synthetic seawater, 1 atm and 2000 psi	S-N curves from 5×10^5 cycles; influence of hydrostatic pressure	73
5086-H117			Smooth cylindrical, continuous radius		33.3	Synthetic seawater, 1 atm and 2000 psi	S-N curves from 5×10^5 cycles	73
5456-H117			Compact tension		30	Seawater	FCG vs ΔK function of applied potential	229
5456-H117			Double cantilever		30	Seawater	FCG vs ΔK	228

(a) An experimental alloy.   (b) 1/6 to 1/3 the salt content of natural seawater, depending on the season and tide.   (c) Welded specimens were tested in the bead-removed condition.
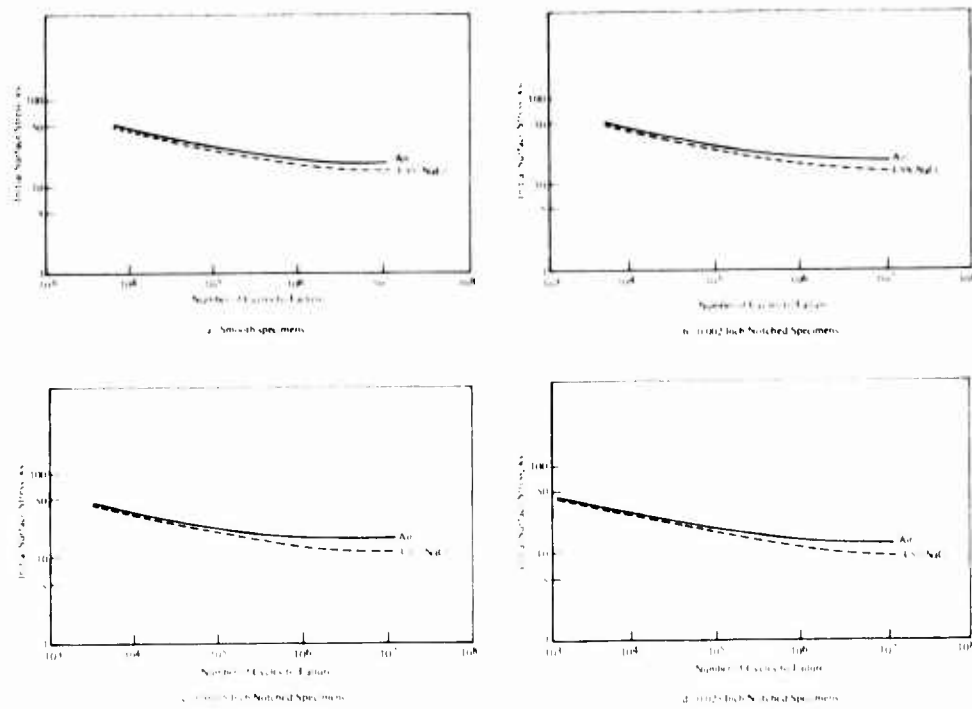
FIGURE 170. Fatigue-Life Curves for Cantilever Bend Specimens of Alloy 5456-H343[231]
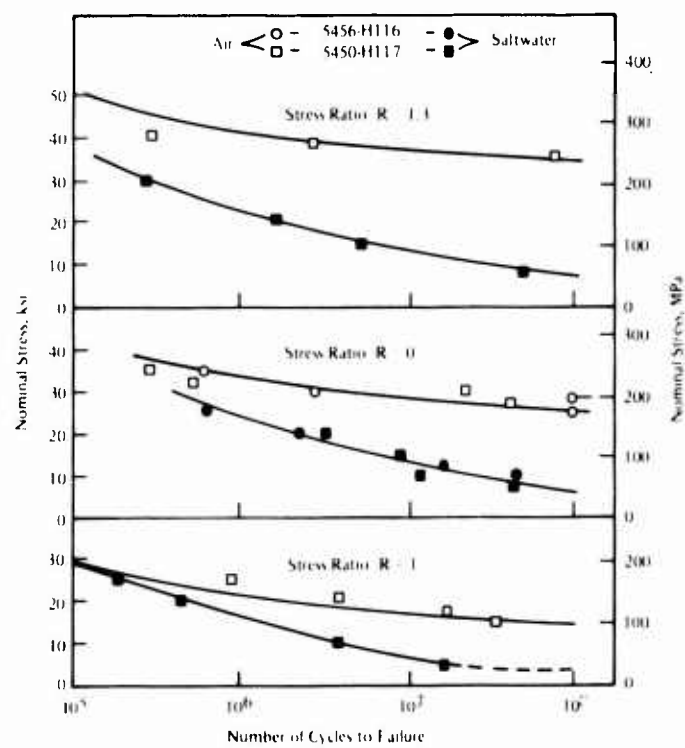
FIGURE 171. High-Cycle Corrosion-Fatigue-Life
Curves for Alloys 5456-H116 and 5456-H117[10]

TABLE 31. Average Fatigue Limit at 10^7 Cycles for Alloy 5456-H343 Specimens[222]

| | Average Fatigue Limit, ksi (MPa) | | | |
| | | Specimens With Notches of Indicated Depths | | |
Environment	Smooth Specimen	0.002 in. (0.050 mm)	0.0115 in. (2.921 mm)	0.025 in. (0.635 mm)
Air	19.2 (132)	18.5 (128)	15.3[a] (105)	13.2 (91)
3.5% NaCl	15.2 (105)	13.7 (94)	11.3 (78)	10[a] (69)

(a) Calculated value.

TABLE 32. Fatigue Strength of 5456-H117 at 10^6 Cycles to Failure[10]

| | Fatigue Strength (Maximum Stress), ksi (MPa) | |
Stress Ratio (R)	In Air	In Saltwater
-1	14 (96.6)	4 (27.6)
0	24 (165.6)	5 (34.5)
1/3	34 (234.6)	7 (48.3)
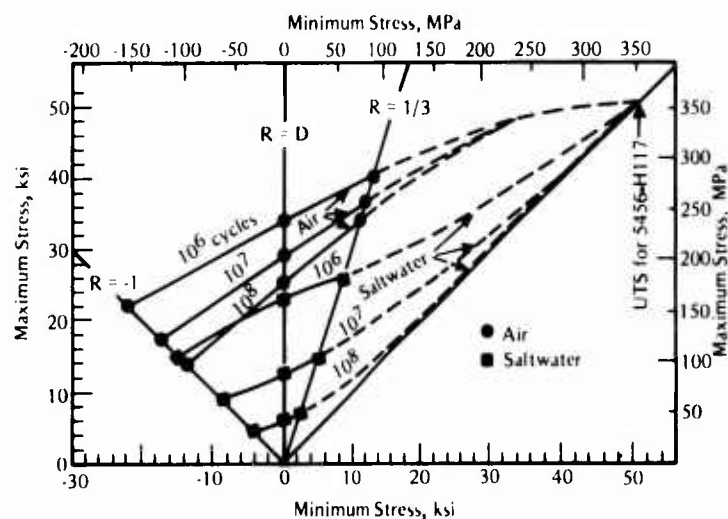
FIGURE 172. Modified Goodman Diagram for Alloy 5456-H117 in Air and in Saltwater
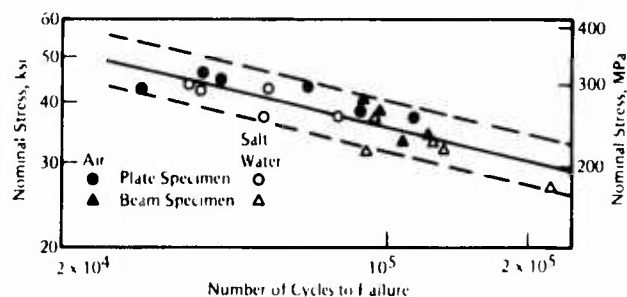
FIGURE 173. Low-Cycle Fatigue-Life Curves for Alloy 5456-H117[10]
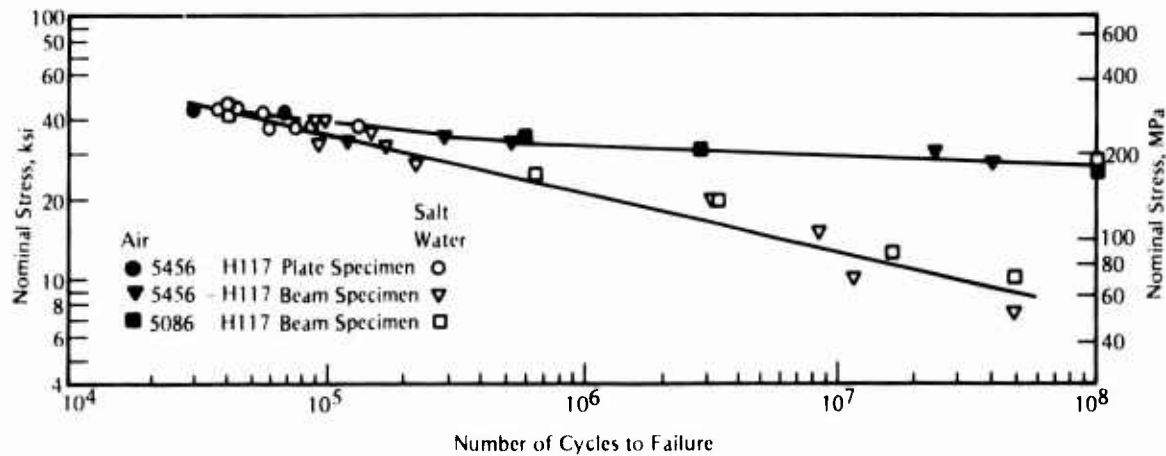
FIGURE 174. Broad Life Corrosion-Fatigue Curves (R = 0) for Alloy 5456-H117[10]

Chu[228] studied the corrosion-fatigue-crack growth of Alloy 5456-H117 in air and in natural seawater. Compact-tension and contoured double-cantilever-beam specimens were tested at 30 Hz in both environments. The fatigue-crack growth rates as a function of ΔK are plotted in Figure 175. Five stress ratios (R) were employed in this study. At all ΔK levels, the fatigue-crack growth rates were higher in seawater than in air. The effect of stress ratio (R) on the crack growth rates was the same for both environments, that is, an increase in R caused a corresponding increase in crack growth rate. Apparently, the presence of seawater did not enhance this effect, since the distances between the fatigue-data scatterbands for seawater and for air were approximately the same.

Crooker et al[17] studied the effects of flowing natural seawater and two applied potentials on the fatigue-crack growth rates of Alloy 5456-H116. The crack growth rate for this alloy as a function of stress intensity factor range is plotted in Figure 176. The application of an anodic potential of -0.750 V SCE and a cathodic potential of -1.300 V SCE to the specimen while it was undergoing testing was beneficial. The crack growth rates of the freely corroding specimen, -0.950 V SCE, were higher than those of specimens in the ambient air with applied potentials. The author found that the applied potentials lessened the detrimental effects of the seawater.

Crooker and Bogar[229] have determined the effects of applied potentials on the corrosion-fatigue-crack growth of Alloy 5456-H117 in seawater. The crack growth rate for this alloy in this environment as a function of stress intensity factor range is shown in Figure 177. Between -1.3 and -1.4 V SCE, the crack growth rate was suppressed at ΔK levels below about 22.75 ksi $\sqrt{\text{in.}}$ (25 MPa $\sqrt{\text{M}}$).

The effect of the dissolved oxygen content in natural seawater on the corrosion-fatigue-crack growth rates of Alloy 5456-H116 was studied by Bogar and Fujii.[231] They found that the fatigue-crack growth rates were higher in flowing natural seawater than in air, as shown in Figure 178. Testing of this alloy in seawater deoxygenated with helium produced crack growth rates similar to those produced when testing in air. Because the corrosion rates were often limited by the cathodic reaction, and because oxygen is an effective depolarizer, the authors concluded that higher oxygen concentrations lead to higher corrosion rates.

Crooker[217] found that Alloy 5456-H321 was moderately sensitive to 2.5 percent NaCl solution. The fatigue-crack growth rates in air and saltwater environments are plotted in Figure 179. This figure shows that the environment was less detrimental in the higher stress intensity factor range.
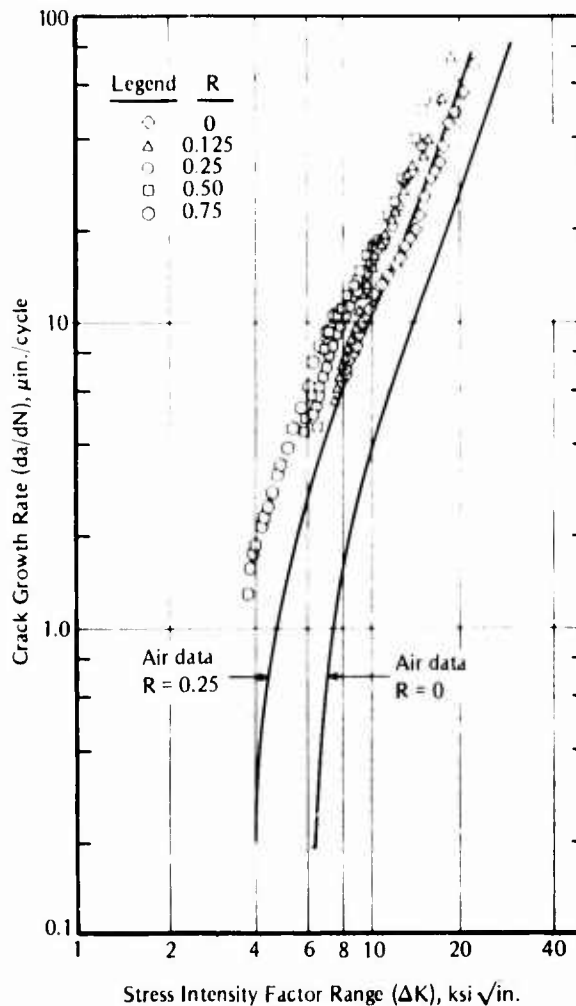
FIGURE 175. Effect of Stress Ratio on Fatigue–Crack Growth Rate for Alloy 5456-H117 in Seawater [228]
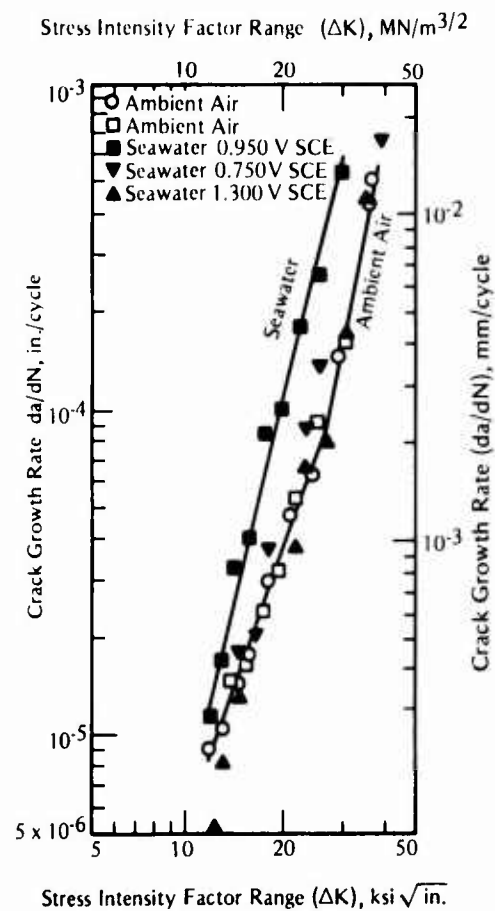
FIGURE 176. Corrosion-Fatigue-Crack Growth for Alloy 5456-H116 in Ambient Air and Seawater [17]

Results from high-cycle fatigue tests on welded specimens of Alloys 5086-H116 and 5456-H117 in air and in seawater are shown in Figure 180.[132] Tests were conducted on specimens made of base plate and on specimens with butt and tee welds. The effects of the seawater overrode any effects the different welding processes might have had on the fatigue strength. At 10^8 cycles to failure, no significant differences were observed among the fatigue strengths of the base metal and the weldments.

Corrosion-fatigue properties of plate and welded specimens of Alloys 5456-H117 and CS19 were evaluated by Rogers et al.[234] Axial fatigue tests in substitute ocean water (ASTM D1141-52) were conducted at 18.3 Hz. For plate specimens at 10^8 cycles to failure, the fatigue strength of Alloy 5456-H117 was approximately 15.52 ksi (97 MPa), or 75 percent of that in air, and the fatigue strength of CS19 was approximately 11 to 12 ksi (76 to 83 MPa).

Transverse butt welds of Alloys 5456-H117 and CS19 were subjected to corrosion-fatigue testing in the as-welded condition and with the weld bead dressed.[234] Testing also was performed in air for comparison. At all stress levels, the specimen fatigue lives were reduced in the synthetic seawater (compared with those in air). The dressing of the weld bead increased the fatigue strength in air and in seawater. The dressing of the weldment decreased the stress

FIGURE 179. Corrosion-Fatigue-Crack Growth for Alloy 5456-H321 in Air and Saltwater[217]

FIGURE 178. Effect of Dissolved Oxygen Content in Seawater on the Corrosion-Fatigue-Crack-Growth Rate of Alloy 5456-H116[231]

FIGURE 177. Effects from Cathodic Potential on the Corrosion-Fatigue-Crack-Growth Resistance of Alloy 5456-H117 in Seawater[229]
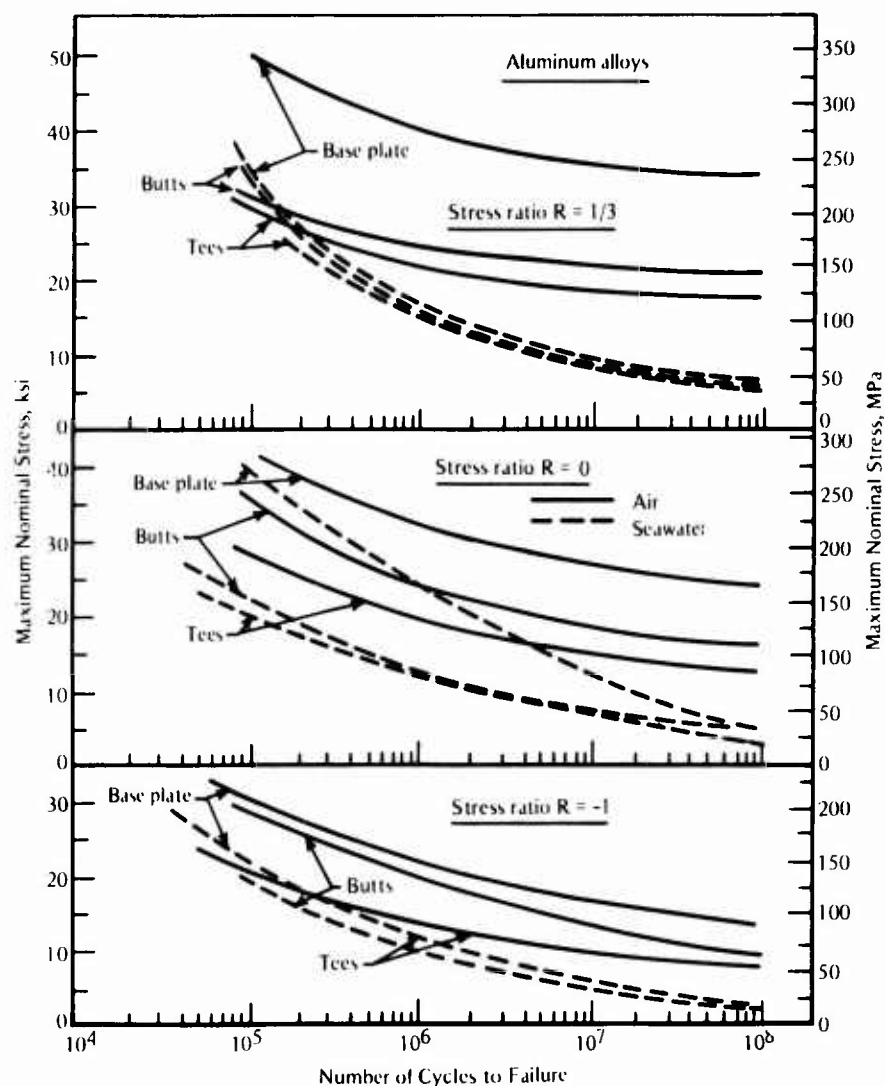
FIGURE 180. Corrosion-Fatigue-Life Curves for Alloys 5086-H116 and 5456-H117[132]

concentration at the weld, so the increased fatigue strength was expected. There were no significant differences between the fatigue strengths of the two alloys.

Czyryca[230] evaluated the high-cycle fatigue properties of Alloys 5083, 5086, and 5456, with a variety of tempers and weldments, in air, Severn River water, and natural seawater. Both saltwater environments produced the same reduction in fatigue strengths. It was noted that the surface corrosion appearance differed for each environment. Samples taken from 1-inch-thick butt weldments of Alloy 5086-H116 and 5456-H117 in the single-vee joint design and of Alloy 5456-H321 in the modified double-U joint design were tested as rotating cantilever-beam specimens at 24.2 Hz.

The fatigue-life curves for the Alloy 5086 and Alloy 5456 base metal tempers are shown in Figures 181 and 182, respectively. Results for Alloy 5086-H116 weldments in air and saltwater are shown in Figure 183; those for Alloy 5456-H117 weldments in air, seawater, and Severn River water are shown in Figure 184; and those for Alloy 5456-H321 base metal in air and Alloy 5456-H321 weldments in air and Severn River water are shown in Figure 185. The specimens containing welds were tested with the weld crown ground flush to the base-metal plate. The
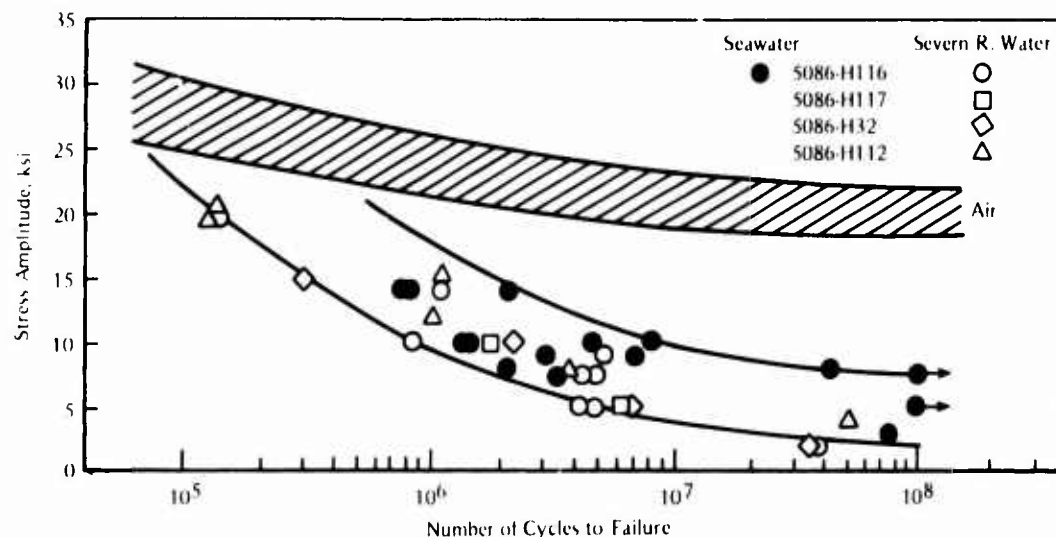
FIGURE 181. Corrosion-Fatigue-Test Results for Alloy 5086 Base Metal Tempers in Saltwater Environments[230]

The shaded scatterband region is reproduced from air environment data.
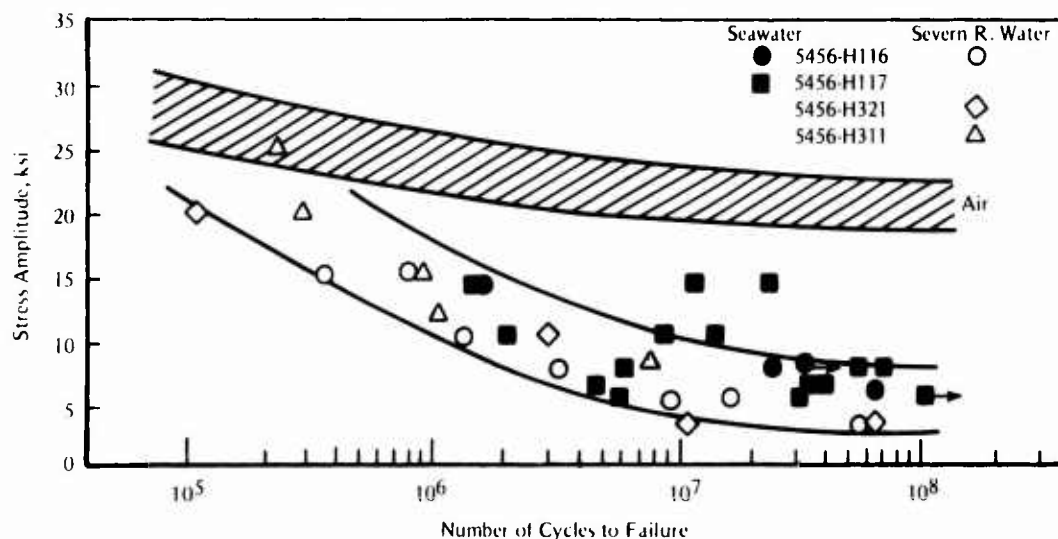
FIGURE 182. Corrosion-Fatigue-Test Results for 5456 Base Metal Tempers in Saltwater Environments[230]

The shaded scatterband region is reproduced from air environment data.

seawater and Severn River water are both detrimental to the fatigue lives of the base metal and the base metal containing weldments. The presence of saltwater decreases the fatigue resistance of the base metal compared with that in air, and the presence of welds further decreases the resistance.

In addition to the results for Alloy 5086 discussed above, the influence of hydrostatic pressure on the corrosion-fatigue properties of Alloy 5086 in the H116 and H117 tempers was studied by Jolliff and Thiruvengadam.[73] This aspect of corrosion fatigue is important for deep-ocean structural applications. High-frequency (20 kHz) tests were performed on smooth
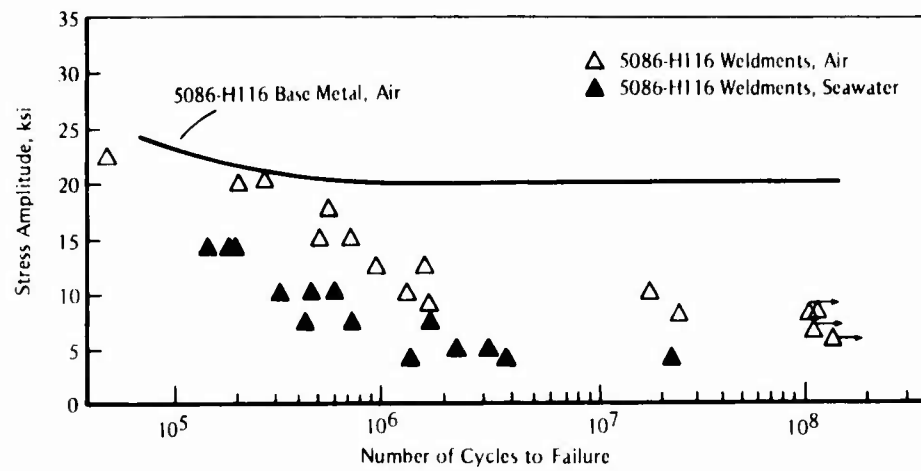
FIGURE 183. Corrosion-Fatigue-Test Results for Alloy 5086-H116
Weldments in Air and Seawater[230]
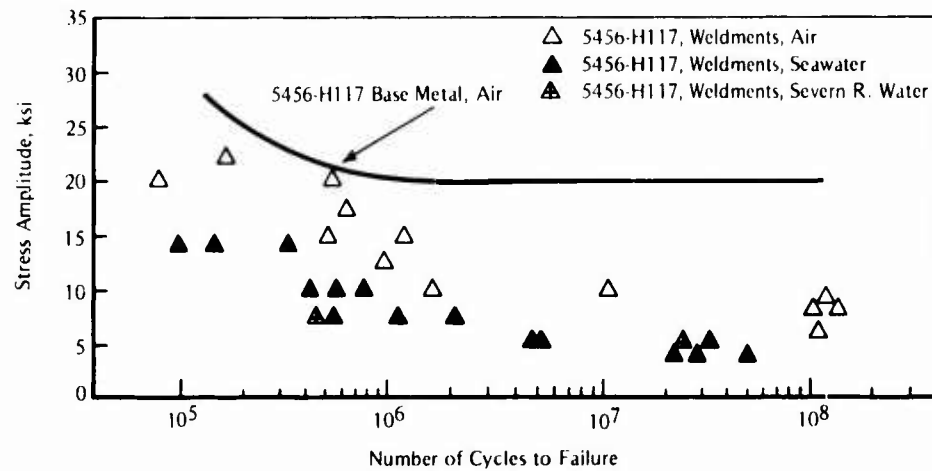
FIGURE 184. Corrosion-Fatigue-Test Results for Alloy 5456-H117
Weldments in Air, Seawater, and Severn River Water[230]
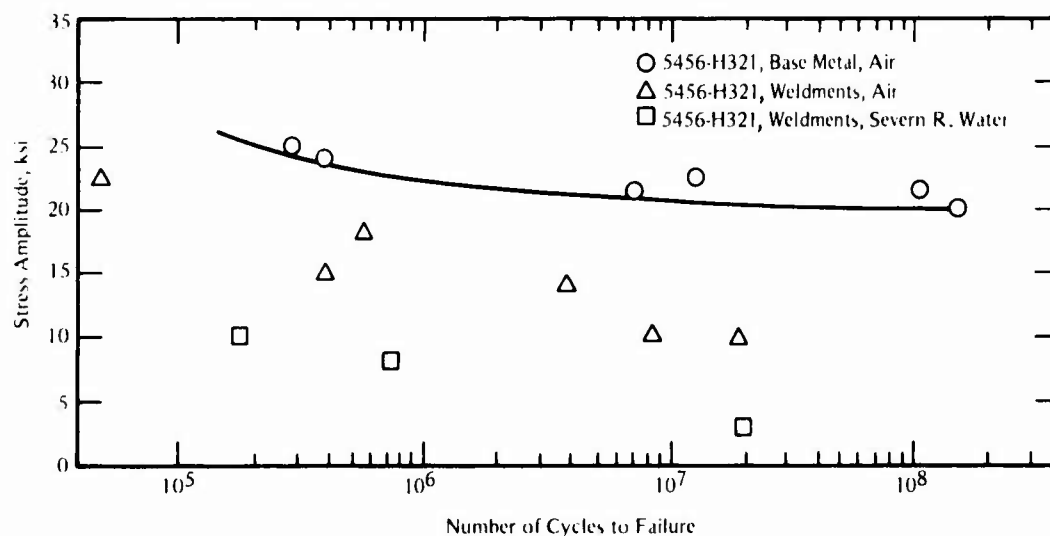
FIGURE 185. Corrosion-Fatigue-Test Results for Alloy 5456-H321 Base Metal and Weldments
in Air and Severn River Water[230]

cylindrical specimens in synthetic seawater at atmospheric pressure and at a pressure of 2000 psi (13.8 MPa). The high-pressure testing simulated conditions at 4500 ft (1372 m).

Results for both materials are shown in Figures 186 and 187. The effect of the hydrostatic pressure on the fatigue strength of Alloy 5086-H117 is shown by the fatigue-life for this alloy in saltwater at 2000 psi (see Figure 186). The fatigue-life curve obtained at hydrostatic pressure lies below that obtained in saltwater at atmospheric pressure over the entire range of data. This is not true for Alloy 5086-H116; instead there was a crossover in curves at approximately 2×10^6 cycles (Figure 187). The influence on fatigue strength hydrostatic pressure was considered to be primarily chemical in nature. The author believes that the seawater is forced to be in more intimate contact with the material's surface (i.e., cracks and microcracks), which results in a more intensive chemical reaction.

Austin[213] evaluated the corrosion-fatigue resistance of Alloys 5052-H32, 5052-H34, and 5086-H34 in air and in artificial seawater. His results are plotted in Figure 188. Alloy 5086-H34 showed the best corrosion-fatigue resistance and Alloy 5052-H32 displayed the worst. Although the corrosive environment did cause a significant reduction in cyclic life, this reduction was not quite as large as that found for Alloys 2014-T6 and 2024-T4 in similar tests (see Figure 157, discussed earlier). At higher stress levels 29.41 ksi (near 200 MPa), all three 5000-series alloys showed inferior corrosion-fatigue resistance to the two 2000-series alloys. However, at lower stress levels near 17.65 ksi (120 MPa), the corrosion-fatigue resistance for the 5000-series alloys was as good as or slightly better than that of the 2000-series alloys.
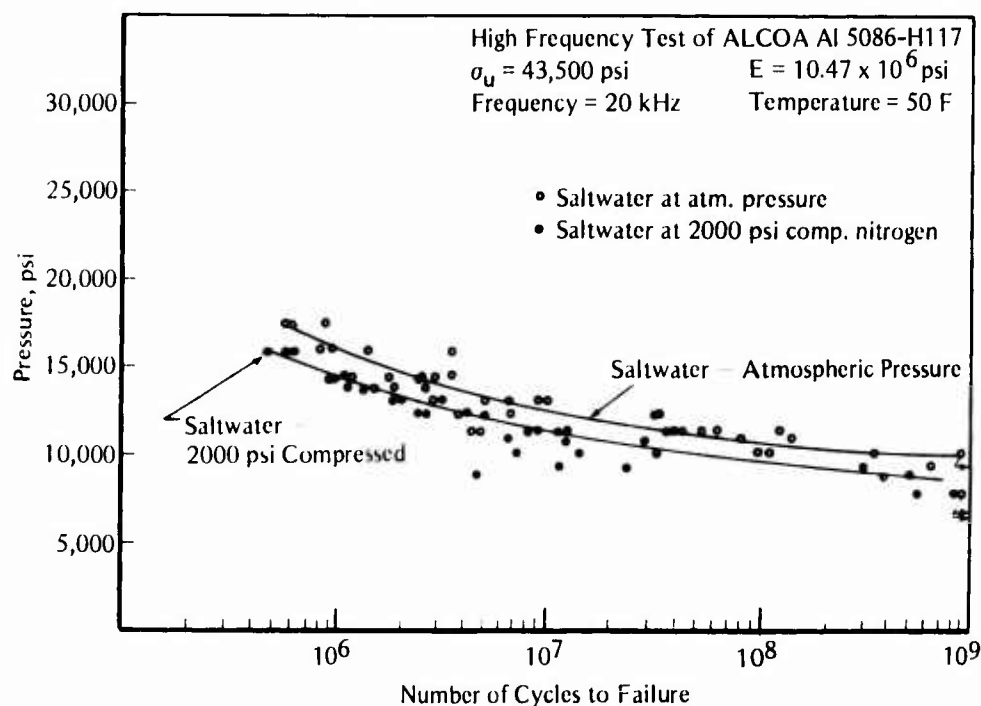
FIGURE 186. Fatigue-Life Curves for Alloy 5086-H117
Tested in Saltwater at High Frequency and High Pressure[73]

High Frequency Test of Reynolds Al 5086-H116
σ_u = 49,760 psi   E = 1049 x 10^6 psi
Frequency = 20 kHz   Temperature = 50 F

ALCOA Al 5086-H117 Smooth Specimen in Air, R = -1

● Saltwater at atm. pressure
● Saltwater at 2000 psi comp. nitrogen
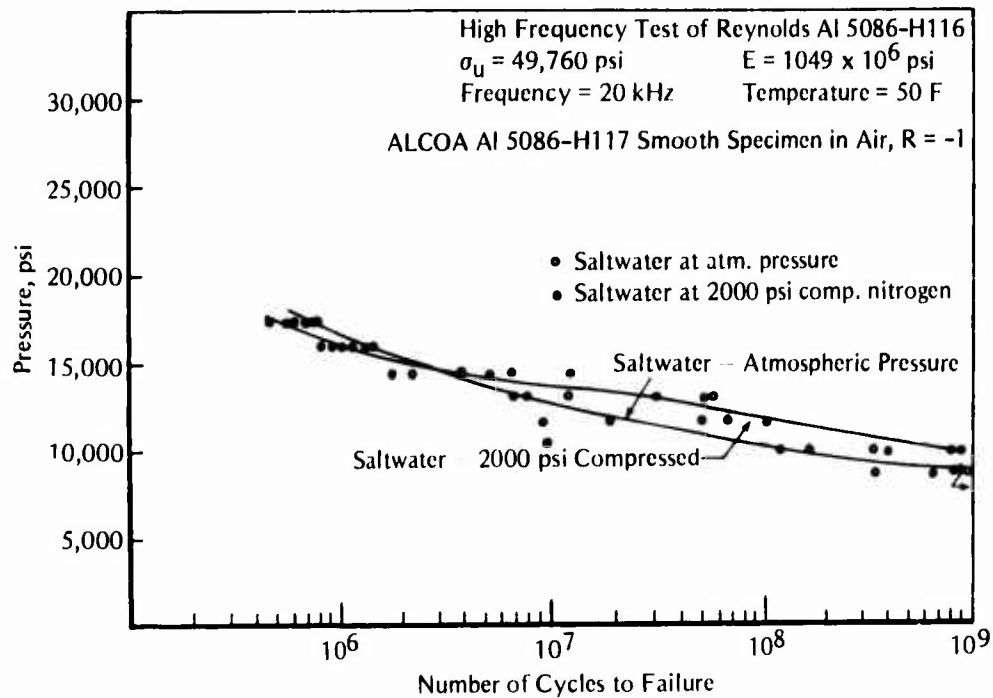
FIGURE 187. Fatigue-Life Curves for Alloy 5086-H116
Tested in Saltwater at High Frequency and High Pressure[73]
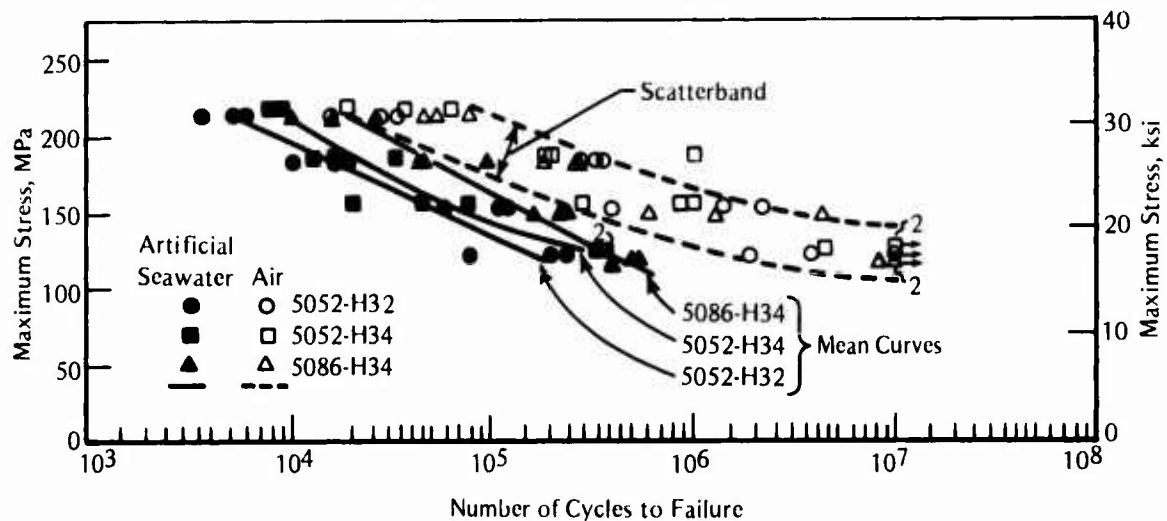
FIGURE 188. Corrosion-Fatigue Resistance of Alloys 5052-H32, 5052-H34, and 5086-H34 in Air
and in Artificial Seawater[213]

6XXX Series Aluminum Alloys

A limited amount of data was available for the 6XXX series aluminum alloys because these alloys have only limited use in the marine and aircraft/aerospace industries. Alloy 6061 is used for both marine and aircraft storage tanks.

Crooker[217] included Alloy 6061-T651 in his corrosion-fatigue-crack growth studies. The data for single-edge-notched specimens in air and 3.5 percent NaCl solution are plotted in Figure 189 in terms of crack growth rate as a function of the stress intensity factor range. At the lower ΔK levels, Alloy 6061-T651 was found to be somewhat sensitive to the saltwater solution, but at ΔK values greater than 25 ksi $\sqrt{\text{in.}}$, this sensitivity decreased.
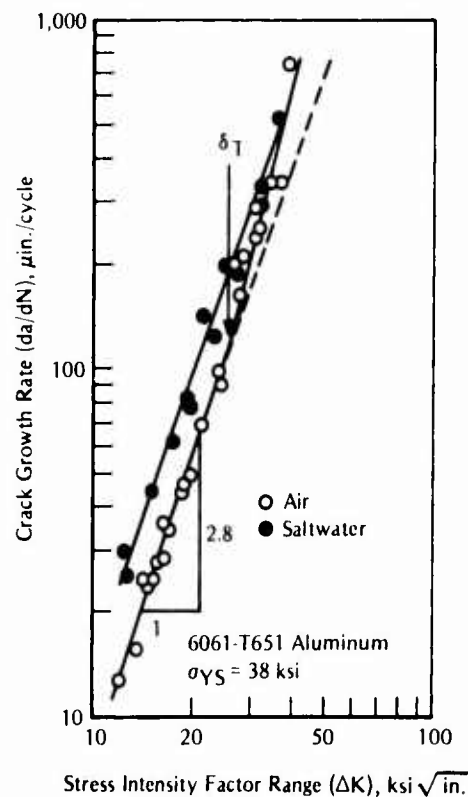
FIGURE 189. Corrosion-Fatigue-Crack Growth for Alloy 6061-T651 in Air and in Saltwater[217]

7XXX Series Aluminum Alloys

The 7XXX series aluminum alloys are popular in the aircraft and aerospace industries because of their high strength-to-weight ratios. The most popular alloy is 7075 in the overaged condition.

The alloys reviewed in this section and the corresponding reference numbers of the articles in which the data appeared are listed in Table 33. The data for the 7XXX series aluminum alloys are summarized in Table 34.

Alloy 7075

Results from tests by Stoltz and Pelloux[237] indicated that for Alloy 7075-T6 in a 3.5 percent NaCl solution, a cathodic potential of -1.400 V SCE reduced corrosion-fatigue-crack growth rates to a level observed in dry argon. Open-circuit potential for this system was -0.820 V SCE.

TABLE 33. 7XXX Series Aluminum Alloys Reviewed

Alloy	Alloy Composition, wt %								Reference
	Cu	Mg	Cr	Zn	Si	Mn	Ti	Zr	
7075	1.6	2.5	0.23	5.6					212, 216, 235 - 240
ZK41	0.03	1.89		3.97	0.05	0.3		0.16	241
7475		2.3	0.22	5.7	1.5				126
7079	0.4	2.9	0.1	3.8	0.3	0.1	0.1		151
7005		1.4	0.13	4.5		0.45	0.04	0.14	217
X166	1.7	2.3		6.0	0.08	0.02	0.02	0.1	242
7175	1.6	2.5	0.23	5.6					243

The authors ran a series of tests to obtain the crack growth rates at stress intensity factors of 10, 15, 20, and 25 ksi $\sqrt{\text{in}}$. and plotted them against the applied potential. Their results are shown in Figure 190. For $\Delta K = 10$ ksi $\sqrt{\text{in}}$., there was a noticeable drop in crack growth rate at the more negative cathodic potentials. At higher ΔK's, there is no such drop.

Smith and Duquette[239] performed corrosion-fatigue tests on axially loaded specimens of a high-purity alloy (Al-Zn-Mg-Cu) similar to Alloy 7075 in a 3.0 percent NaCl environment. Their
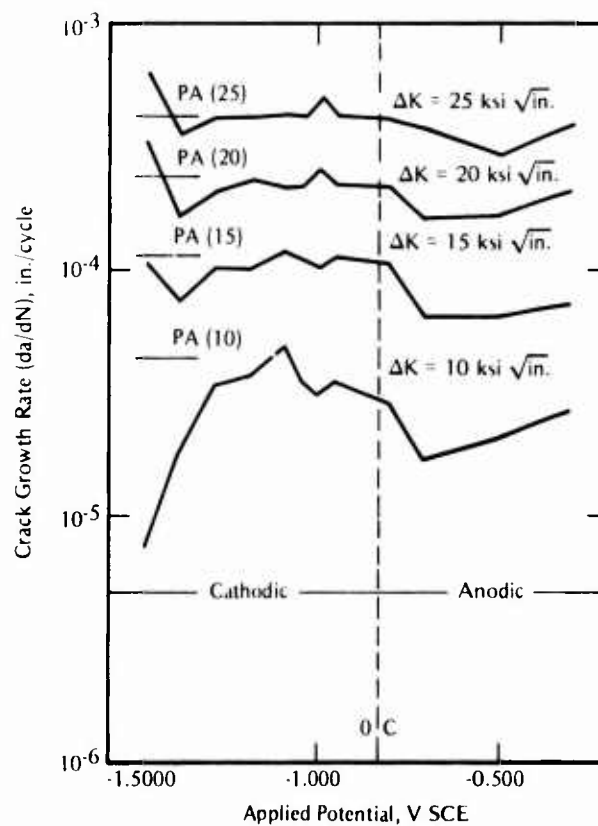
FIGURE 190. Corrosion-Fatigue-Crack-Growth Rates as a
Function of Applied Potential for Alloy 7075 Peak Aged[237]

TABLE 34. Summary of Corrosion-Fatigue Data for the 7XXX Series Aluminum Alloys

Alloy Condition	Tensile Strength, ksi (MPa) Ultimate	Yield	Type of Specimen	Type of Loading	Frequency, Hz	Environment	Types of Data	Note	References
7075-T6	75 (510)	68 (462.4)	Smooth, cylindrical	Axial tension-tension	30	Aerated flowing 0.5N NaCl	S-N curves 10^4 to 10^7 cycles	Free corrosion	235
7075-T6			Smooth, cylindrical	Axial tension-tension	30	Precorroded-tested in air		Precorrosion in 0.5N NaCl for 24 hr before testing	235
7075-T6			Smooth, cylindrical	Axial tension-tension	30	Precorroded-heat treated-tested in air			235
Al-5.5Zn-2.5Mg-1.5Cu(a)			Smooth, plate	Axial tension-tension	30	Aerated flowing 0.5N NaCl	$S-N$ curves 4×10^4 to 10^7 cycles	Free Corrosion	235
Al-5.5Zn-2.5Mg-1.5Cu(a)			Smooth, plate	Axial tension-tension	30	Aerated flowing 0.5N NaCl		Applied cathodic potential of -1.30 and -1.75V SCE	235
7079-T6	75 (510)	68 (462.4)	Smooth, tapered cylindrical, rotating cantilever beam	Constant stress-reversed	24.2	Aerated Severn river water	S-N curve 10^2 to 10^8 cycles		151
7079-T6	75 (510)	68 (462.4)	Notched, cylindrical, rotating cantilever beam	Constant stress-reversed	-1.2	Aerated Severn river water	S-N curve 10^2 to 10^8 cycles		151
7079-T6	75 (510)	68 (462.4)	Smooth, plate, continuous radius	Constant stress-reversed	0.006-1.016	Aerated Severn river water	S-N curve 10^2 to 10^8 cycles		151
7079-T6	75 (510)	68 (462.4)	Notched plate, continuous radius	Constant stress-reversed	0.007-0.016	Aerated Severn river water	S-N curve 10^2 to 10^8 cycles		151
7075(b)			Center-notched plate	Axial tension-tension	1.0	0.2M 3% NaCl solution	Crack growth rate vs ΔK		244
7075-T6			Smooth, hourglass	Axial with superimposed mean stresses of 0, 25, and 40 ksi (0, 170, and 272 MPa)	30	0.5N NaCl solution	S-N curves for each imposed stress, Goodman plot		246
7075-T6	87 (591.6)	80 (544)	Polished, cylindrical	Rotating bending	36.6	Flowing 3% NaCl solution at 77 F	S-N curve 10^4 to 10^7 cycles, variation of cathodic polarization curves with progress of stress cycles		52
7075-T651	Slightly lower than for 7075 alloy		Smooth plate	Constant load, constant deflection, double cantilever, R=0.1, 0.5, 0.8	0.1, 1	3.5% NaCl solution at 72 F, 175 F	Crack growth rate vs intensity factor		245
7475-T651	87 (591.6)	80 (544)		Constant load, double cantilever, R=0.1, 0.5, 0.8	1	3.5% NaCl solution at 72 F	Crack growth rate vs intensity factor		245
7075-T651	87 (591.6)	80 (544)	Surface-flawed plate	Double cantilever, R=0.1, 0.5, 0.8	1	3.5% NaCl solution at 72 F	Crack growth rate vs intensity factor		245
7005-T63	52 (353.6)	46 (312.8)	Single-edge notched	Cantilever, zero to tension	0.1	3.5% NaCl solution	Crack growth rate vs ΔK		217
7039-T6X31	62 (421.5)	52 (353.6)	Single-edge notched	Cantilever, zero to tension	0.1	3.5% NaCl solution	Crack growth rate vs ΔK		217
7106-T63	61 (414.8)	52 (353.6)	Single-edge notched	Cantilever, zero to tension	0.1	3.5% NaCl solution	Crack growth rate vs ΔK		217
7075-T6, peak aged			Center-notched plate	Axial tension-tension	1	3.5% NaCl solution	Crack growth rate vs applied potential	Constant impressed current, reversed anodic-cathodic current (polarity)	23
7075-T6, overaged				Axial tension-tension	1	3.5% NaCl solution	Crack growth rate vs applied potential		237
Al alloy ZF(c)			Center-notched plate	Axial tension-tension	1	3.5% NaCl solution	Crack growth rate vs applied potential	Addition of NaNO3 as inhibitor	237
Al alloy ZC(d)			Center-notched plate	Axial tension-tension	1	3.5% NaCl solution	Crack growth rate vs applied potential	Fractographic studies	237
7075-T651	83.6 (568.5)	74.7 (508)	Plate, smooth with holes	Uniaxial tension, maneuver spectrum	2	Fretted, tested in 3.5% NaCl solution			214
7075-T651-Alodine	83.6 (568.5)	74.7 (508)	Ditto	Ditto	2	Fretted, alternately immersed in 3.5% NaCl solution for 30 days and tested in air	Crack propagation data for test spectrum		214
7075-T73	72.7 (494.4)	58.8 (400)	″	″	2				214
7075-T651	83.6 (568.5)	74.7 (508)	″	″	2				214
7075-T73	72.7 (494.4)	58.8 (400)	″	″	2	Fretted, alternately immersed in 3.5% NaCl solution for 30 days and tested in distilled H2O			214
7075-T651	83.6 (568.5)	74.7 (508)	″	″	2				214

TABLE 34. (Continued)

Alloy Condition	Tensile Strength, ksi (MPa)		Type of Specimen	Type of Loading	Frequency, Hz	Environment	Types of Data	Note	References
	Ultimate	Yield							
7075-T651	83.6 (568.6)	73.7 (508)	...			Tested, alternately immersed in 3.5% NaCl solution for 40 days			214
7075-T651-Alodine	83.6 (568.6)	73.7 (508)	...			and tested in 3.5% NaCl solution			214
7075-T73	72.7 (494.1)	58.3 (400)				Nonfretted, alternately immersed in 3.5% NaCl solution for 40 days,			214
7075-T651	83.6 (568.6)	73.7 (508)	Plate, smooth with holes	Uniaxial tension, maneuver spectrum		and tested in air			214
7075-T6	81.3 (553)	72.1 (504)	Single-edge notched	Constant amplitude	Overload 0.1	3.5% NaCl solution	Constant amplitude FCP	With single overload ratios of 1.5, 2.0, and 2.5	224
7075-T73	72.2 (491)	61.6 (419)	Single-edge notched	Constant amplitude	Overload 0.1	3.5% NaCl solution	Overload and decay crack data, fractographic results		224
7075-T6			Center notched	Axial constant amplitude	0.33	Synthetic seawater	S-N curves 10⁴ to 10⁷ cycles		248
7075-T76			Center notched	Axial constant amplitude	0.33	Synthetic seawater			238
7075-T6			Center notched	Axial constant amplitude	0.33	Synthetic seawater			248
7075-T76	81.6 (555)	71 (484)	Center notched	Axial constant amplitude	0.33	Synthetic seawater	Crack growth rate vs intensity factor		235
7175-T351			Compact tension		Variable	3.5% NaCl solution			225
7075-T651	73.7 (501)	63.1 (428)	Compact tension		Variable	3.5% NaCl solution	Crack growth rate vs intensity factor, effect of specimen thickness and test frequency		226
7075-T6 overaged			Center notched	Tension-tension, R=0.01 to 4	0.1, 1, 10	Aerated 3.5% NaCl solution	Crack growth rate vs intensity factor, crack growth rate vs test frequency		243(c)
7075-T6			Center notched	Tension-tension, R=0.01 to 4	0.1, 1, 10	Aerated 3.5% NaCl solution	Crack growth rate vs intensity factor		
Al alloy Zr			Center notched	Tension-tension, R=0.01 to 4	0.1, 1, 10	Aerated 3.5% NaCl solution	Crack growth rate vs intensity factor		
Al alloy ZC			Center notched	Tension-tension, R=0.01 to 4	0.1, 1, 10	Aerated 0.5N NaCl solution	Crack growth rate vs intensity factor		
High purity analogue alloy of 7075 (T6)	82 (557.6)	72	Polished, plate	Constant load, tension-tension		3% NaCl solution	S-N curves from 4 × 10⁴ to 10⁷ cycles for open-circuit potential and cathodically polarized specimens, fractographic studies	Effect of polarization, 1.6 V and 1-2 V on fatigue strength	239
7075-T6	83 (564.4)	73	Polished, plate	Constant load, tension-tension		3% NaCl solution			
7075-T6	83.5 (567.8)	73.8 (508.6)	Center cracked	Remote wedge, tension-tension	2	3.5% NaCl solution	Crack length vs N		226
7178-T6	91.1 (619.5)	79.1 (537.9)	Center cracked	Remote wedge, tension-tension	2	3.5% NaCl solution	dN vs crack growth rate, fractographic studies		
7175-T651	86.5 (588)	72.2 (491)	Compact tension	R=0.01, 0.5	0.2	30 g/l NaCl solution	Crack-opening displacement		248
2K41(f)-T6	65.7 (446.8)	59.0 (401.2)	Polished cylindrical		30	1% NaCl-O₂ saturated solution, 86 F	Rotating bending; S-N diagrams under various applied potentials, fractographic studies		241

(a) A high purity alloy similar to Alloy 7075

(b) Solution treated at 1652 F for 2 hours, water quenched, aged at 482 F for 8 hours, peak aged at 622 F for 20 hours, overaged

(c) Alloy contains zirconium instead of chromium as a grain growth inhibitor and is given a final cold rolling pass before solution treating with a finer grain size than 7C heat

(d) Alloy contains zirconium instead of chromium as a grain growth inhibitor and is hot rolled to final thickness

(e) Part II of report. Part I is Reference 237.

(f) Instance a, Zr Medallion

results are shown in Figure 191, with air and open-circuit-potential curves for reference. They found that polarization to -1.30 V SCE produced fatigue behavior similar to that under free corrosion conditions, but that potentials of -1.50 and -1.75 V SCE were extremely detrimental.
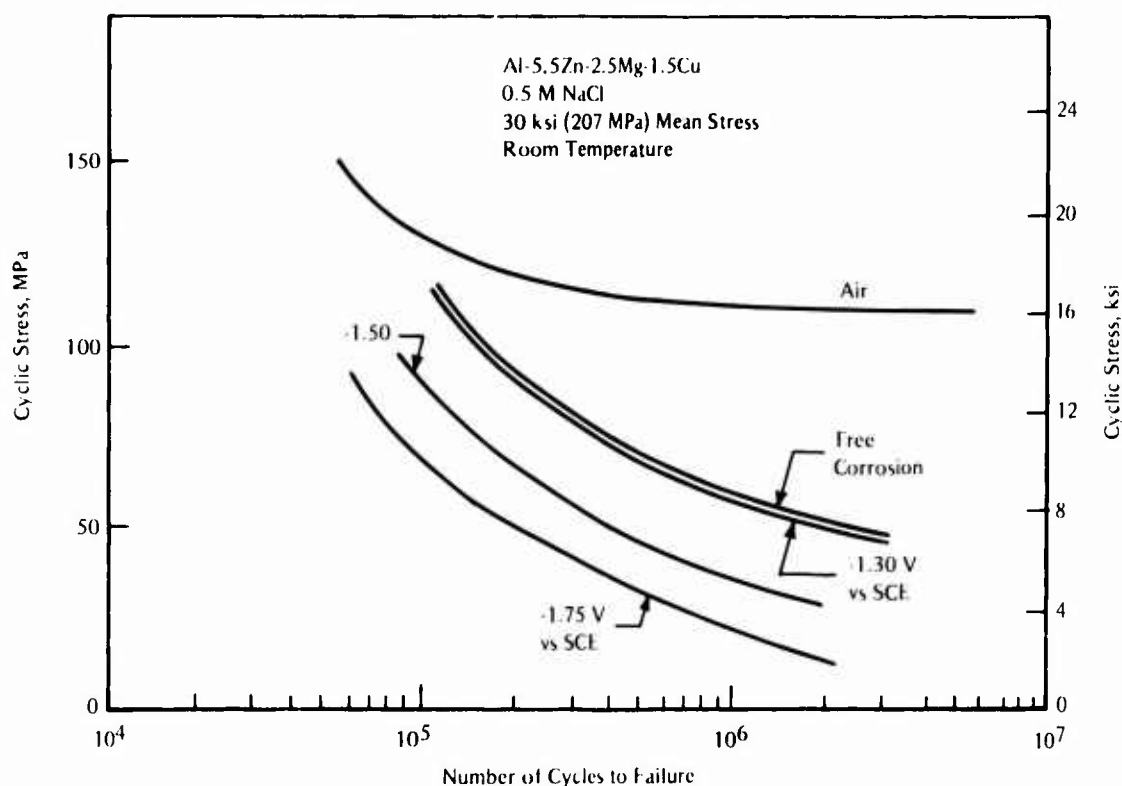
FIGURE 191. Fatigue-Life Curves for Cathodically Polarized Specimens of Al-5.5Zn-2.5Mg-1.5Cu in Saltwater[239]

The addition of sodium nitrate as an inhibitor has been shown to reduce the corrosion-fatigue-crack growth rates for a high-purity Al-Zn-Mg alloy (7075 type) in distilled water and 0.2 M NaCl solution.[244] Center-notched specimens were cycled at 1 Hz and the results of tests in the different environments are shown in Figure 192. The shaded area represents the scatterband of results using inhibitor solutions plus 1.7 M $NaNO_3$ in distilled water. The reduction in fatigue-crack growth rates in the inhibitor solutions is apparent.

The effects of prior corrosion on the fatigue life of Alloys 7075-T6 and 7075-T73 were investigated by Person.[212] Tapered repeated-bending specimens made from these alloys were exposed to a continuous salt fog spray (CASS-ASTM B-369-65). The form of prior corrosion was moderate intergranular attack for the Alloy 7075-T6 specimens exposed to the fog spray for 120 hours and pitting with slight intergranular attack for specimens exposed 278 hours. For specimens of Alloy 7075-T73, the form of prior corrosion was pitting after exposure to the continuous salt fog. Specimens exposed for 120 hours developed pitting attack on 25 percent of the surface while specimens exposed for 240 hours developed pitting attack on 50 to 70 percent of the surface.

Tensile properties of Alloys 7075-T6 and 7075-T73 were measured and compared with those of uncorroded test materials. The average tensile properties are given in Table 35.
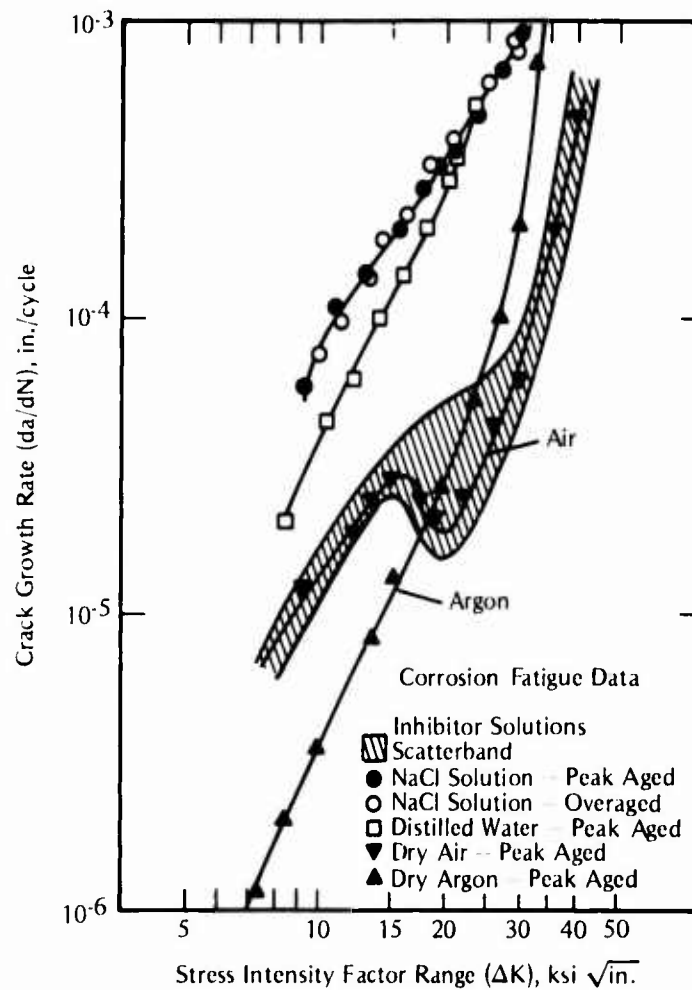
FIGURE 192. Corrosion-Fatigue-Crack-Growth Behavior of a High-Purity Al-Zn-Mg Alloy (7075 Type)[244]

TABLE 35. Average Tensile Properties of 7075-T6 and 7075-T73 Materials[212]

Material	Ultimate Tensile Strength, ksi (MPa)		Yield Strength, ksi (MPa)		Elongation, %
0.125 in. (3.18 mm) 7075-T6					
Uncorroded	86.8	(590.2)	77.3	(525.6)	11.5
Intergranular Attack	82.7	(562.4)	73.0	(496.4)	11.0
Decrease Caused by Intergranular Attack, %	4.7		5.6		4.5
0.125 in. (3.18 mm) 7075-T6					
Uncorroded	85.9	(584.1)	74.5	(506.6)	13.0
Heavy Pitting	80.2	(545.4)	71.0	(482.8)	6.5
Decrease Caused by Pitting, %	6.6		5.8		50.0
0.125 in. (3.18 mm) 7075-T73					
Uncorroded	80.4	(546.7)	69.7	(473.9)	12.5
Light Pitting	76.6	(520.8)	65.6	(446.0)	11.5
Heavy Pitting	75.4	(512.7)	65.4	(444.7)	7.5
Decrease Caused by Heavy Pitting, %	6.2		6.2		40.0

(a) Based on original thickness of uncorroded sheet.

Note: Average values are result of three tests on uncorroded sheet and at least ten tests on corroded sheet.

Corrosion data for each material are plotted in Figures 193 through 195. Uncorroded specimens fatigued in air serve as controls in each figure. The fatigue strengths at 10^5 and 10^8 cycles, along with the reductions in fatigue strength caused by the prior corrosion, are summarized in Table 36.
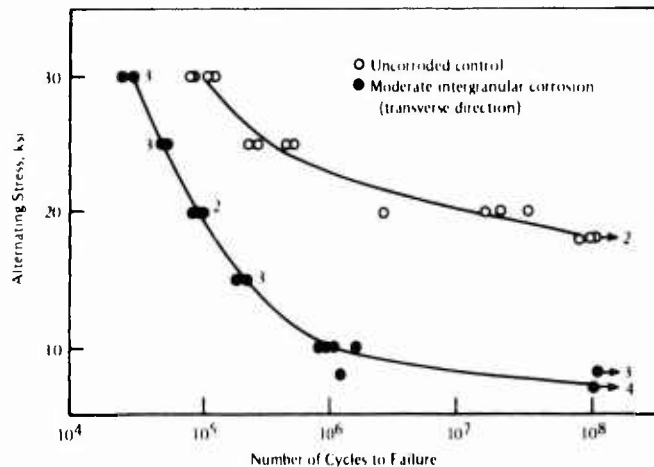
FIGURE 193. Effect of Intergranular Corrosion on Repeated Bending Fatigue Properties of 0.125-Inch-Thick 7075-T6 Sheet[212]
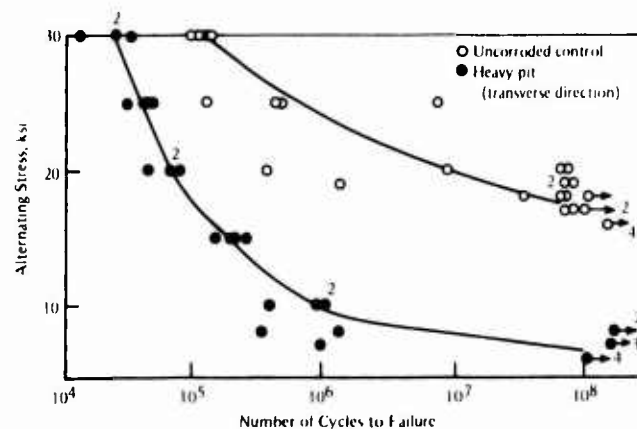
FIGURE 194. Effect of Corrosion Pitting on Repeated Bending Fatigue Properties of 0.125-Inch-Thick 7075-T6 Sheet[212]
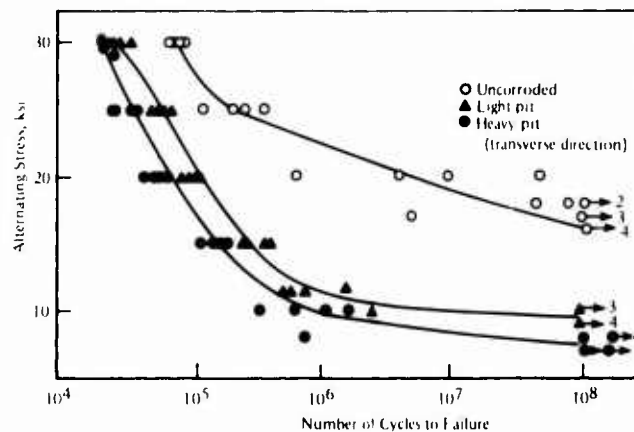
FIGURE 195. Effect of Corrosion Pitting on Repeated Bending Fatigue Properties of 0.125-Inch-Thick 7075-T73 Sheet[212]

For all materials, the previously corroded specimens had lower strengths for the entire cyclic ranges studied. The effect of the prior corrosion was greatest in the low-stress, high-cycle range for all materials, with the heavily pitted 7075-T6 material having the largest reduction in fatigue strength at 10^8 cycles to failure.

The decrease in fatigue strength between Alloy 7075-T73 specimens with light pitting and those with heavy pitting was small compared with that between specimens with no prior corrosion and those with light pitting. This indicates that the initial damage resulting from prior corrosion pitting caused most of the decrease in fatigue strength.

TABLE 36. Effect of Prior Corrosion on Repeated Bending Fatigue Properties of 7075-T6 and 7075-T73 Materials[212]

Alloy	Surface Condition	Pit Depth, in. (mm)	Fatigue Strength[a], ksi (MPa)		Reduction in Fatigue Strength[a],	
			10^5	10^8	10^5	10^8
7075-T6 (Lot A)	Uncorroded		30 (204)	18 (122.4)		
	Moderate inter-granular attack		20 (136)	7.5 (51)	33	58
7075-T6 (Lot B)	Uncorroded		31 (210.8)	17 (115.6)		
	Heavy pitting	6-11 (40.8-74.8)	17.5 (119)	6.5 (44.2)	44	62
7075-T73	Uncorroded		28.5 (193.8)	16 (108.8)		
	Light pitting	3-4.5 (20.4-30.6)	21.5 (146.2)	9.5 (64.6)	25	41
	Heavy pitting	8-13 (54.4-88.4)	18.0 (122.4)	7.5 (51)	37	53

(a) For indicated number of cycles.

Smith et al[235] found that the effects produced by corrosion of Alloy 7075-T6 specimens in 0.5 N NaCl solution for 24 hours prior to testing in air were similar to those produced by simultaneous corrosion and testing in saltwater. These tests were conducted at 30 Hz. The investigators also found that the effects of prior corrosion could be partially reversed by a heat treatment consisting of variable resolution treatment for three hours and peak aging of the precorroded specimens before testing in air. Their results are presented in Figure 196. Fatigue lives of the precorroded and air-fatigued specimens were shorter than those of the free-corrosion fatigue specimens in the high stress range, but in the low stress range the lives of the
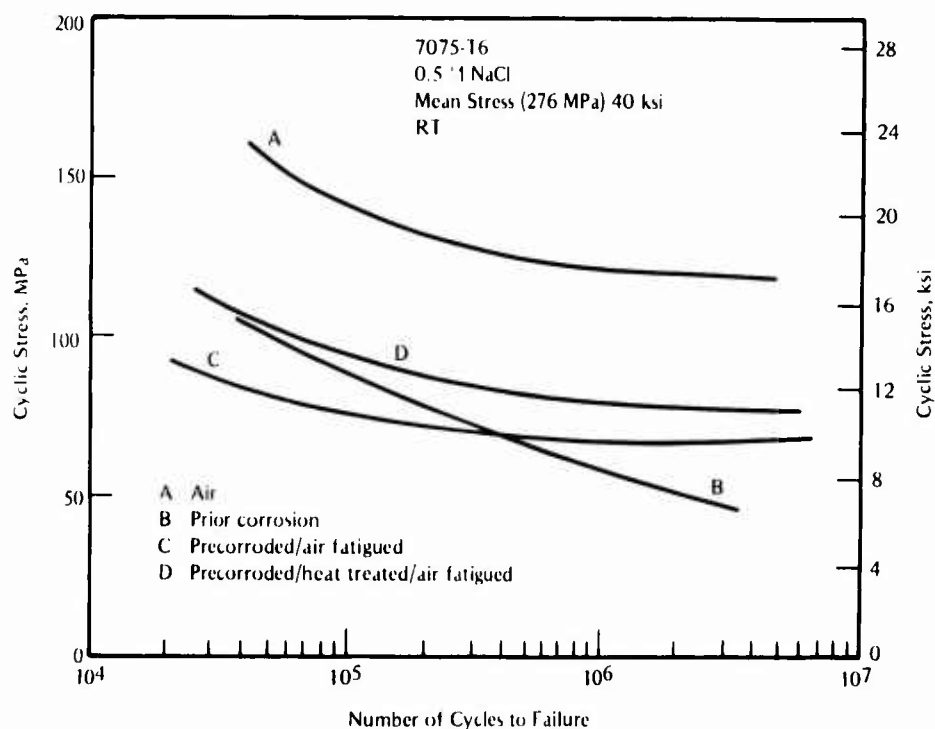
FIGURE 196. Fatigue-Life Curves for Alloy 7075-T6 in Air, in 0.5 N NaCl, Precorroded in 0.5 N NaCl and Cyclically Stressed in Air, and Precorroded, Heat-Treated, and Cyclically Stressed in Air[235]

free-corrosion specimens were longer. The fatigue lives for Alloy 7075-T6 specimens with no prior corrosion and tested in air are longer than those for the precorroded/heat-treated/air-fatigued specimens.

Smith et al[235] also investigated effects of cathodic polarization on a high-purity analogue of Alloy 7075-T6, Al-5.5Zn-2.5Mg-1.5 Cu. The results are shown in Figure 197. The fatigue life of this alloy is significantly decreased by the saltwater environment. Cathodic charging at -1.3 V SCE did not further reduce fatigue life, while cathodic charging at -1.5 V SCE reduced fatigue life considerably.
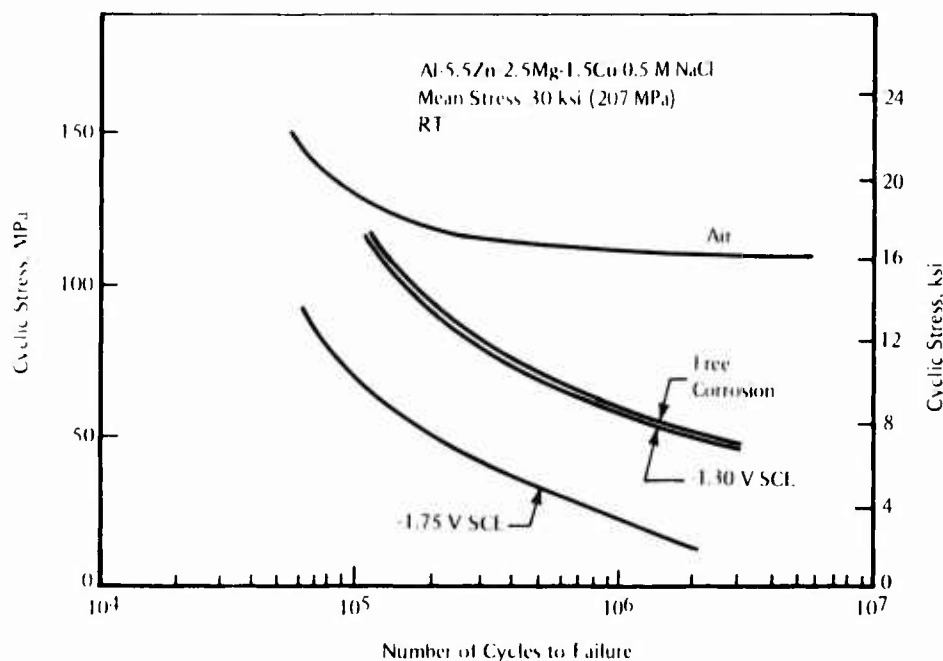
FIGURE 197. Fatigue-Life Curves for Al-5.5Zn-2.5Mg-1.5Cu in Air, in 0.5 N NaCl, in 0.5 N NaCl at -1.30 V SCE, and in 0.5 N NaCl at -1.75 V SCE[235]

Craig[238] found that the effects of synthetic seawater without heavy metals on the fatigue lives of center-notched 7075-T6 and 7075-T76 specimens were longer under high-cycle, low-stress conditions than under low-cycle, high-stress conditions. In the high-stress, low-cycle range, the fatigue lives of these specimens was nearly the same. In the low-stress, high-cycle range, the fatigue life of the 7075-T6 material was longer than that of the 7075-T76 material.

Axial fatigue tests were performed on Alloy 7075-T6 in dry air and in 0.5 N NaCl solution by Corsetti and Duquette.[236] Cylindrical specimens with an hourglass-shaped gage section were electropolished prior to testing at 30 Hz under conditions of 0, 25, and 40-ksi mean stress. The results are shown in Figure 198. For each mean stress, there was a reduction in fatigue life at all applied cyclic stress levels.

Data from fatigue-life curves for 10^5, 10^6, and 10^7 cycles to failure were replotted on a Goodman diagram to show fatigue life as a function of stress amplitude and mean stress (Figure 199). The Goodman diagram showed that the reduction in the fatigue limit associated with the corrosive environment is independent of mean stress. The 0.5 N NaCl solution severely attacked material around nonmetallic inclusions, thereby creating deep longitudinally oriented pits which acted as stress raisers. The authors attributed the accelerated
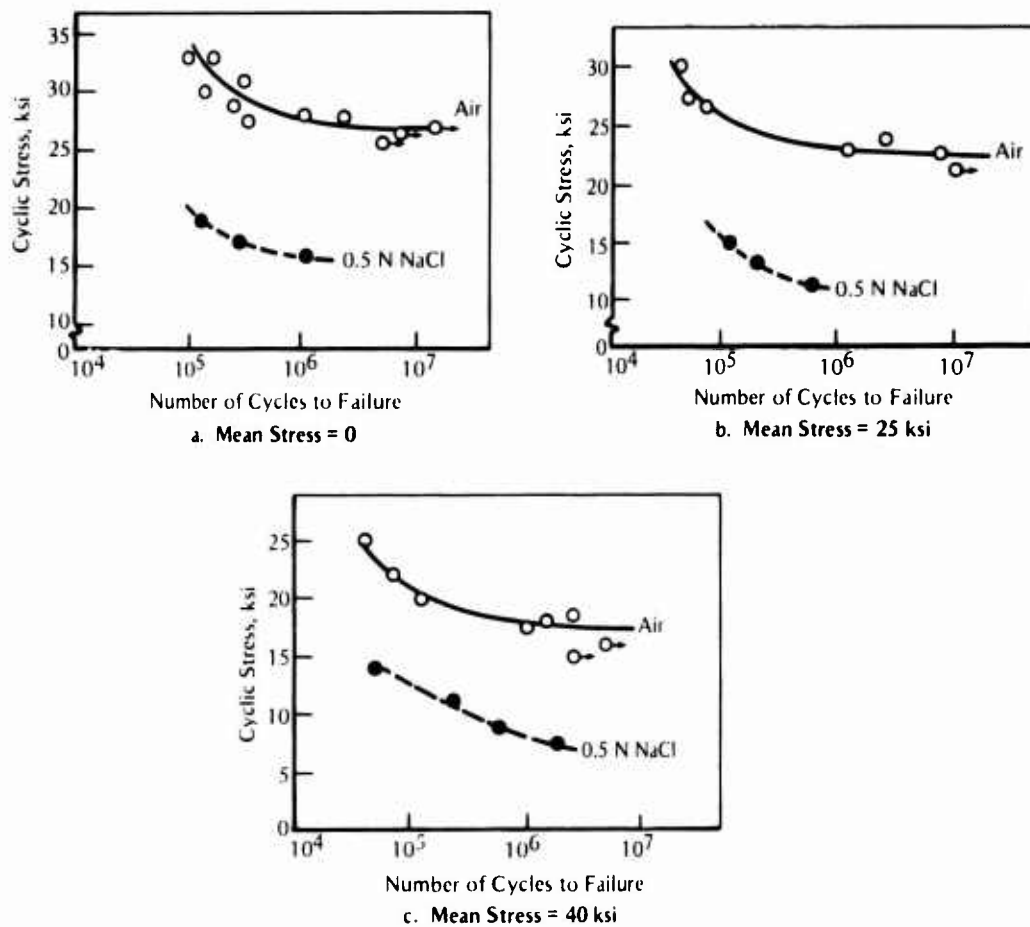
FIGURE 198. Fatigue-Life Curves for Alloy 7075-T6
in Air and in Aerated 0.5 N NaCl Solution[236]

FIGURE 199. Goodman Plot Showing Fatigue Life
as a Function of Stress Amplitude and Mean Stress[236]
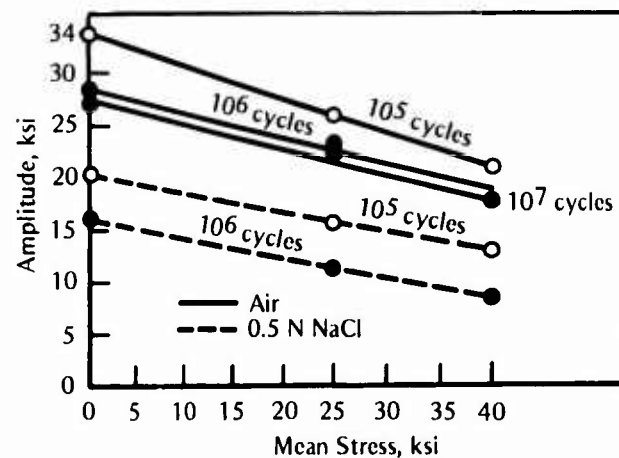
noncrystallographic corrosion-fatigue behavior as experienced in their testing to a localized hydrogen embrittlement phenomenon.

Fatigue-crack-propagation tests on flat specimens of Alloy 7075-T6 in air and seawater were performed by Figge and Hudson.[216] These specimens were axially loaded, R = 0, either at 0.67 Hz for maximum stress levels of 50, 40, 30, and 25 ksi (346, 276, 206, and 173 MPa) or at 20 Hz for maximum stress levels of 20 and 16 ksi (138 and 110 MPa). Fatigue-crack growth for Alloy

7075-T6 in air and in seawater at those stress levels is shown in Figure 200. The fatigue cracks grew approximately twice as fast in seawater as in air at all stress levels.

Fatigue-crack growth rates for Alloy 7075 were studied as a function of environment, frequency, composition, and thermomechanical treatment by Selines et al.[247] This alloy was tested in the peak aged condition, in the T6 temper, and in the overaged condition. An alloy similar to Alloy 7075 was also tested in grain size conditions. In this alloy, the chromium addition which is found in 7075 alloys was replaced by zirconium. Samples labled ZC had a final grain size comparable to that of 7075 alloys, while samples labled ZF had a grain size approximately
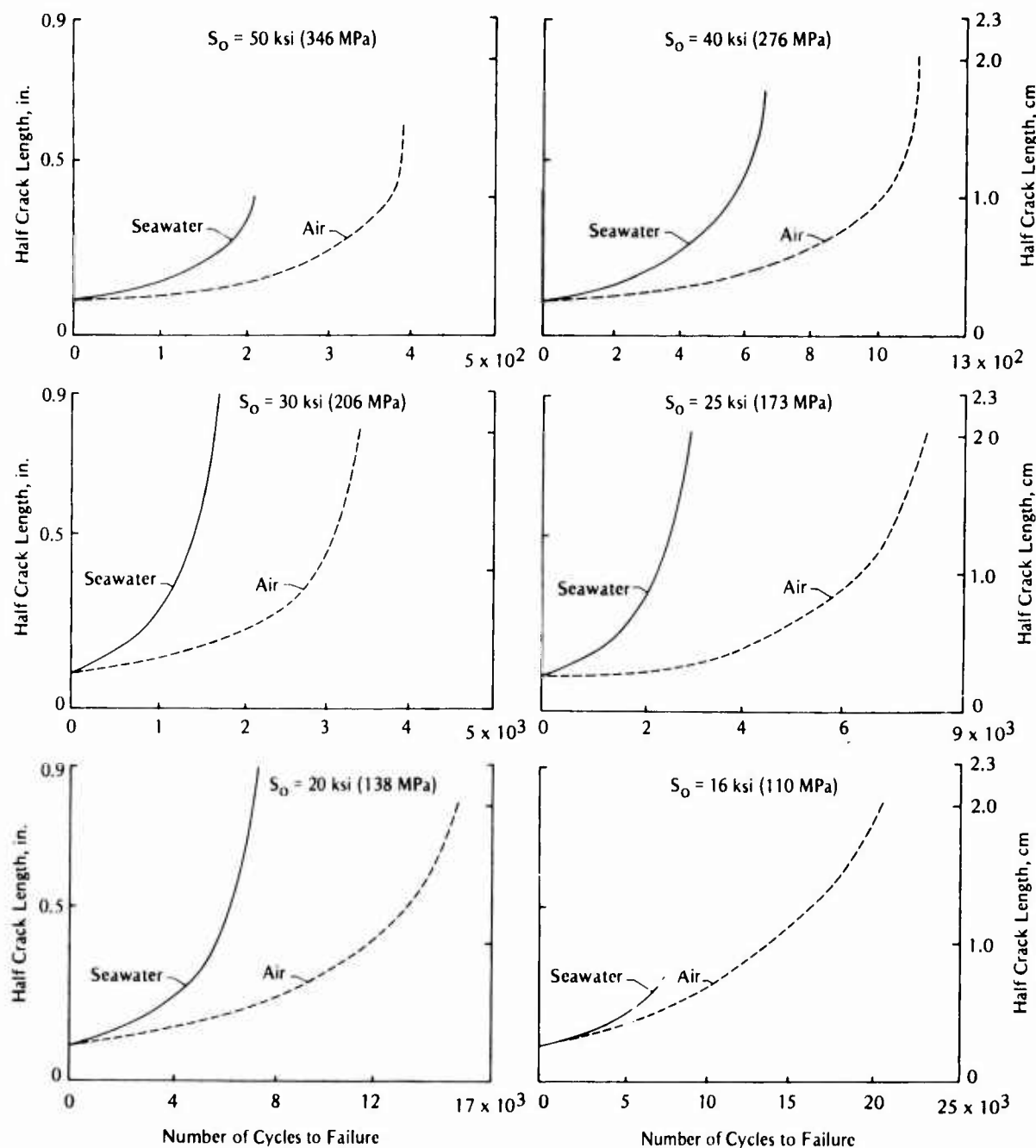
FIGURE 200. Fatigue-Crack Growth for Alloy 7075-T6 Tested in Air or in Seawater, R = 0[216]

one-third that of the ZC alloy and the 7075 alloys. Center-notched specimens were tested at 0.1, 1, and 10 Hz using stress fluctuations in the form of a simusoidal wave, a square wave, a positive-sawtooth wave, and negative-sawtooth wave. Tests were performed in dry argon containing 20 ppm by volume of H_2O, in air containing 225 ppm by volume of H_2O, and in aerated 3.5 percent NaCl solution.

The effect of cyclic frequency on crack growth rates is shown in Figure 201 for Alloy 7075-T6 in saltwater, with test results in argon included as reference. The effect of the corrosive environment was more detrimental in the low stress intensity factor range than at $\Delta K > 20$ ksi $\sqrt{\text{in}}$., which corresponds to K_{Iscc} where the effects of the environment became minimal. The crack-growth rate as a function of ΔK for the 7075 alloys and modified alloys is shown in Figure 202. Neither the small changes in composition nor changes in thermomechanical processing or aging treatment significantly improved the corrosion fatigue resistance of the 7075-type alloys in a saltwater environment below K_{Iscc}. However, overaging 7075-type alloys to a T773 temper was found to be slightly beneficial. The effects of stress wave forms on the corrosion-fatigue-crack growth rate of Alloy 7075 in saltwater at 0.1 Hz are shown in Figure 203. As can be seen, varying the stress wave form did not significantly alter the detrimental effects of the saltwater.
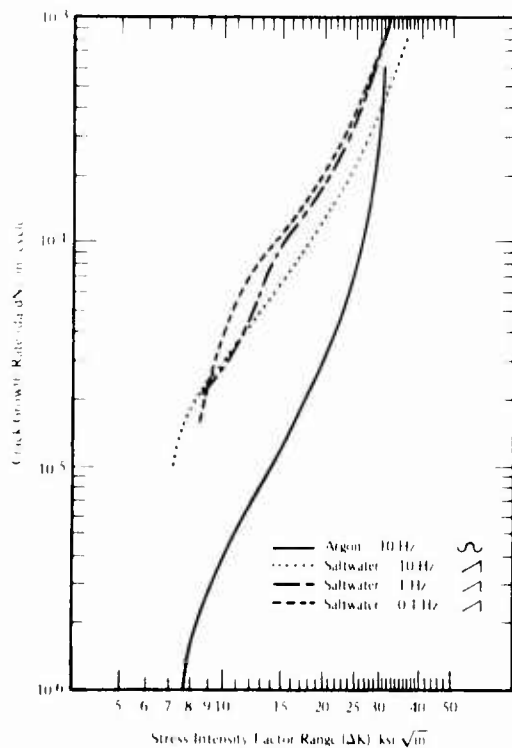
FIGURE 201. Crack Growth Rates for Alloy 7075-T6 in Saltwater at 0.1, 1, and 10 Hz[247]
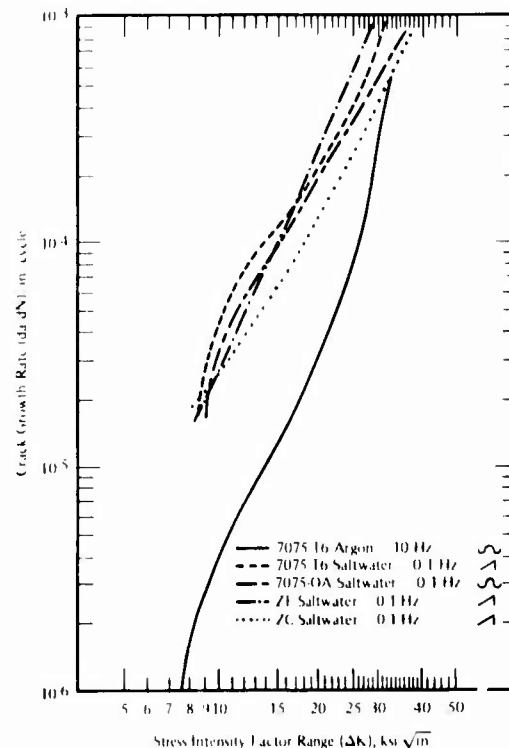
FIGURE 202. Crack Growth Rates in Saltwater for Alloy 7075-Type Materials With Different Compositions and Thermomechanical Treatments[247]
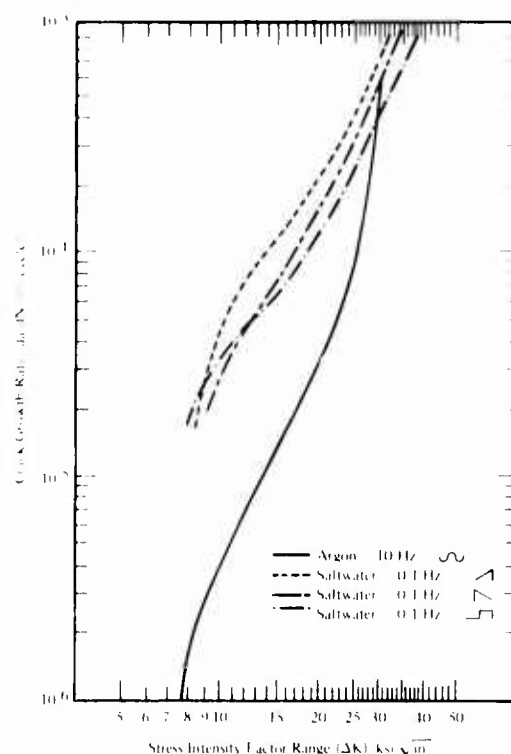
FIGURE 203. Effect of Stress Wave Form on Crack Growth
Rate of Alloy 7075-T6 in Saltwater at 0.1 Hz[247]

Alloy ZK 41

Endo et al[241] studied the effects of cathodic protection on the corrosion-fatigue life of Alloy ZK41-T6, which is similar to the 7XXX series alloys. Fatigue tests were conducted in rotating bending at 30 Hz in a 1 percent NaCl-oxygen saturated environment. Fatigue-life curves for ZK41-T6 in saltwater for applied potentials ranging from -0.8 to -1.75 V SCE are shown in Figure 204. The points for $E = E_c$ denote open-circuit potential. The fatigue lives for the anodic potential, 0.80 V SCE, and for the cathodic potential, 1.75 V SCE, are shorter than those under open-circuit potential for the entire cyclic range. The highest increase in corrosion-fatigue life occurred for the applied potential of -1.3 V SCE, with maximum life occurring between -1.3 and -1.4 V SCE.

Alloy 7475

Bogar and Crooker[126] studied the influence of the bulk solution chemistry on the corrosion-fatigue-crack growth rate of several high-strength alloys. The solutions investigated were: (1) fresh natural seawater; (2) 2.5 percent NaCl solution; (3) ASTM D-1141-75, substitute ocean water with heavy metal additions; and (4) ASTM D-1141-75, substitute ocean water without heavy metal additions. The effects of each solution in the quiescent and flowing conditions were taken into consideration. All the above-mentioned solutions and conditions are frequently employed in marine corrosion studies. Crack growth rates as a function of stress intensity factor range for single-edge-notched cantilever specimens of Alloy 7475-T7351 at
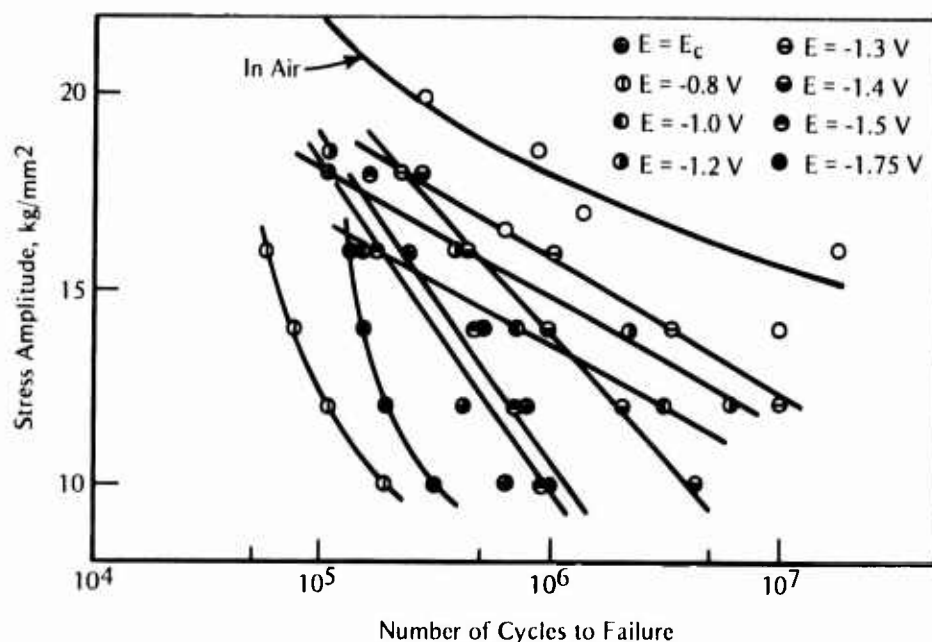
FIGURE 204. Fatigue-Life Curves for ZK41-T6 Under Various Applied Potentials, Where $E = E_c$ is the Open-Circuit Corrosion Potential[241]

Potential was measured against a saturated calomel electrode (SCE).

a frequency of 0.167 Hz are plotted in Figure 205. This figure shows that the variation in growth rates is minimal for Alloy 7475-T7351 in natural seawater and in either of the ASTM artificial seawaters under quiescent or flowing conditions. Test results plotted in Figure 206 reveal a noticeable difference between fatigue-crack growth rates in natural seawater and those in 3.5 percent NaCl solution. The aqueous 3.5 percent NaCl solution was much more detrimental, with crack growth rates being almost double those in natural seawater in the lower stress intensity range. The flow rate had no effect on crack growth rate. In many experiments a 3.5 percent NaCl solution is used to duplicate natural seawater. It is believed that for this particular alloy/condition (7475-T7351) NaCl solutions were more severe than natural seawater.

Alloy 7079

Fatigue lives (pseudo stress amplitude* versus number of cycles to failure) for smooth and notched specimens of Alloy 7079-T6 in air and in aerated Severn River water are shown in Figure 207.[151] At intermediate stress levels, the smooth specimens exhibited longer fatigue lives in air and in saltwater. However, at approximately 10^6 cycles, there was a crossover in the curves for the notched and smooth specimens in saltwater, showing that the notched specimens had longer fatigue lives at the lower stress amplitudes. In air, the presence of notches decreased the fatigue strength of Alloy 7079-T6.

---

*See explanation in earlier section on ship steels (Chapter 3).
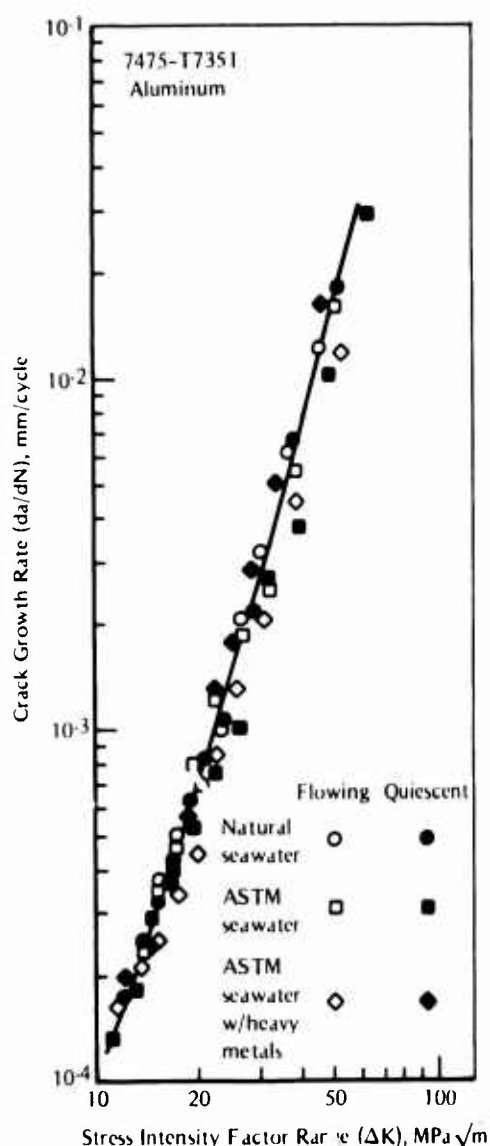
FIGURE 205. Crack Growth Rate for 7475-T7351 in Natural Seawater and in ASTM D 1141-75 Substitute Ocean Water, With and Without Heavy Metals, Under Flowing and Quiescent Conditions[126]
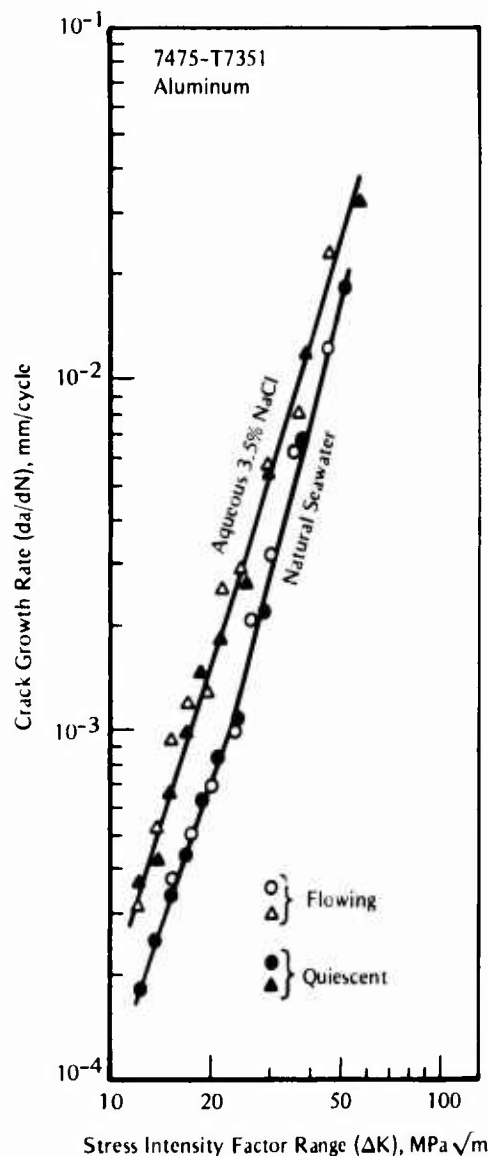
FIGURE 206. Crack Growth Rate for 7475-T7351 in Natural Seawater and in 3.5 Percent NaCl Solution Under Flowing and Quiescent Conditions[126]

Alloy 7005

Of the aluminum alloys included in Crooker's[217] study of corrosion-fatigue-crack growth, Alloy 7005-T63 exhibited the highest degree of sensitivity to 3.5 percent NaCl solution. The other aluminum alloys included in this study were: 2219-T87, 5456-H321, and 6061-T651 (discussed previously). The results of tests conducted on single-edge-notched specimens of Alloy 7005 cycled at 0.1 Hz in ambient room air and in 3.5 percent NaCl solution are shown in Figure 208. The amount of displacement of the saltwater data above the baseline air data was the largest observed for any of the aluminum alloys studied. Alloy 7005-T63 was the only alloy found to be sensitive to saltwater stress-corrosion cracking.
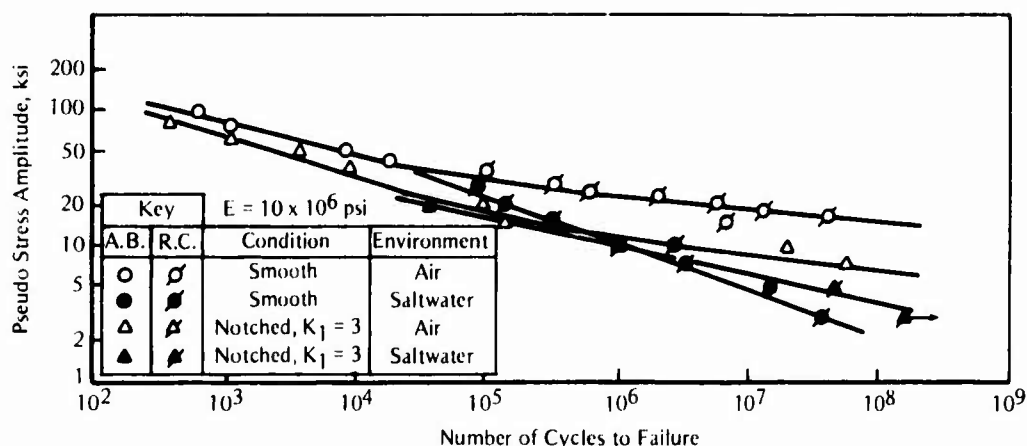
FIGURE 207. Corrosion Fatigue Strength for Alloy 7079–T6[151]

R.C. = rotating cantilever; high–cycle testing
A.B. = Low–cycle testing.

Alloy X166

The corrosion-fatigue resistance of an experimental Al-Zn-Cu alloy, X166, in a salt-fog environment was evaluated by Gunn and Bullett.[242] Dogbone-shaped specimens with a 0.098-in. (2.5-mm) hole in the center of the gage area were tested in fluctuating tension, R = 0.1, at 130 Hz in a spray of 3.5 percent NaCl solution. High-strength X166 was aged for 6 hours at 338 F (170 C) for a T7651 temper, and low-strength X166 was aged for 10 hours at the same temperature for a T73651 temper. Results for a high-strength plate specimen show a reduction of approximately 60 percent in fatigue strength [from 23.82 ksi (162 MPa) to 8.53 ksi (58 MPa)] at 2×10^7 cycles in the fog spray compared with that in laboratory air. For a low-strength X166 plate specimen under the same conditions, the reduction in fatigue strength was 40 percent, or from 19.49 ksi (132.5 MPa) to 11.40 ksi (77.5 MPa).

Alloy 7175

The effect of 30 g/l NaCl solution on the crack-tip opening of Alloy 7175-T651 specimens was studied by Clerivet and Bathias.[248] Compact-tension specimens were tested at 0.2 Hz to determine crack growth rate as a function of maximum crack-opening-displacement. The results are presented in Figure 209. As can be seen in the figure, for the same displacement, the crack growth rate in the salt solution is 3 to 4 times higher than that in air.
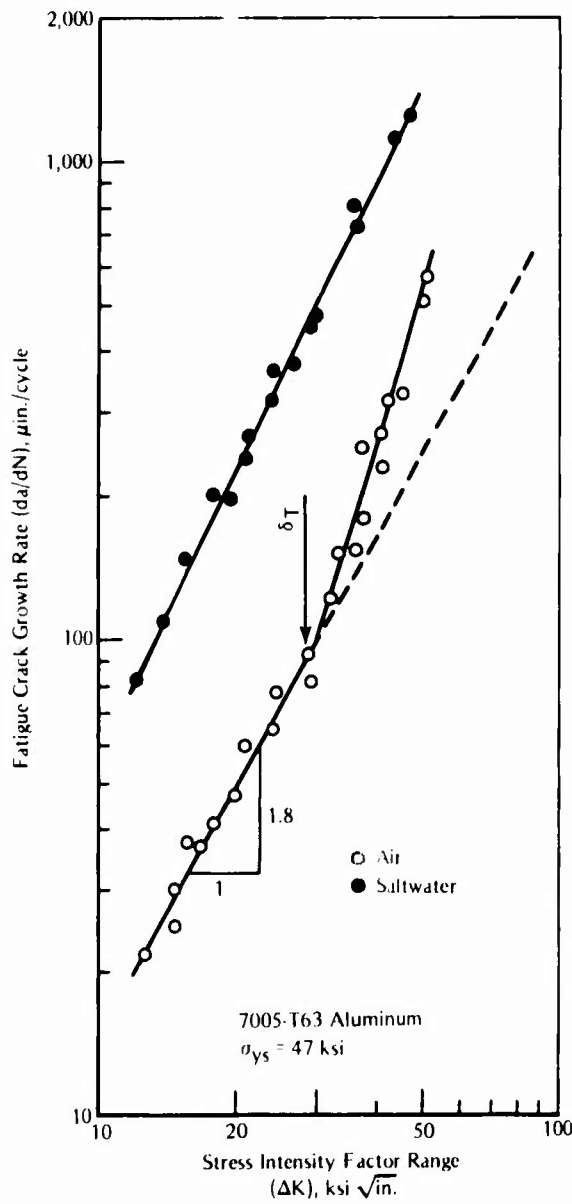
FIGURE 208. Corrosion-Fatigue-Crack Growth Behavior for Alloy 7005-T63 in Air and in Saltwater[217]
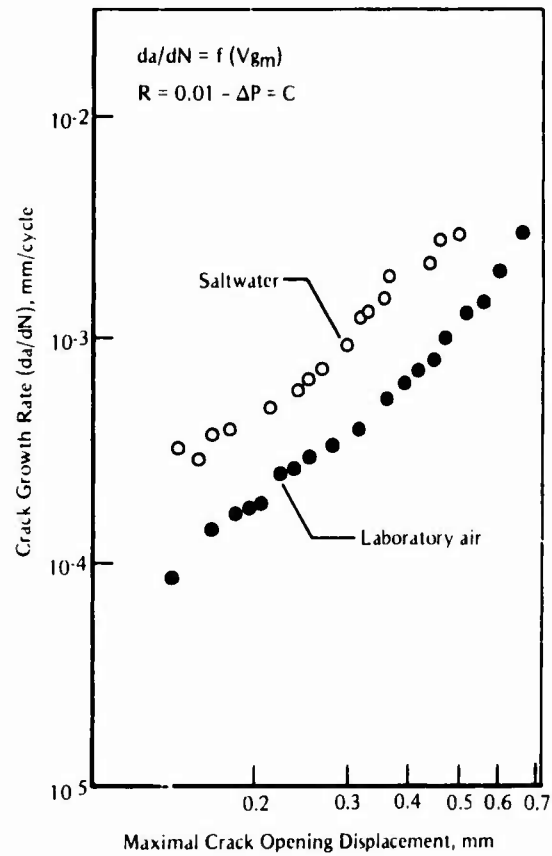
FIGURE 209. Fatigue-Crack Growth Rate as a Function of Crack Opening Displacement[248]

CHAPTER 8
CORROSION-FATIGUE DATA FOR TITANIUM ALLOYS

The corrosion-fatigue data for titanium alloys are reviewed in this section. The alloys covered and the corresponding reference numbers of the articles in which the data appeared are listed in Table 37. The corrosion-fatigue data for titanium alloys are summarized in Table 38. The alloy and types of corrosion-fatigue data are described along with the mechanical properties, types of specimen loading conditions, and environment. Titanium alloys have a high strength-to-weight ratio and excellent corrosion resistance so they are considered for many critical aircraft and marine structure applications.

Ti-6Al-4V

Ti-6Al-4V is the most widely used structural titanium alloy. Changes in fatigue-cracking resistance often can be altered through variations in heat treatments and microstructures.

TABLE 37. Titanium Alloys Reviewed and the References in Which Data Appeared

Alloy	References
Ti-6Al-4V	132, 151, 209, 215, 240, 245, 249, 250-253
Ti-6Al-6V-2Sn	208, 249, 254, 255
Ti-8Al-1Mo-1V	249, 256-258
Ti-6Al-2Cb-1Ta-0.8Mo	17, 132, 259
Ti-7Al-2.5Mo	132, 209
Ti-4Al-3Mo-1V	249
Ti-8Al-2Cb-1Ta	240
Ti-8Al	260
Ti-4Al	261
Ti-6.5Al-3.8Sn-2.5V-2.5Zr	261
Ti-6Al-4V carbon-epoxy laminate	262

201

TABLE 38. Summary of Corrosion Fatigue Data for Titanium Alloys in Seawater and Saltwater

Alloy	Condition[a]	Mechanical Strength, ks (MPa)		Type of Specimen	Frequency, Hz	Environment	Type of Loading	Types of Data[a]	References
		Ultimate	Yield						
Ti-6Al-4V (carbon contaminant)				Flat center notched	Variable	Waterspray with 0.3% NaCl in solution	Axial	Crack growth rates	262
Ti-6Al-4V (ELI)	Rolled and mill annealed	136 (938)	126 (869)	Smooth tapered cylindrical V-notch cylindrical	24, 2	Severn[b] River water	Rotating cantilever, completely reversed		151
Ti-6Al-4V (0.08 O₂) 8	Rolled and mill annealed	126 (869)	108 (744)	Smooth flat flexure V-notch, cylindrical	0.004-0.01	Severn[b] River water	Rotating cantilever, completely reversed	Bar graph summaries of the fatigue strength. Broadline spectrum S-N curves from 10³ to 10⁶ cycles	151
Ti-6Al-2Cb-1Ta-0.8 Mo	As rolled	117 (806.7)	96 (661.9)	Smooth tapered cylindrical cylindrical V-notch		Severn[b] River water	Rotating cantilever, fully reversed	Fracture surfaces	151
Ti-7Al-2.5 Mo	Annealed	150 (1034)	125 (850)	Smooth flat flexure cylindrical V-notch		Severn[b] River water	Rotating cantilever, fully reversed		151
Ti-8Al-1Mo-1V	Mill annealed		138 (951,51)	Center-notched sheet	0.05, 0.5, 2	3.5% NaCl solution	Axial, R=0	Crack growth rate; fractographic studies	265
Ti-8Al	Solution treated	91-93 (627-641)	88-91 (606.8-627)	Single-edge-notched sheet Smooth sheet	20-30 30	3.0% NaCl solution	Fluctuating tension, R=0	Fractographic	260
Ti-8Al	Aged	96-100 (662-689)	96-97 (662-677.7)	Smooth sheet	30	3.0% NaCl solution	Fluctuating tension, R=0	Fractographic	260
Ti-6Al-2Cb-1Ta-0.5 Mo		126 (869)	115 (793)	Single edge-notch cantilever	0.17	Flowing seawater	Cantilever	FCGR vs ΔK at negative imposed potentials of -800 and -1050 mV SCE	17
Ti-6Al-4V BA	Beta annealed	121-152 (834-1048)	108-146 (745-1007)	Double cantilever beam	0.1, 1	3.5% NaCl solution, 72,175 F	Cantilever	FCGR vs ΔK	245
Ti-6Al-4V RA	Recrystallized, annealed	128-155 (882.5-1068.7)	114-155 (779-1068)	Double cantilever beam	0.1, 1	3.5% NaCl solution, 72,175 F		FCGR vs ΔK	245
Ti-6Al-4V BA	Beta annealed	121-152 (834-1048)	108-146 (745-1007)	Tapered double cantilever	1	3.5% NaCl solution, 72 F		FCGR vs ΔK	245
Ti-6Al-4V RA	Recrystallized, annealed	128-155 (882.5-1068.7)	114-145 (779-1007)	Tapered double cantilever	1	3.5% NaCl solution, 72 F		FCGR vs ΔK	245
Ti-6Al-4V BA	Beta annealed	121-152 (834-1048)	108-146 (745-1007)	Surface flawed	1	3.5% NaCl solution, 72 F		FCGR vs ΔK	245
Ti-6Al-4V RA	Recrystallized, annealed	128-155 (882-1068.7)	113-146 (779-1007)	Surface flaw	1	3.5% NaCl solution, 72 F		FCGR vs ΔK	245
Ti-6Al-6V-2Sn	Mill annealed	169 (1165)	160 (1103.2)	Single-edge notched	50, 10, 2, 0.1, 5	0.6 M NaCl solution		FCGR vs ΔK ⎱ Effect of bulk solution ⎰ pH discussed	250
Ti-6Al-4V	Mill annealed	144 (993)	143 (985.99)	Single-edge notched	1, 5, 10	0.6 M NaCl solution	Cantilever, R=0	FCGR vs ΔK	250
Ti-6Al-2Cb-1Ta-0.8 Mo		121 (834)	107 (738)	Single-edge notched with side groove	0.16	Natural seawater	Cantilever, R=0	FCGR vs ΔK, E_corr = -300 mV SCE	259
Ti-6Al-2Cb-1Ta-0.8 Mo		126 (868)	115 (793)	Single-edge notched with side groove	0.16	Natural seawater	Cantilever, R=0	Effects of imposed cathodic potentials of -800 and -1050 mV SCE	259
Ti-8Al-1Mo-1V	Duplex annealed			Center-cracked panels	2	3.5% NaCl solution	Cantilever, R=0	Crack length vs N	239
Ti-CP-5A	Annealed			Center-cracked panels	2	3.5% NaCl solution	Cantilever, R=0	Crack length vs N	239
Iml 679				Center-cracked panels	2	3.5% NaCl solution	Cantilever, R=0	Crack length vs N, FCGR vs ΔK	239
Ti-6Al-6V-2Sn	Beta annealed			Center-cracked panels	2	3.5% NaCl solution	Cantilever, R=0	Crack length vs N, FCGR vs ΔK	239
Ti-6Al-4V	Duplex annealed			Center-cracked panels	2	3.5% NaCl solution	Cantilever, R=0	Crack length vs N, FCGR vs ΔK	239
Ti-4Al-3Mo-1V				Center-cracked panels	2	3.5% NaCl solution	Cantilever, R=0	Crack length vs N, FCGR vs ΔK	239

TABLE 38. (Continued)

| Alloy | Condition[a] | Mechanical Strength, ksi (MPa) | | Type of Specimen | Frequency, Hz | Environment | Type of Loading | Types of Data[a] | References |
		Ultimate	Yield						
Ti-8Al-1V	Actual turbine blades	Variable	Variable	Compact tension	0.5	3% NaCl solution	Axial, R=0.1	Displacement load vs normalized crack length	251
Ti-8Al-1V	Actual turbine blades	Variable	Variable	Single-edge notch	0.5	3% NaCl solution	Axial, R=0.1	FCGR vs ΔK	251
Ti-6Al-2V-2S	Solution treated and aged			Wedge-open load	0.1, 1, 10	3% NaCl solution	Axial R=0.1	FCGR vs ΔK	251
Ti-6Al-2V-2S	Solution treated and aged			Center-cracked through	0.1, 1, 10	3% NaCl solution	Axial, R=0.1 and 0.5	FCGR vs ΔK	251
Ti-6Al-2V-2S	Solution treated and aged			Part-through crack	0.1, 1, 10	3% NaCl solution	Axial, R=0.1 and 0.5	FCGR vs ΔK	251
Ti-6Al-4V welds	Solution treated and aged	164 (1131)	144 (993)	Tapered box beams	3.3	Seven(c) River water	Cantilever, spectrum loading	Fatigue, stress spectrum	252
Ti-6Al-4V-Best	Recrystallized, annealed		120 (827)	Tapered box beams	3.3	Seven(c) River water	Cantilever, spectrum loading	S-N curve from 10⁴ to 10⁸ cycles	251
Ti-6Al-4V	Recrystallized, annealed	165 (1131 910)	145 (1000)	Wedge-open load	0.1, 1, 10	3.5% NaCl solution	Axial, R=0	FCGR vs ΔK	251
Ti-6Al-4V	Recrystallized, annealed	115 (1075)		Center-cracked through	0.1, 10	3.5% NaCl solution	Axial	FCGR vs ΔK	251
Ti-6Al-4V	Recrystallized, annealed			Part-through crack	0.1, 10	3.5% NaCl solution	Axial	FCGR vs ΔK, fractographic studies	251
Ti-6Al-4V	Annealed	108 (745)	98 (677)	Compact tension	20	3.5% NaCl solution	Axial	S-N curves from 1 to 10⁴ cycles	252
Ti-4Al	Annealed	131 (902)	122 (841)	Cylindrical, smooth	0.02?	3.0% NaCl solution	Rotary bending	S-N curves from 1 to 10⁴ cycles	261
Ti-6.5Al-3.85Sn-2.5V-2.6Zr	Annealed	108 (745)	98 (677)	Cylindrical, smooth	0.02?	3.0% NaCl solution	Rotary bending	S-N curves from 1 to 10⁴ cycles	261
Ti-4Al	Annealed	131 (902)	122 (841)	Cylindrical, notched	0.02?	3.0% NaCl solution	Rotary bending	S-N curves from 1 to 10⁴ cycles	261
Ti-6.5Al-3.85Sn-2.5V-2.6Zr	Beta annealed			Cylindrical, notched	0.02?	3.0% NaCl solution	Rotary bending	S-N curves from 1 to 10⁴ cycles	261
Ti-8Al-1Mo-1V	Beta annealed			Compact tension	0.1, 5	3.5% NaCl solution	Axial, R=0.1	FCGR vs ΔK	255
Ti-6Al-4V				Smooth	1	Hanks solution, 98.6 F	Torsion, fully reversed	Open-circuit potential vs time	216
Ti-6Al-4V				Welded cantilever beam	24.2	Seawater	Undirectional bending, R=0	(Comparison with other hydrofoil materials	240
Ti-8Al-2Cb-1Ta				Welded and unwelded cantilever beams	24.2	Seawater	Undirectional bending, R=0		240
Ti-6Al-4V	Mill annealed			Surface-notched plate	0.083	3.5% NaCl solution	Cantilever, fully reversed	FCGR vs total strain	204
Ti-6Al-6V-2Sn-1Cu-.5Fe	Mill annealed			Surface-notched plate	0.083	3.5% NaCl solution	Cantilever, fully reversed	FCGR vs total strain	204
Ti-6Al-4V-1Mo	Mill annealed			Surface-notched plate	0.083	3.5% NaCl solution	Cantilever, fully reversed	FCGR vs total strain	204
Ti-7Al-2.5Mo	Mill annealed			Surface-notched plate	0.083	3.5% NaCl solution	Cantilever, fully reversed	FCGR vs total strain	204

(a) FCGR = Fatigue crack growth rate
   ΔK = Stress intensity factor range
   E_corr = Natural corrosion potential
   N = Number of cycles to failure
   S = Stress.

(b) Brackish estuary water containing one-sixth to one-third the salinity of natural seawater, depending on the season and the tide.

(c) Fifteen heat treatments were analyzed. Mechanical properties for each microstructure are given in the reference paper.

Base Metal Data

In 3.5 percent NaCl solution, mill-annealed and beta-STA-1250 Ti-6Al-4V material have shown approximately the same crack growth rates at a stress intensity factor range (ΔK) of 45 to 70 ksi $\sqrt{\text{in}}$., whereas a duplex-annealed Ti-6Al-4V exhibited lower crack growth rates at similar Δk levels.[249] This behavior is shown in Figure 210 together with the results for Ti-4Al-3Mo-1V. The effect of aging temperature on corrosion-fatigue-crack growth rate of Ti-6Al-4V materials is shown in Figure 211. These data show lowere fatigue-crack growth rates for beta-STA-1250 than for beta-STA-1000 in room air, distilled water, and 3.5 percent NaCl solution.

The corrosion-fatigue properties of Ti-6Al-4V in the mill-annealed condition and in the solution-treated (900 C) and water-quenched condition were compared by Iman et al.[253] The microstructure of the mill-annealed material consisted mainly of α-Ti with a small amount of intergranular β-Ti. The heat-treated material had a microstructure containing large α-Ti grains and martensitic areas of α'-Ti and β-Ti which surrounded areas of α-Ti. The additional heat treating and quenching of mill-annealed Ti-6Al-4V improved the corrosion-fatigue behavior in a saline environment. The mill-annealed material had a corrosion-fatigue life about one-half (2.9 X 10^4 cycles compared with 5.3 X 10^4 cycles) that of the solution-treated and quenched material. The corrosion-fatigue life data for each heat treatment are summarized in Table 39.

These authors[253] also monitored the potential during their corrosion-fatigue tests (reversible torsion) of Ti-6Al-4V in a saline solution [Hanks' solution, pH = 7.4 at 98.6 F (37 C)] to gain information relating the formation of protective films on the metal in solution with the cracking of the oxide film and the metal specimen. The open-circuit potential versus time curves for this alloy in the mill-annealed condition and in a solution-treated [1652 F (900 C)], water-quenched condition are shown in Figure 212. When the fatigue tests began, the electrode potential became more negative. The magnitude of this drop was dependent upon the applied load of the test. This more negative potential indicated dissolution of the film or other film breakdown which led to cracking. As the test progressed, some of the cracks became passivated with an oxide film. This repassivation of some of the cracks under the environmental and mechanical conditions accounted for the positive rise in the potential time curve.[253]

Smooth and notched specimens of Ti-6Al-4V were subjected to low- and high-cycle fatigue testing in air and Severn River water.[151] Fatigue-life curves, plotted in terms of pseudo stress amplitude*, are shown in Figure 213.
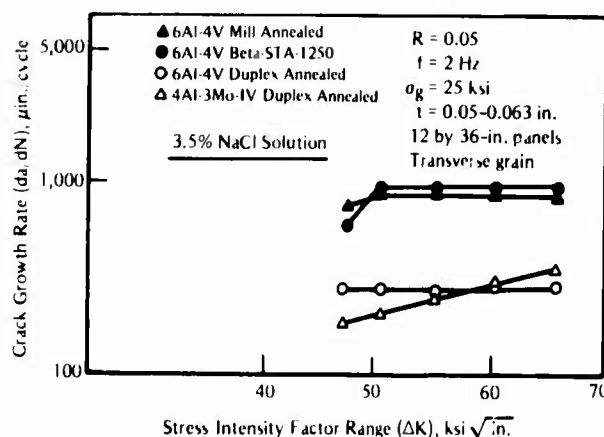
FIGURE 210. Corrosion-Fatigue-Crack Growth Rate for Ti-6Al-4V and Ti-4Al-3Mo-1R in 3.5 Percent NaCl Solution[249]

*Psuedo stress amplitude, as explained in the section on ship steels (Chapter 3), is directly proportional to strain range.

FIGURE 211. Corrosion-Fatigue-Crack Growth Behavior of Ti-6Al-4V
Beta STA-1000 and Beta STA-1250[249]

TABLE 39. Corrosion-Fatigue Life of Ti-6Al-4V
for a Shear Strain of ~0.018[253]

Heat Treatment	Fatigue Life, 10^4 cycles to failure	
	Average	Minimum
Mill Annealed		
1300 (704 C)	2.3283[a]	1.7130
1400 (760 C)	3.5476[a]	3.2463
Total	2.938[b]	1.7130
Solution Treated		
1652 F (900 C)	5.2504[b]	4.229

(a) Two specimens tested.
(b) Four specimens tested.

FIGURE 212. Open Circuit Potential Versus Time Curves for Ti-6Al-4V Specimens During Corrosion-Fatigue Testing (Reversible Torsion) in Hanks' Solution (pH = 7.4) at 98.6 F[253]

The presence of notches decreased the fatigue strength over almost the entire cyclic range, but the notch effect was small at $\leq 5 \times 10^3$ cycles to failure. The saltwater environment did not decrease the fatigue lives or fatigue strengths for either the smooth or notched specimens.

Results of corrosion-fatigue-crack-growth tests by Crooker and Lange[254] (at a frequency of 0.083 Hz) on notched specimens of Ti-6Al-4V, Ti-6Al-6V-2Sn-1Cu-0.5Fe, Ti-6Al-3V-1Mo, and Ti-7Al-2.5Mo are shown in Figure 214 along with scatterband limits from air-environment tests for reference. These results showed no degradation in fatigue-crack-growth resistance in 3.5 percent NaCl solution as compared with results of tests in air. Crooker and Lange noted that the test conditions of sinusoidal loading patterns and laboratory salt solution are possibly not as severe as many actual loading service situations.

Dawson and Pelloux[250] studied the general form of the log da/dN versus log ΔK behavior of many titanium alloys in aqueous halide solutions. These results were compared with those in air and in other inert environments. The effect of frequency is shown schematically in Figure
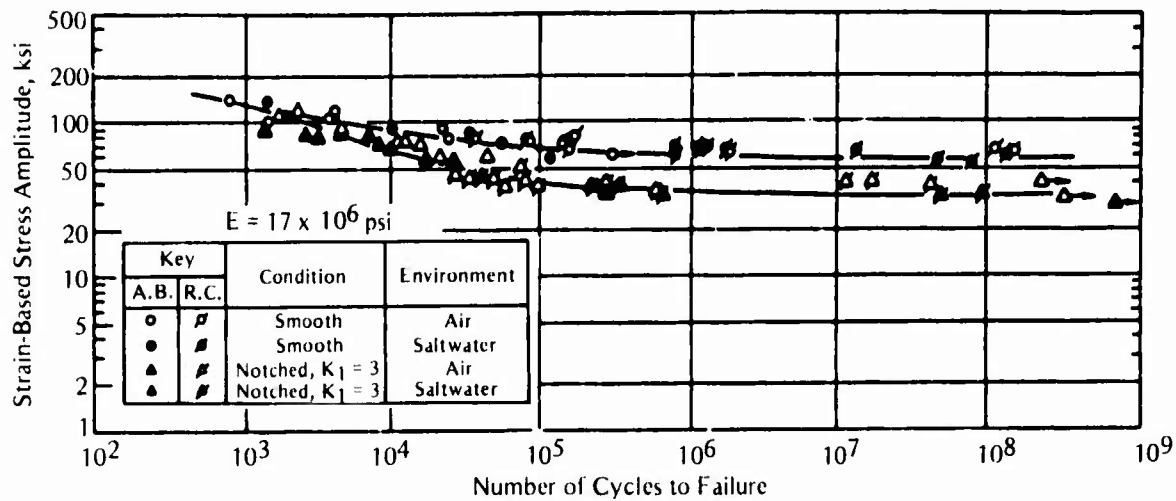
FIGURE 213. Corrosion-Fatigue Strength of Smooth and Notched
Ti-6Al-4V Alloy Specimens in Air and Saltwater[151]
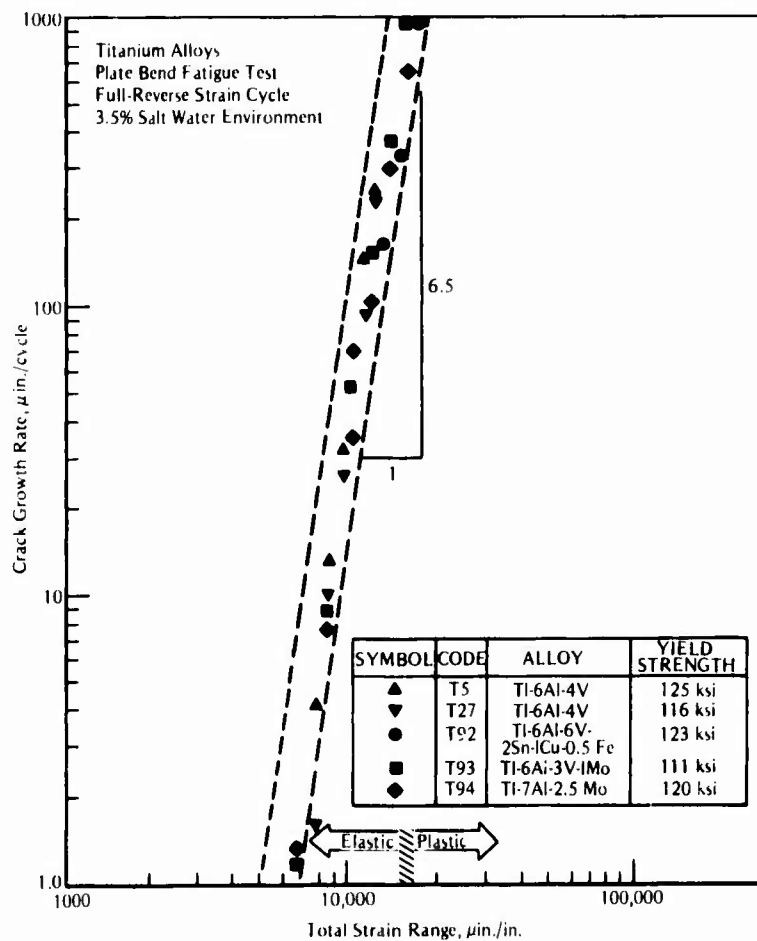
FIGURE 214. Fatigue Crack Growth Rate Versus Total Strain Range for
Titanium Alloys in 3.5 Percent Saltwater Environment[209]

215. The inert-environment fatigue behavior was frequency independent for titanium alloys in air, argon, vacuum, and an aqueous solution containing a corrosion inhibitor (Na_2SO_4). The effect of frequency on the corrosion-fatigue-crack growth of mill-annealed Ti-6Al-4V in aqueous 0.6 M NaCl solution is shown in Figure 216. The salt-solution curves were unique for titanium alloys in aqueous solutions containing halide ions, Cl^- and Br^-. The curves show frequency dependence (da/dN increasing with decreasing frequency), at high stress-intensity factors (ΔK) and a reverse frequency dependence at low ΔK levels. At frequencies of less than 10 Hz, an abrupt increase in the fatigue-crack growth rates with increasing ΔK marked the apparent onset of cyclic stress corrosion cracking (SCC). This particular ΔK value where a rapid increase in da/dN was observed is often referred to ΔK_{scc}, and many times its associated K_{max} level corresponds to K_{Iscc} of that material. This frequency effect is also shown for recrystallized annealed Ti-6Al-4V in 3.5 percent NaCl solution[251] in Figure 217. From these figures, it can be seen that the two alloys exhibited similar frequency effect behavior. That is, for both alloys, as the frequency was lowered from 10 Hz, the crack growth rate increased. The crossing over of the higher frequency curves by the lowest frequency curve at mid-stress-intensity range is very pronounced for both materials.

Crooker and Lange[263] studied accelerated crack-growth behavior for Ti-6Al-4V when exposed to a marine environment. Results of tests at a frequency of 0.083 Hz show that Ti-6Al-4V is insensitive to saltwater up to a ΔK of approximately 50 ksi $\sqrt{in.}$, but at higher ΔK's crack growth rates accelerated rapidly as K_{Iscc} was approached (see Figure 218). Because K_{Iscc} is an approximate stress-intensity level for the onset of SCC under static conditions, K_{Iscc} for Ti-6Al-4V in saltwater at this frequency can also be a limiting factor for corrosion fatigue.

Summer and Creagen[252] investigated the effect of dissolved hydrogen on the corrosion-fatigue-crack-growth behavior of Ti-6Al-4V. The results for furnace-cooled material containing 20 ppm hydrogen and helium-cooled material containing 8 ppm hydrogen are shown in Figures 219 and 220. The difference in hydrogen content of the two materials had no influence on the corrosion-fatigue resistance of Ti-6Al-4V in either saltwater or seawater.

FIGURE 215. Schematic Showing the Reversal of Frequency Effect on Titanium Alloys in an Aqueous NaCl Environment Above and Below ΔK_{SCC}[250]
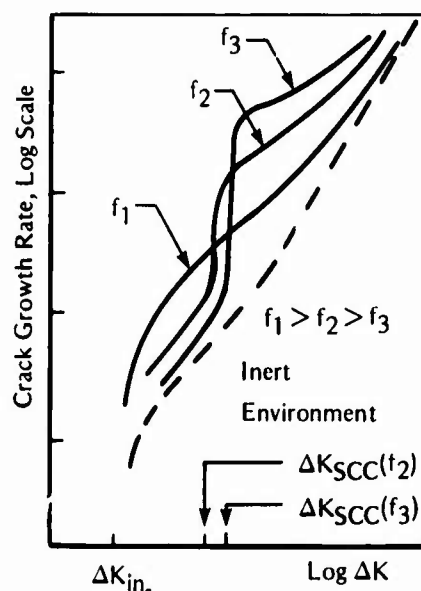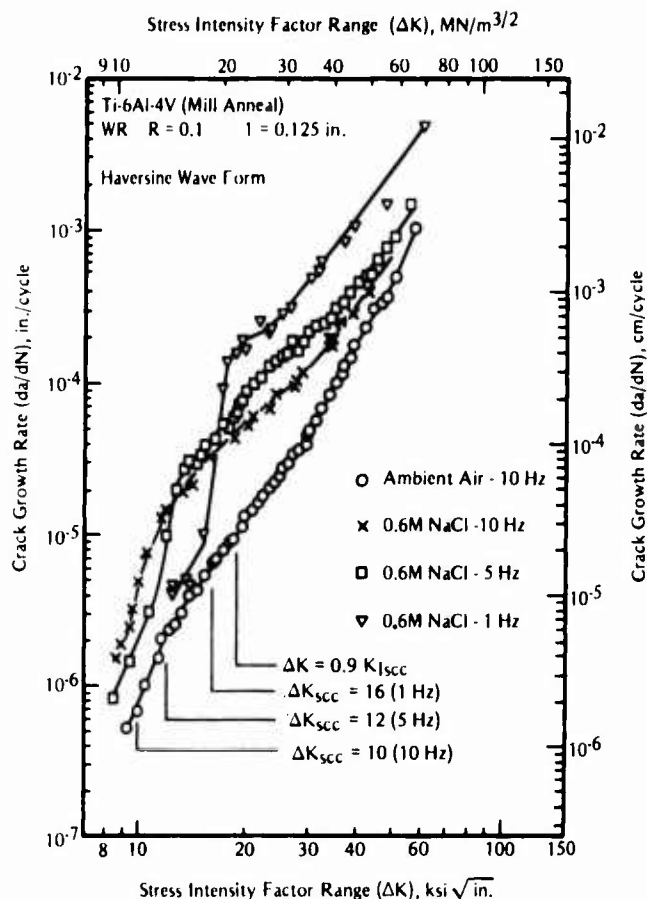
FIGURE 216. Effect of Frequency on Corrosion-Fatigue-Crack Growth Behavior of Ti-6 Al-4V in Aqueous 0.6 M NaCl[250]

Weldment Data

Piper et al[249] investigated the effects of 3.5 percent NaCl solution on the corrosion-fatigue resistance of welded Ti-6Al-4V panels. The results for fusion weldments of mill-annealed Ti-6Al-4V are shown in Figures 221 and 222. The welds were produced by the opposed-arc method and stress relieved at 1250 F for 30 minutes. The data showed that the welds did not decrease the resistance of the base metal to corrosion fatigue in 3.5 percent NaCl solution. However, in general, welding decreases the fatigue strength of titanium alloys if the appropriate heat treatment or stress relief is not employed.

In actual failures, cast propellers of Ti-6Al-4V have failed by corrosion fatigue or stress corrosion cracking, or a combination of the two, at weld repairs. Macco[132] compared the corrosion-fatigue resistance of butt welds and tee welds of Ti-6Al-4V. Fatigue-life curves for these two types of Ti-6Al-4V alloys are shown in Figure 223. The author concluded that differences in performance due to the effects of welding processes were not as significant as the detrimental effect of seawater on the reduction of fatigue strength. Constant-life diagrams comparing these titanium welds with welds of other high-strength materials used in marine structures are shown in Figures 224 and 225. These constant-life diagrams provide a composite
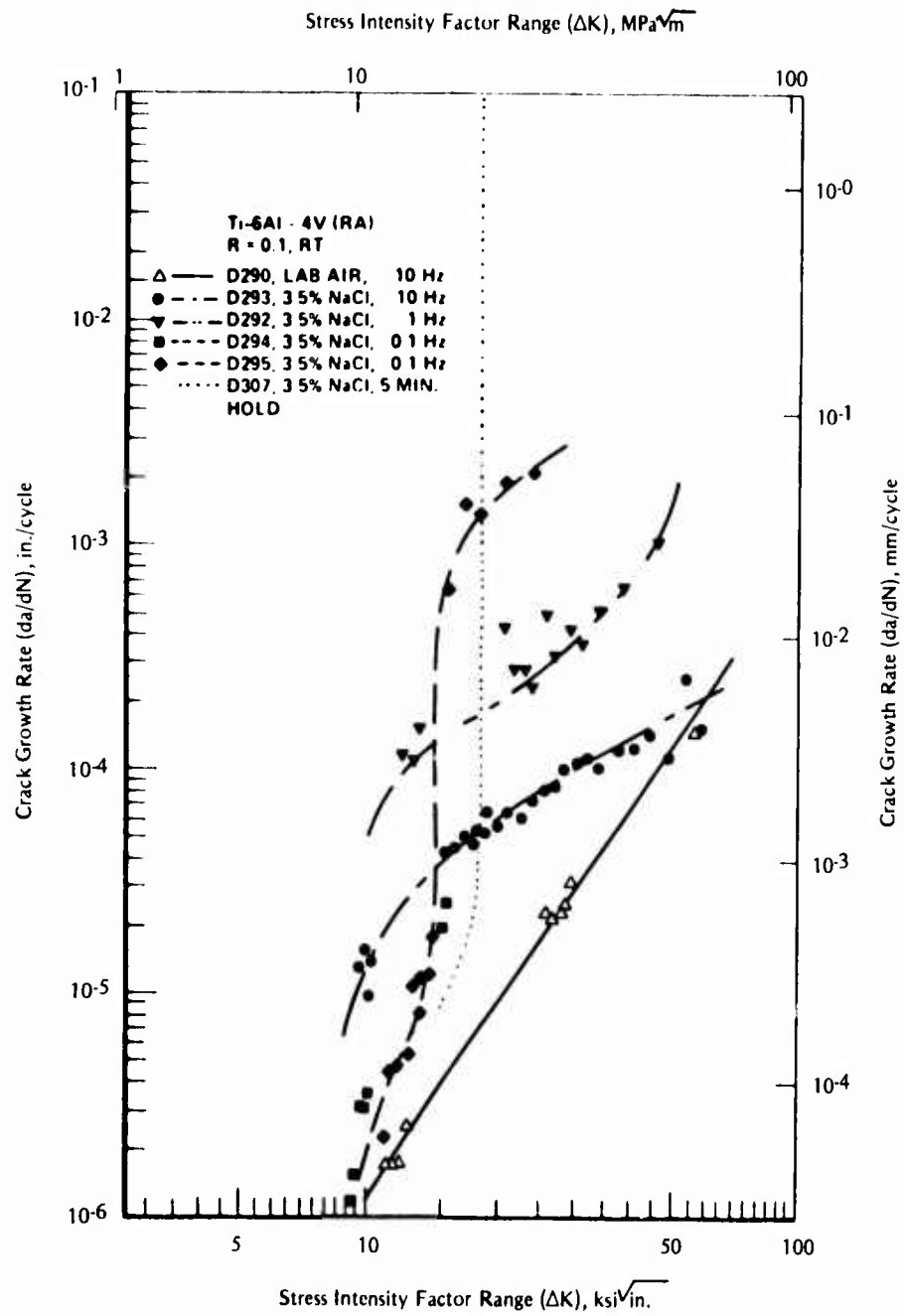
FIGURE 217. Frequency Screening Results for 3/8-in. (9.5-mm) Ti-6Al-4V Specimens in 3.5 Percent NaCl[251]
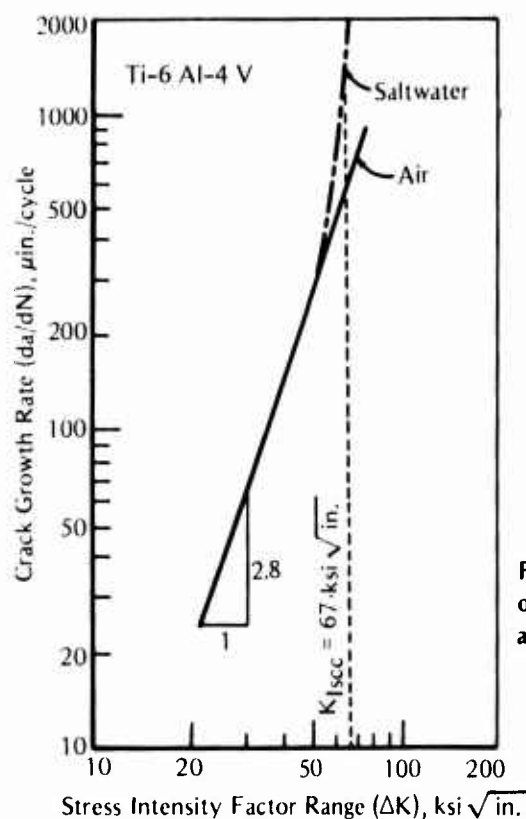
FIGURE 218. Crack Growth Rate as a Function of Stress Intensity for a Ti-6Al-4V Alloy in Air and in Saltwater [263]

representation of the fatigue properties for Ti-6Al-4V and other marine structure materials investigated. Notice that the titanium alloy had the highest corrosion-fatigue strength of the materials evaluated by Macco.

Ti-6Al-6V-2Sn

Crooker and Lange[254] found no effect of environment on fatigue-crack-growth rate for specimens of Ti-6Al-6V-2Sn tested in 3.5 percent NaCl solution at a frequency of 0.083 Hz. Their results for Ti-6Al-6V-2Sn are included in Figure 214 (presented earlier).

Piper et al[249] studied the effect of stress ratio (R) on the fatigue-crack-growth rate of Ti-6Al-6V-2Sn. Tests were performed on center-cracked panels at a frequency of 2 Hz. The authors found that a high mean stress level or R ratio and low cyclic stress amplitude produce higher fatigue-crack growth rates in 3.5 percent NaCl than in air. The crack length versus number of cycles to failure for Ti-6Al-6V-2Sn for R = 0.05 and 0.67 is shown in Figure 226. For both ratios, the crack growth rate was higher in 3.5 percent NaCl solution than in air, and the fatigue life was longer for the higher stress ratio.

Dawson and Pelloux[250] studied the effect of frequency on crack growth rates for Ti-6Al-6V-2Sn using SEN specimens in 0.6 M NaCl solution. Their results are shown in Figure 227. At low ΔK levels, the fatigue-crack growth rate decreased with decreasing frequency. At high ΔK levels, the fatigue crack growth rate increased with decreasing frequency. At the transition stress intensity range, ΔK_{scc}, which marked the onset of stress corrosion cracking (SCC) under cyclic loading, an increase in crack growth rate occurred. The magnitude of this increase was greater with decreasing frequency. This crossover type of frequency effect is unique to titanium alloys in aqueous solutions containing halide ions.
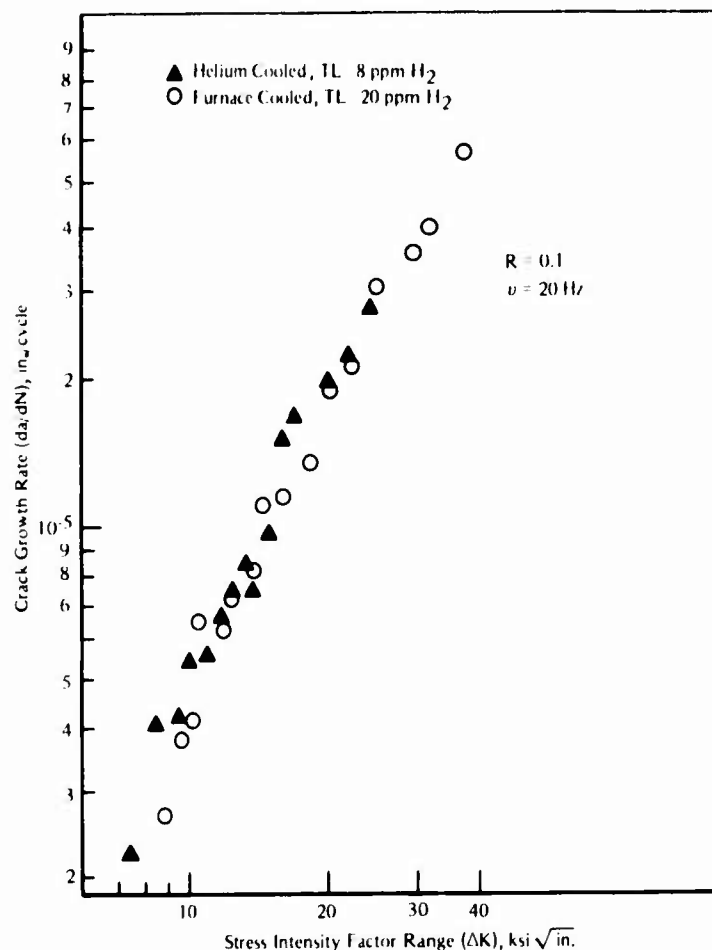
FIGURE 219. Effect of Dissolved Hydrogen on Corrosion-Fatigue-Crack Growth of Basal Transverse Texture Ti-6Al-4V E [252]

Krupp et al[255] evaluated the corrosion-fatigue properties of Ti-6Al-6V-2Sn in the solution-treated and aged condition. A frequency effect was found for this alloy. The general trend was increasing fatigue-crack growth rate with decreasing frequency. Aggressive environments such as 3.5 percent NaCl solution enhanced this frequency effect. This is the same corrosion-fatigue behavior described by Dawson and Pelloux[250] and shown earlier in the schematic log crack growth rate versus log stress intensity factor curves in Figure 215.

Ti-8Al-1Mo-1V

Cullen and Stonesifer[257] determined the fatigue-crack-growth rates of Ti-8Al-1Mo-1V at ambient temperatures in both room air and 3.5 percent NaCl solution for compact-tension specimens made from forged first-stage-turbine fan blades. The blades had been removed from service because of foreign-object damage. The specimens were cut from the blades in such a manner as to simulate the suspected in-service failure path and primary stress. The authors' results are shown in Figure 228. The crack growth rate versus stress intensity factor curves shown were derived by using a version of the tensile-ligament instability model for mathematically characterizing corrosion-fatigue-crack-growth behavior. For further details,
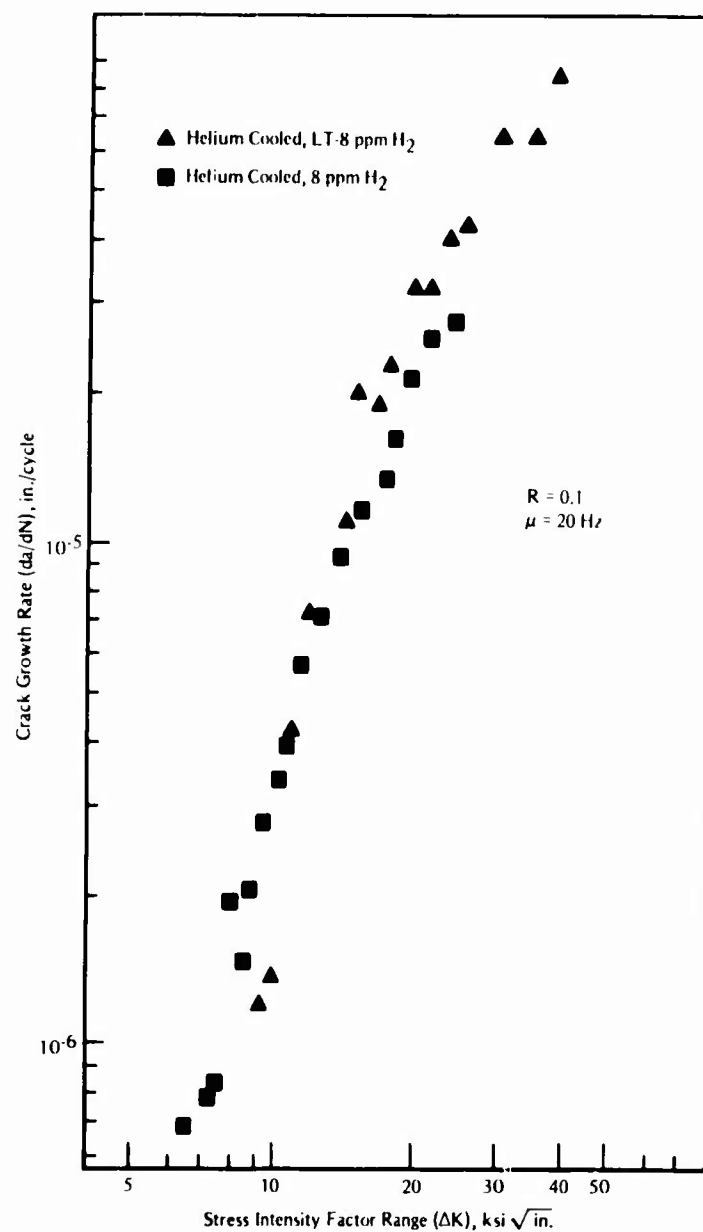
FIGURE 220. Effect of Dissolved Hydrogen on the Corrosion-Fatigue Crack Growth of Basal Transverse Textured Ti-6Al-4V in Seawater [252]
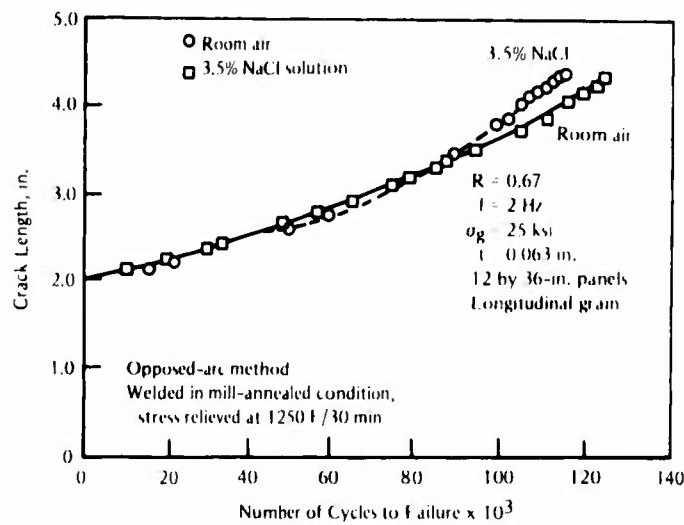
FIGURE 221. Corrosion–Fatigue–Crack Growth Behavior of Ti–6Al–4V Fusion Weldments[249]
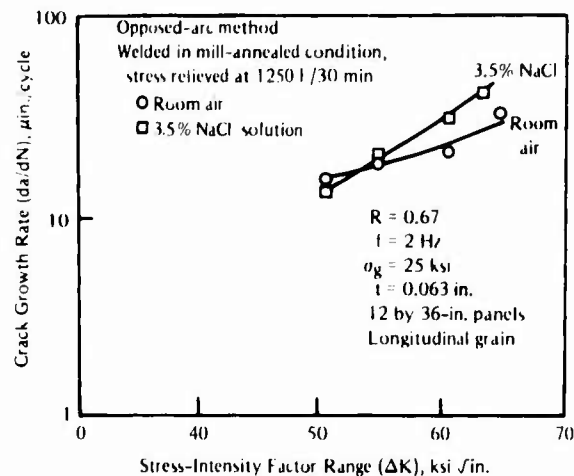
FIGURE 222. Corrosion-Fatigue-Crack Growth Rate in Ti-6Al-4V Fusion Weldments[249]

see the discussion of this model in Chapter 2, or refer to the work of Krafft et al.[33,264] Environment/lower frequency had little effect at low and high ΔK levels but caused a significant increase in crack growth rate at intermediate ΔK levels. The authors compared their data with results for conventionally rolled Ti-8Al-1Mo-1V material and concluded that the fatigue-crack growth rates for their forged specimens were nearly the same as those for the conventionally rolled specimens.

Yoder, Cooley, and Crooker[258,265] studied the fatigue-crack-growth behavior of Ti-8Al-1Mo-1V which had been microstructurally modified through various heat treatments. This commonly used duplex-annealed alloy was altered by 14 different heat treatments. Corrosion-fatigue tests were performed on a duplex-annealed Ti-8Al-1Mo-1V alloy and a beta-annealed
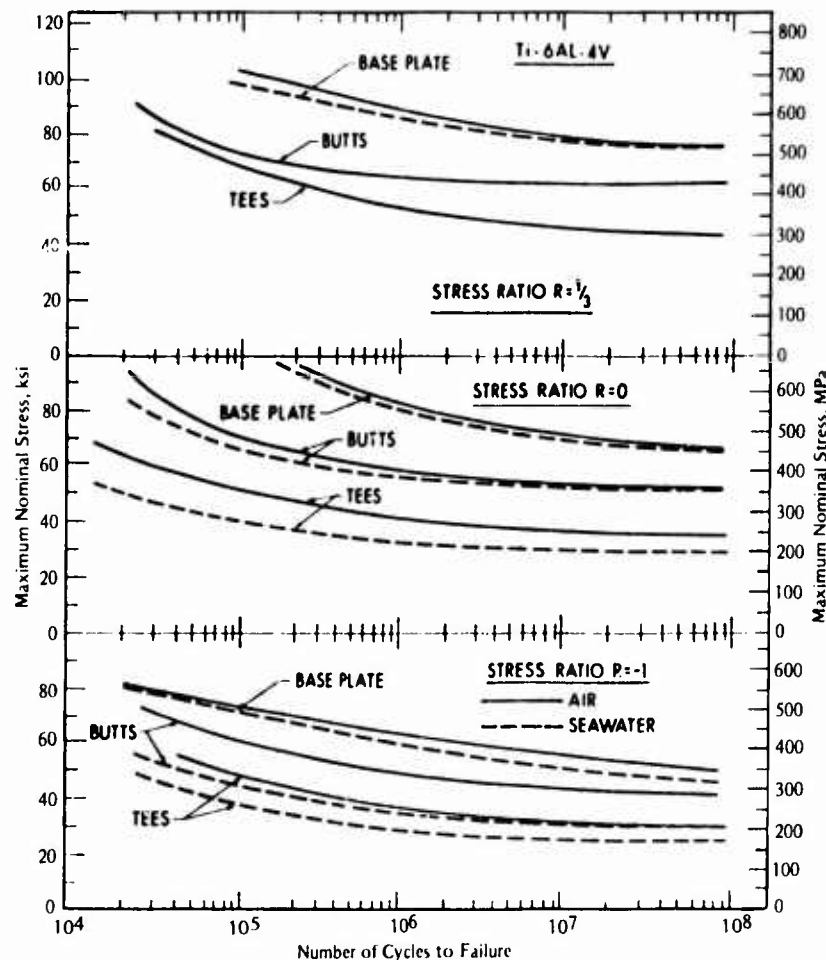
FIGURE 223. Fatigue-Life Curves for Ti-6Al-4V Weldments and Base Metal in Air and Seawater[132]

Ti-8Al-1Mo-1V alloy. The former alloy was selected because it is the one commonly used, and the latter alloy was chosen because it had good resistance to stress-corrosion-crack growth. Compact-type specimens of each material were tested in circulating 3.5 percent NaCl solution and in air. The results of these tests are shown in Figure 229. Growth rates for the beta-annealed material in 3.5 percent NaCl solution were an order of magnitude less than those for the duplex-annealed material in saltwater and were fourfold less than those for the duplex-annealed material in air. In both environments, resistance of the beta-annealed material with a Widmanstätten microstructure to corrosion-fatigue-crack growth was superior to that of the duplex-annealed alloy with an α/β duplex microstructure.

Meyn[256] studied the frequency and amplitude effects on the crack growth behavior in Ti-8Al-1Mo-1V, which exemplifies the group of high-strength alloys susceptible to stress corrosion cracking (SCC). A three-dimensional sketch of crack growth rate, stress intensity factor range, and frequency for Ti-8Al-1Mo-1V in a stress-corrosion-inducing environment such as 3.5 percent NaCl solution is shown in Figure 230. The curve for 30 Hz is considered the base-line curve and is representative of behavior not dependent on cyclic stress corrosion cracking. At 5 Hz, a small hump appeared in the curve for $\Delta K > K_{Iscc}$. This hump became larger and more dominant as the frequency was lowered. At frequencies less than 0.01 Hz, the hump
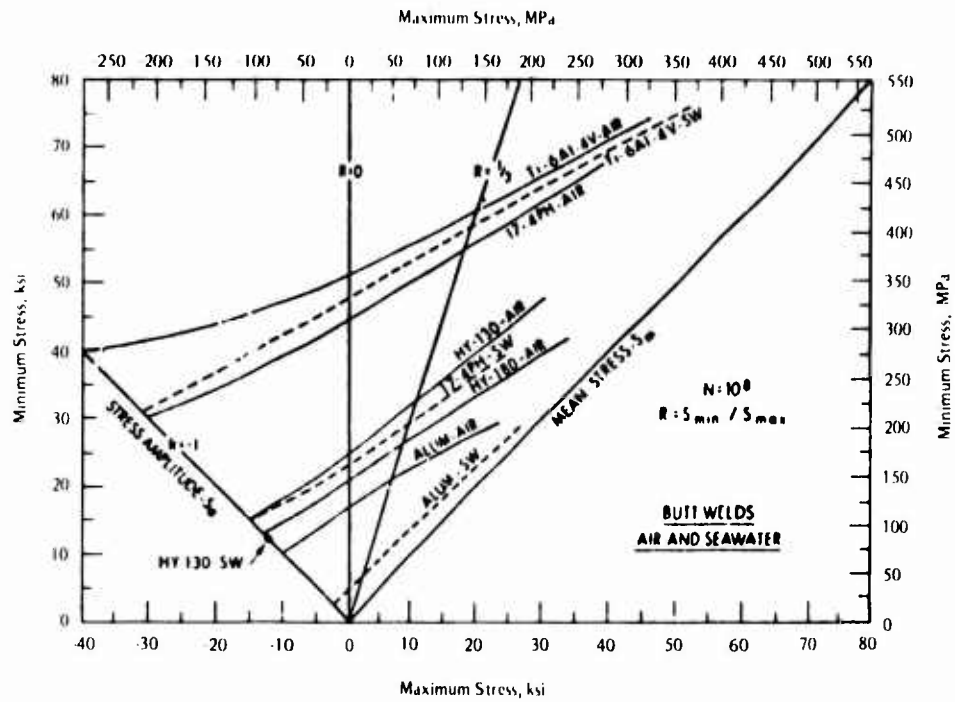
FIGURE 224. Constant-Life Diagrams for Butt-Welded Krouse Specimens[132]
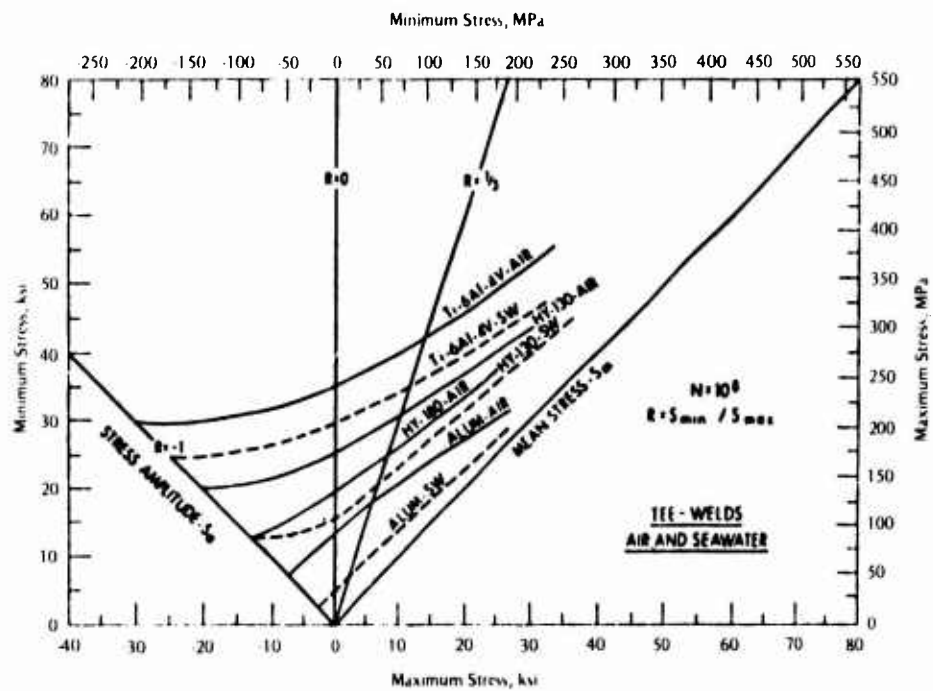
FIGURE 225. Constant-Life Diagrams for Tee-Welded Krouse Specimens[132]
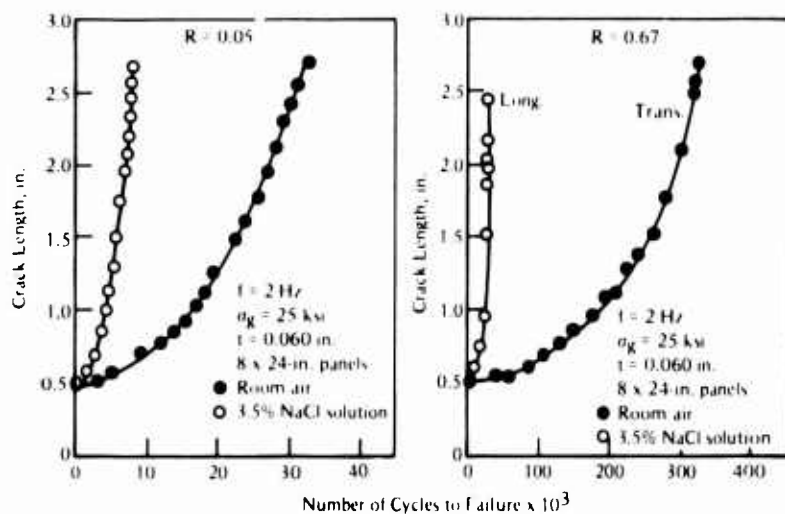
FIGURE 226. Corrosion-Fatigue-Crack Growth in Beta-Annealed Ti-6Al-6V-2Sn[249]

a. At 0.5 and 10 Hz

b. At 0.1 to 50 Hz
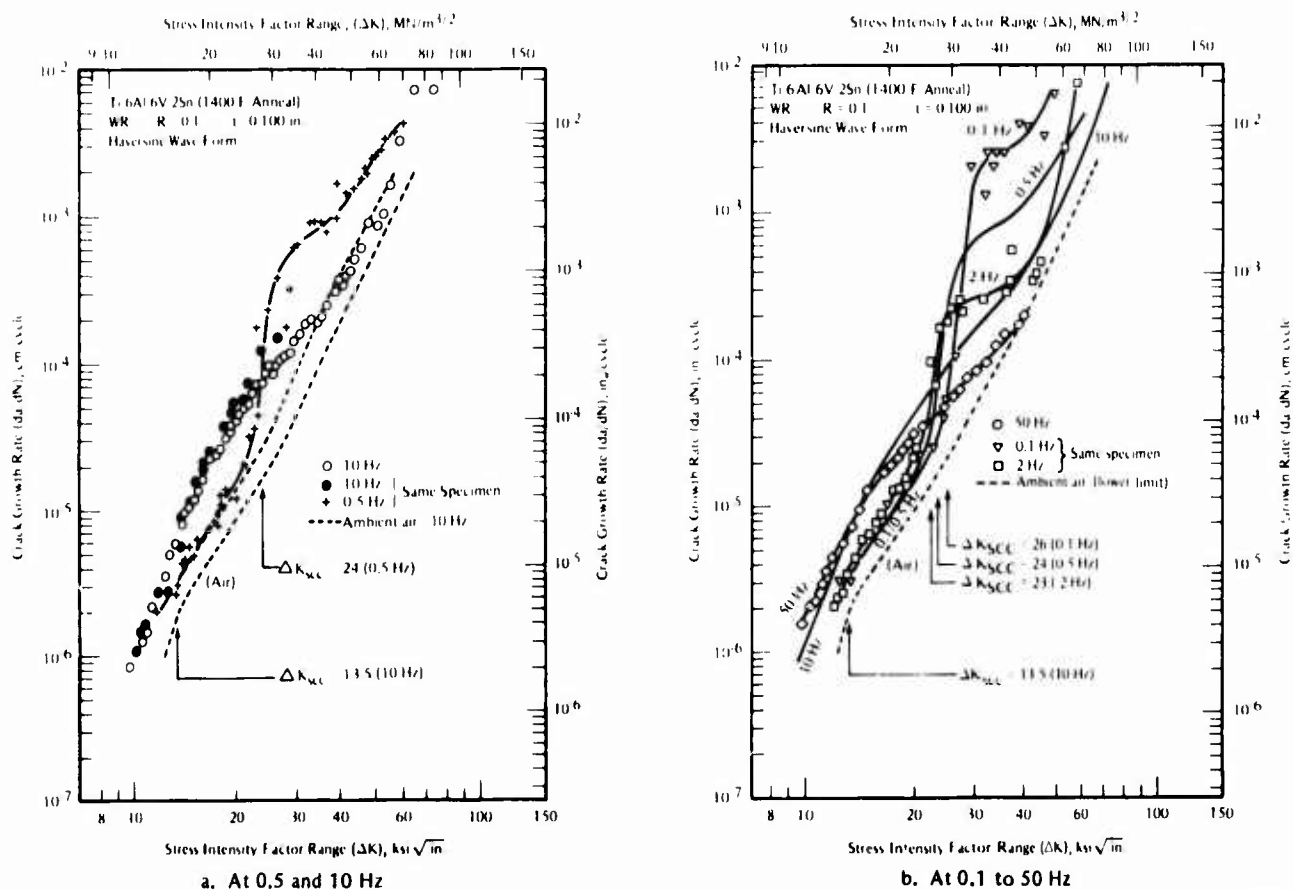
FIGURE 227. Effect of Frequency on Corrosion-Fatigue-Crack Growth Behavior of Ti-6Al-6V-2Sn in Aqueous 0.6 M NaCl[250]

Applied Stress Intensity Factor Range, ksi√in.
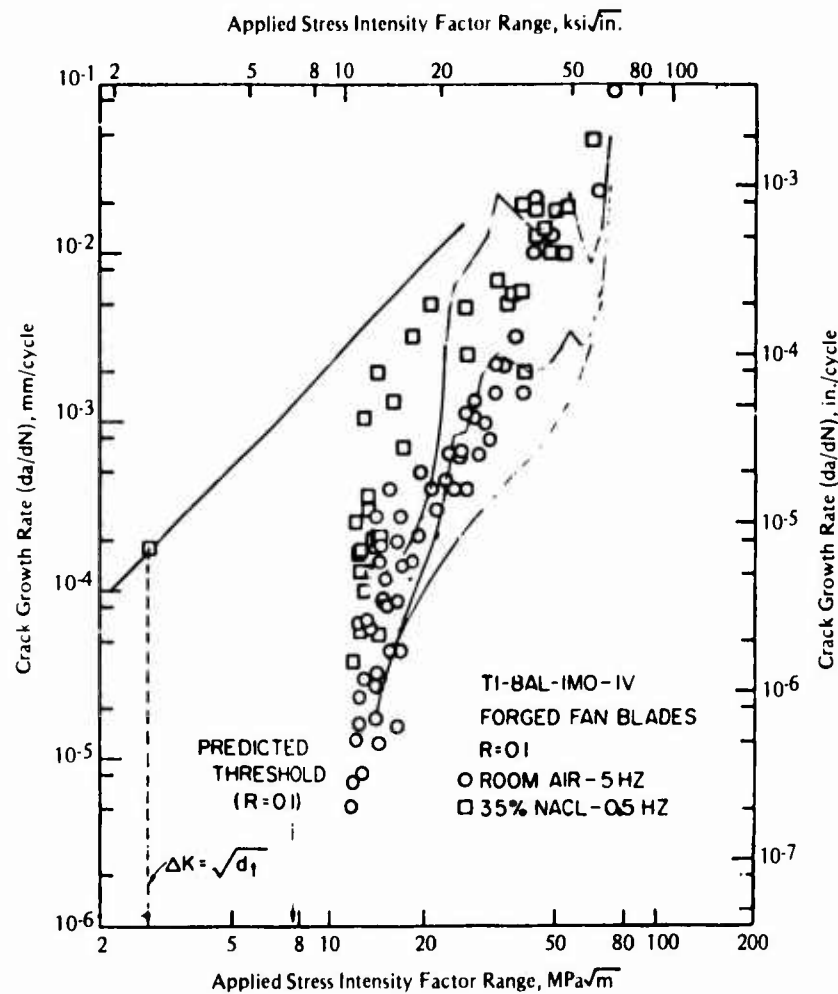
FIGURE 228. Fatigue-Crack Growth Data for Forged-Fan-Blade Specimens
Tested in Room Air and in Saltwater[258]

disappeared and SCC controlled the crack growth rate. At K_{Ic}, mechanical fast-fracture
controlled the crack growth rate.

Piper et al[249] compared the crack growth rate of Ti-8Al-1Mo-1V duplex-annealed alloy to
a commercially pure titanium alloy CP75A, using center-cracked specimens. Both alloys were
found to be sensitive to corrosion fatigue, as shown in Figure 231. The Ti-8Al-1Mo-1V alloy
exhibited better fatigue-crack growth resistance in both air and 3.5 percent NaCl solution.

Ti-6Al-2Cb-1Ta-0.8Mo

Schwab and Czyryca[151] studied the effects of notches and Severn River water on the
fatigue behavior of high-strength structural alloys. Fatigue-life curves*, which incorporate
high- and low-cycle fatigue data, for smooth and notched specimens of Ti-6Al-2Cb-1Ta-0.8Mo
tested in air and in saltwater are shown in Figure 232. Notches decreased the fatigue strength

---

*These curves are plotted in terms of pseudo stress amplitude which is directly proportional to strain range (see section on ship
steels in Chapter 3).
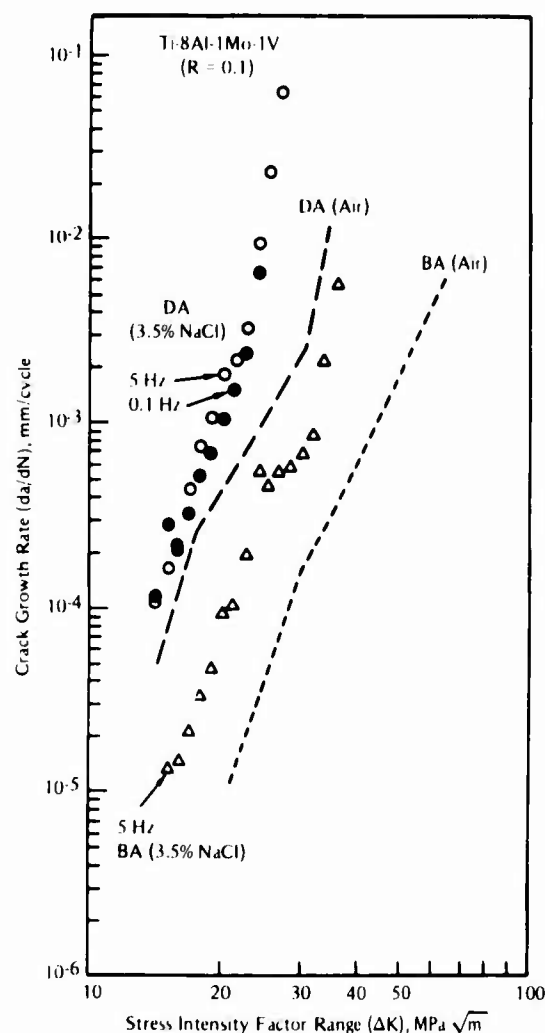
FIGURE 229. Corrosion-Fatigue Crack Growth Rates in 3.5 Percent NaCl
Solution for the Duplex-Annealed (DA) and Beta-Annealed (BA)
Microstructures[258]

Data trend lines (dahsed) for the respective microstructures are shown for
growth rates in ambient air.

of this alloy at all cyclic lives, but the Severn River saltwater had no significant detrimental
effect. The notch effect was much smaller in the low-cycle fatigue range (near 10^3 cycles to
failure) than in the higher cyclic range.

The effects of cathodic polarization on corrosion-fatigue-crack growth for Ti-6Al-2Cb-
1Ta-0.8Mo in air and in natural seawater were reported in two studies.[231,259] The experiments
were conducted on side-grooved SEN cantilever samples at 0.167 Hz under constant-load
amplitude. The results of this study are presented in Figure 233. The corrosion-fatigue-crack-
growth rate was not affected by the two applied cathodic potentials of -0.80 and -1.05 V SCE in
flowing natural seawater. The free-corrosion electrochemical potential of Ti-6Al-2Cb-1Ta-
0.8Mo in natural seawater was -0.30 V SCE. Neither the seawater environments nor the
cathodic potential had a detrimental influence on corrosion-fatigue-crack growth for this
alloy.
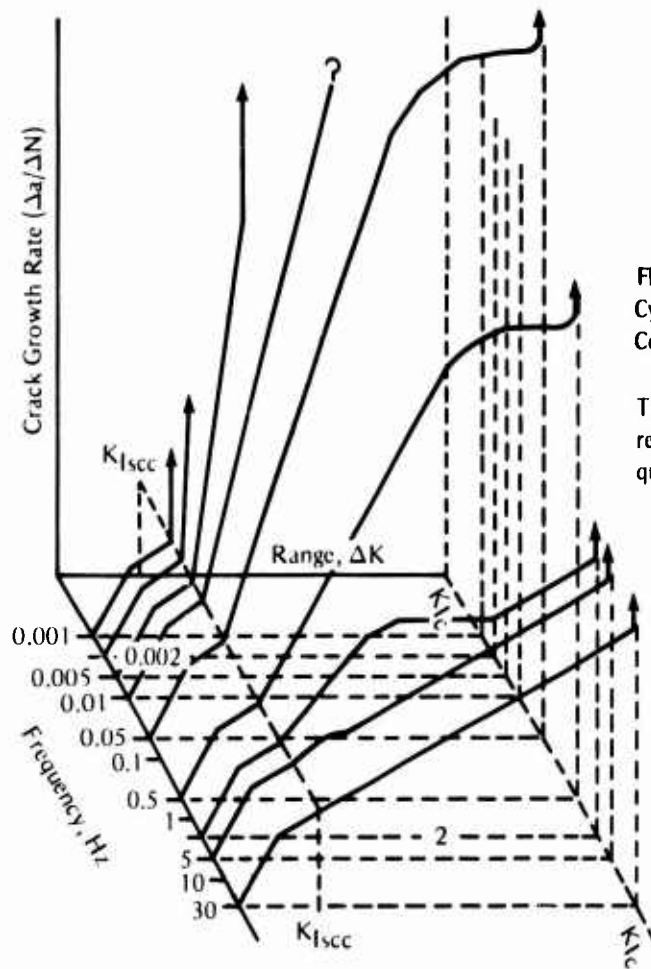
FIGURE 230. Effects of Frequency and ΔK Range on the Cyclic Crack Growth Rate of Ti-8Al-1Mo-1V in a Stress-Corrosion-Inducing Environment[256]

The vertical portions of the lines at 0.005 Hz and less represent complete fracture within the first tensile quarter cycle.
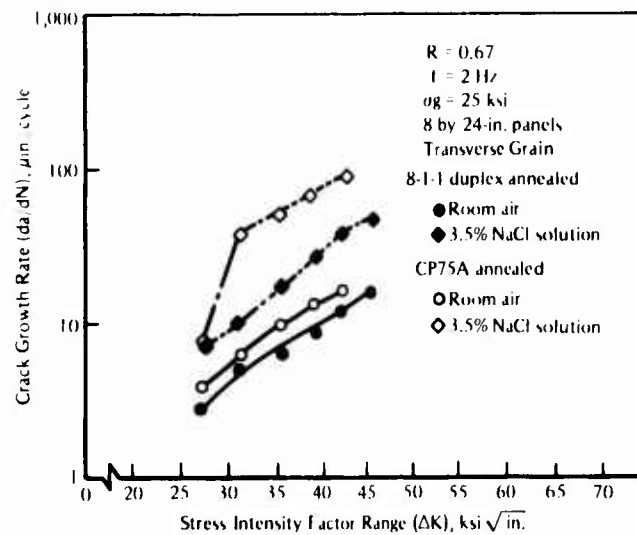
FIGURE 231. Corrosion-Fatigue-Crack Growth Rate for Ti-8Al-1Mo-1V and Ti-CP75A[249]
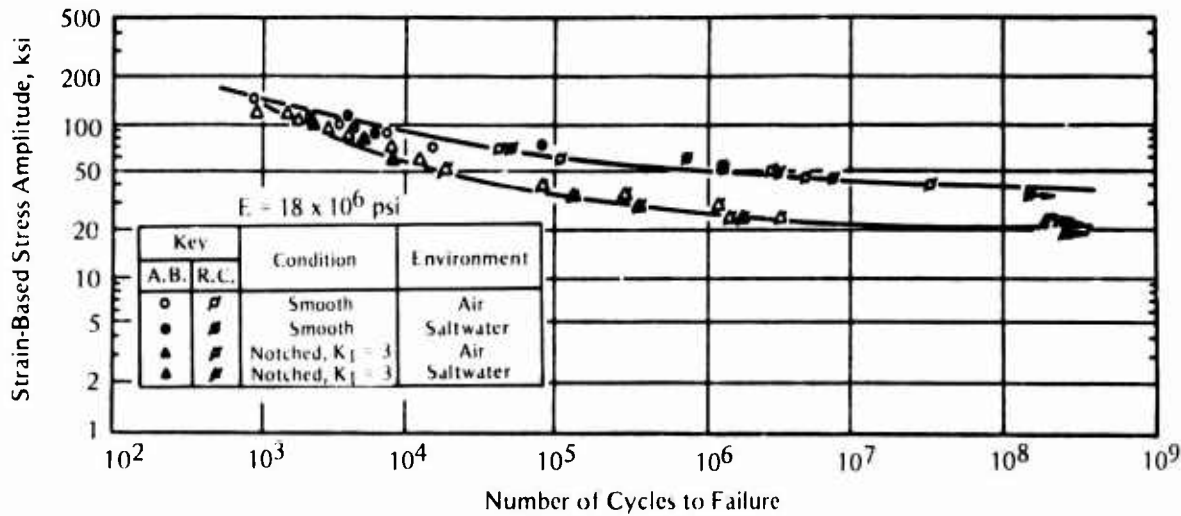
FIGURE 232. Corrosion-Fatigue Curves for Alloy 6Al-2Cb-1Ta-0.8Mo[151]

Ti-7Al-2.5Mo

Data from Crooker and Lange[254] indicated that the corrosion-fatigue-crack-growth behavior of Ti-7Al-2.5Mo was between the scatterband limits found in tests of this same alloy performed in air. The test specimens were cantilever-loaded, center-notched-plate bend specimens cycled at approximately 0.083 Hz, and the environment was a 3.5 percent NaCl solution. These test results, plotted in terms of pseudo stress amplitudes, are shown in Figure 216 presented earlier.*

Schwab and Czyryca[151] studied the effects of notches and saltwater on corrosion-fatigue properties of Ti-7Al-2.5Mo. High-cycle fatigue testing in Severn River saltwater at a frequency of 24.2 Hz was performed using rotating cantilever beams. Fatigue-life curves for smooth and notched specimens in air and seawater are presented in Figure 234. The notched specimens had lower fatigue strengths in the range greater than 5×10^3 cycles. The saltwater had no detrimental effects on the fatigue life of either the smooth or notched specimens under these conditions.

Ti-4Al-3Mo-1V

Piper, Smith, and Carter[248] used center-cracked panels to determine the fatigue-crack-growth behavior in Ti-6Al-4V specimens which had received three different heat treatments. Ti-4Al-3Mo-1V was included as a reference alloy in tests conducted in three environments (air, distilled water, and 3 percent NaCl solution). The test results are shown in Figure 235. In room air and distilled water, Ti-4Al-3Mo-1V and Ti-6Al-4V beta STA-1250 had similar crack growth behavior and both exhibited behavior superior to that of Ti-6Al-4V in either the mill-annealed

---

* Psuedo stress amplitude is directly proportional to strain range (see section on ship steels in Chapter 3).
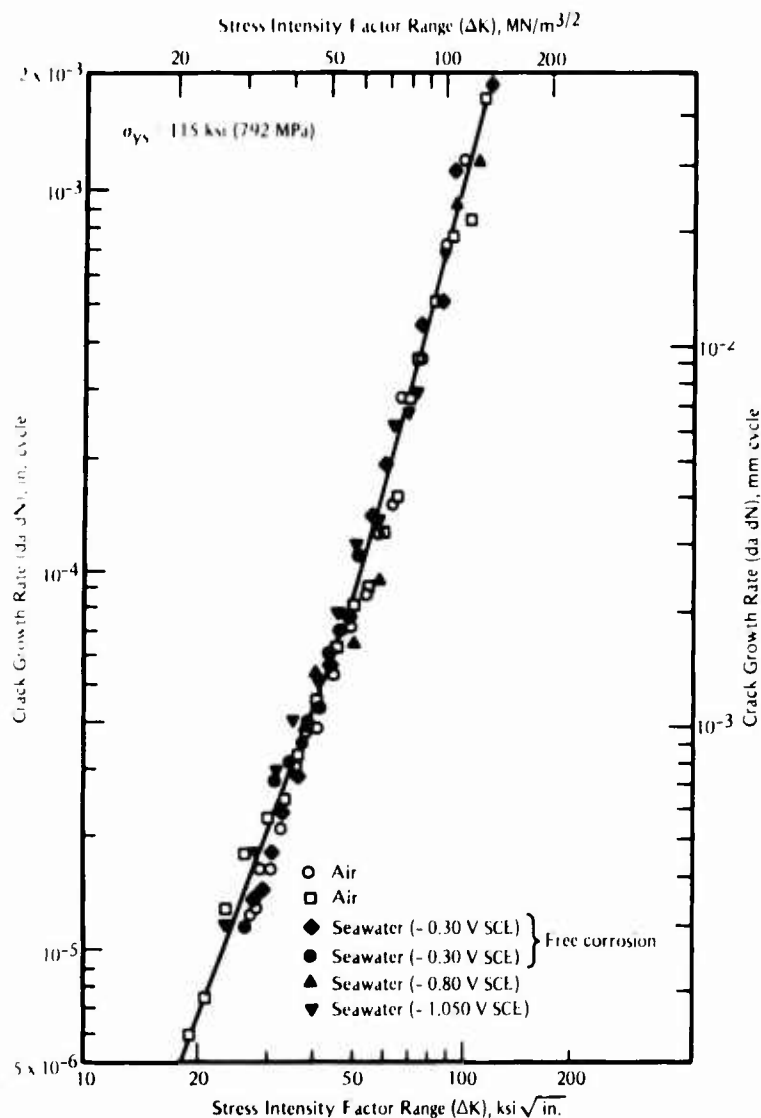
FIGURE 233. Fatigue–Crack Growth Rate for Ti-6Al-2Cb-1Ta-0.8Mo
in Air and Seawater at 0.167 Hz[259]

or duplex-annealed condition. In the 3.5 percent NaCl solution, the crack growth resistance of
the reference alloy, Ti-4Al-3Mo-1V, was slightly better than that for the Ti-6Al-4V in all three
heat-treated conditions.

Ti-8Al-2Cb-1Ta

The corrosion-fatigue properties of welded Ti-8Al-2Cb-1Ta and Ti-6Al-4V were compared
by Hoffman and Kennedy.[240] From corrosion fatigue tests in seawater at a frequency of 24.2 Hz
they determined that the reduction in fatigue strength for the Ti-8Al-2Cb-1Ta specimens was
greater than that for the Ti-6Al-4V specimens.
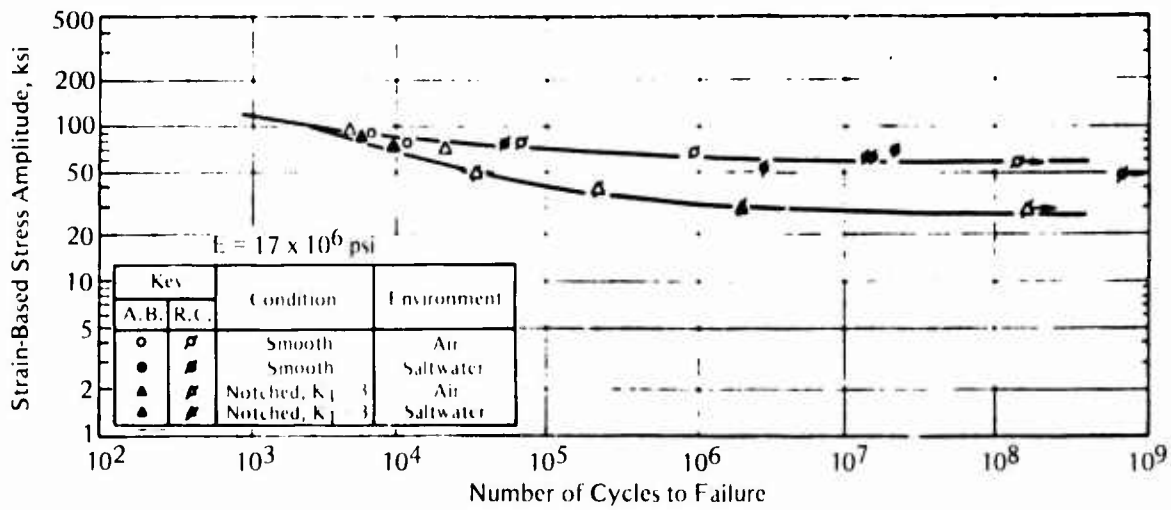
FIGURE 234. Flexural Fatigue Curves for 7Al-2.5Mo Titanium Alloy[151]

△ 6Al-4V mill annealed   R = 0.05   t = 0.05-0.063 in.
O 6Al-4V duplex annealed   f = 2 Hz   12 by 36-in. panels
▲ 6Al-3Mo-1V duplex annealed σ_g = 25 ksi   Transverse grain
● 6Al-4V Beta-STA-1250
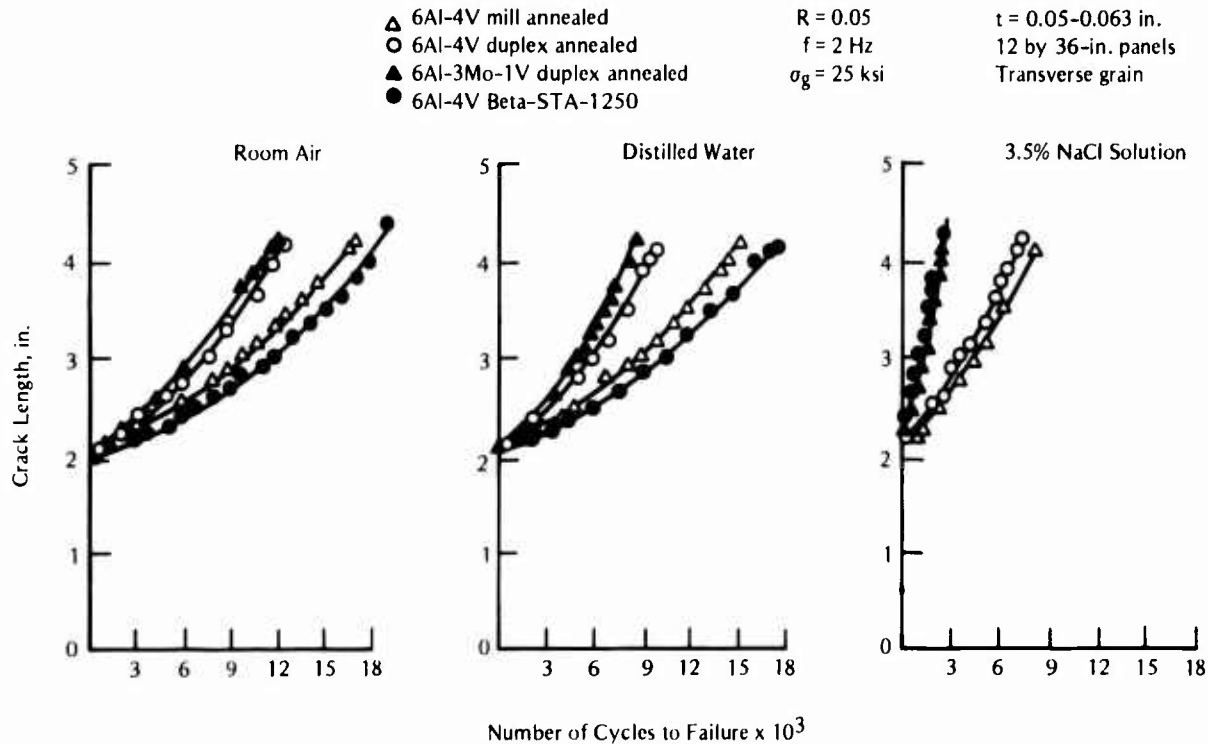
FIGURE 235. Corrosion-Fatigue-Crack Growth Behavior of Ti-6Al-4V and Ti-4Al-3Mo-1V[249]

Ti-8Al

Wanhill[260] determined the fatigue lives of Ti-8Al in both the solution-treated and aged conditions. Unnotched specimens tested in air and 3.0 percent NaCl solution behaved similarly, as shown in Figure 236. The specimens were tested at a frequency of 30 Hz in fluctuating tension.

Ti-4Al

The effect of saltwater (3.0 percent NaCl solution) on the fatigue strength of smooth and notched specimens of Ti-4Al was determined by Glikman and Shekhovtsev.[261] The saltwater had no detrimental effect on the smooth specimens, but did have an adverse effect on the notched specimens. Low-cycle fatigue curves for both the smooth and notched specimens from plate material tested in air, distilled water, and 3.0 percent NaCl solution are shown in Figure 237. As shown by Curve 2c, the notched specimens tested in 3.0 percent NaCl solution had the lowest fatigue strength for the entire stress range. Curves for notched specimens cut from rod material tested in air and saltwater, shown in Figure 238, also reveal a reduction in fatigue resistance of the notched specimens due to saltwater exposure.

Ti-6.5Al-3.8Sn-2.5V-5Zr

The effect of 3.0 percent NaCl solution on the fatigue life of notched specimens of Ti-6.5Al-3.8Sn-2.5V-2.5Zr is shown in Figure 239.[260] The presence of saltwater significantly reduced the fatigue endurance of the notched specimens.
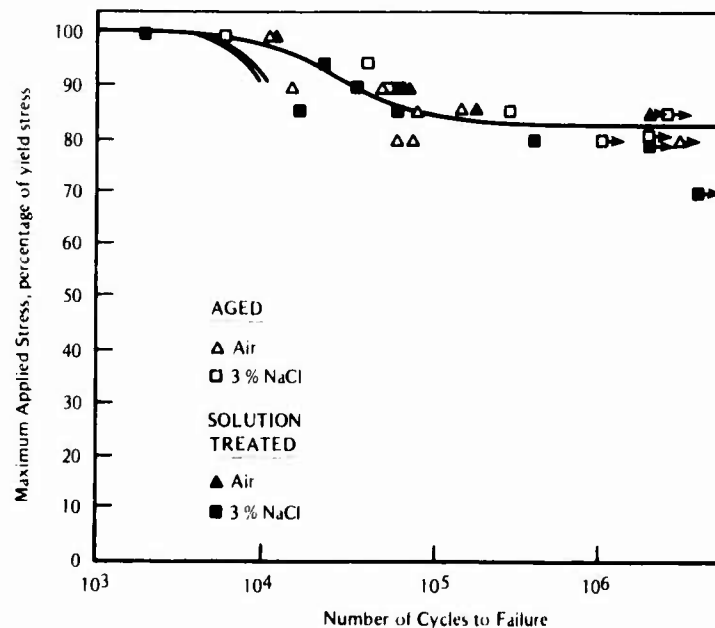
FIGURE 236. Number of Cycles to Failure Versus Maximum Applied Percentage of the 0.2 Percent Offset Yield Stress for Ti-Al in Air and in 0.3 Percent NaCl[261]
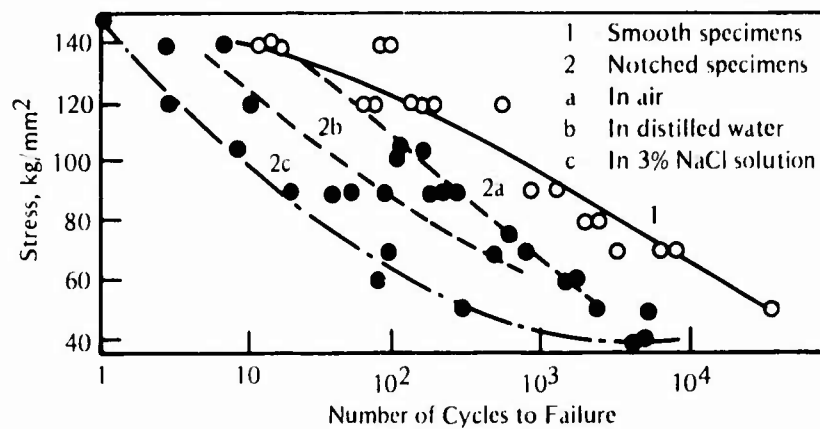
FIGURE 237. Low-Endurance Fatigue Curves for Ti-4Al Specimens (Cut From 25 mm-Thick Plate)[261]
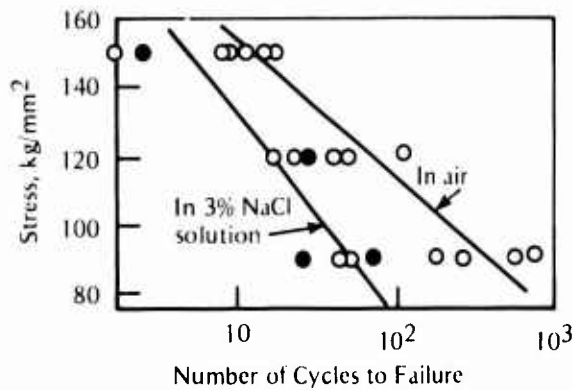
FIGURE 238. Low-Endurance Fatigue Curves for Notched Ti-4Al Specimens (Cut From Rod)[261]
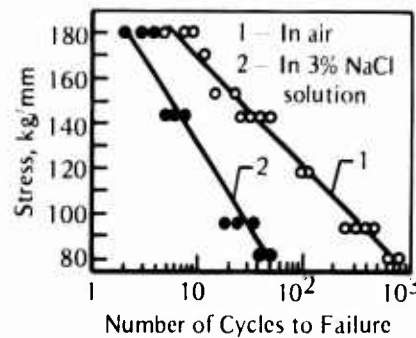
FIGURE 239. Low-Endurance Fatigue Curves for Notched Ti6.5Al-3.8Sn-2.5V-2.5Zr Specimens in Air and in a 3 Percent NaCl Solution[260]

Ti-6Al-4V Carbon-Epoxy Laminate

The fatigue-crack-growth behavior of Ti-6Al-4V/carbon-epoxy laminate was investigated by Wanhill.[262] The tests were carried out on notched specimens under a gust spectrum loading in air and in an air plus saltwater (0.35 percent NaCl) spray environment. The gust spectrum is an average of the scatterband loading spectra for the nine commercial aircraft types. Changing from an air environment to an air/saltwater environment was found to be detrimental. Visible cracking of the carbon-epoxy cores took place in the presence of the saltwater spray.

REFERENCES

1. Swanson, S. R. (Ed.), *Handbook of Fatigue Testing*, ASTM-STP 566 (1974).

2. Ebara, R., Kai, T., and Inoue, K., "Corrosion-Fatigue Behavior of 13Cr Stainless Steel in Sodium-Chloride Aqueous Solution and Steam Environment", ASTM-STP 642, 155-168 (1977).

3. McAdam, D. J. Jr., "Corrosion-Fatigue of Non-Ferrous Metals", *ASTM Proc.*, **27** (1927).

4. McAdam, D. J., Jr., "Fatigue and Corrosion-Fatigue of Spring Material" *Trans. ASME*, **51**, 45-58 (1929).

5. Sedriks, A. J. and Money, K. L., "Corrosion Fatigue Properties of Nickel Containing Materials in Sea Water", Technical Publication, International Nickel Limited, Product Research and Development Department, No. P-BL. **240** (1973).

6. May, T. P., "Corrosion Fatigue of Large Ship Propeller Alloys", Paper presented at Propellers '75 Conference, The Society of Naval Architects and Marine Engineers, Philadelphia, Pennsylvania, July 22-23, 1975.

7. Webb, A.W.O., Eames, C.F.W., and Tuffrey, A., "Factors Affecting Design Stresses in Marine Propellers", Paper presented at Propellers 75 Conference, The Society of Naval Architects and Marine Engineers, Philadelphia, Pennsylvania, July 22-23, 1975.

8. Richards, C. W., *Engineering Materials Science*, Wadsworth Publishing Co., San Francisco (1961).

9. Jaske, C. E., Utah, D. A., and Boyd, W. K., "Corrosion Fatigue of Cast Propeller Alloys", Paper presented at the Propellers '78 Symposium, Society of Naval Architects and Marine Engineers, Virginia Beach, Virginia, May 24-25, 1978.

10. Chu, H. P., and Macco, J. G., "Corrosion Fatigue of 5456-H117 Aluminum Alloy in Saltwater", ASTM-STP 642, 223-239 (1977).

11. American Society for Testing and Materials, "Standard Recommended Practice for Constant Amplitude Axial Fatigue Test of Metallic Materials", ASTM E 466-76, in *Annual Book of ASTM Standards*, Part 10 (1976).

12. "Tentative Recommended Practice for Constant-Amplitude Low-Cycle Fatigue Testing", ASTM E 606-77T, *Annual Book of ASTM Standards*, Part 10 (1977).

13. MTS Systems Corp., *Closed Loop*, **I**, Nos. 1-8, 1965-1968.

14. American Society for Testing and Materials, "Tentative Test Method for Constant-Load-Amplitude Fatigue Crack Growth Rates Above 10^{-8}m/cycle", ASTM E 647-78T, in *Annual Book of ASTM Standards*, Part 10 (1978).

15. Clark, W. G., Jr., and Hudak, S. J., Jr., "Variability in Fatigue Crack Growth Rate Testing", *J. Testing and Eval.*, **3**(6), 454-476 (1975).

16. Bucci, R. J., "Development of a Proposed Standard Practice for Near Threshold Fatigue Crack Growth Rate Measurement", Paper presented at ASTM Symposium on Fatigue Crack Growth Measurement and Data Analysis, Pittsburgh, Pa. October, 1979.

17. Crooker, T. W., Bogar, F. D., and Cares, W. R., "Effects of Flowing Natural Seawater and Electrochemical Potential on Fatigue-Crack Growth in Several High-Strength Marine Alloys", NRL Report 8042 (August 30, 1976).

18. American Society for Testing and Materials, "Specification for Substitute Ocean Water", ASTM D 1141, in *Annual Book of ASTM Standards*, Part 31.

19. Jaske, C. E., Broek, D., Slater, J. E., Utah, D. A., and Martin, C. J., "Corrosion Fatigue of Cathodically Protected, Welded Carbon Steel in Cold Seawater", Final Report to American Petroleum Institute, Committee on Offshore Safety and Antipollution Research, Dallas, Texas (February 11, 1977).

20. Wei, R. P., and Speidel, M. O., "Phenomenological Aspects of Corrosion Fatigue, Critical Introduction", in *Corrosion Fatigue: Chemistry, Mechanics and Microstructure*, **NACE-2**, 379-380 (1972).

21. Laird, C., and Duquette, D. J., "Mechanisms of Fatigue Crack Nucleation", in *Corrosion Fatigue: Chemistry, Mechanics and Microstructure*, **NACE-2**, 88-117 (1972).

22. Duquette, D. J., "Environmental Effect I: General Fatigue Resistance and Crack Nucleation in Metals and Alloys", *Fatigue and Microstructure*, American Society for Metals, Metals Park, Ohio (1979), pp. 335-363.

23. Jaske, C. E., Broek, D., Slater, J. E., and Anderson, W. E., "Corrosion Fatigue of Structural Steels in Seawater and for Offshore Applications", ASTM-STP-642, 19-47 (1978).

24. Hoeppner, D. W., "Model for Prediction of Fatigue Lives Based Upon a Pitting Corrosion Fatigue Process", ASTM-STP 675, 841-870 (1979).

25. Starke, E. A., Jr., and Lütjering, G., "Cyclic Plastic Deformation and Microstructure", in *Fatigue and Microstructure*, American Society for Metals, Metals Park, Ohio (1979), pp. 205-243.

26. Hahn, H. N., and Duquette, D. J., "The Effect of Heat Treatment on the Fatigue and Corrosion Fatigue Behavior of a CuNiCr Alloy", Metallurgical Trans., **10A**(10), 1453-1460 (October, 1979).

27. Mitchell, M. R., "Fundamentals of Modern Fatigue Analysis for Design", *Fatigue and Microstructure*, American Society for Metals, Metals Park, Ohio (1979), pp. 385-437.

28. Jaske, C. E., Slater, J. E., Broek, D., Leis, B. N., Anderson, W. E., Turn, J. C., and Omar, T., "Corrosion Fatigue of Welded Carbon Steel for Application to Offshore Structures", Interpretative Report to American Petroleum Institute, Committee on Offshore Safety and Antipollution Research (February 1, 1977).

29. McEvily, A. J., and Wei, R. P., "Fracture Mechanics and Corrosion Fatigue", in *Corrosion Fatigue: Chemistry, Mechanics and Microstructure*, **NACE-2**, 381-395 (1972).

30. Wei, R. P., "On Understanding Environment Enhanced Fatigue Crack Growth—A Fundamental Approach", ASTM STP 675, 816-840 (1979).

31. Wei, R. P., "Some Aspects of Environment-Enhanced Fatigue-Crack Growth", *Engineering Fracture Mechanics*, **1**, 633-651 (1970).

32. Wei, R. P., and Landes, J. D., "Correlation Between Sustained-Load and Fatigue Crack Growth in High Strength Steels", *Materials Research and Standards*, **9**(7), 25 (1969).

33. Krafft, J. M., and Cull, W. H., Jr., "Organizational Scheme for Corrosion-Fatigue Crack Propagation Data", NRL Memorandum Report 3505 (July 1977).

34. Sullivan, A. M., "Conditions Affecting Fatigue-Crack-Growth Rate: Relevance to Test Method Selection and Data Interpretation", NRL Report 8111 (June 7, 1977), ADA042927.

35. Hartt, W. H., Tennant, J. S., and Hooper, W. C., "Solution Chemistry Modification Within Corrosion-Fatigue Cracks", ASTM-STP 642, 5-18 (1978).

36. Simmons, G. W., Pao, P. S., and Wei, R. P., "Fracture Mechanics and Surface Chemistry Studies of Subcritical Crack Growth in AISI 4340 Steel", *Met. Trans. A*, **9A**(8), 1147-1158 (1978).

37. Wei, R. P., Rao, P. S., Hart, R. G., Weir, T. W., and Simmons, G. W., "Fracture Mechanics and Surface Chemistry Studies of Fatigue Crack Growth in an Aluminum Alloy", *Met. Trans. A*, **11A**(1), 151-158, (1960).

38. Scott, P. M., and Silvester, D.R.V., "The Influence of Mean Tensile Stress on Corrosion Fatigue Crack Growth in Structural Steel Immersed in Seawater", Department of Energy, UK Offshore Steels Research Project, Interim Technical Report UKOSRP 3/02 (May 25, 1977).

39. Vosikovsky, O., "Effects of Stress Ratio on Fatigue Crack Growth Rates in X70 Pipeline Steel in Air and Saltwater", *J. Testing and Eval.*, **8**(2), 68-73 (March, 1980).

40. Boyd, W. K., and Fink, F. W., "Corrosion of Metals in Marine Environments", Metals and Ceramics Information Center, Report No. MCIC-78-37 (March 1978).

41. Leis, B. N., "Fatigue-Life Prediction for Complex Structures", *J. Design Engr.*, **100**(1), 2-9 (January, 1979).

42. Dowling, N. E., "Fatigue Life Prediction for Complex Load Versus Time Histories", in *Decade of Progress in Pressure Vessels and Piping*, to be published by ASME, New York (1980).

43. Leis, B. N., and Forte, T. P., "Fatigue Growth of Initially Physically Short Cracks in Notched Aluminum and Steel Plates", Paper presented at *13th National Symposium on Fracture Mechanics*, June, 1980.

44. Leis, B. N., "An Approach for Fatigue Crack Initiation Life Prediction with Applications to Complex Components", *Proceedings of the 9th ICAF Symposium on Fatigue Life of Structures Under Operational Loads*, May, 1977, ICAF Doc. 960, Laboratorium für Betriebstestigeit, pp. 3.4/1-47.

45. Dowling, N. E., Brose, W. R., and Wilson, W. K., "Notched Member Fatigue Life Predictions by the Local Strain Approach", in *Fatigue Under Complex Loading: Analyses and Experiments*, AE6, The Society of Automotive Engineers, Warrendale, Pa., 1977, pp. 55-84.

46. Dowling, N. E., "Fatigue at Notches and the Local Strain and Fracture Mechanics Approaches", ASTM-STP 677, 247-273 (1979).

47. Ishiguro, T., "Corrosion Fatigue Strength of Steels for Marine Structures", Nippon Steel Technical Report, **9**, 27-36 (April, 1977).

48. Knight, J. W., "Corrosion Fatigue Related to Welded Steel Structures—A Literature Survey" *Welding Research Internat.*, **7**(3), 195-240 (1977).

49. Minami, Y., Ogawa, T., and Kimura, M., "Investigation on the Corrosion-Fatigue and Its Prevention of Steel in Sea Water", *Bull. Faculty of Engineering, Yokohama National University*, **24**, 51-68 (March, 1977).

50. Masumoto, I., and Akaishi, T., "Study on Corrosion Fatigue of Steel Plates and Welded Joints in 3% NaCl Aqueous Solution — 1st Report: Effect of Alloyed Elements on the Corrosion Fatigue of Steel Plate, *J. Japan Welding Soc.*, **44**(3), 236-240 (1975).

51. Masumoto, I., and Akaishi, T., "Study on Corrosion Fatigue of Steel Plates and Welded Joints in 3% NaCl Aqueous Solution — 2nd Report: Effect of the Grain Size and Cementite Configuration of Steels on the Corrosion Fatigue of Steel", *J. Japan Welding Soc.*, **44**(9), 734-738 (1975).

52. Masumoto, I., and Akaishi, T., "Study on Corrosion Fatigue of Steel Plates and Welded Joints in 3% NaCl Aqueous Solution — Report 3", *J. Japan Welding Soc.*, **44**(10), 822-825 (1975).

53. Minami, Y., Ogawa, T., and Hashimoto, K., "Corrosion-Fatigue of Weathering Steel in Sea Water", *J. Soc. of Mater. Sci.*, **17**, 718-722 (August, 1968) (In Japanese; English abstract).

54. Mehdizadeh, P., "Assessment of Corrosion Fatigue Damage by Acoustic Emission and Periodic Proof Tests", *Materials Evaluation*, **34**(3) (March, 1976).

55. Loria, E. A., and Bush, G. W., "Fatigue Properties of Galvanized Steel and Hot Rolled Steel Before and After Exposure to Salt Spray", Paper presented at Automotive Engineering Congress, Society of Automotive Engineers, Detroit, Michigan, February 25 to March 1, 1974.

56. Nishioka, K., Hirakawa, K., and Kitaura, I., "Low Frequency Corrosion Fatigue Strength of Steel Plate", *The Sumitomo Search*, No. 16, 40-54 (November, 1976).

57. Marsh, K. J., Phil, D., Martin, T., and McGregor, J., "The Effect of Random Loading and Corrosive Environment on the Fatigue Strength of Fillet-Welded Lap Joints", NEL Report No. 587 (February, 1975).

58. Nichols, J. L., "Cathodic Protection Reduces Corrosion Fatigue Cracking of Steel in Sea Water", *Materials Protection*, **2**(2), 46-53 (February, 1963).

59. Mehdizadeh, P., McGlasson, R. L., and Landers, J. E., "Corrosion Fatigue Performance of a Carbon Steel in Brine Containing Air, H_2S and CO_2", *Corrosion*, **22**(12), 325-335 (December, 1966).

60. Duquette, D. J., and Uhlig, H. H., "The Critical Reaction Rate for Corrosion Fatigue of 0.18% Carbon Steel and the Effect of pH", *Trans. ASM*, **62**, 839-845 (1969).

61. Duquette, D. J., and Uhlig, H. H., "Effect of Dissolved Oxygen and NaCl on Corrosion Fatigue of 0.18% Carbon Steel", *Trans. ASM*, **61**, 449-456 (1968).

62. Hudgins, C. M., Jr., Casad, B. M., Schroeder, R. L., and Patton, C. C., "The Effect of Cathodic Protection on the Corrosion Fatigue Behavior of Carbon Steel in Synthetic Sea Water", *J. Petroleum Technol.*, **23**, 283-293 (March, 1971).

63. Endo, K., and Komai, K., "Influences of Secondary Stress Fluctuations of Small Amplitude on Low-Cycle Corrosion Fatigue", ASTM-STP 642, (1978), pp 74-97.

64. Endo, K., Komai, K., and Kuroda, T., "Influences of Secondary Stress Fluctuations of Small Amplitude on Low Cycle Corrosion Fatigue", *Bull. JSME*, **18**(122), 769-775 (August, 1975).

65. Endo, K., Komai, K., and Nakagaki, K., "Plastic Strain Fatigue of High Tensile Steel in Corrosive Media", *Bull. JSME*, **11**(47), 791-797 (October, 1968).

66. Radd, F. J., Crowder, L. H., and Wolfe, L. H., "Effect of pH in the Range 6.6-14.0+ on the Aerobic Corrosion Fatigue of Steel", *Corrosion*, **16**, 415-418 (August, 1960).

67. Endo, K., Komai, K., and Kinoshita, S., "Long-Life Corrosion-Fatigue Strength of a Carbon Steel", *Proceedings of the 22nd Japan Congress on Materials Research*, Kyoto, Japan, 1978, pp. 193-198.

68. Koga, M., Terasawa, M., and Asami, K., "Corrosion Fatigue of Tufftrided Steel—Fatigue Tests in Pure Water and in 3% Sodium Chloride Solution", *Proceedings of the 17th Japan Congress on Materials Research*, Kyoto, Japan, 1974, pp. 1-6.

69. Koga, M., Terasawa, M., and Asami, K., "Corrosion Fatigue of Tufftrided Steel—Fatigue Tests in Pure Water and in 3% Sodium Chloride Solution- -2nd Report", *Proceedings of the 19th Japan Congress on Materials Research*, Kyoto, Japan, 1976, pp. 65-70.

70. Gould, A. J., "The Influence of Temperature on the Severity of Corrosion Fatigue", *Engineering*, pp 495-496 (May 8, 1936).

71. Kirk, W. W., Covert, R. A., and May, T. P., "Corrosion Behavior of High-Strength Steels in Marine Environments", *Met. Eng. Quart.*, **8**(4), 31-38 (November, 1968).

72. Thiruvengadam, A., "High-Frequency Fatigue of Metals and Their Cavitation-Damage Resistance", *Trans. ASME, J. Eng. for Ind.*, Series B, **88**(3), 332-340 (August, 1966).

73. Jolliff, J. V., and Thiruvengadam, A., "Effect of Hydrostatic Pressure on Corrosion-Fatigue at High Frequency" *Trans. ASME, J. Eng. for Ind.*, Series B, **96**(3), 1085-1088 (August, 1974).

74. Thiruvengadam, A., "Corrosion Fatigue at High Frequencies and High Hydrostatic Pressures", ASTM-STP 518, 139-154 (1972).

75. Lyashscenko, A. E., Glikman, L. A., and Zobachev, Yu. E., "Some Features of Influence of Cathodic Polarization on the Corrosion Fatigue Strength of Steel Samples with a Notch", *Soviet Mater. Sci.*, **9**(5), 496-499 (September-October, 1973).

76. Endo, K., and Miyao, Y., "Effects of Cyclic Frequency on the Corrosion Fatigue Strength", *Bull. JSME*, **1**, 374-380 (1958).

77. Hartt, W. H., Fluet, J. E., and Henke, T. E., "Cathodic Protection Criteria for Notched Mild Steel Undergoing Corrosion Fatigue In Sea Water", Paper presented at the Seventh Annual Offshore Technology Conference, Houston, Texas, May 5 to 8, 1975.

78. Hooper, W. C., and Hartt, W. H., "The Influence of Cathodic Polarization Upon Fatigue of Notched Structural Steel in Seawater", *Corrosion*, **34**(9), 320-323 (1978).

79. Hartt, W. H., and Hooper, W. C., "Endurance Limit Enhancement of Notched, 1018 Steel in Sea Water—Specimen Size and Frequency Effects", *Corrosion*, **36**(3), 107-112 (March, 1980).

80. Hartt, W. H., Martin, P. E., and Hooper, W. C., "Endurance Limit Enhancement of Structural Steel in Sea Water by Cathodic Protection", *Proceedings of 11th Annual Offshore Technology Conference*, Houston, Texas, April 30 to May 3, 1979, Vol. II, pp. 1331-1340.

81. Dugdale, D. S., "Corrosion Fatigue of Sharply Notched Steel Specimens", *Metallurgica*, pp. 27-28 (January, 1972).

82. Endo, K., Komai, K., and Nakamuro, N., "Estimation of Corrosion Fatigue Strength by Corrosion Resistance and Notch Sensitivity of Materials", *Bull. JSME*, **13**(61), 837-849 (1970).

83. Walter, J. C., Olbjorn, E., Alfstad, O., and Eide, G., "Safety Against Corrosion Fatigue Offshore", Publication No. 94, Det Norske Veritas, Oslo, Norway (April, 1976).

84. Watanabe, M., Mukai, Y., and Naganuma, M., "Corrosion Fatigue Properties of Structural Steel", *Technology Reports of Osaka University*, **24**(1191-1229), 487-494 (1974).

85. Dvoracek, L. M., "Cathodic Over-Protection and Fatigue of Carbon Steel in Sea Water", Preprint of paper for the Pacific Northwest Metals and Minerals Conference, 1977.

86. Dvoracek, L. M., "Influence of Cathodic Over-Protection on Fatigue of Carbon Steel in Sea Water", *Materials Performance*, **16**(9), 21-24 (September, 1977).

87. Popperling, R., Schwenk, W., and Vogt, G., "Potential Dependence of the Corrosion Fatigue of High Strength Sheet Piling Steel in Salt Water", *Werkstoffe and Korrosion (Materials and Corrosion)*, **29**(7), 445-451 (July, 1978).

88. Zamikhovskii, V. S., and Pokhmurskii, V. I., "Effect of Chromium-Nickel Diffusion Coatings on the Mechanical Properties of Medium-Carbon Steel", *Metal Sci. and Heat Treatment*, **15**(3-4), 262-264 (March-April, 1973).

89. Hodgkiess, T., "Corrosion Fatigue of Structural Steel in Seawater", *Proceedings of International Conference on Mechanisms of Environment Sensitive Cracking of Materials*, the University of Surrey, Guildford, England, April 4 to 7, 1977, pp. 348-358.

90. Jarman, R. A., Smith, S., and Williams, R. A., "Simple and Inexpensive Test Rig for Determining Basic S-N Data of Welded Joints in a Corrosive Environment", *Brit. Corrosion J.*, **13**(4), 195-198 (1978).

91. Kochera, J. W., Tralmer, J. P., and Marshall, P. W., "Fatigue of Structural Steel for Offshore Platforms", *Proceedings of 8th Annual Offshore Technology Conference*, Houston, Texas, May 3 to 6, 1976, Vol. II, pp. 831-844.

92. Havens, F. E., and Bench, D. M., "Fatigue Strength of Quenched and Tempered Carbon Steel Plates and Welded Joints in Sea Water", Preprint of Paper No. OTC 1046 presented at the First Annual Offshore Technology Conference, Houston, Texas, May 18-21, 1969.

93. Watanabe, M., and Mukai, Y., "Corrosion Fatigue Properties of Structural Steel and Its Welded Joints in Sea Water—Properties under High Amplitude and Slow Rate of Cyclic Stressing", *Proceedings of International Conference on Welding in Offshore Constructions*, Newcastle-upon-Tyne, England, February 26 to 28, 1974; published by The Welding Institute, Abington, Cambridge, England (1974), Vol. 1, pp 46-53.

94. Berge, S., "Corrosion Fatigue Testing of Welded Joints at Low Frequencies", Preliminary report, Division of Ship Structures, The Norwegian Institute of Technology, Trondheim, Norway (1976).

95. Berge, S., "Constant Amplitude Fatigue Strength of Welds in Sea Water Drip", *Proceedings of Offshore Steels Conference*, Welding Institute, England, November, 1978, pp. 336-346.

96. Booth, G. S., "Constant Amplitude Fatigue Tests on Welded Steel Joints Performed in Sea Water", *Proceedings of Offshore Steels Conference*, Welding Institute, England, November, 1978, pp. 227-252.

97. Booth, G. S., "The Influence of Simulated North Sea Environmental Conditions on the Constant Amplitude Fatigue Strength of Welded Joints", *Proceedings of 11th Annual Offshore Technology Conference*, Houston, Texas, April 30 to May 3, 1979, Vol. I, pp. 547-554.

98. Wildschut, H., De Back, J., Dortland, W., and Van Leeuwen, O. L., "Fatigue Behaviour of Welded Joints in Air and Seawater", *Proceedings of Offshore Steels Conference*, Welding Institute, England, November, 1978, pp. 112-155.

99. Vaessen, G.H.G., and De Back, J., "Fatigue Behavior of Welded Steel Joints in Air and Seawater", *Proceedings of 11th Annual Offshore Technology Conference*, Houston, Texas, April 30 to May 3, 1979, Vol. I, pp. 555-562.

100. Haagensen, P. J., D'Erasmo, P., and Pettersen, B., "Fatigue Performance in Air and Sea Water and Fracture Toughness of TIG Dressed Steel Weldments", *Proceedings of Offshore Steels Conference*, Welding Institute, England, November, 1978, pp. 208-226.

101. Solli, O., "Corrosion Fatigue of Welded Joint in Structural Steels and the Effect of Cathodic Protection", *Proceedings of Offshore Steels Conference*, Welding Institute, England, November, 1978, pp. 253-287.

102. Holmes, R., "Fatigue and Corrosion Fatigue of Welded Joints Under Random Loading Conditions", *Proceedings of Offshore Steels Conference*, Welding Institute, England, November, 1978, pp. 288-335.

103. Nagai, K., Takeuchi, N., and Mori, M., "Effect of Various Improvements on the Corrosion Fatigue Strength of Structural Steel in 3% Sodium Chloride Solution", *Proceedings of the 20th Japan Congress on Materials Research*, Kyoto, Japan, 1977, pp. 71-75.

104. Kitagawa, H., "A Fracture Mechanics Approach to Ordinary Corrosion Fatigue of Unnotched Steel Specimens", *Corrosion Fatigue: Chemistry, Mechanics, and Micro-structure*, **NACE-2**, National Association of Corrosion Engineers, Houston, 1972, pp. 521-528.

105. Hooper, W. C., and Hartt, W. H., "Influence of Cathodic Polarization Upon Fatigue of Notched Structural Steel in Sea Water", Paper No. 38 presented at Corrosion/77, San Francisco, California, March 14 to 18, 1977.

106. Pook, L. P., "Fatigue Crack Growth Data for Various Materials Deduced from Fatigue Lives of Precracked Plates", *Stress Analysis and Growth of Cracks*, Part 1, ASTM-STP 513, 106-124 (1972).

107. Pook, L. P., and Greenan, A. F., "Various Aspects of the Fatigue Crack Growth Threshold in Mild Steel", in *Fatigue Testing and Design*, Vol. 2, The Society of Environmental Engineers, London (April, 1976).

108. Crooker, T. W., and Lange, E. A., "Low Cycle Fatigue Crack Propagation in A201B, A302B, and A517F Pressure Vessel Steels", *Welding J.*, **46**, 322-s-328-s (July, 1967).

109. Sullivan, A. M., and Crooker, T. W., "Fatigue Crack Growth in A516-60 Steel—Effects of Specimen Thickness, Saline Environment, and Electrochemical Potential" *Procedings of International Conference on Fracture Mechanics and Technology*, Hong Kong, March 21-25, 1977, Vol. 1, pp. 687-698.

110. Telseren, A., and Doruk, M., "Temperature Dependence of Water-Inhanced Fatigue-Crack Growth in Mild Steel", *Engineering Fracture Mechanics*, **6**(2), 283-286 (September, 1974).

111. Nagai, K-I., "Environmental Strength and Fracture Mechanics", *J. Japan Welding Soc.*, **45**(11), 926-937 (1976).

112. Socie, D. F., and Antolovich, S. D., "Subcritical Crack Growth Characteristics in Welded ASTM A537 Steel", *Welding J.*, **53**(6), 267-s-271-s (June, 1974).

113. Vosikovsky, O., "Fatigue-Crack Growth in an X-65 Line-Pipe Steel at Low Cyclic Frequencies in Aqueous Environments", *Trans. ASME, J. Eng. Mater. and Technol.*, Series H, **97**(4), 298-304 (October, 1975).

114. Endo, K., Komai, K., and Suzuki, Y., "Influences of Stress Cycle Frequency on Propagation of Corrosion Fatigue Cracks", *Bull. JSME*, **18**(115), 9-16 (January, 1975).

115. Endo, K., Komai, K., and Kimura, K., "Cathodic Protection Against Propagation of Corrosion Fatigue Cracks of a Mild Steel", *Bull. JSME*, **21**(161), 1565-1570 (November, 1978).

116. Misawa, T., and Kobayashi, Y., "Effect of pH on Corrosion Fatigue Crack Propagation in a Low Carbon Steel", *Boshoku Gijutsu*, **25**(8), 493-497 (1976).

117. Bristoll, P., and Opdam, J.J.G., "Fatigue of Offshore Structures: The Prediction of Fatigue Crack Propagation Under Conditions of Random Loading", Paper presented at Oceanology International, 1975.

118. Bristoll, P., and Roeleveld, J. A., "Fatigue of Offshore Structures: Effect of Seawater on Crack Propagation in Structural Steel", *Proceedings of Offshore Steels Conference*, Welding Institute, England, November, 1978, pp. 439-458.

119. Bardal, E., and Haagensen, P. J., "Corrosion Fatigue Crack Propagation Tests on Steels for Offshore Structures", *Proceedings of 9th Annual Offshore Technology Conference*, Houston, Texas, May 2 to 5, 1977, Vol. II, pp. 381-390.

120. Haagensen, P. J., and Dagestad, V., "Random Load Crack Propagation in Sea Water in a Medium Strength Structural Steel", *Proceedings of Offshore Steels Conference*, Welding Institute, England, November, 1978, pp. 531-547.

121. Haagensen, P. J., "Fatigue Crack Growth of Steel in Air and Sea Water Under Constant Amplitude and Random Loading", Paper presented at The Fourth International Conference on Fracture, University of Waterloo, Ontario, Canada, June, 1977.

122. Johnson, R., Bretherton, I., Tomkins, B., Scott, P. M., and Silvester, D.R.V., "The Effect of Sea Water Corrosion in Fatigue Crack Propagation in Structural Steel", *Proceedings of Offshore Steels Conference*, Welding Institute, England, November, 1978, pp. 387-414.

123. Scott, P. M., and Silvester, D.R.V., "The Influence of Seawater on Fatigue Crack Propagation Rates in Structural Steel", Department of Energy, UK Offshore Steels Research Project, Interim Technical Report UKOSRP 3/03, (December 19, 1975).

124. Bardal, E., Sondenfor, J. M., and Gartland, P. O., "Slow Corrosion Fatigue Crack Growth in a Structural Steel in Artificial Sea Water at Different Potentials, Crack Depths and Loading Frequencies", *Proceedings of Offshore Steels Conference*, Welding Institute, England, November, 1978, pp. 415-438.

125. Austen, I. M., "Factors Affecting Corrosion Fatigue Crack Growth in Steels", *Proceedings of Offshore Steels Conference*, Welding Institute, England, November, 1978, pp. 364-386.

126. Bogar, F. D., and Crooker, T. W., "The Influence of Bulk-Solution-Chemistry Conditions on Marine Corrosion Fatigue Crack Growth Rate", *J. Test. and Eval. (JTEVA)*, **7**(3), 155-159 (May, 1979).

127. Bogar, F. D., and Crooker, T. W., "Influence of Bulk-Solution-Chemistry Conditions on Corrosion-Fatigue Crack-Growth Rate", NRL Report 8265 (August 21, 1978), ADA061119.

128. Kawai, S., and Koibuchi, K., "Effect of Waveform on Corrosion Fatigue Crack Growth", *Fatigue of Engineering Materials and Structures*, **1**(4), 395-407 (1979).

129. Austen, I. M., and Walker, E. F., "Quantitative Understanding of the Effects of Mechanical and Environmental Variables on Corrosion Fatigue Crack Growth Behaviour", Paper presented at Institution of Mechanical Engineers Conference, The Influence of Environment on Fatigue, London, England, May 18 to 19, 1977.

130. Barsom, J. M., "Effect of Cyclic Stress Form on Corrosion Fatigue Crack Propagation Below K_{Iscc} in a High Yield Strength Steel", in *Corrosion Fatigue: Chemistry, Mechanics and Microstructure*, **NACE-2,** 424-435 (1972).

131. Hasson, D. F., Zanis, C., Aprigliano, L., and Fraser, C., Research and Development Center, Annapolis, Maryland. "Surfacing of 3.25% Nickel Steel with Inconel 625 by the Gas Metal Arc Welding-Pulsed Arc Process", *Welding Journal*, 57(1), 1-s-8-s (January, 1978).

132. Macco, J. G., "High-Cycle Flexural Fatigue Properties of Materials for Hydrofoil Strut/Foil Structures", Naval Ship Research and Development Report No. DTNSRDC-76-0045 (August, 1976), ADB013285L.

133. Gross, M. R., and Czyryca, E. J., "Effects of Notches and Saltwater Corrosion on the Flexural Fatigue Properties of Steels for Hydrospace Vehicles", MEL Research and Development Report, No. 420/66 (October, 1966), AD644147.

134. Smith, J. A., Peterson, M. H., and Brown, B. F., "Effect of Cathodic Protection on Low-Cycle Corrosion Fatigue of HY-80 Steel at Slow Cycle Rates", Interim Report No. NRL-MR-1302 (April, 1962), ADA067622.

135. Brown, B. F., "*Corrosion Fatigue in Naval Structures*", Corrosion Fatigue: Chemistry, Mechanics, and Microstructure, **NACE**-25-29 (1972).

136. Wacker, G. A., "Effects of Marine Environment on High-Strength Steels", ASTM-STP 445, 68-87 (1969).

137. Vassilaros, M. G., and Czyryca, E. J., "Low-Cycle Fatigue Crack Initiation in HY-130 System Metals; Effects of Marine Environments, Cathodic Protection, Frequency, and Hold-Time", Research and Development Report MAT-77-57 (September, 1977), ADB021330L.

138. Gross, M. R., "The Mechanical, Thermal, and Fatigue Properties of HY-100 Steel", Report NAVENGRXSTA-910153 (April, 1961), AD833690.

139. Gallagher, J. P., "Corrosion Fatigue Crack Growth Behavior Above and Below K_{Iscc}", Final Report NRL-7064 (May 28, 1970), AD708377.

140. Hartt, W. H., and Adamson, J. H., "Fatigue and Corrosion Fatigue of HY-80 Steel, as Applicable to Anchor Bolt Failures", Final Report, Contract N00014-78-C-0307 (July, 1979), ADA072067.

141. Knight, J. W., "Corrosion Fatigue of Welded Quenched and Tempered Steels", *Welding Research Internat.*, 7(5), 385-411 (1977).

142. Clark, W. G., Jr., and Kim, D. S., "Effect of Synthetic Sea Water on the Crack Growth Properties of HY140 Steel Weldments", *Engineering Fracture Mechanics*, 4(3), 499-510 (September, 1972).

143. Vosikovsky, O., "Frequency, Stress Ratio, and Potential Effects on Fatigue Crack Growth of HY130 Steel in Salt Water", *J. Test. and Eval. (JTEVA)*, 6(3), 175-182 (May, 1978).

144. Congleton, J., Craig, I. H., Denton, B. K., and Parkins, R. N., "Crack Growth in HY80 and HY130 Steels by Corrosion Fatigue", *Metal Sci.*, 13(7), 436-443 (July, 1979).

145. Ryder, J. T., and Gallagher, J. P., "Temperature Influence on Corrosion Fatigue Behavior of 5Ni-Cr-Mo-V Steel", *J. Test. and Eval. (JTEVA)*, **2**(3), 180-189 (May, 1974).

146. Davis, D. A., and Czyryca, E. J., "The Effects of Environment and Cathodic Protection on the Low-Cycle Fatigue Crack Growth Characteristics of a 5Ni-Cr-Mo-V Steel", Paper presented at ASME Pressure Vessels and Piping Technology Conference, San Francisco, August, 1980.

147. Gallagher, J. P., Ryder, J. T., and Hadley, J. C., "The Salt Water Corrosion Fatigue Crack Propagation Behavior of Two Steels", *Proceedings of the 1971 International Conference on Mechanical Behavior of Materials*, Japan, August 15 to 20, 1971, Vol. III, pp. 328-340.

148. Beach, J. E., Marchica, N. V., and Ichter, L. L., "A Fatigue Comparison of High Strength Steel, Stainless Steel, and Titanium in a Simulated Ocean Environment", *Proceedings of 10th Annual Offshore Technology Conference*, Houston, Texas, May 8 to 11, 1978, Vol. III, pp. 1737-1745.

149. Lennox, T. J., Jr., Peterson, M. H., Brown, B. F., Groover, R. E., Newbegin, R. L., Smith, J. A., and Waldron, L. J., "Marine Corrosion Studies—Stress Corrosion Cracking, Deep Ocean Technology, Cathodic Protection, Corrosion Fatigue", Memorandum Report, Fourth Interim Report of Progress, NRL-MR-1711 (May, 1966), AD639599.

150. Pettit, D. E., Hoeppner, D. W., and Hyler, W. S., "Evaluation of Methods to Alleviate Corrosion Fatigue in Type 135 Drill-Pipe Steel for Offshore-Drilling Applications", ASTM-STP 462, 241-257 (1970).

151. Schwab, R. C., and Czyryca, E. J., "Effects of Notches and Salt Water Corrosion on the Flexural Fatigue Behavior of High-Strength Structural Alloys", Naval Ship R&D Laboratory Research and Development Report No. 2854 (May, 1969), AD852521.

152. Davis, D. A., and Czyryca, E. J., "Mechanical Properties of Astralloy-V Forged Shaft", Naval Ship Research and Development Center Report MAT-75-67 (January, 1976), ADB008764L.

153. Taniguchi, K., Oda, T., Ueda, S., and Nakajima, M., "Development of New High Strength Special Steel Propeller for Big Ship", *Japan Shipbuilding and Marine Engineering*, pp. 20-28 (January, 1969).

154. Harbage, A. B., "Fatigue Study of a Monel Inlaid Shaft Exposed to Seawater", Naval Ship Research and Development Center Report No. 7-353 (April, 1970), AD869198.

155. Levy, M., and Morrossi, J. L., "Corrosion Fatigue Behavior of Coated 4340 Steel for Blade Retention Bolts of the AH-1G Helicopter", Final Report No. AMMRC-TR-76-34 (October 11, 1976), ADA033253.

156. Lee, H. H., and Uhlig, H. H., "Corrosion Fatigue of Type 4140 High Strength Steel", *Metall. Trans.*, **3**(11), 2949-2957 (November, 1972).

157. Hasan, S. Z., Ghali, E. L., and Dumais, J., "Influence of pH and Specimen Orientation on Corrosion Fatigue Behavior of 18% Ni (300) Maraging Steel in Chloride Environments", *SAMPE Quart.*, **7**(1), 20-27 (October, 1975).

158. Hutchings, J., and Sanderson, G., "The Influence of Tempering Temperature, Minor Alloying Elements, and Cathodic Polarization on the Low Frequency Fatigue Resistance of 18% Ni Maraging Steel", *Corrosion Sci.*, **16**(8), 545-549 (1976).

159. Baxa, M. S., Chang, Y. A., and Burck, L. H., "Effects of Sodium Chloride and Shot Peening on Corrosion Fatigue of AISI 6150 Steel", *Metall. Trans.*, **9A**(8), 1141-1146 (August, 1978).

160. Chait, R., and Campbell, M. D., "Corrosion Fatigue and Stress-Corrosion Cracking of High-Hardness Laminar Composite Steel", ASTM-STP 610, 226-242 (1976).

161. Bellow, D. G., and Faulkner, M. G., "Salt Water and Hydrogen Sulfide Corrosion Fatigue of Work-Hardened, Threaded Elements", *J. Test. and Eval. (JTEVA)*, **4**(2), 141-147 (March, 1976).

162. Heller, S. R. Jr., Matanzo, F., and Metcalf, J. T., "Axial Fatigue of Wire Rope in Sea Water", Final Report (June 15, 1972), AD743924.

163. Gutman, E. M., Abdullin I. G., and Kleiner, L. M., "Use of Low-Carbon Martensitic Steels Without Nickel for Deep-Well Sucker Rods", *Fiz-Khim. Mekh. Mater.*, **15**(1), 67-68 (1979).

164. Endo, K., Komai, K., and Imashiro, N., "Environmental Effects on Initiation and Propagation of Fatigue Cracks in High Strength Steel", *Bull. JSME*, **20**(143), 513-520 (May, 1977).

165. Rollins, V., Arnold B., and Lardner, E., "Corrosion Fatigue in High Carbon Steel", *Brit. Corrosion J.*, **5** (January, 1970).

166. Crooker, T. W., and Lange, E. A., "Corrosion-Fatigue Crack Propagation Studies of Some New High-Strength Structural Steels", *Trans. ASME, J. Basic Engineering*, Series D, **91**(4), 570-574 (December, 1969).

167. Austen, I. M., and Walker, E. F., "The Influence of Environmental Aggression on the Corrosion Fatigue Behavior of Steels", *Proceedings of International Conference on Mechanisms of Environment Sensitive Cracking of Materials*, University of Surrey, Guildford, England, April 4 to 7, 1977, pp. 334-347.

168. Austen, I. M., West, J. M., and Brook, R., "Corrosion Fatigue in Nickel Steels", *Metal Sci.*, **12**(2), 77-82 (February, 1978).

169. Pettit, D. E., Ryder, J. T., Krupp, W. E., and Hoeppner, D. W., "Environmental Aspects of Subcritical Crack Growth", *Proceedings of Second International Conference on Mechanical Behavior of Materials*, August 16 to 20, 1976, pp. 680-684.

170. Barsom, J. M., "Corrosion-Fatigue Crack Propagation below K_{Iscc}", *Engineering Fracture Mechanics*, **3**, 15-25 (July, 1971).

171. Eisenstadt, R., and Rajan, K. M., "Effect of Salt Water Temperature on the Crack Growth Characteristics of 12 Chrome Steel", *J. Eng. Mater. and Technol.*, Series H, **96**(2), 81-87 (April, 1974).

172. Preiser, H. S., "Research on the Corrosion Behavior of 17-4 PH Stainless Steel in High Velocity Seawater", Final Report No. TR-838-F (September, 1969), AD859795L.

173. Redmond, J. R., "Seawater Corrosion Fatigue of CA-6NM, CA-15 and a High-Molybdenum Modification of CA-6NM", Climax Molybdenum Co. Report No. RP-33-75-20 (December 9, 1976).

174. Tenge, P., and Gjertsen, G., "Corrosion Fatigue Cracking from Surface Defects in Marine Propeller Blades", *Proceedings of 7th Scandinavian Corrosion Congress*, Trondheim, Norway, May 26 to 28, 1975, pp. 279-296.

175. Ueda, S., Daikoku, T., and Matsuo, S., "Development of High Strength Steel for Propeller", *Japan Shipbuilding and Marine Eng.*, **12**(4), 17-24 (1978).

176. Ebara, R., Kai, T., and Inoue, K., "Long Life Corrosion Fatigue Behavior of 13Cr Stainless Steel in NaCl Aqueous Solution", *Proceedings of the 21st Japan Congress on Materials Research*, Tokyo, Japan, October, 1977, pp. 89-92.

177. Amzallag, C., Rabbe, P., and Desestret, A., "Corrosion-Fatigue Behavior of Some Special Stainless Steels", ASTM-STP 642, 117-132 (1977).

178. Ebara, R., Mihara, M., Kino, H., Kai, T., Katayama, K., and Shiota, K., "Corrosion Fatigue Behavior of 13Cr Stainless Steel for Turbine Moving Blade", Mitsubishi Heavy Industries, Mitsubishi Technical Bulletin, No. 129 (November, 1978).

179. Ebara, R., Kano, H., Takano, Y., Hakjima, K., and Nathano, K., "Influence of Dissolved Oxygen Contents and Stress Concentration Factor on Corrosion Fatigue Strength of Turbine Moving Blade", Mitsubishi Heavy Industries, Ltd., Technical Review (October, 1979).

180. Clark, W. G., Jr., "The Fatigue Crack Growth Rate Properties of Type 403 Stainless Steel in Marine Turbine Environments", Book of papers, presented at a Symposium on Corrosion Problems in Energy Conversion and Generation, Fall Meeting of the Electrochemical Society, New York City, October 15 to 17, 1974, pp. 359-367.

181. Abrego, L., Begley, J. A., "Fatigue Crack Propagation of 403 Stainless Steel in Aqueous Solutions at 100 C", Paper No. 235 presented at Corrosion/80, Chicago, Illinois, March 3 to 7, 1980.

182. Collins, J. D., "The Effects of Residual Magnetism on the Corrosion Fatigue Properties of Type 410 Stainless Steel Compressor Blades", *Corrosion*, 32(3), 109-113 (March, 1976).

183. Amzallag, C., Rabbe, P., and Truchon, M., "Failure of Stainless Steels by Corrosion-Fatigue", *Proceedings of the Fourth International Conference on Fracture*, held at University of Waterloo, Ontario, Canada, June, 1977, Vol. 2B, pp. 873-878.

184. Bock, H. E., "On the Stress and Fatigue Corrosion Cracking Behavior of Nitrogen-Alloyed Austenitic and Ferritic-Austenitic Chromium-Nickel-(Molybdenum) Steels", *Tech. Mitt. Krupp Forschungsber*, 36(2), (August, 1978) (In German).

185. Journeaux, G. E., Martin, J. W., and Talbot, D.E.J., "The Role of Electrochemistry in Corrosion-Fatigue", *Proceedings of International Conference on Mechanisms of Environment Sensitive Cracking of Materials*, University of Surrey, Guildford, England, April 4 to 7, 1977, pp. 322-333.

186. Richardson, W. H., Guha, P., and Machin, R., "The Development of a High Strength Ductile Stainless Steel of Improved Corrosion Resistance in Marine and Chemical Environments", *Proceedings of Third International Congress on Marine Corrosion and Fouling*, Gaithersburg, Maryland, October 2 to 6, 1972, pp. 528-536.

187. Karpenko, G. V., Tkachenko, N. N., Potapov, V. V., Zafiiovskii, Yu. M., Kiliushko, B. F., and Kolosov, I. E., "Corrosion-Fatigue Strength of Steel OCr18Ni10Ti in Aqueous NaCl and $MgCl_2$ Solutions at High Temperatures and Pressures", *Soviet Mater. Sci.*, 5(3), 223-225 (May to June, 1969).

188. Ellinghausen, H. C., "Endurance and Stressless Corrosion Fatigue Tests of Ni-Cu Alloys and Tobin Bronze in Sea Water", U.S. Naval Engineering Experiment Station, Research and Development Report No. PB168687 (April 15, 1957).

189. Newcombe, G., "Some Copper Alloy Weld Fabrications and Their Performance in Sea Water", Paper presented at CDA-ASM Conference on Copper, Cleveland, Ohio, October 16 to 19, 1972.

190. Stewart, W. C., and Williams, W. L., "Investigation of Materials for Marine Propellers", *Proc. ASTM*, **46**, 836-845 (1946).

191. Anon., "The Corrosion of Metals—Part VI—The Corrosion of Copper and Its Alloys", *Sheet Metal Ind.*, **24**(1), 145-153 (January, 1947).

192. Gross, M. R., and Schwab, R. C., "Fatigue Properties of Nonferrous Alloys for Heat Exchangers, Pumps, and Piping", Technical Report No. MEL 232/66 (May, 1966).

193. Gross, M. R., "Low-Cycle Fatigue of Materials for Submarine Construction", NAVEN-GRXSTA Report No. 91 197D (February 14, 1963).

194. Czyryca, E. J., and Gross, M. R., "Low Cycle Fatigue of Nonferrous Alloys for Heat Exchangers and Salt-Water Piping, Phase IV", NAVSHIPS, Report No. MEL 26/66 (February, 1966), AD627929.

195. Gatzoulis. J., Werchniak, W., and Czyryca, E. J., "Fatigue Behavior of Large Propellers", *Naval Engineers J.*, **86**, 65-77 (October, 1974).

196. Tokuda, S., Okuyama, Y., Inoue, H., and Denoh, S., "Fatigue Failure in Marine Propeller Blades", Paper presented at the Propellers '78 Symposium, Virginia Beach, Virginia, May 24 to 25, 1978.

197. Masuda, H., and Duquette, D. J., "The Effect of Surface Dissolution on Fatigue Crack Nucleation in Polycrystalline Copper", *Metall. Trans.*, **6A**(1), 87-94 (January, 1975).

198. Birley, S. S., and Tromans, D., "Corrosion Fatigue of Copper and Alpha Brass", *J. Electrochem. Soc.*, **119**(10), 1278-1285 (October, 1972).

199. Duquette, D., Andresen, P., and Masuda, H., "Corrosion Fatigue Crack Initiation in Cu and 7.8% Al", RPI Technical Report No. 9741.2-MC (1973), AD770209.

200. Gough, H. J., and Sopwith, D. G., "The Resistance of Some Special Bronzes to Fatigue and Corrosion-Fatigue", *J. Inst. of Metals*, **LX**(1), 143-158 (1937).

201. Richards, J. T., "Corrosion Resistance of Beryllium Copper", *Corrosion*, **9**(10), 359-371 (October, 1953).

202. Langham, J. M., and Webb, A.W.O., "The New High Strength Copper-Manganese-Aluminium Alloys—Their Development, Properties and Applications", *Brit. Foundryman*, **55**, 246-262 (June, 1962).

203. Elin, I. A., Zhur, N. V., Kvurt, O. S., Shekhovtsev, Ye. D., and Smiryagin, A. P., "Copper Alloys for Screw Propellers of Sea Vessels", *Transactions of the Central Scientific Research Institute of Merchant Marine, Technical Maintenance of Merchant Marine, New Materials in Ship Technology, Prevention of Corrosion*, No. 116, pp. 32-38 (1969).

204. Leoni, M., and Fortina, G., "Investigation of the Structural, Mechanical and Corrosion-Resistance Properties of Complex Co-Bearing Aluminum Bronzes", Final Report to INCRA, New York (January, 1971).

205. Veyngarten, A. M., Ozhiganov, Yu. G., Vsorov, Yu. K., Gubarev, M. R., and Taratuta, M. V., "Cathodic Protection of Bronze AZhN-9-4-4 in Sea Water from Corrosion Fatigue", *Protection of Metals*, **9**(6), 735-736 (1973) (Translation).

206. Solumsmoen, O. H., "Marine Propeller Materials Evaluation of Corrosion Fatigue Strength", *European Shipbuilding*, **21**(3/4), 42-48 (1972).

207. Veingarten, A. M., Taratuta, M. V., Ozhiganov, Yu. G., Vzorov, Yu. K., and Gubarev, M. K., "Raising the Corrosion Resistance and Corrosion-Fatigue Strength of Screw Propellers Made of Brass LMtsZh 55-3-1 by Cathodic Polarization", *Soviet Materials Sci.*, **10**(3), 303-305 (October, 1975).

208. Czyryca, E. J., and Niederberger, R. B., "Mechanical, Fatigue and Corrosion Properties of Propeller Bronzes", Paper presented at Propellers '75 Conference, The Society of Naval Architects and Marine Engineers, Philadelphia, Pennsylvania, July 22-23, 1975.

209. Cross, D. G., "Materials Design, Processing, and Performance Data for Construction of Seawater Systems", *Proceedings of Inter-Nav. Corrosion Conference*, New Zealand Government Printer, Auckland, N.Z. (1976).

210. Collins, P., and DuQuette, D. J., "Corrosion Fatigue Behavior of a Duplex Aluminum Bronze Alloy", *Corrosion*, **34**(4), 119-124 (April, 1978).

211. Smith, K. N., Watson, P., and Topper, T. H., "A Stress-Strain Function for Fatigue of Metals", *J. of Materials*, Vol. 5, No. 4, 1970, pp. 767-778.

212. Person, N. L., "Fatigue Properties of Prior-Corroded Aluminum Sheet Alloys", *Materials Performance*, **14**(12), 22-26 (December, 1975).

213. Austin, C. W., "Rotating Beam Fatigue and Corrosion Fatigue Properties of Aluminum and Magnesium Alloys", Summary Report No. ABMA-DS-TN-169 (February, 1958), AD606552.

214. Gruff, J. J., and Hutcheson, J. G., "Spectrum Corrosion Fatigue Test of Various Aluminum Alloys—Phases I and II—RA-5C Extended Service Life Program", Report No. NR69H-425 (August, 1969), AD875665.

215. Harmsworth, C. L., "Effect of Corrosion on the Fatigue Behavior of 2024-T4 Aluminum Alloy", Report No. ASD-TR-61-121 (July, 1961), AD268569.

216. Figge, I. E., and Hudson, C. M., "Crack Propagation Delayed Failure, and Residual Static Strength of Titanium, Aluminum, and Stainless Steel Alloys in Aqueous Environments", NASA-TN-D-3825 (February, 1967).

217. Crooker, T. W., "Fatigue and Corrosion-Fatigue Crack Propagation in Intermediate-Strength Aluminum Alloys", *Trans. ASME, J. Eng. Mater. Technol.*, Series H, **95**(3), 150-156 (July, 1973).

218. Branco, C. M., Radon, J. C., and Culver, L. E., "An Analysis of the Influence of Mean Stress Intensity and Environment on Fatigue Crack Growth in a New High Strength Aluminum Alloy", *J. Test. and Eval. (JTEVA)*, **3**(6), 407-413 (November, 1975).

219. Radon, J. C., "Influence of Environment on Threshold in Fatigue Crack Growth", *Metal Sci.*, **13**(7), 411-419 (July, 1979).

220. Karlashov, A. V., Gainutdinov, R. G., and Pankov, A. T., "Relationship of Efficiency of Cladding D16 Alloy Sheet to Environmental Attack in Corrosion Fatigue", *Soviet Mater. Sci.*, **9**(3), 262-265 (May-June, 1973).

221. Maksimovich, G. G., Yanchishin, F. P., Shchepanskii, Ya. S., Nagirnyi, S. V., and Kalichak, T. N., "Corrosion-Fatigue Strength of Duralumin D16 Previously Deformed in Tension", *Soviet Mater. Sci.*, **7**(3), 265-267 (May-June, 1971).

222. Karlashov, A. F., Gainutdinov, R. G., and Pankov, A. T., "Comparative Study of the Effect of Anodizing and of Cladding Followed by Anodizing on the Cyclic Strength of D16T Sheet Material", *Soviet Mater. Sci.*, **12**(1), 76-79 (January-February, 1976).

223. Shavyrin, V. N., and Suvorova, G. S., "Effect of a Polymer Coating on Corrosion-Fatigue Strength of Welded Joints in Aluminum Alloys", *Soviet Mater. Sci.*, **8**(2), 150-152 (March-April, 1972).

224. Chanani, G. R., "Investigation of Effects of Saltwater on Retardation Behavior of Aluminum Alloys", ASTM-STP 642, 51-73 (1977).

225. Bathias, C., "Corrosion Fatigue of Aluminum Alloys", Paper presented at 44th Meeting of the Structures and Materials Panel of AGARD, April, 1977.

226. Feeney, J. A., McMillan, J. C., and Wei, R. P., "Environmental Fatigue Crack Propagation of Aluminum Alloys at Low Stress Intensity Levels", Boeing Co. Research Report No. D6-60114 (May, 1969), ARPA Contract N00014-66-C0365.

227. Karlashov, A. V., and Pryakhin, I. I., "Increase in the Corrosion-Fatigue Strength of Aluminum Alloy with Treatment by Magnetic Field", *Soviet Mater. Sci.*, 9(4), 383-385 (July-August, 1973).

228. Chu, H. P., "Fatigue Crack Propagation in a 5456-H117 Aluminum Alloy in Air and Sea Water", *Trans. ASME, J. Eng. Mater. and Technol.*, Paper No. 74-MAT-4 (1974), AD769467.

229. Crooker, T. W., and Bogar, F. D., "Engineering Consideration of Electrochemistry in Corrosion-Fatigue Crack Propagation", Paper presented at the 14th Annual Meeting of the Society for Engineering Science, Inc., Lehigh University, Bethlehem, Pennsylvania, November 14 to 16, 1977.

230. Czyryca, E. J., and Vassilaros, M. G., "Corrosion Fatigue of Marine Aluminum Alloys in Salt Water Environments", Paper No. 24 presented at Tri-Service Conference on Corrosion (1972).

231. Bogar, F. D., and Fujii, C. T., "The Effect of Dissolved Oxygen in Natural Seawater on the Corrosion-Fatigue Behavior of 5456-H116 Aluminum Alloy", Report of NRL Progress, pp. 32-34 (November, 1978).

232. Tinkel, T. L., "Corrosion Fatigue of a Marine Aluminum Alloy (5456-H343) in the Presence of Shallow Cracks", Master's Thesis (June, 1978), ADA072562.

233. Flodder, S. P., and Hartt, W. H., "Corrosion Fatigue of 5086-H34 Aluminum in Sea Water", *Proceedings of 4th Annual Conference on Ocean Thermal Energy Conversion*, 1977, Section VII, pp. 41-45, published by Technical Information Center, Oak Ridge, Tennessee.

234. Rogers, R. W., Jr., Vernam, W. D., and Shumaker, M. B., "Test and Exploratory Development of an Optimum Aluminum Alloy System for Ship Structures", NAVSHIPS 56-AC223 (July 23, 1974), AD787568.

235. Smith, E. F., Jacko, R., and Duquette, D. J., "Hydrogen Assisted Fatigue Cracking of High Strength Aluminum Alloys", Technical Report from RPI to ONR (August, 1975), ADA014477.

236. Corsetti, L. V., and Duquette, D. J., "The Effect of Mean Stress and Environment on Corrosion Fatigue Behavior of 7075-T6 Aluminum", RPI Technical Report No. 2 to ONR (April 10, 1973), AD763455.

237. Stoltz, R. E., and Pelloux, R. M., "Mechanisms of Corrosion Fatigue Crack Propagation in Al-Zn-Mg Alloys", *Metall. Trans.*, 3(9), 2433-2441 (September, 1972).

238. Craig, W. J., "Fatigue and Stress Corrosion Characteristics of 7075-T6 Aluminum Alloy Extrusion", Report No. LR-24663 and GIDEP-502.22.10.41-FB-02 (March, 1972), ADB007165L.

239. Smith, E. F., III, and Duquette, D. J., "The Corrosion Fatigue Behavior of a High Purity Al-Zn-Mg-Cu Alloy", RPI Technical Report to ONR, Contract N00014-75-C-0466 (November, 1979), ADA077461.

240. Hoffman, A. E., and Kennedy, W. L., "Corrosion and Materials Selection Problems on Hydrofoil Craft", *Materials Protection*, **2**, 56, 58-68 (September, 1963).

241. Endo, K., Komai, K., and Watase, Y., "Cathodic Protection in Corrosion Fatigue of an Aluminum-Zinc-Magnesium Alloy", *Proceedings of the 19th Japan Congress on Materials Research*, Kyoto, Japan, 1976, pp. 71-76.

242. Gunn, N.J.F., and Ballett, J. T., "The Axial Loading Corrosion Fatigue Properties of 25mm Thick High and Low Strength X166 Plate (DTD 5120 and DTD 5130)", Report No. RAE-TR-78114 and DRIC-BR-65880 (September, 1978), ADA071434.

243. Bowen, A. W., "Corrosion Fatigue of Aluminum and Titanium Alloys and Steels", Paper presented at the 44th Meeting of the Structures and Materials Panel of AGARD, April, 1977.

244. Stoltz, R. E., and Pelloux, R. M., "Inhibition of Corrosion Fatigue in 7075 Aluminum Alloys", *Corrosion*, **29**(1), 13-17 (January, 1973).

245. Hall, L. R., Finger, R. W., and Spurr, W. F., "Corrosion Fatigue Crack Growth in Aircraft Structural Materials", AFML-TR-73-204 (September, 1973), AD916695.

246. Stoltz, R. E., and Pelloux, R. M., "Corrosion Fatigue of High Strength Aircraft Structural Materials—Crystallographic Dependence of Fracture Path in Al-Zn-Mg (7075) Alloys", Report No. AFML-TR-77-36 (December, 1977), ADA053743.

247. Selines, R. J., Stoltz, R. E., and Pelloux, R. M., "Corrosion Fatigue Crack Propagation in Aluminum Alloys—Part I: Effect of Cyclic Stress Wave Form on Corrosion Fatigue Crack Propagation in AL-Zn-MG Alloys—Part II: Mechanisms of Corrosion Fatigue Crack Propagation in Al-Zn-Mg Alloys", AFML TR-72-21-Pt-1/2 (February, 1972, AD747709.

248. Clerivet, A., and Bathias, C., "Study of Crack Tip Opening Under Cyclic Loading Taking into Account the Environment and R Ratio", *Engineering Fracture Mechanics*, **12**(4), 599-611 (1979).

249. Piper, D. E., Smith, S. H., and Carter, R. V., "Corrosion Fatigue and Stress-Corrosion Cracking in Aqueous Environments", **8**, 50-63 (August, 1968).

250. Dawson, D. B., and Pelloux, R. M., "Corrosion Fatigue Crack Growth of Titanium Alloys in Aqueous Environments", *Metall. Trans.*, **5**(3), 723-731 (March, 1974).

251. Ryder, J. T., Krupp, W. E., Pettit, D. E., and Hoeppner, D. W., "Corrosion-Fatigue Properties of Recrystallization Annealed Ti-6Al-4V", ASTM-STP-642, 202-222 (1977).

252. Sommer, A. W., and Creager, M., "Research Toward Developing and Understanding of Crystallographic Texture on Mechanical Properties of Titanium Alloys", Interim Quarterly Report (November, 1975), AFSC, Contract F33615-74-C-5107.

253. Imam, M. A., Gilmore, C. M., and Franker, A. C., "Corrosion-Fatigue Properties of the Ti-6Al-4V Alloy", *Proceedings of Conference on Environmental Degradation of Engineering Materials*, Blacksburg, Va., October 10 to 12, 1977, pp. 783-790.

254. Crooker, T. W., and Lange, E. A., "Effects of a 3.5 Percent Sodium Chloride Aqueous Saline Environment on the Fatigue Crack Propagation Characteristics of Titanium Alloys", ASTM-STP 432, 251-267 (1968).

255. Krupp, W. E., Ryder, J. T., Pettit, D. E., and Hoeppner, D. W., "Corrosion Fatigue Properties of Ti-6Al-6V-2Sn (STOA)", ASTM-STP 631, 345-364 (1977).

256. Meyn, D. A., "An Analysis of Frequency and Amplitude Effects on Corrosion Fatigue Crack Propagation in Ti-8Al-1Mo-1V", *Metall. Trans.*, **2**(3), 853-865 (March, 1971).

257. Cullen, W. H., and Stonesifer, F. R., "Fatigue-Crack-Growth Analysis of Titanium Gas-Turbine Fan Blades", NAVAIR, NRL-MR-3378 (October, 1976), ADA031836.

258. Yoder, G. R., Cooley, L. A., and Crooker, T. W., "Improvement of Environmental Crack Propagation Resistance in Ti-8Al-1Mo-1V Through Microstructural Modification", Final Report No. NRL-MR-3955 (March, 1979), ADA069084.

259. Cares, W. R., and Crooker, T. W., "Fatigue-Crack Growth of Ti-6Al-2Cb-1Ta-0.8Mo Alloy in Air and Natural Sea Water Environments", NRL Memorandum Report 2617 (June, 1973), AD765318.

260. Wanhill, R.J.H., "Fractography of Stress Corrosion in Ti-8Al Tested in Fatigue", *Corrosion*, **29**(7), 261-267 (July, 1973).

261. Glikman, L. A., and Shekhovtsev, E. D., "Corrosion-Fatigue of Titanium Alloys in the Low Endurance Range", *Soviet Mater. Sci.*, **5**(6), 633-634 (November-December, 1969).

262. Wanhill, R.J.H., "Environmental Fatigue Crack Propagation in Metal/Composite Laminates", *Fatigue of Engineering Materials and Structures*, **2**(3), 319-330 (1979).

263. Crooker, T. W., and Lange, E. A., "Failure of Structural Alloys by Slow Crack Growth", Naval Research Laboratory Report 6944 (October, 1969), AD175243.

264. Krafft, J. M., Lamb, C. L., and Simmonds, K. E., "Corrosion- and Creep-Induced Instability—Modeling of Fatigue Cracking in Various Alloys", NRL Memorandum Report 2399 (February, 1972).

265. Yoder, G. R., Cooley, L. A., and Crooker, T. W., "Corrosion Fatigue Resistance of Beta-Annealed Ti-8Al-1Mo-1V in 3-1/2% Salt Water", Report of NRL Progress, pp. 7-8 (September, 1978).

266. Levy, M., and Morrossi, J. L., "Corrosion Fatigue Behavior of Coated 4340 Steel for Blade Retention Bolts of the AH-1 Helicopter", *Corrosion-Fatigue Technology*, ASTM Special Tech. Pub. 642, 300-312 (1978).

267. Levy, M., Dawson, D. B., Sklover, G. N., and Seitz, D. W., Jr., "The Corrosion Behavior of Titanium Alloys in Chloride Solutions: Materials for Surgical Implants", in *Titanium Science and Technology* (R. I. Jaffe and H. M. Burte, Eds.), Vol. 4, Plenum Publishing Company, New York, N.Y., 1973.

CONVERSION FACTORS

1 cpm	=	0.0166 cps
1 cps	=	1 Hz
1 Hz	=	1 cps
1 inch	=	25.4 mm
1 kg/mm^2	=	1.422 ksi
1 ksi	=	6.89 MPa
1 ksi $\sqrt{\text{in.}}$	=	1.0989 MN/m$^{3/2}$
1.422 ksi	=	1 kg/mm^2
25.4 mm	=	1 inch
1.0989 MN/m$^{3/2}$	=	1 ksi $\sqrt{\text{in.}}$
1 MPa	=	1 N/mm^2
6.89 MPa	=	1 ksi
1 N/m^2	=	1 Pa
1 N/mm^2	=	1 MPa
1 Pa	=	1 N/m^2